frontiers | Research Topics

Evolution of phytochemicals and phytotherapies in the treatment and management of cancer: Targeted strategies in cancer precision medicine

Edited by
Mohd Adnan, Mitesh Patel and Visweswara Rao Pasupuleti

Published in
Frontiers in Pharmacology
Frontiers in Oncology

ISSN 1664-8714
ISBN 978-2-8325-3958-3
DOI 10.3389/978-2-8325-3958-3

About Frontiers

Frontiers is more than just an open access publisher of scholarly articles: it is a pioneering approach to the world of academia, radically improving the way scholarly research is managed. The grand vision of Frontiers is a world where all people have an equal opportunity to seek, share and generate knowledge. Frontiers provides immediate and permanent online open access to all its publications, but this alone is not enough to realize our grand goals.

Frontiers journal series

The Frontiers journal series is a multi-tier and interdisciplinary set of open-access, online journals, promising a paradigm shift from the current review, selection and dissemination processes in academic publishing. All Frontiers journals are driven by researchers for researchers; therefore, they constitute a service to the scholarly community. At the same time, the *Frontiers journal series* operates on a revolutionary invention, the tiered publishing system, initially addressing specific communities of scholars, and gradually climbing up to broader public understanding, thus serving the interests of the lay society, too.

Dedication to quality

Each Frontiers article is a landmark of the highest quality, thanks to genuinely collaborative interactions between authors and review editors, who include some of the world's best academicians. Research must be certified by peers before entering a stream of knowledge that may eventually reach the public - and shape society; therefore, Frontiers only applies the most rigorous and unbiased reviews. Frontiers revolutionizes research publishing by freely delivering the most outstanding research, evaluated with no bias from both the academic and social point of view. By applying the most advanced information technologies, Frontiers is catapulting scholarly publishing into a new generation.

What are Frontiers Research Topics?

Frontiers Research Topics are very popular trademarks of the *Frontiers journals series*: they are collections of at least ten articles, all centered on a particular subject. With their unique mix of varied contributions from Original Research to Review Articles, Frontiers Research Topics unify the most influential researchers, the latest key findings and historical advances in a hot research area.

Find out more on how to host your own Frontiers Research Topic or contribute to one as an author by contacting the Frontiers editorial office: frontiersin.org/about/contact

Evolution of phytochemicals and phytotherapies in the treatment and management of cancer: Targeted strategies in cancer precision medicine

Topic editors
Mohd Adnan — University of Hail, Saudi Arabia
Mitesh Patel — Parul University, India
Visweswara Rao Pasupuleti — REVA University, India

Citation
Adnan, M., Patel, M., Pasupuleti, V. R., eds. (2023). *Evolution of phytochemicals and phytotherapies in the treatment and management of cancer: Targeted strategies in cancer precision medicine*. Lausanne: Frontiers Media SA.
doi: 10.3389/978-2-8325-3958-3

Table of contents

frontiers | Frontiers in Pharmacology

TYPE Editorial
PUBLISHED 02 November 2023
DOI 10.3389/fphar.2023.1326474

OPEN ACCESS

EDITED AND REVIEWED BY
Olivier Feron,
Université catholique de Louvain,
Belgium

*CORRESPONDENCE
Mohd Adnan,
drmohdadnan@gmail.com

RECEIVED 23 October 2023
ACCEPTED 30 October 2023
PUBLISHED 02 November 2023

CITATION
Adnan M, Pasupuleti VR and Patel M (2023), Editorial: Evolution of phytochemicals and phytotherapies in the treatment and management of cancer: targeted strategies in cancer precision medicine.
Front. Pharmacol. 14:1326474.
doi: 10.3389/fphar.2023.1326474

Editorial: Evolution of phytochemicals and phytotherapies in the treatment and management of cancer: targeted strategies in cancer precision medicine

Mohd Adnan[1]*, Visweswara Rao Pasupuleti[2] and Mitesh Patel[3]

[1]Department of Biology, College of Science, University of Ha'il, Ha'il, Saudi Arabia, [2]Center for International Collaboration and Research, REVA University, Bangalore, Karnataka, India, [3]Research and Development Cell, Department of Biotechnology, Parul Institute of Applied Sciences, Parul University, Vadodara, India

KEYWORDS

phytomedicine, precision medicine, natural products, phytotherapies, cancer

Editorial on the Research Topic
Evolution of phytochemicals and phytotherapies in the treatment and management of cancer: targeted strategies in cancer precision medicine

There is a rising recurrence of cancers in humans and related complications of chemotherapeutic agents that reduce the clinical potency of numerous anticancer agents, including those which are currently in use. Hence, there is a consistent need for the development of alternative or synergistic anticancer drugs with lower side complications. Plants are predicted to have innumerable functional phytochemical constituents with potent features, and aid as prime source and candidates for the discovery of anticancer drugs. Therefore, considering the fact, this Research Topic of Frontiers in Pharmacology aims to cover the current trends and advancements in phytotherapies with an emphasis on targeted strategies in cancer precision medicine. Total of 17 manuscripts, which includes 10 research and 7 review articles were published in this Research Topic covering the recent advances in phytochemicals and phytotherapies for targeted cancer therapy.

First paper focuses on the treatment of rhabdomyosarcoma (RMS), the most common type of pediatric soft tissue sarcoma. Since RMS efficiently activates mechanisms of resistance to therapies, despite improvements, the prognosis remains still largely unsatisfactory. Here, authors have showed the therapeutic properties of PBI-05204, an extract from *Nerium oleander* containing the CG oleandrin, which is already studied in phase I and II clinical trials for cancer patients, were investigated, *in vitro* and *in vivo*, against FN- and FP-RMS cancer models. They found that PBI-05204 efficiently counteracted the transformed and intrinsically radioresistant phenotype of RMS by concomitantly inducing cytostatic and cytotoxic effects, promoting RT-induced G2 cell cycle arrest and restraining the ability of RMS cells to repair RT-induced DNA damage. These results suggest that PBI-05204 could have therapeutic and radiosensitizing properties on RMS (Vaccaro et al.).

Second paper highlights the role of dietary flavone apigenin (4′,5,7-trihydroxyflavone) in interacting and inhibiting the topoisomerase 1 and upregulating the CD26/DPP4 on colorectal carcinoma cells (CRC). They observed a unique synergistic interaction with the CRC chemotherapeutic agent irinotecan. The interplay between apigenin and irinotecan was not observed when apigenin was combined with other chemotherapeutic drugs including the topoisomerase 2 inhibitors doxorubicin or etoposide. Authors conclude that apigenin has a unique fit into the Topo1-DNA functional complex that leads to direct inhibition of Topo1 activity, and suggest that this is the basis for the exceptional interaction with the CRC drug irinotecan. A combined action of these two agents may therefore exert a role to limit local signals that facilitate tumour progression (Fux et al.).

Third paper focuses on locating the potential interactions of the diosgenin-regulated proteins and attributable pathways implicated in breast cancer using a range of system biology techniques, *i.e.,* gene ontology (GO) analysis, molecular docking, and molecular dynamics (MD) simulations, and reinforcing its findings using diverse functional biomarkers using *in vitro* experiments. Authors identified the probable action of the diosgenin against breast cancer via FoxO, PI3K-Akt, p53, Ras, and MAPK signaling pathways. This work will open the way for the development of novel therapeutic techniques and/or medication candidates for breast cancer (Khanal et al.).

Fourth paper presents a comprehensive review focussed on the potential anticancer benefits of bromelain, analyzing the cytotoxic, apoptotic, necrotic, autophagic, immunomodulating, and anti-inflammatory effects in cancer cells and animal models. Bromelain, the main medicinal component of pineapple, is an enzyme with numerous pharmacological properties, as it can act on different health disorders, including osteoporosis and osteoarthritis, diarrhea, chronic wounds, surgical debridement, edema, inflammation, and cancer. The anticancer properties of bromelain are extensively documented *in vitro* experiments, but such demonstrations *in vivo* animal models are far less. Here, authors have presented the novel approaches to cancer chemotherapy, which are warmly urgent and bromelain could be regarded as an important tool in the cancer fight (Pezzani et al.).

Fifth paper aimed to investigate the effects and mechanism of HQ (*Astragalus membranaceus* (Fisch.) Bunge (Huang Qi in Chinese), a well-known Chinese herbal medicine, and its bioactive ingredients FMNT (isoflavonoid, formononetin) and CS (isoflavonoid, calycosin) against colon cancer using network pharmacology analysis coupled with experimental validation and molecular docking. The findings suggested that the HQ exerted good therapeutic effects against colon cancer by mainly inhibiting the ERK1/2 signaling pathway. FMNT and CS were two bioactive ingredients responsible for the inhibitory effects of HQ against colon cancer. The current study expands our knowledge pertaining to the effects and mechanism of HQ against colon cancer, and suggests that FMNT and CS will hopefully serve as prospective compounds for colon cancer treatment (Hu et al.).

Sixth paper presents a systematic review focussed on the wide range of anticancer effects of licochalcones in gastric, lung, colon, breast, liver, and bladder cancer. After analyzing and collating the literature, authors concluded that the regulation of multiple signaling pathways by licochalcones includes the EGFR/ERK, PI3K/Akt/mTOR, p38/JNK, JAK2/STAT3, MEK/ERK, Wnt/β-catenin, and MKK4/JNK signaling pathways, which is the key to their antineoplastic effects. Among all the examined licochalcones, licochalcone A (LA) not only has antineoplastic effects, but also can be used to reduce drug efflux from cancer cells and reduce adverse reactions caused by other antitumor drugs. Authors therefore believe that the use of LA as an adjunct to anticancer drugs holds great promise (Deng et al.).

Seventh paper summarizes the antitumor activity and associated mechanisms of the organosulfur compounds of garlic in breast carcinoma. Authors presented in this review that garlic extract, its bioactive compounds, and their use in nanoformulations can prevent breast cancer in all of its stages, including initiation, promotion, and progression. Additionally, these bioactive compounds may affect cell signaling for cell cycle arrest and survival along with lipid peroxidation, nitric oxide synthase activity, epidermal growth factor receptor, nuclear factor kappa B (NF-κB), and protein kinase C in breast carcinoma. Altogether, in this review, authors have demonstrated the anticancer potential of garlic phytoconstituents and its nanoformulations as beneficial nutraceuticals and pharmaceuticals for the efficient management of human breast cancer (Pandey et al).

Eighth paper discusses the specific mechanisms and molecular targets of calotropin, a pharmacologically active compound isolated from milkweed plants like *Calotropis procera, Calotropis gigantea,* and *Asclepias currasavica* in cancer treatment. Calotropin is identified as a highly potent cardenolide that has a similar chemical structure to cardiac glycosides (such as digoxin and digitoxin). During the last few years, cytotoxic and antitumor effects of cardenolides glycosides have been reported more frequently. Among cardenolides, calotropin is identified as the most promising agent. Authors demonstrated that calotropin can be a potential chemotherapeutic/chemopreventive adjunctive agent in cancer pharmacotherapeutic management (Rajkovic et al.).

Ninth paper demonstrates the antitumor effects and potential mechanisms underlying the impact of 5-Demethylnobiletin (5-DMN), the active ingredient in citrus polymethoxyflavones on Glioblastoma (GBM) for the first time both *in vitro* and *in vivo*. Authors elucidated that 5-DMN promoted G0/G1 phase arrest and apoptosis in glioblastoma cells by restraining the ERK1/2, AKT and STAT3 signaling pathways. The results will help to evaluate the potential applications of 5-DMN as a clinical agent for glioblastoma (Zhang et al.).

Tenth paper investigates the inhibitory mechanisms of Polymethoxyflavonoids (PMFs) from *Citrus reticulata* 'Chachi' (CRCP) on nasopharyngeal carcinoma (NPC) growth *in vivo* and *in vitro*. The results of this study demonstrated for the first time that heptamethoxyflavone (HMF) purified from CRCP significantly inhibited the proliferation and induced apoptosis of NPC cells (CNE-2 and 5–8F), and also inhibited NPC cell migration and invasion. The results of the tumor transplantation experiment in nude mice confirmed the inhibitory effect of HMF on NPC cell growth *in vivo*. These findings provide a preliminary experimental basis for treating NPC and the development and utilization of PMFs in CRCP (Yang et al.).

Eleventh paper aimed to determine whether the administration of cocoa bean extract reduces doxorubicin-induced organ damage in mice with Ehrlich ascites carcinoma (EAC) without compromising doxorubicin efficacy. Authors demonstrated the protective effect of cocoa extract (COE) against doxorubicin-induced organ toxicities (heart, liver, and kidney), but also indicated synergistic potential with the anticancer activity of doxorubicin. Furthermore, the study also demonstrated the efficacy of COE to neutralize the free radicals

generated by doxorubicin; maintaining the cell integrity, along with the inherent anti-cancer properties; and prolonging the survival time of EAC mice. These findings exhibit the promising nutraceutical properties toward cardioprotective, hepatoprotective, and nephroprotective effects, when supplemented with doxorubicin (Patil et al.).

Twelfth paper aims to summarize and understand the mechanisms behind the anticancer potential of sulforaphane (SFN). Authors from this review concludes that SFN provides cancer protection through the alteration of various epigenetic and non-epigenetic pathways. It is a potent anticancer phytochemical that is safe to consume with minimal side effects. However, there is still a need for further research regarding SFN and the development of a standard dose. This will point to new therapeutic perspectives towards the possible development of new sulforaphane-based anticancer drugs (Ali et al.).

Thirteenth paper focuses on exploring the anticancer attributes of Cucurbitacin-B (Cur-B) against androgen-dependent prostate adenocarcinoma (PCa) LNCaP cells. Authors concluded that Cur-B suppressed the growth of PCa cells, which is associated with apoptosis induction, caspase activation, ROS generation, dissipation of mitochondrial membrane potential, and modulation of genes associated with apoptosis and cell cycle arrest. As a result, the data suggests the plausible potential of Cur-B as an alternative and complementary medicine for the treatment of PCa (Alafnan et al.).

Fourteenth paper focuses on details regarding the traits of the pentacyclic triterpenes known as boswellic acids (BAs), their roles as anti-cancer agents, the mechanism underlying their activities, and the function of their semi-synthetic derivatives in managing and treating certain cancers. The review also explores the biological sources of BAs, how they are conserved, and how biotechnology might help preserve and improve *in vitro* BA production. Authors conclude that the BAs and their semi-synthetic derivatives are effective against a broad spectrum of cancer cell lines. This comprehensive review can be helpful for researchers to gain more information about BAs and BA-based medications for efficient and cost-effective cancer treatments (Trivedi et al.).

Fifteenth paper is the first study to summarize the research progress on various compounds, including natural products and derivatives, that target the canonical Wnt pathway in lung cancer (LC) to develop safer and more targeted drugs or alternatives. Authors have particularly presented the impact of Wnt in mediating clinically relevant therapies for LC, such as chemotherapy, radiotherapy, EGFR-TKI, immunotherapy, and even anti-angiogenic therapy. Therefore, Wnt combination therapy is a good strategy for overcoming drug resistance in LC, and should be an overriding direction for future research. Many naturally occurring small molecules used as Wnt inhibitors have good effects, when used in combination with chemotherapy and targeted drugs, with the advantage of inhibiting proliferation and overcoming drug resistance (Shen et al.).

Sixteenth paper aimed to explore the efficacy of diallyl trisulfide (DATS) combined with cisplatin (DDP) for gastric cancer treatment and its underlying mechanism based on network pharmacology. Here, authors demonstrated that the combination of DDP and DATS significantly increased cytotoxicity and cell apoptosis compared to the DATS or DDP treatment group *in vitro*. In addition, continuous intraperitoneal injection of DATS markedly improved the tumor inhibitory effect of DDP in the SGC-7901 tumor-bearing mouse model. Authors further revealed that the combination of DATS and DDP synergistically enhanced antitumor activity by regulating endoplasmic reticulum stress and inhibiting STAT3/PKC-δ and MAPK signaling pathways. This study offers a new adjuvant strategy based on DATS and DDP for the treatment of gastric cancer (Lv et al.).

Seventeenth and final paper report the synthesis of methotrexate-conjugated zinc oxide nanoparticles (MTX-ZnONPs) and their high efficacy against lung cancer cells. The results of the current study have illustrated the conjugation of MTX with ZnONPs with high drug-loading efficiency. Authors emphasized the efficient delivery of MTX to lung cancer cells via ZnONPs as nanocarriers and showed that MTX could induce apoptosis in lung cancer cells via both caspase-dependent and caspase-independent pathways (Mishra et al.).

Existing therapeutic approaches to treat cancer in humans are invasive and often exhibit long-lasting side effects. Furthermore, there are a limited number of treatments available to treat different types of cancers, which represents a major challenge for cancer drug discovery. It is therefore necessary to develop new anticancer drugs. Improving fundamental understanding of the mechanisms underlying the cascade of cancer progression is of key importance towards transforming the landscape of cancer research and developing new and improved treatments of numerous cancerous cell types. Finally, the Guest Editors would like to sincerely thank all the authors and reviewers for their valuable contributions.

Author contributions

MA: Conceptualization, Supervision, Validation, Writing–original draft. VP: Data curation, Writing–review and editing. MP Data curation, Writing–review and editing.

Funding

The author(s) declare that no financial support was received for the research, authorship, and/or publication of this article.

Conflict of interest

The authors declare that the research was conducted in the absence of any commercial or financial relationships that could be construed as a potential conflict of interest.

Publisher's note

frontiers | Frontiers in Pharmacology

TYPE Original Research
PUBLISHED 01 December 2022
DOI 10.3389/fphar.2022.1071176

OPEN ACCESS

EDITED BY
Mitesh Patel,
Parul University, India

REVIEWED BY
Priyankar Dey,
Thapar Institute of Engineering and Technology, India
Patrick Valere Tsouh Fokou,
The University of Bamenda, Cameroon
Sindhu Subramanian,
Amrita Vishwa Vidyapeetham University, India

*CORRESPONDENCE
Francesco Marampon,
francesco.marampon@uniroma1.it

†These authors share first authorship

‡These authors have contributed equally to this work and share last authorship

SPECIALTY SECTION
This article was submitted to Pharmacology of Anti-Cancer Drugs, a section of the journal Frontiers in Pharmacology

RECEIVED 15 October 2022
ACCEPTED 16 November 2022
PUBLISHED 01 December 2022

CITATION
Vaccaro S, Rossetti A, Porrazzo A, Camero S, Cassandri M, Pomella S, Tomaciello M, Macioce G, Pedini F, Barillari G, Marchese C, Rota R, Cenci G, Tombolini M, Newman RA, Yang P, Codenotti S, Fanzani A, Megiorni F, Festuccia C, Minniti G, Gravina GL, Vulcano F, Milazzo L and Marampon F (2022), The botanical drug PBI-05204, a supercritical CO_2 extract of *Nerium oleander*, sensitizes alveolar and embryonal rhabdomyosarcoma to radiotherapy *in vitro* and *in vivo*. *Front. Pharmacol.* 13:1071176. doi: 10.3389/fphar.2022.1071176

The botanical drug PBI-05204, a supercritical CO_2 extract of *Nerium oleander*, sensitizes alveolar and embryonal rhabdomyosarcoma to radiotherapy *in vitro* and *in vivo*

Sara Vaccaro[1,2†], Alessandra Rossetti[3†], Antonella Porrazzo[1,4†], Simona Camero[5], Matteo Cassandri[1,4], Silvia Pomella[4,6], Miriam Tomaciello[1], Giampiero Macioce[2], Francesca Pedini[2], Giovanni Barillari[6], Cinzia Marchese[7], Rossella Rota[4], Giovanni Cenci[8,9], Mario Tombolini[10], Robert A. Newman[11], Peiying Yang[12], Silvia Codenotti[13], Alessandro Fanzani[13], Francesca Megiorni[7], Claudio Festuccia[3], Giuseppe Minniti[14,15], Giovanni Luca Gravina[16], Francesca Vulcano[2‡], Luisa Milazzo[2‡] and Francesco Marampon[1‡*]

[1]Department of Radiotherapy, Policlinico Umberto I, "Sapienza" University of Rome, Rome, Italy, [2]Department of Oncology and Molecular Medicine, Istituto Superiore di Sanità, Rome, Italy, [3]Department of Biotechnological and Applied Clinical Sciences, Laboratory of Radiobiology, University of L'Aquila, L'Aquila, Italy, [4]Department of Oncohematology, Bambino Gesù Children's Hospital, IRCCS, Rome, Italy, [5]Department of Maternal, Infantile and Urological Sciences, "Sapienza" University of Rome, Rome, Italy, [6]Department of Clinical Sciences and Translational Medicine, University of Rome Tor Vergata, Rome, Italy, [7]Department of Experimental Medicine, "Sapienza" University of Rome, Rome, Italy, [8]Dipartimento Biologia e Biotecnologie "C. Darwin," "Sapienza" University of Rome, Rome, Italy, [9]Istituto Pasteur Italia-Fondazione Cenci Bolognetti, Rome, Italy, [10]Otolaryngology Department, San Giovanni-Addolorata Hospital, Rome, Italy, [11]Phoenix Biotechnology Inc., San Antonio, TX, United States, [12]Department of Palliative, Rehabilitation and Integrative Medicine, The University of Texas MD Anderson Cancer Center, Houston, TX, United States, [13]Department of Molecular and Translational Medicine, Division of Biotechnology, University of Brescia, Brescia, Italy, [14]Radiation Oncology Unit, Department of Medicine, Surgery and Neurosciences, University of Siena, Siena, Italy, [15]IRCCS Neuromed, Pozzilli, IS, Italy, [16]Department of Biotechnological and Applied Clinical Sciences, Radiotherapy Oncology Unit, St Salvatore Hospital, University of L'Aquila, L'Aquila, Italy

Treatment of rhabdomyosarcoma (RMS), the most common a soft tissue sarcoma in childhood, provides intensive multimodal therapy, with radiotherapy (RT) playing a critical role for local tumor control. However, since RMS efficiently activates mechanisms of resistance to therapies, despite improvements, the prognosis remains still largely unsatisfactory, mainly in RMS expressing chimeric oncoproteins PAX3/PAX7-FOXO1, and fusion-positive (FP)-RMS. Cardiac glycosides (CGs), plant-derived steroid-like compounds with a selective inhibitory activity of the Na^+/K^+-ATPase pump (NKA), have shown antitumor and radio-sensitizing properties. Herein, the therapeutic properties of PBI-05204, an extract from *Nerium oleander* containing the CG oleandrin already studied in phase I and II clinical trials for cancer patients, were investigated, *in vitro* and *in vivo*, against FN- and FP-

RMS cancer models. PBI-05204 induced growth arrest in a concentration dependent manner, with FP-RMS being more sensitive than FN-RMS, by differently regulating cell cycle regulators and commonly upregulating cell cycle inhibitors $p21^{Waf1/Cip1}$ and $p27^{Cip1/Kip1}$. Furthermore, PBI-05204 concomitantly induced cell death on both RMS types and senescence in FN-RMS. Notably, PBI-05204 counteracted *in vitro* migration and invasion abilities and suppressed the formation of spheroids enriched in $CD133^+$ cancer stem cells (CSCs). PBI-05204 sensitized both cell types to RT by improving the ability of RT to induce G2 growth arrest and counteracting the RT-induced activation of both Non-Homologous End-Joining and homologous recombination DSBs repair pathways. Finally, the antitumor and radio-sensitizing proprieties of PBI-05204 were confirmed *in vivo*. Notably, both *in vitro* and *in vivo* evidence confirmed the higher sensitivity to PBI-05204 of FP-RMS. Thus, PBI-05204 represents a valid radio-sensitizing agent for the treatment of RMS, including the intrinsically radio-resistant FP-RMS.

KEYWORDS

PBI-05204, oleandrin, rhabdomyosarcoma, Na/K +ATPase, radiotherapy, radiosenisitizing agent

Introduction

Rhabdomyosarcoma (RMS) is the most common pediatric soft tissue sarcoma. The two major subtypes are the alveolar (ARMS), more frequently expressing the pro-oncogenic fusion proteins PAX3/7-FOXO1 (PAX3/7-FKHR), namely "fusion positive" RMS (FP-RMS), and the embryonal (ERMS), characterized by different mutations, "fusion negative" (FN-RMS). However, despite the status of fusion proteins, ARMS and ERMS present similar molecular perturbations, this indicating some commonality in the molecular driving forces in RMS (Sorensen et al., 2002; Davicioni et al., 2009; Rudzinski et al., 2015, 2017; Skapek et al., 2019). Treatment of RMS, currently consists of neoadjuvant radiotherapy (RT), with or without adjuvant chemotherapy (CHT), followed by a delayed excision (PDQ Pediatric Treatment Editorial Board, 2002; Cecchetto et al., 2007; Gallego et al., 2021). RT is critical to improve survival in RMS patients (Terezakis and Wharam, 2013; Mandeville, 2019). However, RMS has been shown to aberrantly express several mechanisms that sustain the resistance to RT (Marampon et al., 2011; 2019b; 2019c; 2019a; Ciccarelli et al., 2016; Gravina et al., 2016; Megiorni et al., 2017; Camero et al., 2019, 2020, 2021; Giannattasio et al., 2019; Petragnano et al., 2020a; 2020b; Casey et al., 2021; Cassandri et al., 2021; Codenotti et al., 2021; Rossetti et al., 2021; Perrone et al., 2022)., potentially responsible of the high relapse rate after apparent complete remission (Heske and Mascarenhas, 2021). Notably, the use of larger dose of radiations, has not improved the therapeutic efficiency of radiation (Kalbasi et al., 2020; Parsai et al., 2020) suggesting that new radiosensitizing strategies are urgently needed in order to improve patient overall survival.

RT kills cancer cells by inducing the accumulation of potentially repairable DNA single strand breaks (SSBs) and their transformation into non-repairable DNA double strand breaks (DSBs) (Baskar et al., 2014). cancer cells can efficiently repair SBSs, preventing the formation of DSBs formation, ability that result to be higher in the cancer stem cell (CSC) subpopulations (Wang, 2015), thus resulting the real responsible of intrinsic radioresistance (Rycaj and Tang, 2014; Wang, 2015; Schulz et al., 2019; Arnold et al., 2020). Cardiac glycosides (CGs) (e.g., digitoxin, digoxin, ouabain, and oleandrin) are selective inhibitors of the Na^+/K^+-ATPase pump (NKA), , commonly used to treat heart failure (Pavlovic, 2020). The aberrant expression/activity of NAK has been found in several cancer types (Mijatovic et al., 2012; Durlacher et al., 2015), including RMS (Liepkans, 1990). Thus, CGs have shown towards some types of malignant tumors, both *in vitro* and *in vivo* (López-Lázaro et al., 2005; Kumavath et al., 2021), working at concentrations commonly found in the plasma of cardiopathic patients treated with CGs (López-Lázaro et al., 2005). Thus, CGs have been tested in clinical trials for the treatment of cancer demonstrating satisfactory safety and efficacy (Mekhail et al., 2006; Menger et al., 2013; Hong et al., 2014; Frankel et al., 2017; Roth et al., 2020). Furthermore, considering that CGs to act as potent inhibitors of DSB repair (Wha Jun et al., 2013; Surovtseva et al., 2016; Tian et al., 2020), increasing evidence suggests their use as effective radiosensitizers (Verheye-Dua and Böhm, 1998; Nasu et al., 2002; Lee et al., 2017; Zhang et al., 2017; Du et al., 2018; Colapietro et al., 2022). Notably no studies have been still conducted on RMS.

We have recently show that PBI-05204, a defined supercritical CO_2 extract of *N. oleander*, has anticancer and radiosensiting effects towards glioblastoma (Colapietro et al., 2020; Colapietro et al., 2022). Herein, we have investigated the therapeutic potential of PBI-05204, alone and in combination

with RT, towards RMS, by using, *in vitro* and *in vivo,* RD (FN-RMS) and RH30 (FP-RMS), the most representative RMS cell lines. Herein we found that PBI-05204 efficiently counteracted the transformed and intrinsically radioresistant phenotype of RMS by concomitantly inducing cytostatic and cytotoxic effects, promoting RT-induced G2 cell cycle arrest and restraining the ability of RMS cells to repair RT-induced DNA damage. Notably, PBI-05204 showed important *in vivo* effects, enhanced by RT. Altogether, these results suggest that PBI-05204 could have therapeutic and radiosensitizing properties on RMS.

Materials and methods

Cell lines and pharmacological treatment

RD (ERMS, FN-RMS) and RH30 (ARMS, FP-RMS) human cell lines were purchased from American Type Culture Collection (Manassas, VA, United States), cultured, in Dulbecco's Modified Eagle's and RPMI medium (DMEM) containing 10% Fetal Bovine Serum (Hyclone, Logan, UT, United States) supplemented with glutamine and gentamycin (GIBCO-BRL Gaithersburg, MD, United States), dissociated using 0.25% trypsin and 0.02% EDTA solution and resuspended into a fresh medium once every 2–3 days (Camero et al., 2019b). GenePrint 10 System (Promega Corporation, Madison, WI, United States) was used to authenticate cell cultures by comparing the DNA profiles of cell lines with those found in GenBank. Multipotent mesenchymal stromal cells (MSCs) were previously described (Vulcano et al., 2016). The supercritical CO_2 extract of *N. oleander* PBI-05204 was provided by Phoenix Biotechnology, Inc., (San Antonio, Texas) and characterized by using an AccuTOF-DART mass spectrometer (Jeol UAS, Peabody, MA). Specific molecular content of the extract was previously reported (Siddiqui et al., 1995; Dunn et al., 2011).

Viability of cells

RD and RH30 cells were seeded into 6-well tissue culture plates at a density of 8,500 cells/cm^2 and treated with PBI-05204 24 (hours) h later. Trypan blue (Thermofisher) dye exclusion test was used to assess cell viability. A Countess II Automated Cell Counter (ThermoFisher Scientific, Waltham, MA, United States) was used to assess the number of the cells. "Quest Graph™ IC_{50} Calculator" (AAT Bioquest, Inc.,) was used to calculate IC_{50} values (AAT Bioquest, 2022).

Migration and invasion assays

Migration was assessed using wound healing assays that were performed as previously described (Gravina et al., 2017). Briefly, RD and RH30 cells were plated in 6-well plates and incubated with or without PBI-05204 for 24 h. The following day, a sterile pipette tip was used to scratch the cell monolayer (4–5 parallel scratches/plate). Cells were washed with PBS, photographed to mark scratched tracks, and incubated for an additional 24 h to evaluate cell migration into the injured areas. Wound healing was quantified using ImageJ 1.47v software. For the invasion assay, RD and RH30 cells (8×10^5 cells/ml) were seeded in the upper portion of a Boyden chamber separated from the lower compartment, containing DMEM with 10% FBS added with PBI-05204 (IC_{50}) or DMSO, by a matrigel-coated PVP-free polycarbonate filter with 8 mm pore size (Costar, Cambridge, United States). After incubation at 37°C for 6 h, migrated cells were stained with Diff-Quik (Dade-Behring, Milan, Italy) (Codenotti et al., 2019). The number of migrated cells was quantified using ImageJ 1.47v software. Experiments were carried out in triplicate.

Sphere culture and sphere formation

Sphere-forming cells were obtained as previously described (Ciccarelli et al., 2016; Camero et al., 2020; Megiorni et al., 2021). Briefly, RD and RH30 cells were cultured in anchorage-independent conditions (ultra-low attachment flasks or plates, Corning) in stem cell (SC)-medium consisting of DMEM: F12 medium (Gibco-Invitrogen) and B27 (ThermoFischer). Fresh human epidermal growth factor (20 ng/ml) and fibroblast growth factor (20 ng/ml) (PeproTech, London, United Kingdom) were added twice/week until cells formed floating spheres. To evaluate the primary sphere formation, cells from sub-confluent (70–80%) monolayer cultures were plated at a density of 100, 500 or 1,000 cells in a 24-well culture plate (Corning Inc., Corning, NY, United States). For the sphere formation assay, the number of primary tumor spheres was determined.

Flow cytometer analysis of cell cycle distribution and stem cell markers

For cell cycle analysis, a BD Cycletest Plus DNA Kit (BD Biosciences) was used for DNA staining. Following trypsinization, cells were adjusted to a concentration of 1×10^6 cells/ml and treated using reagent kit, according to the manufacturer's instructions. The cell cycle status was analyzed by flow cytometry using propidium iodide (PI). Analysis was performed using a flow cytometer (FACSCalibur), and the cell-cycle distribution was analyzed using the Mod-Fit LT software (Verity Software House, Topsham, ME, United States). Stem cell markers in RMS cells were evaluated by staining with monoclonal antibodies conjugated with phycoerythrin (PE) anti–CD133 (BD Biosciences, Buccinasco,

Italy). Appropriate isotype controls for non-specific binding were used for each antibody. A minimum of 50,000 events were acquired for each sample by the flow cytometer and the CellQuest software (BD Biosciences) was used for both data acquisition and analysis (Marampon et al., 2019d).

Protein extraction,western blot and protein simple WES western analysis

For total protein extraction, RD and RH30 cells were lysed in 2% SDS containing 2 mM phenyl-methyl sulphonyl fluoride (PMSF) (Sigma-Aldrich (St. Louis, MO, United States), 10 μg/ml antipain, leupeptin and trypsin inhibitor, 10 mM sodium fluoride and 1 mM sodium orthovanadate (all from Sigma-Aldrich, St. Louis, MO, United States) and sonicated for 30 s (sec). Protein concentration was estimated by BCA assay and equal amounts were separated on SDS-PAGE. Proteins were transferred to a nitrocellulose membrane (ThermoFisher Scientific, Waltham, MA, United States) by electroblotting. The balance of total protein levels was confirmed by staining the membranes with Ponceau S (Sigma-Aldrich (St. Louis, MO, United States). Membranes were blocked for 1 h in 5% non-fat dry milk in Tris-buffered saline and Tween-20 (TBS-T) and then incubated at 4 °C overnight with primary antibodies. The primary antibodies used were: $p21^{Waf1/Cip1}$ (C-19) and $p27^{Cip1/Kip1}$ (F-8), Cyclin A (BF683), Cyclin B1 (H-20), Cyclin E (HE12), myelocytomatosis virus oncogene cellular homolog (c-Myc) (9E10), N-Myc (B.8.4.B), phosphorylated extracellular signal-regulated kinase 1/2 ($ERK1/2^{PO4}$) (E-4), extracellular signal-regulated kinase (ERK1/2) (C-14), phosphorylated protein kinase B (Akt^{PO4}) (C-11), e phosphorylated protein kinase B (Akt) (5C10), and vinculin (7F9) by Santa Cruz Biotechnology (Dallas, TX, United States). Appropriate horseradish peroxidase (HRP)-conjugated secondary antibodies (Santa Cruz Biotechnology (Dallas, TX, United States) were used for 1 h at room temperature (Gravina et al., 2019; Menna et al., 2022). Western blots for ATM, ATM^{PO4}, DNA-PKCs, $DNA\text{-}PKCs^{PO4}$ and vinculin were performed using a Protein Simple WES Western instrument (San Jose, CA). Cell and tissue lysates were prepared as described above. Protein simple (6 μl) was mixed with 5x fluorescent master mix (Protein Simple) to achieve a finial concentration of 1x master mix buffer according to manufacturer's instructions. Samples were then denatured at 95°C for 5 min. All materials and solutions added onto the assay plate were purchased from Protein Simple except primary antibodies. Antibody diluent (10 μl), protein normalizing reagent, primary antibodies, secondary antibodies, chemiluminescent substrates, 3 μl of sample, and 500 μl of wash buffer were prepared and dispensed into the assay plate. Assay plates were loaded into the instrument and proteins were separated within individual capillaries. Protein detection and digital images were collected and analyzed with Compass software (Protein Simple) and data were reported as area under the peak, which represents the intensity of the signal. For primary antibody, phospho-ATM (D6H9, Ser 1981, used at 1:25), phospho-DNA-PKCs (E9J4G, Ser 2056, used at 1:25) and DNA-PKCs (E6U3A, used at 1:100) by Cell Signaling (Danvers, MA, United States); ATM (G-12, used at 1:50) by Santa Cruz Biothecnology (Dallas, TX, United States) were mixed with vinculin (hVIN-1, used at 1:100) by Sigma-Aldrich Inc. (Saint Louis, MO, United States). Anti-mouse HRP and anti-rabbit HRP secondary antibodies from Protein Simple were used (Kannan et al., 2018; Hui et al., 2020). Quantification of Western blot data was performed by using a ChemiDoc MP (Bio-Rad) imager.

Radiation exposure and clonogenic assay

Radiation was delivered at room temperature using a x-6 MV photon linear accelerator. The total single dose of 4 Gy was delivered with a dose rate of 2 Gy/min using a source-to-surface distance (SSD) of 100 cm. A plate of Perspex thick 1.2 cm was positioned below the cell culture flasks in order to compensate for the build-up effect. Tumor cells were then irradiated placing the gantry angle at 180°. Non-irradiated controls were handled identically to the irradiated cells with the exception of radiation exposure. The absorbed dose was measured using a Duplex dosimeter (PTW). For clonogenic survival assay, exponentially growing RD and RH30 cells in 25-cm^2 flasks were treated with PBI-05204 or vehicle and irradiated 24 h later. Three h after irradiation, cells were harvested, counted, diluted serially to appropriate densities, plated in triplicate in six multi-well plates with 2 ml of complete drug-free medium/each well. Fourteen days (d) later, cells were fixed with methanol:acetic acid (10:1, v/v), and stained with crystal violet. Colonies containing >50 cells were counted.

Animal research ethics statement and in vivo xenograft experiments

The recommendations of the European Community (EC) guidelines (2010/63/UE and DL 26/2014 for the use of laboratory animals) and the Istituto Superiore di Sanità guidelines, complying with the Italian government regulation n.116 27 January 1992 for the use of laboratory animals code 221/2022-PR (D9997.140) approved 4 April 2022 were followed to undertake *in vivo* experiments. Before any invasive manipulation, mice were anesthetized with a mixture of ketamine (25 mg/ml)/xylazine (5 mg/ml). For xenotransplants exponentially growing RD or RH30 cells were detached by trypsin-EDTA, washed twice in PBS, and resuspended in saline solution at cell densities of 1×10^6/200 μl. Xenotransplants were done in 45-day-old female nude

CD1 mice from Charles River Laboratories Italia, SRL (Calco, Italy), by subcutaneously injection in the leg using a 21-gauge needle on a tuberculin syringe. Treatments were started when tumors reached a volume of 0.3–0.5 cm^3 (Cassandri et al., 2021). Mice were irradiated at room temperature using an Elekta 6-MV photon linear accelerator. Three fractions of 2 Gy were delivered every other day, the first, third and fifth d, for a total dose of 6 Gy. A dose rate of 1.5 Gy/min was used with a source-to-surface distance (SSD) of 100 cm. Prior to irradiation, mice were anesthetized and were protected from off-target radiation by a 3 mm lead shield. Before tumor inoculation mice were randomly assigned to four experimental groups. Each group was composed of eight mice. One control group received 200 µl carrier solution by mouth (PO); PBI-05204 (20 mg/kg/5 Day/week (PO); one group received RT (3 fractions of 2 Gy delivered every other day to a total dose of 6 Gy); PBI-05204 (20 mg/kg/5 Day/week, (PO) coupled with RT (3 fractions of 2 Gy delivered every other day to a total dose of 6 Gy) (Colapietro et al., 2022). During treatment, mice with significant body weight loss approaching (10–15%) were euthanized early per protocol, by using Carbon Dioxide, following the AVMA Guidelines for the Euthanasia of Animals (AVMA, 2019). The effects on tumor growth because of different treatments were evaluated as follows: tumor volume was measured during and at the end of the experiment; tumor volume was assessed every 4 days with a Vernier caliper (length × width); the volume of the tumor was expressed in mm^3 according to formula $4/3\pi\ r^3$, measuring tumor weight at the end of the experiment and defining tumor progression (TP), the doubling of the tumor volume.

Statistical analysis and data analysis

Three independent experiments, each performed in triplicate, were carried out and the results were expressed as the mean ± SD. Assessment of normal distribution of data was confirmed by Shapiro–Wilk, D'Agostino and Pearson and Kolmogorov–Smirnov tests. Real-time PCR experiments were evaluated by one-way (ANOVA) with a Tukey's post hoc test using $2^{-\Delta\Delta CT}$ values for each sample. Flow cytometry data were analyzed by ANOVA with a Bonferroni post hoc test. All analyses were performed using the SAS System (SAS Institute Inc., Cary, NC, United States) and GraphPad Prism 6.1.

Results

PBI-05204 Induces Concomitant Growth Arrest and Cell Death in RMS but not in MSCs Cell Lines *in vitro*.

Trypan blue dye exclusion test showed that increasing doses (0–50 ng/ml) of PBI-05204 treatment, performed for 24, 48 and 72 h, significantly reduced the number of live cells in a concentration-dependent manner, both in RD (Figure 1A, Left Panel) and RH30 cells (Figure 1A, Right Panels), with an average of 50% cell viability at a concentration of 4.8 ng/ml on RD (Figure 1B, Left Panel) and 2.2 ng/ml on RH30 cell line (Figure 1B, Right Panel). RMS cultures were treated with PBI-05204 (IC_{50}) for 8 days. As shown in Figure 1C, 4 days of PBI-05204 (IC_{50}) treatment reduced the number of living cells by 71.4 ± 4.7% in RD (Figure 1C, Left Panel, 4 d, Live Cells) and 78.3 ± 3.7% in RH30 cells (Figure 1C, Right Panel, 4 d, Live Cells). Prolonged drug exposure resulted in the total absence of viable cells (Figure 1C, RD, Left Panel, and RH30, Right Panel, Time 8 days, Live Cells). Concomitantly, the number of dead cells was progressively and persistently induced by the presence of PBI-05204 (Figure 1C, RD, Left Panel, and RH30, Right Panel. Notably, PBI-05204-treated adherent cells exhibited a substantial change in their morphology, with larger cellular bodies at 4 d post-exposure (Figure 1D, RD, Left Panel, and RH30, Right Panel, 4 d). Cell fragments and cells almost devoid of cytoplasm appeared after 8 days of continuous treatment (Figure 1D, RD, Left Panel, and RH30, Right Panel, 8 days). The IC_{50} of PBI-05204 was of 93.7 ng/ml for MSCs cells (Supplementary Data S1; Figure 1A), 19.5 and 42.5 times higher than RD and RH30, respectively. Notably, treating MSCs did not induce any statistically significant increase in dead cells (Supplementary Data S1; Figure 1B). Altogether, these data indicate that PBI-05204 induces concomitant growth arrest and cell death in RMS but not in the normal counterpart with FP-RMS being more sensitive to the drug than FN-RMS.

PBI-05204 Causes G_1 Phase Cell Cycle Arrest of Both FN-RMS and FP-RMS and Senescence in FN-RMS.

Cell cycle distribution analysis, performed by flow cytometry on RMS cells treated for 24 h and 4 days with PBI-05204 (IC_{50}), showed that in RD cells this drug significantly, but transiently, arrested cells in the G_1 phase. After 24 h of treatment with PBI-05204 the percentage of cells in G_1 phase significantly increased (Figure 2A, RD 24 h, 33% ± 1.1 PBI-05204 vs. 21% ± 1.3 Untreated) by primarily reducing the number of cells in S phase (Figure 2A, RD 24 h, 36% ± 1.3 PBI-05204 vs. 53% ± 2.2 Untreated) while no statistically significant differences on cell cycle distribution were observed after 4 days of treatment (Figure 2A, RD 4 days). In RH30 cells, PBI-05204 induced a rapidly (24 h) and persistently (4 days) cell cycle arrest as indicated by the increase of cell number in the G_1 phase (Figure 2A, RH30 24 h, G_1 phase: 65% ± 2 PBI-05204 vs. 41% ± 1.2 Untreated and 4 days, G_1 phase: 62% ± 1.4 PBI-05204 vs. 45% ± 1.1 Untreated) and the concomitant reduction in both the S phase (Figure 2A, RH30 24 h, S phase: 29% ± 3 PBI-05204 vs. 42% ± 2 Untreated and 4 days, S phase: 33% ± 2.1 PBI-05204 vs. 44% ± 2 Untreated) and the G_2 phase (Figure 2A, RH30 24 h, G_2 phase: 6% ± 1 PBI-05204 vs. 17% ± 0.6 Untreated and 4 d, G_2 phase: 4% ± 0.4 PBI-05204 vs. 11% ± 1 Untreated). RD cells treated with PBI-05204 downregulated the expression of the cell cycle promoters

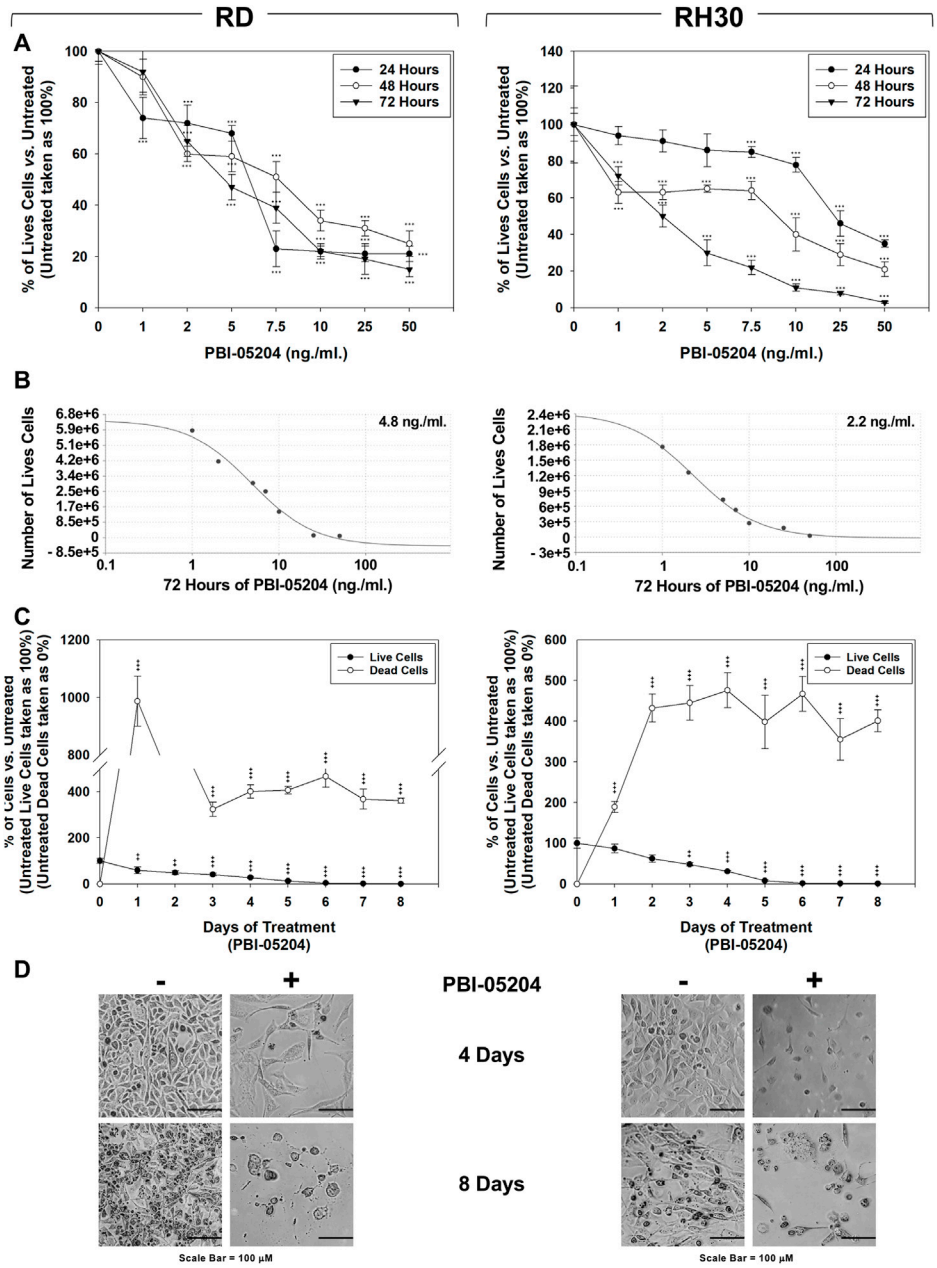

FIGURE 1
PBI-05204 induces concomitant cell death and growth arrest in FN-RMS and FP-RMS cells. RD (Left) and RH30 (Right) cell lines were treated for 24, 48 and 72 h with increasing concentrations (0, 1, 2, 5, 7.5, 10, 25, 50 ng/ml) of the drug. Surviving **(A)** cells were counted using Trypan blue dye exclusion test. **(B)** Concentration of PBI-05204 able to reduce by 50% the cell survival of RD (Left) and RH30 (Right) cell lines. **(C)** Effect of PBI-05204 IC_{50} on cell number of live and dead RD (Left) and RH30 (Right) cells. Surviving cells were counted using Trypan blue dye exclusion test. Results represent the mean values of three independent experiments ±SD. Statistical significance: $*p \leq 0.05$, $**p \leq 0.01$, $***p \leq 0.001$ vs. Untreated. **(D)** Cellular morphology of RD (Left) and RH30 (Right), untreated or treated with PBI-05204 (IC50) for 4 d was analyzed under light microscope at ×200 magnification.

c-Myc (Figure 2B, RD, c-Myc), but not of Cyclin A1 (Figure 2B, RD, Cyclin A1), Cyclin B1 (Figures 2B,D, Cyclin B1), Cyclin E (Figure 2B, RD, Cyclin E), CDK1 (Figure 2B, RD, CDK1) and CDK2 (Figure 2B, RH30, CDK2), and upregulated the expression of cell cycle inhibitors $p21^{Waf1/Cip1}$ and $p27^{Cip1/Kip1}$ (Figure 2B, RD, $p21^{Waf1/Cip1}$ and $p27^{Cip1/Kip1}$). On the other hand, consistent with G_1 cell cycle arrest, RH30 cells treated with PBI-05204 showed the a downregulation of Cyclin A1 (Figure 2B,

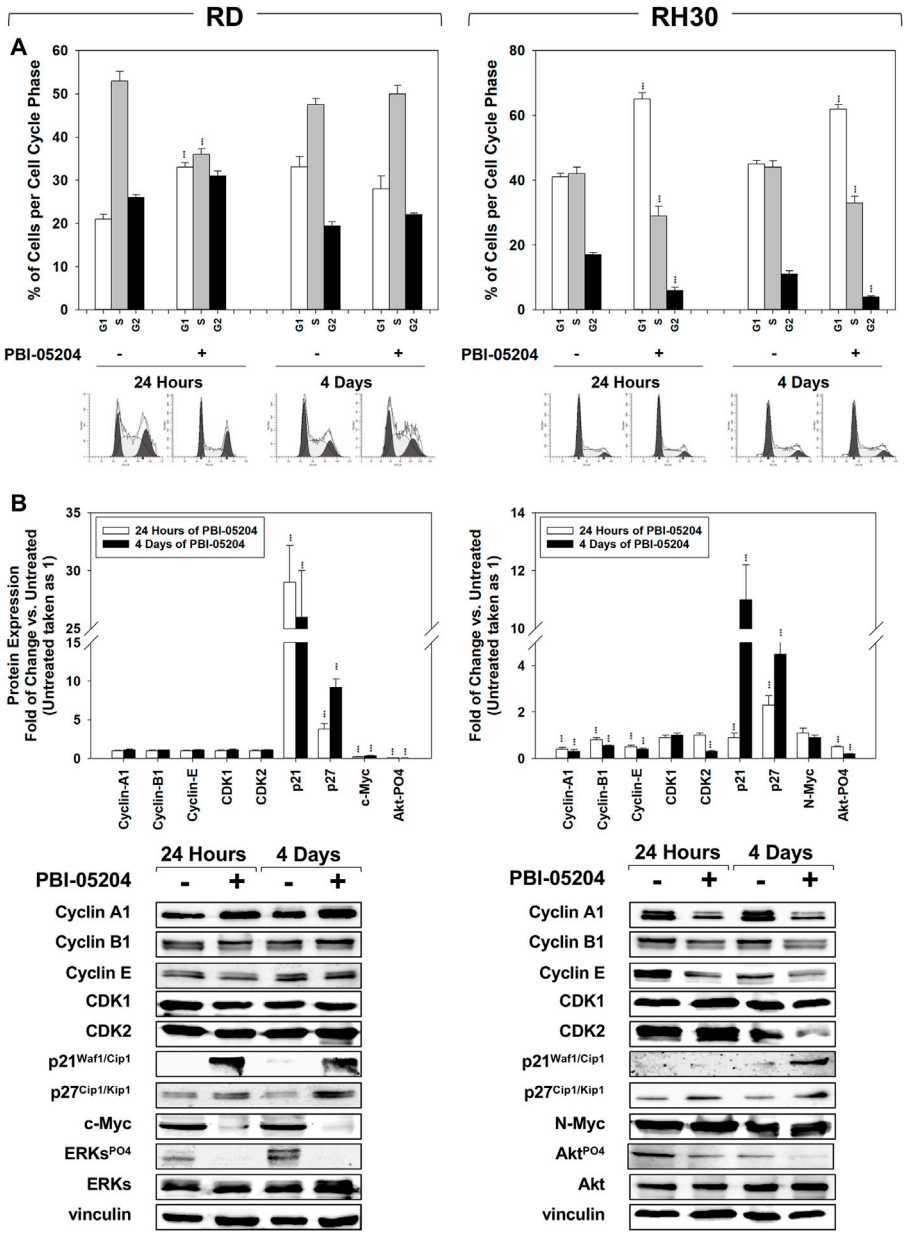

FIGURE 2
PBI-05204 affects cell cycle distribution. **(A)** FACS analysis performed on RD (Left) and RH30 (Right) untreated or treated for 4 with PBI-05204 (IC50). Data (Up) indicates the percentage of cells in each cell cycle phase representing the mean value of three independent experiments. (Down) Representative data of three independent experiments is shown. **(B)** Cell lysates from RD (Left) and RH30 (Right) cells treated for 24 h and 4 d with PBI-05204 (IC50) were analyzed by immunoblotting with specific antibodies for the indicated proteins; vinculin expression was used as a loading control. Histograms (Up) of densitometric analysis represent the mean values of three independent experiments ±SD. Statistical significance: $^{**}p \leq 0.01$, $^{***}p \leq 0.001$ vs. Untreated cells. Representative data from three independent experiments is shown (Down).

RH30, Cyclin A1), Cyclin B1 (Figure 2B, RH30, Cyclin B1), Cyclin E (Figure 2B, RH30, Cyclin E) and CDK2 expression levels (Figure 2B, RH30, CDK2), and an the upregulation of the expression of $p21^{Waf1/Cip1}$ and $p27^{Cip1/Kip1}$ cell cycle inhibitors (Figure 2B, RH30, $p21^{Waf1/Cip1}$ and $p27^{Cip1/Kip1}$), whilst no changes were observed in N-Myc and CDK1 protein levels (Figure 2B, RH30, N-Myc). Furthermore, PBI-05204 affected the phosphorylation/activation of ERKs in RD (Figure 2B, RD, ERKsPO4) and of Akt in RH30 (Figure 2B, RD, AktPO4, RH30). Due to PBI-05204-induced upregulation of $p21^{Waf1/Cip1}$ and $p27^{Cip1/Kip1}$, biomarkers of senescent cells (Flores et al., 2014; Kumari and Jat, 2021), the induction of

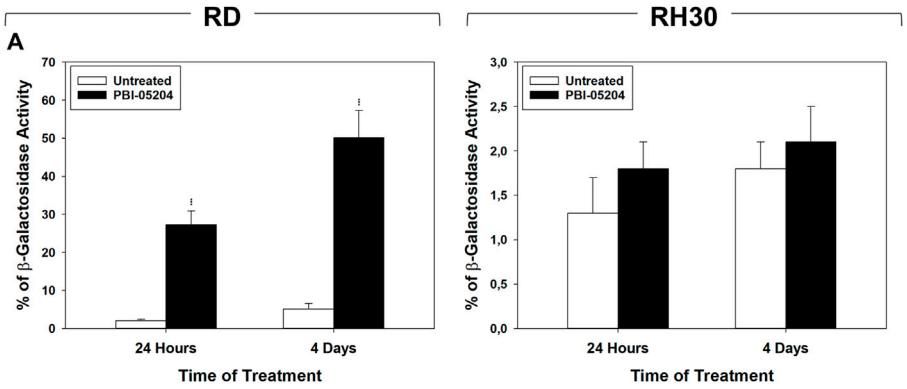

FIGURE 3
PBI-05204 induces senescence in FN-RMS but not in FP-RMS cells. **(A)** b-Galactosidase test performed on RD (Left) and RH30 (Right) cells untreated or treated for 24 h and 4 d with PBI-05204 (IC_{50}). Data represent the mean value of three independent experiments ±SD. Statistical significance: $^{**}p \leq 0.01$, $^{***}p \leq 0.001$ vs. Untreated cells.

senescence-associated β-galactosidase activity (SA-β-Gal), considered to be an important hallmark of cell senescence (Dimri et al., 1995), was evaluated on RMS cells after 24 h and 4 days of PBI-05204 (IC_{50}) treatment. As shown in Figure 3, PBI-05204 increased SA-β-Gal 24 h later (Figure 3, RD 24 h, 26.3% ± 4,1 PBI-05204 vs. 2.3% ± 0,2 Untreated), up to 4 days (Figure 3, RD cell lines 4 d, 50.1% ± 8,3 PBI-05204 vs. 5.2% ± 0,6 Untreated) in RD whilst no statistically significant differences were obtained in RH30 (Figure 4, RH30 24 h and 3 days, PBI-05204 vs. Untreated). Thus, these data indicate that PBI-05204 induce the growth arrest of FP- and FN-RMS in two different ways: persistently perturbing the cell cycle distribution of RH30 cells and promoting the senescence in RD cells.

PBI-05204 Inhibits the Ability of RMS to Migrate and Invade.

The ability of PBI-05204 to affect the migration/invasion ability of RMS cells was investigated. As shown in Figure 4A, PBI-05204 (IC_{50}) reduced RMS cell migration as assessed by wound healing assays in which the same fields of confluent cells were pictured immediately after the scratch (time 0 h) and again after 6, 12, 18 and 24 h following drug pre-incubation. Particularly, 24 h after the scratch, PBI-05204 decreased the level of wound closure to 41.1% ± 4.9% for RD (Figure 4A, RD, 24 h Untreated vs. PBI-05204) and 42.4% ± 3.8% for RH30 of the control sample (Figure 4A, RH30, 24 h Untreated vs. PBI-05204). Furthermore, PBI-05204 inhibited the ability of both RD of 92.3% ± 2.1% and RH30 of 98.7% ± 1.1% to invade chambers coated with Matrigel (Figure 4B, RD and RH30 Untreated vs. PBI-05204). Altogether, these data indicate that PBI-05204 can also counteract the *in vitro* ability of RMS to migrate and invade.

PBI-05204 sensitizes RMS cells to radiation affecting also the intrinsically radioresistant stem-like cell population

The ability of PBI-05204 to sensitize cells to ionizing radiation was assessed through colony formation assay performed on RMS cells (Figure 5A) and RMS-derived CSC-like cells (Figure 5B) pre-treated for 24 h with PBI-05204 (IC_{50}) and then irradiated with a dose of 4 Gy. The combination of RT and PBI-05204 improved the ability of this treatment to affect the clonogenic ability (Figure 5A) and to form tumor-spheres (Figure 5B) in both cell lines. The clonogenic ability was affected by RT alone of 39.1% ± 8% in RD (Figure 5A, RD, RT vs. Untreated) and 18% ± 8% in RH30 (Figure 5A, RH30, RT vs. Untreated), by PBI-05204 alone of 76% ± 3% in RD (Figure 5A, RD, PBI-05204 vs. Untreated) and 79% ± 5% in RH30 (Figure 5A, RH30, PBI-05204 vs. Untreated), and by RT combined with PBI-05204 by 94% ± 0.8% in RD (Figure 5A, RD, PBI-05204 + RT vs. Untreated) and 98% ± 0.4% in RH30 (Figure 5A, RH30, PBI-05204 + RT vs. Untreated). Drug treatment in combination with RT significantly reduced the rhabdosphere formation by 94.3% ± 0.6% in RD (Figure 5A, RD, PBI-05204 + RT vs. Untreated) and 98.2% ± 0.4% in RH30 (Figure 5A, RH30, PBI-05204 + RT vs. Untreated), significantly improving the efficiency of RT alone by 92.8% ± 2.9% in RD (Figure 5A, RD, PBI-05204 + RT vs. RT) and 97.5% ± 3.2% in RH30 (Figure 5A, RH30, PBI-05204 + RT vs. RT) and PBI-05204 alone by 77.3% ± 3.1% in RD (Figure 5A, RD, PBI-05204 + RT vs. PBI-05204) and 90.8% ± 2.4% in RH30 (Figure 6A, RH30, PBI-05204 + RT vs. PBI-05204). Notably, 24 h of PBI-05204 pre-treatment alone affected the formation of tumorspheres in RD by 90.5% ± 3.8% (Figure 5B, RD, Upper Panel, PBI-05204 vs.

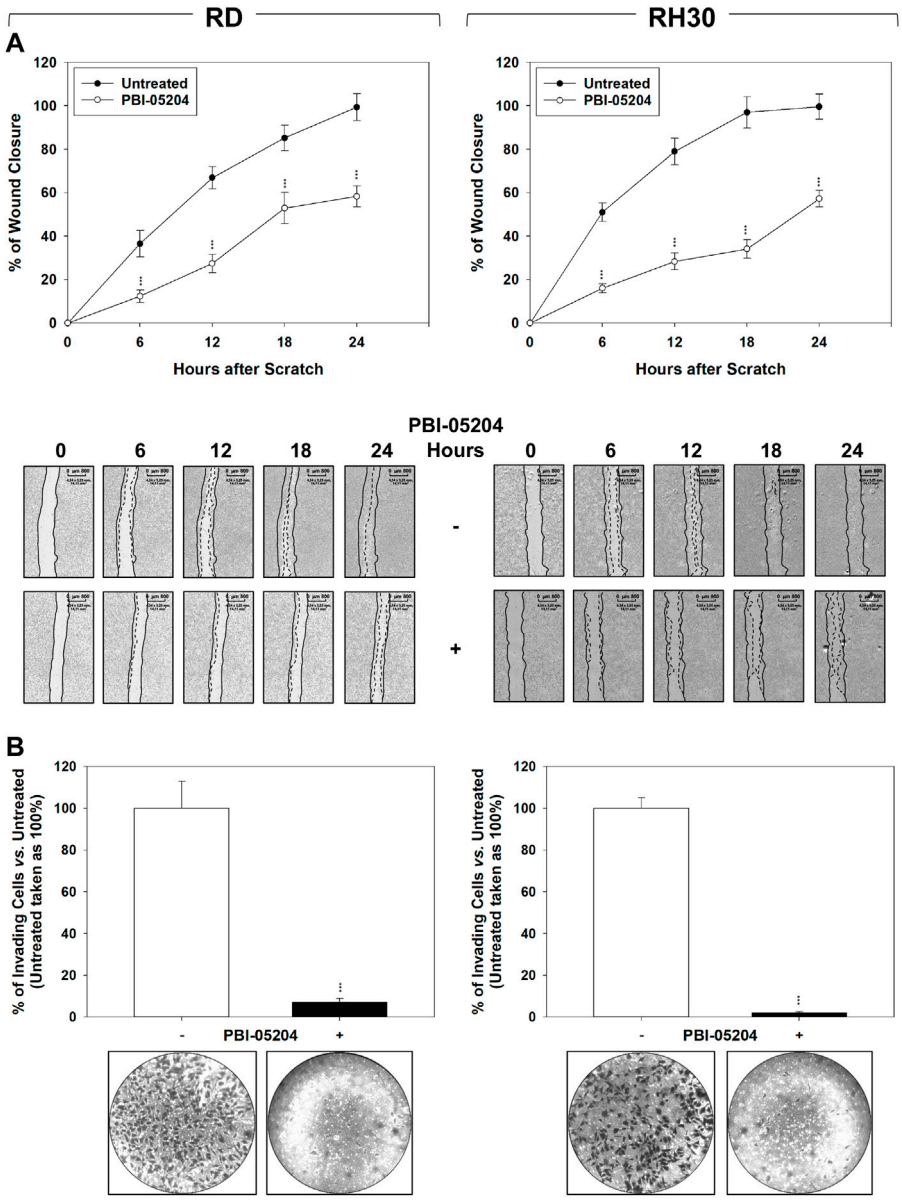

FIGURE 4
PBI-05204 impairs migration and invasion as determined by wound closure by FN-RMS and FP-RMS cells. **(A)** Wound healing experiments in RD (Left) and RH30 (Right) cell lines, treated or not with PBI-05204 IC_{50}. The scratch and then PBI-05204 treatment was made at time 0 and maintained or not for 24 h. The dotted lines represent the edges of the wound. Photographs (Left Panel) were taken under light microscope (×10 magnification). The migration index was plotted in bar graphs as the % of wound area (Right Panel). Lines (Up) represent the mean values of three independent experiments ±SD. Statistical significance: $^{**}p \leq 0.01$, $^{***}p \leq 0.001$ vs. Untreated cells. Representative data from three independent experiments is shown (Down). **(B)** Matrigel invasion assay using a Transwell system. Results represent the mean values of three independent experiments ±SD (Up). Statistical significance: $^{*}p \leq 0.05$, $^{**}p \leq 0.01$, $^{***}p \leq 0.001$ vs. Untreated. Representative data from three independent experiments is shown (Down).

Untreated) and in RH30 by 98.8% ± 2.6% (Figure 5B, RH30, Upper Panel, PBI-05204 vs. Untreated) and, parallelly, the number of the $CD133^{+}$ RMS cells (Figure 5B, RD and RH30, Lower Panel, PBI-05204 vs. Untreated). Thus, PBI-05204 can radiosensitize RMS independently from FP status, also targeting the CSC subpopulation.

PBI-05204 promotes RT-induced G_2 phase cell cycle arrest and impairs DNA double-strand break repair in RMS

The effects of PBI-05204 on cell cycle distribution and DNA repair were investigated. Cell cycle distribution analysis

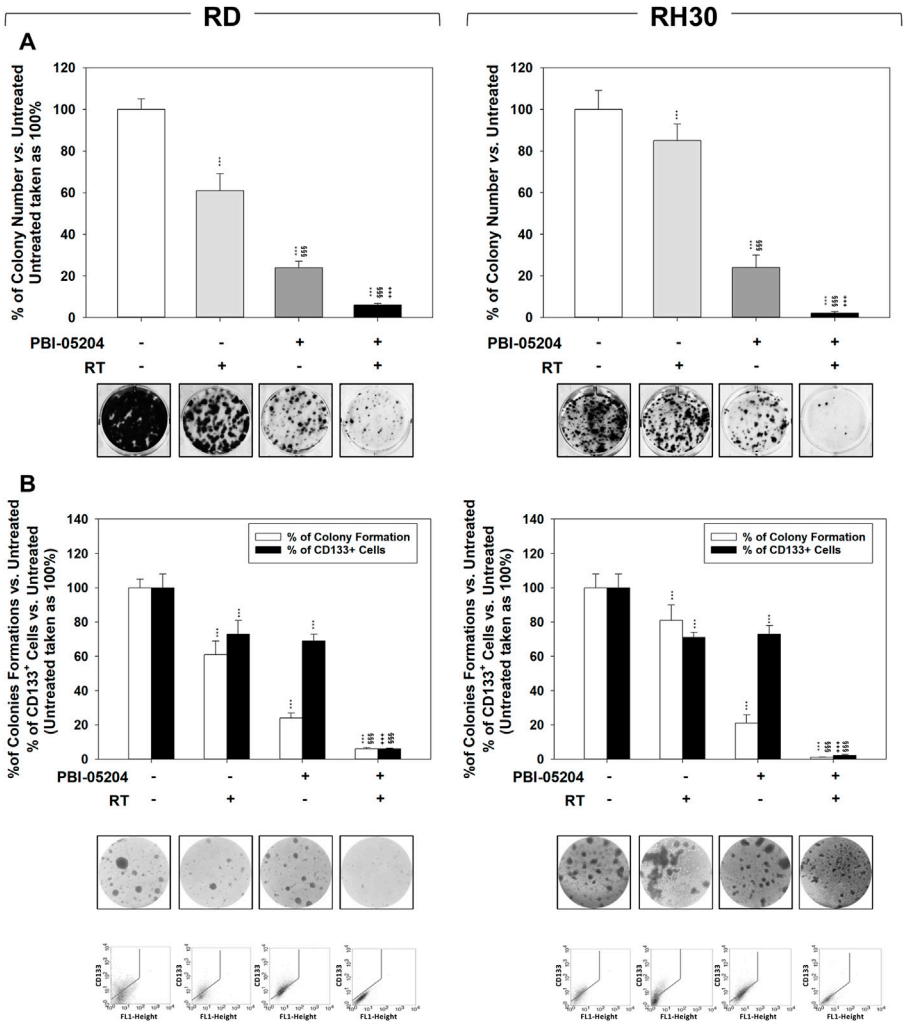

FIGURE 5
PBI-05204 radiosensitizes FN-RMS and FP-RMS cell lines and cancer-stem like derived cells. **(A)** Colony formation assay of RD (Left) and RH30 (Right) treated with PBI-05204 IC_{50}, RT alone or with the combination. Three h after RT (4 Gy), cells were seeded at low concentrations for colony assays. Colony forming efficiency was calculated by crystal violet absorbance after 14 d of PBI-05204 treatment. **(B)** The formation of spheres enriched in stem-like cells and the expression of CD133 were assessed in RD (Left) and RH30 (Right) treated with PBI-05204 (IC50), RT alone or with the combination. Results represent the mean values ±SD of three independent experiments (Up). Representative data from three independent experiments is shown (Down). Statistical significance: $^{*}p \leq 0.05$, $^{**}p \leq 0.01$, $^{***}p \leq 0.001$, vs. Untreated, §$p \leq 0.05$, §§$p \leq 0.01$, §§§$p \leq 0.001$ vs. RT, $+p \leq 0.05$, $++p \leq 0.01$, $+++p \leq 0.001$ vs. PBI-05204.

was performed by flow cytometry on RMS cells pre-treated for 24 h with PBI-05204 (IC_{50}) and then irradiated with 4 Gy, 24 h, and 4 days after RT. As shown in Figure 6A, on RD cells, PBI-05204 pre-treatment increased the percentage of cells arrested in the G_2 cell cycle phase by RT, 4 days after irradiation (Figure 6A, RD, 4 d, 30.7% ± 1.3% PBI-05204 + RT vs. 24.6% ± 2.3% RT). On RH30, PBI-05204 pre-treatment induced an early, 24 h (Figure 6A, RH30, 24 h, 43.3% ± 0.6% PBI-05204 + RT vs. 7.6% ± 1.2% RT), and stable G_2 cell cycle phase arrest following 4 d (Figure 6A, RH30, 4 d, 28.3% ± 1.6% PBI-05204 + RT vs. 17.4% ± 1.1% RT) of drug exposure. The phosphorylation/activation status of DNA-PKcs and ATM, respectively upstream of Non-Homologous End-Joining (NHEJ) and Homologous Recombination (HR) DSB repair pathways, were also investigated. Pre-treating cells with PBI-05204 counteracted the RT-induced phosphorylation/activation of DNA-PKcs (Figure 6B, DNA-PKcsPO4 PBI-05204 + RT vs. RT), and ATM (Figure 6B, ATMPO4 PBI-05204 + RT vs. RT) in both RD and RH30 cells. Thus, the data suggest that PBI-05204 can sensitize FN-RMS and FP-RMS to RT by promoting the accumulation of cells in the G_2, the most radiosensitive phase of the cell cycle (Pawlik and Keyomarsi, 2004), thereby impairing the ability of FN-RMS and FP-RMS to repair RT-induced DSBs.

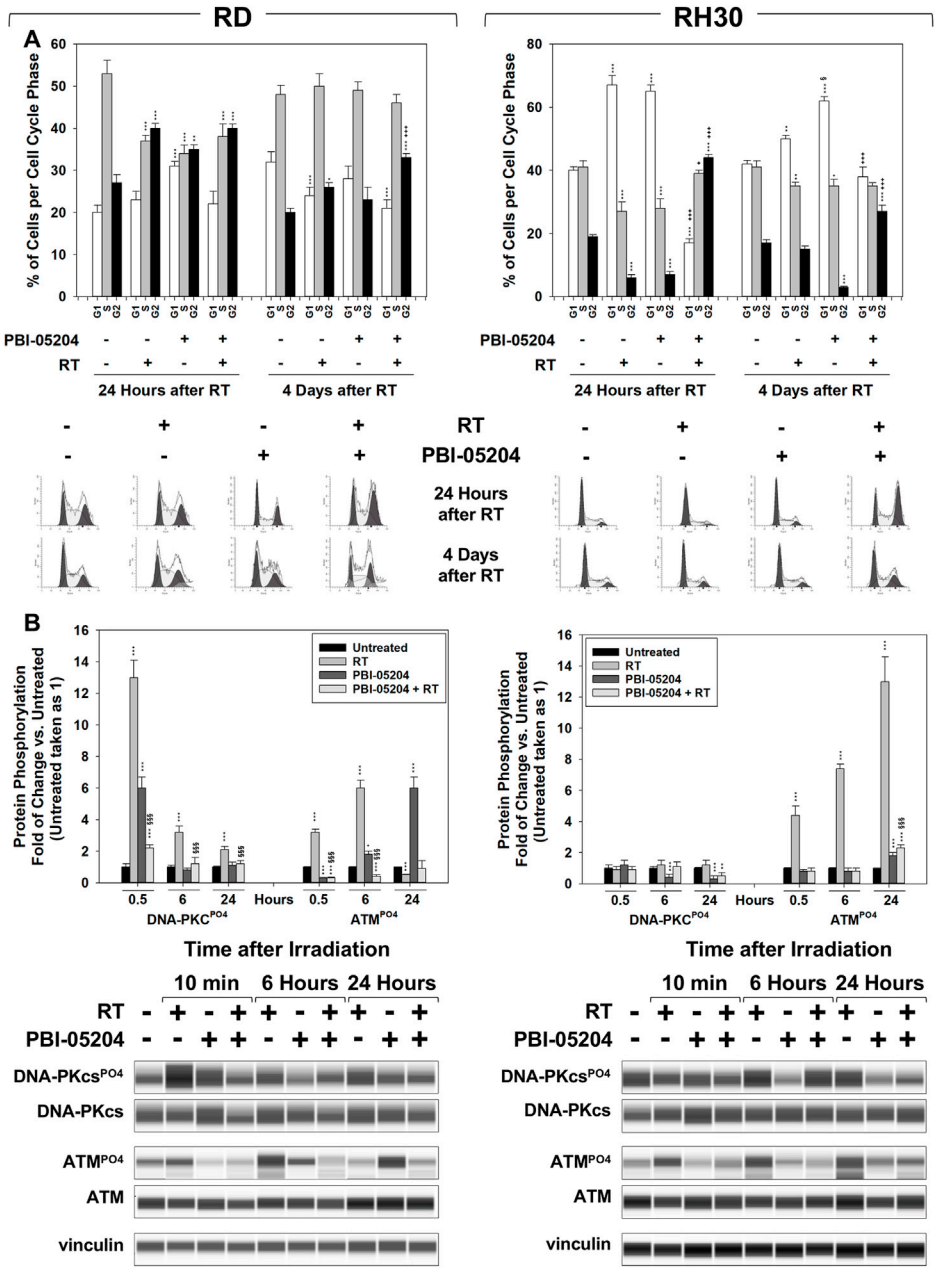

FIGURE 6
PBI-05204 promotes RT-induced accumulation of cancer cells in the G2 phase of the cell cycle and counteracts the ability of FN-RMS and FP-RMS to repair damaged DNA. **(A)** FACS analysis performed on RD (Left) and RH30 (Right) treated with PBI-05204 (IC_{50}), RT alone or with the combination. Data (Up) show the percentage of cells in each cell cycle phase representing the mean value of three independent experiments. (Down) Representative data from three independent experiments is shown. **(B)** Cell lysates from RD (Left) and RH30 (Right) cells pre-treated for 24 h with PBI-05204 (IC50) and then irradiated with 4 Gy were collected 10 min, 6 and 24 h after RT. Cell lysates were analyzed by immunoblotting with specific antibodies for the indicated proteins; vinculin expression was used as a loading control. Histograms (Up) of densitometric analysis represent the mean values of three independent experiments ±SD. Statistical significance: $^{**}p \leq 0.01$, $^{***}p \leq 0.001$ vs. Untreated cells, §$p \leq 0.05$, §§$p \leq 0.01$, §§§$p \leq 0.001$ vs. RT, $+p \leq 0.05$, $++p \leq 0.01$, $+++p \leq 0.001$ vs. PBI-05204. A representative of three independent experiments is shown (Down).

PBI-05204 radiosensitizes RMS cells *in vivo*

In vivo experiments were then performed by subcutaneously injecting (SC) RMS cells in nude mice. When the tumor volume reached 0.5 cm^3 (T0), mice received PBI-05204 (20 mg/kg) (Colapietro et al., 2022) or vehicle (PBS) by mouth once daily for five consecutive d (see Methods) and then were irradiated, or not, with 2 Gy on the 1st, 3rd, and fifth d with PBI-05204 given 1 h before RT. Tumor volumes were measured every 5 days for a

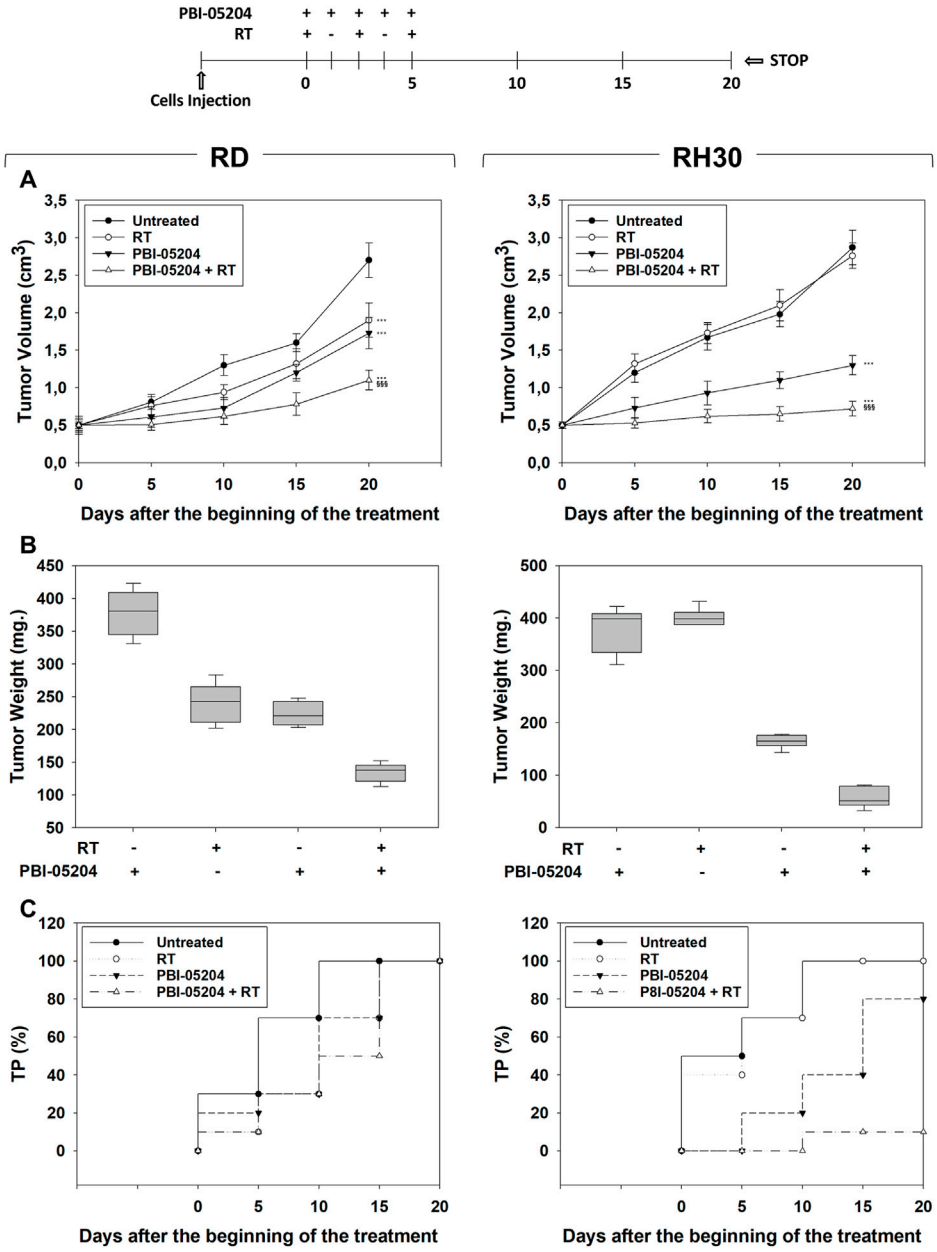

FIGURE 7
Effect of PBI-05204 combined or not with irradiation on *in vivo* tumor growth. The diagram above all the figures indicates the experiment procedure. **(A)** Growth curve of tumor volumes from xenografted RD and RH30 cell lines, untreated, PBI-05204-treated, irradiated (RT), PBI-05204-pre-treated and irradiated (RT + PBI-05204). Tumor volumes were evaluated as described in methods and represent the mean ± SEM of eight mice per group. The graphs show the sequential treatments of xenografted mice started when tumors reached an initial volume of approximately 0.5 cm^3. Results represent the mean values ±SD. Statistical significance: $^{**}p \leq 0.01$, $^{***}p \leq 0.001$ vs. Untreated mice; \$\$\$ $p \leq 0.001$ vs. RT-treated mice; ###$p \leq 0.001$ vs. PBI-05204-treated mice. **(B)** Tumor weights from mice injected with RD (Left) and RH30 (Right) and treated with PBI-05204 and RT alone or in combination. **(C)** Kaplan–Meier estimates for rates of progression for untreated, PBI-05204, RT, or PBI-05204 + RT combination in RMS-derived tumors.

period of 20 days after the start of treatment. Compared to single treatments, combining RT and PBI-05204 significantly improved the therapeutic efficiency of RT resulting in 60.4% ± 6.3% volume reduction in RD (Figure 7A, RD, PBI-05204 + RT vs. RT) and 83.3% ± 6.2% in RH30 (Figure 7A, RH30, PBI-05204 + RT vs. RT) xenografts compared to RT alone, and of 37.5% ± 5.7% in RD (Figure 7A, RD, PBI-05204 + RT vs. PBI-05204) and 54.4% ± 8.1% in RH30 (Figure 7A, RH30, PBI-05204 + RT vs. PBI-05204)

xenografts compared to PBI-05204 alone. Notably, PBI-05204 alone significantly affected the *in vivo* tumor growth of RD by 44% ± 3.9% (Figure 7A, RD, PBI-05204 vs. Untreated) and of RH30 by 52.1% ± 7.1% (Figure 7A, RH30, PBI-05204 vs. Untreated). Accordingly, tumor weights of xenografts from mice co-treated with PBI-05204 and RT decreased significantly compared to those of untreated mice and single treatments (Figure 7B, RH30, PBI-05204 vs. Untreated). In both RD and RH30 xenografted mice PBI-05204 and RT co-treatment slowed the tumor progression (TP) compared to PBI-05204 (Figure 7C, RD and RH30, PBI-05204 + RT vs. PBI-05204) or RT (Figure 7C, RD and RH30, PBI-05204 + RT vs. RT) alone. Taken together, these findings highlight the ability of PBI-05204 to radiosensitize both FN-RMS and FP-RMS with a greater effect on FP-RMS.\

Discussion

Herein, the therapeutic potential of PBI-05204, a supercritical CO_2 extract of *N. oleander* (Colapietro et al., 2022) already clinically successfully tested for its tolerability and safety in cancer patients (Hong et al., 2014; Roth et al., 2020), has been investigated in RMS cells, as a single agent and in combination with RT.

As previously demonstrated with *in vitro* and *in vivo* models of pancreatic cancer (Pan et al., 2015) and glioblastoma (Colapietro et al., 2020, 2022), PBI-05204 counteracted, *in vitro*, the aberrant proliferation of RMS, by concomitantly inducing cytostatic and cytotoxic effects in a concentration dependent manner. Notably, the half maximal inhibitory concentration (IC_{50}) able to induce growth arrest was 4.8 ng/ml in FN- and 2.2 ng/ml in FP-RMS, suggesting a higher sensitivity to PBI-20054 of the most aggressive RMS subtype. Furthermore, prolonged treatment induced the death of all cells, suggesting that the initial cytostatic effect induced by PBI-05204 could be a failed attempt by cells to resist the cytotoxic action of the drug.

Treatment of FP-RMS resulted rapidly (24 h) and persistently (4 days) in an arrest in the G_2/M phase of the cell cycle, while FN-RMS was transiently restrained in the G_1/S phase, with a different molecular pattern between RMS subtypes.

In FP-RMS, PBI-05204 downregulated the expression of cyclin A1 and cyclin B1, promoters of G_2/M transition (Jackman and Pines, 1997), and upregulated the expression of $p21^{Waf1/Cip1}$ and $p27^{Cip1/Kip1}$, cell cycle inhibitors globally acting in any phase of the cell cycle (Abukhdeir and Park, 2008). According to previously reported evidence (Hong et al., 2014), PBI-05204 inhibited the PI3-kinase/AKT protein kinase pathway. PI3-kinase/AKT signaling, known to be aberrantly activated and sustained in the transformed phenotype of FP-RMS (Sorensen et al., 2002; Davicioni et al., 2009; Rudzinski et al., 2015, 2017; Skapek et al., 2019), has multiple roles in regulation of cell cycle progression (Liang and Slingerland, 2003), including the G_2/M phase (Shtivelman et al., 2002) in part by phosphorylating/inhibiting $p21^{Waf1/Cip1}$ and $p27^{Cip1/Kip1}$ (Chen et al., 2019). Furthermore, targeted inhibition of the PI3K/AKT pathway has been shown to enhance cell death in FP-RMS (Liu et al., 2009; Crose and Linardic, 2011). Thus, we believe that the cytostatic and cytotoxic effects concomitantly induced by PBI-05204 could be related to PI3K/AKT pathway inhibition. Notably, we noticed that PBI-05204 also downregulated the expression of cyclin E/CDK2 complex, known to be a G_1 cell cycle promoter (Hinds et al., 1992). However, it has been shown that cyclin E/CDK2 complex can also promote non-cell cycle-related (Hydbring et al., 2016; Liu et al., 2019) pro-oncogenic functions (Hwang and Clurman, 2005; Pang et al., 2020), including in FP-RMS (Takahashi et al., 2004; Tamura et al., 2022). Thus, although we cannot exclude a possible role in growth arrest, we believe that PBI-05204-induced cyclin E/CDK2 downregulation is relevant in terms of affecting the relative aggressiveness FP-RMS.

In contrast to FP-RMS, PBI-05204-treatment did not modulate the expression of cyclins and/or CDKs in FN-RMS but downregulated the expression of the oncoprotein c-Myc. Similarly, PBI-05204 upregulated the expression of $p21^{Waf1/Cip1}$ and $p27^{Cip1/Kip1}$. We have previously shown that overexpression of $p21^{Waf1/Cip1}$ (Ciccarelli et al., 2005) or downregulation of c-Myc itself (Gravina et al., 2016) can induce growth arrest in FN-RMS. Considering that PBI-05204 induces the dephosphorylation/inhibition of ERKs, known to be aberrantly activated in FN-RMS (Sorensen et al., 2002; Davicioni et al., 2009; Rudzinski et al., 2015, 2017; Skapek et al., 2019), upregulates $p21^{Waf1/Cip1}$ (Ciccarelli et al., 2005) and downregulates c-Myc (Marampon et al., 2006) expression, the molecular modulations induced by PBI-05204 in FN-RMS may occur through disruption of the MEKs/ERKs signaling and consequent c-Myc-downregulation-mediated p21Waf1/Cip1 expression (Gartel et al., 2001) and $p27^{Cip1/Kip1}$ phosphorylation/activation (García-Gutiérrez et al., 2019). Notably, according to the proposed roles of $p21^{Waf1/Cip1}$ and $p27^{Cip1/Kip1}$ as key master regulators of cellular senescence (Flores et al., 2014), a potentially reversible type of cell cycle arrest (Flores et al., 2014; Kumari and Jat, 2021), it was demonstrated that PBI-05204 increased the expression levels of SA-β-Gal, a marker of cell senescence (Dimri et al., 1995), in FN-RMS but not in FP-RMS. It has been recently shown that senescence is not always definitive and that arrested cancer cells can use senescence as an adaptive pathway to restart proliferation (Guillon et al., 2019). Thus, we speculate that the lower sensitivity of FN-RMS to PBI-05204 could be related to an ability of this RMS subtype to activate a program of senescence-mediated cellular protection in which an inability to be activated in FP-RMS makes the latter more sensitive to the drug.

The potential therapeutic efficiency of PBI-05204 is also suggested by its ability to counteract the growth of the cancer stem cell (CSC) subpopulation, as suggested by the assays based

on the formation of CSCs-like enriched tumorspheres and the reduction in the expression of the stem cell marker CD133. The subpopulation of CSCs has been shown to drive tumor initiation, resistance to therapies and be responsible for local relapses and distant metastases (Phi et al., 2018; Arnold et al., 2020). Notably, according to the role of CSCs in promoting cancer metastases and the ability of PBI-05204 to counteract RMS stemness, the treatment reduced the ability of FN- and FP-RMS to migrate and invade. It has been recently shown that MEKs/ERKs signaling in FN-RMS and PI3K/AKTs signaling in FP-RMS sustain CSCs and a pro-metastatic phenotype (Ciccarelli et al., 2016; Manzella et al., 2020; Ramadan et al., 2020; Skrzypek et al., 2020). Thus, inhibition of these pathways by PBI-05204 could be explained at least in part by its ability to counteract stemness and the migratory behavior/metastatic potential of RMS cancer cells.

Since monotherapy frequently fails to adequately control tumor proliferation and RT has been shown to play a critical role in treating RMSs patients, the ability of PBI-05204 to increase the therapeutic efficacy of RT was investigated. PBI-05204 radiosensitized both FN- and FP-RMS, as indicated by the impaired clonogenic survival of PBI-05204-pre-treated non-CSCs and CSCs RMS cells. Since CSCs have been shown to contribute significantly to radiation resistance, and PBI-05204 has recently been shown to radiosensitize CSCs of GBM (Colapietro et al., 2022), it is suggested that this botanical drug is a strong candidate for use as a radiosensitizer in the treatment of RD. The molecular mechanisms involved in radioresistance are not fully understood (Arnold et al., 2020), even though DNA repair remains the mechanism primarily responsible for resistance of cancer cells to radiation (Schulz et al., 2019). A tumor cell's ability to effectively repair DNA damage can enable it to: 1) resume proliferation, abandoning the redistribution of the cell cycle induced by radiation; 2) effectively repopulate the portion of cancer cells killed by radiation; 3) counteract the radiosensitizing phenomenon of reoxygenation; and, 4) acquire a more aggressive phenotype capable of increasing intratumoral heterogeneity, reducing the immunostimulating potential of RT (Boustani et al., 2019). Homologous recombination (HR), mediated by ATM signaling, and NHEJ, mediated by DNA-PKcs signaling, are the two major pathways for repair of DSBs, (Toulany, 2019). PBI-05204 efficiently, stably, and persistently counteracted the phosphorylation/activation of ATM on both FN- and FP-RMS. ATM contributes to radioresistance of several cancer cell types (Tribius et al., 2001; ZHOU et al., 2013; Bernardino-Sgherri et al., 2021; Cao et al., 2021; Zhang et al., 2022), resulting in an important pathway for DSB repair (Helleday, 2010), as also confirmed by García et al., 2022. Recently, a Phase I clinical trial investigating the radiosensitizing efficiency of M3541, a selective inhibitor of ATM, has closed unsuccessfully (Waqar et al., 2022), while another, assessing the safety and tolerability of the ATM inhibitor AZD1390 in combination to RT in patients with brain cancer is ongoing (NCT03423628). It has been largely shown that cancer cells can activate alternative survival pathways as a major mechanism of drug resistance and this also involves resistance to DNA repair inhibitors (Baxter et al., 2022). In this context, having available a drug capable of inhibiting the main pathways responsible for rhabdomyosarcomagenesis and DNA repair is certainly an advantage. That PBI-05204 can counteract in a stable and persistent way the state of phosphorylation/activation of DNA-PKcs, and thereby abolish repair of DSBs in the most aggressive and radioresistant subtype of RMS, the FP-RMS, represents a further point in favor of the use of PBI-05204 as a radiosensitizing agent. Further research is required to understand why inhibition of DNA-PKcs is transient in FN-RMS and whether this can be interpreted as a potential attempt to activate a resistance mechanism. However, PBI-05204 efficiently counteracted the ability of RMS to escape from RT-induced G2/M growth arrest on both FN- and FP-RMS, predisposing cancer cells to a higher sensitivity to subsequent fractions of irradiation (Toulany, 2019).

Finally, PBI-05204 radiosensitized FN- and FP-RMS in *in vivo* xenograft models of RMS as indicated by the ability of RT to counteract tumor growth and progression more efficiently in PBI-05204 pre-treated mice. The dose of PBI-05204 (20 mg/kg) (Colapietro et al., 2022) herein used in *in vivo* experiments is effectively higher than used in the phase I clinical trial (Hong et al., 2014). This is explained by the fact that mice lack expression of the Na, K-ATPase alpha3 subunit, which is important for efficient uptake of oleandrin, the major bioactive component of PBI-05204 (Yang et al., 2009), which leads to a relatively low absorption. However, no differences were noticed between the blood concentration of oleandrin in treated mice (Pan et al., 2015) and patients treated with the highest dose of PBI-05204 (Hong et al., 2014). Additional research requires that lower doses of PBI-05204 will need to be evaluated.

RT remains a pivotal treatment in the management of RMS even though a significant number of patients experience local and/or distant recurrences. The use of hypofractionated schedules has not improved the therapeutic efficiency of RT. Therefore, there is an urgent need to identify new radiosensitizing strategies. The data reported herein suggests that PBI-05204 could be an important new radiosensitizer with strong activity toward FP-RMS, the most aggressive type of RMS.

Data availability statement

The original contributions presented in the study are included in the article/Supplementary Materials, further inquiries can be directed to the corresponding author.

Ethics statement

The animal study was reviewed and approved by The recommendations of the European Community (EC) guidelines (2010/63/UE and DL 26/2014 for the use of

laboratory animals) and the Istituto Superiore di Sanità guidelines, complying with the Italian government regulation n.116 27 January 1992 for the use of laboratory animals code 221/2022-PR (D9997.140) approved 4 April 2022 were used to undertake *in vivo* experiments.

Author contributions

SV, AR, and AP conceptualized and designed the study. SCa, MC, SP, and MT, performed the experiments and acquired data. GMa, FP, GB, CM, RR, GC, MT, RN, and PY, analysed and interpreted the data. SCo, AF, FMe, CF, GMi, and GG, drafted the manuscript. FV, LM, and FMa critically revised the manuscript. All authors read and approved the final version of the manuscript.

Funding

The research leading to these results has received funding from AIRC under IG 2020—ID. 24696 project—P.I. FM. SCa was supported by "Io, domani..." Associazione per la lotta contro i tumori infantili Onlus with a post-doctoral fellowship. SCo was supported by Fondazione Umberto Veronesi.

Acknowledgments

We are grateful to the Italian Association for Cancer Research (AIRC) for the support given to our studies.

Conflict of interest

RN was employed by Phoenix Biotechnology, Inc.

The remaining authors declare that the research was conducted in the absence of any commercial or financial relationships that could be construed as a potential conflict of interest.

Publisher's note

Supplementary material

The Supplementary Material for this article can be found online at: https://www.frontiersin.org/articles/10.3389/fphar.2022.1071176/full#supplementary-material

SUPPLEMENTAL FIGURE S1
Multipotent mesenchymal stromal cells (MSCs) are slightly sensitive to PBI-05204. Dose of PBI-05204 able to reduce by 50% the cell survival of MSCs cells. **(B)** Effect of PBI-05204 IC50 on cell number of dead MSCs cells. Surviving cells were counted using Trypan blue dye exclusion test. Results represent the mean values of three independent experiments ± SD. Statistical significance: *$p \leq 0.05$, **$p \leq 0.01$, ***$p \leq 0.001$, Live Cells, Untreated vs. PBI-05204.

References

AAT Bioquest (2022). Quest GraphTM IC50 calculator. Available at: https://www.aatbio.com/tools/ic50-calculator.

Abi Jaoude, J., Thunshelle, C. P., Kouzy, R., Nguyen, N. D., Lin, D., Prakash, L., et al. (2021). Stereotactic versus conventional radiation therapy for patients with pancreatic cancer in the modern era. *Adv. Radiat. Oncol.* 6, 100763. doi:10.1016/j.adro.2021.100763

Abukhdeir, A. M., and Park, B. H. (2008). p21 and p27: roles in carcinogenesis and drug resistance. *Expert Rev. Mol. Med.* 10, e19. doi:10.1017/S1462399408000744

Alamilla-Presuel, J. C., Burgos-Molina, A. M., González-Vidal, A., Sendra-Portero, F., and Ruiz-Gómez, M. J. (2022). Factors and molecular mechanisms of radiation resistance in cancer cells. *Int. J. Radiat. Biol.* 98, 1301–1315. doi:10.1080/09553002.2022.2047825

Arnold, C. R., Mangesius, J., Skvortsova, I.-I., and Ganswindt, U. (2020). The role of cancer stem cells in radiation resistance. *Front. Oncol.* 10, 164. doi:10.3389/fonc.2020.00164

AVMA (2019). Proposed 2019 updates to the AVMA guidelines for the Euthanasia of animals. [Cited 11 February 2020]Available at: https://www.avma.org/KB/Policies/Documents/Interim-2019-marked-changes-for-comment-period.pdf.

Balagurumoorthy, P., James Adelstein, S., and Kassis, A. I. (2011). Novel method for quantifying radiation-induced single-strand-break yields in plasmid DNA highlights 10-fold discrepancy. *Anal. Biochem.* 417, 242–246. doi:10.1016/j.ab.2011.06.023

Baskar, R., Dai, J., Wenlong, N., Yeo, R., and Yeoh, K.-W. (2014). Biological response of cancer cells to radiation treatment. *Front. Mol. Biosci.* 1, 24. doi:10.3389/fmolb.2014.00024

Baxter, J. S., Zatreanu, D., Pettitt, S. J., and Lord, C. J. (2022). Resistance to DNA repair inhibitors in cancer. *Mol. Oncol.* 16, 3811–3827. doi:10.1002/1878-0261.13224

Bernardino-Sgherri, J., Siberchicot, C., Auvré, F., Busso, D., Brocas, C., el Masri, G., et al. (2021). Tumor resistance to radiotherapy is triggered by an ATM/TAK1-dependent-increased expression of the cellular prion protein. *Oncogene* 40, 3460–3469. doi:10.1038/s41388-021-01746-0

Botelho, A. F. M., Pierezan, F., Soto-Blanco, B., and Melo, M. M. (2019). A review of cardiac glycosides: Structure, toxicokinetics, clinical signs, diagnosis and antineoplastic potential. *Toxicon* 158, 63–68. doi:10.1016/j.toxicon.2018.11.429

Boustani, J., Laurent, P. A., Mirjolet, C., and Apetoh, L. (2019). The 6th R of radiobiology: Reactivation of anti-tumor immune response. *Cancers (Basel)* 11, 860. doi:10.3390/cancers11060860

Calderón-Montaño, J. M., Burgos-Morón, E., Orta, M. L., Maldonado-Navas, D., García-Domínguez, I., and López-Lázaro, M. (2014). Evaluating the cancer therapeutic potential of cardiac glycosides. *Biomed. Res. Int.* 2014, 794930–794939. doi:10.1155/2014/794930

Camero, S., Camicia, L., Marampon, F., Ceccarelli, S., Shukla, R., Mannarino, O., et al. (2020). BET inhibition therapy counteracts cancer cell survival, clonogenic potential and radioresistance mechanisms in rhabdomyosarcoma cells. *Cancer Lett.* 479, 71–88. doi:10.1016/j.canlet.2020.03.011

Camero, S., Ceccarelli, S., de Felice, F., Marampon, F., Mannarino, O., Camicia, L., et al. (2019). PARP inhibitors affect growth, survival and radiation susceptibility of human alveolar and embryonal rhabdomyosarcoma cell lines. *J. Cancer Res. Clin. Oncol.* 145, 137–152. doi:10.1007/s00432-018-2774-6

Camero, S., Vitali, G., Pontecorvi, P., Ceccarelli, S., Anastasiadou, E., Cicchetti, F., et al. (2021). DNMT3A and DNMT3B targeting as an effective radiosensitizing strategy in embryonal rhabdomyosarcoma. *Cells* 10, 2956. doi:10.3390/cells10112956

Cao, K., Chen, Y., Zhao, S., Huang, Y., Liu, T., Liu, H., et al. (2021). Sirt3 promoted DNA damage repair and radioresistance through ATM-chk2 in non-small cell lung cancer cells. *J. Cancer* 12, 5464–5472. doi:10.7150/jca.53173

Casey, D. L., Pitter, K. L., Wexler, L. H., Slotkin, E. K., Gupta, G. P., and Wolden, S. L. (2021). TP53 mutations increase radioresistance in rhabdomyosarcoma and Ewing sarcoma. *Br. J. Cancer* 125, 576–581. doi:10.1038/s41416-021-01438-2

Cassandri, M., Pomella, S., Rossetti, A., Petragnano, F., Milazzo, L., Vulcano, F., et al. (2021). MS-275 (entinostat) promotes radio-sensitivity in PAX3-FOXO1 rhabdomyosarcoma cells. *Int. J. Mol. Sci.* 22, 10671. doi:10.3390/ijms221910671

Cecchetto, G., Bisogno, G., de Corti, F., Dall'Igna, P., Inserra, A., Ferrari, A., et al. (2007). Biopsy or debulking surgery as initial surgery for locally advanced rhabdomyosarcomas in children? *Cancer* 110, 2561–2567. doi:10.1002/cncr.23079

Chen, Y., Liu, X., Wang, H., Liu, S., Hu, N., and Li, X. (2019). Akt regulated phosphorylation of GSK-3β/cyclin D1, p21 and p27 contributes to cell proliferation through cell cycle progression from G1 to S/G2M phase in low-dose arsenite exposed HaCat cells. *Front. Pharmacol.* 10, 1176. doi:10.3389/fphar.2019.01176

Ciccarelli, C., Marampon, F., Scoglio, A., Mauro, A., Giacinti, C., de Cesaris, P., et al. (2005). p21WAF1 expression induced by MEK/ERK pathway activation or inhibition correlates with growth arrest, myogenic differentiation and onco-phenotype reversal in rhabdomyosarcoma cells. *Mol. Cancer* 4, 41. doi:10.1186/1476-4598-4-41

Ciccarelli, C., Vulcano, F., Milazzo, L., Gravina, G. L., Marampon, F., Macioce, G., et al. (2016). Key role of MEK/ERK pathway in sustaining tumorigenicity and *in vitro* radioresistance of embryonal rhabdomyosarcoma stem-like cell population. *Mol. Cancer* 15, 16. doi:10.1186/s12943-016-0501-y

Codenotti, S., Faggi, F., Ronca, R., Chiodelli, P., Grillo, E., Guescini, M., et al. (2019). Caveolin-1 enhances metastasis formation in a human model of embryonal rhabdomyosarcoma through Erk signaling cooperation. *Cancer Lett.* 449, 135–144. doi:10.1016/j.canlet.2019.02.013

Codenotti, S., Marampon, F., Triggiani, L., Bonù, M. L., Magrini, S. M., Ceccaroli, P., et al. (2021). Caveolin-1 promotes radioresistance in rhabdomyosarcoma through increased oxidative stress protection and DNA repair. *Cancer Lett.* 505, 1–12. doi:10.1016/j.canlet.2021.02.005

Colapietro, A., Yang, P., Rossetti, A., Mancini, A., Vitale, F., Chakraborty, S., et al. (2022). The botanical drug PBI-05204, a supercritical CO_2 extract of Nerium oleander, is synergistic with radiotherapy in models of human glioblastoma. *Front. Pharmacol.* 13, 552428. doi:10.3389/fphar.2020.552428

Colapietro, A., Yang, P., Rossetti, A., Mancini, A., Vitale, F., Martellucci, S., et al. (2020). The botanical drug PBI-05204, a supercritical CO_2 extract of Nerium oleander, inhibits growth of human glioblastoma, reduces akt/mTOR activities, and modulates GSC cell-renewal properties. *Front. Pharmacol.* 11, 552428. doi:10.3389/fphar.2020.552428

Crose, L. E. S., and Linardic, C. M. (2011). Receptor tyrosine kinases as therapeutic targets in rhabdomyosarcoma. *Sarcoma* 2011, 756982–756993. doi:10.1155/2011/756982

Davicioni, E., Anderson, M. J., Finckenstein, F. G., Lynch, J. C., Qualman, S. J., Shimada, H., et al. (2009). Molecular classification of rhabdomyosarcoma-genotypic and phenotypic determinants of diagnosis: A report from the children's oncology group. *Am. J. Pathol.* 174, 550–564. doi:10.2353/ajpath.2009.080631

Dearnaley, D., Syndikus, I., Mossop, H., Khoo, V., Birtle, A., Bloomfield, D., et al. (2016). Conventional versus hypofractionated high-dose intensity-modulated radiotherapy for prostate cancer: 5-year outcomes of the randomised, non-inferiority, phase 3 CHHiP trial. *Lancet. Oncol.* 17, 1047–1060. doi:10.1016/S1470-2045(16)30102-4

Dimri, G. P., Lee, X., Basile, G., Acosta, M., Scott, G., Roskelley, C., et al. (1995). A biomarker that identifies senescent human cells in culture and in aging skin *in vivo*. *Proc. Natl. Acad. Sci. U. S. A.* 92, 9363–9367. doi:10.1073/pnas.92.20.9363

Du, J., Shang, J., Chen, F., Zhang, Y., Yin, N., Xie, T., et al. (2018). A CRISPR/Cas9-Based screening for Non-Homologous End Joining inhibitors reveals ouabain and penfluridol as radiosensitizers. *Mol. Cancer Ther.* 17, 419–431. doi:10.1158/1535-7163.MCT-17-0090

Dunn, D. E., He, D. N., Yang, P., Johansen, M., Newman, R. A., and Lo, D. C. (2011). *In vitro* and *in vivo* neuroprotective activity of the cardiac glycoside oleandrin from Nerium oleander in brain slice-based stroke models. *J. Neurochem.* 119, 805–814. doi:10.1111/j.1471-4159.2011.07439.x

Durlacher, C. T., Chow, K., Chen, X.-W., He, Z.-X., Zhang, X., Yang, T., et al. (2015). Targeting Na^+/K^+ -translocating adenosine triphosphatase in cancer treatment. *Clin. Exp. Pharmacol. Physiol.* 42, 427–443. doi:10.1111/1440-1681.12385

Flores, J. M., Martín-Caballero, J., and García-Fernández, R. A. (2014). p21 and p27 a shared senescence history. *Cell Cycle* 13, 1655–1656. doi:10.4161/cc.29147

Fowler, J. F. (1989). The linear-quadratic formula and progress in fractionated radiotherapy. *Br. J. Radiol.* 62, 679–694. doi:10.1259/0007-1285-62-740-679

Frankel, A. E., Eskiocak, U., Gill, J. G., Yuan, S., Ramesh, V., Froehlich, T. W., et al. (2017). Digoxin plus trametinib therapy achieves disease control in BRAF wild-type metastatic melanoma patients. *Neoplasia* 19, 255–260. doi:10.1016/j.neo.2017.01.010

Fruci, D., Cho, C. S. W., Romania, P., Nobili, V., Locatelli, F., and Alisi, A. (2016). Drug transporters and multiple drug resistance in pediatric solid tumors. *Curr. Drug Metab.* 17, 308–316. doi:10.2174/1567205010666131212110948

Gallego, S., Bernabeu, D., Garrido-Pontnou, M., Guillen, G., Hindi, N., Juan-Ribelles, A., et al. (2021). GEIS-SEHOP clinical practice guidelines for the treatment of rhabdomyosarcoma. *Clin. Transl. Oncol.* 23, 2460–2473. doi:10.1007/s12094-021-02654-1

García, M. E. G., Kirsch, D. G., and Reitman, Z. J. (2022). Targeting the ATM kinase to enhance the efficacy of radiotherapy and outcomes for cancer patients. *Semin. Radiat. Oncol.* 32, 3–14. doi:10.1016/j.semradonc.2021.09.008

García-Gutiérrez, L., Bretones, G., Molina, E., Arechaga, I., Symonds, C., Acosta, J. C., et al. (2019). Myc stimulates cell cycle progression through the activation of Cdk1 and phosphorylation of p27. *Sci. Rep.* 9, 18693. doi:10.1038/s41598-019-54917-1

Gartel, A. L., Ye, X., Goufman, E., Shianov, P., Hay, N., Najmabadi, F., et al. (2001). Myc represses the p21 (WAF1/CIP1) promoter and interacts with Sp1/Sp3. *Proc. Natl. Acad. Sci. U. S. A.* 98, 4510–4515. doi:10.1073/pnas.081074898

Giannattasio, S., Megiorni, F., di Nisio, V., del Fattore, A., Fontanella, R., Camero, S., et al. (2019). Testosterone-mediated activation of androgenic signalling sustains *in vitro* the transformed and radioresistant phenotype of rhabdomyosarcoma cell lines. *J. Endocrinol. Invest.* 42, 183–197. doi:10.1007/s40618-018-0900-6

Goodhead, D. T. (1994). Initial events in the cellular effects of ionizing radiations: Clustered damage in DNA. *Int. J. Radiat. Biol.* 65, 7–17. doi:10.1080/09553009414550021

Gravina, G. L., Festuccia, C., Popov, V. M., di Rocco, A., Colapietro, A., Sanità, P., et al. (2016). c-Myc sustains transformed phenotype and promotes radioresistance of embryonal rhabdomyosarcoma cell lines. *Radiat. Res.* 185, 411–422. doi:10.1667/RR14237.1

Gravina, G. L., Mancini, A., Colapietro, A., Monache, S. D., Sferra, R., Vitale, F., et al. (2019). The small molecule ephrin receptor inhibitor, GLPG1790, reduces renewal capabilities of cancer stem cells, showing anti-tumour efficacy on preclinical glioblastoma models. *Cancers (Basel)* 11, E359. doi:10.3390/cancers11030359

Gravina, G. L., Mancini, A., Colapietro, A., Vitale, F., Vetuschi, A., Pompili, S., et al. (2017). The novel CXCR4 antagonist, PRX177561, reduces tumor cell proliferation and accelerates cancer stem cell differentiation in glioblastoma preclinical models. *Tumour Biol.* 39, 1010428317695528. doi:10.1177/1010428317695528

Guillon, J., Petit, C., Toutain, B., Guette, C., Lelièvre, E., and Coqueret, O. (2019). Chemotherapy-induced senescence, an adaptive mechanism driving resistance and tumor heterogeneity. *Cell Cycle* 18, 2385–2397. doi:10.1080/15384101.2019.1652047

Helleday, T. (2010). Homologous recombination in cancer development, treatment and development of drug resistance. *Carcinogenesis* 31, 955–960. doi:10.1093/carcin/bgq064

Heske, C. M., and Mascarenhas, L. (2021). Relapsed rhabdomyosarcoma. *J. Clin. Med.* 10, 804. doi:10.3390/jcm10040804

Hinds, P. W., Mittnacht, S., Dulic, V., Arnold, A., Reed, S. I., and Weinberg, R. A. (1992). Regulation of retinoblastoma protein functions by ectopic expression of human cyclins. *Cell* 70, 993–1006. doi:10.1016/0092-8674(92)90249-C

Hong, D. S., Henary, H., Falchook, G. S., Naing, A., Fu, S., Moulder, S., et al. (2014). First-in-human study of pbi-05204, an oleander-derived inhibitor of akt, fgf-2, nf-κB and p70s6k, in patients with advanced solid tumors. *Invest. New Drugs* 32, 1204–1212. doi:10.1007/s10637-014-0127-0

Hui, C., Tomilov, A., Garcia, C., Jiang, X., Fash, D. M., Khdour, O. M., et al. (2020). Novel idebenone analogs block Shc's access to insulin receptor to improve insulin sensitivity. *Biomed. Pharmacother.* 132, 110823. doi:10.1016/j.biopha.2020.110823

Hwang, H. C., and Clurman, B. E. (2005). Cyclin E in normal and neoplastic cell cycles. *Oncogene* 24, 2776–2786. doi:10.1038/sj.onc.1208613

Hydbring, P., Malumbres, M., and Sicinski, P. (2016). Non-canonical functions of cell cycle cyclins and cyclin-dependent kinases. *Nat. Rev. Mol. Cell Biol.* 17, 280–292. doi:10.1038/nrm.2016.27

Jackman, M. R., and Pines, J. N. (1997). Cyclins and the G2/M transition. *Cancer Surv.* 29, 47–73.

Jones, C. M., Spencer, K., Hitchen, C., Pelly, T., Wood, B., Hatfield, P., et al. (2019). Hypofractionated radiotherapy in oesophageal cancer for patients unfit for systemic therapy: A retrospective single-centre analysis. *Clin. Oncol.* 31, 356–364. doi:10.1016/j.clon.2019.01.010

Kalbasi, A., Kamrava, M., Chu, F.-I., Telesca, D., van Dams, R., Yang, Y., et al. (2020). A phase II trial of 5-day neoadjuvant radiotherapy for patients with high-risk primary soft tissue sarcoma. *Clin. Cancer Res.* 26, 1829–1836. doi:10.1158/1078-0432.CCR-19-3524

Kannan, A., Bhatia, K., Branzei, D., and Gangwani, L. (2018). Combined deficiency of Senataxin and DNA-PKcs causes DNA damage accumulation and neurodegeneration in spinal muscular atrophy. *Nucleic Acids Res.* 46, 8326–8346. doi:10.1093/nar/gky641

Kılıç, L., Ekenel, M., Karabulut, S., Ağaoğlu, F., and Darendeliler, E. (2017). Neoadjuvant sequential chemoradiotherapy versus radiotherapy alone for treatment of high-risk extremity soft tissue sarcoma: A single-institution experience. *Contemp. Oncol.* 1, 60–65. doi:10.5114/wo.2017.66658

Koseła-Paterczyk, H., Szacht, M., Morysiński, T., Ługowska, I., Dziewirski, W., Falkowski, S., et al. (2014). Preoperative hypofractionated radiotherapy in the treatment of localized soft tissue sarcomas. *Eur. J. Surg. Oncol.* 40, 1641–1647. doi:10.1016/j.ejso.2014.05.016

Kumari, R., and Jat, P. (2021). Mechanisms of cellular senescence: Cell cycle arrest and senescence associated secretory phenotype. *Front. Cell Dev. Biol.* 9, 645593. doi:10.3389/fcell.2021.645593

Kumavath, R., Paul, S., Pavithran, H., Paul, M. K., Ghosh, P., Barh, D., et al. (2021). Emergence of cardiac glycosides as potential drugs: Current and future scope for cancer therapeutics. *Biomolecules* 11, 1275. doi:10.3390/biom11091275

Lee, J. Y., Kim, M.-S., Lee, M. S., Ju, J. E., Chung, N., and Jeong, Y. K. (2017). Digoxin enhances radiation response in radioresistant A549 cells by reducing protein phosphatase 2A. *Biosci. Rep.* 37, BSR20171257. doi:10.1042/BSR20171257

Li, F., Zhou, K., Gao, L., Zhang, B., Li, W., Yan, W., et al. (2016). Radiation induces the generation of cancer stem cells: A novel mechanism for cancer radioresistance. *Oncol. Lett.* 12, 3059–3065. doi:10.3892/ol.2016.5124

Liang, J., and Slingerland, J. M. (2003). Multiple roles of the PI3K/PKB (Akt) pathway in cell cycle progression. *Cell Cycle* 2, 336–342. doi:10.4161/cc.2.4.433

Liepkans, V. A. (1990). Monosialoganglioside biosynthesis by subcellular membranes of rhabdomyosarcoma cell lines differing in metastatic potential. *Int. J. Cancer* 45, 961–967. doi:10.1002/ijc.2910450531

Liu, P., Cheng, H., Roberts, T. M., and Zhao, J. J. (2009). Targeting the phosphoinositide 3-kinase pathway in cancer. *Nat. Rev. Drug Discov.* 8, 627–644. doi:10.1038/nrd2926

Liu, S.-T., Chan, G. K., and Li, W. (2019). Editorial: Non-cell cycle functions of cell cycle regulators. *Front. Cell Dev. Biol.* 7, 122. doi:10.3389/fcell.2019.00122

López-Lázaro, M., Pastor, N., Azrak, S. S., Ayuso, M. J., Austin, C. A., and Cortés, F. (2005). Digitoxin inhibits the growth of cancer cell lines at concentrations commonly found in cardiac patients. *J. Nat. Prod.* 68, 1642–1645. doi:10.1021/np050226l

MacDermed, D. M., Miller, L. L., Peabody, T. D., Simon, M. A., Luu, H. H., Haydon, R. C., et al. (2010). Primary tumor necrosis predicts distant control in locally advanced soft-tissue sarcomas after preoperative concurrent chemoradiotherapy. *Int. J. Radiat. Oncol. Biol. Phys.* 76, 1147–1153. doi:10.1016/j.ijrobp.2009.03.015

Mandeville, H. C. (2019). Radiotherapy in the management of childhood rhabdomyosarcoma. *Clin. Oncol.* 31, 462–470. doi:10.1016/j.clon.2019.03.047

Manzella, G., Schreck, L. D., Breunis, W. B., Molenaar, J., Merks, H., Barr, F. G., et al. (2020). Phenotypic profiling with a living biobank of primary rhabdomyosarcoma unravels disease heterogeneity and AKT sensitivity. *Nat. Commun.* 11, 4629. doi:10.1038/s41467-020-18388-7

Marampon, F., Ciccarelli, C., and Zani, B. M. (2019a). Biological rationale for targeting MEK/ERK pathways in anti-cancer therapy and to potentiate tumour responses to radiation. *Int. J. Mol. Sci.* 20, E2530. doi:10.3390/ijms20102530

Marampon, F., Ciccarelli, C., and Zani, B. M. (2006). Down-regulation of c-Myc following MEK/ERK inhibition halts the expression of malignant phenotype in rhabdomyosarcoma and in non muscle-derived human tumors. *Mol. Cancer* 5, 31. doi:10.1186/1476-4598-5-31

Marampon, F., Codenotti, S., Megiorni, F., del Fattore, A., Camero, S., Gravina, G. L., et al. (2019b). NRF2 orchestrates the redox regulation induced by radiation therapy, sustaining embryonal and alveolar rhabdomyosarcoma cells radioresistance. *J. Cancer Res. Clin. Oncol.* 145, 881–893. doi:10.1007/s00432-019-02851-0

Marampon, F., di Nisio, V., Pietrantoni, I., Petragnano, F., Fasciani, I., Scicchitano, B. M., et al. (2019c). Pro-differentiating and radiosensitizing effects of inhibiting HDACs by PXD-101 (Belinostat) in *in vitro* and *in vivo* models of human rhabdomyosarcoma cell lines. *Cancer Lett.* 461, 90–101. doi:10.1016/j.canlet.2019.07.009

Marampon, F., Gravina, G. L., di Rocco, A., Bonfili, P., di Staso, M., Fardella, C., et al. (2011). MEK/ERK inhibitor U0126 increases the radiosensitivity of rhabdomyosarcoma cells *in vitro* and *in vivo* by downregulating growth and DNA repair signals. *Mol. Cancer Ther.* 10, 159–168. doi:10.1158/1535-7163.MCT-10-0631

Marampon, F., Leoni, F., Mancini, A., Pietrantoni, I., Codenotti, S., Letizia, F., et al. (2019d). Histone deacetylase inhibitor ITF2357 (givinostat) reverts transformed phenotype and counteracts stemness in *in vitro* and *in vivo* models of human glioblastoma. *J. Cancer Res. Clin. Oncol.* 145, 393–409. doi:10.1007/s00432-018-2800-8

Megiorni, F., Camero, S., Pontecorvi, P., Camicia, L., Marampon, F., Ceccarelli, S., et al. (2021). OTX015 epi-drug exerts antitumor effects in ovarian cancer cells by blocking GNL3-mediated radioresistance mechanisms: Cellular, molecular and computational evidence. *Cancers (Basel)* 13, 1519. doi:10.3390/cancers13071519

Megiorni, F., Gravina, G. L., Camero, S., Ceccarelli, S., del Fattore, A., Desiderio, V., et al. (2017). Pharmacological targeting of the ephrin receptor kinase signalling by GLPG1790 *in vitro* and *in vivo* reverts oncophenotype, induces myogenic differentiation and radiosensitizes embryonal rhabdomyosarcoma cells. *J. Hematol. Oncol.* 10, 161. doi:10.1186/s13045-017-0530-z

Mekhail, T., Kaur, H., Ganapathi, R., Budd, G. T., Elson, P., and Bukowski, R. M. (2006). Phase 1 trial of Anvirzel in patients with refractory solid tumors. *Invest. New Drugs* 24, 423–427. doi:10.1007/s10637-006-7772-x

Menger, L., Vacchelli, E., Kepp, O., Eggermont, A., Tartour, E., Zitvogel, L., et al. (2013). Trial watch: Cardiac glycosides and cancer therapy. *Oncoimmunology* 2, e23082. doi:10.4161/onci.23082

Menna, M., Fiorentino, F., Marrocco, B., Lucidi, A., Tomassi, S., Cilli, D., et al. (2022). Novel non-covalent LSD1 inhibitors endowed with anticancer effects in leukemia and solid tumor cellular models. *Eur. J. Med. Chem.* 237, 114410. doi:10.1016/j.ejmech.2022.114410

Meyer, J. M., Perlewitz, K. S., Hayden, J. B., Doung, Y.-C., Hung, A. Y., Vetto, J. T., et al. (2013). Phase I trial of preoperative chemoradiation plus sorafenib for high-risk extremity soft tissue sarcomas with dynamic contrast-enhanced MRI correlates. *Clin. Cancer Res.* 19, 6902–6911. doi:10.1158/1078-0432.CCR-13-1594

Mijatovic, T., Dufrasne, F., and Kiss, R. (2012). Na +/K + -ATPase and cancer. *Pharm. Pat. Anal.* 1, 91–106. doi:10.4155/ppa.12.3

Murray Brunt, A., Haviland, J. S., Wheatley, D. A., Sydenham, M. A., Alhasso, A., Bloomfield, D. J., et al. (2020). Hypofractionated breast radiotherapy for 1 week versus 3 weeks (FAST-Forward): 5-year efficacy and late normal tissue effects results from a multicentre, non-inferiority, randomised, phase 3 trial. *Lancet* 395, 1613–1626. doi:10.1016/S0140-6736(20)30932-6

Nasu, S., Milas, L., Kawabe, S., Raju, U., and Newman, R. A. (2002). Enhancement of radiotherapy by oleandrin is a caspase-3 dependent process. *Cancer Lett.* 185, 145–151. doi:10.1016/S0304-3835(02)00263-X

Pan, Y., Rhea, P., Tan, L., Cartwright, C., Lee, H.-J., Ravoori, M. K., et al. (2015). PBI-05204, a supercritical CO_2 extract of Nerium oleander, inhibits growth of human pancreatic cancer via targeting the PI3K/mTOR pathway. *Invest. New Drugs* 33, 271–279. doi:10.1007/s10637-014-0190-6

Pang, W., Li, Y., Guo, W., and Shen, H. (2020). Cyclin E: A potential treatment target to reverse cancer chemoresistance by regulating the cell cycle. *Am. J. Transl. Res.* 12, 5170–5187.

Parsai, S., Lawrenz, J., Kilpatrick, S., Rubin, B., Hymes, C., Gray, M., et al. (2020). Early outcomes of preoperative 5-fraction radiation therapy for soft tissue sarcoma followed by immediate surgical resection. *Adv. Radiat. Oncol.* 5, 1274–1279. doi:10.1016/j.adro.2020.06.024

Pavlovic, D. (2020). Endogenous cardiotonic steroids and cardiovascular disease, where to next? *Cell Calcium* 86, 102156. doi:10.1016/j.ceca.2019.102156

Pawlik, T. M., and Keyomarsi, K. (2004). Role of cell cycle in mediating sensitivity to radiotherapy. *Int. J. Radiat. Oncol. Biol. Phys.* 59, 928–942. doi:10.1016/j.ijrobp.2004.03.005

PDQ Pediatric Treatment Editorial Board (2002). *Childhood rhabdomyosarcoma treatment (PDQ®): Health professional version*.

Pennington, J. D., Eilber, F. C., Eilber, F. R., Singh, A. S., Reed, J. P., Chmielowski, B., et al. (2018). Long-term outcomes with ifosfamide-based hypofractionated preoperative chemoradiotherapy for extremity soft tissue sarcomas. *Am. J. Clin. Oncol.* 41, 1154–1161. doi:10.1097/COC.0000000000000443

Perrone, C., Pomella, S., Cassandri, M., Pezzella, M., Milano, G. M., Colletti, M., et al. (2022). MET inhibition sensitizes rhabdomyosarcoma cells to NOTCH signaling suppression. *Front. Oncol.* 12, 835642. doi:10.3389/fonc.2022.835642

Petragnano, F., Pietrantoni, I., Camero, S., Codenotti, S., Milazzo, L., Vulcano, F., et al. (2020a). Clinically relevant radioresistant rhabdomyosarcoma cell lines: Functional, molecular and immune-related characterization. *J. Biomed. Sci.* 27, 90. doi:10.1186/s12929-020-00683-6

Petragnano, F., Pietrantoni, I., di Nisio, V., Fasciani, I., del Fattore, A., Capalbo, C., et al. (2020b). Modulating the dose-rate differently affects the responsiveness of human epithelial prostate- and mesenchymal rhabdomyosarcoma-cancer cell line to radiation. *Int. J. Radiat. Biol.* 96, 823–835. doi:10.1080/09553002.2020.1739774

Phi, L. T. H., Sari, I. N., Yang, Y.-G., Lee, S.-H., Jun, N., Kim, K. S., et al. (2018). Cancer stem cells (CSCs) in drug resistance and their therapeutic implications in cancer treatment. *Stem Cells Int.* 2018, 5416923–5416939. doi:10.1155/2018/5416923

Ramadan, F., Fahs, A., Ghayad, S. E., and Saab, R. (2020). Signaling pathways in Rhabdomyosarcoma invasion and metastasis. *Cancer Metastasis Rev.* 39, 287–301. doi:10.1007/s10555-020-09860-3

Rodin, D., Tawk, B., Mohamad, O., Grover, S., Moraes, F. Y., Yap, M. L., et al. (2021). Hypofractionated radiotherapy in the real-world setting: An international ESTRO-GIRO survey. *Radiother. Oncol.* 157, 32–39. doi:10.1016/j.radonc.2021.01.003

Rossetti, A., Petragnano, F., Milazzo, L., Vulcano, F., Macioce, G., Codenotti, S., et al. (2021). Romidepsin (FK228) fails in counteracting the transformed phenotype of rhabdomyosarcoma cells but efficiently radiosensitizes, *in vitro* and *in vivo*, the alveolar phenotype subtype. *Int. J. Radiat. Biol.* 97, 943–957. doi:10.1080/09553002.2021.1928786

Roth, M. T., Cardin, D. B., Borazanci, E. H., Steinbach, M., Picozzi, V. J., Rosemury, A., et al. (2020). A phase II, single-arm, open-label, bayesian adaptive efficacy and safety study of PBI-05204 in patients with stage IV metastatic pancreatic adenocarcinoma. *Oncologist* 25, e1446–e1450. doi:10.1634/theoncologist.2020-0440

Rudzinski, E. R., Anderson, J. R., Chi, Y.-Y., Gastier-Foster, J. M., Astbury, C., Barr, F. G., et al. (2017). Histology, fusion status, and outcome in metastatic rhabdomyosarcoma: A report from the children's oncology group. *Pediatr. Blood Cancer* 64, e26645. doi:10.1002/pbc.26645

Rudzinski, E. R., Anderson, J. R., Hawkins, D. S., Skapek, S. X., Parham, D. M., and Teot, L. A. (2015). The world health organization classification of skeletal muscle tumors in pediatric rhabdomyosarcoma: A report from the children's oncology group. *Arch. Pathol. Lab. Med.* 139, 1281–1287. doi:10.5858/arpa.2014-0475-OA

Ryan, C. W., Montag, A. G., Hosenpud, J. R., Samuels, B., Hayden, J. B., Hung, A. Y., et al. (2008). Histologic response of dose-intense chemotherapy with preoperative hypofractionated radiotherapy for patients with high-risk soft tissue sarcomas. *Cancer* 112, 2432–2439. doi:10.1002/cncr.23478

Rycaj, K., and Tang, D. G. (2014). Cancer stem cells and radioresistance. *Int. J. Radiat. Biol.* 90, 615–621. doi:10.3109/09553002.2014.892227

Schulz, A., Meyer, F., Dubrovska, A., and Borgmann, K. (2019). Cancer stem cells and radioresistance: DNA repair and beyond. *Cancers (Basel)* 11, 862. doi:10.3390/cancers11060862

Siddiqui, B. S., Begum, S., Siddiqui, S., and Lichter, W. (1995). Two cytotoxic pentacyclic triterpenoids from Nerium oleander. *Phytochemistry* 39, 171–174. doi:10.1016/0031-9422(94)00855-N

Skapek, S. X., Ferrari, A., Gupta, A. A., Lupo, P. J., Butler, E., Shipley, J., et al. (2019). *Nat. Rev. Dis. Prim.* 5, 1. doi:10.1038/s41572-018-0051-2

Skrzypek, K., Kot, M., Konieczny, P., Nieszporek, A., Kusienicka, A., Lasota, M., et al. (2020). SNAIL promotes metastatic behavior of rhabdomyosarcoma by increasing EZRIN and AKT expression and regulating MicroRNA networks. *Cancers (Basel)* 12, 1870. doi:10.3390/cancers12071870

Sorensen, P. H. B., Lynch, J. C., Qualman, S. J., Tirabosco, R., Lim, J. F., Maurer, H. M., et al. (2002). PAX3-FKHR and PAX7-FKHR gene fusions are prognostic indicators in alveolar rhabdomyosarcoma: A report from the children's oncology group. *J. Clin. Oncol.* 20, 2672–2679. doi:10.1200/JCO.2002.03.137

Soyfer, V., Corn, B. W., Kollender, Y., Issakov, J., Dadia, S., Flusser, G., et al. (2013). Hypofractionated adjuvant radiation therapy of soft-tissue sarcoma achieves excellent results in elderly patients. *Br. J. Radiol.* 86, 20130258. doi:10.1259/bjr.20130258

Spalek, M., Koseła-Paterczyk, H., Borkowska, A., Wągrodzki, M., Szumera-Ciećkiewicz, A., Cieszanowski, A., et al. (2019). OC-0069 5x5 Gy with chemotherapy in borderline resectable soft tissue sarcomas: Early results of a trial. *Radiotherapy Oncol.* 133, S31–S32. doi:10.1016/S0167-8140(19)30489-X

Spałek, M., Koseła-Paterczyk, H., Borkowska, A., Wągrodzki, M., Szumera-Ciećkiewicz, A., Pałucki, J., et al. (2019). Hypofractionated radiotherapy in locally advanced myxoid liposarcomas of extremities or trunk wall: Results of a single arm prospective clinical trial. *Int. J. Radiat. Oncology*Biology*Physics* 105, S63. doi:10.1016/j.ijrobp.2019.06.506

Spencer, R. M., Aguiar Junior, S., Ferreira, F. O., Stevanato Filho, P. R., Kupper, B. E., Silva, M. L., et al. (2017). Neoadjuvant hypofractionated radiotherapy and chemotherapy in high-grade extremity soft tissue sarcomas: Phase 2 clinical trial protocol. *JMIR Res. Protoc.* 6, e97. doi:10.2196/resprot.6806

Surovtseva, Y. v., Jairam, V., Salem, A. F., Sundaram, R. K., Bindra, R. S., and Herzon, S. B. (2016). Characterization of cardiac glycoside natural products as potent inhibitors of DNA double-strand break repair by a whole-cell double immunofluorescence assay. *J. Am. Chem. Soc.* 138, 3844–3855. doi:10.1021/jacs.6b00162

Takahashi, Y., Oda, Y., Kawaguchi, K., Tamiya, S., Yamamoto, H., Suita, S., et al. (2004). Altered expression and molecular abnormalities of cell-cycle-regulatory proteins in rhabdomyosarcoma. *Mod. Pathol.* 17, 660–669. doi:10.1038/modpathol.3800101

Tamura, S., Hayashi, T., Ichimura, T., Yaegashi, N., Abiko, K., and Konishi, I. (2022). Characteristic of uterine rhabdomyosarcoma by algorithm of potential biomarkers for uterine mesenchymal tumor. *Curr. Oncol.* 29, 2350–2363. doi:10.3390/curroncol29040190

Temple, W. J., Temple, C. L. F., Arthur, K., Schachar, N. S., Paterson, A. H. G., and Crabtree, T. S. (1997). Prospective cohort study of neoadjuvant treatment in conservative surgery of soft tissue sarcomas. *Ann. Surg. Oncol.* 4, 586–590. doi:10.1007/BF02305541

Terezakis, S. A., and Wharam, M. D. (2013). Radiotherapy for rhabdomyosarcoma: Indications and outcome. *Clin. Oncol.* 25, 27–35. doi:10.1016/j.clon.2012.07.009

Tian, D., Tang, J., Geng, X., Li, Q., Wang, F., Zhao, H., et al. (2020). Targeting UHRF1-dependent DNA repair selectively sensitizes KRAS mutant lung cancer to chemotherapy. *Cancer Lett.* 493, 80–90. doi:10.1016/j.canlet.2020.08.008

Toulany, M. (2019). Targeting DNA double-strand break repair pathways to improve radiotherapy response. *Genes (Basel)* 10, 25. doi:10.3390/genes10010025

Tounekti, O., Kenani, A., Foray, N., Orlowski, S., and Mir, L. M. (2001). The ratio of single- to double-strand DNA breaks and their absolute values determine cell death pathway. *Br. J. Cancer* 84, 1272–1279. doi:10.1054/bjoc.2001.1786

Tribius, S., Pidel, A., and Casper, D. (2001). ATM protein expression correlates with radioresistance in primary glioblastoma cells in culture. *Int. J. Radiat. Oncol. Biol. Phys.* 50, 511–523. doi:10.1016/S0360-3016(01)01489-4

Verheye-Dua, F., and Böhm, L. (1998). Na+, K+-ATPase inhibitor, ouabain accentuates irradiation damage in human tumour cell lines. *Radiat. Oncol. Investig.* 6, 109–119. doi:10.1002/(SICI)1520-6823(1998)6:3<109::AID-ROI1>3.0.CO;2-1

Vlashi, E., and Pajonk, F. (2015). Cancer stem cells, cancer cell plasticity and radiation therapy. *Semin. Cancer Biol.* 31, 28–35. doi:10.1016/j.semcancer.2014.07.001

Vulcano, F., Milazzo, L., Ciccarelli, C., Eramo, A., Sette, G., Mauro, A., et al. (2016). Wharton's jelly mesenchymal stromal cells have contrasting effects on proliferation and phenotype of cancer stem cells from different subtypes of lung cancer. *Exp. Cell Res.* 345, 190–198. doi:10.1016/j.yexcr.2016.06.003

Wang, L., Hensch, N. R., Bondra, K., Sreenivas, P., Zhao, X. R., Chen, J., et al. (2021). SNAI2-Mediated repression of BIM protects rhabdomyosarcoma from ionizing radiation. *Cancer Res.* 81, 5451–5463. doi:10.1158/0008-5472.CAN-20-4191

Wang, Q.-E. (2015). DNA damage responses in cancer stem cells: Implications for cancer therapeutic strategies. *World J. Biol. Chem.* 6, 57–64. doi:10.4331/wjbc.v6.i3.57

Waqar, S. N., Robinson, C., Olszanski, A. J., Spira, A., Hackmaster, M., Lucas, L., et al. (2022). Phase I trial of ATM inhibitor M3541 in combination with palliative radiotherapy in patients with solid tumors. *Invest. New Drugs* 40, 596–605. doi:10.1007/s10637-022-01216-8

Wha Jun, D., Hwang, M., Kim, H. J., Hwang, S. K., Kim, S., and Lee, C.-H. (2013). Ouabain, a cardiac glycoside, inhibits the fanconi anemia/BRCA pathway activated by DNA interstrand cross-linking agents. *PLoS One* 8, e75905. doi:10.1371/journal.pone.0075905

Widmark, A., Gunnlaugsson, A., Beckman, L., Thellenberg-Karlsson, C., Hoyer, M., Lagerlund, M., et al. (2019). Ultra-hypofractionated versus conventionally fractionated radiotherapy for prostate cancer: 5-year outcomes of the HYPO-RT-PC randomised, non-inferiority, phase 3 trial. *Lancet* 394, 385–395. doi:10.1016/S0140-6736(19)31131-6

Zhang, J., Wu, Q., Zhu, L., Xie, S., Tu, L., Yang, Y., et al. (2022). SERPINE2/PN-1 regulates the DNA damage response and radioresistance by activating ATM in lung cancer. *Cancer Lett.* 524, 268–283. doi:10.1016/j.canlet.2021.10.001

Zhang, X., Huang, Q., Wang, X., Xu, Y., Xu, R., Han, M., et al. (2017). Bufalin enhances radiosensitivity of glioblastoma by suppressing mitochondrial function and DNA damage repair. *Biomed. Pharmacother.* 94, 627–635. doi:10.1016/j.biopha.2017.07.136

Zhou, W., Sun, M., Li, G.-H., Wu, Y.-Z., Wang, Y., Jin, F., et al. (2013). Activation of the phosphorylation of ATM contributes to radioresistance of glioma stem cells. *Oncol. Rep.* 30, 1793–1801. doi:10.3892/or.2013.2614

frontiers | Frontiers in Pharmacology

TYPE Original Research
PUBLISHED 22 December 2022
DOI 10.3389/fphar.2022.1086894

OPEN ACCESS

EDITED BY
Visweswara Rao Pasupuleti,
REVA University, India

REVIEWED BY
Gulam M. Rather,
The State University of New Jersey,
United States
Ali Hafez El-Far,
Damanhour University, Egypt

*CORRESPONDENCE
Jonathan Blay,
jonathan.blay@uwaterloo.ca

†These authors have contributed equally to this work

‡Present address: Émilie C. Lefort, DePuy Synthes, Markham, ON, Canada

SPECIALTY SECTION
This article was submitted to Pharmacology of Anti-Cancer Drugs, a section of the journal Frontiers in Pharmacology

RECEIVED 01 November 2022
ACCEPTED 12 December 2022
PUBLISHED 22 December 2022

CITATION
Fux JE, Lefort ÉC, Rao PPN and Blay J (2022), Apigenin directly interacts with and inhibits topoisomerase 1 to upregulate CD26/DPP4 on colorectal carcinoma cells.
Front. Pharmacol. 13:1086894.
doi: 10.3389/fphar.2022.1086894

Apigenin directly interacts with and inhibits topoisomerase 1 to upregulate CD26/DPP4 on colorectal carcinoma cells

Julia E. Fux[1†], Émilie C. Lefort[2†‡], Praveen P. N. Rao[1] and Jonathan Blay[1,2*]

[1]School of Pharmacy, University of Waterloo, Waterloo, ON, Canada, [2]Department of Pathology, Dalhousie University, Halifax, NS, Canada

Introduction: CD26/dipeptidyl peptidase IV (DPP4) is a cell-surface glycoprotein present on most epithelial cells that modulates the local response to external signals. We have previously shown that the dietary flavone apigenin (4′,5,7-trihydroxyflavone) upregulates cell-surface CD26/DPP4 on human colorectal carcinoma (CRC) cells and regulates its activities. We observed a unique synergistic interaction with the CRC chemotherapeutic agent irinotecan, which through its metabolite SN38 elevates CD26 at doses that are sub-cytotoxic. As SN38 interacts with topoisomerase 1 (Topo1) we evaluated whether apigenin influences Topo1 activity.

Methods: We used a radioimmunoassay to selectively measure CD26 at the cell surface of HT-29 cells following various treatments. Topoisomerase 1 mRNA expression was measured by q-RT-PCR and protein abundance by western blot analysis. Direct inhibition of topoisomerase activity was measured using an assay of DNA supercoil relaxation with recombinant human Topo1. The role of Topo1 in the effect of apigenin was shown both pharmacologically and by siRNA silencing of Topo1. Molecular docking analysis was done with SBD computational software using the CDOCKER algorithm.

Results: The interplay between apigenin and irinotecan was not observed when apigenin was combined with other chemotherapeutic drugs including the topoisomerase 2 inhibitors doxorubicin or etoposide. There was no enhancement of irinotecan action if apigenin was replaced with its hydroxylated metabolite luteolin (3′,4′,5,7-tetrahydroxyflavone) or emodin (6-methyl-1,3,8-trihydroxyanthraquinone), which is an inhibitor of the principal kinase target of apigenin, casein kinase 2 (CK2). Apigenin did not alter Topo1 mRNA expression, but siRNA knockdown of functional Topo1 eliminated the effect of apigenin and itself increased CD26 levels. Apigenin inhibited Topo1 activity in intact HT-29 cells and showed comparable inhibition of purified recombinant human Topo1 enzyme activity to that of SN-38, the active metabolite of irinotecan. Apigenin fits into the complex of Topo1 with DNA to directly inhibit Topo1 enzyme activity.

Discussion: We conclude that apigenin has a unique fit into the Topo1-DNA functional complex that leads to direct inhibition of Topo1 activity, and suggest

that this is the basis for the exceptional interaction with the CRC drug irinotecan. A combined action of these two agents may therefore exert a role to limit local signals that facilitate tumour progression.

KEYWORDS

apigenin, DPP4 (CD26), CK2 (casein kinase II), topoisomerase 1 (Top1), irinotecan (CPT-11)

Introduction

Apigenin (4′,5,7-trihydroxyflavone; 5,7-dihydroxy-2-(4-hydroxyphenyl)-4H-1-benzopyran-4-one) is one of many bioactive compounds found in the diet, being present at significant levels in many fruits, vegetables, herbs, and spices and particularly abundant in parsley and chamomile (Birt et al., 2001; Yang et al., 2001; Lefort and Blay 2013). As a flavonoid, it has the potential to impact multiple cellular signalling pathways and consequent cell behaviour, giving it the capacity to alter the relationship of cells with their surroundings and potentially affect cell disposition in both normal and pathological situations. We have reviewed these actions and how they might impact on cancer, particularly in neoplasias situated in, or associated with, the gastrointestinal tract (Lefort and Blay 2013). Most importantly, we have recently shown that the use of oral supplements of apigenin in a semi-purified form should be able to reach circulating blood levels capable of causing the cellular changes that are predicted to be beneficial against cancers, including those of the gastrointestinal tract (DeRango-Adem and Blay 2021). This may be achieved using dosing quantities comparable with those currently accepted for other natural product supplements (DeRango-Adem and Blay 2021).

Amongst its actions, we have shown that apigenin is able to upregulate CD26 at the surface of human colorectal carcinoma (CRC) cells, including those of the HT-29, HRT-18 and Caco-2 cultured cell lines (Lefort and Blay 2011; Lefort et al., 2020). CD26 is a 110-kDa membrane glycoprotein that is normally found at the apical surface of mature intestinal epithelial cells including those of the colon (Darmoul et al., 1991; Lefort and Blay 2013). It shows changes in expression and distribution in cancer (Balis 1985; Kotackova et al., 2009). CD26 is a multifunctional protein and in its mature, dimeric form it is enzymatically active at the cell surface and has an intrinsic hydrolase activity (dipeptidyl peptidase IV, DPP4) that cleaves N-terminal dipeptides from certain extracellular signalling peptides (De Meester et al., 1999; Havre et al., 2008). Amongst its substrates that are key cell mediators are the cell-directing peptides known as chemokines, and the highest affinity of DPP4 is for CXCL12 (stromal-derived factor-1, SDF-1), which is the ligand for the receptor CXCR4, a regulator of cell migration that is itself regulated by constituents of the tumour microenvironment (Richard et al., 2006; Richard et al., 2007; Richard and Blay 2008). CD26 also (i) functions as the major cellular binding protein for adenosine deaminase (ADA), a soluble ecto-enzyme that inactivates the immunosuppressive metabolite adenosine (Dong et al., 1997), and (ii) directly interacts with the extracellular matrix (ECM) proteins collagen and fibronectin (Loster et al., 1995; Cheng et al., 2003). CD26 is therefore a nexus of regulation governing the cell's relationship with its extracellular milieu, and it is regulated by apigenin.

We have recently shown (Lefort et al., 2020) that apigenin's ability to upregulate CD26 is dependent upon its ability to inhibit the activity of casein kinase 2 (CK2). CK2 is a ubiquitous cellular Ser/Thr-protein kinase that has downstream effects on cell proliferation, cell viability, modulation of DNA damage, contractility, and cellular invasion through the extracellular matrix (Pinna and Meggio 1997; Morales and Carpenter 2004; Kim et al., 2018; Suhas et al., 2018). Apigenin is well known for its ability to inhibit CK2 and has been used experimentally as a CK2 inhibitor (Ahmad et al., 2006; Kroonen et al., 2012; Jung et al., 2014; Kim et al., 2018; Suhas et al., 2018). However, it is uncertain that apigenin exerts its effect on cellular behaviours including regulation of interactions with the extracellular matrix, cellular contractility and the function of molecules including CD26 (Lefort and Blay 2011; Kim et al., 2018; Suhas et al., 2018) solely through CK2. Apigenin and related flavonoids differ from synthetic CK2 inhibitors both in terms of the stereochemistry of their interaction with CK2 and their observed effect in experimental cellular systems (Sarno et al., 2002; Suhas et al., 2018). Furthermore, However, the protracted time course of the change in CD26 levels [maximum reached after 24 h–48 h, (Lefort and Blay 2011)] suggests that there are additional or subsequent events necessary in order to have changes in CD26.

In our earlier work (Lefort and Blay 2011) we noted that apigenin has a distinct property in how it interacts with the anti-cancer drug irinotecan at the cellular level. Multiple chemotherapeutic agents also have the property, independent of their cytotoxic action, of upregulating CD26 (Cutler et al., 2015). However while the effects of combining apigenin with, for example, 5-fluorouracil or oxaliplatin are simply additive, the combination with irinotecan shows a marked synergism, with irinotecan enhancing the potency for apigenin to increase CD26 by 30-fold (Lefort and Blay 2011). The primary mode of action of irinotecan, through its active metabolite SN-38, is to poison the nuclear enzyme DNA topoisomerase 1 (Topo1) (Liu et al., 2000). We therefore hypothesized that apigenin might somehow also be acting on Topo1, which would lead to an interaction with SN38 and explain the synergism with irinotecan in elevating CD26.

In this work we show that apigenin can directly interact with and inhibit the activity of topoisomerase, that the interaction is selective for Topo1, and that the resultant inhibition is a part of the ability of apigenin to upregulate CD26/DPP4.

Materials and methods

Culture of human colorectal carcinoma cells

HT-29 human colorectal carcinoma (CRC) cells were obtained from the American Type Culture Collection (ATCC, Manassas, VA, United States) and were maintained at 37°C in a humidified atmosphere of 90% air/10% CO_2. The stocks used have been confirmed for genotype, and cultures were negative for *mycoplasma* contamination when tested using a PCR-based approach. All responses have been confirmed in cells within 4 passages of receipt from ATCC.

Cells were cultured in 80-cm^2 flasks (Corning, Nepean, ON, Canada), containing Dulbecco's modified Eagle medium (DMEM), supplemented with 10% (v/v) heat-inactivated newborn calf serum (NCS; Life technologies, Burlington, ON, Canada) and passaged with brief exposure to TrypLE™ Express (Life technologies, Burlington, ON, Canada). For experimental purposes, cells were seeded at density of 90,000 cells/ml unless otherwise indicated. Once cultures reached 60%–70% of confluent density, they were treated with compounds of interest or with control vehicle, as specified in figure legends.

Chemotherapeutic treatments were irinotecan (Sandoz, Montreal, QC, Canada), etoposide (Novopharm, Toronto, ON, Canada) and doxorubicin (Mayne Pharma, Montreal, QC, Canada). Bovine serum albumin (BSA), dimethyl sulfoxide (DMSO), apigenin, luteolin (3′,4′,5,7-tetrahydroxyflavone), 6-methyl-1,3,8-trihydroxyanthraquinone (emodin), and the irinotecan active metabolite SN-38 (7-Ethyl-10-hydroxycamptothecin) were obtained from Sigma-Aldrich (St. Louis, MO. United States). Flavonoids were dissolved in DMSO to make stock solutions and subsequently further diluted in medium to give a final DMSO concentration in whole cell assays of less than 0.02% (v/v), a concentration that does not affect CD26 levels (Tan et al., 2004).

Radioimmunoassay for cell-surface CD26

Following a 48 h treatment, cell-surface CD26 was quantified using a radioimmunoassay as previously described (Tan et al., 2004). All washes and incubations were performed at 4°C. Wells from a 48- (or 24-) well plate were washed once with 500 µl (750 µl for 24-well plate) of ice-cold phosphate-buffered saline (PBS; 137 mM NaCl, 24.8 mM Tris-HCl, 5mM KCl, 0.7 mM Na_2HPO_4, 0.5 mM $MgSO_4$ and 1 mM $CaCl_2$; pH 7.2) containing 0.2% (w/v) BSA and incubated for 1 h with 125 µl (200 µl for a 24-well plate) PBS containing 1% (w/v) BSA and 1 µg/ml mouse anti-human CD26 (clone M-A261) monoclonal antibody (mAb) or mouse IgG isotype-matched control mAb (clone W3/25). Following the incubation period, cells were washed twice with 500 µl (750 µl for a 24-well plate) PBS containing 0.2% (w/v) BSA and were incubated for 1 h with 125 µl (200 µl for a 24-well plate) PBS containing 1% (w/v) BSA and 1 µCi/ml ^{125}I-labeled goat anti-mouse IgG mAb obtained from (PerkinElmer Life Sciences, NEN, Boston, MA, United States). Cells received two final washes with 500 µl (750 µl for a 24-well plate) PBS containing 0.2% ($^{w}/_{v}$) BSA. Finally, 500 µl of 0.5 M NaOH was added to each well in order to solubilize the cells, and radioactivity was assessed using a gamma counter (Model 1,480 Wizard™ 3, Wallac Co., Turku, Finland). Radioactive counts were corrected for both non-specific binding relative to an isotype control and the number of viable cells as assessed by a Coulter® Model ZM151183 particle counter (Beckman Coulter, Mississauga, ON, Canada).

Topoisomerase 1 mRNA expression using q-RT-PCR

Total RNA was extracted from HT-29 cells grown in 6-well plates (VWR International, Mississauga, ON, Canada) using the TRIzol® reagent (Life technologies, Burlington, ON, Canada), as indicated by the manufacturer. RNA concentrations were quantified by spectrophotometric analysis at 280 nm/260 nm wavelengths. RNA (1 µg) was reverse-transcribed using an M-MLV reverse transcriptase enzyme, 5 mM deoxyribonucleotide triphosphate, 0.5 µM oligo (dT), dithiothreitol, 5x First Strand buffer, all obtained from Life technologies (Burlington, ON, Canada) and DEPC-H_2O (GE Healthcare Life Sciences, Baie D'Ufré, QC, Canada) in a total volume of 20 µl. Custom primers (Life technologies, Burlington, ON, Canada) were designed to amplify specific regions in the transcript and the sequences used were: Topo1 forward primer 5′- TCCGGAACCAGTATCGAGAAGA-3′ and reverse primer 5′- CCTCCTTTTCATTGCCTGCTC-3′. For each of the samples, mRNA levels were normalized to cyclophilin A, sequence forward: 5′-TTCATCTGCACTGCCAAGAC-3′, reverse: 5′-TCGAGTTGTCCACAGTCAGC-3′. Amplification reactions included an initial cycle of denaturation for 10 min at 95°C, followed by 40 cycles of denaturation at 95°C for 20 s, annealing at 60°C for 18 s, and extension at 70°C for 30 s, with brilliant SYBR Green detection, and a final melting curve cycle of 95°C for 1 min, 65°C for 30 s, and 95°C for 30 s in a Stratagene Mx3000P thermocycler (Cedar Creek, TX, United States). Relative *Topo1* expression as indicated by the fluorescence was analyzed using the comparative Ct method.

Western blot analysis for topoisomerase 1

HT-29 cells were seeded into 6-well plates and were grown to 60%–70% confluency, after which they were exposed to apigenin over a time period of 0 h–60 h. Cells were washed twice with ice-cold PBS and dissolved in lysis buffer (50 mM Tris-HCl, pH 7.4, 1% Nonidet P-40, 0.25% sodium deoxycholate, 150 mM NaCl) supplemented with 1 mM EDTA, 1 mM NaF, 1 mM phenylmethyl sulfonyl fluoride and 1X protease inhibitor cocktail

set 1 (EMD Canada Inc. Mississauga, ON, Canada). Samples were incubated on a plate rotator for 20 min at 4°C and cell lysates then clarified by centrifugation (12,000 x *g* for 20 min). Cellular protein was quantified using Bio-Rad Protein Assay Dye Reagent (Bio-Rad Laboratories Inc. Mississauga, ON, Canada).

HT-29 cells were seeded into 6-well plates and were grown to 60%–70% confluency, after which they were exposed to apigenin over a time period of 0 h–60 h. Cells were washed twice with ice-cold PBS and dissolved in lysis buffer (50 mM Tris-HCl, pH 7.4, 1% Nonidet P-40, 0.25% sodium deoxycholate, 150 mM NaCl) supplemented with 1 mM EDTA, 1 mM NaF, 1 mM phenylmethyl sulfonyl fluoride and 1X protease inhibitor cocktail set 1 (EMD Canada Inc. Mississauga, ON, Canada). Samples were incubated on a plate rotator for 20 min at 4°C and cell lysates then clarified by centrifugation (12,000 x *g* for 20 min). Cellular protein was quantified using Bio-Rad Protein Assay Dye Reagent (Bio-Rad Laboratories Inc. Mississauga, ON, Canada). Samples were denatured in Laemmli buffer at 95°C for 5 min and 15 μg of protein per lane was separated by SDS-PAGE using 4% stacking and 10% resolving gels as previously described [27]. Gels were then electroblotted onto a nitrocellulose membrane, blocked with 3% BSA (CD26) and probed overnight at 4°C with IgM mouse anti-human DNA Topo1 (clone C-21) (BD Pharmingen, San Diego, CA, United States). Membranes were washed 5 times with Tris-buffered saline with 0.1% Tween 20 and then incubated with horseradish peroxidase (HRP)-conjugated polyclonal IgM goat anti-mouse secondary Ab (BD Pharmingen, San Diego, CA. United States), for 1 h at room temperature. Protein expression was detected using an enhanced chemiluminescence detection system (Thermo scientific, Ottawa, ON, Canada). To confirm equal protein loading in each sample, the membrane was re-probed with a IgG rabbit anti-human α–tubulin (11H10) primary Ab (Cell Signaling Technology®, Pickering, ON, Canada), followed by an IgG HRP-conjugated goat anti-rabbit secondary mAb (BD Pharmingen, San Diego, CA, United States).

Assay of inhibition of recombinant topoisomerase 1

Recombinant human DNA topoisomerase 1 (rhTopo1; Prospec-Tany Technogene Ltd., East Brunswick, NJ, United States) was diluted to 10 μg/ml in 10 mM Tris-HCl, pH 7.9, 150 mM NaCl, 1 mM EDTA, 5% glycerol, 0.1 mM spermidine and 0.1% BSA, and used at 10 ng per reaction. The rhTopo1 was pre-incubated with flavonoids for 15min at room temperature, followed by incubation for 25 min at 37°C with 250 ng supercoiled pHOT1 plasmid substrate from a commercial topoisomerase 1 assay kit (Topogen Inc., Buena Vista, CO, United States). Bands were visualized after electrophoresis for 2 h at 70V on 1% ($^{w}/_{v}$) agarose with 0.01% ($^{w}/_{v}$) SDS and staining with GelRed (Biotium, Fremont, CA, United States) for 30 min.

Assay of topoisomerase 1 inhibition in cells

HT-29 cells at ~60% of confluent density were treated with apigenin or SN38 for 48 h. Cells were then rinsed with PBS, released by trypsinisation, and pelleted by centrifugation (200 x *g*, 10 min, 4°C). The pellet (~10^7 cells) was washed 3 times with cold PBS and resuspended in 180 μl ice-cold low-salt buffer (20 mM Tris-HCl, pH7.5, containing 5 mM KCl, 1 mM dithiothreitol, 10% ($^{v}/_{v}$) glycerol) and 1x HALT® (Pierce Biotechnology, Rockford, IL, United States) protease inhibitors for a total of 10 min at 4°C and then physically disrupted by trituration 5x through a 27G needle. After further incubation for 30 min at 4°C, the homogenate was centrifuged (15,000 x *g*, 3 min, 4°C) and the nuclear pellet resuspended in 180 μl ice-cold high-salt buffer (low-salt buffer supplemented with 355 mM KCl) for total of 80 min at 4°C. The sample was then recentrifuged (15,000 x *g*, 10 min, 4°C) and the supernatant containing extracted nuclear proteins assayed for topoisomerase activity. Topoisomerase 1 activity was assessed as described (Webb and Ebeler 2003; Nitiss et al., 2012) using 5 μg protein, 200 ng supercoiled pEGFP DNA plasmid (Clontech Laboratories Inc., Mountain View, CA, United States) and incubation for 10 min at 37°C.

Silencing of topoisomerase 1 using siRNA transfection

Small interfering RNA (siRNA) transfection of HT-29 cells was carried out according to the manufacture's instructions, using 3.0 μl/well siPORT™ *Amine* Transfection Agent (AM4503) in 24-well plates. *Silencer* ® Select negative control #1 siRNA was used as a negative control. Cells were seeded in 10% NCS DMEM at a density of 240,000 cells/ml and were transfected with an optimized concentration of 7.5 nM, using validated silencer® Select siRNA specific for Topo1. 24 h following seeding, cells received a medium change in order to reduce cellular cytotoxicity. 48 h following siRNA transfection (when the knock-down became established as evaluated through western blot), cells were treated with 60 μM apigenin or its equivalent DMSO control. To examine the effect of apigenin on Topo1 knocked-down cells, cell-surface CD26 levels were assessed through a radioimmunoassay 48 h following treatment; this corresponded to 96 h after transfection.

Molecular docking studies

Molecular docking studies were carried out using the computational software Discovery Studio Structure Base Design (SBD) suite from BIOVIA v17.1.0.16143 (Dassault Systemes, France). Flavonoids apigenin, luteolin, kaempferol and genistein were built in 3D and subjected to energy minimization by 500 steps each of steepest descent and

conjugate gradient minimization respectively (RMS gradient 0.1 kcal/mol), using the CHARMm force field, distance-dependent dielectric constant and SHAKE algorithm using the *small molecules* tool in SBD. The x-ray coordinates of human Topo1-DNA complex were obtained from PDB (pdb id: 1K4T), water molecules were removed and the protein configuration was prepared using the *macromolecules* tool in SBD. The bound ligand topotecan was then used to create a 10 Å sphere to define the active site and the ligand (both cyclic lactone and open carboxylate) was deleted. In the next step, docking studies of flavonoids were carried out using the CDOCKER algorithm which is based on a simulated-annealing protocol using the CHARMm force field, 2,000 heating steps, 700 K target temperature and 5,000 cooling steps with a target temperature of 300 K to obtain 10 docked ligand poses with the Topo1-DNA complex. The binding poses were ranked using CDOCKER energy in kcal/mol, by determining the polar and non-polar interactions and bond distance parameters.

Statistical analysis

Unless otherwise noted, figures are representative of independent experiments conducted on at least three separate occasions. Statistical analyses were performed using Prism 8.0 software (GraphPad, San Diego, CA, United States). Comparisons of data were performed using two-way ANOVA with Bonferroni's comparison test to compare the replicate means unless otherwise indicated. For all analyses a p-value <0.05 was considered as the minimum for statistical significance.

Results

Other inhibitors of CK2 do not reproduce the ability of apigenin to interact with irinotecan

In our original work showing that apigenin can upregulate the protein CD26 on human colon carcinoma cells we noted that apigenin had a unique interaction with the anticancer drug irinotecan (Lefort and Blay 2011). We have since documented how multiple chemotherapeutic agents have the additional property, independent of their cytotoxic action, of upregulating CD26 (Cutler et al., 2015). However while the effects of combining apigenin with, for example, 5-fluorouracil or oxaliplatin are no more than additive, the interaction with irinotecan is highly synergistic.

Irinotecan enhances the *potency* for apigenin to increase CD26 by 30-fold (Lefort and Blay 2011). Conversely, apigenin itself enhances the *potency* of the irinotecan effect; it leads to a 4.2-fold enhancement of irinotecan potency, with 30 μM apigenin causing a reduction in the irinotecan EC_{50} from 4.7 μg/ml to 1.1 μg/ml (Lefort and Blay 2011).

We have recently shown (Lefort et al., 2020) that the ability of apigenin to elevate CD26 involves and requires inhibition of the activity of the kinase CK2. Furthermore, multiple synthetic CK2 inhibitors (Emodin, 6-methyl-1,3,8-trihydroxyanthraquinone; TBB, 4,5,6,7-tetrabromobenzotriazole; and DRB, 5,6-dichlorobenzimidazole 1-β-D-ribofuranoside) also upregulate CD26 (Lefort et al., 2020). We first examine whether CK2 inhibition is also necessary and sufficient for the ability to interact synergistically with irinotecan.

Consistent with our earlier work (Lefort et al., 2020) the CK2 inhibitor emodin was itself able to elevate cell-surface CD26 (Figure 1A). Furthermore, the apigenin metabolite luteolin (3′,4′,5,7-tetrahydroxyflavone), which is also an inhibitor of CK2 (Li et al., 2009; Lolli et al., 2012) was itself able to upregulate CD26 in a dose-dependent fashion (Figures 1B, C). As well, treating the cells with irinotecan produced a dose-dependent elevation of CD26 (Figures 1A, C) comparable to that we had observed before (Lefort and Blay 2011). However, neither emodin nor luteolin showed an ability to interact productively with irinotecan, nor the ability to increase the potency of irinotecan to act on CD26 (Figures 1A, C). Indeed, with the single exception of emodin at the highest dose of irinotecan, the effect of irinotecan was to mask the positive effect of the CK2 inhibitors.

Therefore, we conclude that although CK2 kinase inhibition is a key step in allowing flavonoids to elevate CD26, it is not sufficient to generate a synergism with irinotecan. Furthermore, this aspect of apigenin action has structural specificity in that it is not shared with its metabolite luteolin, which differs from apigenin only in the addition of a further hydroxyl group in the 3′ ring position. Apigenin also is more efficaceous in elevating CD26 and its associated activities than its isoflavone equivalent genistein or kaempferol, an analogue with an additional hydroxyl in the 3 position (Lefort and Blay 2011).

The apigenin interaction with irinotecan is not seen with topoisomerase 2 inhibitors

We next asked if this interaction would be present if apigenin were combined with type 2 topoisomerase-targeted anticancer drugs. As anticipated, given the breadth of chemotherapeutic triggers to this response, Topo2-active agents were able to elevate the level of CD26 on viable CRC cells (Figure 2). The response to the standard Topo2 drug etoposide was quantitatively similar to that for irinotecan (Figures 2A, B), and CD26 upregulation was also seen with another such agent, doxorubicin (Figure 2D). However, neither etoposide nor doxorubicin gave a further elevation of CD26 when combined with apigenin, unlike irinotecan (Figures 2C, D). Indeed, the response to apigenin was reduced to below statistical significance in the presence of both Topo2 inibitors. This is in agreement with our prior findings

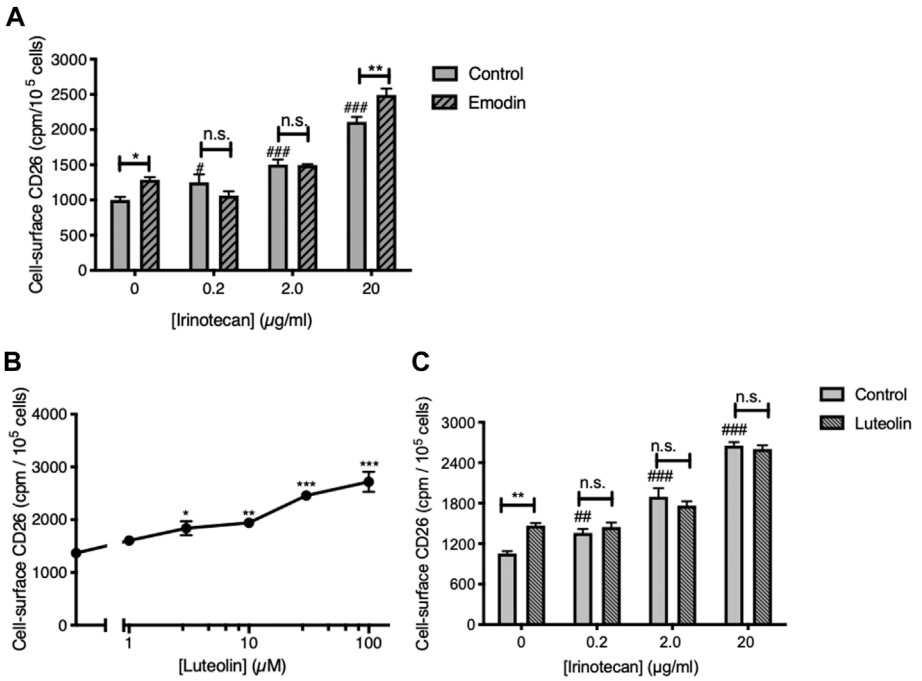

FIGURE 1
Neither CK2 inhibition, nor use of the apigenin metabolite luteolin, reproduce the interaction with apigenin seen with irinotecan. **(A)** The CK2 inhibitor emodin does not enhance the upregulation of CD26 by irinotecan. HT-29 cells were treated with irinotecan in the absence or presence of emodin (20 μM) as indicated, and cell-surface CD26 was assessed 48 h afterward. Data are means ± SEM (n = 4); *p < 0.05, **p < 0.01, enhancement by emodin; n.s., not significant; #p < 0.05 and ###p < 0.001 enhancement by irinotecan. **(B)** Luteolin enhances cell-surface CD26 in a dose-dependent manner. Means ± SEM (n = 4); *p < 0.05, **p < 0.01 and ***p < 0.001. **(C)** Luteolin does not enhance the upregulation of CD26 by irinotecan. Means ± SEM (n = 4); **p < 0.01, enhancement by luteolin (30 μM); n.s., not significant; ##p < 0.01 and ###p < 0.001 enhancement by irinotecan.

(Lefort and Blay 2011) that the synergistic potential of apigenin in elevating CD26 is restricted to the agent irinotecan, of the broad variety of anticancer drugs from different classes of activity, which now includes 5-FU, oxaliplatin, and irinotecan (Lefort and Blay 2011), cisplatin, vinblastine, methotrexate (Cutler et al., 2015) and etoposide and doxorubicin (this study).

The ability of apigenin to upregulate CD26 involves Topo1 but is not due to altered Topo1 expression

Topo1 mRNA expression showed some variation over a 60-h time course (Figure 3A), likely reflecting cell cycle-dependent changes as we have noted for chemokine receptor CXCR4 (Richard et al., 2006). Apigenin treatment led to a modified time profile but no aggregate change in *Topo1* expression over the entire experimental period. The abundance of cellular Topo1 protein similarly showed no change relative to α–tubulin (Figure 3B). Apigenin does not therefore substantially alter the amount of Topo1 mRNA or protein.

To further probe for the importance of Topo1 in apigenin action, we knocked down expression using an siRNA approach with a combination of 3 validated siRNA constructs, and then subsequently tested the cells to see whether apigenin would still enhance CD26 levels. We were able to substantially (> 75%) knock down Topo1 protein at 48 h (Figure 3C) while retaining good cellular viability, which is also taken into account in our CD26 radioimmunoassay. The reduction in Topo1 was largely preserved at 96 h, which represents the total period covered for apigenin treatment and CD26 immunoassay (Figure 3C).

As shown in Figure 3D, the sham-transfected cells retained a robust apigenin response for the elevation of CD26 (mean increase, 114%). The baseline CD26 at the cell surface, and the ability to be upregulated by apigenin, were unaltered using a scrambled siRNA negative control. However, with Topo1 knockdown (i) the control-treated cells showed a significant increase in CD26, and (ii) the apigenin-treated cells showed no increase in CD26 above sham and scrambled controls that had received apigenin, and had lost their response to apigenin relative to the appropriate knock-down control (Figure 3D). This provides

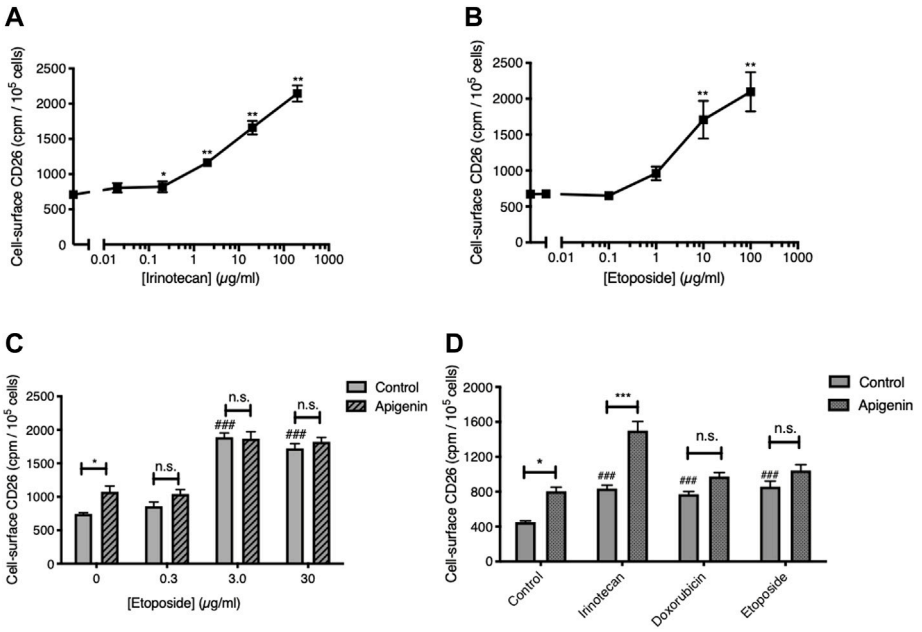

FIGURE 2
Topoisomerase 2 inhibitors elevate CD26 but do not reproduce the interaction with apigenin. **(A,B)** Topoisomerase 1 and 2 inhibitors both enhance cell-surface CD26. HT-29 cells treated for 48 h. Means ± SE (n = 4), one-way ANOVA followed by Dunnett's test; *p < 0.05 and **p < 0.01, enhancement in CD26 by topoisomerase inhibitors. **(C)** Apigenin does not enhance the action or potency of etoposide. Means + SE (n = 4); *p < 0.05, enhancement by apigenin (30 μM); ###p < 0.001 up-regulation by etoposide. **(D)** Apigenin interacts solely with the Topo1 inhibitor irinotecan. Means + SE (n = 4); *p < 0.05, ***p < 0.01 enhancement by apigenin (30 μM); ###p < 0.001 up-regulation by topoisomerase inhibitors. Concentrations are: Irinotecan, 2 μg/ml; doxorubicin, 1 μg/ml; etoposide, 10 μg/m.

direct evidence for the involvement of Topo1 activity in the CD26 upregulatory response, and suggests that apigenin's effect may depend on functional Topo1.

Apigenin directly suppresses topoisomerase 1 activity

The evidence that apigenin might act through Topo1, and the unique interaction with the Topo1 poison irinotecan, suggest that apigenin might affect topoisomerase 1 activity. We assessed this directly in both whole cells and an *in vitro* enzyme system.

We first tested whether apigenin treatment led to inhibition of the topoisomerase 1 activity isolated from pretreated whole cells. As illustrated in Figure 4A recoverable Topo1 leads to progressive uncoiling of supercoiled plasmid DNA ('Sup') to produce a series of products culminating in the fully relaxed and slowest-migrating (topmost) band. Treating the cells for 48 h with apigenin over its active concentration range 0 μM–100 μM led to progressive inhibition of the topoisomerase activity in those cells with greater preservation of supercoiled structure on the final assay. Maximal effect in this system was at 60 μM apigenin, consistent with its effect in elevating cellular CD26. The efficacy of apigenin was equivalent to that of a maximally effective dose (30 nM) of the irinotecan active metabolite SN38, which is a cell-permeable direct inhibitor of Topo1 (Cutler et al., 2015) (Figure 4A). The inhibitory effect of apigenin was observable at culture confluencies between 30% and post-confluent, and for cultures with apigenin treatment times of 6 h–48 h (data not shown).

When apigenin was added directly into an assay of topoisomerase 1 activity using purified rhTopo1, it substantially inhibited the uncoiling of supercoiled DNA (Figure 4B). Inhibition was substantial (greater than 30%) with 10 μM apigenin (Figure 4C), which is below the EC_{50} of 32.8 μM ± 1.1 μM seen in whole cells (Lefort and Blay 2011). Inhibition of activity exceeded 80% with apigenin present at 100 μM, the highest exposure to which whole cells may be exposed without substantial acute toxicity (Lefort and Blay 2011), and was essentially complete (3 independent experiments) with apigenin present at 1 mM. The solvent vehicle, DMSO, slightly interfered with Topo1 activity (Figure 4C), but this did not exceed 10% inhibition at the highest concentration (1.7%$^{v}/_{v}$) used in these assays.

Luteolin, over the concentration range 0 μM–100 μM, within which it is able to elevate CD26 levels in whole cell assays (Figure 1B) did not directly inhibit Topo1 in these assays (Figure 4C). It had a minor (< 15%) effect at the highest concentration used (1 mM), which exceeds that attainable with whole cells.

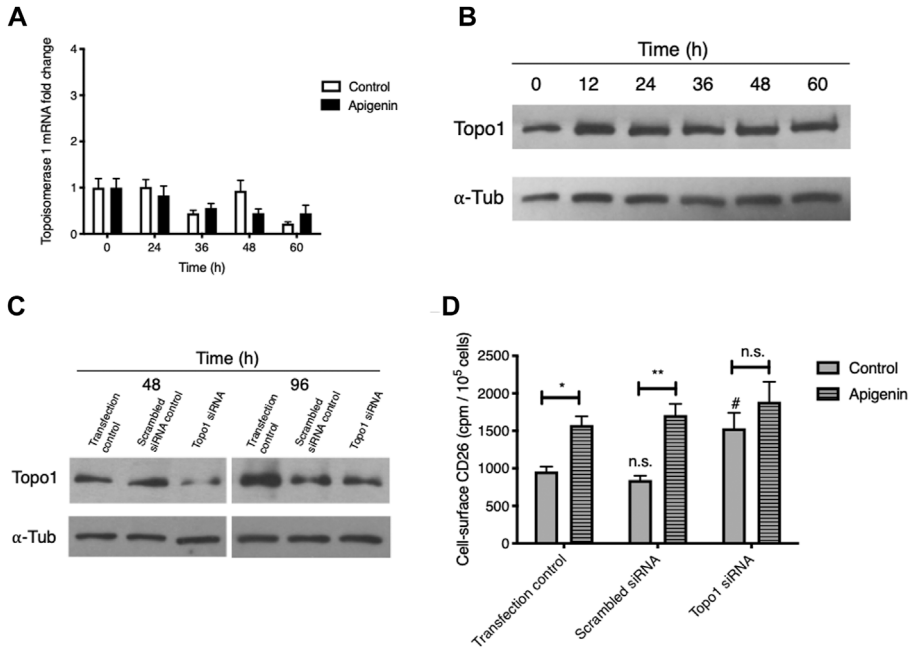

FIGURE 3
Apigenin's ability to upregulate CD26 requires Topo1 but does not come from changes in Topo1 expression. **(A)** Apigenin does not alter *Topo1* mRNA expression. HT-29 cells were treated with apigenin (30 μM) or vehicle control for the times indicated and *Topo1* mRNA levels were quantified by q-RT-PCR. Values are means ± SEM (n = 3). **(B)** Apigenin does not alter Topo1 protein expression. HT-29 cells were treated with apigenin (60 μM) for the times indicated and Topo1 protein levels were quantified by western blotting relative to a-tubulin as loading control. **(C)** siRNA knock-down of Topo1. Topo1 protein levels were measured after 48 h or 96 h by western blot. **(D)** Knock-down of Topo1 enhances cell-surface CD26 and abrogates the apigenin upregulation of CD26. CD26 levels were evaluated 48 h following apigenin (60 μM) treatment. Values are means ± SEM (n = 4), from 3 independent experiments. #, $p < 0.05$, enhancement by knock-down; *, $p < 0.05$ and **, $p < 0.01$, enhancement by apigenin. n.s., not significant.

Apigenin therefore: (i) inhibits Topo1 activity in whole cells over the same concentration range at which it elevates CD26, (ii) inhibition is present over the time course in which it produces progressive elevation of CD26 (Lefort and Blay 2011), (iii) it inhibits Topo1 activity directly in an *in vitro* assay with recombinant enzyme, (iv) luteolin the predominant metabolite of apigenin, which is also able to elevate CD26 but does *not* exhibit synergy with irinotecan (SN-38) in this response, is *unable* to inhibit the activity of Topo1. We therefore propose that the ability of apigenin to interact synergistically with irinotecan in causing elevation of cell-surface CD26 is due to direct interaction with Topo1 enzyme.

Apigenin has a direct fit into the Topo1-DNA complex

We propose that Topo1 is one of the components of the pathway(s) that cause cells to express increased amounts of CD26 on their cell surface, and that apigenin has a particular fit to Topo1 that enables its unique interaction with irinotecan. We used computational modeling of binding interactions to assess the feasibility of this proposal.

The binding interactions of apigenin, luteolin, kaempferol and genistein with human DNA-topoisomerase 1 (Topo1) complex were investigated by molecular docking studies. The x-ray crystal structure of human Topo1-DNA in complex with its known inhibitor topotecan [pdb id: 1K4T; (Staker et al., 2002)] was used as the basis for these studies.

Computational analysis of molecular interaction with the Topo1-DNA complex showed that each of these flavones in planar conformation is able to intercalate at the site of DNA cleavage (Figures 5, 6).

For apigenin (4′,5,7-trihydroxyflavone, Figure 5A) after intercalation the flavone structure undergoes several hydrophobic π-π stacking interactions with the DNA base pairs adenine, guanine, thymine and cytosine (distance range = 4.0 Å–5.2 Å). Furthermore, bound apigenin is in contact with the Topo1 enzyme *via* polar interactions, with the C7 OH undergoing a hydrogen bond with the Glu356 side chain (distance <2.9 Å), the benzopyran-4-one ketone forming a hydrogen bonding interaction with the Arg364 side chain (distance <1.8 Å) and the C2 phenolic group undergoing hydrogen bonding interaction with the side chain of Asn722 (distance <2.6 Å), as shown in Figure 5A.

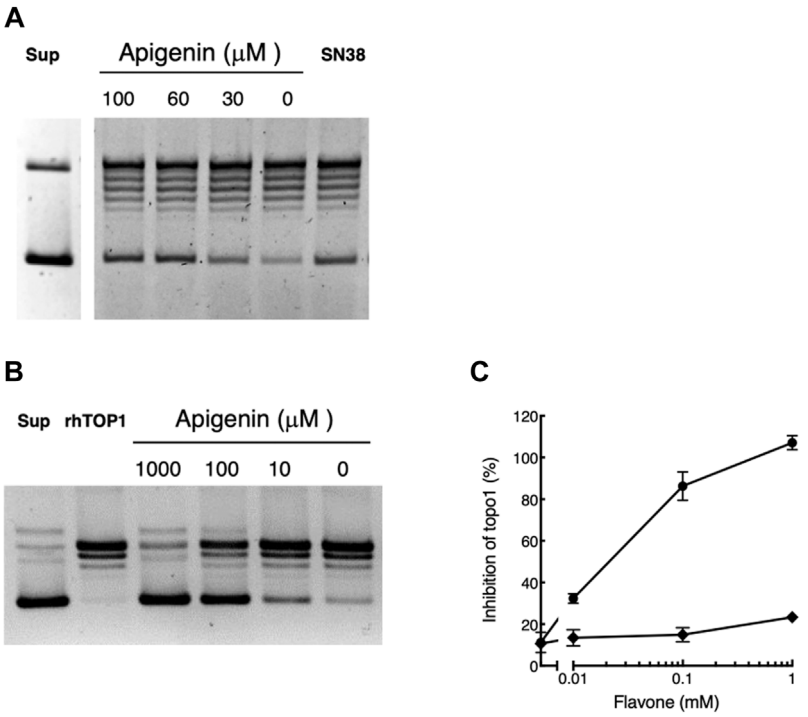

FIGURE 4
Apigenin suppresses topoisomerase 1 activity. **(A)** Apigenin suppresses topoisomerase 1 activity in whole cells. HT-29 cells were treated with apigenin for 48 h at the concentrations indicated. The original supercoiled DNA is shown ('Sup') as well as the effect of treating cells with 30 nM SN38 (positive control for Topo1 inhibition). The lowest band is the supercoiled DNA that is successively uncoiled (ladder) by cellular Topo1 activity to yield the final uncoiled structure (topmost band). Maximal uncoiling is present with untreated cells ("0 μM apigenin") and this is inhibited by increasing concentrations of apigenin or exposure to SN38 (more intense lowest band). Representative of three independent experiments. **(B)** Representative result showing the gel separation of supercoiled plasmid ("Sup"), the effect of incubation with rhTopo1 alone and the result of co-incubation with apigenin at concentrations shown. As for panel A the lowest band is input supercoiled DNA that shows uncoiling to higher bands in the presence of Topo1, in this case rhTopo1. Increasing concentrations of apigenin added directly to the reaction mixture inhibit Topo1 activity, such that at 1,000 μM apigenin the uncoiling activity of the enzyme is essentially blocked. **(C)** rhTopo1 activity was measured in the presence of apigenin (●) or luteolin (◆) at the concentrations shown. Representative of three independent experiments.

Luteolin (3′,4′,5,7-tetrahydroxyflavone, Figure 5B) is the 3′-hydroxylated metabolite of apigenin. Modeling luteolin in the Topo1-DNA complex showed that it is also able to intercalate between DNA base pairs. Compared to apigenin, it exhibits a completely different binding mode where the planar benzopyran-4-one ring is primarily interacting with guanine and thymine base pairs on either sides instead of adenine and cytosine (distance <5.5 Å). These π-π stacking interactions lead to a more stable complex (CDOCKER energy = −42.02 kcal/mol) compared to apigenin (CDOCKER energy = −37.35 kcal/mol). In addition, luteolin was also in contact with amino acids of Topo1 *via* hydrogen bonding interactions (Glu356, Arg364, and Asn722; distance <2.8 Å) as shown in Figure 5B.

Kaempferol (3,4′,5,7-tetrahydroxyflavone), which differs from apigenin in the addition of a hydroxyl at the 3 position, exhibited a similar binding mode to luteolin in the Topo1-DNA complex (Figure 5C). It was able to intercalate between DNA base pairs by several π-π stacking interactions and also formed hydrogen bonding interactions with Topo1 amino acid residues Arg364 and Asn722. The ternary complex energy (CDOCKER energy = −38.11 kcal/mol) showed that it was able to exhibit slightly superior binding compared to apigenin.

The flavonoid genistein (4′,5,7-trihydroxyisoflavone), which is apigenin's isoflavone analogue, shows a similar binding mode to apigenin (Figure 5D) in which the benzopyran-4-one is flanked by guanine, adenine and cytosine *via* π-π stacking interactions. Genistein also undergoes additional polar interactions with Topo1 amino acids Glu356, Arg364, and Thr718 (distance <3.0 Å). Genistein exhibited a less stable ternary complex than the other flavones (CDOCKER energy = −30.69 kcal/mol).

The fit of apigenin into the topotecan-stabilized Topo1-DNA complex, and key interaction distances, are summarized in Figure 6. The molecular modeling studies show that all of these flavones potentially act as DNA base pair mimics, and that their planar conformation enables them to intercalate at the site of DNA cleavage. In this way they are similar to other natural products with planar structures that are able to intercalate into the DNA helix and have been found to inhibit the activities of

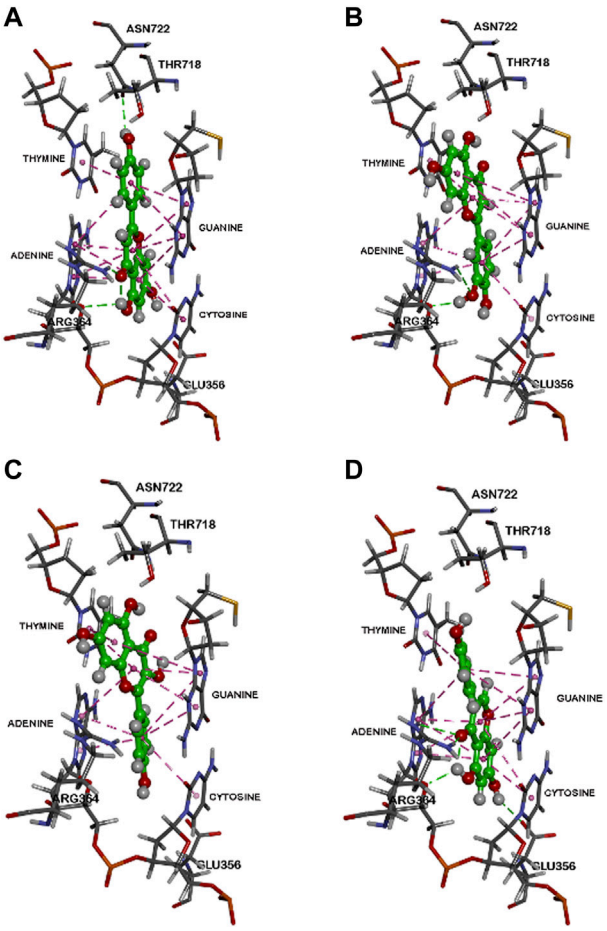

FIGURE 5
Binding modes of flavonoids within the human Top 1-DNA complex. The binding modes within the human Topo1-DNA complex (pdb id: 1K4T) are shown for, **(A)** apigenin, **(B)** luteolin, **(C)** kaempferol, and **(D)** genistein. Polar and non-polar interactions are colored coded and details are provided in text.

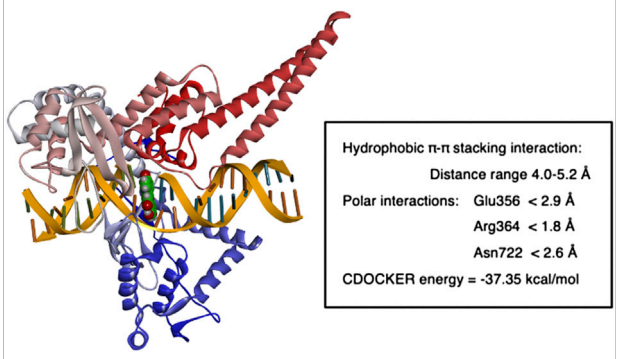

FIGURE 6
Molecular modeling of apigenin fit within in human Top 1-DNA complex. The figure shows the result of computational modeling for apigenin bound within the Topo1-DNA complex and key interaction distances.

both types 1 and 2 topoisomerases. It may be that apigenin's action is like that of topotecan (Staker et al., 2002) and that it can bind and stabilize the Topo1-DNA complex to prevent DNA religation (Drwal et al., 2011; Jadaun et al., 2017). However, the affinity of binding under these conditions may be less important to the effect on Topo1 activity than the nature of the specific interactions with particular base pair combinations and/or Topo1 amino acid residue side chains. Our data show that luteolin, which has the greatest overall binding potency, does not reproducibly inhibit Topo1 activity to a substantial degree.

Discussion

The ability to elevate cell-surface CD26 is a feature of many chemotherapeutic agents, including 5-fluorouracil, cisplatin, vinblastine, methotrexate, oxaliplatin and irinotecan (Lefort and Blay 2011; Cutler et al., 2015), etoposide and doxorubicin (this paper). It is also seen to different degrees extent with flavones such as apigenin, genistein, kaempferol (Lefort and Blay 2011) and luteolin (this paper). Transduction of the enabling signal involves a network of protein kinases, including CK2 (Lefort et al., 2020) and MAPK (Lefort and Blay, unpublished data) kinases. We have though noted a pharmacologic interaction only between apigenin and irinotecan, a chemotherapeutic drug that acts as a topoisomerase 1 inhibitor. Taken together, our findings here provide evidence for a unique involvement of the irinotecan (SN38) target Topo1 in CD26 upregulation by apigenin.

We have previously observed that multiple chemotherapeutic drugs have the ability to upregulate CD26 over a prolonged period (beginning 24 h–72 h after initial exposure), at doses below those causing cytotoxicity (Lefort and Blay 2011; Cutler et al., 2015). Our data here confirm that irinotecan, etoposide and doxorubicin have this action in HT-29 cells, producing elevations in cell-surface CD26 within the range 71%–212%. This phenomenon is seen in cells from different cancers including prostate, breast, lung and colon and is consistently demonstrable in different cell lines from a given cancer (Lefort and Blay 2011; Cutler et al., 2015). The increased abundance of CD26 is found at the cell surface and accompanied by elevations in dipeptidyl peptidase IV (DPP4) and adenosine deaminase (ADA)-binding activities, which are the functionalities of the CD26 protein (Lefort and Blay 2011; Cutler et al., 2015). As these functions serve to dampen external pathways that facilitate tumour progression, we have proposed that is an additional beneficial action of anticancer drugs due to the activation of antimetastatic pathways secondary to their cytotoxic action (Cutler et al., 2015).

Separately, we have shown that apigenin increases cell-surface CD26 on CRC cancer cells (Lefort and Blay 2011).

This is common to relatively differentiated CRC cell lines (HT-29, HRT-18 and Caco-2) but not seen in less-differentiated cells such as those of the HCT-116, SW480 and SW620 lines, which express very low intrinsic levels of CD26 (Lefort et al., 2020). The apigenin enhancement of CD26 in CRC cells is independent of detectable cytotoxicity, but is accompanied by subsequent decreases in cell growth and profileration as measured by assays of DNA synthesis, energy metabolism and cell population number (Lefort and Blay 2011). We have also shown that elevation of CD26 by apigenin is preceded by inhibition of the activity of the kinase CK2 (Lefort et al., 2020). The cellular distribution of CK2 in a cancer cell differs from that of a normal cell. In the former, CK2 is mainly localized in a diffuse pattern in the nucleus and the cytoplasm whereas in a cancer cell, CK2 levels are higher in the nuclear compartment (Faust et al., 1999; Laramas et al., 2007). This raises the possibility that apigenin's actions on CK2 might directly interplay with its ability to target Topo1 as reported here.

Topo1 plays a role in the pathway to elevate CD26. In addition to the ability of the Topo1 inhibitors irinotecan and SN38 to upregulate CD26, we show here that direct knockdown of Topo1 with a specific siRNA leads to a substantial (mean, 96.5%) increase in CD26. Moreover, there is a unique interaction with apigenin. Our molecular modeling shows that all 4 related flavones tested, apigenin, luteolin, kaempferol, and genistein, have the capacity to bind within the Topo1-DNA complex, but that the binding of apigenin is unique in terms of its angle relative to the base-pair structure, potentially giving apigenin the ability to interfere with topoisomerase function. Direct measurements of topoisomerase activities, both in whole cells and with purified recombinant Topo1, showed that apigenin has the ability to directly inhibit Topo1 activity, and that this occurs within the concentration range that is non-toxic and able to elevate CD26 on whole cells.

Although luteolin, the primary hydroxylated metabolite of apigenin, is itself able to elevate CD26, it does not inhibit topoisomerase activity (Figure 4C) and does not yield a synergistic effect with irinotecan (Figure 1C). These two actions are unique to apigenin. We propose that the unique ability of apigenin to sensitize cells to irinotecan (4.2-fold reduction in the EC_{50}, (Lefort and Blay 2011)) and conversely that of irinotecan to increase sensitivity to apigenin (29.8-fold reduction in EC_{50}, (Lefort and Blay 2011)) follow from direct cooperation of apigenin and the active metabolite of irinotecan SN-38 in modulating the activity of Topo1.

We conclude that apigenin has a unique fit into the Topo1-DNA functional complex that leads to direct inhibition of Topo1 activity, and suggest that this is the basis for the unique interaction with the CRC drug irinotecan. The combined action of these two agents in elevating cell-surface CD26, which may play a role in limiting local signals that facilitate tumour progression, may allow an approach to enhance the beneficial action of irinotecan in CRC, independently of its direct cytotoxic action. This is consistent with findings that irinotecan analogues may have beneficial clinical actions in cancer patients that are independent of their ability to inhibit Topo1 (Li et al., 2017).

Data availability statement

The original contributions presented in the study are included in the article/Supplementary Material, further inquiries can be directed to the corresponding author.

Author contributions

JB and EL conceived and planned the research, experiments were carried out by JF and EL with guidance from JB, PR performed docking and molecular analyses, the manuscript was written by JB and EL with contributions from JF and PR, all authors reviewed and edited.

Funding

Supported by grants from the Canadian Institutes for Health Research (CIHR; FRN 84361) and Natural Sciences and Engineering Research Council of Canada (NSERC; RGPIN 121624) awarded to JB. EL was supported by a CRTP studentship award from the Beatrice Hunter Cancer Research Institute (BHCRI). JB is a Senior Scientist of the BHCRI.

Conflict of interest

The authors declare that the research was conducted in the absence of any commercial or financial relationships that could be construed as a potential conflict of interest.

Publisher's note

References

Ahmad, K. A., Wang, G., and Ahmed, K. (2006). Intracellular hydrogen peroxide production is an upstream event in apoptosis induced by down-regulation of casein kinase 2 in prostate cancer cells. *Mol. Cancer Res. May* 4, 331–338. doi:10.1158/1541-7786.MCR-06-0073

Balis, M. E. (1985). Adenosine deaminase and malignant cells. *Ann. N. Y. Acad. Sci.* 451, 142–149. doi:10.1111/j.1749-6632.1985.tb27105.x

Birt, D. F., Hendrich, S., and Wang, W. (2001). Dietary agents in cancer prevention: Flavonoids and isoflavonoids. *Pharmacol. Ther. May-Jun* 90, 157–177. doi:10.1016/s0163-7258(01)00137-1

Cheng, H. C., Abdel-Ghany, M., and Pauli, B. U. (2003). A novel consensus motif in fibronectin mediates dipeptidyl peptidase IV adhesion and metastasis. *J. Biol. Chem. Jul* 4 (278), 24600–24607. doi:10.1074/jbc.M303424200

Cutler, M. J., Lowthers, E. L., Richard, C. L., Hajducek, D. M., Spagnuolo, P. A., and Blay, J. (2015). Chemotherapeutic agents attenuate CXCL12-mediated migration of colon cancer cells by selecting for CXCR4-negative cells and increasing peptidase CD26. *BMC Cancer* 15 (15), 882. doi:10.1186/s12885-015-1702-2

Darmoul, D., Rouyer-Fessard, C., Blais, A., Voisin, T., Sapin, C., Baricault, L., et al. (1991). Dipeptidyl peptidase IV expression in rat jejunal crypt-villus axis is controlled at mRNA level. *Am. J. Physiol. Nov.* 261, G763–G769. doi:10.1152/ajpgi.1991.261.5.G763

De Meester, I., Korom, S., Van Damme, J., and Scharpe, S. (1999). CD26, let it cut or cut it down. *Immunol. today Aug* 20, 367–375. doi:10.1016/s0167-5699(99)01486-3

DeRango-Adem, E. F., and Blay, J. (2021). Does oral apigenin have real potential for a therapeutic effect in the context of human gastrointestinal and other cancers? *Front. Pharmacol.* 12, 681477. doi:10.3389/fphar.2021.681477

Dong, R. P., Tachibana, K., Hegen, M., Munakata, Y., Cho, D., Schlossman, S. F., et al. (1997). Determination of adenosine deaminase binding domain on CD26 and its immunoregulatory effect on T cell activation. *J. Immunol.* 159, 6070–6076.

Drwal, M. N., Agama, K., Wakelin, L. P., Pommier, Y., and Griffith, R. (2011). Exploring DNA topoisomerase I ligand space in search of novel anticancer agents. *PLoS One* 6, e25150. doi:10.1371/journal.pone.0025150

Faust, R. A., Niehans, G., Gapany, M., Hoistad, D., Knapp, D., Cherwitz, D., et al. (1999). Subcellular immunolocalization of protein kinase CK2 in normal and carcinoma cells. *Int. J. Biochem. Cell Biol. Sep.* 31, 941–949. doi:10.1016/s1357-2725(99)00050-3

Havre, P. A., Abe, M., Urasaki, Y., Ohnuma, K., Morimoto, C., and Dang, N. H. (2008). The role of CD26/dipeptidyl peptidase IV in cancer. *Front. Biosci.* 13, 1634–1645. doi:10.2741/2787

Jadaun, A., Subbarao, N., and Dixit, A. (2017). Allosteric inhibition of topoisomerase I by pinostrobin: Molecular docking, spectroscopic and topoisomerase I activity studies. *J. Photochem Photobiol. B. Feb* 167, 299–308. doi:10.1016/j.jphotobiol.2017.01.010

Jung, E. B., Kim, Y. J., and Lee, C. S. (2014). Casein kinase 2 inhibition attenuates cholesterol oxidation product-induced apoptosis by suppressing the activation of the mitochondrial pathway and the caspase-8- and bid-dependent pathways. *Neurochem. Int. Jan.* 65, 30–39. doi:10.1016/j.neuint.2013.12.010

Kim, J. M., Noh, E. M., Song, H. K., You, Y. O., Jung, S. H., Kim, J. S., et al. (2018). Silencing of casein kinase 2 inhibits PKCinduced cell invasion by targeting MMP9 in MCF7 cells. *Mol. Med. Rep.* 17, 8397–8402. doi:10.3892/mmr.2018.8885

Kotackova, L., Balaziova, E., and Sedo, A. (2009). Expression pattern of dipeptidyl peptidase IV activity and/or structure homologues in cancer. *Folia Biol. (Praha)* 55, 77–84.

Kroonen, J., Artesi, M., Capraro, V., Nguyen-Khac, M. T., Willems, M., Chakravarti, A., et al. (2012). Casein kinase 2 inhibition modulates the DNA damage response but fails to radiosensitize malignant glioma cells. *Int. J. Oncol. Aug* 41, 776–782. doi:10.3892/ijo.2012.1489

Laramas, M., Pasquier, D., Filhol, O., Ringeisen, F., Descotes, J. L., and Cochet, C. (2007). Nuclear localization of protein kinase CK2 catalytic subunit (CK2alpha) is associated with poor prognostic factors in human prostate cancer. *Eur. J. Cancer. Mar.* 43, 928–934. doi:10.1016/j.ejca.2006.11.021

Lefort, E. C., and Blay, J. (2013). Apigenin and its impact on gastrointestinal cancers. *Mol. Nutr. Food Res. Jan.* 57, 126–144. doi:10.1002/mnfr.201200424

Lefort, E. C., and Blay, J. (2011). The dietary flavonoid apigenin enhances the activities of the anti-metastatic protein CD26 on human colon carcinoma cells. *Clin. Exp. Metastasis* 28, 337–349. doi:10.1007/s10585-010-9364-6

Lefort, E. C., Diaconu, B., Bentley, V. L., and Blay, J. (2020). Apigenin upregulation of CD26/DPPIV on colon epithelial cells requires inhibition of casein kinase 2. *Food Sci. Nutr.* 8, 5321–5329. doi:10.1002/fsn3.1823

Li, C., Liu, X., Lin, X., and Chen, X. (2009). Structure-activity relationship of 7 flavonoids on recombinant human protein kinase CK2 holoenzyme. *Zhong nan da xue xue bao Yi xue ban = J. Central South Univ. Med. Sci.* 34, 20–26.

Li, F., Jiang, T., Li, Q., and Ling, X. (2017). Camptothecin (CPT) and its derivatives are known to target topoisomerase I (Top1) as their mechanism of action: Did we miss something in CPT analogue molecular targets for treating human disease such as cancer? *Am. J. Cancer Res.* 7, 2350–2394.

Liu, L. F., Desai, S. D., Li, T. K., Mao, Y., Sun, M., and Sim, S. P. (2000). Mechanism of action of camptothecin. *Ann. N. Y. Acad. Sci.* 922, 1–10. doi:10.1111/j.1749-6632.2000.tb07020.x

Lolli, G., Cozza, G., Mazzorana, M., Tibaldi, E., Cesaro, L., Donella-Deana, A., et al. (2012). Inhibition of protein kinase CK2 by flavonoids and tyrphostins. A structural insight. *Biochemistry* 51 (51), 6097–6107. doi:10.1021/bi300531c

Loster, K., Zeilinger, K., Schuppan, D., and Reutter, W. (1995). The cysteine-rich region of dipeptidyl peptidase IV (CD 26) is the collagen-binding site. *Biochem. Biophys. Res. Commun.* 217, 341–348. doi:10.1006/bbrc.1995.2782

Morales, J. C., and Carpenter, P. B. (2004). Breaking in a new function for casein kinase 2. *Sci. Aging Knowl. Environ.* 2004, pe24. doi:10.1126/sageke.2004.22.pe24

Nitiss, J. L., Soans, E., Rogojina, A., Seth, A., and Mishina, M. (2012). Topoisomerase assays, *Curr. Protoc. Pharmacol.* 1(10):e250. doi:10.1002/cpz1.250

Pinna, L. A., and Meggio, F. (1997). Protein kinase CK2 ("casein kinase-2") and its implication in cell division and proliferation. *Prog. Cell Cycle Res.* 3, 77–97. doi:10.1007/978-1-4615-5371-7_7

Richard, C. L., and Blay, J. (2008). CXCR4 in cancer and its regulation by PPARgamma. *PPAR Res.* 2008, 769413. doi:10.1155/2008/769413

Richard, C. L., Lowthers, E. L., and Blay, J. (2007). 15-Deoxy-delta(12, 14)-prostaglandin J(2) down-regulates CXCR4 on carcinoma cells through PPARgamma- and NFkappaB-mediated pathways. *Exp. Cell Res.* 313, 3446–3458. doi:10.1016/j.yexcr.2007.06.027

Richard, C. L., Tan, E. Y., and Blay, J. (2006). Adenosine upregulates CXCR4 and enhances the proliferative and migratory responses of human carcinoma cells to CXCL12/SDF-1alpha. *Int. J. Cancer. Nov.* 1119, 2044–2053. doi:10.1002/ijc.22084

Sarno, S., Moro, S., Meggio, F., Zagotto, G., Dal Ben, D., Ghisellini, P., et al. (2002). Toward the rational design of protein kinase casein kinase-2 inhibitors. *Pharmacol. Ther. Feb-Mar* 93, 159–168. doi:10.1016/s0163-7258(02)00185-7

Staker, B. L., Hjerrild, K., Feese, M. D., Behnke, C. A., Burgin, A. B., Jr., and Stewart, L. (2002). The mechanism of topoisomerase I poisoning by a camptothecin analog. *Proc. Natl. Acad. Sci. U. S. A. Nov.* 26 (99), 15387–15392. doi:10.1073/pnas.242259599

Suhas, K. S., Parida, S., Gokul, C., Srivastava, V., Prakash, E., Chauhan, S., et al. (2018). Casein kinase 2 inhibition impairs spontaneous and oxytocin-induced contractions in late pregnant mouse uterus. *Exp. Physiol.* 103, 621–628. doi:10.1113/EP086826

Tan, E. Y., Mujoomdar, M., and Blay, J. (2004). Adenosine down-regulates the surface expression of dipeptidyl peptidase IV on HT-29 human colorectal carcinoma cells: Implications for cancer cell behavior. *Am. J. Pathol. Jul* 165, 319–330. doi:10.1016/S0002-9440(10)63299-3

Webb, M. R., and Ebeler, S. E. (2003). A gel electrophoresis assay for the simultaneous determination of topoisomerase I inhibition and DNA intercalation. *Anal. Biochem.* 321, 22–30. doi:10.1016/s0003-2697(03)00459-7

Yang, C. S., Landau, J. M., Huang, M. T., and Newmark, H. L. (2001). Inhibition of carcinogenesis by dietary polyphenolic compounds. *Annu. Rev. Nutr.* 21, 381–406. doi:10.1146/annurev.nutr.21.1.381

frontiers | Frontiers in Pharmacology

TYPE Original Research
PUBLISHED 04 January 2023
DOI 10.3389/fphar.2022.1052849

OPEN ACCESS

EDITED BY
Mitesh Patel,
Parul University, India

REVIEWED BY
Mohammad Jahoor Alam,
University of Hail, Saudi Arabia
Mejdi Snoussi,
University of Hail, Saudi Arabia

*CORRESPONDENCE
Pukar Khanal,
pukarkhanal58@gmail.com
Darasaguppe R. Harish,
drharish49@gmail.com

†These authors have contributed equally to this work and share first authorship

SPECIALTY SECTION
This article was submitted to Pharmacology of Anti-Cancer Drugs, a section of the journal Frontiers in Pharmacology

RECEIVED 24 September 2022
ACCEPTED 05 December 2022
PUBLISHED 04 January 2023

CITATION
Khanal P, Patil VS, Bhandare VV, Patil PP, Patil BM, Dwivedi PSR, Bhattacharya K, Harish DR and Roy S (2023), Systems and *in vitro* pharmacology profiling of diosgenin against breast cancer. *Front. Pharmacol.* 13:1052849. doi: 10.3389/fphar.2022.1052849

Systems and *in vitro* pharmacology profiling of diosgenin against breast cancer

Pukar Khanal[1*†], Vishal S. Patil[2†], Vishwambhar V. Bhandare[3], Priyanka P. Patil[4], B. M. Patil[5], Prarambh S. R. Dwivedi[1], Kunal Bhattacharya[6,7], Darasaguppe R. Harish[2*] and Subarna Roy[2]

[1]Department of Pharmacology, NGSM Institute of Pharmaceutical Sciences (NGSMIPS), Nitte (Deemed to be University), Mangalore, India, [2]ICMR-National Institute of Traditional Medicine, Belagavi, Karnataka, India, [3]Department of Microbiology, Shivaji University, Kolhapur, India, [4]Department of Pharmacology, KLE College of Pharmacy Belagavi, KLE Academy of Higher Education and Research (KAHER), Belagavi, India, [5]PRES's Pravara Rural College of Pharmacy Pravaranagar, Loni, Maharashtra, India, [6]Pratiksha Institute of Pharmaceutical Sciences, Guwahati, Assam, India, [7]Royal School of Pharmacy, The Assam Royal Global University, Guwahati, Assam, India

Aim: The purpose of this study was to establish a mode of action for diosgenin against breast cancer employing a range of system biology tools and to corroborate its results with experimental facts.

Methodology: The diosgenin-regulated domains implicated in breast cancer were enriched in the Kyoto Encyclopedia of Genes and Genomes database to establish diosgenin-protein(s)-pathway(s) associations. Later, molecular docking and the lead complexes were considered for molecular dynamics simulations, MMPBSA, principal component, and dynamics cross-correlation matrix analysis using GROMACS v2021. Furthermore, survival analysis was carried out for the diosgenin-regulated proteins that were anticipated to be involved in breast cancer. For gene expression analyses, the top three targets with the highest binding affinity for diosgenin and tumor expression were examined. Furthermore, the effect of diosgenin on cell proliferation, cytotoxicity, and the partial Warburg effect was tested to validate the computational findings using functional outputs of the lead targets.

Results: The protein-protein interaction had 57 edges, an average node degree of 5.43, and a *p*-value of 3.83e-14. Furthermore, enrichment analysis showed 36 KEGG pathways, 12 cellular components, 27 molecular functions, and 307 biological processes. In network analysis, three hub proteins were notably modulated: *IGF1R*, *MDM2*, and *SRC*, diosgenin with the highest binding affinity with *IGF1R* (binding energy −8.6 kcal/mol). Furthermore, during the 150 ns molecular dynamics (MD) projection run, diosgenin exhibited robust intermolecular interactions and had the least free binding energy with *IGF1R* (−35.143 kcal/mol) compared to *MDM2* (−34.619 kcal/mol), and *SRC* (-17.944 kcal/mol). Diosgenin exhibited the highest cytotoxicity against MCF7 cell lines (IC_{50} 12.05 ± 1.33) μg/ml. Furthermore, in H_2O_2-induced oxidative stress, the inhibitory constant (IC_{50} 7.68 ± 0.51) μg/ml of diosgenin was lowest in MCF7 cell lines. However, the reversal of the Warburg effect by diosgenin seemed to be maximum in non-cancer Vero cell lines (EC_{50}

15.27 ± 0.95) μg/ml compared to the rest. Furthermore, diosgenin inhibited cell proliferation in SKBR3 cell lines more though.

Conclusion: The current study demonstrated that diosgenin impacts a series of signaling pathways, involved in the advancement of breast cancer, including FoxO, PI3K-Akt, p53, Ras, and MAPK signaling. Additionally, diosgenin established a persistent diosgenin-protein complex and had a significant binding affinity towards *IGF1R*, *MDM2*, and *SRC*. It is possible that this slowed down cell growth, countered the Warburg phenomenon, and showed the cytotoxicity towards breast cancer cells.

KEYWORDS

breast cancer, computational pharmacology, diosgenin, gene ontology analysis, system biology

Introduction

Breast cancer spreads through the inner layer of the milk gland or lobules and ducts (Sariego, 2010), and it is one of the second leading causes of mortality for women between the ages of 45 and 55 (Jemal et al., 2009). It includes age, iodine deficiency (Venturi, 2001; Aceves et al., 2005; Stoddard et al., 2008), high hormone levels (Russo and Russo, 2006; Yager and Davidson, 2006), and age-related (Steiner et al., 2008) risk factors. This incident potentially results in the breast being surgically removed entirely or in requiring chemo-, radio-, or hormone-therapy (HeraviKarimovi et al., 2006). However, these practises are preoccupied with multiple side effects that are not specific to the breast tumor. Furthermore, the currently used chemotherapeutic drugs in medical care result in anemia, exhaustion, mouth soreness, vomiting, and diarrhea. This suggests the requirement to discover a novel therapeutic agent against breast cancer.

Diosgenin is a phyto steroid sapogenin obtained from the hydrolysis by strong bases, acids, or enzymes of saponin. It is commercially used as a precursor to synthesis various hormones and steroid products like pregnenolone, and cortisone including progesterone (Marker and Krueger, 1940) for the early manufacture of combined oral contraceptive pills (Djerassi, 1992). Additionally, diosgenin has the potential to inhibit activated pro-inflammatory and pro-survival signaling pathways and promote the death of a variety of cancer cells (Shishodia and Aggarwal, 2006). Additionally, diosgenin inhibits the growth of oestrogen receptor-positive MCF-7 cells by activating caspase three and upregulating the p53 tumor suppressor gene. Further, BCL2 is downregulated in estrogen receptor-negative MDA-MB-231 breast cancer cells (Srinivasan et al., 2009). Although the potential of diosgenin to treat breast cancer has been demonstrated its interaction with proteins involved in the progenesis of breast cancer has yet to be investigated.

As a result, the current study focuses on locating the potential interactions of the diosgenin-regulated proteins and attributable pathways implicated in breast cancer using a range of system biology techniques *i.e.*, gene ontology (GO) analysis, molecular docking, and molecular dynamics (MD) simulations, and reinforcing its findings using diverse functional biomarkers using *in vitro* experiments in four distinct cell lines.

Materials and methods

Computational pharmacology

The detected diosgenin-regulated proteins were enriched to determine the altered pathways. Later, diosgenin was docked with proteins, and the proteins with the maximum diosgenin binding affinity were chosen for MD simulation. Furthermore, the diosgenin-regulated proteins involved in breast cancer were examined for survival and gene expression in normal and tumor cell lines, including the three hub proteins determined by molecular docking.

ADMET profile of diosgenin and its targets

Canonical SMILES of diosgenin (Figure 1) were retrieved from the PubChem database (https://pubchem.ncbi.nlm.nih.gov/) and ADME profile was predicted by SwissADME (Daina et al., 2017; http://www.swissadme.ch/) and ADMETlab 2.0 (Xiong et al., 2021; https://admetmesh.scbdd.com) and adverse effects from ADVERPred (Ivanov et al., 2018; http://www.way2drug.com/adverpred/).

Diosgenin-modulated targets were predicted using SwissTargetPrediction (Daina et al., 2019; http://www.swisstargetprediction.ch/), DIGEP-Pred (Lagunin et al., 2013; http://www.way2drug.com/ge/), and BindingDB (Liu et al., 2007; https://www.bindingdb.org/bind/index.jsp) and any duplicates were eliminated. In addition, the semantic type (neoplastic process) oestrogen receptor-positive breast cancer targets (UMLS CUI: C2938924), were retrieved from DisGeNET (https://www.disgenet.org/). Later, the

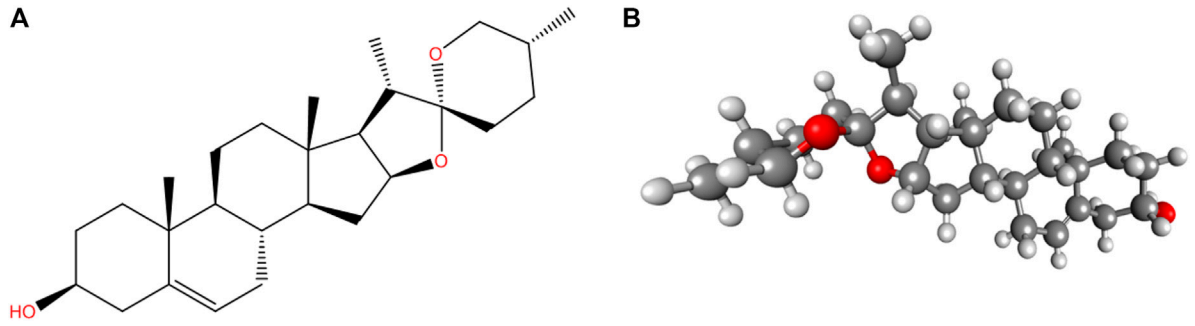

FIGURE 1
Structure of Diosgenin **(A)** 2D and **(B)** 3D (ball and stick). PubChem CID: 99474, Molecular Formula: $C_{27}H_{42}O_3$, Synonyms: Nitogenin, UNII-K49P2K8WLX, (3β, 25R)-spirost-5-en-3-ol, Molecular Weight: 414.6.

diosgenin-modulated targets were compared with DisGeNET-recorded targets to trace the reported targets involved in oestrogen receptor-positive breast cancer using PivotTable (Microsoft excel 2007; https://www.microsoft.com/en-in/microsoft-365/excel).

GO and cluster analysis

The diosgenin-modulated targets involved in oestrogen receptor-positive breast cancer were queried in STRING (Szklarczyk et al., 2021; https://string-db.org/) ver 11.5 for "*Homo sapiens*" to trace three GO terms i.e., cellular components, molecular function, and biological processes. In addition, probable regulations of multiple pathways were also traced concerning the KEGG database (https://www.genome.jp/kegg/pathway.html) with whole genome statistical background. Also, the regulated proteins were concerned with subcellular location (COMPARTMENT), protein domains and features (InterPro), protein domain (Pfam), and tissue expression (TISSUES). Later, the protein-protein interaction (PPI) was also assessed for the cluster analysis via k means clustering to identify three lead distinct clusters.

Network construction and analysis

The network between diosgenin, its targets (involved in oestrogen receptor-positive breast cancer), and the regulated pathways were constructed using Cytoscape ver 3.5.1 (Shannon et al., 2003; https://cytoscape.org/). The constructed network was recognized as directed and inspected by translating node size and color to low values corresponding to small sizes and low values corresponding to bright colors toward edge count. In addition, the edge size and color were mapped to edge betweenness, with low values corresponding to small sizes and low values equating to bright colors.

Molecular docking

The regulation of insulin-like growth factor 1 receptor (*IGF1R*), E3 ubiquitin-protein ligase Mdm2 (*MDM2*), and proto-oncogene tyrosine-protein kinase Src (*SRC*) were majorly triggered in the network interaction among diosgenin-target(s)-pathway(s). As a result, these three proteins were considered for molecular docking studies.

Ligand preparation: The ligand's 3D conformation, diosgenin, was obtained from the PubChem database (https://pubchem.ncbi.nlm.nih.gov) and converted to .pdb using Discovery Studio Visualizer (https://discover.3ds.com/discover-studio-visualizer-download) *ver*. 2019. The ligand's energy was minimized using the mmff94 force field (Halgren 1996) and saved in .pdbqt format.

Preparation of macromolecule: Diosgenin was docked against *IGF1R* (PDB: 3I81), *MDM2* (PDB: 3LBL), and *SRC* (PDB: 1O43); retrieved from a protein data bank maintained by the Research Collaboratory for Structural Bioinformatics (RCSB; https://www.rcsb.org). All proteins were refined and saved in .pdb format after eliminating all heteroatoms and pre-complex ligands.

Ligand–protein docking: Diosgenin was docked against the aforementioned targets using AutoDock Vina, which was run through the POAP pipeline (Trott and Olson 2010; Samdani and Vetrivel 2018; Patil et al., 2022). Nine different poses of ligand were obtained after docking. Docking results were analysed based on the binding affinity, and number of interactions as explained previously (Dwivedi et al., 2021; Badraoui et al., 2022). Further, the diosgenin pose with the lowest binding energy was chosen to visualize the ligand-protein interactions and perform MD simulation (Samdani and Vetrivel 2018).

MD simulation

To examine the structural stabilities and intermolecular interactions of diosgenin with *IGF1R*, *MDM2*, and *SRC*, an all-atom MD simulation in an explicit solvent was performed for 150 ns. We used the GROMACS software package, *ver*. 2021.3

(https://www.gromacs.org/) and Amber *ff99SB-ildn* force field to run MD simulations (Berendsen et al., 2005; Saeed et al., 2020; Dwivedi et al., 2022). The topological parameters of the ligands and the entire complex were calculated using the AmberTool's xleap module (https://ambermd.org/AmberTools.php) and the partial charges of the small molecules were calculated using an antechamber with a "bcc" charge model. The built systems were solvated in a rectangular box with 10.0 Å boundary conditions from the protein's borders in all directions using the TIP3P water model. The required amounts of counter ions were introduced to the prepared systems to neutralize the charges. The steepest descent and conjugate gradient energy reduction methods were used to discover the least energy conformations of the near-global state. To equilibrate the systems for 1 ns, "Canonical (NVT) and isobaric (NPT) ensembles" were used. A modified Berendsen thermostat approach was utilized to keep the volume and temperature consistent during NVT equilibration (300 K). During NPT equilibration, a Parrinello-Rahman barostat was used to keep the pressure constant at 1 bar. Furthermore, the Particle Mesh Ewald approximation with a cut-off value of 1 nm was used to calculate the long-range electrostatic interactions, van der Waals, and Coulomb interactions. A similar LINear Constraint Solver method was used to constrain bond length. Every complex went through a 150 ns production run with coordinates recorded every 2 fs. Other software programs, in addition to the built-in gromacs tools, were utilized to perform specific analyses on the acquired trajectories as required.

Analysis of free binding energy of complexes utilizing molecular mechanics Poisson–Boltzmann surface area (MM-PBSA)

In MD simulations and thermodynamic calculations, the relative binding energy of a ligand-protein complex was employed to investigate the binding free energies. The relative binding free energy and its contribution to individual residues were calculated using the MM-PBSA method and the "g_mmpbsa" tool (Kumari et al., 2014; Dwivedi et al., 2022). The parameters for binding free energy calculations were taken from our previous study (Khanal et al., 2022). The binding free energy (ΔG) was calculated using 50 representative snapshots taken throughout the stable trajectory observed between 100 and 150 ns. The change in entropy (ΔS) was calculated using the Schlitter formula and finally, accurate binding free energy was calculated using the formula, $\Delta G = \Delta H - T\Delta S$, where, ΔG = Gibbs free energy, ΔH = enthalpy change, T = temperature (Kelvin), and ΔS = entropy change.

Principal component (PCA) and dynamic cross-correlation matrix (DCCM) analysis

PCA was performed over the stable MD trajectory to examine various forms of molecular motion (Amadei et al., 1993; Amadei et al., 1996; Bhandare and Ramaswamy 2018). To accomplish this, the "*least square fit*" to the reference structure was used to account for the molecular translational and rotational motion. The collection of eigenvectors obtained by diagonalizing a covariance matrix was produced by a linear transform of cartesian coordinate space to reflect the direction of the molecular motion. The energy contribution of each eigenvector to the motion was presented by the eigenvalue associated with the respective eigenvector. The "*time-dependent motions*" that the components carry out in an atomic vibrational mode were demonstrated by projecting the trajectory onto a particular eigenvector. The atomic vibrational components' contribution to this form of coordinated motion was shown by the projection's time average (Amadei et al., 1993; Van Aalten et al., 1995; Amadei et al., 1996; Bhandare and Ramaswamy 2018).

DCCM evaluates the magnitude of each pairwise cross-correlation coefficient to determine whether or not atomic pair motion is correlated *i.e.,* positive or negative (Khanal et al., 2021). We examined each DCCM component in this section, where $Cij = 1$ denotes the same period and phase (positive correlation), $Cij = 0$ indicates a lack of correlation, and $Cij = -1$ indicates a negative correlation between the fluctuations of *i* and j (Khanal et al., 2021).

Survival analysis of hub genes

To assess the prognostic values of hub genes of diosgenin-regulated oestrogen receptor-positive breast cancer targets, the Kaplan–Meier plotter breast cancer database (http://kmplot.com/analysis/) was used with *APP*, *AR*, *CDK4*, *CRHR1*, *CYP17A1*, *CYP19A1*, *CYP3A4*, *FASN*, *FGFR2*, *GRM1*, *IGF1R*, *LYN*, *MDM2*, *MDM4*, *NR3C1*, *PDGFRB*, *PRCP*, *PTPN1*, *RET*, *SRC*, and *STAT3* probe ID. Patients were divided into two groups with "*auto-detected best cutoff*"; overall survival was analyzed against $n = 2{,}976$ samples with a follow-up of 20 years of data. Also, the subtype analysis was restricted to lymph node status ($n = 2{,}887$), *ER* status ($n = 2{,}789$), *PGR* status (n = 2,662), *HER2* status (n = 2,875), *KI67* status ($n = 1{,}360$), Nottingham histologic grade ($n = 2{,}917$), and PAM50 subtype (n = 2,976) and cohort restriction *i.e.,* endocrine treated ($n = 2{,}955$) and chemo treated ($n = 2{,}956$). The difference among the groups was considered to be statistically significant if $p < 0.05$.

Gene expression analysis in tumor, normal and metastatic tissues

Herein, we evaluated the top three genes based on the log-rank test from survival analysis, and *in silico* molecular docking was evaluated for the gene expression in normal, tumor, and metastatic tissues using RNA sequence data in the platform of tumor, normal and metastatic samples. These data were analyzed using Kruskal Wallis and Dunn test.

Experimental pharmacology

Through different *in vitro* pharmacology profiling, we investigated the influence of diosgenin on breast cancer cell

lines. To begin, brine shrimp lethality (BSL) bioassay was used to assess its cytotoxicity and the effect was compared with doxorubicin. Later, the effect of diosgenin on breast cancer cell lines (MCF7, MDA-MB-231, SKBR3, and T47D) was compared to normal epithelial cell lines (Vero) by emphasizing on cell viability, proliferation, and Warburg effect.

BSL bioassay

The brine shrimp lethality bioassay was performed as explained by McLaughlin et al. (1998) with minor modifications. Here, *Artemia salina* Leach. eggs from Seamonk international Artemia cyst 003 were used for the assay. Briefly, 10–12 brine shrimps were incubated within the different concentrations of diosgenin and doxorubicin (prepared in seawater) for 24 h. Controls were used without the test agents. After 24 h, the survived shrimps were counted and the % cytotoxicity was calculated as

$$\%\,cytotoxicity = \left(\frac{Total\ shrimps\ added - live\ shrimps}{Total\ shrimps}\right) \times 100$$

The LC_{50} was calculated using a linear regression curve.

In vitro MTT assay tumor and non-tumor cell lines

The cytotoxic activity of diosgenin and doxorubicin on tumor and normal cell lines was performed using an MTT assay (Mosmann, 1983) with minor modifications. Briefly, cell lines were plated onto 96-well flat-bottom plates, maintaining the cell density (20,000 cells/well), and were allowed to proliferate (24 h). After that, the cells were treated with different concentrations of diosgenin and doxorubicin maintaining the final volume of 250 µL after adding DMEM media (supplemented with 3% FBS) and incubated (37°C, 48 h, 5% CO_2). Next, 20 µL of MTT reagent was added and incubated (37°C in 5% CO_2, 4 h). After incubation, the wells were washed (PBS, 3X) to discard the MTT. Then, formazan crystals were dissolved in DMSO (99.5% v/v, 100 µL) by gentle shaking. The absorbance was then recorded (570 nm) using an ELISA plate reader. The cell viability was calculated as

$$\%\,viability = \left(\frac{Absorbance\ of\ control - Absorbance\ of\ sample}{Absorbance\ of\ control}\right) \times 100$$

In vitro scratch assay

In vitro scratch assay was performed as explained by Bolla et al (2019) with minor modifications. Briefly, a stock solution (200 µg/ml) of diosgenin and doxorubicin was prepared and sterilized by filtering using a sterile membrane filter (0.22 µm). Later the solution was diluted using geometric series up to 1.56 µg/ml. This series of concentrations were chosen based on the number of experiments (trial and error). All the cells were seeded (2×10^5 cells/well) in 12-well tissue culture plates to obtain the confluence of 80–90% after 24 h of culture. After 24 h of post-seeding, the cell monolayers were scraped to create scratches of (300 µm). The detached cells and debris were washed with phosphate buffer. The media containing the samples were added to each well. Suitable controls were used by adding the minimal media and the scratch coverage was recorded at 0, 12, 24, 48, and 72 h after sample addition. The percentage scratch coverage was calculated using the following formula

$$\%\,scratch\ coverage = \left(\frac{Scratch\ length\ at\ (0\ min - t\ min)}{Scratch\ length\ at\ 0\ min}\right) \times 100$$

Effect of diosgenin on Warburg effect

The effect of diosgenin on the Warburg phenomena was evaluated by evaluating glucose uptake *via* the above-mentioned cancer cell lines vs. normal cell lines (Vero). Initially, the cells were grown in six well plates and incubated (37°C, 48 h) in a CO_2 incubator. After the formation of the confluent monolayer, the culture was renewed (DMEM consisting of 0.2% BSA) and again incubated (37°C, 18 h) in the CO_2 incubator. After incubation, the media was discarded and washed with KRP buffer. The cells were then treated with diosgenin and metformin in the presence of insulin followed by the addition of glucose (1 M) and incubated (30 min). The remaining amount of glucose was quantified from the supernatant. The percentage glucose uptake was calculated as the difference between the initial and final glucose content in the incubated medium (Gupta et al., 2009).

Statistical analysis

For the enrichment analysis, the whole-genome statistical background was used. The inhibitory constant (IC_{50}) and effective concentration (EC_{50}) were calculated using linear regression in GraphPad Prism (https://www.graphpad.com/) *ver* 5.0.

Results

Computational pharmacology

Diosgenin ADMET profile and its targets

Diosgenin has molecular weight of 414.62 g/mol with 3 *H*-bond acceptors and 1 *H*-bond donor. Diosgenin was predicted to possess the high human intestinal absorption (>30). In addition, it also showed the plasma protein binding, fraction unbound in plasma, and its volume of distribution 97.743%, 1.872%, and 1.695 L/kg, respectively. It was predicted as no inhibitory action towards *CYP1A2*, *CYP2C19*, *CYP2C9*, *CYP2D6*, and *CYP3A4* and showed

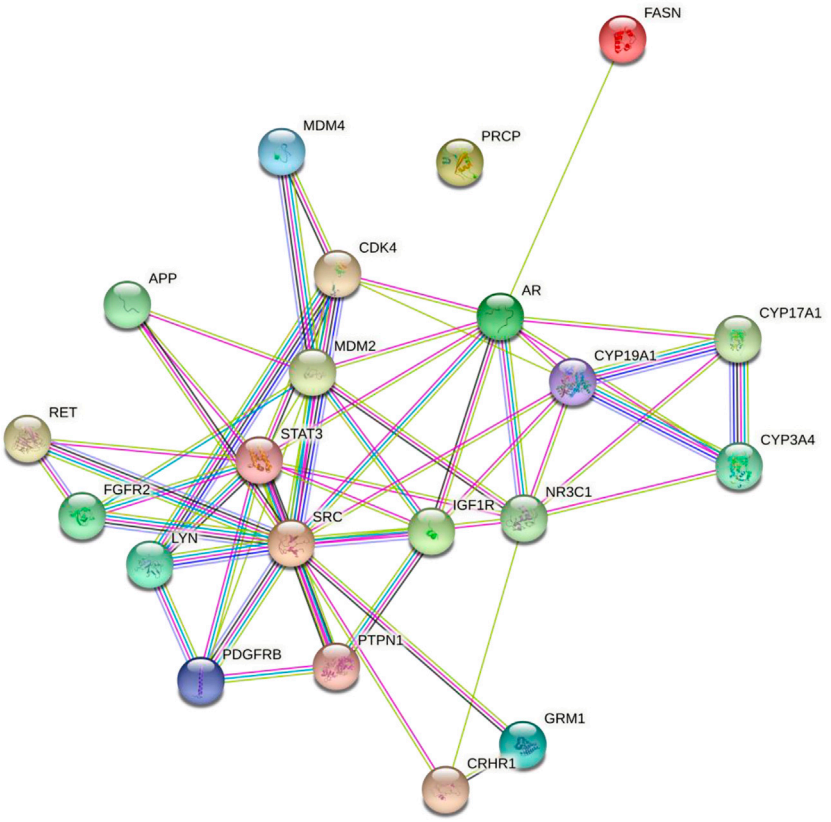

FIGURE 2
Protein-protein interaction of the diosgenin-triggered protein. Node color; colored nodes: query proteins and first shell of interactors, white nodes: second shell of interactors, Node content; empty nodes: proteins of unknown 3D structure, filled nodes: some 3D structure is known or predicted, Known Interactions; *from curated databases*, *experimentally determined*, Predicted Interactions; *gene neighborhood*, *gene fusions*, *gene co-occurrence* and Others; *text mining*, *co-expression*, *protein homology*.

high clearance rate of 23.332 ml/min/kg. In addition, it was not predicted for any side effects based on the ADVERPred server projection.

Diosgenin was predicted to regulate 105 targets in SwissTargetPrediction and four in DIGEP-Pred and BindingDB. The predicted targets in BindingDB were in common with SwissTargetPrediction. Similarly, a total of 510 different targets were recorded in DisGeNET for the neoplastic process of oestrogen receptor-positive breast cancer targets (UMLS CUI: *C2938924*). In general, the Diosgenin targeted 21 different proteins involved in breast cancer compared to recorded targets in DisGeNET (UMLS CUI: *C2938924*); Supplementary Figure S1.

Gene set enrichment analysis

The interaction of diosgenin-targeted 21 proteins had a total of 57 edges, 5.43 average node degree, 0.701 average local clustering coefficient, 17 edges (expected), and 3.83e-14 enrichment *p*-value (Figure 2).

KEGG enrichment analysis

Concerning the KEGG record, the PPI reflected the regulation of 36 different pathways in which *EGFR* tyrosine kinase inhibitor resistance (*hsa01521*) had the lowest false discovery rate *i.e.*, 1.06E-05 *via* the regulation of five genes *i.e.*, *PDGFRB*, *STAT3*, *IGF1R*, *SRC*, and *FGFR2* against 78 background genes at 1.78 strength. Additionally, eight different pathways were detected for keyword "*cancer*" *i.e.* pathways in cancer; *hsa05200* (regulated eight genes *i.e.* *CDK4*, *MDM2*, *PDGFRB*, *STAT3*, *IGF1R*, *RET*, *AR*, and *FGFR2* against 517 background genes at 1.16 strength and 1.06E-05 false discovery rate), prostate cancer; *hsa05215* (regulated five genes *i.e.* *MDM2*, *PDGFRB*, *IGF1R*, *AR*, and *FGFR2* against 96 background genes at 1.69 strength and 1.06E-05 false discovery rate), bladder cancer; *hsa05219* (regulated three genes *i.e.* *CDK4*, *MDM2*, and *SRC* against 41 background genes at 1.83 strength and 0.00062 false discovery rate), microRNAs in cancer; *hsa05206* (regulated four genes *i.e.* *MDM2*, *PDGFRB*, *STAT3*, and *MDM4* against

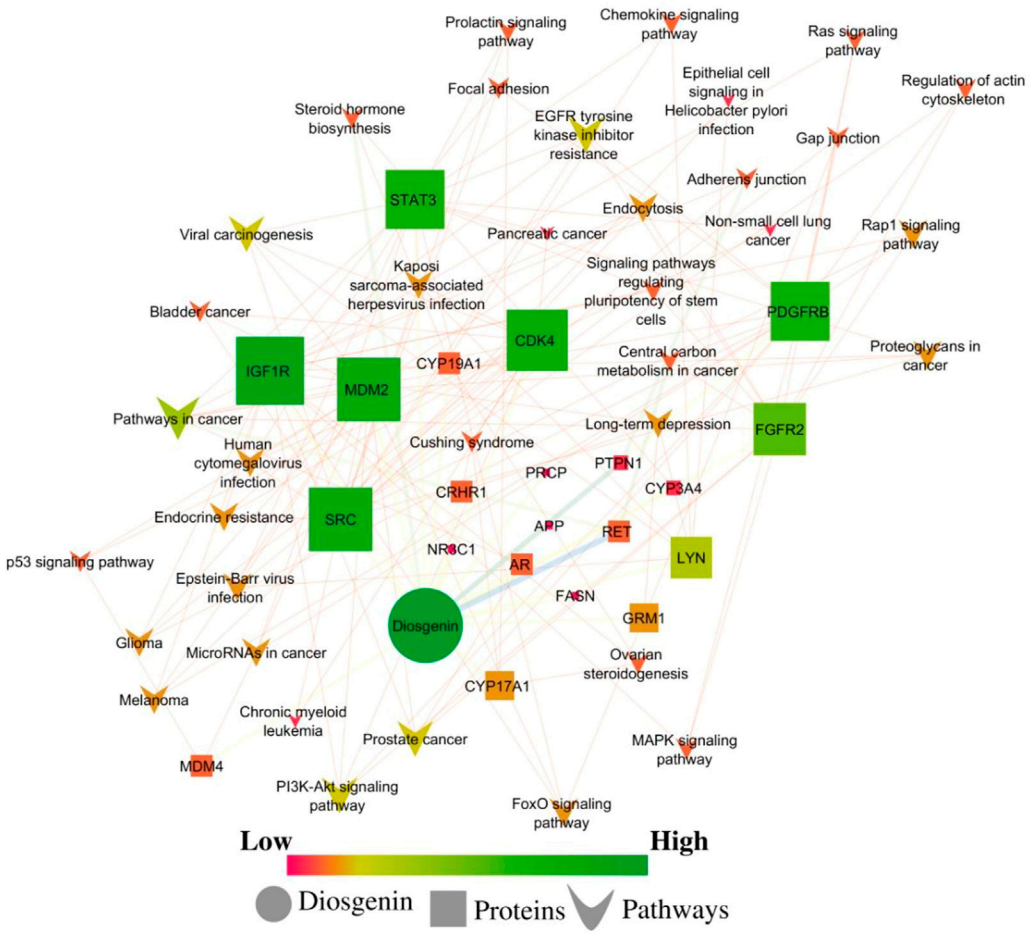

FIGURE 3
Network interaction of diosgenin-regulated proteins and respective pathways. Pink color presents a low edge count and green color presents a high edge count. A large node size presents a higher edge count and a smaller edge count presents a lower edge count.

160 background genes at 1.37 strength and 0.00099 false discovery rate), proteoglycans in cancer; *hsa05205* (regulated four genes *i.e. MDM2*, *STAT3*, *IGF1R*, and *SRC* against 196 background genes at 1.28 strength and 0.0015 false discovery rate), central carbon metabolism in cancer; *hsa05230* (regulated three genes *i.e. PDGFRB*, *RET*, and *FGFR2* against 69 background genes at 1.61 strength and 0.0015 false discovery rate), non-small cell lung cancer; *hsa05223* (regulated two genes *i.e. CDK4* and *STAT3* against 68 background genes at 1.44 strength and 0.0349 false discovery rate), and pancreatic cancer; *hsa05212* (regulated two genes *i.e. CDK4* and *STAT3* against 73 background genes at 1.41 strength and 0.0387 false discovery rate). Also, a total of 129 genes were modulated in 36 different pathways in which insulin-like growth factor-1 receptor (*IGF1R*) was majorly triggered in 18 different pathways *i.e., EGFR* tyrosine kinase inhibitor resistance; *hsa01521*, pathways in cancer; *hsa05200*, prostate cancer; *hsa05215*, long-term depression; *hsa04730*, glioma; *hsa05214*, melanoma; *hsa05218*, endocrine resistance; *hsa01522*, ovarian steroidogenesis; *hsa04913*, signaling pathways regulating pluripotency of stem cells; hsa04550, adherens junction; *hsa04520*, proteoglycans in cancer; *hsa05205*, endocytosis; *hsa04144*, focal adhesion; *hsa04510*, and Ras; *hsa04014*, MAPK; *hsa04010*, FoxO; *hsa04068*, PI3K-Akt; *hsa04151*, and Rap1 signaling pathway; *hsa04015* (Supplementary File S1; Supplementary Sheet S1). The modulated genes in the KEGG pathways were observed to be common with three GO terms *i.e.,* cellular components, molecular function, and biological processes (Supplementary Figure S2); detailed below. Further, the interaction between the diosgenin-modulated targets and triggered pathways is presented in Figure 3. The associated protein-pathways interaction with respective false discovery rate and strengths is presented in Figure 4.

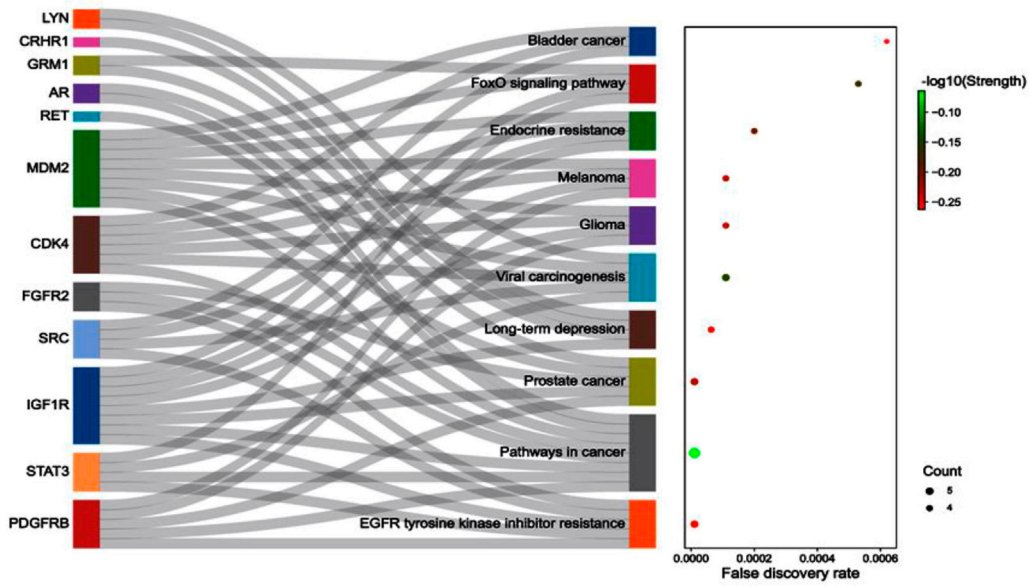

FIGURE 4
The associated protein-pathways interaction with respective false discovery rate and strength.

GO analysis

GO analysis identified 12 GO terms for cellular components in which receptor complex; GO:*0043235* had the lowest false discovery rate *i.e.,* 0.00025 regulated seven genes *i.e., PDGFRB*, *IGF1R*, *APP*, *RET*, *GRM1*, *FGFR2*, and *LYN* against 381 genes at 1.23 strength. Also, a total of 21 genes were triggered in multiple cellular components in which tyrosine-protein kinase Lyn (*LYN*) was majorly triggered in 11 cellular components except for cytoplasmic vesicles; GO:*0031410* (Supplementary File S1; Supplementary Sheet S1). In addition, the Pearson *p*-value for cellular components was 0.795 strength vs. false discovery rate, 0.0003 strength vs. observed gene count, 0.8093 false discovery rate vs. observed gene count, 2.684e-004 observed gene count vs. strength, and 0.809 observed gene count vs. false discovery rate. In addition, the minimum observed Pearson r was −0.084 and the maximum was 1.000 (Supplementary Figure S3). The proteins modulated by the diosgenin in the different cellular compartments are presented in Figure 5.

Likewise, 27 different molecular functions GO terms were identified *via* the PPI in which protein tyrosine kinase activity; GO:*0004713* had the lowest false discovery rate *i.e.,* 3.53E-05 to trigger six genes *i.e., PDGFRB*, *IGF1R*, *RET*, *SRC*, *FGFR2*, and *LYN* against 137 background genes at 1.61 strength. Herein, a total of 22 genes were triggered in 27 molecular functions in which proto-oncogene tyrosine-protein kinase Src (*SRC*) was involved in 18 molecular functions except hormone binding; GO:*0042562*, transmembrane receptor protein tyrosine kinase activity; GO: *0004714*, transition metal ion binding; GO:*0046914*, steroid hydroxylase activity; GO:*0008395*, oxygen binding; GO:*0019825*, nuclear receptor activity; GO:*0004879*, peptide hormone binding; GO:*0017046*, platelet-derived growth factor receptor binding; GO: *0005161*, and steroid-binding; GO:*0005496* (Supplementary File S1; Supplementary Sheet S3). Herein, the correlation *p* values were 0.130 strength vs. false discovery rate, 2.0510e-009 strength vs. observed gene count, and 0.753 false discovery rate vs. observed gene count. Within the interaction of strength, false discovery rate, and observed gene count, −0.877 and 1.000 were minimum and maximum r values for molecular function (Supplementary Figure S3).

Similarly, a total of 307 biological processes was traced due to PPI in which cellular response to oxygen-containing compound; GO:*1901701* had the lowest false discovery rate *i.e.,* 2.72E-09 in modulating 14 genes *i.e., NR3C1*, *CDK4*, *MDM2*, *PDGFRB*, *STAT3*, *IGF1R*, *APP*, *RET*, *PTPN1*, *SRC*, *AR*, *CRHR1*, *FGFR2*, and *LYN* against 1,055 background proteins at 1.09 strength. In addition, a total of 21 genes were triggered for 307 biological processes *via* the 21 proteins associated with breast cancer in which *SRC* was involved and linked with 213 biological processes. In addition, the order of triggered genes in multiple pathways was as *CYP17A1* (**17**) < *CYP3A4* (**22**) < *PRCP* (**33**) < *CRHR1* (**35**) < *FASN* (**42**) < *GRM1* (**52**) < *CYP19A1* (**59**) < *NR3C1* (**60**) < *MDM4* (**71**) < *CDK4* (**111**) < *IGF1R* (**113**) < *PTPN1* (**114**) < RET (**130**) < *MDM2* (**134**) < *AR* (**139**) < *STAT3* (**140**) < *FGFR2* (**149**) < *PDGFRB* (**160**) < *LYN* (161) < *APP* (**198**) < *SRC* (**213**). The detailed biological processes of participation of the above genes are supplemented in Supplementary File S1; Supplementary Sheet S4. The Pearson correlation *p*-value was found to be 0.034 strength vs. false discovery rate,

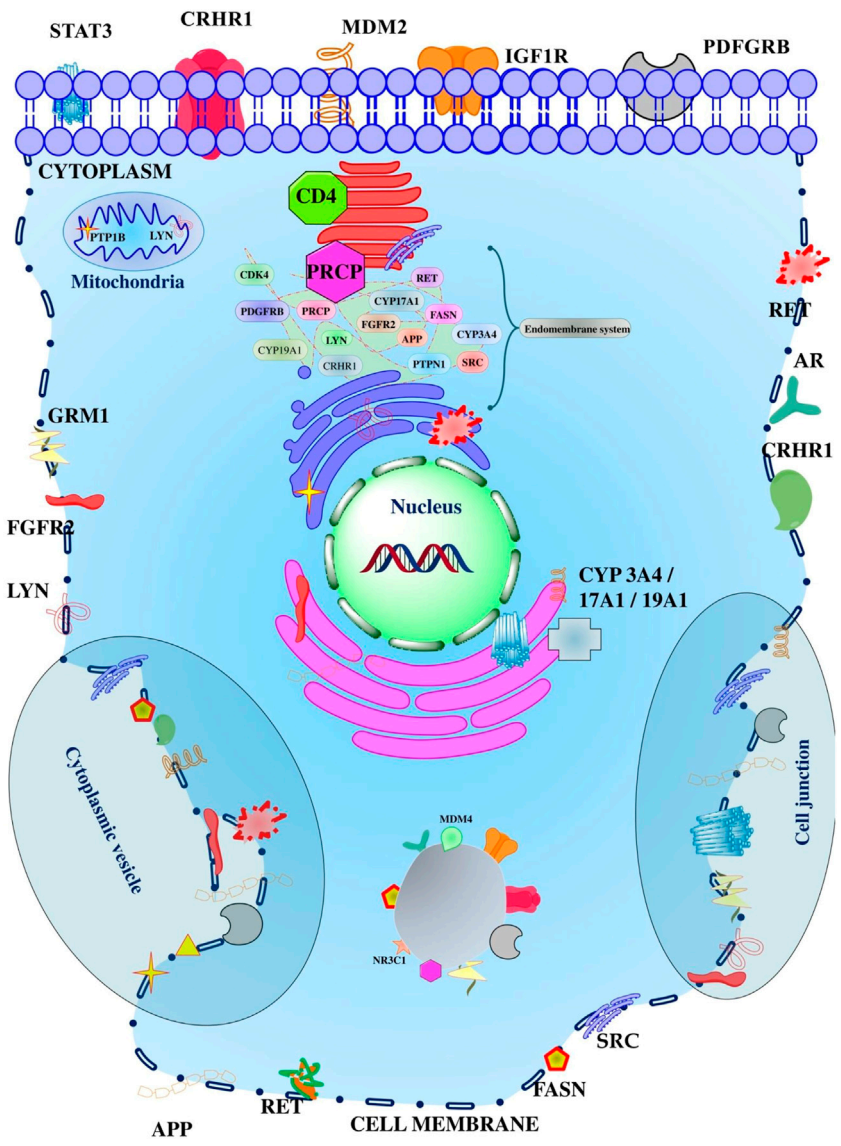

FIGURE 5
Different proteins affected by the diosgenin in the various compartment of the cell. The cellular organelles presented reflect the membrane-bounded organelle or intracellular organelle.

1.0622e-063 strength vs. observed gene count, and 8.1767e-017 false discovery rate vs. observed gene count. In addition, the minimum Pearson *r* values for biological processes were -0.779 and 1.000 respectively (Supplementary Figure S3).

Compartments enrichment analysis

The PPI reflected the modulation of proteins in 16 different compartments in which the intrinsic component of plasma membrane; GOCC:*0031226* had the lowest false discovery rate *i.e.*, 0.00027 in regulating nine genes *i.e.*, *PDGFRB*, *STAT3*, *IGF1R*, *APP*, *RET*, *GRM1*, *CRHR1*, *FGFR2*, and *LYN* against 841 background genes at 1 strength. Herein, a total 21 were triggered in 16 compartments in which *LYN* was traced in all; the order of genes regulation in multiple enriched compartments was *MDM4* (**5**) < *NR3C1* (**6**) = *AR* (**6**) < *CYP17A1* (**7**) < *CYP19A1* (**8**) = *CYP3A4* (**8**) = *CDK4* (**8**) = *GRM1* (**8**) = *MDM2* (**8**) < *FASN* (**9**) = *PDGFRB* (**9**) = *PRCP* (**9**) = *PTPN1* (**9**) = *SRC* (**9**) < *CRHR1* (**12**) = *FGFR2* (**12**) < *IGF1R* (**13**) < *RET* (**14**) = *STAT3* (**14**) < *APP* (**15**) < *LYN* (**16**); Supplementary File S1; Supplementary Sheet S5.

InterPro enrichment analysis

Protein-protein enrichment analysis traced seven InterPro in which tyrosine-protein kinase, catalytic domain; *IPR020635* was

traced with minimum false discovery rate *i.e.,* 8.42E-06 to regulate six genes *i.e., PDGFRB*, *IGF1R*, *RET*, *SRC*, *FGFR2*, and *LYN* against 79 background genes at 1.85 strength. Herein, in the enrichment of InterPro analysis, a total of nine genes were triggered in order as *MDM2* (**1**) = *MDM4* (**1**) < *CDK4* (**3**) < *FGFR2* (**6**) = *IGF1R* (**6**) = *LYN* (**6**) = *PDGFRB* (**6**) = *RET* (**6**) = *SRC* (**6**); Supplementary File S1; Supplementary Sheet S6.

Pfam enrichment analysis

Enrichment analysis concerning to Pfam database traced the regulation of protein kinase domain; *PF00069* and protein tyrosine kinase; *PF07714* at the false discovery rate of 0.0068 to regulate seven genes *i.e., CDK4*, *PDGFRB*, *IGF1R*, *RET*, *SRC*, *FGFR2*, and *LYN* at 1.13 strength against 486 and 481 background genes respectively; Supplementary File S1; Supplementary Sheet S7.

Tissues enrichment analysis

Enrichment analysis of PPI for TISSUES traced 13 different TISSUES terms in which erythroleukemia cell; BTO:*0000426* was traced with the lowest false discovery rate *i.e.,* 0.0088 in regulating five genes *i.e., MDM2*, *STAT3*, *PTPN1*, *SRC*, and *LYN* at 1.32 strength against 225 background genes. Herein, there was a regulation of 21 genes *i.e. APP*, *AR*, *CDK4*, *CRHR1*, *CYP17A1*, *CYP19A1*, *CYP3A4*, *FASN*, *FGFR2*, *GRM1*, *IGF1R*, *LYN*, *MDM2*, *MDM4*, *NR3C1*, *PDGFRB*, *PRCP*, *PTPN1*, *RET*, *SRC*, and *STAT3* in which nuclear receptor subfamily 3, group C, member 1 (*NR3C1*) was majorly triggered in 10 different TISSUES *i.e.* bone marrow cancer cell (BTO:*0000583*), organism form (BTO:*0000284*), leukemia cell (BTO:*0001271*), fibroblast (BTO:*0000452*), liver (BTO:*0000759*), whole body (BTO:*0001489*), reproductive system (BTO:*0000081*), embryonic structure (BTO:*0000174*), endocrine gland (BTO:*0001488*) and connective tissue (BTO:*0000421*); Supplementary File S1; Supplementary Sheet S8.

Cluster analysis

K means analysis of PPI against the whole genome of *Homo sapiens* traced three sets of clusters which are indicated by red (cluster 1; included *AR*, *CYP17A1*, *CYP19A1*, *CYP3A4*, *FASN*, *NR3C1*, and *PRCP*), green (cluster 2; included *APP*, *CDK4*, *CRHR1*, *FGFR2*, *GRM1*, *IGF1R*, *LYN*, *PDGFRB*, *PTPN1*, *RET*, *SRC*, and *STAT3*) and blue (cluster 3; included *MDM2* and *MDM4*); Supplementary Table S1.

In cluster 1, the interaction of seven nodes corresponded to 11 edges with 3.14 average node degree, 0.8 average local clustering coefficients, 1 expected edge, and 1.07e-09 PPI enrichment *p*-value. Herein, a total of nine molecular functions were traced in which steroid hydroxylase activity (GO:*0008395*) and oxygen binding (GO:*0019825*) scored the lowest false discovery rate *i.e.,* 0.0013 *via* the regulation of three genes *i.e., CYP3A4*, *CYP17A1*, and *CYP19A1* against 36 background genes at 2.37 strength. Similarly, Steroid binding (GO:*0005496*) showed 0.0082 false discovery rate and regulated three genes *i.e., NR3C1*, *CYP3A4*, and *AR* against 104 background genes at a strength of 1.91. Similarly, two KEGG pathways *i.e.,* steroid hormone biosynthesis (*hsa00140*) and ovarian steroidogenesis (*hsa04913*) were traced. Herein, steroid hormone biosynthesis was identified with a false discovery rate of 0.00048 to regulate three genes *i.e., CYP3A4*, *CYP17A1*, and *CYP19A1* against 59 background genes at 2.15 strength. In addition, ovarian steroidogenesis regulated two genes *i.e., CYP17A1* and *CYP19A1* against 50 genes at 2.05 strength and 0.0327 false discovery rate. Also, two different biological processes *i.e.,* androgen metabolic process (GO:*0008209*) and organic cyclic compound biosynthetic process (GO:*1901362*) were identified to regulate three genes *i.e., CYP3A4*, *CYP17A1*, and *CYP19A1* against 27 background genes at 2.47 strength and 0.002 false discovery rate and six genes (*NR3C1*, *FASN*, *CYP3A4*, *CYP17A1*, *AR*, and *CYP19A1I*) against 1,211 background genes at 1.14 strength and 0.0033 respectively (Supplementary File S2; Supplementary Sheet S1).

In cluster 2, 12 protein interactions traced 25 edges with 4.17 average node degree, 0.843 average local clustering coefficient, seven expected edges, and 3.83e-07 PPI enrichment *p*-value. Herein, a total of 25 enriched cellular components were traced in which receptor complex (GO:*0043235*), an integral component of the plasma membrane (GO:*0005887*), and cell junction (GO:*0030054*) were majorly enriched at a false discovery rate of 2.03E-06, 0.001, and 0.0033 and strength of 1.48, 0.91, and 0.8 respectively. Herein, the receptor complex was enriched with seven genes *i.e., PDGFRB*, *IGF1R*, *APP*, *RET*, *GRM1*, *FGFR2*, and *LYN*, an integral component of the plasma membrane with eight genes *i.e., PDGFRB*, *IGF1R*, *APP*, *RET*, *GRM1*, *CRHR1*, *FGFR2*, and *LYN* and cell junction with eight genes *i.e., CDK4*, *PDGFRB*, *STAT3*, *APP*, *GRM1*, *SRC*, *FGFR2*, and *LYN*. Also, a total of 21 enriched molecular functions were traced for cluster 2 in which protein tyrosine kinase activity; GO:*0004713* (regulated six genes *i.e. PDGFRB*, *IGF1R*, *RET*, *SRC*, *FGFR2*, and *LYN* against 137 background genes at 1.85 strength and 6.36E-07 false discovery rate), insulin receptor binding; GO:*0005158* (regulated four genes *i.e. IGF1R*, *APP*, *PTPN1*, and *SRC* against 24 background genes at 2.43 strength and 4.29E-06 false discovery rate) and ephrin receptor binding; GO:*0046875* (regulated four genes *i.e. APP*, *PTPN1*, *SRC*, and *LYN* against 28 background genes at 2.37 strength and 5.02E-06 false discovery rate). A total of 45 KEGG pathways were traced within the PPI of cluster 2 in which *EGFR* tyrosine kinase inhibitor resistance; *hsa01521* (regulated five genes *i.e. PDGFRB*, *STAT3*, *IGF1R*, *SRC*, and *FGFR2* against 78 background genes at 2.02 strength and 4.26E-07 false discovery rate), long-term depression; *hsa04730* (regulated four genes *i.e. IGF1R*, *GRM1*, *CRHR1*, and *LYN* against 59 background genes at 2.04 strength and 1.07E-05 false discovery rate), and pathways in cancer;

hsa05200 (regulated six genes *i.e. CDK4*, *PDGFRB*, *STAT3*, *IGF1R*, *RET*, and *FGFR2* against 517 background genes at 1.28 strength and 4.31E-05 false discovery rate) were identified to be top three majorly triggered pathways. Similarly, a total of 222 biological processes were traced within the PPI of cluster 2 in which cellular response to oxygen-containing compound; GO:*1901701* (regulated 11 genes *i.e. CDK4*, *PDGFRB*, *STAT3*, *IGF1R*, *APP*, *RET*, *PTPN1*, *SRC*, *CRHR1*, *FGFR2*, and *LYN* against 1,055 background genes at 1.23 strength and 2.37E-09 false discovery rate), regulation of protein serine/threonine kinase activity; GO:*0071900* (regulated nine genes *i.e. CDK4*, *PDGFRB*, *IGF1R*, *APP*, *RET*, *GRM1*, *PTPN1*, *SRC*, and *LYN* against 521 genes at 1.45 strength and 1.31E-08 false discovery rate), and regulation of protein phosphorylation; GO:*0001932* (regulated 11 genes *i.e. CDK4*, *PDGFRB*, *STAT3*, *IGF1R*, *APP*, *RET*, *GRM1*, *PTPN1*, *SRC*, *FGFR2*, and *LYN* against 1,459 background genes at 1.09 strength and 1.93E-08 false discovery rate (Supplementary File S2; Supplementary Sheet S2).

In cluster 3 the interaction of the nodes had 1 edge count, average node degree, and average local clustering coefficient with 0.0398 PPI enrichment *p*-values. Here, only two KEGG pathways and eight biological processes were traced. In KEGG pathways, the p53 signaling pathway; *hsa04115,* and microRNAs in cancer; *hsa05206* were associated with two genes *i.e., MDM2* and *MDM4* against 72 and 160 background genes, 2.43 and 2.09 strength and 0.0064 and 0.0155 false discovery rate respectively. Further, interaction between *MDM2* and *MDM4* triggered eight biological processes *i.e.* atrioventricular valve morphogenesis; GO:*0003181* (24 background genes at 2.91 strength and 0.0274 false discovery rate), endocardial cushion morphogenesis; GO:*0003203* (34 background genes at 2.76 strength and 0.0274 false discovery rate), ventricular septum development; GO:*0003281* (73 background genes at 2.43 strength and 0.0274 false discovery rate), atrial septum development; GO:*0003283* (23 background genes at 2.93 strength and 0.0274 false discovery rate), DNA damage response, signal transduction by p53 class mediator resulting in cell cycle arrest; GO:*0006977* (59 background genes, 2.52 strength and 0.0274 false discovery rate), negative regulation of cell cycle arrest; GO:*0071157* (23 background genes, 2.93 strength and 0.0274 false discovery rate), regulation of signal transduction by p53 class mediator; GO:*1901796* (182 background genes, 2.03 strength, and 0.0376 false discovery rate), and cellular response to hypoxia; GO:*0071456* (189 background genes, 2.02 strength and 0.0395 false discovery rate); Supplementary File S2; Supplementary Sheet S3.

Diosgenin-targets-protein network analysis

The combined interaction between the diosgenin, its targets, and regulated pathways traced *IGF1R*, *MDM2*, *SRC*, *CDK4*, and *PDGFRB* as the top five lead hub proteins. In addition, pathways in cancer; *hsa05200*, *EGFR* tyrosine kinase inhibitor resistance;

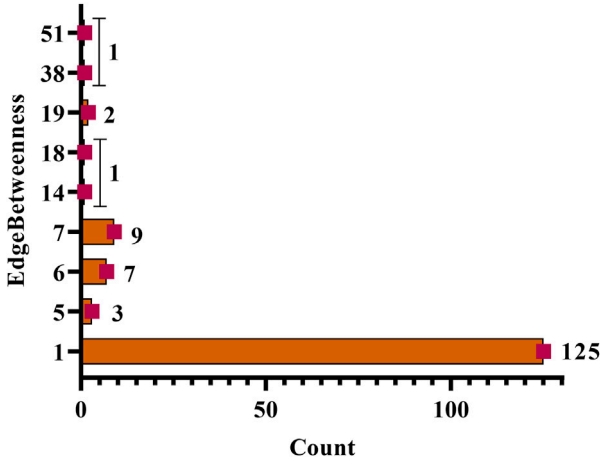

FIGURE 6
Edgebetweenness of network interaction and node interaction count. The highest edge betweenness was 51 (1 interaction) and the lowest was 1 (125 interactions).

hsa01521 prostate cancer; *hsa05215*, viral carcinogenesis; *hsa05203*, and PI3K-Akt signaling pathway; *hsa04151* were traced as the top five lead hub pathways modulated within diosgenin-targets-pathways interactions.

In diosgenin-targets-pathways interactions, none of the nodes were single or undirected. Herein, two pathways' nodes *i.e.,* adherens junction and central carbon metabolism in cancer had a maximum average shortest path length *i.e.,* 2.67. Herein, 33 nodes *i.e.* diosgenin, PI3K-Akt signaling pathway, *EGFR* tyrosine kinase inhibitor resistance, viral carcinogenesis, prostate cancer, endocrine resistance, proteoglycans in cancer, glioma, melanoma, human cytomegalovirus infection, endocytosis, Rap1 signaling pathway, FoxO signaling pathway, Kaposi sarcoma-associated herpesvirus infection, Epstein-Barr virus infection, MicroRNAs in cancer, long-term depression, focal adhesion, bladder cancer, signaling pathways regulating pluripotency of stem cells, Ras signaling pathway, *MAPK* signaling pathway, regulation of actin cytoskeleton, chemokine signaling pathway, p53 signaling pathway, prolactin signaling pathway, gap junction, ovarian steroidogenesis, Cushing syndrome, chronic myeloid leukemia, non-small cell lung cancer, pancreatic cancer, and epithelial cell signaling in *Helicobacter pylori* infection had the maximum closeness centralities *i.e.* 1. Further, the *CYP3A4* node had the maximum clustering coefficient *i.e.,* 0.5. Likewise, three pathways nodes *i.e.,* adherens junction, central carbon metabolism in cancer, and pathways in cancer had maximum eccentricity *i.e.,* 3. In addition, node diosgenin had the maximum stress *i.e.,* 101 followed by 21°, 0.03 betweenness centrality, 21 directed nodes, 0.85 radiality, 22 edge count, and, 19 outdegrees. Further, four nodes i.e. *NR3C1*, *PRCP*, *APP*,

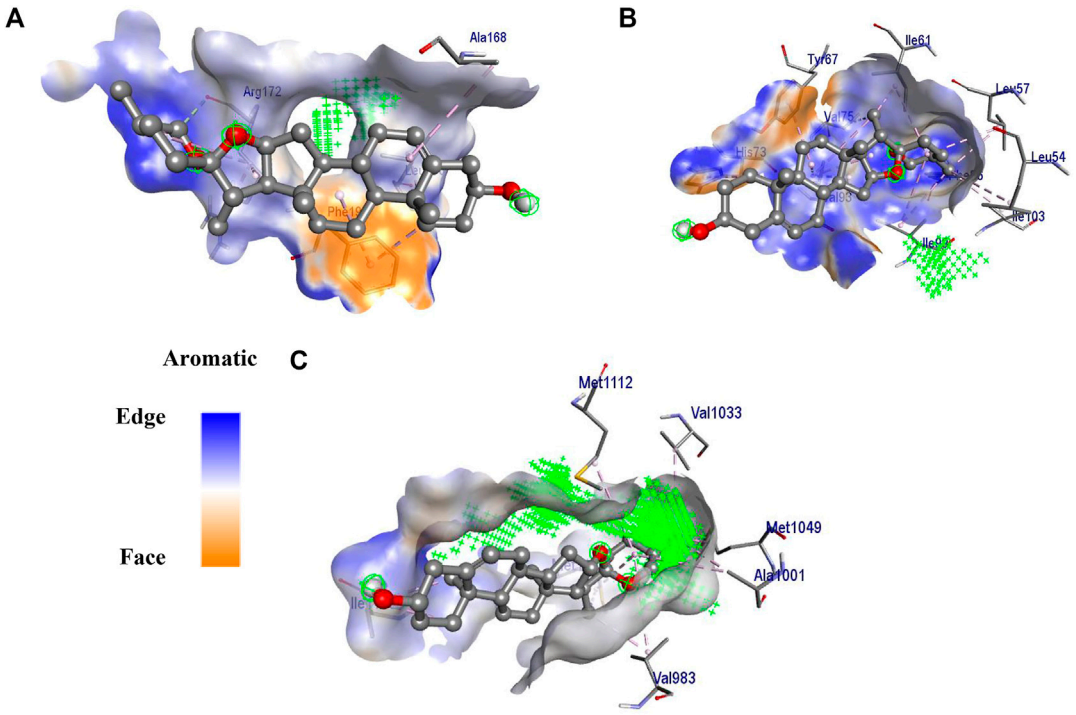

FIGURE 7
3D interaction of diosgenin with **(A)** *SRC*, **(B)** *MDM2* and **(C)** *IGF1R*. The surface around the ligand presents an aromatic surface. The ligand was presented in ball and stick. Amino acid residues were presented on a stick and the active site of the protein was presented with +++.

and *FASN* had maximum neighborhood connectivity *i.e.,* 22. In addition, the *AR* node had the maximum topological coefficient *i.e.,* 0.79 and *IGF1R* had maximum indegree *i.e.,* 19 (Supplementary File S3; Supplementary Sheet S1).

In a network a total of nine categories of edge betweenness were traced *i.e.,* 1 (125 interactions), 5 (3 interactions), 6 (7 interactions), 7 (9 interactions), 19 (2 interactions), 14, 18, 38, and 51 had the 1 interaction (Figure 6). Herein, within the whole network, 51 edge betweenness was within the *RET* and diosgenin interaction, 38 with *PTP1B* and diosgenin interaction, 19 with adherens junction interaction with *PTPN1*, and central carbon metabolism in cancer interaction with *RET*, 18 with steroid hormone biosynthesis with diosgenin, and 14 with pathways in cancer with *RET* (Supplementary File S3; Supplementary Sheet S2).

Molecular docking

Among the three studied targets, diosgenin was predicted to possess a maximum binding affinity with *IGF1R* (ΔG = −8.6 kcal/mol, 11 alkyl interactions with *Val983*, *Met1126*, *Val1033*, *Met1112*, *Met1049*, *Ala1001*, and *Ile1130*) compared to *MDM2* (ΔG = -8.5 kcal/mol, 16 alkyl interactions with *Ile61*, *Val75*, *Phe86*, *Ile99*, *Leu54*, *Ile103*, *Leu57*, *Val93*, *Tyr67*, and *His73* and three van der Walls interactions with *Phe91*, *Gly58*, and *His96*) and *SRC* (ΔG = -7.4 kcal/mol, five alkyl interactions with *Phe194*, *Leu200*, and *Ala168*, four van der Waals interaction and three carbon-hydrogen bond with *Arg172*); Figure 7.

Molecular dynamics simulation

Stability of diosgenin–*IGF1R* complex

The diosgenin-*IGF1R* complex showed stable dynamics up to 150 ns after a 20 ns equilibration phase. Initial backbone and complex RMSD values climbed steadily increased from 1.0 Å to 3.1 Å and ~1.4 Å to ~3.7 Å, respectively from 0 to 20 ns After 20 ns, it was discovered that the backbone and complex RMSD (~2.5 Å and 3.0 Å, respectively) were stabilized with lesser fluctuations (Figure 8A). The loop-forming residues *Leu1064* to *Pro1077* showed comparatively greater fluctuations (7.0 Å). On the other hand, residues *Leu975*, *Val983*, *Ala1001*, *Glu1050*, *Asp1123*, and *Ile1130* that interacted with diosgenin during docking studies didn't exhibit fluctuation because they were involved in stable non-bonded interactions. Additionally, it was discovered that residues *Gly1122* to *Tyr1131* forming the loop region were involved in ligand binding and showed the least RMS fluctuation (~2.0 Å) (Figure 8B, Supplementary Movie S1). There was a formation of a compact globular shape, which was supported by a gradual drop in R*g* value from 20.5 Å to 19.6 Å and was further found to be stable at 20.0 Å (Figure 8C). The initial and final surface

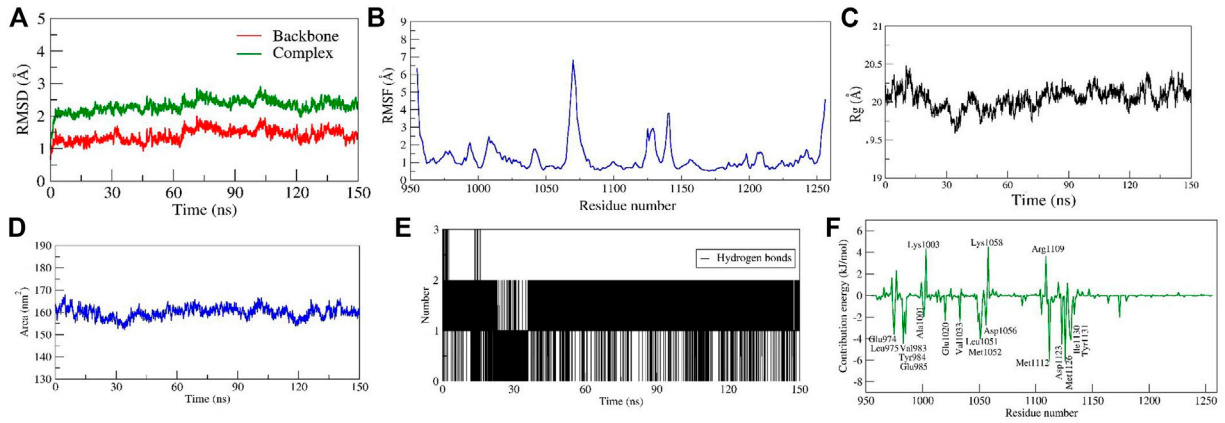

FIGURE 8
Parameters representing the structural stability of the Diosgenin-IGF1R complex. **(A)** Backbone and complex RMSD, **(B)** RMSF, **(C)** Rg, **(D)** SASA, **(E)** number of H-bond interactions, and **(F)** contribution energy plot demonstrates the significance of the ligand binding domain residues in stable complex formation.

area occupied by *IGF1R* and diosgenin docked complex was 163.825 nm^2 and 159.1106 nm^2. The complex typically occupied 159.95 nm^2 (Figure 8D). The complex formed 3 H-bonds of which two were consistent during the simulation (Figure 8E). It was discovered that diosgenin and *IGF1R* had relative binding energy of −35.143 ± 3.03 kcal/mol. Supplementary Table S2 summarizes the free energy contribution of diosgenin with *IGF1R*, *MDM2*, and *SRC*. The per residue contribution energy revealed that 16 residues from the binding pocket i.e. *Glu974*, *Leu975*, *Val983*, *Tyr984*, *Glu985*, *Ala1001*, *Glu1020*, *Val1033*, *Leu1051*, *Met1052*, *Asp1056*, *Met1112*, *Asp1123*, *Met1126*, *Ile1130*, and *Tyr1131* significantly contributed to the formation of a stable complex. These residues also scored the least per residue decomposition/contribution energy which ranged from −2.0 kJ/mol to −6.8 kJ/mol whereas the positive contribution energy of 4.0 kJ/mol was achieved by residues *Lys1003*, *Lys1058*, and *Arg1109* (Figure 8F).

Stability of diosgenin–*MDM2* complex

Throughout a 150 ns production run, the Diosgenin-*MDM2* complex exhibited stable dynamics. The initial and final backbone RMSD values were 0.62 and 1.21, respectively, and an average was 1.40 Å. Similar to this, the initial and final RMSD of the docked complex *MDM2* and diosgenin were 0.92 and 2.13 respectively with an average of ~2.30 Å (Figure 9A). The loop forming *Met17* to *Ser22* residues at the N-terminus had substantially greater fluctuations (~4.2 Å). Further, residues interacting with diosgenin during docking studies (*Leu57*, *Tyr67*, *Phe91*, *Val93*, and *Ile99*) did not exhibit variations as they were involved in stable non-bonded interactions (Figure 9B and Supplementary Movie S2). By monitoring a stable Rg, a more compact and stable complex was formed. The complex's initial and final Rg values were determined to be 13.2 Å and 1.31 Å. Similarly, the initial and final surface area occupied by *IGF1R* and diosgenin docked complex was 63.90 nm^2 and 61.57 nm^2. The complex had an average surface area of 62.89 nm^2 (Figure 9D). Two H-bonds were established by the complex of which one was consistent during MD simulation (Figure 9E). The relative binding energy between diosgenin and *IGF1R* was discovered to be −34.619 ± 2.81 kcal/mol. Further, seven residues (*Leu57*, *Gly58*, *Ile61*, *Met62*, *Tyr67*, *Val93*, and *Ile99*) from the binding pocket scored the lowest per residue decomposition/contribution energy, ranging from −3.65 kJ/mol to −8.87 kJ/mol. These residues contributed significantly to forming the stable complex according to the per residue decomposition/contribution energy. The residue *Glu69* had positive contribution energy of 2.68 kJ/mol (Figure 9F).

Stability of diosgenin–*SRC* complex

Another diosgenin–*SRC* complex also showed stable dynamics with the RMSD value of < 2Å after the equilibration period of 50 ns(Figure 10A). In addition, the RMSD of the complex showed a sharp increase in its values after 40 ns to 8 Å (Figure 10A). The careful observation of the entire complex trajectory and representative snapshots extracted from the region reveal the structural transition of diosgenin from its primary binding pocket to the neighboring alternate pocket which formed a stable complex during the entire simulation period. Thus, for the first time, we report the existence of an alternate binding site other than the primary binding site on *SRC*. From the simulation movie (Supplementary Movie S3) it was observed that the complex undergoes major conformational changes in the

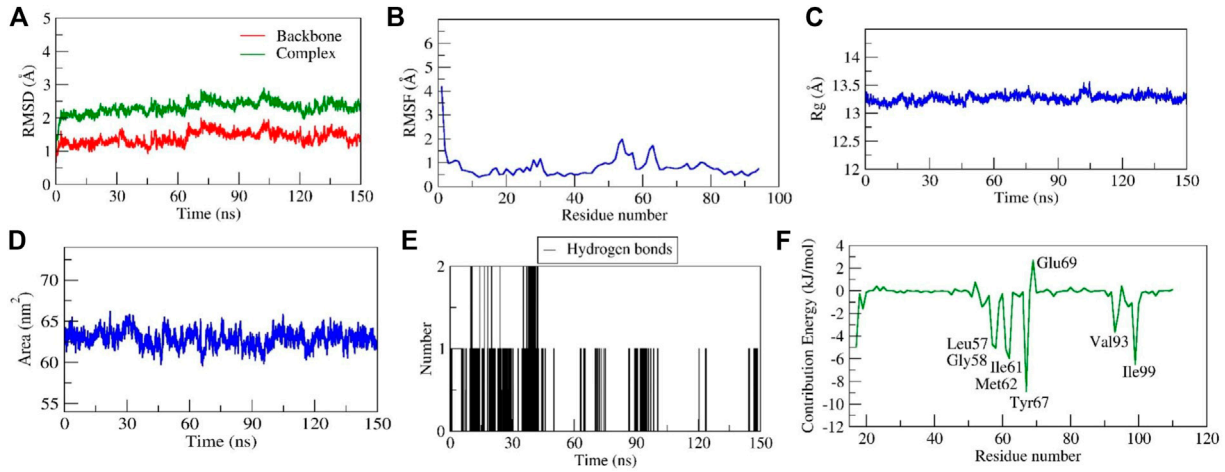

FIGURE 9
Parameters representing the structural stability of the Diosgenin-MDM2 complex. **(A)** Backbone and complex RMSD, **(B)** RMSF, **(C)** Rg, **(D)** SASA, **(E)** number of H-bond interactions, and **(F)** contribution energy plot demonstrates the significance of the ligand binding domain residues in stable complex formation.

secondary structure of the protein including the primary binding pocket, leading to the increased conformational flexibility of *SRC*, hence the diosgenin switches its original position from the primary binding pocket to the reported alternate binding pocket (formed by the residues *Tyr152* to *Leu164*). The residual fluctuations observed show fewer C-alpha fluctuations (<2.2Å), interestingly the residues from the primary binding pocket as well as new reported alternate binding pocket show the least RMSF values ~0.5Å (Figure 10B), mainly due to the stable non-bonded interactions shown by them. The complex diosgenin–*SRC* gains a compact globular shape during the simulation, thus we propose the stable complex formation was favored after the equilibration period of MD simulation (Figure 10C). The solvent-accessible surface area represents an exposure of the hydrophobic residues to the solvent, here in this complex SASA exhibited a similar trend as that of Rg values. SASA value decreased gradually till the equilibration state and further, it stabilized till the simulation end (Figure 10D), suggesting the proper folding of the hydrophobic core including both the binding sites. Two H-bonds were established by the complex of which one was consistent during MD simulation (Figure 10E). The relative binding energy between diosgenin to *SRC* was discovered to be −17.994 ± 5.67 kcal/mol. In addition, three residues *i.e.*, *Ile156*, *Thr157*, and *Leu164* from the binding pocket scored the lowest energy contribution per residue. These residues contributed significantly to forming the stable complex according to the per residue decomposition/contribution energy. The residue *Ile156* had the least contribution energy of −8.9 kJ/mol (Figure 10F).

Principal component and dynamic cross-correlation matrix

PCA is a statistical technique being used to study the dynamics of bimolecular complexes as it limits the 3 N (N = number of atoms in the protein) degrees of freedom describing functionally crucial motions of the protein. It was observed that in all the complexes maximum dynamics during the simulation have been captured by the first 10 eigenvectors, of which the first two contributed significantly to the collective motions exerted by all the simulated complexes (Figures 14A–C). Hence, we examined the collective motion sampled by the first two principal components (PCs), and 2D projections for PC1 and PC2 were plotted (Figures 11D–F). The complexes of diosgenin with *MDM2* and *SRC* express the compact clusters in the conformational spaces those range from -1.5 to 1.5. In the MD trajectory of complexes Diosgenin-*SRC* and Diosgenin-*MDM2*, PC1 and PC2 (top two modes) showed the uniform distribution across the configurational space while the remaining complex of Diosgenin-*IGF1R* showed a large diversity in the conformational space and was widely clustered in the range of -4.5 to 4.5 (Figure 11D). MD trajectory sampled three states of the protein as seen by the three individual clusters in the scatterplot of PC1 v/s PC2. Herein, we propose that the Diosgenin-*IGF1R* complex has undergone significant conformational changes in the secondary structure during the simulation those favored in forming a stable complex. However, other complexes namely Diosgenin-*SRC* and Diosgenin-*MDM2* were well stabilized and undergone comparatively lesser conformational changes in the secondary structure hence exhibited compact cluster in the conformations space. Further, the convergence of sampling was also analyzed by calculating the

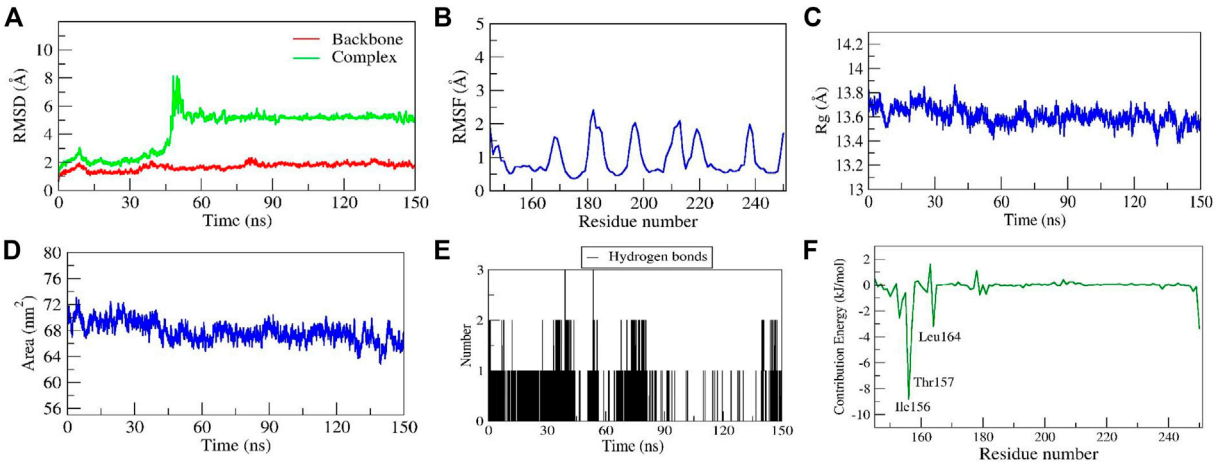

FIGURE 10
Parameters representing the structural stability of the Diosgenin-SRC complex. **(A)** Backbone and complex RMSD, **(B)** RMSF, **(C)** Rg, **(D)** SASA, **(E)** number of H-bond interactions, and **(F)** contribution energy plot demonstrates the significance of the ligand binding domain residues in stable complex formation.

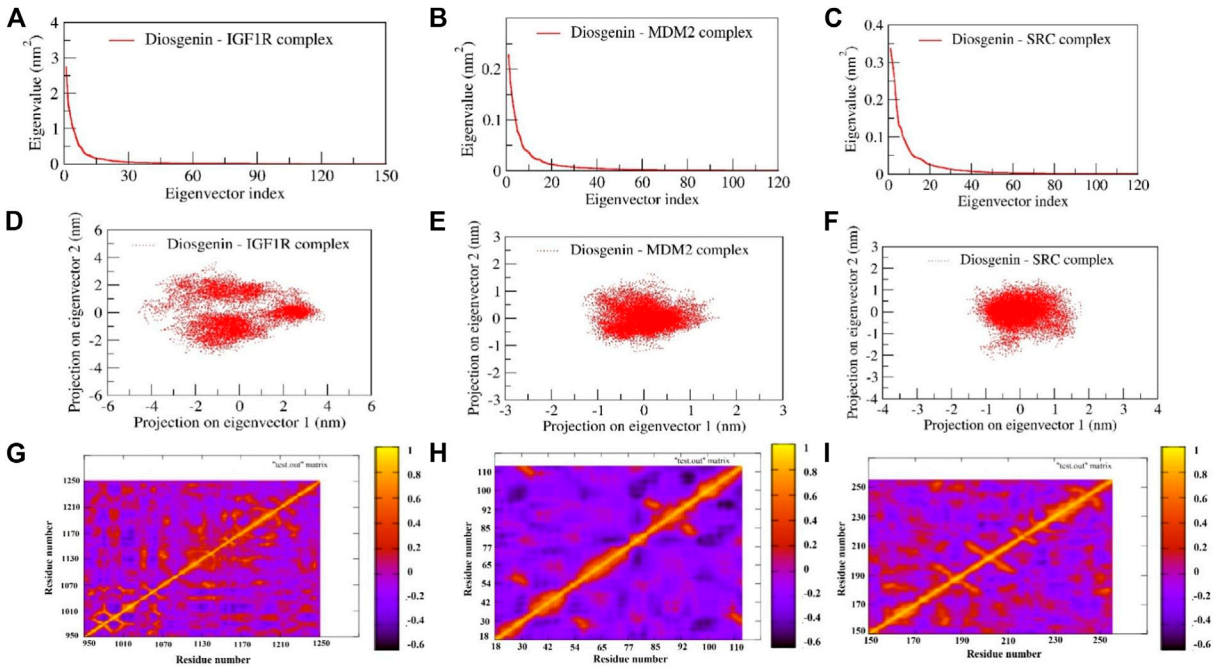

FIGURE 11
Represents the principal component analysis and dynamic cross-correlation matrix of complexes: The first 120 eigenvectors were plotted v/s eigenvalues for diosgenin with **(A)** *IGF1R* **(B)** *MDM2*, and **(C)** *SRC*. The collective motions of diosgenin with **(D)** *IGF1R* **(E)** *MDM2*, and **(F)** *SRC* using projections of MD trajectories on two eigenvectors corresponding to the first two principal components. Dynamic cross-correlation matrix of Cα atoms observed in diosgenin with **(G)** *IGF1R* **(H)** *MDM2*, and **(I)** *SRC*. The amber-colored positive regions reflect strongly correlated Cα atom movements (C*ij* = 1), whereas the blue-colored negative regions show anticorrelated motions (C*ij* = -1).

cosine content of all the trajectories obtained. The cosine content was calculated for the trajectories of the first top two principal components (PC1 and PC2) for complexes Diosgenin-*SRC* and Diosgenin-*MDM2*, and Diosgenin-*IGF1R* is observed as 0.024225, 0.0175249 and 0.158163 respectively. It has been reported that the value of cosine content for the first few PCs

close to 1 indicated bad sampling of the trajectory pointing to all our simulation trajectories being well converged and properly sampled in the free energy landscape.

The concerted motion exerted by the three complexes during the simulation was examined using DCCM (dynamic cross-correlation matrix). The calculation of the correlation matrix is utilized to depict the dynamical information of proteins in two dimensions. To observe the correlation in the dynamics of the binding site correlation matrix over the stable trajectory of all the complexes were plotted (Figures 11F,G). The diagonal orange-red line indicates the self-correlation of the individual residues with themselves. The orange-red region in the correlation map signifies the concerted movement of the residues in the same direction whereas the dark blue region represents anti-correlated fluctuations. The N- and C-terminal region of the complex Diosgenin-*MDM2* represents strong anticooperative movement with each other. Comparatively, this complex exhibited a maximum amplitude of negative correlation across all the residues. The maximum region in the complex Diosgenin-*IGF1R* showed positive correlation mainly at the binding pocket region (residues *Glu974, Leu975, Val983, Tyr984, Glu985, Ala1001, Glu1020, Val1033, Leu1051, Met1052, Asp1056, Met1112, Asp1123, Met1126, Ile1130,* and *Tyr1131*). This signifies the closure movement observed at the binding pocket region facilitating stable complex formation (Supplementary Movie S1). Similarly, in the Diosgenin-*SRC* complex, the binding pocket residues (*Arg158*, *Glu181*, *Thr182*, *Cys188*, *Lys203-Lys206*) showed moderately positive cooperative motion compared to other regions in the *SRC* structures. Interestingly, the residues from the alternate binding region show the cooperative motion results in stable non-bonded contact with the newly reported alternate binding pocket.

In general, the conformational flexibility of all the complexes *i.e.,* Diosgenin-*IGF1R*, Diosgenin-*MDM2*, and Diosgenin-*SRC* varies greatly as observed in the DCCM plot and the collective dynamics nature observed in the PCA and DCCM plot favors the stable complex formation during the simulation.

Survival analysis of hub genes

To evaluate the prognostic significance of genes, we analyzed the survival curves of each gene. Among 21 genes, 17 genes were observed to had the significant effect over the Kaplan–Meier survival analysis *i.e., APP* (log-rank $p = 0.0018$), *AR* (log-rank $p = 0.0033$), *CDK4* (log-rank $p = 0.0062$), *CYP19A1* (log-rank $p = 0.036$), *FGFR2* (log-rank $p = 2.9 \times 10^{-5}$), *GRM1* (log-rank $p = 0.027$), *IGF1R* (log-rank $p = 3.2 \times 10^{-05}$), *LYN* (log-rank $p = 0.017$), *MDM2* (log-rank $p = 0.0012$), *MDM4* (log-rank $p = 0.044$), *NR3C1* (log-rank $p = 0.00038$), *PDGFRB* (log-rank $p = 1.2 \times 10^{-06}$), *PRCP* (log-rank $p = 0.015$), *PTPN1* (log-rank $p = 0.00041$), *RET* (log-rank $p = 0.03$), *SRC* (log-rank $p = 0.0039$), and *STAT3* (log-rank $p = 1.4 \times 10^{-06}$). Similarly, four genes *i.e., CRHR1* (log-rank $p = 0.09$), *CYP17A1* (log-rank $p = 0.14$), *CYP3A4* (log-rank $p = 0.056$), and *FASN* (log-rank $p = 0.15$) were insignificantly linked with disease prognosis; Table S3.

Gene expression analysis in tumor, normal and metastatic tissues

Kruskal Wallis test revealed the significant expression (p = 5.96e-04) of the *PDGFRB* gene in breast invasive carcinoma compared to normal and metastatic samples. In addition, the similar observations were also noted for the *FGFR2* (p = 3.03e-08) and *STAT3* (p = 9.51e-02) genes. In addition, Dunn test pointed the difference in *PDGFRB* expression in the normal vs. tumor (p = 7.74e-05), tumor vs. metastasis (p = 5.66e-02), normal vs. metastasis (p = 2.61e-01), *FGFR2* in normal vs. tumor (p = 2.31e-04), tumor vs. metastasis (p = 2.98e-02), and normal vs. metastasis (p = 3.41e-01) and *STAT3* normal vs. tumor (p = 1.59e-02), tumor vs. metastasis (p = 4.26e-01), and normal vs. metastasis (p = 3.57e-01); Figure 12).

Among *IGF1R*, *SRC*, and *MDM2*, all the genes had a significant difference in gene expression compared to three different tissues *i.e., IGF1R* (p = 2.07e-01), *SRC* (p = 2.71e-18), and *MDM2* (p = 1.91e-02) which were evaluated using Kruskal Wallis test. In addition, there was a significant difference in *MDM2* expression in normal vs. tumor (p = 3.83e-03), tumor vs. metastasis (6.87e-02), and normal vs. metastasis (2.03e-01) as revealed by the Dunn test. Likewise, there was a significant difference in *SRC* expression in normal vs. tumor (p = 1.72e-19), tumor vs. metastasis (1.92e-03), and normal vs. metastasis (2.62e-01). Likewise, there was a significant difference in *IGF1R* expression in normal vs. tumor (p = 4.25e-02), tumor vs. metastasis (p = 4.91e-01), and normal vs. metastasis (p = 3.19e-01); Figure 13.

In vitro pharmacology

BSL bioassay

Exposure to the different concentrations of diosgenin and doxorubicin showed concentration-dependent brine shrimp lethality. In addition, the LC_{50} was found to be 19.15 and 0.71 μg/ml respectively reflecting the doxorubicin to be 27.06 times more potent than diosgenin (Supplementary Figure S4).

In vitro MTT assay

Here, the MTT assay showed the IC_{50} of the diosgenin to be significantly higher than that of the doxorubicin in MCF7 ($p < 0.001$), MDA-MB-231 ($p < 0.05$), SKBR3 ($p < 0.05$) and Vero ($p < 0.001$) compared to the doxorubicin. *In vitro* MTT assay on MCF7 cell lines reflected the doxorubicin (IC_{50} 3.21 ± 0.29 μg/ml) to be 3.7 times more potent than the diosgenin (IC_{50} 12.05 ± 1.33 μg/ml). In addition, over the MDA-MB-231 cell lines, the IC_{50} of diosgenin was found to be (45.54 ± 23.41) μg/ml compared to doxorubicin (6.30 ± 2.67) μg/ml which suggests the doxorubicin to be 7.2 times more potent than diosgenin. In addition, the diosgenin and doxorubicin had the IC_{50} (15.11 ± 5.32) μg/ml and (5.47 ± 1.09) μg/ml respectively over SKBR3 reflecting the doxorubicin to be 2.76 times more potent than that of diosgenin. In addition, the IC_{50} of diosgenin and doxorubicin was found to be (17.78 ± 7.86)

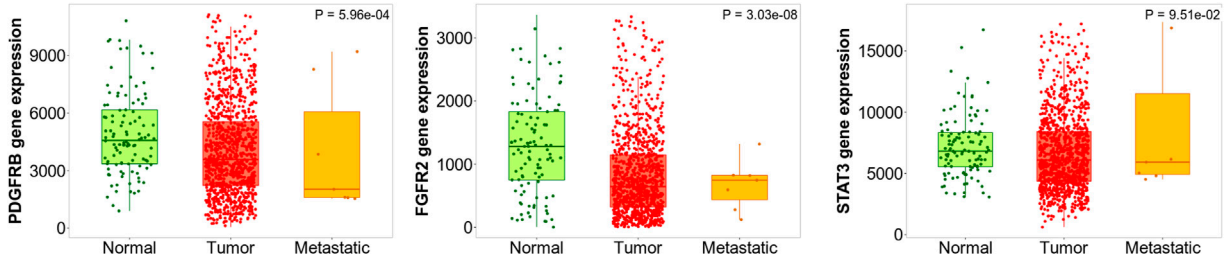

FIGURE 12
Differential gene expression analysis of *PDGFRB*, *FBFR2*, and *STAT3* in tumor, normal and metastatic tissues. These genes were identified to possess the least log-rank test.

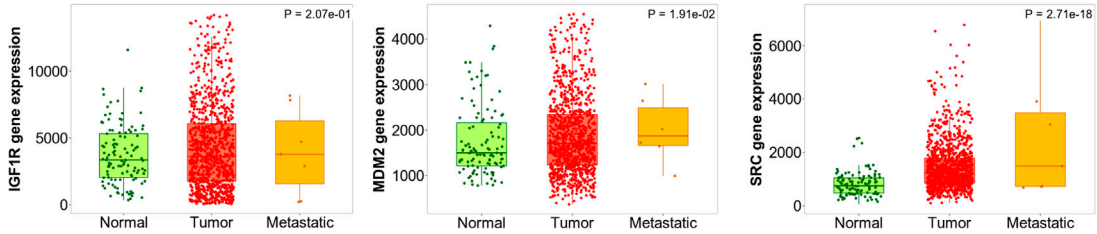

FIGURE 13
Differential gene expression analysis of *IGF1R*, *MDM2*, and *RSC* in tumor, normal and metastatic tissues. Diosgenin was predicted to possess the highest binding affinity with these targets.

and (8.18 ± 8.18) μg/ml respectively over the T47D cell lines to point doxorubicin to be 2.17 times more potent. Further, diosgenin and doxorubicin had the IC_{50} of (38.59 ± 4.03) and (7.05 ± 0.69) μg/ml respectively in which the doxorubicin was found to be 7 times more cytotoxic than Vero cell lines; Supplementary Figure S5; Supplementary Table S4.

In vitro scratch assay

After the 72-h exposure to different cells, it was observed that diosgenin (200 μg/ml) had the highest effect on SKBR3 cell lines (18.22 ± 1.237%) to prevent cell migration compared to the rest. In addition, we observed a significant difference in percentage scratch closure within MCF vs. SKBR3 ($p < 0.01$), MDA-MB-231 vs. SKBR3 ($p < 0.05$), SKBR3 vs. T47D ($p < 0.01$) and SKBR3 vs. Vero ($p < 0.001$) cell lines (Supplementary Figure S6). In addition, the concentration and time-dependent effect of the diosgenin on scratch closure are presented in Supplementary Figure S7.

Effect of diosgenin and doxorubicin over H_2O_2-induced stress in cell lines

Upon the 24 h exposure of the H_2O_2, it was observed that diosgenin has an equivalent effect to ascorbic acid over MCF cell lines with an IC_{50} (7.68 ± 0.51) μg/ml and (7.13 ± 0.31) μg/ml respectively. In addition, diosgenin and ascorbic acid showed the IC_{50} of (13.58 ± 0.90) μg/ml and (10.60 ± 1.60) μg/ml respectively over the MDA-MB-231 cell lines. However, diosgenin (IC_{50} 6.68 ± 0.67 μg/ml) had more effect over the SKBR3 compared to ascorbic acid (9.39 ± 3.09 μg/ml). Similarly, diosgenin and doxorubicin had the IC_{50} (8.90 ± 0.98) and (9.14 ± 0.78) μg/ml respectively over T47D cell lines. Further, the diosgenin and ascorbic acid had the IC_{50} (13.72 ± 1.83) μg/ml and (12.68 ± 4.53) μg/ml respectively over the Vero cell lines (Supplementary Table S5). The concentration-dependent effect of diosgenin and ascorbic acid is presented in Supplementary Figure S8.

Effect of diosgenin on Warburg effect

It was observed that diosgenin had efficacy in dealing glucose uptake in tumor cells. The EC_{50} of the diosgenin was observed to be significantly higher in glucose uptake in MCF7 ($p < 0.001$), SKBR3 ($p < 0.05$), T47D ($p < 0.001$), and Vero ($p < 0.01$) cell lines compared to metformin in the presence of insulin. It was observed that diosgenin had a comparatively higher EC_{50} (26.19 ± 2.77) μg/ml compared to metformin (3.10 ± 0.99) μg/ml which showed the diosgenin to possess a comparatively lower glucose uptake efficacy than metformin in

MCF7 cell lines. In addition, in MDA-MB-231 cell lines, diosgenin and metformin had an equivalent EC_{50} in promoting glucose uptake *i.e.,* EC_{50} (17.92 ± 1.19) and (17.03 ± 2.59) μg/ml respectively. Furthermore, it was observed that diosgenin had comparatively higher the EC_{50} in promoting the glucose uptake in SKBR3 (EC_{50} 19.99 ± 2.91 μg/ml), T47D (EC_{50} 37.47 ± 1.75 μg/ml), and Vero (EC_{50} 15.27 ± 0.95 μg/ml) compared to metformin (EC_{50} SKBR3; 11.74 ± 3.19 μg/ml, T47D; 12.50 ± 1.42 μg/ml, and Vero; 11.79 ± 1.65 μg/ml); Supplementary Table S6; Supplementary Figure S9

Discussion

The present study focused on tracing the targets of diosgenin and evaluates the probably triggered pathways *via* the PPI in breast cancer. In this regard initially, we predicted the targets using three open-source platforms *i.e.* SwissTargetPrediction, DIGEP-Pred, and BindingDB; matched with estrogen receptor-positive breast cancer targets (UMLS CUI: *C2938924*); retrieved from DisGeNET in which diosgenin was predicted to target 21 different proteins *i.e. APP*, *CDK4*, *CRHR1*, *CYP17A1*, *CYP19A1*, *CYP3A4*, *FASN*, *FGFR2*, *GRM1*, *IGF1R*, *LYN*, *MDM2*, *MDM4*, *PDGFRB*, *PRCP*, *PTPN1*, *RET*, and *SRC*, (predicted in SwissTargetPrediction) *AR* and *NR3C1* (predicted in DIGEP-Pred), and *STAT3* (predicted in SwissTargetPrediction and BindingDB) in the breast cancer. Herein concerning the KEGG database, it was observed that 36 different pathways were triggered in which 12 pathways *i.e.* pathways in cancer; *hsa05200*, prostate cancer; *hsa05215*, viral carcinogenesis; *hsa05203*, glioma; *hsa05214*, melanoma; *hsa05218*, bladder cancer; *hsa05219*, MicroRNAs in cancer; *hsa05206*, Kaposi sarcoma-associated herpesvirus infection; *hsa05167*, proteoglycans in cancer; *hsa05205*, central carbon metabolism in cancer; *hsa05230*, non-small cell lung cancer; *hsa05223*, and pancreatic cancer; *hsa05212* were identified which explores the anti-cancer pharmacological spectra of the diosgenin.

Breast cancer is one of the main causes of death among women. Chiefly, the cells lining the milk-forming duct of the mammary glands are the origination of breast cancer (Herbein and Kumar, 2014) which can be further subdivided based on the presence or absence of the hormone receptors *i.e.,* estrogen and progesterone subtypes and human epidermal growth factor receptor-2 (*HER2*). In addition, the estrogen receptor pathway triggers hormone receptor-positive breast cancer (Rani et al., 2019). Similarly, in *HER2*-positive breast cancer, *HER2* triggers RAS/RAF/MAPK and PI3K/AKT signaling pathways that stimulate cell growth, survival, and differentiation (Dittrich et al., 2014). We discovered 21 diosgenin-regulated proteins that are involved with oestrogen receptor-positive breast cancer (UMLS CUI: *C2938924*) targets in this investigation. In addition, three pathways *i.e.,* PI3K-Akt (modulated five genes *i.e., CDK4*, *MDM2*, *PDGFRB*, *IGF1R*, and *FGFR2*), Ras (modulated three genes *i.e., PDGFRB*, *IGF1R*, and *FGFR2*), and MAPK (modulated three genes *i.e., PDGFRB*, *IGF1R*, and *FGFR2*) signaling pathways associated to *HER2* positive breast cancer were modulated. Since diosgenin modulated three pathways closely associated with *HER2*-linked pathogenesis, it can be speculated that diosgenin could act *via* the manipulation of *HER2*.

It has previously been proposed that Akt activation influences endocrine resistance in metastatic breast cancer. In addition, Akt activation in the downstream pathway of *HER2* could resist the endocrine therapy of breast cancer (Tokunaga et al., 2006). Furthermore, Ras proteins activate the cytoplasm and extracellular signaling networks *via* receptor tyrosine kinase and are involved in cell proliferation, survival, growth, metabolism, motility, and apoptosis, and their hyperactivation promotes the growth and progression of breast cancer. In addition, Ras's intracellular localization, activation, and signaling have been used in developing therapeutic candidates against breast cancer *via* the enzymes involved in posttranslational modification of Ras *e.g.,* farnesyltransferase and geranylgeranyltransferase 1 (Moon, 2021). Further, *MAPK* links the extracellular mitogenic signals to cell proliferation which may be concerned with or act independently towards estrogen-mediated events in breast cancer cells (Yue et al., 2002). In the present study, we identified the modulation of the above-modulated pathways *i.e.,* PI3K-Akt signaling pathway (false discovery rate: 0.0011, strength: 1.12), Ras signaling pathway (false discovery rate: 0.0263, strength: 1.09), and MAPK signaling pathway (false discovery rate: 0.0446, strength: 0.99). This suggests the probability of involvement of these pathways linked to *HER2* function which could be modulated by diosgenin in breast cancer.

The role of *EGFR* dysregulation or mutation in cancer etiology, particularly breast cancer, has been proposed previously. However, resistance towards *EGFR* tyrosine kinase inhibitors may occur due to secondary mutations (T790M), activation of secondary pathways (AXL, c-Met, HGF), aberrant downstream pathways (K-RAS mutations, loss of *PTEN*), deregulation of the *EGFR* tyrosine kinase-mediated apoptosis, histological transformation, and ATP binding cassette transporter effusion, etc (Huang and Fu 2015).

The FoxO signaling system interacts with the PI3K-Akt signaling pathway and relates to cancer progression, particularly breast cancer advancement (Farhan et al., 2017). In addition, FoxO negatively regulates activated *EGFR* signaling which was demonstrated *via* the *in vitro* cell line culture method and *in vivo* models (Sangodkar et al., 2012). Here, in the present study, we identified the regulation of the FoxO signaling pathway *via* the modulation of four genes *i.e. MDM2*, *STAT3*, *IGF1R*, and *GRM1* which could support the functioning of the PI3K-Akt and *EGFR* signal against breast cancer pathogenesis.

Furthermore, the Rap1 signal has been linked to tumor cell proliferation, invasion, and metastasis through regulating integrin- or cadherin-mediated cell function, cytoskeletal alterations, protease (metal metalloprotease) production, and cell adhesion (Zhang et al., 2017). In addition, Rap1 has been traced to attenuate metastasis and *EGFR*-triggered carcinoma (Huang et al., 2012). Since breast cancer progression is closely linked to *EGFR* tyrosine kinase signal; it can be speculated that diosgenin-mediated Rap1 signal could attenuate tumor invasion and metastasis; was observed to be modulated *via* the modulation of three genes *i.e., PDGFRB*, *IGF1R*, and *FGFR2*.

The p53 acts as a transcription factor for p21 *via* cyclin-CDK interactions which is important for the transition of the G2 phase to the mitosis phase (Alam et al., 2015). In addition, p21 protects cells from apoptosis, regulates the cell cycle, causes apoptosis, and decreases cell proliferation in tumor cells (Wang et al., 2021). Mutant p53 has been pointed to as the guardian of the cancer cells (Mantovani et al., 2019) and is also associated with worsening breast cancer affecting overall survival (Gasco et al., 2002). In the present study, we identified the regulation of the three genes *i.e., CDK4*, *MDM2*, and *MDM4* which could activate the p53 signal against breast cancer. Furthermore, excessive plasma prolactin levels have been associated with an increased risk of breast cancer in both premenopausal and postmenopausal women; is more prominent in estrogen or progestogen receptor cancer type (Tworoger et al., 2004; Tworoger et al., 2006). Here, in the present study, we identified the diosgenin to regulate the prolactin signaling pathway *via* the regulation of three genes *i.e., STAT3*, *CYP17A1*, and *SRC* which could avoid estrogen or progestogen receptor-mediated breast cancer progression. In addition, chemokine signals are not limited to tissue differentiation, hematopoiesis, inflammation, and immune regulation but also process tumor development by triggering angiogenesis, metastasis, drug resistance, and immunity of breast cancer (Liu et al., 2020). In the present study, we identified the diosgenin to trigger the chemokine signaling pathway, and regulated three genes *i.e., STAT3*, *SRC*, and *LYN* at 1.18 strength and 0.0168 false discovery rate). In addition, in enrichment analysis *i.e.,* tissues, Pfam, InterPro, and compartments enrichment analysis we observed the multiple proteins that are concerned with the breast cancer prognosis.

Also, in the present study, we identified three proteins *i.e., IGF1R*, *MDM2*, and *SRC* in diosgenin-protein(s)-pathway(s) interaction. Hence, these were further considered for post-network analysis *i.e.,* molecular docking and molecular dynamics simulation. Apart from handling the transcription, *IGF1R* can trigger the growth and metastasis of malignant melanoma cells through the PI3K-Akt signaling pathway (Ekyalongo and Yee, 2017). Diosgenin was anticipated to interact with *IGF1R* in the current investigation, potentially preventing breast cancer metastasis and tumor invasion, which could be PI3K-Akt driven, as previously discussed.

The *IGF1R* is a transcription factor that binds to DNA and influence transcription. Both ERK1/2 and AKT are involved in the transcriptional control of the *IGF1R* gene. MicroRNA-139-5p modulates the growth and metastasis of malignant melanoma cells *via* the PI3K/AKT signaling pathway by binding to *IGF1R* (binding energy -8.6 kcal/mol). Previously, *MDM2* amplification has been reported to relate to estrogen receptor status and its presence has been indicated in human breast cancer cell (Quesnel et al., 1994); was observed to be manipulated with diosgenin in the third cluster of the PPI binding (binding energy −8.5 kcal/mol). Likewise, another modulated protein *i.e.,* SRC has been reported to increase its expression in human breast cancer by 4–30 fold which was evidenced *via* both immunohistochemistry and immunoblotting (Verbeek et al., 1996); was also predicted to be modulated by diosgenin interaction (binding energy -7.4 kcal/mol). In addition, since 17 genes i.e. *APP*, *AR*, *CDK4*, *CYP19A1*, *FGFR2*, *GRM1*, *IGF1R*, *LYN*, *MDM2*, *MDM4*, *NR3C1*, *PDGFRB*, *PRCP*, *PTPN1*, *RET*, *SRC*, and *STAT3* were observed to have a significant role in disease prognosis, it can be speculated that the above-modulated proteins are primarily concerned with breast cancer management with diosgenin treatment.

The docking study revealed diosgenin to interact with active site residues of three potential targets involved in breast cancer *via IGF1R, MDM2*, and *SRC*. Diosgenin formed stable intermolecular interactions throughout 150 ns MD simulation revealing them as the best lead. Among the interactions of diosgenin with *IGF1R*, diosgenin interactions with *Leu975, Val983, Met1112, Met1126*, and *Ile1130* were consistent in both docking and MD simulation. Multiple studies have demonstrated these residues involve the pocket as a primary binding site (also validated by PrankWeb server; https://prankweb.cz/) for inhibition of *IGF1R* (Munshi et al., 2002; Li et al., 2009; Guo et al., 2015). This indicates, that diosgenin as a potent lead hit against *IGF1R*. Similarly, diosgenin scored the lowest binding energy of -8.5 kcal/mol and binding free energy of -34.619 kcal/mol and formed stable interactions *Leu57*, *Gly58*, *Ile61*, *Met62*, *Tyr67*, *Val93*, and *Ile99* throughout the 150 ns MD production run. Both docking and MD simulation revealed diosgenin as a potent lead hit for targeting *MDM2*. Interestingly, a study by Li et al. (2021) identified AG-690/37072075 and AO-022/43452814 as potent anticancer lead hits against *MDM2*. These molecules were predicted to interact with the residues "*Leu57, Gly58, Ile61, Met62, Tyr67, Val93,* and *Ile99*" and were also found to inhibit p53-MDM2 interaction in wild-type p53 cells. Hence, we believe that diosgenin may interfere with the p53-*MDM2* interaction (*MDM2* inhibits the transcriptional activity of p53 by attaching to its transactivation domain), and further experimental studies are required to validate our findings. Further, diosgenin scored -7.4 kcal/mol binding energy against SRC and formed interaction with *Ala168*, *Arg172*, *Phe194*, and *Leu200*. The structural shift of diosgenin from its initial binding pocket to the neighboring alternative pocket was revealed through MD simulation, and the complex remained stable throughout the entire simulation. As a result, we are the first to disclose the discovery of a secondary binding site in the *SRC*.

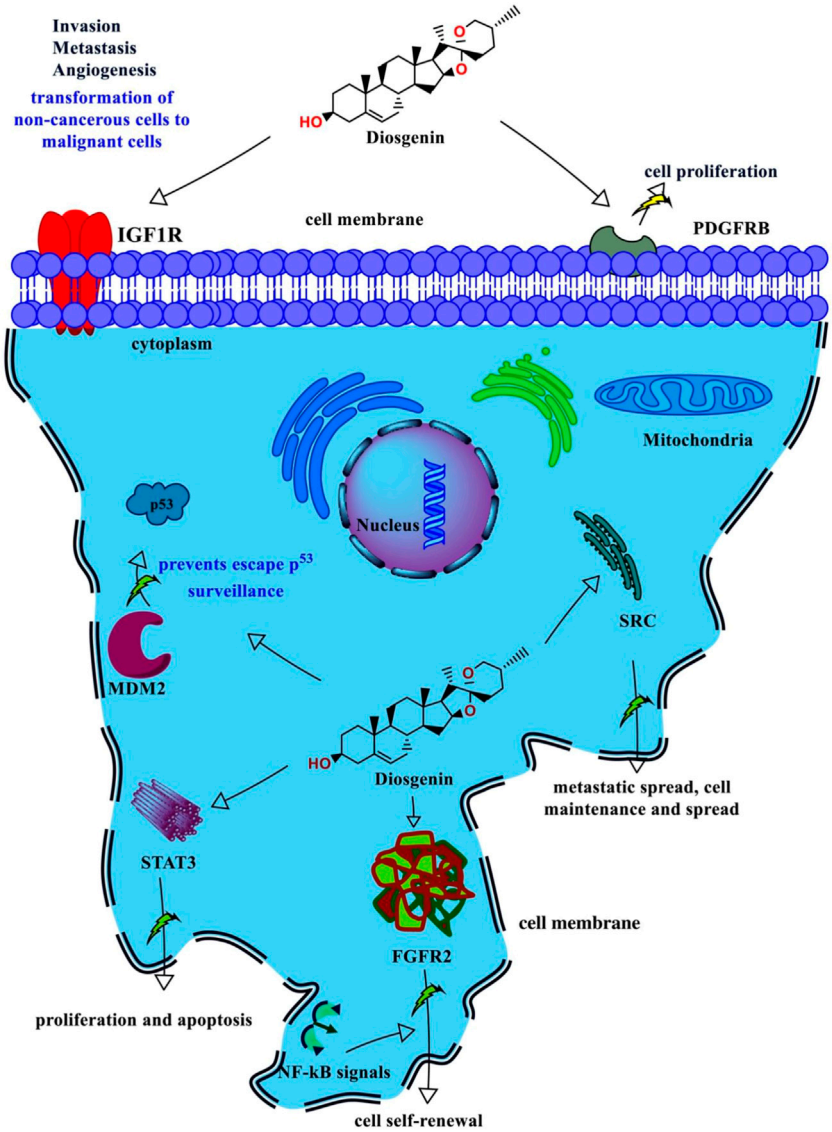

FIGURE 14
Mechanism of action of diosgenin against oestrogen receptor-positive breast cancer. Diosgenin acts on the two cell surface proteins *IGF1R* and *PDGFRB* and inhibits invasion, metastasis, angiogenesis, and cell proliferation. In addition, it acts on the four cytoplasmic proteins i.e., *MDM2*, *STAT3*, *FGFR2*, and *SRC*. Diosgenin may inhibit the cell to escape p53 surveillance by binding with *MDM2*, inhibit cell proliferation and promote apoptosis by binding to *STAT3*, interfere with *NF-kB* signals check the cancer cell self-renewal, and inhibit the metastatic spread by inhibiting the SRC action.

The simulation movie (Supplementary Movie S3) shows that the complex undergoes significant conformational changes in the protein's secondary structure, including the primary binding pocket, increasing the conformational flexibility of *SRC* and causing diosgenin to switch positions from the primary binding pocket to the alternate binding pocket that has been reported. The PCA and DCCM revealed that diosgenin with *IGF1R*, *MDM2*, and *SRC* exhibited significant differences in conformational flexibility and also support the stable complex formation during the simulation.

During the differential gene expression analysis of diosgenin-regulated genes, we observed that *PDGFRB*, *FBFR2*, and *STAT3* possess maximum gene expression in tumor and metastatic vs. normal tissues. In addition, molecular docking and simulation also identified *IGF1R*, *MDM2*, and *SRC* could be the prime diosgenin-modulated targets against breast cancer. Hence, to confirm this we further assessed the functional role of each target using cell line studies. The *PDGF* family (*PDFGRB*) has been reported to use *PDGF* ligands released by cancer stromal cells from breast cancer cells to drive cell proliferation (Farooqi and

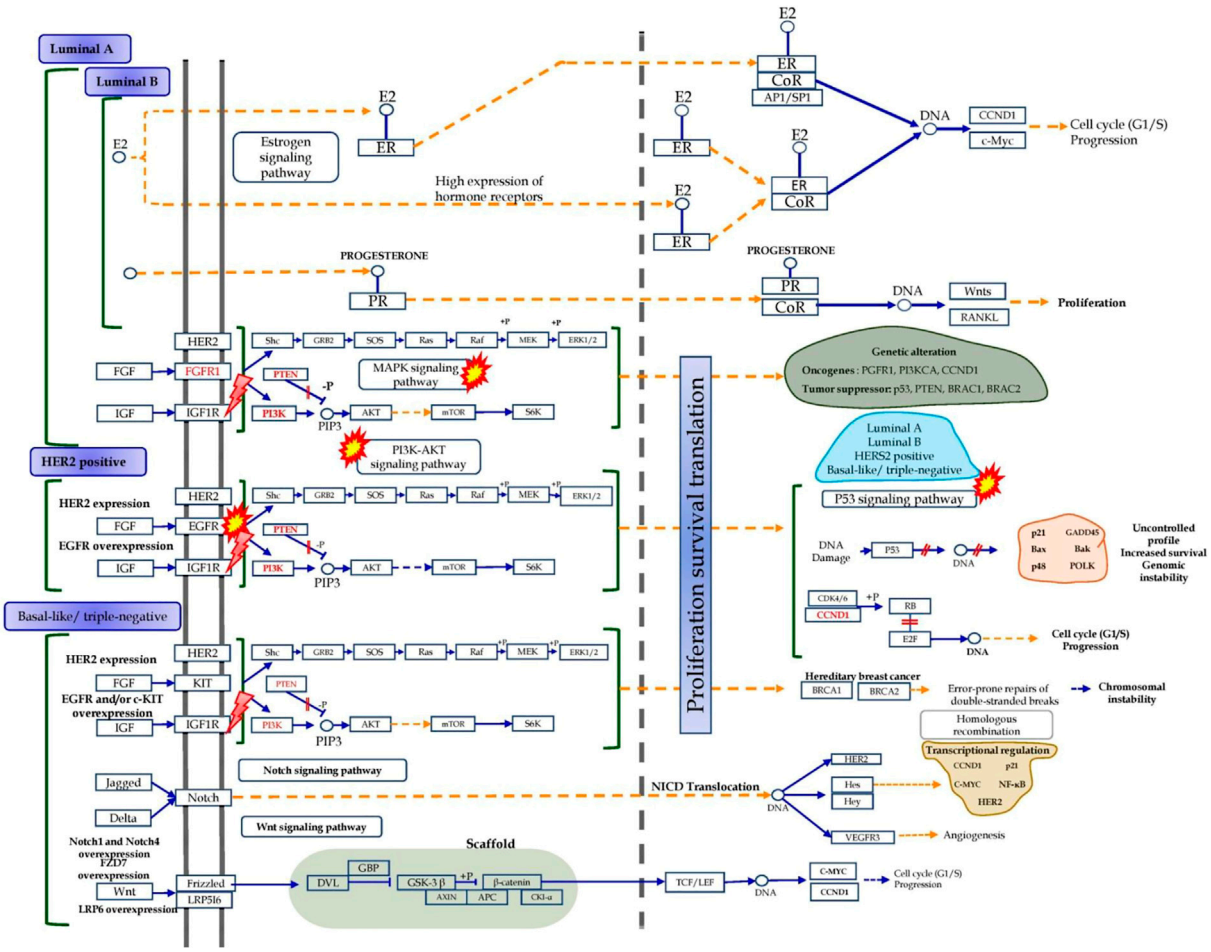

FIGURE 15
Probable checkpoints affected by the diosgenin in the pathogenesis of breast cancer (*Homo sapiens* (human); *hsa05224*) targets/ pathways. In the KEGG pathway analysis, it was diosgenin-regulated targets involved in breast cancer were also identified to trigger EGFR, PI3K-Akt, MAPK, and p53 signaling pathways.

Siddik, 2015). Similarly, *FBFR2* has been reported to promoting cell self-renewal by interacting with NF-kB signals (Kim et al., 2013). Likewise in previous studies, *STAT3* inhibition has been reported to decrease cell proliferation and apoptosis promotion in various cancers including breast cancer (Kanai et al., 2003; Pancotti et al., 2012; Chen et al., 2013). In this regard, because these targets were directly triggered by diosgenin and were also significantly higher in the tumor than in the normal, diosgenin may limit cell proliferation and promote apoptosis by interfering with the self-renewal process. This hypothesis was further supported by the MTT and scratch assays. Previously, an increase in glucose uptake has been reported in the cancer cell which supports ATP production and acts as a fuel (Adekola et al., 2012). This glucose uptake can be reduced by blocking insulin's impact on cancer cells. In comparison to metformin, the current investigation found a considerably greater effective concentration to limit glucose uptake. As a result, diosgenin may inhibit glucose uptake in cancer cells. In the current investigation, however, the glucose absorption assay was done in the presence of insulin. As a consequence, more research is needed to determine its role in glucose uptake in the absence of insulin. Similarly, *MDM2* helps cancer cells to escape p53 surveillance and avoid cellular apoptosis (Momand et al., 1998). In the present study, since, diosgenin had a significant binding affinity with *MDM2*, it could probably promote the apoptosis that needs to be further confirmed. In addition, *SRC* has been indicated for cancer metastasis and also helps in cancer progression and development which is an indicator of cell proliferation (Wheeler et al., 2009). In the current investigation, we discovered that diosgenin inhibited cell proliferation in a variety of cell lines. This may be due to the blockage of the *SRC* generated by diosgenin by binding to it. This could have prevented cell multiplication, as revealed by the scratch assay. Based on the information presented above, it is

reasonable to believe that diosgenin may act against breast cancer by reducing glucose utilization, invasion, and metastasis *via* the surface protein *IGF1R*. Furthermore, it may limit cancer cell proliferation by acting on another surface protein, *PDGFRB*. In addition, the diosgenin may also act over the *MDM2* and prevent the cancer cell to escape the p53 surveillance in the cytoplasm. Also, diosgenin may primarily act over two cytoplasmic targets *FGFR2* and *SRC* to prevent the interaction with NF-kB (prevents cell self-renewal) and metastatic spread respectively (Figure 14) and may also modulate other pathways within the breast cancer pathogenesis (Figure 15) which was evidenced during KEGG pathway analysis.

Although diosgenin inhibited cell growth, was cytotoxic, and had an effect on the various cellular compartments of the tumor cell, the inhibitory constant efficacy was found to be greater than that of doxorubicin. In addition, the previous drug discovery process utilized the concept of the "*lock and key*" approach in which a designed drug is specific to a single protein e.g. doxorubicin complexes with DNA by intercalation and inhibits topoisomerase II. However, this approach has often failed many times and molecules were potent cytotoxic to normal cells which was also observed in the present study. However, a single compound preferably from a natural source tends to act through a polypharmacology approach in which a single molecule can target multiple proteins based on the concept "*master key can unlock multiple locks*" to target multiple proteins and pathways (Chandran et al., 2017). If it happens, the amount of concentration required is a bit high; however, approaches should be made through the targeted drug delivery to breast cancer which is yet to be studied. This issue could be remedied by increasing diosgenin's cellular permeability and promoting anti-cancer action against breast tumors *via* a novel drug delivery mechanism, as established in previous studies (Dhamecha et al., 2015; Jagwani et al., 2020; Dhamecha et al., 2021; Ramasamy et al., 2021). In addition, the effect of diosgenin on the hub genes (*SRC*, *MDM2,* and *IGF1R*) expression is based on the computational models which need to be further evaluated using real-time or reverse transcriptase polymerase chain reaction even though the present study pointed their functional effect *via* the glucose uptake, cell proliferation, and apoptosis which is the perspective of the present findings.

Conclusion

The present study utilized a series of system biology tools to trace the potential action of diosgenin against breast cancer. Herein, we identified the probable action of the diosgenin against breast cancer *via* FoxO, PI3K-Akt, p53, Ras, and MAPK signaling pathways. In addition, we traced the selectivity of the diosgenin to manipulate the action of three hub genes *i.e.*, *IGF1R*, *MDM2*, and *SRC*. Our molecular modeling study reveals that the stable complex formation is primarily facilitated by the cooperative closure motion exerted by the primary binding pocket residues in diosgenin-*MDM2*, and diosgenin-*IGF1R* complex while, in Diosgenin-*SRC* similar compact closure dynamics are also observed at the alternate binding pocket. Conformational flexibility and convergence of the trajectories during MD have been investigated using PCA. Diosgenin showed stable non-bonded interactions forming stable binary complexes with all three screened targets namely *SRC*, *MDM2*, and *IGF1R*. Thus, we proposed that these stable interactions of Diosgenin would trigger the successful inhibition of *SRC*, *MDM2*, and *IGF1R*; the newly identified targets in breast cancer. The results of our computer modeling investigations agree well with the results of the experimental cell line tests. As a result, we hope that this work will open the way for the development of novel therapeutic techniques and/or medication candidates for breast cancer.

Data availability statement

The original contributions presented in the study are included in the article/Supplementary Material, further inquiries can be directed to the corresponding authors.

Author contributions

PK: Conceptualized, experimented, drafted, edited, reviewed, and supervised the entire work. VP: Equal contribution in experimentation, drafting, editing, and reviewing the draft. VVB, PPP, PSRD, KB: Assisted in experimentation and editing. BMP, DRH, and SR: Reviewed, edited, and approved the entire work.

Funding

The work was partially supported by the Indian Council of Medical Research-National Institute of Traditional Medicine (ICMR-NITM), Belagavi, Karnataka, India (Intramural funds).

Acknowledgments

The authors gratefully acknowledge the NGSMIPS-Cell culture lab and Bioinformatics center of ICMR-NITM for providing resources.

Conflict of interest

The authors declare that the research was conducted in the absence of any commercial or financial relationships that could be construed as a potential conflict of interest.

Publisher's note

All claims expressed in this article are solely those of the authors and do not necessarily represent those of their affiliated organizations, or those of the publisher, the editors and the reviewers. Any product that may be evaluated in this article, or claim that may be made by its manufacturer, is not guaranteed or endorsed by the publisher.

Supplementary material

The Supplementary Material for this article can be found online at: https://www.frontiersin.org/articles/10.3389/fphar.2022.1052849/full#supplementary-material

References

Aceves, C., Anguiano, B., and Delgado, G. (2005). Is iodine a gatekeeper of the integrity of the mammary gland? *J. Mammary Gland. Biol. Neoplasia* 10 (2), 189–196. doi:10.1007/s10911-005-5401-5

Adekola, K., Rosen, S. T., and Shanmugam, M. (2012). Glucose transporters in cancer metabolism. *Curr. Opin. Oncol.* 24 (6), 650–654. doi:10.1097/CCO.0b013e328356da72

Alam, M. J., Kumar, S., Singh, V., and Singh, R. K. B. (2015). Bifurcation in cell cycle dynamics regulated by p53. *PLoS ONE* 10 (6), e0129620. doi:10.1371/journal.pone.0129620

Amadei, A., Linssen, A. B., and Berendsen, H. J. (1993). Essential dynamics of proteins. *Proteins* 17 (4), 412–425. doi:10.1002/prot.340170408

Amadei, A., Linssen, A. B., De Groot, B. L., Van Aalten, D. M., and Berendsen, H. J. (1996). An efficient method for sampling the essential subspace of proteins. *J. Biomol. Struct. Dyn.* 13 (4), 615–625. doi:10.1080/07391102.1996.10508874

Badraoui, R., Saoudi, M., Hamadou, W. S., Elkahoui, S., Siddiqui, A. J., Alam, J. M., et al. (2022). Antiviral effects of artemisinin and its derivatives against SARS-CoV-2 main protease: Computational evidences and interactions with ACE2 allelic variants. *Pharmaceuticals* 15 (2), 129. doi:10.3390/ph15020129

Berendsen, H. J., Hess, B., Lindahl, E., Van Der Spoel, D., Mark, A. E., and Groenhof, G. (2005). GROMACS: Fast, flexible, and free. *J. Comput. Chem.* 26 (16), 1701–1718. doi:10.1002/jcc.20291

Bhandare, V. V., and Ramaswamy, A. (2018). The proteinopathy of D169G and K263E mutants at the RNA recognition motif (RRM) domain of tar DNA-binding protein (tdp43) causing neurological disorders: A computational study. *J. Biomol. Struct. Dyn.* 36 (4), 1075–1093. doi:10.1080/07391102.2017.1310670

Bolla, S. R., Mohammed Al-Subaie, A., Yousuf Al-Jindan, R., Papayya, B. J., Kanchi, R. P., Veeraraghavan, V. P., et al. (2019). *In vitro* wound healing potency of methanolic leaf extract of Aristolochiasaccata is possibly mediated by its stimulatory effect on collagen-1 expression. *Heliyon* 5 (5), e01648. doi:10.1016/j.heliyon.2019.e01648

Chandran, U., Mehendale, N., Patil, S., Chaguturu, R., and Patwardhan, B. (2017). Network pharmacology. *Innovative Approaches Drug Discov.* 2017, 127–164. doi:10.1016/B978-0-12-801814-9.00005-2

Chen, H., Yang, Z., Ding, C., Chu, L., Zhang, Y., Terry, K., et al. (2013). Discovery of O-alkylamino tethered niclosamide derivatives as potent and orally bioavailable anticancer agents. *ACS Med. Chem. Lett.* 4 (2), 180–185. doi:10.1021/ml3003082

Daina, A., Michielin, O., and Zoete, V. (2017). SwissADME: a free web tool to evaluate pharmacokinetics, drug-likeness and medicinal chemistry friendliness of small molecules. *Sci. Rep.* 7 (1), 42717–42723. doi:10.1038/srep42717

Daina, A., Michielin, O., and Zoete, V. (2019). SwissTargetPrediction: updated data and new features for efficient prediction of protein targets of small molecules. *Nucleic Acids Res.* 47 (W1), W357–W364. doi:10.1093/nar/gkz382

Dhamecha, D., Jalalpure, S., and Jadhav, K. (2015). Doxorubicin functionalized gold nanoparticles: Characterization and activity against human cancer cell lines. *Process Biochem.* 50 (12), 2298–2306. doi:10.1016/j.procbio.2015.10.007

Dhamecha, D., Le, D., Chakravarty, T., Perera, K., Dutta, A., and Menon, J. U. (2021). Fabrication of PNIPAm-based thermoresponsive hydrogel microwell arrays for tumor spheroid formation. *Mater. Sci. Eng. C Mat. Biol. Appl.* 125, 112100. doi:10.1016/j.msec.2021.112100

Dittrich, A., Gautrey, H., Browell, D., Tyson-Capper, A., and Tyson-Capper, A. (2014). The HER2 signaling network in breast cancer-like a spider in its web. *J. Mammary Gland. Biol. Neoplasia* 19 (3-4), 253–270. doi:10.1007/s10911-014-9329-5

Djerassi, C. (1992). Steroid research at syntex: "the pill" and cortisone. *Steroids* 57 (12), 631–641. doi:10.1016/0039-128x(92)90016-3

Dwivedi, P. S. R., Patil, R., Khanal, P., Gurav, N. S., Murade, V. D., Hase, D. P., et al. (2021). Exploring the therapeutic mechanisms of Cassia glauca in diabetes mellitus through network pharmacology, molecular docking and molecular dynamics. *RSC Adv.* 11 (62), 39362–39375. doi:10.1039/d1ra07661b

Dwivedi, P. S. R., Patil, V. S., Khanal, P., Bhandare, V. V., Gurav, S., Harish, D. R., et al. (2022). System biology-based investigation of Silymarin to trace hepatoprotective effect. *Comput. Biol. Med.* 142, 105223. doi:10.1016/j.compbiomed.2022.105223

Ekyalongo, R. C., and Yee, D. (2017). Revisiting the IGF-1R as a breast cancer target. *NPJ Precis. Oncol.* 1, 14. doi:10.1038/s41698-017-0017-y

Farhan, M., Wang, H., Gaur, U., Little, P. J., Xu, J., and Zheng, W. (2017). FOXO signaling pathways as therapeutic targets in cancer. *Int. J. Biol. Sci.* 13 (7), 815–827. doi:10.7150/ijbs.20052

Farooqi, A. A., and Siddik, Z. H. (2015). Platelet-derived growth factor (PDGF) signalling in cancer: rapidly emerging signalling landscape. *Cell biochem. Funct.* 33 (5), 257–265. doi:10.1002/cbf.3120

Gasco, M., Shami, S., and Crook, T. (2002). The p53 pathway in breast cancer. *Breast Cancer Res.* 4 (2), 70–76. doi:10.1186/bcr426

Guo, F. J., Sun, J., Gao, L. L., Wang, X. Y., Zhang, Y., Qian, S. S., et al. (2015). Discovery of phenylpiperazine derivatives as IGF-1R inhibitor with potent antiproliferative properties *in vitro*. *Bioorg. Med. Chem. Lett.* 25 (5), 1067–1071. doi:10.1016/j.bmcl.2015.01.011

Gupta, R. N., Pareek, A., Suthar, M., Rathore, G. S., Basniwal, P. K., and Jain, D. (2009). Study of glucose uptake activity of Helicteresisora Linn. fruits in L-6 cell lines. *Int. J. Diabetes Dev. Ctries.* 29 (4), 170–173. doi:10.4103/0973-3930.57349

Halgren, T. A. (1996). Merck molecular force field. V. Extension of MMFF94 using experimental data, additional computational data, and empirical rules. *J. Comput. Chem.* 17, 616–641. doi:10.1002/(sici)1096-987x(199604)17:5/6<616::aid-jcc5>3.0.co;2-x

HeraviKarimovi, M., Pourdehqan, M., JadidMilani, M., Foroutan, S. K., and Aieen, F. (2006). Study of the effects of group counseling on quality of sexual life of patients with breast cancer under chemotherapy at Imam Khomeini Hospital. *J. MazandaranUniv Med. Sci.* 16 (54), 43–51.

Herbein, G., and Kumar, A. (2014). The oncogenic potential of human cytomegalovirus and breast cancer. *Front. Oncol.* 4, 230. doi:10.3389/fonc.2014.00230

Huang, L., and Fu, L. (2015). Mechanisms of resistance to EGFR tyrosine kinase inhibitors. *Acta Pharm. Sin. B* 5 (5), 390–401. doi:10.1016/j.apsb.2015.07.001

Huang, M., Anand, S., Murphy, E. A., Desgrosellier, J. S., Stupack, D. G., Shattil, S. J., et al. (2012). EGFR-dependent pancreatic carcinoma cell metastasis through Rap1 activation. *Oncogene* 31 (22), 2783–2793. doi:10.1038/onc.2011.450

Ivanov, S. M., Lagunin, A. A., Rudik, A. V., Filimonov, D. A., and Poroikov, V. V. (2018). ADVERPred–Web service for prediction of adverse effects of drugs. *J. Chem. Inf. Model.* 58 (1), 8–11. doi:10.1021/acs.jcim.7b00568

Jagwani, S., Jalalpure, S., Dhamecha, D., Jadhav, K., and Bohara, R. (2020). Pharmacokinetic and pharmacodynamic evaluation of resveratrol loaded cationic liposomes for targeting hepatocellular carcinoma. *ACS Biomater. Sci. Eng.* 6 (9), 4969–4984. doi:10.1021/acsbiomaterials.0c00429

Jemal, A., Siegel, R., Ward, E., Hao, Y., Xu, J., and Thun, M. J. (2009). Cancer statistics, 2009. *CA. Cancer J. Clin.* 59 (4), 225–249. doi:10.3322/caac.20006

Kanai, M., Konda, Y., Nakajima, T., Izumi, Y., Kanda, N., Nanakin, A., et al. (2003). Differentiation-inducing factor-1 (DIF-1) inhibits STAT3 activity involved in gastric cancer cell proliferation via MEK-ERK-dependent pathway. *Oncogene* 22 (4), 548–554. doi:10.1038/sj.onc.1206109

Khanal, P., Zargari, F., Far, B. F., Kumar, D., Mogana, R., Mahdi, Y. K., et al. (2021). Integration of system biology tools to investigate huperzine A as an anti-Alzheimer agent. *Front. Pharmacol.* 12, 785964. doi:10.3389/fphar.2021.785964

Khanal, P., Patil, V. S., Bhandare, V. V., Dwivedi, P. S., Shastry, C. S., Patil, B. M., et al. (2022). Computational investigation of benzalacetophenone derivatives against SARS-CoV-2 as potential multi-target bioactive compounds. *Comput. Biol. Med.* 146, 105668. doi:10.1016/j.compbiomed.2022.105668

Kim, S., Dubro ka, A., Salamone, R. J., Walker, J. R., Grandinetti, K. B., Bonamy, G. M., et al. (2013). FGFR2 promotes breast tumorigenicity through maintenance of breast tumor-initiating cells. *PLoS One* 8 (1), e51671. doi:10.1371/journal.pone.0051671

Kumari, R., Kumar, R., and Lynn, A.Open Source Drug Discovery Consortium (2014). g_mmpbsa-a GROMACS tool for high-throughput MM-PBSA calculations. *J. Chem. Inf. Model.* 54 (7), 1951–1962. doi:10.1021/ci500020m

Lagunin, A., Ivanov, S., Rudik, A., Filimonov, D., and Poroikov, V. (2013). DIGEP-pred: Web service for *in silico* prediction of drug-induced gene expression profiles based on structural formula. *Bioinformatics* 29 (16), 2062–2063. doi:10.1093/bioinformatics/btt322

Li, R., Pourpak, A., and Morris, S. W. (2009). Inhibition of the insulin-like growth factor-1 receptor (IGF1R) tyrosine kinase as a novel cancer therapy approach. *J. Med. Chem.* 52 (16), 4981–5004. doi:10.1021/jm9002395

Li, B. H., Ge, J. Q., Wang, Y. L., Wang, L. J., Zhang, Q., and Bian, C. (2021). Ligand-based and docking-based virtual screening of MDM2 inhibitors as potent anticancer agents. *Comput. Math. Methods Med.* 2021, 3195957. doi:10.1155/2021/3195957

Liu, T., Lin, Y., Wen, X., Jorissen, R. N., and Gilson, M. K. (2007). BindingDB: a web-accessible database of experimentally determined protein-ligand binding affinities. *Nucleic Acids Res.* 35, D198–D201. doi:10.1093/nar/gkl999

Liu, H., Yang, Z., Lu, W., Chen, Z., Chen, L., Han, S., et al. (2020). Chemokines and chemokine receptors: A new strategy for breast cancer therapy. *Cancer Med.* 9 (11), 3786–3799. doi:10.1002/cam4.3014

Mantovani, F., Collavin, L., and Del Sal, G. (2019). Mutant p53 as a guardian of the cancer cell. *Cell Death Differ.* 26 (2), 199–212. doi:10.1038/s41418-018-0246-9

Marker, R. E., and Krueger, J. (1940). Sterols. CXII. Sapogenins. XLI. The preparation of Trillin and its conversion to progesterone. *J. Am. Chem. Soc.* 62 (12), 3349–3350. doi:10.1021/ja01869a023

McLaughlin, J., Rogers, L. L., and Anderson, J. E. (1998). The use of biological assays to evaluate botanicals. *Drug Inf. J.* 32 (2), 513–524. doi:10.1177/009286159803200223

Momand, J., Jung, D., Wilczynski, S., and Niland, J. (1998). The MDM2 gene amplification database. *Nucleic Acids Res.* 26 (15), 3453–3459. doi:10.1093/nar/26.15.3453

Moon, A. (2021). Ras signaling in breast cancer. *Adv. Exp. Med. Biol.* 1187, 81–101. doi:10.1007/978-981-32-9620-6_4

Mosmann, T. (1983). Rapid colorimetric assay for cellular growth and survival: Application to proliferation and cytotoxicity assays. *J. Immunol. Methods* 65 (1-2), 55–63. doi:10.1016/0022-1759(83)90303-4

Munshi, S., Kornienko, M., Hall, D. L., Reid, J. C., Waxman, L., Stirdivant, S. M., et al. (2002). Crystal structure of the apo, unactivated insulin-like growth factor-1 receptor kinase: implication for inhibitor specificity. *J. Biol. Chem.* 277 (41), 38797–38802. doi:10.1074/jbc.M205580200

Pancotti, F., Roncuzzi, L., Maggiolini, M., and Gasperi-Campani, A. (2012). Caveolin-1 silencing arrests the proliferation of metastatic lung cancer cells through the inhibition of STAT3 signaling. *Cell. Signal.* 24 (7), 1390–1397. doi:10.1016/j.cellsig.2012.02.015

Patil, V. S., Harish, D. R., Vetrivel, U., Deshpande, S. H., Khanal, P., Hegde, H. V., et al. (2022). Pharmacoinformatics analysis reveals flavonoids and diterpenoids from *Andrographis paniculata* and *Thespesia populnea* to target hepatocellular carcinoma induced by hepatitis B virus. *Appl. Sci.* 12 (21), 10691. doi:10.3390/app122110691

Quesnel, B., Preudhomme, C., Fournier, J., Fenaux, P., and Peyrat, J. P. (1994). MDM2 gene amplification in human breast cancer. *Eur. J. Cancer* 30A (7), 982–984. doi:10.1016/0959-8049(94)90128-7

Ramasamy, S., Dhamecha, D., Kaliyamoorthi, K., Pillai, A. S., Alexander, A., Dhanaraj, P., et al. (2021). Magnetic hydroxyapatite nanomaterial–cyclodextrin tethered polymer hybrids as anticancer drug carriers. *Mater. Adv.* 2 (10), 3315–3327. doi:10.1039/d1ma00142f

Rani, A., Stebbing, J., Giamas, G., and Murphy, J. (2019). Endocrine resistance in hormone receptor positive breast cancer-from mechanism to therapy. *Front. Endocrinol.* 10, 245. doi:10.3389/fendo.2019.00245

Russo, J., and Russo, I. H. (2006). The role of estrogen in the initiation of breast cancer. *J. Steroid Biochem. Mol. Biol.* 102 (1-5), 89–96. doi:10.1016/j.jsbmb.2006.09.004

Saeed, M., Saeed, A., Alam, M. J., and Alreshidi, M. (2020). Identification of persuasive antiviral natural compounds for COVID-19 by targeting endoribonuclease NSP15: A structural-bioinformatics approach. *Molecules* 25 (23), 5657. doi:10.3390/molecules25235657

Samdani, A., and Vetrivel, U. (2018). POAP: A GNU parallel based multithreaded pipeline of open babel and AutoDock suite for boosted high throughput virtual screening. *Comput. Biol. Chem.* 74, 39–48. doi:10.1016/j.compbiolchem.2018.02.012

Sangodkar, J., Dhawan, N. S., Melville, H., Singh, V. J., Yuan, E., Rana, H., et al. (2012). Targeting the FOXO1/KLF6 axis regulates EGFR signaling and treatment response. *J. Clin. Invest.* 122 (7), 2637–2651. doi:10.1172/JCI62058

Sariego, J. (2010). Breast cancer in the young patient. *Am. Surg.* 76 (12), 1397–1400. doi:10.1177/000313481007601226

Shannon, P., Markiel, A., Ozier, O., Baliga, N. S., Wang, J. T., Ramage, D., et al. (2003). Cytoscape: a software environment for integrated models of biomolecular interaction networks. *Genome Res.* 13 (11), 2498–2504. doi:10.1101/gr.1239303

Shishodia, S., and Aggarwal, B. B. (2006). Diosgenin inhibits osteoclastogenesis, invasion, and proliferation through the downregulation of Akt, I kappa B kinase activation and NF-kappa B-regulated gene expression. *Oncogene* 25 (10), 1463–1473. doi:10.1038/sj.onc.1209194

Srinivasan, S., Koduru, S., Kumar, R., Venguswamy, G., Kyprianou, N., and Damodaran, C. (2009). Diosgenin targets Akt-mediated prosurvival signaling in human breast cancer cells. *Int. J. Cancer* 125 (4), 961–967. doi:10.1002/ijc.24419

Steiner, E., Klubert, D., and Knutson, D. (2008). Assessing breast cancer risk in women. *Am. Fam. Physician* 78 (12), 1361–1366.

Stoddard, F.R., 2nd, Brooks, A. D., Eskin, B. A., and Johannes, G. J. (2008). Iodine alters gene expression in the MCF7 breast cancer cell line: evidence for an anti-estrogen effect of iodine. *Int. J. Med. Sci.* 5 (4), 189–196. doi:10.7150/ijms.5.189

Szklarczyk, D., Gable, A. L., Nastou, K. C., Lyon, D., Kirsch, R., Pyysalo, S., et al. (2021). The STRING database in 2021: customizable protein-protein networks, and functional characterization of user-uploaded gene/measurement sets. *Nucleic Acids Res.* 49 (D1), D605–D612. doi:10.1093/nar/gkaa1074

Tokunaga, E., Kimura, Y., Mashino, K., Oki, E., Kataoka, A., Ohno, S., et al. (2006). Activation of PI3K/Akt signaling and hormone resistance in breast cancer. *Breast Cancer* 13 (2), 137–144. doi:10.2325/jbcs.13.137

Trott, O., and Olson, A. J. (2010). AutoDock Vina: improving the speed and accuracy of docking with a new scoring function, efficient optimization, and multithreading. *J. Comput. Chem.* 31 (2), 455–461. doi:10.1002/jcc.21334

Tworoger, S. S., Eliassen, A. H., Rosner, B., Sluss, P., and Hankinson, S. E. (2004). Plasma prolactin concentrations and risk of postmenopausal breast cancer. *Cancer Res.* 64 (18), 6814–6819. doi:10.1158/0008-5472.CAN-04-1870

Tworoger, S. S., Sluss, P., and Hankinson, S. E. (2006). Association between plasma prolactin concentrations and risk of breast cancer among predominately premenopausal women. *Cancer Res.* 66 (4), 2476–2482. doi:10.1158/0008-5472.CAN-05-3369

Van Aalten, D. M., Findlay, J. B., Amadei, A., and Berendsen, H. J. (1995). Essential dynamics of the cellular retinol-binding protein evidence for ligand-induced conformational changes. *Protein Eng.* 8 (11), 1129–1135. doi:10.1093/protein/8.11.1129

Venturi, S. (2001). Is there a role for iodine in breast diseases? *Breast* 10 (5), 379–382. doi:10.1054/brst.2000.0267

Verbeek, B. S., Vroom, T. M., Adriaansen-Slot, S. S., Ottenhoff-Kalff, A. E., Geertzema, J. G., Hennipman, A., et al. (1996). c-Src protein expression is increased in human breast cancer. An immunohistochemical and biochemical analysis. *J. Pathol.* 180 (4), 383–388. doi:10.1002/(SICI)1096-9896(199612)180:4<383::AID-PATH686>3.0.CO;2-N

Wang, L., Han, H., Dong, L., Wang, Z., and Qin, Y. (2021). Function of p21 and its therapeutic effects in esophageal cancer. *Oncol. Lett.* 21 (2), 136–137. doi:10.3892/ol.2020.12397

Wheeler, D. L., Lida, M., and Dunn, E. F. (2009). The role of Src in solid tumors. *Oncologist* 14 (7), 667–678. doi:10.1634/theoncologist.2009-0009

Xiong, G., Wu, Z., Yi, J., Fu, L., Yang, Z., Hsieh, C., et al. (2021). ADMETlab 2.0: an integrated online platform for accurate and comprehensive predictions of ADMET properties. *Nucleic Acids Res.* 49 (W1), W5–W14. doi:10.1093/nar/gkab255

Yager, J. D., and Davidson, N. E. (2006). Estrogen carcinogenesis in breast cancer. *N. Engl. J. Med.* 354 (3), 270–282. doi:10.1056/NEJMra050776

Yue, W., Wang, J. P., Conaway, M., Masamura, S., Li, Y., and Santen, R. J. (2002). Activation of the MAPK pathway enhances sensitivity of MCF-7 breast cancer cells to the mitogenic effect of estradiol. *Endocrinology* 143 (9), 3221–3229. doi:10.1210/en.2002-220186

Zhang, Y. L., Wang, R. C., Cheng, K., Ring, B. Z., and Su, L. (2017). Roles of Rap1 signaling in tumor cell migration and invasion. *Cancer Biol. Med.* 14 (1), 90–99. doi:10.20892/j.issn.2095-3941.2016.0086

frontiers | Frontiers in Oncology

TYPE Review
PUBLISHED 09 January 2023
DOI 10.3389/fonc.2022.1068778

OPEN ACCESS

EDITED BY
Visweswara Rao Pasupuleti,
REVA University, India

REVIEWED BY
Meraj Ansari,
National Institute of Pharmaceutical Education and Research Mohali, India
David Morris,
University of New South Wales, Australia

*CORRESPONDENCE
Javad Sharifi-Rad
javad.sharifirad@gmail.com
Christophe Hano
hano@univ-orleans.fr
Daniela Calina
calinadaniela@gmail.com
Paolo Zucca
pzucca@unica.it

SPECIALTY SECTION
This article was submitted to Pharmacology of Anti-Cancer Drugs, a section of the journal Frontiers in Oncology

RECEIVED 13 October 2022
ACCEPTED 12 December 2022
PUBLISHED 09 January 2023

CITATION
Pezzani R, Jiménez-Garcia M, Capó X, Sönmez Gürer E, Sharopov F, Rachel TYL, Ntieche Woutouoba D, Rescigno A, Peddio S, Zucca P, Tsouh Fokou PV, Martorell M, Gulsunoglu-Konuskan Z, Ydyrys A, Bekzat T, Gulmira T, Hano C, Sharifi-Rad J and Calina D (2023) Anticancer properties of bromelain: State-of-the-art and recent trends. *Front. Oncol.* 12:1068778. doi: 10.3389/fonc.2022.1068778

Anticancer properties of bromelain: State-of-the-art and recent trends

Raffaele Pezzani[1,2], Manuel Jiménez-Garcia[3], Xavier Capó[4], Eda Sönmez Gürer[5], Farukh Sharopov[6], Tchokouaha Yamthe Lauve Rachel[7], David Ntieche Woutouoba[8], Antonio Rescigno[9], Stefania Peddio[9], Paolo Zucca[9]*, Patrick Valere Tsouh Fokou[10], Miquel Martorell[11,12], Zehra Gulsunoglu-Konuskan[13], Alibek Ydyrys[14,15], Tynybekov Bekzat[16], Tussupbekova Gulmira[17], Christophe Hano[18]*, Javad Sharifi-Rad[19]* and Daniela Calina[20]*

[1]Phytotherapy Lab, Endocrinology Unit, Department of Medicine (DIMED), University of Padova, Padova, Italy, [2]Associazione Italiana per la Ricerca Oncologica di Base (AIROB), Padova, Italy, [3]Laboratory of Neurophysiology, Biology Department, University of Balearic Islands (UIB), Palma de Mallorca, Spain, [4]Research Group in Community Nutrition and Oxidative Stress and Health Research Institute of the Balearic Islands (IdISBa), University of Balearic Islands, Palma de Mallorca, Spain, [5]Faculty of Pharmacy, Department of Pharmacognosy, Sivas Cumhuriyet University, Sivas, Turkey, [6]Research Institution "Chinese-Tajik Innovation Center for Natural Products" of the National Academy of Sciences of Tajikistan, Dushanbe, Tajikistan, [7]Institute of Medical Research and Medicinal Plants Studies (IMPM), Yaounde, Cameroon, [8]Antimicrobial and Biocontrol Agents Unit, Department of Biochemistry, Faculty of Science, University of Yaounde, Yaounde, Cameroon, [9]Department of Biomedical Sciences, University of Cagliari, Cagliari, Italy, [10]Department of Biochemistry, Faculty of Science, University of Bamenda, Bambili, Cameroon, [11]Department of Nutrition and Dietetics, Faculty of Pharmacy, and Centre for Healthy Living, University of Concepción, Concepción, Chile, [12]Universidad de Concepción, Unidad de Desarrollo Tecnológico, UDT, Concepción, Chile, [13]Faculty of Health Science, Nutrition and Dietetics Department, Istanbul Aydin University, Istanbul, Turkey, [14]Biomedical Research Centre, Al-Farabi Kazakh National University, Almaty, Kazakhstan, [15]The Elliott School of International Affairs, George Washington University, Washington, DC, United States, [16]Department of Biodiversity and Bioresources, Al-Farabi Kazakh National University, Almaty, Kazakhstan, [17]Department of Biophysics, Biomedicine and Neuroscience, Al-Farabi Kazakh National University, Almaty, Kazakhstan, [18]Department of Biological Chemistry, University of Orleans, Chartres, France, [19]Facultad de Medicina, Universidad del Azuay, Cuenca, Ecuador, [20]Department of Clinical Pharmacy, University of Medicine and Pharmacy of Craiova, Craiova, Romania

Bromelain is a key enzyme found in pineapple (*Ananas comosus (L.) Merr.*); a proteolytic substance with multiple beneficial effects for human health such as anti-inflammatory, immunomodulatory, antioxidant and anticarcinogenic, traditionally used in many countries for its potential therapeutic value. The aim of this updated and comprehensive review focuses on the potential anticancer benefits of bromelain, analyzing the cytotoxic, apoptotic, necrotic, autophagic, immunomodulating, and anti-inflammatory effects in cancer cells and animal models. Detailed information about Bromelain and its anticancer effects at the cellular, molecular and signaling levels were collected from online databases such as PubMed/MedLine, TRIP database, GeenMedical, Scopus, Web of Science and Google Scholar. The results of the analyzed studies showed that Bromelain possesses corroborated pharmacological activities,

such as anticancer, anti-edema, anti-inflammatory, anti-microbial, anti-coagulant, anti-osteoarthritis, anti-trauma pain, anti-diarrhea, wound repair. Nonetheless, bromelain clinical studies are scarce and still more research is needed to validate the scientific value of this enzyme in human cancer diseases.

KEYWORDS

bromelain, cancer, chemotherapeutics, cytotoxicity, apoptosis, molecular targets

1 Introduction

Cancer has become a global problem, with a negative impact on patients, their families and the whole of society. Tumor cells can affect any part of the body and are characterized by proliferation caused by the loss of control of cell division, reducing the possibility of repairing cell DNA mutations, the ability to avoid genetically programmed cell death (apoptosis), to form new blood vessels (angiogenesis), to invade other tissues and develop metastases, the ability to hide from the action of the immune system or the loss of abilities to fulfil a function in the body (1, 2). The main objectives of oncological treatments are the remission or cure of the disease, the extension of the duration and the improvement of the patient's quality of life. The effectiveness of oncological therapies depends on early detection, accurate diagnosis of cancer, compliance with standards of care and the correct way of administering treatments. Chemotherapy is a systemic treatment, administered to destroy tumor cells or stop their multiplication (3). The cytotoxic action also manifests itself in healthy cells that multiply rapidly (eg hair, and cells of the intestinal mucosa), causing adverse reactions (4). Chemotherapy is administered strictly according to the type of tumor cell and the patient's response to treatment (5, 6). Today, there are a variety of natural cancer treatments that may be able to provide results comparable to chemotherapy and radiation therapy (7, 8). They are much less toxic and invasive compared to standard methods of cytostatic treatment. Some of the most successful cancer treatment plans involve a combination of therapies (9–11).

Bromelain is an enzyme with a particular proteolytic activity that can be easily obtained from the pineapple stem (*Ananas comosus* (L.) Merr.). Bromelain is also present in other parts of the pineapple and is found in association with other cysteine proteases (12). Bromelain is traditionally extracted from the juice following ultrafiltration and centrifugation, with an end process culminating in lyophilization (13). However, the growing request for this substance induced the research to develop new purification techniques, i.e. ion exchange chromatography, gel filtration, aqueous two-phase extraction, affinity chromatography, reverse micelle chromatography, and recombinant DNA technology, with the final aim to contain costs and increase the production yield (14). Given the elevated costs of production and a market that needs a highly purified and certified bromelain, pineapple cultivation is widespread in many tropical and subtropical areas, i.e. South-East Asia, Africa, and Central-South America (15). At the basis of this great request for bromelain, there are the extraordinary properties that make it indispensable for numerous processes related to foods production, cosmetics, pharmaceuticals, and textile industries (13, 15–18). In addition, since its discovery, bromelain demonstrated interesting pharmacological and potential medical applications. In 1875, bromelain was first analyzed as a specific substance obtained by pineapple (19) and later in 1892, other researchers defined their matter of investigation as "bromelin" (20). After in 1962, Seligman and collaborators demonstrated the anti-inflammatory effect of bromelain (21). Since this finding, bromelain has been increasingly studied in different settings, leading to the discovery of numerous properties in human health, i.e. treatment of osteoporosis and osteoarthritis, diarrhea, treatment of chronic wounds, surgical debridement, anti-edema and anti-inflammatory processes, trauma pain, burn eschars, and many others (Figure 1) (22–29). Certainly, such clinical studies have been based on previous animal or cellular experiments. Indeed, a plethora of preclinical works have been published on this substance as they will be reported in this review. In particular, this updated review is focused on the anti-cancer effect of bromelain, an activity that emerged since 1972, when a first work explored the use of the enzyme in malignant tumors with notable remissions in some anecdotal cases (30).

2 Review methodology

To carry out this updated review on the anticancer effects of bromelain, published studies were searched in specialized databases such as PubMed/MedLine, TRIP database, GeenMedical, Scopus, Web of Science and Google Scholar, using the next MeSH terms: 'Animals", "Anticarcinogenic Agents/pharmacology",

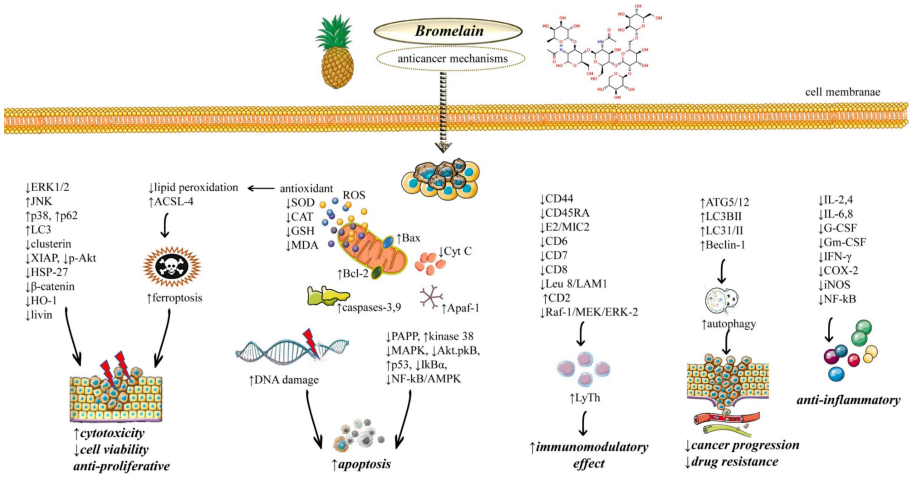

FIGURE 1
Illustrative diagram with the most representative anticancer molecular mechanisms of Bromelain. Abbreviations and symbols: ↑increase, ↓decrease, extracellular signal-related kinase (ERK), c-Jun N-terminal kinase (JNK), X-linked inhibitor of apoptosis protein (XIAP), Heat shock protein 27 (HSP27), Heme oxygenase-1 (HO-1), long-chain fatty acyl-CoA synthetase 4 (ACSL4), reactive oxygen species (ROS), superoxide dismutase.(SOD), Glutathione (L-γ-glutamyl-L-cysteinyl-glycine; GSH), malondialdehyde (MDA), Bcl-2 Associated X (Bax), B-cell lymphoma 2 (Bcl-2), Pro-Apoptotic Apoptosis Protease–Activating Factor 1 (Apaf-1), mitogen-activated protein kinase (MAPK), serine/threonine protein kinase (Akt), nuclear factor-kappa B (NF-κB), cluster of differentiation 44 (CD44), serine/threonine kinase (Raf1), mitogen-activated protein kinase (MEK), Autophagy related 5 protein (ATG5), Microtubule-associated protein 1A/1B-light chain 3 (LC3), IL (interleukin), Interferon-gamma (IFNγ), cyclooxygenase-2 (COX-2), Granulocyte-macrophage colony-stimulating factor (GM-CSF), granulocyte-colony stimulating factor (G-CSF).

"Antineoplastic Agents/pharmacology", "Bromelain/pharmacology", "Bromelain/administration and dosage", "Bromelain/chemistry", "Cell Line, Tumor", "Cell Survival/drug effects", "Dose-Response Relationship", "Drug, Humans", "Nanocapsules/administration and dosage", "Neoplasms/drug therapy", "Neoplasms, Experimental/pathology", "Signal Transduction/drug effects", "Treatment Outcome". Each article published before 1 August 2022, written in English, and their significance was evaluated by analyzing the title and abstract. All studies written in preclinical and clinical language that highlighted the anticancer molecular mechanisms, signaling pathways and action targets of bromelain were included. Duplicate studies, abstracts, presentations at conferences or that had associated homeopathic preparations were excluded. The chemical forms were validated with Chemspider and the scientific names of the plant species were validated according to WorldFloraOnline (31, 32).

3 Chemistry data of bromelain

3.1 Physicochemical characteristics

The term "bromelain" initially referred to a mixture of proteases produced by any member of the *bromeliaceae* family (14). However, the extraction is most common from pineapple fruit (*Ananas comosus*). These extracts usually contain several enzymes (including proteases, phosphatases, nucleases, oxidoreductases, and glycosidases), but the most characteristics among them are some cysteine endopeptidases that specifically hydrolytically cleave non-terminal peptide bonds (33, 34). Four main enzymes have been identified, as shown in Table 1.

Proteolytic activity is present in almost all parts of the plants, but the stem and fruit are indeed richer. The main enzyme is bromelain. This is α + β protein that can be extracted both from the stem (EC: 3.4.22.32) and from fruit (EC: 3.4.22.33). The first is

TABLE 1 summary of the most prominent characteristics of pineapple cysteine proteases (adapted from (Colletti et al., 2021; Murachi, 1976; Rowan & Buttle, 1994) (33).

Protease	M_r (kDa)	pI	Optimum pH	Glycoprotein
Bromelain (fruit)	25-31	4.6	3-8	Yes
Bromelain (stem)	23.8-27	9.5	6-7	Yes
Ananain	23.4-25	>10	~7	No
Comosain	24.5	>10	~7	Yes

the most abundant showing MW of about 23.8 kDa, a pI of 9.5 and a pH optimum around neutrality (33). Bromelain from the fruit on the contrary has a slightly higher MW (25 kDa), a more acidic pI (4.6) and a broader pH optimum (3-8). All these differences on the whole may be, at least in part, responsible for the very different results observed in all the clinical and preclinical studies (33, 35). Stem bromelain is a single polypeptide chain (211/212 aminoacids), presenting at least a single glycosylation point accountable for the 23.8 kDa MW. A crucial glutamate residue (Glu68) has been suggested responsible for the preference for positively charged substrates (36). Both enzymes could undergo however complex glycosylation patterns, increasing the global MW. These reactions depend on a lot of factors and are still largely poorly known (34). The aminoacidic sequence of stem bromelain is quite homologous to other plant cysteine-peptidases such as papain, chymopapain and actinidin (37). Nonetheless, several authors reported that this proteolytic activity could be only marginally connected to the pharmacological effects. Other components (protein and non-protein) could be responsible for a complex network of interactions and synergistic actions resulting in pharmacological effects (16). Stem bromelain is very stable when frozen at -20°C, whereas a complete loss activity occurs when boiled at 100°C for 10' (38). Optimum activity has been found at 30°C and neutrality for the glycosylated form. Both heating (40-60°C) and acidification (pH 3-4) led to significant inactivation (39). The deglycosylated form was found to be more susceptible to temperature and organic solvent inactivation, suggesting an important role of the oligosaccharide portion in the retention of the enzyme's native form (39).

Fruit bromelain showed a similar pH optimum around neutrality and a loss of activity for a pH higher than 8.0 (40). The enzyme retained a part of catalytic activity (respectively 22% and 44%) after 30 days of storage at 30°C and 60 days of storage at 4°C (41). On the contrary, 180 days of freezing at -4°C led to an almost complete retaining (75%) of proteolytic power. Slightly different results were obtained by Chaurasiya and colleagues (40). In this study after 9 days at 5-8°C the loss of activity was significant (around 30% residual activity) (40). These differences could be explained by the different degrees of purification. Glutaraldehyde crosslinking has been shown to increase thermal and pH stability, up to 60°C and pH 8 (42). Even the effect of different organic solvents led to less marked losses of proteolytic activity. Recently, Zhou and coworkers showed that thermal inactivation followed the first-order reaction, and that half-life from 45 to 75°C decreased from 81' to 5' (43).

3.2 Purification of bromelain

Protein purification is always a challenging task since all proteins show similar physicochemical properties (being constituted always by the same 20 aminoacidic building blocks). In addition, all the required purification techniques must be performed under very controlled conditions to avoid protein inactivation (and consequently the complete loss of commercial value of the protein). Temperature, pH, presence of organic solvents, ionic strength, dilution or concentration, and various chemical and biological contaminants are all factors that should be carefully monitored and controlled during purification, affecting the overall cost of the process. In accordance, a lot of attention has been paid to the purification strategies, looking for the most effective approaches, also from an economical point of view. Up to now the most used protocol encompass the preparation of a crude bromelain extract, using conventional low-resolution techniques (44). After cleaning, peeling and cutting down the whole pineapple, cell lysis is usually obtained mechanically without any further water addition. This homogenization, after centrifugation, allows for recovering an active extract presenting however several impurities. The product can be then concentrated to improve the purification fold. Size exclusion membranes (cut-off > 5-10kDa) are usually the basis for ultrafiltration techniques, giving encouraging results (45–47). Such a strategy is quite simple and the costs are relatively low. A more expensive way to concentrate protein is lyophilization (freeze-dry). The transition of water from solid to gas form under a deep vacuum requires a high amount of energy but allows a complete solvent removal (not possible with membrane filtration). On the negative side, the stability of bromelain during freeze-drying is not high (35, 48) possibly suggesting the use of a stabilizer. All these approaches lead to a crude extract in which bromelain has been isolated from non-protein contaminants, but no real protein purification has been done. This can be achieved with high-resolution techniques, that greatly increase the final cost of the purified product. Usually low- and high-resolution isolation steps are combined following the purpose of the purified extract (Arshad et al., 2014). One of the easiest ways to fractionate proteins is reversible precipitation. Several approaches can be used, including salts, isoelectric, organic solvents and non-ionic polymer precipitation. All these techniques have been tested for bromelain, with various results (40). Ethanol precipitation gave better yields than isoelectric, PEG and ammonium sulfate (48, 49). PEG can be also used in aqueous two-phase systems, preserving bromelain activity (50, 51). Precipitation is a very affordable option, with quite good recovery yields. However, the obtained purification fold factors are not very high, and the product could be contaminated by salts or polymers (33).

To improve protein purification fold, the golden standard in biochemistry is chromatography. This term encompassed all the techniques using a combination of two immiscible phases, moving one on the other. The analytes are separated giving their different affinity for the two phases. Chromatographic separation typically highly increases the protein purification yields, but with higher operational costs. Often chromatography is employed in combination with fractionated precipitation (52). Ion exchange chromatography relies on

reversible electrostatic interaction between a resin and charged analytes. Such an approach has been proved able to remove contaminant polysaccharides (35), increasing bromelain-specific activity (even more than salt precipitation) (53, 54). Ion exchange has been also tested in combination with size exclusion chromatography, resulting in a 41% recovery of initial activity (55).

Affinity chromatography (AC) is a very potent separation technique, relying on a specific interaction between a protein and a ligand-functionalized chromatographic column (56). This could allow (theoretically) to completely purify proteins in a single step. Bobb and colleagues achieved a similar result using an e-aminocaproic-D-tryptophan methyl ester coupled with Sepharose 4B (57). In this case stem, bromelain was effectively purified to a single SDS-PAGE band in one step. Alternatively, Rowan et al. used acetone precipitation and a Sepharose- Ahx-Phe-GlySc resin to purify fruit bromelain (Rowan et al., 1990). In both cases, mercury was used to allow elution after sample application and resin washing of unbound. The downside of such approaches is the high costs of similarly functionalized resins. In the case of recombinant bromelain, His-tag could be inserted allowing AC purification based on nickel/nitriloacetic aced-based resins (58, 59). High recovery yields of bromelain have been also obtained using reversed micellar extraction (RME) process (40, 60, 61). RME relies on the inclusion of proteins into micellar inner cores, and the subsequent release in the aqueous phase. The works reported good bromelain recovery and significant enhancement in the purification fold.

3.3 Determination of bromelain activity

Casein and azocasein are the most used substrates for the spectrophotometric determination of bromelain activity. Casein is chosen due to its low cost and high availability (62). The reaction is performed in 0.5-1% casein solutions at neutral pH. After 5-30' at 37°C trichloroacetic is added to stop the reaction and the resulting soluble peptides are spectrophotometrically detected at 280 nm, comparing absorbance with a tyrosine standard curve (48, 63). Reducing thiols and EDTA is required to, respectively, prevent oxidation of cysteine in the active site and chelate interfering metals (64, 65). Upon proteolysis, azocasein releases instead diazo sulphonic analogues of Tyr and His residues, quantifiable at 440 nm. Operational conditions are like casein, but alkali addition is necessary to develop color (66). Also, in this case, the reaction is performed at 37°C. As alternatives, several synthetic substrates are available usually based on chromogenic or fluorogenic moieties (such as *p*-nitrophenol or *p*-nitroaniline) coupled to small peptides. For instance, Z-Arg-Arg-p-nitroaniline, Bz-Phe-Val-Arg-pNA, *p*Glu-Phe-Leu-*p*-nitroanilide and N-Cbz-L-Gln-*p*-nitrophenyl ester hydrolysis leads in solution to chromophores easy detectable at 405 nm (67, 68). These approaches are easy, convenient and quick. One more advantage is the fact that different substrates present different specificity for various bromelain forms. For instance, Z-Arg-Arg is more specific for stem enzymes (69, 70). On the other hand, fruit bromelain showed a preference for Bz-Phe-Val-Arg.

4 Bromelain as an emerging anticancer agent: Molecular mechanisms, signaling pathways and therapeutic targets

To elucidate in detail the potential mechanisms of anticancer action, bromelain has been extensively studied in numerous studies (16, 71–73). Bromelain anticancer effects were evaluated in both "*in vivo*" in animal models and "*in vitro*" as a potential agent against several cancer lines such as gastrointestinal, colorectal, breast, mesothelioma, lung, hepatic, pancreatic, epidermoid, and melanoma (71) (Table 2 and Figure 1).

4.1 Cytotoxicity

The cytotoxic properties of bromelain have been known since ancient times, as it was used in traditional Asian medicine. Cytotoxic or anticancer bromelain effects are associated with its protease activity (16). In SCC25 human oral squamous carcinoma cells, cell viability decreased in a dose- and time-dependent manner after 24-hr treatment with bromelain, from 95.16% (at 0.78 μg/mL) to 69.93% (at 25 μg/mL) (85). It has been reported that bromelain-induced cytotoxic activity in human gastrointestinal cancer cells (76, 96), breast cancer cells (76, 80), and hepatocellular carcinoma cell lines (97). It is also evidenced that bromelain presented antiproliferative properties in gastric and colon carcinoma cells. For example in human gastrointestinal cell lines, in the case of MKN45 cells, the enzyme in a range of concentration from 100 to 600 μg/mL but non-dose dependently reduced cell survival at 72h of treatment (81). In the case of KATO-III cells, antiproliferative effects were shown at concentrations above 100 μg/mL, while in LS174 cells, cytotoxic properties of bromelain were evidenced above 30 μg/mL and its cytotoxicity increased with higher bromelain concentrations at 72h (81). Cytotoxicity of bromelain was also evaluated in other human gastric carcinoma cells (AGS cells) at concentrations from 5 to 600 μg/mL, whereas the first anti-proliferative effects (25% growth reduction) were observed at concentrations >50 μg/mL in a dose-dependent manner at 24h of treatment (76). Another study demonstrated a reduction of almost 75% cell viability after 12 hours of treatment with a concentration of 50 μg/mL bromelain in DLD-1 colorectal carcinoma cells (89).

Cytotoxic properties of bromelain were also tested in hepatocellular carcinoma cells (HepG2). Cells treated for 48

TABLE 2 Table with summarized anticancer mechanisms of Bromelain from *in vitro* studies.

Type of tested cancer cell lines	Effects	Results/Potential Mechanisms	Ref
MDA-MB231breast adenocarcinoma A2058 melanoma OCI-LY19 non-adherent human B cell lymphoma HL-60 human leukemia cells	↑cytotoxicity anti-proliferative	IC_{50} = 0.3 μM ↑ cancer cells death in MDA-MB231, A2058 IC_{50} = 1 μM ↑ cancer cells death in OCI-LY19, HL-60	(36)
MCF-7, MDA-MB-231 breast adenocarcinoma	↑cytotoxicity ↑autophagy ↑apoptosis	IC_{50} = 1 μg/mL ↓ cancer cells viability: 20% for MCF-7, 30% for MDA-MB-231 IC_{50} = 100 μg/mL ↓cancer cell viability, ↓caspase 9, ↓ERK½, ↑JNK, ↑p38 60% for MCF-7, 80% for MDA-MB-231 ↑autophagic markers: ↑LC3BII, ↑beclin-1	(74)
MCF-7 breast adenocarcinoma	↓ proliferation	nanocapsules of bromelain ↓cells proliferation 72.6% at IC_{50} = 1.25 μg/mL 66.4% at IC_{50} = 0.625 μg/mL	(75)
	↓cells viability	↑cytotoxicity IC_{50} = >75 μg/mL	(76)
	↓cells viability	anti-proliferative 80% similar to taxol at IC_{50} > 50 μg/mL	(77)
4T1 breast adenocarcinoma	↓tumor mass ↑cytotoxicity	combination treatment of bromelain + cisplatin reduced tumor cells growth ↓GREM1 ↓IL-1β, ↓IL-4, ↓NF-kB, ↓PTGS2, ↓NO	(78)
MDA-MB-231 breast adenocarcinoma	↓cells viability ↑apoptosis	combination treatment bromelain IC_{50} = 2 μM + cisplatin IC_{50} = 1.5 μM ↓ cell viability to 50% bromelain IC_{50} = 0.9 μM + cisplatin IC_{50} = 4.0 μM ↓ cell viability to 70% ↓anti-apoptotic proteins: ↓cIAP 1, ↓Bcl-2, ↓CAT, ↓clusterin, ↓HO-1, ↓livin, ↓XIAP, ↓claspin, ↓HSP27 ↓IkB kinase, ↓NF-kB no effect on pro-apoptotic protein Bax	(79)
GI-101A breast adenocarcinoma	↓cells viability ↑apoptosis ↑cytotoxicity	IC_{50} = 5, 10, 20, 40, 50 μg/mL ↓cell viability 36% ↑apoptosis ↑DNA fragmentation ↑JNK, ↑kinase 38 ↑caspase-3, ↑caspase-9	(80)
MKN45, KATO-III, LS174 gastrointestinal carcinoma	↓cells survival ↑autophagy ↑apoptosis ↑mucin depletion	↓cells survival IC_{50} = 100 -600 μg/mL for MKN45, KATO-III IC_{50} = 30 μg/mL for LS174 synergic anticancer effects with N-acetylcysteine ↑caspase-3, 7, 8, ↓PARP, ↓cytochrome C ↓LC3-II, ↓Bcl-2, ↓ p-Akt, ↓Atg3, ↓Atg5, ↓Atg7, ↓Atg12, ↓Beclin 1, ↓MUC2, ↓MUC5AC	(81, 82)
AGS gastric carcinoma	↑cytotoxicity anti-proliferative	↑cytotoxicity IC_{50} >50 μg/mL	(76)
MPM malignant peritoneal mesothelioma	↓cells viability ↑autophagy ↑apoptosis	↓cell viability 60% at IC_{50} = 100 μg/mL ↑caspase-3, 7, 8, 9, ↑Cyt C ↓PARP, ↓ p-Ikkb, ↓NF-κB,↓ p-Akt	(83, 84)
SCC25 oral squamous carcinoma	↓cells viability	↓cell viability 31.07% at IC_{50} = 25 μg/mL	(85)
HepG2 hepatocellular carcinoma	↓cells survival ↑apoptosis ↓ cells proliferation ↓cells growth	↓cell viability IC_{50} = 25 μg/mL antioxidant in cell cancers: ↓SOD, ↓CAT, ↓GSH, ↓MDA	(86)

(Continued)

TABLE 2 Continued

Type of tested cancer cell lines	Effects	Results/Potential Mechanisms	Ref
	↑ cell cycle arrest in G2/M phase	↑apoptosis: ↑p53 ↓β- catenin	
PC3 prostate cancer	↓cell survival ↑apoptosis	↓cell viability 25% at IC_{50} >50 μg/mL	(76)
A431 epidermoid carcinoma A375 melanoma	↓cell survival ↑apoptosis	↑cytotoxicity IC_{50} = 200mg/mL for A431 IC_{50} = 400mg/mL for A375 cells ↑Bax, ↑Apaf-1, ↑caspases-3, 9, ↓Bcl-2	(87)
DLD-1, HT-29, HCT116 colorectal carcinoma	↑cytotoxicity ↑autophagy	IC_{50} = 50 μg/ml for HCT116 IC_{50} = 70 μg/ml for HT-29, DLD-1 ↑AIF, ↑Endo G, ↑caspases -3, -8, -9, ↑PARP-1, ↑ATG5/12, ↑Beclin, ↑p62, ↑LC3	(88)
Non-*Kras* mutant (Caco2 and NCI-H508) *Kras* mutant (HCT-116, DLD-1) colorectal carcinoma	↓cell viability ↑ferroptosis	↑cytotoxicity IC_{50} = 50 μg/mL Kras mutant cells were more susceptible ↓ACSL-4, ↑ miRNAs in Caco2 cells ↑ROS, ↑feroptosis *Kras* mutant cells	(89)
DMBA-TPA-induced mouse skin cancer cells	↑apoptosis ↓papilloma cells development	↓tumorigenesis ↓IκBα, ↓NF-κB, ↓COX-2, ↓Bcl-2, ↑Bax, ↑caspase 3, 9, ↑p53, ↓ERK1/2, ↓MAPK, ↓Akt	(90)
K562 human acute myeloid leukemia	↑apoptosis	↑peroxidase, ↑ROS, ↑Bax, ↑caspase-3, ↑Cyt C, ↓Bcl2, ↑p53	(91)
DLA Ascitic Dalton's lymphoma cells from mice	↑apoptosis	↑ROS, ↓Cyt C, ↓Bad, ↓Bax protein ↑NF-kB, ↑Bcl-2, x↑serum vitamin C, E	(92)
Mouse lung adenocarcinoma cells	↓carcinogenesis ↓inflammation ↓oxidative stress	bromelain plus ethanolic olive leaf extract ↑Nrf2, ↓NF-κB translocation, ↓IL-6, ↓TNF-α, ↓MMP2, ↓MMP9, ↑LPO, ↑ROS	(93)
TFK-1, SZ-1, cholangiocarcinoma cells	↑cytotoxicity ↑apoptosis	↓cells viability IC_{50} = 150 μM ↓NF-κB/AMPK, ↓p-AKT, ↓p-ERK, ↓p-STAT3, ↓MMP9 ↑PARP, ↑p-AMPK	(94)
C57BL/6N strain mice musculocutaneous flaps	↓necrotic inflammation	↓tissue necrosis by 25% ↓apoptotic cells, ↑angiogenesis	(95)

↑increase, ↓decrease, tumor inflammatory genes Gremlin (GREM1), interleukin 1β (IL-1β), interleukin-4 [IL-4], nuclear factor κB subunit 1 (NFκB1), and prostaglandin-endoperoxide synthase 2 (PTGS2), extracellular signal-regulated kinase ½ (ERK½), c-jun N-terminal kinase (JNK), light chain 3 protein B II (LC3BII), c-Jun N-terminal kinase (JNK), poly(ADP ribose) polymerase (PARP)-1, nuclear factor-kappa B (NF-kappaB), cyclooxygenase-2 (Cox-2), extracellular signal-regulated protein kinase (ERK1/2), mitogen-activated protein kinase (MAPK), 7,12-dimethylbenz(a)anthracene (DMBA)-initiated and 12-O-tetradecanoylphorbol-13-acetate (TPA), metalloproteinases MMP.

hours with bromelain at 25 μg/mL, 50 μg/mL, 100 μg/mL, and 125 μg/mL, showed a decrease in cell viability in a concentration-dependent manner (86). Bromelain cytotoxic effects were also tested in malignant Peritoneal Mesothelioma (MPM cells). This study showed a reduction of 60% in cell viability after 4 hours of treatment with 100 μg/mL, while at 72 hours of treatment the reduction in cell viability was much higher (>80%) (83).

Human breast cancer cells were frequently used to study the cytotoxic effects of different bioactive compounds (98–100). Azarcan and their collaborators showed that bromelain at 0.3 μM induced high mortality in breast adenocarcinoma and melanoma cell lines (36). Bhui and colleagues showed that bromelain in a dose and time-dependent manner induced a cytotoxic response in MCF-7 cells after 72 or 96 hours of treatment (74). Bromelain induced a reduction in cell proliferation of 72.6% (at 1.25 μg/mL) and 66.5% (at 0.625 μg/mL) at 24h in MCF-7 cells, however in this case bromelain was mobilized in nanocapsules surface by coordination with Zn^{+2} facilitating the entry into the cell (75). Similarly to previous data, Raeisi and collaborators tested the effects of bromelain in MCF-7 cells, where concentrations >75 μg/mL was able to induce cytotoxicity greater than 70% at 24h of treatment (76). Again in MCF-7 cells, another work established that bromelain at 50 μg/mL for 48h could reduce by 80% cell viability in a similar way that taxol (77). In GI-101A cells human breast cancer line, a decrease in viable cell number after 24h of treatment with different concentrations of bromelain (5, 10, 20, 40, and 50 μg/mL) was demonstrated (80). In particular, at 20 μg/mL, bromelain diminished the percentage of viable cells to 36%,

while higher doses caused cell death in the range of 95% or greater (80). Cytotoxic effects were also reported in another human cell line (PC3 prostate cancer cells) where a 25% reduction of cell viability was observed at concentrations >50 μg/mL in a dose-dependent manner (Raeisi et al., 2019).

4.2 Apoptosis

Apoptosis is a basic cell death mechanism, is vital in physiological processes, maintaining cellular homeostasis, and is detrimental in pathological processes, for example in tumour suppression (98, 101–104). This cell death process can be responsible for blocking cancer cell spread, intervening in the inhibition of the metastasis process (105, 106). Apoptosis has two pathways to be carried out, one that is considered internal, in which various families of proteins are implicated, and a second pathway, in this case external, in which different ligands bind to specific receptors (107). In both cases, various caspases, key proteins in executing the apoptotic signals, will be activated (108–110). Bromelain has been extensively studied for its implication in cell death, indeed it can intervene in the expression of Bcl-2, a type of protein with an anti-apoptotic effect but can also positively regulates the expression of apoptotic genes, such as Bax, Apaf-1, and caspases-9 and -3 (87). *In vitro* studies have shown that bromelain can induce apoptosis. In breast cancer cells, specifically in GI-101A cells, the use of this proteolytic enzyme positively regulates the N-terminal kinase c-Jun and kinase 38, in addition to improving the activity of caspases -3 and -9 at 24h (80). Moreover, bromelain's capacity to increase apoptosis has been shown in other cancer types. In different lines of colorectal cancer, the levels of apoptosis-inducing factor (AIF), Endo G, and caspases -3, -8, and -9 increased once the cells have been treated with bromelain (88). In another study with colorectal cancer cell lines, bromelain stimulated a process called ferroptosis (89).

Ferroptosis is a type of cell death, also programmed, which depends on iron, and is characterized by an accumulation of lipid peroxides. Currently, this type of cell death is being studied as a mechanism to combat cancer cells (111) (112). In this study, an increase in the expression of ACSL-4 has been observed after treatment with bromelain in Caco2 cells (89). This protein is responsible for ferroptosis to take place, thus bromelain also exerted cytotoxic effects against colorectal cancer cells and could reduce polyp number and submucosal layer length in mice (89). From another study, it has been possible to corroborate the effect of bromelain with other enzymes or pathways that intervene in apoptotic processes. This is the case of cyclooxygenase-2 (Cox-2) or the MAPK and Akt/protein kinase B (PKB) pathways, all of which downregulate their expression (90). In particular, bromelain acted by inhibiting the phosphorylation of IκBα, which triggers the retention of NF-κB in the cytosol, decreasing the expression level of Cox-2 (90).

In human cholangiocarcinoma cells (TFK-1, SZ-1), bromelain (and papain) blocked NF-κB/AMPK signalling, inducing cytotoxic effects through the activation of apoptosis in both cell lines after 48h of treatment (94). Apart from apoptosis, the anti-cancer effects of bromelain appear to be also controlled by necrosis, a process in which cell death occurs because of adverse external cell conditions such as injury, trauma, or infections that lead to unregulated digestion of cell components (113). In a recent study with C57BL/6N strain mice, the use of bromelain reduced tissue necrosis by 25% (95). A higher density of functional microvessels was lost compared to controls, as well as a decrease in myeloperoxidase-positive neutrophils, and a reduction in apoptotic cells (95). Therefore, the use of bromelain could be considered in the future as a therapy to prevent cell necrosis, a harmful cell process that often results in inflammation and tissue damage (95).

4.3 Autophagy

Another process in which the implication of bromelain has been verified is autophagy. This mechanism focuses on the degradation and recycling of cellular components (107, 114, 115). In the case of cancer, this process has a dual activity, since it is capable of promoting the survival of cancer cells, through protective autophagy, or participating in the death of these cells, inducing cytotoxic autophagy (116, 117). In normal tissues, autophagy at the basal level is necessary as it provides housekeeping functions as well as increased apoptosis (118, 119). Even in periods of stress and hunger, the autophagy process is necessary (120). Differently, in cancer cells this process can allow them to survive metabolic stress, for example, being a source of energy in the face of a possible lack of nutrients, which is why its inhibition or activation in cancer cells is not completely understood (120). Although autophagy may present this duality, various studies showed that bromelain participated in the reduction of cells of different cancer types through the activation of this process. In MCF-7 cells treatment with bromelain increased the autophagic process and slow down their growth (74). In that same study, pre-treated cells with 3-methyladenine (autophagy inhibitor) demonstrated a decrease in the apoptotic process, thus showing that autophagy can affect the onset of apoptosis (74). In colorectal cancer cells, it has been shown an increased level (2 to 3 times) of autophagy with the creation of lysosomes in the cells treated with bromelain. Concurrently, levels of proteins related to autophagy were enhanced, such as ATG5/12, Beclin-1, p62, and LC3I/II (88).

4.4 Immunomodulatory

The immunomodulatory effects of bromelain have been studied extensively, showing that it can activate or suppress the mammalian immune system (121). One of the first researches was conducted on human T cells from bromelain-

treated PBMC stimulated by mitogenic CD2 mAb to explore the migration and activation of lymphocytes (122). Bromelain acted by removing the extracellular domains of the CD44, CD45RA, E2/MIC2, CD6, CD7, CD8, and Leu 8/LAM1 surface molecules and thus enhancing T cell activation through CD2. The continuation of the research expanded the use of bromelain in monocytes and granulocytes and extended the surface molecules affected by the enzyme, again remarking on the promoting effects on adhesion and activation of immune cells (123). Also, human peripheral blood lymphocytes were pretreated with bromelain to study the anti-proliferative activity in different cancer cell lines (124). The authors reported that lymphocytes were boosted by the enzyme and could enhance the immune system response to the fight against cancer at least *in vitro* experiments. More strictly to human studies, in 16 breast cancer patients treated for 10 days, bromelain could reduce CD44 expression (similar to above), while augmenting CD11a and CD62L expression (125). The work was done on PBMC of breast cancer patients, where also monocytic activity was increased, suggesting that bromelain could stimulate the suppressed immunocytotoxicity of monocytes at least in a proportion of breast cancer patients (only 40% responded to the enzyme). Opposite effects of bromelain were also reported, such as those blocking signal transduction through Raf-1/MEK/ERK-2 signaling pathway in stimulated T helper cells (126). The inhibition was probably unspecific, as it acted on ERK-2 and p21ras of T cells, however proteolytic-dependent, evoked by selective cysteine protease inhibitor in further experiments.

In another tissue cell model (splenocyte cultures), the enzyme could induce TCR-mediated T cell proliferation, but not $CD4^+$ or $CD8^+$ lymphocytes, with concomitant inhibition of TCR-mediated IL-2 production albeit T cells growth (127). In addition, the work showed that Ag-specific B cell antibody response was expanded in bromelain-treated mice, though IL-2 mRNA expression was simultaneously blocked. The authors remarked as bromelain could concurrently boost and inhibit T cell responses, depending on the immune environment and consequently, the enzyme could be potentially implicated in T cell autoimmunity. Bromelain was also studied in the innate immune system, where it could enhance and sustain the process. In a recent study, murine macrophages (RAW 264.7 cells and primary macrophages) were challenged with the enzyme, that caused IFN-γ-mediated nitric oxide and TNFα production to strengthen human defences (128). In addition, in murine natural killer, bromelain was able to augment IL-2- and IL-12-mediated IFN- γ production, IL-6, and Gm-CSF, while reducing T helper cells activation.

4.5 Inflammation

One important property of bromelain is its anti-inflammatory action. Since ancient times, pineapple as the main source of bromelain has been widely applied against inflammation disorders (34). The main applications of bromelain concern the edema processes of an inflammatory nature in the medical and surgical fields. Bromelain administered i.p. and orally at doses of 5-10, mg/kg reduces edema and inflammation in animals due to histamine, formalin, dextran, carrageenan and egg albumin. At the level of inflammatory tissue, bromelain reduces vasodilation, and increased capillary permeability, leukocyte migration and local pain by inhibiting the formation of bradykinin and serotonin. In addition to these, bromelain exhibited anticancer activity and the ability to induce apoptotic, necrotic and autophagic mechanisms.

More recently, the inflamed colon tissue was used as a model to evaluate the bromelain anti-inflammatory role. For example, in spontaneous colitis (in C57BL/6 IL-10-/- mice) the enzyme was able to reduce histological and clinical signs of inflammation (129). The research was expanded with the use of pineapple juice or purified bromelain in the same animal model, showing that both treatments could lessen colon inflammation and neoplastic lesions (130). Previously in colon biopsies from patients affected by ulcerative colitis and Crohn's disease, bromelain *in vitro* experiments resulted in diminished amounts of IL-2, IL-6, IL-4, G-CSF, Gm-CSF, IFN-γ, CCL4/macrophage inhibitory protein (MIP)-1β, and TNF, implying a role in inflamed colon against pro-inflammatory cytokines and chemokines (131). Moreover, in the murine inflammatory bowel disease model, a reduction in neutrophil migration was demonstrated through the blockade of the CD128 chemokine receptor (132). Reduced cytokines/chemokines expression and alteration of white blood cell trafficking can impact on tumor microenvironment, another possible immune-mediated and anti-cancer effect of bromelain.

In another inflammatory disorder, bromelain has notably been shown to reduce inflammation in the gastro-enteric environment (133). In particular, using 3 different cell lines as digestion simulated models (AGS, Caco-2, and SW1353 cells), the authors demonstrated that a proprietary bromelain extract could decrease IL-8, COX-2, iNOS, and TNF-α without affecting cell viability. In addition, bromelain inhibited the iNOS and COX-2 expression in LPS-stimulated RAW 264.7 cells presumably as a result of inhibiting ERK (extracellular signal-regulated kinase) and p-38 phosphorylation (134).

Zhou and co-authors have reported that purified fruit bromelain could stop epithelial TNF-α receptors in rat colitis models and intestinal cell line IEC-6 and Caco-2 cells (43). The work reported that colitis symptoms were ameliorated, together with reduced macroscopic damage, decreased mucosal inflammation, and tight junction barrier recovery.

Bromelain can accelerate tissue repair processes as a result of the depolymerization of intercellular structures and modification of vascular permeability (135). The biological effects of bromelain have been partially associated with the modulation of the arachidonic acid cascade (124), similar to another study that showed the alteration of arachidonic acid metabolism with anti-inflammatory and antiplatelet effects of

bromelain (135). Bromelain therapy resulted in platelet formation reduction with increased resistance to aggregation (136). It experimentally induced inflammatory reactions in the rat with the interference of eicosanoid formation in the arachidonic acid cascade (124) and could modulate the immune system as an anti-inflammatory factor (71).

Habashi and co-authors have also reported that bromelain potentially exerted anti-inflammatory effects by reducing nitric oxide synthesis *in vitro* without cytotoxicity (137). Bromelain downregulated COX-2 and PGE-2 (prostaglandin E2) expression levels in cells (138). Bhui and co-authors explored that bromelain inhibits COX-2 expression by blocking the activation of MAPK-regulated NF-kappa B against skin tumor initiation triggering the mitochondrial death pathway (139). Bromelain was able to inhibit PGE2 production (56.3%) in doses of 40 mg/kg in the rat (140). In addition, after 10 and 20 mg/kg oral application of bromelain in rats, it reduced inflammations mediators, such as PGE2 and substance P (tachykinin family of peptides) production in plasma and peripheral tissues (141).

Anti-inflammatory effects of bromelain were observed at 100 μg/mL in LPS-induced human U937 macrophages by suppressing macrophage inflammatory protein-1 (MIP-1α and MIP-1β), monocyte chemoattractant protein-1 (MCP-1), IL-8, IL-1 β, IL-6 and COX-2 (142). Moreover, bromelain (50-100 μg/ml) reduced TNF-α, IL-1β and IL-6 from LPS-induced peripheral blood mononuclear cells and monocytic leukemia THP-1 cells (143). Similarly, another work suggested that bromelain could regulate inflammatory cytokines and growth factors, including TNF-α, IL-1β, IL-6, and IFNγ (144). Moreover, 2.5 mg/kg intragastrically application of cross-linked bromelain with organic acids and polysaccharides (CL-bromelain) for 7 days considerably showed anti-inflammatory effects *via* reduction of NF-κB activity and COX-2 mRNA expression in rat livers (145). In addition, CL-bromelain was reported for its suppression of ERK, c-Jun N-terminal kinase, and p38 mitogen-activated protein kinase (145). Kalra and others have reported that bromelain regulates p53, NF-kB, and COX-2 expression by targeting the mitogen-activated protein kinase pathway in mouse skin (90). Plasma prekallikrein and kininogen notably decreased fifteen minutes after a single injection of bromelain (10 mg/kg) in rats and gradually recovered over 72 hours (146).

Another hypothetic role of bromelain is in the inflammation caused by advanced glycation end-products (AGEs). It has been shown that the enzyme could increase the soluble form of receptor for advanced glycation end products (sRAGE) in 11 patients affected by chronic kidney disease (CDK). It is known that kidneys are implicated in the removal of sRAGE and circulating AGEs and non-AGE ligands are present in CKD (128). The authors suggested that the rise of sRAGE in CDK patients was associated with an improved detaching of the cell surface RAGE, however, bromelain's role in CDK or AGE removal is still unclear, in particular for the small number of patients analyzed (147).

5 Synergistic anticancer effects of bromelain combined with chemotherapeutics or other bioactive compounds

Bromelain delivery in association with other molecules is often used to obtain a synergistic effect. Although bromelain alone has shown apoptotic effects in cancer cell lines, other studies combining this enzyme with other compounds or extracts have been developed. An example is the combination of this enzyme with peroxidase, indeed their association produced additive effects with an intensification of intracellular ROS level and disruption of mitochondrial membrane potential, leading to acute myeloid cells (K562) growth inhibition. In addition, they participated in the regulation of the expression of Bax, Bcl2, caspase-3, and cytochrome, which are highly related to apoptosis, as well as promoting a positive regulation of p53, a key molecule involved in cell death (91). In another study, the combination of olive leaf extract (*Olea europaea* L.) and bromelain could have promising effects against lung cancer (93). Combining ethanolic olive leaf extract (EOLE) with bromelain increased Nrf2 translocation from the cytoplasm to the nucleus and terminated the translocation of NF-κB from the cytoplasm to the nucleus. Furthermore, the levels of IL-6 and TNF-α, as well as some metalloproteinases, decreased, suggesting that this association could reduce lung carcinogenesis through the regulation of inflammation and oxidative stress (93).

The combination of curcumin, harpagophytum and bromelain has been shown to reduce inflammation and pain in osteoarthritic human synovial cells, through the decrease of prostaglandin E2, Nerve Growth Factor (NGF), IL-6 (148). Similarly to the previous study, the combination treatment of bromelain, trypsin, and rutin resulted in a significant reduction in pain and inflammation in 103 patients with osteoarthritis of the knee (149). This randomized double-blind study demonstrated that the combination regimen was efficacy in 51.4% of the osteoarthritis patients (while for the control group, diclofenac treatment, was 37.2%), thus sufficiently better to induce the authors to suggest this treatment as a new potential tool for osteoarthritis.

Bromelain may increase the cytotoxicity of cisplatin in the treatment of breast cancer as reported in 2 studies with MDA-MB-231 and 4T1 Breast Tumor cell lines (78, 79). Besides the use of bromelain as a single drug, there are studies in which the effect of bromelain has been combined with other molecules, such as N-acetylcysteine. The combination of the two compounds in different gastrointestinal cancer cell lines showed significant

inhibition of cell proliferation, with an increase in autophagosomal markers such as LC3-II (81). In another study, malignant peritoneal mesothelioma (MPM) cells were exposed to the combination of bromelain with cisplatin and fluorouracil, showing cytotoxic effects against these cells in the mixture between bromelain and cisplatin (84).

Bromelain and N-acetylcysteine (NAC) constitute two active ingredients capable of inhibiting the growth and proliferation of induced peritoneal tumors in mice as model animals. Intraperitoneal administration of tumor cells in association with bromelain and NAC showed that bromelain/NAC as a single agent or combination treatment on alternate days inhibited tumor growth and the number of peritoneal nodules in a dose-dependent manner (82). This activity can be traced back to the proteolytic activity of bromelain and the mucolytic activity of NAC. It is known that some mucins, highly glycosylated high molecular weight proteins (i.e. MUC2 and MUC5AC), are involved in the pathogenesis of cancer. Some tumors may use mucins during invasion, metastasis and growth in otherwise inhospitable sites (Byrd & Bresalier, 2004). Besides, extracellular mucus presents a clinically relevant barrier to effective therapy in mucinous cancers. Thus, extracellular mucolytic would decrease compressive effects from bulky mucinous tumor burden. Such an effect was observed when a combination of bromelain + NAC was used to lysate extracellular mucus in the experimental animal model. Bromelain is made up of a mixture of hydrolytic enzymes, not only with endopeptidase activity, hydrolyzes esters, amides and glycosidic bonds, while NAC can reduce disulfide bridges. Such a combination impaired the complex lattice framework of mucus thus improving drug delivery and increasing cytotoxic effects (150).

Bromelain-based mucus-disrupting strategies are also gaining much attention as an effective tool in decreasing the mucus barrier. However, this effect of bromelain may be ineffective, if not harmful, in some circumstances. Non-Small Cell Lung Cancer (NSCLC) is any type of epithelial lung cancer other than small cell lung cancer (SCLC). There are different types of NSCLC which represent about 90% of all lung cancer cases. A significant percentage of these NSCLC cases are characterized by the expression of the anaplastic lymphoma kinase (ALK) protein. Inhibition of ALK is a target for slowing proliferation in NSCLC. Commercial bromelain was tested to evaluate efficacy during the administration of certain ALK inhibitor drugs such as alectinib (ALC), ceritinib (CER), and crizotinib (CRZ). Interestingly, bromelain administration in male Wistar rats caused a significant decrease in plasma levels of CER and CRZ along with an increase in the apparent clearance. However, no significant effect was noticed with ALC (151). Thus, the well-known bromelain muco-permeation enhancing effect can sometimes have unwanted effects.

Even the simple administration of bromelain in mice challenged with 4T1 triple-negative breast cancer cells can increase the effectiveness of anticancer drugs with severe side effects. Animals receiving cisplatin and bromelain jointly showed more significant effects in tumor shrinkage than those receiving bromelain and cisplatin separately by modulating the tumor environmental inflammation (78).

Significant benefits could be obtained if the administration of bromelain allowed the total elimination of synthetic drugs with anticancer activity, which often cause severe side effects. An interesting attempt was made against Dalton's ascites lymphoma tumor model in Swiss albino mice. When bromelain was used in association with peroxidase, the two enzymatic systems were able to counteract some of the typical effects of lymphoma. In fact, during the progression of the tumor the white blood cell count was increased as well as the number of abnormal leukocytes, while the red blood cell count decreased. These negative effects were mitigated following the administration of bromelain and peroxidase, both enzymatic systems found in some pineapple extracts. This may be due to the increase in tumor cell apoptosis (92) resulting from the increase of pro-apoptotic protein factors and the restoration of ROS levels by controlling the activity of antioxidant enzymes.

A similar approach aims to replace drugs with antioxidant substances extracted from plants rich in phenolic compounds. For this purpose, ethanol extract of *Olea europaea* leaves (EOLE) in combination with bromelain was used to evaluate the amelioration of various hallmarks associated with benzo(a)pyrene-induced lung carcinogenesis in male Swiss albino mice (Majumder et al., 2021). The combined treatment of bromelain and EOLE significantly restored body weight and lung weight in treated animals thus suggesting protection due to the inactivation of excess ROS and/or through inhibition of inflammation or deactivating inflammatory markers. The same kind of antioxidant protection can explain the observed general improvement in lung tissue architecture. Hydroxytyrosol and oleuropein are the main components of the polyphenolic fraction of *Olea europaea*, and their antioxidant potential has long been recognized. On the other side, inflammation provides various molecules essential to the formation of a microenvironment suitable for tumor development. Such molecules include growth factors, survival factors, proangiogenic factors and extracellular matrix-modifying enzymes (Ben-Baruch, 2006). Treatment with bromelain-EOLE reduced some crucial proinflammatory cytokines (TNF-α and IL-6), and also interrupted the NF-kB translocation. Altogether, a combination of EOLE and bromelain alleviated the benzo(a) pyrene-induced lung carcinogenesis associated with pulmonary oxidative stress and inflammation (Majumder et al., 2021).

The various strategies for the fight against cancer include also radiotherapy, the effectiveness of which can be limited by the radioresistance of some tumors as well as by the undesirable effects affecting normal tissues. The development of radiosensitizing drugs has therefore found application in the treatment of tumors by radiotherapy. Radiosensitizers are intended to enhance tumor cell killing while having much less effect on normal surrounding tissues. Some drugs target different physiological characteristics of the tumor, particularly hypoxia

of the solid tumor tissue which is considered a major cause associated with radioresistance. From this perspective, the hypothesis that bromelain acts as a radiosensitizer and radioprotector becomes suggestive. Mekkawy and coworkers make this hypothesis their own through *in vivo* studies in Ehrlich solid tumor (EST) bearing mice (152). The size and weight of tumors in gamma-irradiated EST-bearing mice treated with bromelain decreased significantly with a significant amelioration in the histopathological examination (Mekkawy et al., 2020). The benefits could be linked to the gene expression of some nuclear factors (poly ADP ribose polymerase-I, NF-κB), and peroxisome proliferator-activated receptor α together with restored liver function. Besides, bromelain radiosensitizing action could be expressed through increasing lipid peroxidation and ROS production in tumor tissue, inhibition of repair of DNA strand breaks and inhibition of proliferation (153).

6 Clinical studies

The administration of bromelain in tumor patients has been also tested in a few numbers of clinical studies and could represent an adjuvant treatment in cancer care. The immunotoxicity effect of monocytes and lymphocytes against target cells of mammary carcinoma (K562 and MDA-MB-231) was tested *in vitro* after 10 days of oral bromelain administration in breast cancer patients (daily up to a dose of 7800 mg) as above mentioned (paragraph 4.4) (Eckert et al., 1999). Eckert and coworkers found that the intake of the bromelain increases the activity b-MAk and MAK of patient monocytes about 2-fold; in the responder patients, it was recorded an increase in cytotoxicity of b-MAK and MK cells respectively from 7.8% to 54% and from 16% to 47%. No detectable IL-1β from monocyte was found in patients before, during and after the treatment in contrast with what was recorded in healthy blood donors, and no effects were observed in NK and LAK-cell activity in the patient cohort. Moreover, the oral intake of bromelain reduced the expression of the cell surface markers CD44 but poorly increased the expression of CD11a and CD62L without changing the level of CD16. These effects were observed also *in vitro* with a higher decrease in the expression of CD16 and CD44. On the whole, the bromelain's capacity to improve the monocytic cytotoxicity of breast tumor patients makes it suitable as alternative support care in combating cancer.

The anti-cancer properties of bromelain, in combination with N-acetylcysteine, were used also to produce a new drug (BromAc®) which has been recently proved effective in the recurrent thoracic pseudomyxoma peritonei (PMP) treatment (154). According to the bromelain-based mucus-disrupting activity (see above), the mucolytic properties of BromAc® help the tumor dissolution when it was injected directly into mucinous disease. However, its effectiveness is related to neoplastic characteristics. Tumors with soft or intermediate textures are more susceptible to the drug's action. In the first two cases reported, effectively, large response differences were reported, possibly due to the tumor consistency (Lam et al., 2021). The safety profile was however good as also the objective response.

In a phase I study, the safety of bromelain treatment was tested on 20 patients affected by inoperable mucinous cancer. Among the patients, 13 had intra-tumoral treatment and 7 had intraperitoneal treatment (Valle et al., 2021). Intra-tumoral doses consisted of 30-45 mg of bromelain and 1.5 g of NAC while intraperitoneal doses of 45-60 mg of bromelain and 1.5-2 g of acetylcysteine, administrated in 5% glucose. The volume of the fluidized tumor removed was measured and collected for laboratory analysis. The side effects of treatment were recorded after 24 h. Adverse effects were observed in 85% of patients. The main side effects were fever (35%), pain in the injection site (30%), rise in C-reactive protein (CRP)(80%) and white blood cells (WBC) (55%). No death or anaphylactic reactions were recorded. Although the study was carried out on a small number of patients, it was nevertheless promising as in 15 patients (75%) a reduction in tumor-related symptoms after BromAc® administration was reported with manageable side effects.

BromAc® safety was investigated also using blood parameters in 25 patients (mean age 64) with inoperable PMP pre and post-treatment administration (Ke et al., 2021). Patients received bromelain mean dosage of 124 mg and 4.9 g of NAC for each period of treatment, which consisted of an average of 3.8 drug administration on different days. It was tested in the high and low-dose subgroups (mean of 64 mg of bromelain + 2.7 g of NAC and 183 mg of bromelain plus 7.2 g of NAC respectively). An increase in CRP values and WBC, neutrophils and monocytes in both high and low-dose subgroups was found, with a concomitant decrease in albumin and lymphocyte levels suggesting an inflammatory reaction. The other blood parameters, including liver enzymes or coagulation parameters, have not undergone any alteration. This aspect is important in the evaluation of BromAc® safety, that have not shown liver or kidney toxicity.

The role of bromelain (in combination with papain, sodium selenite and *Lens culinaris* lectin) has been also tested as a complementary medicine on more than 600 breast cancer patients to reduce the side effects caused by the administration of the adjuvant hormone therapy. Side effects were measured by scoring from 1 (no side-effects/optimal tolerability) to 6 (extreme side-effects/extremely poor tolerability) The main side effects, arthralgia and mucosal dryness, were drastically reduced after 4 weeks ($p<0.001$) and 8 weeks ($p<0.0001$) of treatment (155, 156).

On the whole, these results support further studies on the role of bromelain in the treatment of tumors possibly representing a non-invasive treatment for people suffering from cancer. Despite these promising effects, the number of clinical trials is low and limited to early stages. More efforts are

thus desirable to validate a promising new strategy for inoperable neoplastic cases.

7 Toxicity and safety data

The recent studies underline its safety and easy of administration with sufficient bioavailability and tolerability both in animal and human studies. Indeed toxicity studies showed a lethal dose of LD50 greater than 10 g/kg in mice, without carcinogenic or teratogenic effects at dosages of 1.5 g/kg per day (157, 158). Other recent studies have shown few side effects arising as a result of taking bromelain in both animals and humans, thus bromelain is considered relatively safe. The main side effects are attributable to the gastrointestinal system (stomach pain and diarrhea), although allergic reactions are always possible in predisposed individuals (159). Bromelain is considered to be safe and it is an effective agent in burn debridement. In Europe, bromelain is approved as a non-steroidal anti-inflammatory agent for oral and topical use for surgical wounds, inflammation, and debridement of deep burns (159, 160). A single 4-hour application of the bromelain-based agent completely debrides deep partial-thickness burns in a validated porcine model (161).

8 Limitations, challenges and prospects

Numerous studies in the literature were focused on the anti-cancer role of bromelain, highlighting its importance in cell processes such as apoptosis and necrosis (95). Available data on bromelain also suggested that the enzyme possesses anti-inflammatory activity in acute and chronic inflammation which are associated with cancer. Bromelain can modulate the metabolism of arachidonic acid affecting the production or activity of cytokines and growth factors involved in the inflammatory process. There are numerous published data on the potential mechanism of action of bromelain in anti-inflammatory activity. Nonetheless, they are not exhaustive and leave many questions unanswered: additional anti-inflammatory works are necessary for a better understanding of its mechanism of action. Many preclinical pharmacological studies showed that Bromelain affected cell viability of cancer cells, however, the exact mechanisms of action produced by bromelain are rarely explored. Nonetheless, it is reported that bromelain could act as an immunomodulator by improving the weakened immunocytotoxicity. Other recent studies showed that bromelain stimulates autophagy which is involved in cancer progression and drug resistance. The activation of autophagosome and lysosome formation by bromelain induces cancer cell death, a key factor that should be more profitably exploited in future research.

A complex picture of the effects of bromelain on the immune system is also perceived. Indeed, most of the published papers reported an immunomodulatory activity of bromelain, with a different behavior based on a specific tissue or cell type. Preclinical pharmacological experiments represent the vast majority of research on the effects of bromelain on the immune system, from which it appears that in the future it is necessary to test bromelain in larger clinical studies in humans. Moreover, its cytotoxic effects in cancer cells could be triggered by proteolytic activity, or by platelet aggregation-inhibitory activity or anti-inflammatory properties (16). Tumour cells with such compromised processes are potential targets of bromelain. In addition, it is known that cancer cell death can be induced in different ways, such as *via* apoptosis, necrosis, and autophagy.

The lack of wide clinical trials leaves the opportunity to further test bromelain in humans, giving the possibility to clinicians to lay clear indications of its use. Another issue to be expanded in future research will be bromelain association with other compounds, as above mentioned in some successful works (78, 82, 84, 92–94, 162–164). The possibilities are enormous, and should not be limited to chemotherapeutic drugs (78, 84, 162–164), but expanded to other drug categories, such as anti-hypertensives, hypoglycemics, anti-asthmatics, anti-microbials, immunomodulators, etc. Moreover, it should be kept in mind that bromelain is highly attractive for the industry, given its indispensable nature in foods, cosmetics, pharmaceuticals, and textiles.

A key limitation factor for the successful use of bromelain as a potential anticancer agent is its production and method of extraction: the more these are reduced and the more the market expands. Indeed, more economical but equally effective bromelain will be highly competitive with other products or other sources and will facilitate its use among both the population and industry. This could in turn generate a scientific relapse with the initiation and extension of new and old research in this field. It is expected that in the next future bromelain will be deeply studied and explored, especially focusing on its anti-cancer activity, as this kind of disease is considered the second leading cause of death all over the world (165).

New perspectives and strategies have been proposed to increase the anti-cancer effects of Bromelain from the bench to bedside. The most promising approach is to enhance the bioavailability of bioactive compounds using new pharmaceutical nanoformulations (166). Thus and simple bromelain delivery may require high doses of the active principle also due to the characteristics of the extracellular matrix (ECM) which constitutes a barrier that slows down or prevents the spread of drugs in the parenchyma of the tumor. For this reason, other delivery methods have been investigated. NPs-based delivery systems can offer an effective alternative. The proteolytic activity of bromelain can pave the way for these

antitumor drug delivery systems by increasing their penetration into the cell, weakening the resistance of ECM proteins. Thus, doxorubicin, a potent anticancer drug, but with heavy side effects, was delivered in association with chemically immobilized bromelain, by lactobionic acid-modified chitosan NPs. *In vivo* drug biodistribution and antitumor activity in ICR, male mice model lead to higher drug concentration in tumor area and superior antitumor effect (Wang et al., 2018).

Pancreatic cancer is one of the most difficult cancers to treat largely because of the inability of anticancer drugs to penetrate the malignant tissue as a result of the dense ECM (167). This can limit the effect of bromelain in degrading the tumor ECM due to the short half-life of bromelain in the blood. An interesting technology has recently been developed capable of increasing blood retention of proteins termed "Self-assembly PEGylation Retaining Activity (SPRA)" (Higashi et al., 2020). This technology based on reversible poly (ethylene glycol) (PEG) modification was applied to stabilization of bromelain *in vivo*, thus enhancing antitumor activities of doxorubicin and doxorubicin encapsulated in PEGylated liposomes (DOXIL) in tumour-bearing mice. The release rate of doxorubicin can be increased by using nanocarriers prepared by crosslinking bromelain with an ortho-ester-based crosslink agent. The release of bromelain in tumour-bearing mice by pH-sensitive NPs increased the hydrolysis of the ECM favoring the penetration of the anticancer drug (164). Bromelain can also be uploaded to obtain poly(lactic-co-glycolic acid) NPs (bromelain-PLGA NPs). Such a delivery system was evaluated for its anti-cancer efficacy in 7,12-dimethylbenz[a]anthracene (DMBA)-induced and 12-O-tetradecanoylphorbol-13-acetate (TPA) promoted 2-stage skin tumorigenesis model in Swiss albino mice. Bromelain-PLGA NPs showed the most significant chemopreventive and chemotherapeutic effects when compared with free bromelain (Bhatnagar et al., 2015). Bromelain-NPs possibly acted by maintaining a balance between the positive and negative regulators of apoptosis and triggering more cells to apoptosis than free bromelain.

9 Conclusions

Bromelain, the main medicinal component of pineapple, was discovered in the late 1800s and since that time research continues to increase available data on its potential benefits. Bromelain is an enzyme with numerous pharmacological properties, as it can act on different health disorders, including osteoporosis and osteoarthritis, diarrhea, chronic wounds, surgical debridement, edema, inflammation, and cancer. Nonetheless, clinical uses of bromelain are limited and poorly representative. The anticancer properties of bromelain are extensively documented *in vitro* experiments, but such demonstrations *in vivo* animal models are far less. The methods and techniques of administration/delivery of bromelain vary significantly. Modalities were tested that involved both the administration of bromelain alone, and in association with other molecules, but the most promising use was the formulation of nanoparticles. Novel approaches to cancer chemotherapy are warmly urgent and bromelain could be regarded as an important tool in the cancer fight.

Several clinical properties have been ascribed to bromelain *vide supra* including anticancer activity. Besides, the utility of these proteins also comprises the cosmetic field, food and beverage production and textile industries as a consequence, the industrial demand in the last few years increased. This phenomenon further affected the final price of the product. However, the protein isolation and purification costs are responsible for more than half of the final commercial price.

Author contributions

All authors made a significant contribution to the work reported, whether that is in the conception, study design, execution, acquisition of data, analysis, and interpretation, or in all these areas - that is, revising or critically reviewing the article; giving final approval of the version to be published; agreeing on the journal to which the article has been submitted; and confirming to be accountable for all aspects of the work. All authors have read and agreed to the published version of the manuscript.

Acknowledgments

MM wants to thank ANID FONDECYT Iniciación 11190641 and ANID CENTROS BASALES ACE210012.

Conflict of interest

The authors declare that the research was conducted in the absence of any commercial or financial relationships that could be construed as a potential conflict of interest.

Publisher's note

All claims expressed in this article are solely those of the authors and do not necessarily represent those of their affiliated organizations, or those of the publisher, the editors and the reviewers. Any product that may be evaluated in this article, or claim that may be made by its manufacturer, is not guaranteed or endorsed by the publisher.

References

1. Mitrut P, Docea AO, Kamal AM, Mitrut R, Calina D, Gofita E, et al. Colorectal cancer and inflammatory bowel disease. colorectal cancer - from pathogenesis to treatmen. IntechOpen Rodrigo L, editor (2016), pp. 185–99. doi: 10.5772/63408

2. Jain D, Chaudhary P, Varshney N, Bin Razzak KS, Verma D, Zahra TRK, et al. Tobacco smoking and liver cancer risk: Potential avenues for carcinogenesis. *J Oncol* (2021) 2021. doi: 10.1155/2021/5905357

3. Sharifi-Rad J, Quispe C, Patra JK, Singh YD, Panda MK, Das G, et al. Paclitaxel: Application in modern oncology and nanomedicine-based cancer therapy. *Oxid Med Cell Longevity* (2021) 2021:3687700. doi: 10.1155/2021/3687700

4. Yokoyama Y, Kubo-Kaneda M, Sunada K, Teishikata Y, Kitamura A, Okamoto K, et al. Adverse events associated with long-term treatment of epithelial ovarian cancer with bevacizumab and chemotherapy. *Anticancer Res* (2022) 42(8):4165–71. doi: 10.21873/anticanres.15916

5. Dhyani P, Quispe C, Sharma E, Bahukhandi A, Sati P, Attri DC, et al. Anticancer potential of alkaloids: A key emphasis to colchicine, vinblastine, vincristine, vindesine, vinorelbine and vincamine. *Cancer Cell Int* (2022) 22 (1):206. doi: 10.1186/s12935-022-02624-9

6. Sharifi-Rad J, Quispe C, Butnariu M, Rotariu LS, Sytar O, Sestito S, et al. Chitosan nanoparticles as a promising tool in nanomedicine with particular emphasis on oncological treatment. *Cancer Cell Int* (2021) 21(1):318–8. doi: 10.1186/s12935-021-02025-4

7. Quetglas-Llabrés MM, Quispe C, Herrera-Bravo J, Catarino MD, Pereira OR, Cardoso SM, et al. Pharmacological properties of bergapten: Mechanistic and therapeutic aspects. *Oxid Med Cell Longev* (2022) 2022:8615242. doi: 10.1155/2022/8615242

8. fSharifi-Rad J, Dey A, Koirala N, Shaheen S, El Omari N, Salehi B, et al. *Cinnamomum* species: Bridging phytochemistry knowledge, pharmacological properties and toxicological safety for health benefits. *Front Pharmacol* (2021) 12:600139–9. doi: 10.3389/fphar.2021.600139

9. Sharifi-Rad J, Bouyahya A, El Menyiy N, El Omari N, Shahinozzaman M, Ara Haque Ovey M, et al. Ethnobotany, phytochemistry, biological activities, and health-promoting effects of the genus *Bulbophyllum*. *Evid Based Complement Alternat Med* (2022) 2022:6727609. doi: 10.1155/2022/6727609

10. Taheri Y, Quispe C, Herrera-Bravo J, Sharifi-Rad J, Ezzat SM, Merghany RM, et al. *Urtica dioica*-derived phytochemicals for pharmacological and therapeutic applications. *Evid Based Complement Alternat Med* (2022) 2022:4024331. doi: 10.1155/2022/4024331

11. Painuli S, Quispe C, Herrera-Bravo J, Semwal P, Martorell M, Almarhoon ZM, et al. Nutraceutical profiling, bioactive composition, and biological applications of lepidium sativum l. *Oxid Med Cell Longevity* (2022) 2022:2910411. doi: 10.1155/2022/2910411

12. Matagne A, Bolle L, El Mahyaoui R, Baeyens-Volant D, Azarkan M. The proteolytic system of pineapple stems revisited: Purification and characterization of multiple catalytically active forms. *Phytochemistry* (2017) 138:29–51. doi: 10.1016/j.phytochem.2017.02.019

13. Arshad ZI, Amid A, Yusof F, Jaswir I, Ahmad K, Loke SP. Bromelain: An overview of industrial application and purification strategies. *Appl Microbiol Biotechnol* (2014) 98(17):7283–97. doi: 10.1007/s00253-014-5889-y

14. Ramli AN, Aznan TN, Illias RM. Bromelain: From production to commercialisation. *J Sci Food Agric* (2017) 97(5):1386–95. doi: 10.1002/jsfa.8122

15. Gonzalez-Rabade N, Badillo-Corona JA, Aranda-Barradas JS, Oliver-Salvador Mdel C. Production of plant proteases *in vivo* and *in vitro*–a review. *Biotechnol Adv* (2011) 29(6):983–96. doi: 10.1016/j.biotechadv.2011.08.017

16. Maurer HR. Bromelain: Biochemistry, pharmacology and medical use. *Cell Mol Life Sci* (2001) 58(9):1234–45. doi: 10.1007/PL00000936

17. Aehle W. *Enzyme in industry: Production and application. 3°*. Frankfurt, Germany: Wiley-VCH Verlag GmbH and Co (2007).

18. Koh J, Kang S-M, Kim S-J, Cha M-K, Kwon Y-J. Effect of pineapple protease on the characteristics of protein fibers. *Fibers Polymers* (2006) 7(2):180–5. doi: 10.1007/BF02908264

19. Taussig SJ, Batkin S. Bromelain, the enzyme complex of pineapple (Ananas comosus) and its clinical application. an update. *J Ethnopharmacol* (1988) 22 (2):191–203. doi: 10.1016/0378-8741(88)90127-4

20. Chittenden RH, Joslin EP, Meara FS. On the ferments contained in the juice of the pineapple (*Ananassa sativa*). (1891).

21. Seligman B. Bromelain: An anti-inflammatory agent. *Angiology* (1962) 13:508–10. doi: 10.1177/000331976201301103

22. Cohen A, Goldman J. Bromelains therapy in rheumatoid arthritis. *Pa Med J* (1964) 67:27–30.

23. Tilwe GH, Beria S, Turakhia NH, Daftary GV, Schiess W. Efficacy and tolerability of oral enzyme therapy as compared to diclofenac in active osteoarthrosis of knee joint: An open randomized controlled clinical trial. *J Assoc Physicians India* (2001) 49:617–21.

24. Al Mahmud Z, Emran TB, Qais N, Bachar SC, Sarker M, Uddin MM. Evaluation of analgesic, anti-inflammatory, thrombolytic and hepatoprotective activities of roots of premna esculenta (Roxb). *J Basic Clin Physiol Pharmacol* (2016) 27(1):63–70. doi: 10.1515/jbcpp-2015-0056

25. Ordesi P, Pisoni L, Nannei P, Macchi M, Borloni R, Siervo S, et al. Therapeutic efficacy of bromelain in impacted third molar surgery: A randomized controlled clinical study. *Quintessence Int* (2014) 45(8):679–84. doi: 10.3290/j.qi.a32237

26. Masson M. [Bromelain in blunt injuries of the locomotor system. a study of observed applications in general practice]. *Fortschr Med* (1995) 113(19):303–6.

27. Cirelli MG, Smyth RD. Effects of bromelain anti-edema therapy on coagulation, bleeding, and prothrombin times. *J New Drugs* (1963) 3:37–9. doi: 10.1002/j.1552-4604.1963.tb00060.x

28. Rosenberg L, Shoham Y, Krieger Y, Rubin G, Sander F, Koller J, et al. Minimally invasive burn care: a review of seven clinical studies of rapid and selective debridement using a bromelain-based debriding enzyme (Nexobrid(R)). *Ann Burns Fire Disasters* (2015) 28(4):264–74.

29. Chakraborty AJ, Mitra S, Tallei TE, Tareq AM, Nainu F, Cicia D, et al. Bromelain a potential bioactive compound: A comprehensive overview from a pharmacological perspective. *Life (Basel)* (2021) 11(4). doi: 10.3390/life11040317

30. Gerard G. [Anticancer treatment and bromelains]. *Agressologie* (1972) 13 (4):261–74.

31. Chemspider. *Chemspider* (2022). Available at: http://www.chemspider.com/.

32. WFO. *WFO the world flora online* (2021). Available at: http://www.worldfloraonline.org/.

33. Colletti A, Li S, Marengo M, Adinolfi S, Cravotto G. Recent advances and insights into bromelain processing, pharmacokinetics and therapeutic uses. *Appl Sci* (2021) 11(18):8428. doi: 10.3390/app11188428

34. Rajan PK, Dunna NR, Venkatabalasubramanian S. A comprehensive overview on the anti-inflammatory, antitumor, and ferroptosis functions of bromelain: An emerging cysteine protease. *Expert Opin Biol Ther* (2022) 22 (5):615–25. doi: 10.1080/14712598.2022.2042250

35. Bresolin IRAP, Bresolin ITL, Silveira E, Tambourgi EB, Mazzola PG. Isolation and purification of bromelain from waste peel of pineapple for therapeutic application. *Braz Arch Biol Technol* (2013) 56:971–9. doi: 10.1590/S1516-89132013000600012

36. Azarkan M, Maquoi E, Delbrassine F, Herman R, M'Rabet N, Calvo Esposito R, et al. Structures of the free and inhibitors-bound forms of bromelain and ananain from ananas comosus stem and *in vitro* study of their cytotoxicity. *Sci Rep* (2020) 10(1):1–18. doi: 10.1038/s41598-020-76172-5

37. Bean LS, et al. The electrochemical behaviour of ferrocene in a photocurable poly (methyl methacrylate-co-2-hydroxylethyl methacrylate) film for a glucose biosensor. *Bioelectrochemistry* (2005) 65(2):157–62. doi: 10.1016/j.bioelechem.2004.11.003

38. Rowan AD, Buttle DJ. Pineapple cysteine endopeptidases. *Methods Enzymol* (1994) 244:555–68. doi: 10.1016/0076-6879(94)44040-9

39. Khan RH, Rasheedi S, Haq SK. Effect of pH, temperature and alcohols on the stability of glycosylated and deglycosylated stem bromelain. *J Biosci* (2003) 28 (6):709–14. doi: 10.1007/BF02708431

40. Chaurasiya RS, Hebbar HU. Extraction of bromelain from pineapple core and purification by RME and precipitation methods. *Separation Purification Technol* (2013) 111:90–7. doi: 10.1016/j.seppur.2013.03.029

41. Bhattacharya R, Bhattacharyya D. Preservation of natural stability of fruit "bromelain" from ananas comosus (pineapple). *J Food Biochem* (2009) 33(1):1–19.

42. Banerjee S, Arora A, Vijayaraghavan R, Patti AF. Extraction and crosslinking of bromelain aggregates for improved stability and reusability from pineapple processing waste. *Int J Biol Macromol* (2020) 158:318–26. doi: 10.1016/j.ijbiomac.2020.04.220

43. Zhou Z, Wang L, Feng P, Yin L, Wang C, Zhi S, et al. Inhibition of epithelial TNF-α receptors by purified fruit bromelain ameliorates intestinal inflammation and barrier dysfunction in colitis. *Front Immunol* (2017) 8:1468. doi: 10.3389/fimmu.2017.01468

44. Gautam SS, Mishra SK, Dash V, Goyal AK, Rath G. Comparative study of extraction, purification and estimation of bromelain from stem and fruit of pineapple plant. *Thai J Pharm Sci* (2010) 34(2):1468. doi: 10.1016/j.ijbiomac.2020.04.220

45. Chao MA, Wu MY, Qiao X, Song Y, Zhao Y. Study on purification of stem bromelain by nano-TiO2 and ultrafiltration. *Food Sci Technol* (2009) 34:167–70.

46. Doko B, Bassani V, Casadebaig J, Cavailles L, Jacob M. Preparation of proteolytic enzyme extracts from *Ananas comosus L. Merr.* fruit juice using semi permeable membrane, ammonium sulfateextraction, centrifugation and freeze-drying processes. *Int Immunopharmacol.* (2005) 5:783–93.

47. Lopes FLG, Severo Júnior JB, de Souza RR, Ehrhardt DD, Santana JCC, Tambourgi EB, et al. Concentration by membrane separation processes of a medicinal product obtained from pineapple pulp. *Braz Arch Biol Technol* (2009) 52:457–64. doi: 10.1590/S1516-89132009000200024

48. Soares PAG, et al. Purification of bromelain from pineapple wastes by ethanol precipitation. *Separation purification Technol* (2012) 98:389–95. doi: 10.1016/j.seppur.2012.06.042

49. Silvestre MPC, Carreira RL, Silva MR, Corgosinho FC, Monteiro MRP, Morais HA. Effect of pH and temperature on the activity of enzymatic extracts from pineapple peel. *Food Bioprocess Technol* (2012) 5(5):1824–31. doi: 10.1007/s11947-011-0616-5

50. Ketnawa S, Chaiwut P, Rawdkuen S. Extraction of bromelain from pineapple peels. *Food Sci Technol Int* (2011) 17(4):395–402. doi: 10.1177/1082013210387817

51. Sankaran K, Vadanasundari V, Hemavathy RV, Thirunavukkarasu AA. A comparative study on determining the efficacy of salt precipitation and biphasic system in the extraction of bromelain from ananas comosus. *Asian J Sci Technol* (2011) 2(1):016–22.

52. Rowan AD, Buttle DJ, Barrett AJ. The cysteine proteinases of the pineapple plant. *Biochem J* (1990) 266(3):869–75.

53. Devakate RV, Patil V, Waje SS, Thorat BN. Purification and drying of bromelain. *Separation Purification Technol* (2009) 64(3):259–64. doi: 10.1016/j.seppur.2008.09.012

54. Badar S, et al. Comparison of proteolytic, cytotoxic and anticoagulant properties of chromatographically fractionated bromelain to un-fractionated bromelain. *Am J Transl Res* (2021) 13(5):4309–21.

55. Hernández-Maldonado AJ, Yang FH, Qi G, Yang RT. Desulfurization of transportation fuels by π-complexation sorbents: Cu (I)-, Ni (II)-, and zn (II)-zeolites. *Appl Catalysis B: Environ* (2005) 56(1-2):111–26. doi: 10.1016/j.apcatb.2004.06.023

56. Ciulu-Costinescu F, Calina D, Chirigiu L, Averis LME, Rosulescu E, Bubulica MV. Identification and quantification of capsaicin from capsicum annuum l. by RP-HPLC. *Rev Chimie* (2015) 66(12):1946–9.

57. Bobb D. Isolation of stem bromelain by affinity chromatography and its partial characterization by gel electrophoresis. *Preparative Biochem* (1972) 2 (4):347–54. doi: 10.1080/00327487208065671

58. Amid A, Ismail NA, Yusof F, Salleh HM. Expression, purification, and characterization of a recombinant stem bromelain from ananas comosus. *Process Biochem* (2011) 46(12):2232–9. doi: 10.1016/j.procbio.2011.08.018

59. Muntari B, et al. Recombinant bromelain production in escherichia coli: Process optimization in shake flask culture by response surface methodology. *AMB Express* (2012) 2:12. doi: 10.1186/2191-0855-2-12

60. Umesh Hebbar H, Sumana B, Raghavarao KS. Use of reverse micellar systems for the extraction and purification of bromelain from pineapple wastes. *Bioresour Technol* (2008) 99(11):4896–902. doi: 10.1016/j.biortech.2007.09.038

61. Chaurasiya RS, et al. Efficacy of reverse micellar extracted fruit bromelain in meat tenderization. *J Food Sci Technol* (2015) 52(6):3870–80.

62. Corzo CA, Waliszewski KN, Welti-Chanes J. Pineapple fruit bromelain affinity to different protein substrates. *Food Chem* (2012) 133(3):631–5. doi: 10.1016/j.foodchem.2011.05.119

63. Ketnawa S, Sai-Ut S, Theppakorn T, Chaiwut P, Rawdkuen S. Partitioning of bromelain from pineapple peel (Nang lae cultv.) by aqueous two phase system. *Asian J Food Agro-Industry* (2009) 2(4):457–68. doi: 10.1016/j.biortech.2007.09.038

64. Giles NM, Giles GI, Jacob C. Multiple roles of cysteine in biocatalysis. *Biochem Biophys Res Commun* (2003) 300(1):1–4. doi: 10.1016/S0006-291X(02)02770-5

65. Shukor MY, Masdor N, Baharom NA, Jamal JA, Abdullah MP, et al. An inhibitive determination method for heavy metals using bromelain, a cysteine protease. *Appl Biochem Biotechnol* (2008) 144(3):283–91. doi: 10.1007/s12010-007-8063-5

66. Novaes LC, Ebinuma Vde C, Mazzola PG, Pessoa A Jr. Polymer-based alternative method to extract bromelain from pineapple peel waste. *Biotechnol Appl Biochem* (2013) 60(5):527–35. doi: 10.1002/bab.1121

67. Muntari B, Maizirwan M, Mohamed SJ, Azura A, Hamzah MS. Kinetic studies on recombinant stem bromelain. *Adv Enzyme Res* (2013) 2013. doi: 10.1016/s0006-291x(02)02770-5

68. Esti M, et al. Effect of wine inhibitors on free pineapple stem bromelain activity in a model wine system. *J Agric Food Chem* (2011) 59(7):3391–7. doi: 10.1021/jf104919v

69. Harrach T, et al. Isolation and characterization of two forms of an acidic bromelain stem proteinase. *J Protein Chem* (1998) 17(4):351–61. doi: 10.1023/A:1022507316434

70. Napper A, et al. Purification and characterization of multiple forms of the pineapple-stem-derived cysteine proteinases ananain and comosain. *Biochem J* (1994) 301(3):727–35. doi: 10.1042/bj3010727

71. Hikisz P, Bernasinska-Slomczewska J. Beneficial properties of bromelain. *Nutrients* (2021) 13(12). doi: 10.3390/nu13124313

72. Beuth J. Proteolytic enzyme therapy in evidence-based complementary oncology: Fact or fiction? *Integr Cancer Ther* (2008) 7(4):311–6. doi: 10.1177/1534735408327251

73. Chobotova K, Vernallis AB, Majid FA. Bromelain's activity and potential as an anti-cancer agent: Current evidence and perspectives. *Cancer Lett* (2010) 290 (2):148–56. doi: 10.1016/j.canlet.2009.08.001

74. Bhui K, Tyagi S, Prakash B, Shukla Y. Pineapple bromelain induces autophagy, facilitating apoptotic response in mammary carcinoma cells. *Biofactors* (2010) 36(6):474–82. doi: 10.1002/biof.121

75. Oliveira CP, Prado WA, Lavayen V, Büttenbender SL, Beckenkamp A, Martins BS, et al. Bromelain-functionalized multiple-wall lipid-core nanocapsules: Formulation, chemical structure and antiproliferative effect against human breast cancer cells (MCF-7). *Pharm Res* (2017) 34(2):438–52. doi: 10.1007/s11095-016-2074-2

76. Raeisi F, Raeisi E, Heidarian E, Shahbazi-Gahroui D, Lemoigne Y. Bromelain inhibitory effect on colony formation: An *in vitro* study on human AGS, PC3, and MCF7 cancer cells. *J Med Signals Sens* (2019) 9(4):267–73. doi: 10.4103/jmss.JMSS_42_18

77. Fouz N, Amid A, Hashim YZ. Cytokinetic study of MCF-7 cells treated with commercial and recombinant bromelain. *Asian Pac J Cancer Prev* (2014) 14 (11):6709–14.

78. Mohamad NE, Abu N, Yeap SK, Alitheen NB. Bromelain enhances the anti-tumor effects of cisplatin on 4T1 breast tumor model in vivo. (2019) 18:1534735419880258. doi: 10.1177/1534735419880258

79. Pauzi AZ, Yeap SK, Abu N, Lim KL, Omar AR, Aziz SA, et al. Combination of cisplatin and bromelain exerts synergistic cytotoxic effects against breast cancer cell line MDA-MB-231 *in vitro*. *Chin Med* (2016) 11:46. doi: 10.1186/s13020-016-0118-5

80. Dhandayuthapani S, Perez HD, Paroulek A, Chinnakkannu P, Kandalam U, Jaffe M, et al. Bromelain-induced apoptosis in GI-101A breast cancer cells. *J Med Food* (2012) 15(4):344–9. doi: 10.1089/jmf.2011.0145

81. Amini A, Masoumi-Moghaddam S, Ehteda A, Morris DL. Bromelain and n-acetylcysteine inhibit proliferation and survival of gastrointestinal cancer cells *in vitro*: significance of combination therapy. *J Exp Clin Cancer Res* (2014) 33(1):014–0092.

82. Amini A, et al. Depletion of mucin in mucin-producing human gastrointestinal carcinoma: Results from *in vitro* and *in vivo* studies with bromelain and n-acetylcysteine. *Oncotarget* (2015) 6(32):33329–44. doi: 10.18632/oncotarget.5259

83. Pillai K. Anticancer property of bromelain with therapeutic potential in malignant peritoneal mesothelioma. *Cancer Invest* (2013) 31(4):241–50. doi: 10.3109/07357907.2013.784777

84. Pillai K, Ehteda A, Akhter J, Chua TC, Morris DL. Anticancer effect of bromelain with and without cisplatin or 5-FU on malignant peritoneal mesothelioma cells. *Anticancer Drugs* (2014) 25(2):150–60. doi: 10.1097/CAD.0000000000000039

85. Lee JH, Lee JT, Park HR, Kim JB. The potential use of bromelain as a natural oral medicine having anticarcinogenic activities. *Food Sci Nutr* (2019) 7(5):1656–67. doi: 10.1002/fsn3.999

86. Murthy SS, Narsaiah TB. Cytotoxic effect of bromelain on HepG2 hepatocellular carcinoma cell line. *Appl Biochem Biotechnol* (2021) 193(6):1873–97. doi: 10.1007/s12010-021-03505-z

87. Bhui K, Tyagi S, Srivastava AK, Singh M, Roy P, Singh R, et al. Bromelain inhibits nuclear factor kappa-b translocation, driving human epidermoid carcinoma A431 and melanoma A375 cells through G(2)/M arrest to apoptosis. *Mol Carcinog* (2012) 51(3):231–43. doi: 10.1002/mc.20769

88. Chang TC, Wei PL, Makondi PT, Chen WT, Huang CY, Chang YJ. Bromelain inhibits the ability of colorectal cancer cells to proliferate via activation of ROS production and autophagy. *PLos One* (2019) 14(1). doi: 10.1371/journal.pone.0210274

89. Park S, Oh J, Kim M, Jin EJ. Bromelain effectively suppresses kras-mutant colorectal cancer by stimulating ferroptosis. *Anim Cells Syst* (2018) 22(5):334–40. doi: 10.1080/19768354.2018.1512521

90. Kalra N, Bhui K, Roy P, Srivastava S, George J, Prasad S, et al. Regulation of p53, nuclear factor kappaB and cyclooxygenase-2 expression by bromelain through targeting mitogen-activated protein kinase pathway in mouse skin. *Toxicol Appl Pharmacol* (2008) 226(1):30–7. doi: 10.1016/j.taap.2007.08.012

91. Debnath R, Chatterjee N, Das S, Mishra S, Bose D, Banerjee S, et al. Bromelain with peroxidase from pineapple are more potent to target leukemia growth inhibition - a comparison with only bromelain. *Toxicol In Vitro* (2019) 55:24–32. doi: 10.1016/j.tiv.2018.11.004

92. Debnath R, Majumder D, Nath P, Ghosh D, Maiti D. Bromelain plus peroxidase reduces non-Hodgkin lymphoma progression in *in vivo* via up-regulation of antioxidant enzymes and modulating apoptotic protein expression. *Nutr Cancer* (2020) 72(7):1200–10. doi: 10.1080/01635581.2019.1670217

93. Majumder D, Majumder D, Nath P, Ghosh D, Maiti D. Bromelain and *Olea europaea* (L.) leaf extract mediated alleviation of benzo(a)pyrene induced lung cancer through Nrf2 and NFκB pathway. (2021) 28(34):47306–26.

94. Müller A, Barat S, Chen X, Bui KC, Bozko P, Malek NP, et al. Comparative study of antitumor effects of bromelain and papain in human cholangiocarcinoma cell lines. *Int J Oncol* (2016) 48(5):2025–34. doi: 10.3892/ijo.2016.3411

95. Weinzierl A, Harder Y, Schmauss D, Menger MD, Laschke MW. Bromelain protects critically perfused musculocutaneous flap tissue from necrosis. *Biomedicines* (2022) 10(6). doi: 10.3390/biomedicines10061449

96. Amini A, Ehteda A, Masoumi Moghaddam S, Akhter J, Pillai K, Morris DL. Cytotoxic effects of bromelain in human gastrointestinal carcinoma cell lines (MKN45, KATO-III, HT29-5F12, and HT29-5M21). *Onco Targets Ther* (2013) 6:403–9. doi: 10.1080/01635581.2019.1670217

97. Lee JS, et al. Classification and prediction of survival in hepatocellular carcinoma by gene expression profiling. *Hepatology* (2004) 40(3):667–76. doi: 10.1002/hep.20375

98. Sharifi-Rad J, Bahukhandi A, Dhyani P, Sati P, Capanoglu E, Docea AO, et al. Recent advances in the therapeutic potential of emodin for human health. *Biomedicine Pharmacother* (2022) 154:113555. doi: 10.1016/j.biopha.2022.113555

99. Kitic D, Miladinovic B, Randjelovic M, Szopa A, Sharifi-Rad J, Calina D, et al. Anticancer potential and other pharmacological properties of prunus armeniaca l.: An updated overview. *Plants* (2022) 11(14):1885. doi: 10.3390/biomedicines10061449

100. Sharifi-Rad J, Bahukhandi A, Dhyani P, Sati P, Capanoglu E, Docea AO, et al. Therapeutic potential of neoechinulins and their derivatives: An overview of the molecular mechanisms behind pharmacological activities. *Front Nutr* (2021) 8:664197. doi: 10.3389/fnut.2021.664197

101. Kaczanowski S. Apoptosis: Its origin, history, maintenance and the medical implications for cancer and aging. *Phys Biol* (2016) 13(3):1478–3975. doi: 10.1088/1478-3975/13/3/031001

102. Hossain R, Ray P, Sarkar C, Islam MS, Khan RA, Khalipha ABR, et al. Natural compounds or their derivatives against breast cancer: A computational study. *BioMed Res Int* (2022) 2022:5886269. doi: 10.1155/2022/5886269

103. Salehi B, Sestito S, Rapposelli S, Peron G, Calina D, Sharifi-Rad M, et al. Epibatidine: A promising natural alkaloid in health. *Biomolecules* (2019) 9(1):6. doi: 10.3390/biom9010006

104. Calina D, Buga AM, Mitroi M, Buha A, Caruntu C, Scheau C, et al. The treatment of cognitive, behavioural and motor impairments from brain injury and neurodegenerative diseases through cannabinoid system modulation-evidence from *in vivo* studies. *J Clin Med* (2020) 9(8):28. doi: 10.3390/jcm9082395

105. Ali ES, Akter S, Ramproshad S, Mondal B, Riaz TA, Islam MT, et al. Targeting ras-ERK cascade by bioactive natural products for potential treatment of cancer: an updated overview. *Cancer Cell Int* (2022) 22(1):246. doi: 10.1186/s12935-022-02666-z

106. Musat G, et al. Rare amyloidoma of the tongue base: A case report and review of the literature. *Mol Clin Oncol* (2020) 12(3):258–62. doi: 10.3892/mco.2020.1972

107. Tsoukalas D, Fragkiadaki P, Docea AO, Alegakis AK, Sarandi E, Vakonaki E, et al. Association of nutraceutical supplements with longer telomere length. *Int J Mol Med* (2019) 44(1):218–26. doi: 10.3892/ijmm.2019.4191

108. Javed Z, Khan K, Herrera-Bravo J, Naeem S, Iqbal MJ, Raza Q, et al. Myricetin: targeting signaling networks in cancer and its implication in chemotherapy. *Cancer Cell Int* (2022) 22(1):239. doi: 10.1186/s12935-022-02663-2

109. Ianoși SL, Batani A, Ilie MA, Tampa M, Georgescu SR, Zurac S, et al. Non-invasive imaging techniques for the *in vivo* diagnosis of bowen's disease: Three case reports. *Oncol Lett* (2019) 17(5):4094–101. doi: 10.1186/s12935-022-02666-z

110. Buga AM, Docea AO, Albu C, Malin RD, Branisteanu DE, Ianosi G, et al. Molecular and cellular stratagem of brain metastases associated with melanoma. *Oncol Lett* (2019) 17(5):4170–5. doi: 10.3892/ol.2019.9933

111. Liu T, Chen X, Guan G, Zou C, Shen S, Wu J, et al. Ferroptosis, as the most enriched programmed cell death process in glioma, induces immunosuppression and immunotherapy resistance. *Neuro Oncol* (2022) 24(7):1113–25. doi: 10.1093/neuonc/noac033

112. Asgharian P, et al. Potential mechanisms of quercetin in cancer prevention: Focus on cellular and molecular targets. *Cancer Cell Int* (2022) 22(1):257. doi: 10.1186/s12935-022-02677-w

113. Krysko DV, Vanden Berghe T, D'Herde K, Vandenabeele P. Apoptosis and necrosis: Detection, discrimination and phagocytosis. *Methods* (2008) 44(3):205–21. doi: 10.1016/j.ymeth.2007.12.001

114. Zlatian OM, Comanescu MV, Rosu AF, Rosu L, Cruce M, Gaman AE, et al. Histochemical and immunohistochemical evidence of tumor heterogeneity in colorectal cancer. *Romanian J Morphol Embryol* (2015) 56(1):175–81. doi: 10.3892/ol.2019.9933

115. Docea AO, Mitrut P, Grigore D, Pirici D, Calina DC, Gofita E. Immunohistochemical expression of TGF beta (TGF-beta), TGF beta receptor 1 (TGFBR1), and Ki67 in intestinal variant of gastric adenocarcinomas. *Romanian J Morphol Embryol* (2012) 53(3):683–92.

116. Russo M, Russo GL. Autophagy inducers in cancer. *Biochem Pharmacol* (2018) 153:51–61. doi: 10.1016/j.bcp.2018.02.007

117. Dhyani P, Sati P, Sharma E, Attri DC, Bahukhandi A, Tynybekov B, et al. Sesquiterpenoid lactones as potential anti-cancer agents: An update on molecular mechanisms and recent studies. *Cancer Cell Int* (2022) 22(1):305. doi: 10.1186/s12935-022-02721-9

118. Iqbal MJ, et al. Biosensing chips for cancer diagnosis and treatment: A new wave towards clinical innovation. *Cancer Cell Int* (2022) 22(1):354. doi: 10.1186/s12935-022-02777-7

119. Scheau C, et al. Cannabinoids and inflammations of the gut-Lung-Skin barrier. *J Pers Med* (2021) 11(6). doi: 10.3390/jpm11060494

120. Mathew R, Karantza-Wadsworth V, White E. Role of autophagy in cancer. *Nat Rev Cancer* (2007) 7(12):961–7. doi: 10.1038/nrc2254

121. Alshehri MM, Quispe C, Herrera-Bravo J, Sharifi-Rad J, Tutuncu S, Aydar EF, et al. A review of recent studies on the antioxidant and anti-infectious properties of *Senna* plants. *Oxid Med Cell Longev* (2022) 2022:6025900. doi: 10.1155/2022/6025900

122. Hale LP, Haynes BF. Bromelain treatment of human T cells removes CD44, CD45RA, E2/MIC2, CD6, CD7, CD8, and leu 8/LAM1 surface molecules and markedly enhances CD2-mediated T cell activation. *J Immunol* (1992) 149 (12):3809–16. doi: 10.1186/s12935-022-02777-7

123. Hale LP, Greer PK, Sempowski GD. Bromelain treatment alters leukocyte expression of cell surface molecules involved in cellular adhesion and activation. *Clin Immunol* (2002) 104(2):183–90. doi: 10.1006/clim.2002.5254

124. Vellini M, Desideri D, Milanese A, Omini C, Daffonchio L, Hernandez A, et al. Possible involvement of eicosanoids in the pharmacological action of bromelain. *Arzneimittelforschung* (1986) 36(1):110–2. doi: 10.1038/nrc2254

125. Eckert K, Grabowska E, Stange R, Schneider U, Eschmann K, Maurer HR. Effects of oral bromelain administration on the impaired immunocytotoxicity of mononuclear cells from mammary tumor patients. *Oncol Rep* (1999) 6(6):1191–9. doi: 10.3892/or.6.6.1191

126. Mynott TL, Ladhams A, Scarmato P, Engwerda CR. Bromelain, from pineapple stems, proteolytically blocks activation of extracellular regulated kinase-2 in T cells. *J Immunol* (1999) 163(5):2568–75.

127. Engwerda CR, Andrew D, Ladhams A, Mynott TL. Bromelain modulates T cell and b cell immune responses *in vitro* and *in vivo*. *Cell Immunol* (2001) 210 (1):66–75. doi: 10.1006/cimm.2001.1807

128. Steenbeke M, De Decker I, Marchand S, Glorieux G, Van Biesen W, Lapauw B, et al. Dietary advanced glycation end products in an elderly population with diabetic nephropathy: An exploratory investigation. *Nutrients* (2022) 14 (9):1818. doi: 10.3390/nu14091818

129. Hale LP, Greer PK, Trinh CT, Gottfried MR. Treatment with oral bromelain decreases colonic inflammation in the IL-10-deficient murine model of inflammatory bowel disease. *Clin Immunol* (2005) 116(2):135–42. doi: 10.1016/j.clim.2005.04.011

130. Hale LP, et al. Dietary supplementation with fresh pineapple juice decreases inflammation and colonic neoplasia in IL-10-deficient mice with colitis. *Inflammation Bowel Dis* (2010) 16(12):2012–21. doi: 10.1002/ibd.21320

131. Onken JE, et al. Bromelain treatment decreases secretion of pro-inflammatory cytokines and chemokines by colon biopsies *in vitro*. *Clin Immunol* (2008) 126(3):345–52. doi: 10.1016/j.clim.2007.11.002

132. Fitzhugh DJ, Shan S, Dewhirst MW, Hale LP. Bromelain treatment decreases neutrophil migration to sites of inflammation. *Clin Immunol* (2008) 128(1):66–74. doi: 10.1016/j.clim.2008.02.015

133. Bottega R, Persico I, De Seta F, Romano F, Di Lorenzo G. Anti-inflammatory properties of a proprietary bromelain extract (Bromeyal^{TM}) after *in vitro* simulated gastrointestinal digestion. *Int J Immunopathol Pharmacol* (2021) 35:20587384211034686. doi: 10.1177/20587384211034686

134. Lee J-H, Lee J-B, Lee J-T, Park H-R, Kim J-B. Medicinal effects of bromelain (*Ananas comosus*) targeting oral environment as an anti-oxidant and anti-inflammatory agent. *J Food Nutr Res* (2018) 6(12):773–84. doi: 10.12691/jfnr-6-12-8

135. Savinova AA, Rybitsky MG, Surovikina DA. Enzymes in the national economy. *Bull Donesk State Agrarian Univ* (2017) 26:112–23. doi: 10.1002/ibd.21320

136. Felton GE. Fibrinolytic and antithrombotic action of bromelain may eliminate thrombosis in heart patients. *Med Hypotheses* (1980) 6(11):1123–33. doi: 10.1016/0306-9877(80)90134-6

137. Abbasi Habashi S, Sabouni F, Moghimi A, Ansari Majd S, Tafreshi AP. Reduction of NO production in LPS-stimulated primary rat microglial cells by bromelain. *J Cell Mol Res* (2011) 3(2):57–65. doi: 10.1016/j.clim.2008.02.015

138. Rathnavelu V, et al. Potential role of bromelain in clinical and therapeutic applications. *BioMed Rep* (2016) 5(3):283–8. doi: 10.3892/br.2016.720

139. Bhui K, George J, Shukla Y. Bromelain inhibits COX-2 expression by blocking the activation of MAPK regulated NF-kappa b against skin tumor-initiation triggering mitochondrial death pathway. *Cancer Lett* (2009) 282 (2):167–76. doi: 10.1016/j.canlet.2009.03.003

140. Sudjarwo SA. The signal transduction of bromelain as antiinflamatory in carrageenan-induced rat paw edema. *Brawijaya Med Magazine* (2005) 21:1–5. doi: 10.3389/fimmu.2017.01468

141. Gaspani L, Limiroli E, Ferrario P, Bianchi M. *In vivo* and *in vitro* effects of bromelain on PGE(2) and SP concentrations in the inflammatory exudate in rats. *Pharmacology* (2002) 65(2):83–6. doi: 10.1159/000056191

142. Kasemsuk T, Vivithanaporn P, Unchern S. Anti-inflammatory effects of bromelain in lps-induced human U937 macrophages. *Chiang Mai J Sci* (2018) 45 (1):299–307. doi: 10.1016/0306-9877(80)90134-6

143. Huang JR, et al. Bromelain inhibits lipopolysaccharide-induced cytokine production in human THP-1 monocytes via the removal of CD14. *Immunol Invest* (2008) 37(4):263–77. doi: 10.1080/08820130802083622

144. Siavash Hosseinpour C. Bromelain as an anti-inflammatory and anti-cancer compound. *Int J Res Pharm Sci Technol* (2019) 1(2):53–7. doi: 10.3892/br.2016.720

145. Hou RC-W, et al. Cross-linked bromelain inhibits lipopolysaccharide-induced cytokine production involving cellular signaling suppression in rats. *J Agric Food Chem* (2006) 54(6):2193–8. doi: 10.1021/jf052390k

146. Uchida Y, Katori M. Independent consumption of high and low molecular weight kininogens *in vivo*. *Adv Exp Med Biol* (1986) 198 Pt A:113–8. doi: 10.1007/978-1-4684-5143-6_16

147. Foroncewicz B, Mucha K, Heidland A, Ciszek M, Imiela J, Helle F, et al. Modulation of serum levels of sRAGE by bromelain in patients with chronic kidney disease: a pilot study. *Pol Arch Med Wewn* (2012) 122(10):514–6. doi: 10.20452/pamw.1427

148. Brochard S, et al. Benefit of combining curcumin, harpagophytum and bromelain to reduce inflammation in osteoarthritic synovial cells. *Osteoarthritis Cartilage* (2021) 29:429. doi: 10.1016/j.joca.2021.02.556

149. Akhtar NM, et al. Oral enzyme combination versus diclofenac in the treatment of osteoarthritis of the knee–a double-blind prospective randomized study. *Clin Rheumatol* (2004) 23(5):410–5. doi: 10.1007/s10067-004-0902-y

150. Dilly AK, et al. Improved chemosensitivity following mucolytic therapy in patient-derived models of mucinous appendix cancer. *Trans Res* (2021) 229:100–14. doi: 10.1016/j.trsl.2020.10.005

151. Maher HM, Almomen A, Alzoman NZ, Shehata SM, Alanazi AA. Development and validation of UPLC-MS/MS method for the simultaneous quantification of anaplastic lymphoma kinase inhibitors, alectinib, ceritinib, and crizotinib in wistar rat plasma with application to bromelain-induced pharmacokinetic interaction. *J Pharm BioMed Anal* (2021) 204:114276. doi: 10.1016/j.jpba.2021.114276

152. Mekkawy MH, Fahmy HA, Nada AS, Ali OS. Study of the radiosensitizing and radioprotective efficacy of bromelain (a pineapple extract): *In vitro* and *in vivo*. (2020) 19:1534735420950468. doi: 10.1177/1534735420950468

153. Mekkawy MH, Fahmy HA, Nada AS, Ali OS. Radiosensitizing effect of bromelain using tumor mice model via ki-67 and PARP-1 inhibition. (2021) 20:15347354211060369. doi: 10.1177/15347354211060369

154. Lam AR, et al. Novel use of bromelain and acetylcysteine (BromAc®) for pleural involvement in pseudomyxoma peritonei. *Case Rep Oncol* (2021) 14 (1):628–33. doi: 10.1159/000514273

155. Uhlenbruck G, et al. Reduced side-effects of adjuvant hormone therapy in breast cancer patients by complementary medicine. *In Vivo* (2010) 24(5):799–802. doi: 10.1007/s10067-004-0902-y

156. Beuth J, van Leendert R, Schneider B, Uhlenbruck G. Complementary medicine on side-effects of adjuvant hormone therapy in patients with breast cancer. *In Vivo* (2013) 27(6):869–71.

157. Taussig SJ, Yokoyama MM, Chinen A, Onari K, Yamakido M. Bromelain: A proteolytic enzyme and its clinical application. a review. *Hiroshima J Med Sci* (1975) 24(2-3):185–93. doi: 10.1016/j.jpba.2021.114276

158. Moss JN, Frazier CV, Martin GJ. BROMELAINS. THE PHARMACOLOGY OF THE ENZYMES. *Arch Int Pharmacodyn Ther* (1963) 145:166–89. doi: 10.1177/1534735420950468

159. Gupta AA, et al. Comparative efficacy of bromelain and aceclofenac in limiting post-operative inflammatory sequelae in surgical removal of lower impacted third molar: A randomized controlled, triple blind clinical trial. *J Dent Anesth Pain Med* (2022) 22(1):29–37. doi: 10.17245/jdapm.2022.22.1.29

160. Muhammad ZA, Ahmad T. Therapeutic uses of pineapple-extracted bromelain in surgical care - a review. *J Pak Med Assoc* (2017) 67(1):121–5. doi: 10.1159/000514273

161. Goradia E. *Comparison of the effects of a bromelain and collagenase-based enzymatic agent on inflammation and eschar debridement in a partial thickness porcine model*. NY: Stony Brook University Hospital (2021).

162. Pillai K, et al. Enhancing the potency of chemotherapeutic agents by combination with bromelain and n-acetylcysteine - an *in vitro* study with pancreatic and hepatic cancer cells. *Am J Transl Res* (2020) 12(11):7404–19.

163. Wang X, et al. Bromelain-immobilized and lactobionic acid-modified chitosan nanoparticles for enhanced drug penetration in tumor tissues. *Int J Biol Macromol* (2018) 115:129–42. doi: 10.1016/j.ijbiomac.2018.04.076

164. Wang X, et al. pH-sensitive bromelain nanoparticles by ortho ester crosslinkage for enhanced doxorubicin penetration in solid tumor. *Mater Sci Eng C Mater Biol Appl* (2020) 113:111004. doi: 10.1016/j.msec.2020.111004

165. Viale PH. The American cancer society's facts & figures: 2020 edition. *J Adv Pract Oncol* (2020) 11(2):135–6. doi: 10.17245/jdapm.2022.22.1.29

166. Quispe C, et al. Therapeutic applications of curcumin nanomedicine formulations in cystic fibrosis. *Prog Biomaterials* (2022).

167. Ferrara B, et al. The extracellular matrix in pancreatic cancer: Description of a complex network and promising therapeutic options. (2021) 13(17):.

frontiers | Frontiers in Pharmacology

TYPE Original Research
PUBLISHED 23 January 2023
DOI 10.3389/fphar.2023.1111912

OPEN ACCESS

EDITED BY
Mitesh Patel,
Parul University, India

REVIEWED BY
Daniela Calina,
University of Medicine and Pharmacy of Craiova, Romania
JianLi Gao,
Zhejiang Chinese Medical University, China

*CORRESPONDENCE
Jinjun Wu,
wujinjun@gzucm.edu.cn
Xin Yang,
chemist_yx@163.com

†These authors have contributed equally to this work

SPECIALTY SECTION
This article was submitted to Pharmacology of Anti-Cancer Drugs, a section of the journal Frontiers in Pharmacology

RECEIVED 30 November 2022
ACCEPTED 13 January 2023
PUBLISHED 23 January 2023

CITATION
Hu Y, Zhai W, Tan D, Chen H, Zhang G, Tan X, Zheng Y, Gao W, Wei Y, Wu J and Yang X (2023), Uncovering the effects and molecular mechanism of *Astragalus membranaceus* (Fisch.) Bunge and its bioactive ingredients formononetin and calycosin against colon cancer: An integrated approach based on network pharmacology analysis coupled with experimental validation and molecular docking.
Front. Pharmacol. 14:1111912.
doi: 10.3389/fphar.2023.1111912

Uncovering the effects and molecular mechanism of *Astragalus membranaceus* (Fisch.) Bunge and its bioactive ingredients formononetin and calycosin against colon cancer: An integrated approach based on network pharmacology analysis coupled with experimental validation and molecular docking

Yu Hu[1†], Wenjuan Zhai[1†], Duanling Tan[2†], Haipeng Chen[1], Guiyu Zhang[1], Xuanjing Tan[1], Yuting Zheng[1], Wenhui Gao[3], Yijie Wei[1], Jinjun Wu[1*] and Xin Yang[2*]

[1]Guangdong Provincial Key Laboratory of Translational Cancer Research of Chinese Medicines, Joint International Research Laboratory of Translational Cancer Research of Chinese Medicines, School of Pharmaceutical Sciences, International Institute for Translational Chinese Medicine, Guangzhou University of Chinese Medicine, Guangzhou, Guangdong, China, [2]Key Laboratory of Molecular Target and Clinical Pharmacology and the State, NMPA Key Laboratory of Respiratory Disease, School of Pharmaceutical Sciences and The Fifth Affiliated Hospital, Guangzhou Medical University, Guangzhou, China, [3]Affiliated Cancer Hospital and Institute of Guangzhou Medical University, Guangzhou, Guangdong, China

Colon cancer is a highly malignant cancer with poor prognosis. *Astragalus membranaceus* (Fisch.) Bunge (Huang Qi in Chinese, HQ), a well-known Chinese herbal medicine and a popular food additive, possesses various biological functions and has been frequently used for clinical treatment of colon cancer. However, the underlying mechanism is not fully understood. Isoflavonoids, including formononetin (FMNT) and calycosin (CS), are the main bioactive ingredients isolated from HQ. Thus, this study aimed to explore the inhibitory effects and mechanism of HQ, FMNT and CS against colon cancer by using network pharmacology coupled with experimental validation and molecular docking. The network pharmacology analysis revealed that FMNT and CS exerted their anticarcinogenic actions against colon cancer by regulating multiple signaling molecules and pathways, including MAPK and PI3K-Akt signaling pathways. The

Abbreviations: CHMs, Chinese herbal medicines; HQ, *Astragalus membranaceus* (Fisch.) Bunge (Huang Qi); FMNT, Formononetin; CS, Calycosin; PPI, Protein-protein interaction; GO, Gene Ontology; KEGG, Kyoto Encyclopedia of Genes and Genomes; BP, Biological process; CC, cellular component; MF, Molecular function; 5-FU, 5-Fluorouracil; IC_{50}, 50% inhibitory concentration; DC, Degree centrality; EMT, Epithelial–mesenchymal transformation; EGFR, Epidermal growth factor receptor; MAPK, Mitogen-activated protein kinase; mTOR, Mammalian target of rapamycin; COX-2, Cyclooxygenase-2; VEGF, vascular endothelial growth factor.

experimental validation data showed that HQ, FMNT and CS significantly suppressed the viability and proliferation, and promoted the apoptosis in colon cancer Caco2 and HT-29 cells. HQ, FMNT and CS also markedly inhibited the migration of Caco2 and HT-29 cells, accompanied by a marked increase in E-cadherin expression, and a notable decrease in N-cadherin and Vimentin expression. In addition, HQ, FMNT and CS strikingly decreased the expression of ERK1/2 phosphorylation (p-ERK1/2) without marked change in total ERK1/2 expression. They also slightly downregulated the p-Akt expression without significant alteration in total Akt expression. Pearson correlation analysis showed a significant positive correlation between the inactivation of ERK1/2 signaling pathway and the HQ, FMNT and CS-induced suppression of colon cancer. The molecular docking results indicated that FMNT and CS had a strong binding affinity for the key molecules of ERK1/2 signaling pathway. Conclusively, HQ, FMNT and CS exerted good therapeutic effects against colon cancer by mainly inhibiting the ERK1/2 signaling pathway, suggesting that HQ, FMNT and CS could be useful supplements that may enhance chemotherapeutic outcomes and benefit colon cancer patients.

KEYWORDS

colon cancer, *Astragalus membranaceus* (Fisch.) Bunge, formononetin, calycosin, network pharmacology, ERK1/2

1 Introduction

Colon cancer is among the most prevalent cancers, which has a complex aetiology consisting of environmental component and genetic component (Fagunwa et al., 2017; Kong et al., 2020). Evidence exists that colon cancer arises from two types of precursor polyps *via* two distinct pathways: conventional adenomas by the conventional adenoma-to-carcinoma sequence and serrated adenomas according to the serrated adenoma-to-carcinoma theory (Cappell, 2008). Currently, colon cancer is the third most common diagnosis and second deadliest malignancy for both sexes combined. It is estimated that colon cancer will cause 1.1 million deaths by 2030 (Kong et al., 2020). Current clinical treatment of colon cancer mainly includes operation, radiotherapy and chemotherapy. Despite advances in the development of these therapies, the prognosis in colon cancer patients remains poor and the recurrence rate is still high (Kong et al., 2020). Moreover, long-term use of these therapies easily produces severe toxicities side effects, including hepatotoxicity, vomiting, diarrhea and immunosuppression (Kong et al., 2020). Thus, alternative therapies with pronounced effectiveness but low toxicity are necessary.

Nowadays, the interest in Chinese herbal medicines (CHMs) has increased worldwide due to their health-beneficial properties. The obvious advantages of CHMs in the prevention and treatment of colon cancer has been widely recognized and confirmed (Ye et al., 2015; Yan et al., 2017; Kong et al., 2020). *Astragalus membranaceus* (Fisch.) Bunge (Huang Qi in Chinese, HQ), one of the most well-known CHMs, is frequently used as a major component in over 200 Chinese medicine formulas to treat a wide variety of diseases and body disorders, including chronic fatigue, weakness, wounds, anemia, fever, uterine bleeding, allergies and cancer (Guo et al., 2019; Lou et al., 2019). Moreover, as a health-beneficial additive in some food, HQ is popularly consumed to strengthen the immune system and reinforce vital energy (Guo et al., 2019). Pharmacological evidence revealed that HQ manifests various biological functions, such as anti-inflammation, anti-oxidant, antiviral, immunomodulation, and anti-carcinogenic activities without any appreciable toxicity (Guo et al., 2019; Lou et al., 2019; An et al., 2020). Previous studies demonstrated that HQ has a utility in clinical applications for the colon cancer treatment. For example, HQ could not only inhibit the proliferation, cause cell cycle arrest and promote apoptosis of colon cancer cells, but also suppress the migration of colon cancer cells (Tseng et al., 2016; Tan et al., 2019). HQ could effectively inhibit the tumors of human colon cancer cells grafted into nude mice without obvious side effect (Tseng et al., 2016), which demonstrated that HQ might be a potential chemopreventive drug for colon cancer therapy. What is more, HQ exerted potent anti-tumor activity through simultaneous modulation of mammalian target of rapamycin (mTOR) and cyclooxygenase-2 (COX-2) signaling, which together decreased vascular endothelial growth factor (VEGF) expression to effectively suppress angiogenesis in tumor xenograft and human colon cancer cells (Auyeung et al., 2016). Although increasing evidence supports the potent inhibitory activity of HQ against colon cancer, the molecular mechanism underlying the action has yet to be fully elucidated. Moreover, colon cancer is a systemic and complicated disease with involvement of multiple signaling molecules. It is essential to further investigate the underlying mechanisms of HQ in the suppression of colon cancer.

Numerous ingredients have been isolated and identified from HQ (Guo et al., 2019). Formononetin (FMNT) and calycosin (CS), two main bioactive isoflavone ingredients isolated from HQ, contribute to the therapeutic efficacy and pharmacological activities of HQ (Guo et al., 2019). It was reported that FMNT could suppress the growth and induce apoptosis of colon cancer cells, which were associated with caspase activation and decrease in protein levels of Bcl-2 and Bcl-x(L). FMNT also inhibited angiogenesis and invasion of colon cancer cells, thereby supporting its potential application in advanced and metastatic colon therapies (Auyeung et al., 2012). CS, as an important marker for monitoring the HQ quality, is pharmacologically beneficial due to its antioxidative, cytoprotection, hypolipemic, neuroprotection, and hypoglycemic effects (Gong et al., 2021; Li et al., 2022). Moreover, CS has potent anti-carcinogenic activities, including action against colon cancer. It was reported that CS notably inhibited proliferation and induced apoptosis of colon cancer cells through regulating the ERβ/MiR-95, IGF-1R and PI3K-Akt signaling pathways (Zhao et al., 2016). CS also promoted apoptosis of human colon cancer cells through

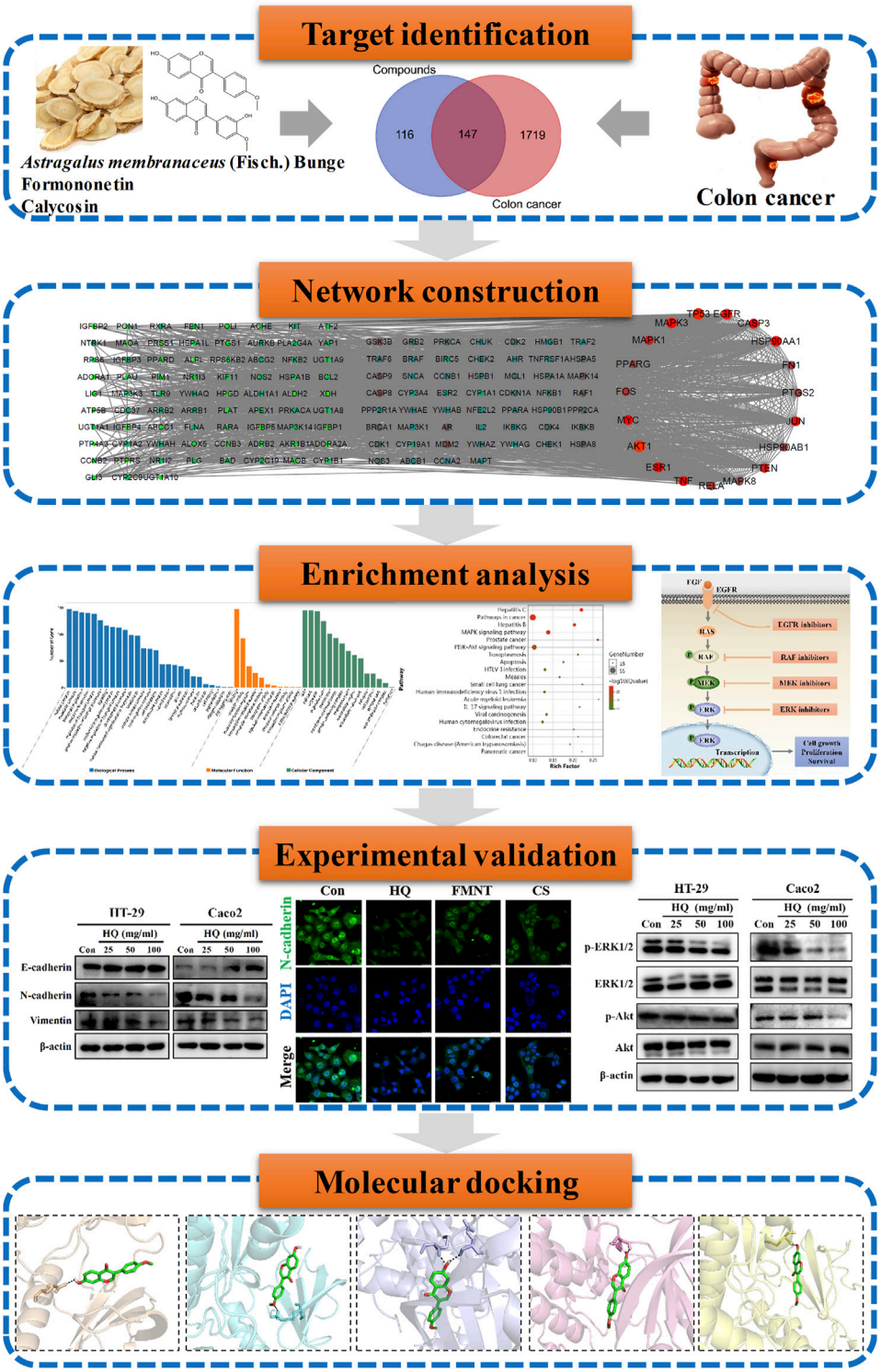

FIGURE 1
Technological road-map. The whole technical roadmap was divided into five steps, including target identification, network construction, enrichment analysis, experimental validation and a molecular docking study.

modulation of ERβ/miR-17 signaling pathway (Chen et al., 2015b). These studies indicate that FMNT and CS may be used as candidate agents for clinical treatment of colon cancer in the future. However, the network molecular mechanisms of FMNT and CS against colon cancer has not been well defined.

Network pharmacology is an emerging methodology that attempts to eliminate drug actions and reveal the interactions between drugs and targets (Hopkins, 2007). As a powerful tool, network pharmacology can combine network biology and polypharmacology approaches to provide evidence for the molecular targets and the

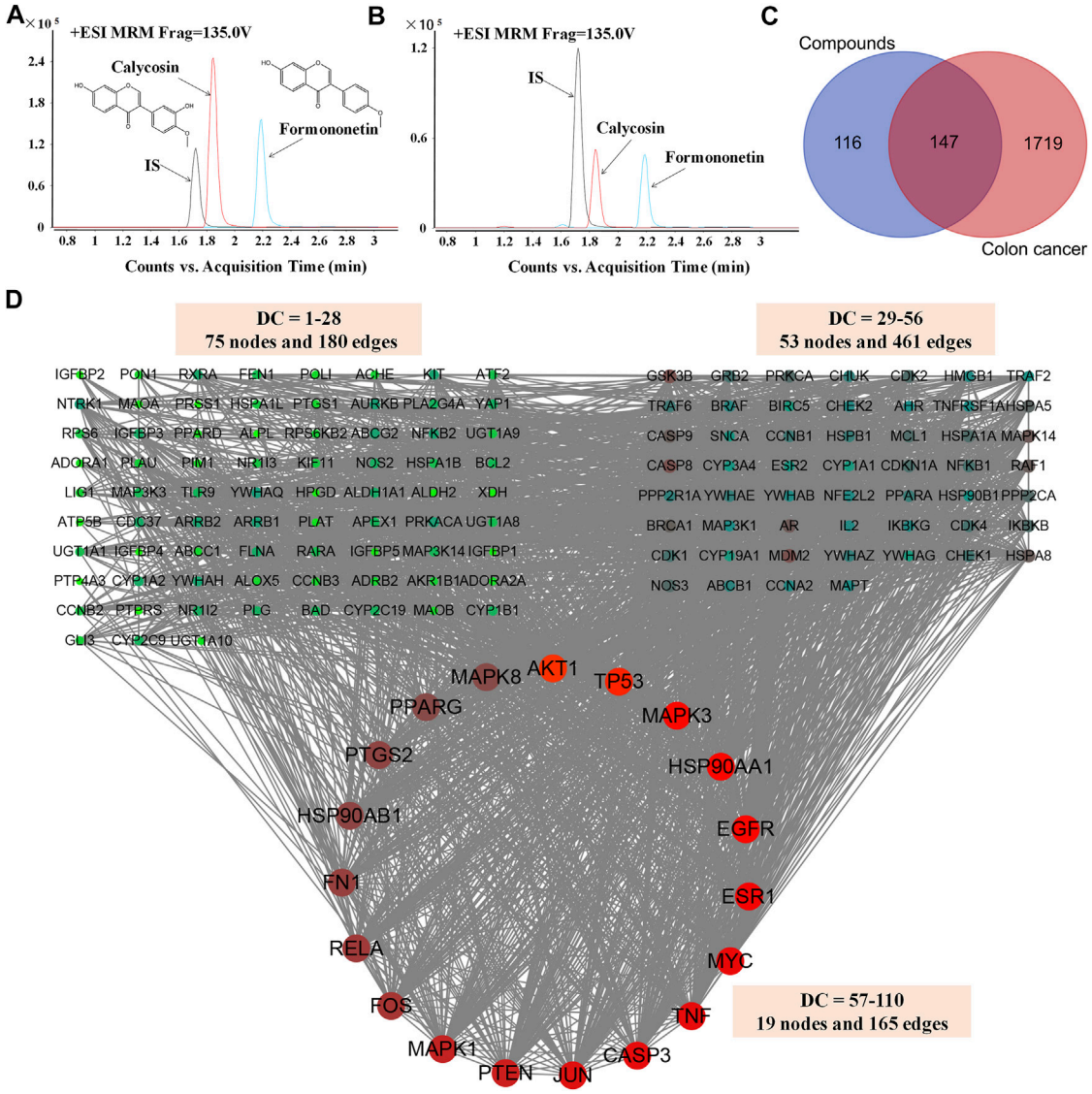

FIGURE 2
Screening and analysis of the common targets of FMNT and CS for the treatment of colon cancer. The content of FMNT and CS were quantitated in HQ water extract using erlotinib as an internal standard (IS) **(A)** A chromatogram of FMNT and CS standard solution **(B)** A chromatogram of FMNT and CS in HQ water extract **(C)** Venn diagram of compounds (FMNT and CS)-colon cancer intersection targets. The 1866 targets of colon cancer were mapped to the 263 targets of FMNT and CS to screen out the 147 common targets **(D)** The PPI network of the 147 nodes. The red nodes represent the big hub nodes, the green nodes represent the other nodes. The node size is proportional to its degree.

potential mechanisms of action of CHMs (Gan et al., 2019; An et al., 2020). Thus, this current study integrates network pharmacology with experimental validation and molecular docking to clarify the effects and potential mechanism of HQ, FMNT and CS against colon cancer (Figure 1). The objectives of the current study were: 1) to determine the content of FMNT and CS in the water extract of HQ for quality control; 2) to screen the potential targets of FMNT and CS against colon cancer; 3) to explore the potential mechanism of FMNT and CS against colon cancer by using network pharmacology; 4) to evaluate the inhibitory effects of HQ water extract, FMNT and CS against colon cancer HT-29 and Caco-2 cells, and to elucidate the potential mechanism by using experimental validation; 5) to investigate the binding ability between FMNT and CS and key targets by using molecular docking. Our results may expand our current knowledge about the mechanism of HQ as a therapeutic candidate for colon cancer therapy.

2 Materials and methods

2.1 Preparation of HQ water extract and UHPLC-MS/MS analysis

One hundred-gram pieces of HQ were weighed. Preparation of HQ water extract (1 g/mL) were performed as previously described (Shi et al., 2015; Lou et al., 2019). Chemical profiling and standardization of HQ water extract using FMNT and CS was performed *via* UHPLC-MS/MS analysis by using an Agilent

1290 infinity LC system (Supplementary materials and methods). The content of FMNT and CS were quantitated in HQ water extract at levels of 0.3338 mg/g and 0.1998 mg/g, respectively (Figures 2A, B).

2.2 Prediction of the targets for FMNT and CS

Several databases, including TCMSP (http://tcmspw.com/) (Tan et al., 2022), SuperPred (http://prediction.charite.de/) (An et al., 2020), SwissTargetPrediction (http://www.swisstargetprediction.ch/) (Tan et al., 2022), PubChem (https://pubchem.ncbi.nlm.nih.gov/) (An et al., 2020) and STITCH (http://stitch.embl.de/) (An et al., 2020) databases, which limit species for "*Homo sapiens*", were used to collect the potential targets of FMNT and CS. Finally, the UniProt database (https://www.uniprot.org/) was used to identify all the targets (An et al., 2020).

2.3 Screening of potential targets for colon cancer

Keywords of "colon cancer", "colon adenocarcinoma" and "colorectal cancer" were used to identify targets related to colon cancer from GeneCards (https://www.genecards.org/) (Tan et al., 2022), OMIM (https://www.omim.org/) (Amberger et al., 2015), TTD (http://db.idrblab.net/ttd/) (Tan et al., 2022), DisGeNET (https://www.disgenet.org/) (Tan et al., 2022) and CTD (http://ctdbase.org) (Tan et al., 2022) databases. Finally, the UniProt database (https://www.uniprot.org/) was used to identify all the targets (An et al., 2020).

2.4 Network construction and analysis

Venn diagram (http://bioinformatics.psb.ugent.be/webtools/Venn/) was used to collect the common targets of FMNT and CS and colon cancer. The detectable targets in the protein-protein interaction (PPI) of FMNT and CS against colon cancer were constructed by the STRING database (https://string-db.org/) and were further visualized by using Cytoscape software (An et al., 2020; Xu et al., 2022). Crucial biotargets of FMNT and CS against colon cancer were obtained according to the degree values in the Cytoscape settings.

2.5 Gene ontology and pathway enrichment analysis

The Omicshare Online tools (https://www.omicshare.com/tools), a free online platform for data analysis, was used to understand the role of the potential targets in gene functions and signaling pathways, including the Gene Ontology (GO) and Kyoto Encyclopedia of Genes and Genomes (KEGG) pathway enrichment analysis (An et al., 2020). GO (https://geneontology.org/) is one of the main resources of biological information, which provides a specific definition of protein functions. GO is subdivided into three non-overlapping ontologies: biological process (BP), cellular component (CC), and molecular function (MF) terms (Ashburner et al., 2000). Those terms with a $p < 0.05$ were chosen for further analysis and the top 20 of GO terms enrichment were displayed. KEGG (https://www.kegg.jp/) is a database resource for the biological interpretation by genome sequencing and other high-throughput experimental technologies (Chen et al., 2015a; An et al., 2020). Those terms with an $p < 0.05$ were chosen for further analysis and the top 25 enriched KEGG pathways were mapped.

2.6 Chemicals and reagents

Astragalus membranaceus (Fisch.) Bunge was purchased from Daxiang Chinese Pharmaceutical Co., Ltd. (Guangdong, China). FMNT and CS (purity ≥98%) were purchased from Chengdu Must Biotechnology Co., Ltd. (Chengdu, China). MTT were bought from Solarbio Science and Technology Co., Ltd. (Beijing, China). BeyoClick™ EdU cell proliferation kitwas bought from Beyotime Biotechnology (Haimen, China). Annexin V-fluorescein isothiocyanate (FITC)/propidium iodide (PI) apoptosis detection kit was purchased from Absin Bioscience Inc. (Shanghai, China). DMSO and HEPES were purchased from GBCBIO Technologies (Guangzhou, China). p-Akt (Ser473); Akt, p-ERK1/2 (Thr202/Tyr204), ERK1/2, and β-actin antibodies were purchased from Cell Signaling Technology (Danvers, MA, United States). N-cadherin, E-cadherin and Vimentin antibodies were purchased from Affinity Biosciences (OH, United States). All other chemicals not mentioned here were of analytical reagent grade or better.

2.7 Cell culture

HT29 and Caco2 human colon carcinoma cells were purchased from American Type Culture Collection (ATCC, Manassas, VA, United States) and then routinely cultured in DMEM medium (Gibco, United States) containing 10% (v/v) fetal bovine serum (FBS) (Gibco, United States) and 100 U/mL streptomycin-penicillin solution (Gibco, United States) in a humidified atmosphere containing 5% CO_2 at 37°C.

2.8 MTT assay

Cell viability was measured by MTT assay. HT29 and Caco2 cells were seeded in 96-well plates and cultured with the vehicle, HQ (3.125–100 mg/mL), FMNT (3.125–200 μM) or CS (3.125–200 μM) for 48 h. 5-Fluorouracil (5-FU) (25 μM) was used as a positive control. Then, the medium was removed and each well was added 200 μL MTT solution (0.5 mg/mL) and incubated at 37°C for additional 4 h. After that, supernatant was discarded and 150 μl DMSO was added to each well to dissolve formazan crystals. Optical density (OD) values were measured at 490 nm by a microplate reader (PerkinElmer, Waltham, MA, United States). Finally, cell inhibitory rates and 50% inhibitory concentration (IC_{50}) values were calculated for each group.

2.9 5-Ethynyl-2′-Deoxyuridine (EdU) assay

Cell proliferation ability was measured by EdU assay following the manufacturer's instructions. HT29 and Caco2 cells were seeded in 96-well plates and cultured with the vehicle, HQ (25, 50, and 100 mg/mL),

FMNT (25, 50, and 100 μM) or CS (25, 50, and 100 μM) for 48 h. 5-FU (25 μM) was used as a positive control. Then, cells were incubated with EdU labeling medium (50 mM) at 37°C for 2 h. Other details of the procedure are described in literature (Wu et al., 2020). Finally, the images were captured using a fluorescence microscope (Leica, Germany) and analyzed by ImageJ software.

2.10 Wound healing assay

HT29 and Caco2 cells were seeded in 6-well plates. Scratch lines were drawn on the monolith of the fused cells using 10 μL pipette tips. Then, the cells were cultured with the vehicle, HQ (25, 50, and 100 mg/mL), FMNT (25, 50, and 100 μM) or CS (25, 50, and 100 μM) for 12, 24 or 48 h, respectively. Pictures of the scratch lines were captured using a microscope (Leica, Germany) at 0, 12, 24 and 48 h, respectively. The cell migration ratio of linear wounds was calculated by using ImageJ software.

2.11 Cell apoptosis assay

HT29 and Caco2 cells were stained with Annexin V-FITC/PI and evaluated for apoptosis by flow cytometry according to the manufacturer's instructions. Briefly, HT29 and Caco2 cells were seeded in 6-well plates and exposed to the vehicle, HQ (25, 50, and 100 mg/mL), FMNT (25, 50, and 100 μM) or CS (25, 50, and 100 μM) for 48 h. Then, cells were collected and stained with Annexin V-FITC and PI for 20 min at room temperature in dark. Finally, cell apoptosis was analyzed by the flow cytometry (BD Biosciences, San Diego, CA, United States).

2.12 Western blot assay

HT29 and Caco2 cells were seeded in 6-well plates and exposed to the vehicle, HQ (25, 50, and 100 mg/mL), FMNT (25, 50, and 100 μM) or CS (25, 50, and 100 μM) for 48 h. After that, the cells were washed with cold PBS and harvested. Total proteins were extracted from cells using the RIPA lysis reagent containing a protease inhibitor and then quantified using a BCA estimation kit. Western blotting was performed as previously described (An et al., 2020) using primary antibodies against p-Akt, Akt, p-ERK1/2, ERK1/2, N-cadherin, E-cadherin, Vimentin or β-actin (1:1000). Protein bands were detected by a gel imaging analysis system and were analyzed using ImageJ software.

2.13 Immunofluorescence

HT29 and Caco2 cells were seeded on confocal dishes and exposed to the vehicle, HQ (100 mg/mL), FMNT (100 μM) or CS (100 μM) for 48 h. At the end of the incubation, the cells were fixed in paraformaldehyde, permeabilized with TritonX-100 and blocked with bovine serum albumin. Then, the cells were incubated with a N-cadherin, an E-cadherin, or a Vimentin (1:200) antibody at 4°C overnight and then stained with a secondary fluorescent antibody (1:200; Alexa Fluor 488). Finally, the cells were incubated with DAPI for 20 min. Fluorescence signals were detected using a Leica TCS SP8 confocal fluorescence microscope (Leica, Germany). The relative fluorescence of N-cadherin, E-cadherin and Vimentin were analyzed by ImageJ software.

2.14 Molecular docking

Molecular docking was carried out by AutoDock Vina software to measure the interactions between the two compounds and the key upstream molecules of ERK1/2 signaling pathway, including EGFR, BRAF, MEK1/2 and ERK1/2. The crystal structures of EGFR, BRAF, MEK1/2 and ERK1/2 were retrieved from the Protein Data Bank (Table 1). The mol2 file format structures of the FMNT and CS were obtained from the PubChem database. Details of the procedure are described in literature (Ruan et al., 2020). After docking, conformations with the lowest docking energy were selected for the binding conformations between the ligands (FMNT and CS) and the target proteins. Finally, the analysis and visualization of the ligand-protein complexes were performed by PyMOL software.

2.15 Statistical analysis

All assays were performed in triplicate. Results were expressed as mean with standard deviations (mean ± SD). One-way analysis of variance (ANOVA) was performed to compare the differences between different groups by SPSS 19.0. Correlation analyses were performed using Pearson product–moment correlation by SPSS 19.0. Statistical significance of differences was accepted at $p < 0.05$, $p < 0.01$ and $p < 0.001$.

3 Results

3.1 Potential targets for compounds and colon cancer

A total of 263 potential targets for FMNT and CS were identified after screening the databases of TCMSP, SuperPred, SwissTargetPrediction, STITCH and PubChem, (Figure 2C). Through the GeneCards, OMIM, TTD, CTD and DisGeNET databases, a total of 1866 colon cancer targets were obtained (Figure 2C).

3.2 Network construction

Then, compound targets and colon cancer-related targets were mapped using a Venn diagram, 147 common targets were obtained as the potential targets of FMNT and CS against colon cancer (Figure 2C). The PPI network of the 147 targets were established by Cytoscape 3.7.2 software (An et al., 2020) (Figure 2D). There were 147 nodes and 2,382 edges in the PPI network with a medium degree centrality (DC) value of 28 (Figure 2D). Afterwards, hub nodes for FMNT and CS against colon cancer were established based on DC values. Finally, a total of 19 hub nodes were screened when the thresholds were set at DC ≥ 57. These 19 crucial targets with higher DC values were identified as the candidate targets of FMNT and CS against colon cancer, including AKT1, TP53, MAPK3, EGFR,

TABLE 1 Molecular docking of FMNT and CS and corresponding targets.

Targets	Protein data bank ID	Compounds	Binding energy (kcal/mol)
EGFR	1M17	formononetin	−7.9
EGFR	1M17	calycosin	−8.3
BRAF	4EHG	formononetin	−9.2
BRAF	4EHG	calycosin	−9.5
MEK1	7B9L	formononetin	−8.5
MEK1	7B9L	calycosin	−9.0
MEK2	1S9I	formononetin	−7.8
MEK2	1S9I	calycosin	−8.3
ERK1	4QTB	formononetin	−9.3
ERK1	4QTB	calycosin	−9.6
ERK2	4ZZN	formononetin	−7.3
ERK2	4ZZN	calycosin	−7.3

HSP90AA1, ESR1, MYC, CASP3, TNF, JUN, PTEN, MAPK1, FOS, RELA, FN1, PTGS2, HSP90AB1, MAPK8 and PPARG (Figure 2D).

3.3 GO analysis and KEGG pathway enrichment analysis

To evaluate the pharmacological effects of FMNT and CS against colon cancer. The potential 147 targets were further utilized for the GO analysis and KEGG pathway enrichment analysis. GO analysis showed that the majority of these 147 targets were enriched in cells with molecular function of protein binding. Specifically, these targets were abundantly enriched in cellular process, metabolic process, biological regulation and response to stimuli (Figure 3A). These results implicated that various cellular functions could be involved in the diverse and synergistic effects of FMNT and CS against colon cancer. The top 20 of GO terms enrichment were mapped (Figures 3B, C). The results showed that targets were closely related to multiple biological processes (BPs), including cellular response to chemical stimuli, response to chemical, response to oxygen-containing compounds, response to organic substances, regulation of programmed cell death, regulation of cell death, regulation of apoptotic process, and apoptotic process, etc (Figure 3B). In molecular functions (MFs), the significant terms were mainly enriched in enzyme binding, kinase binding, protein kinase binding, ubiquitin-like protein ligase binding, protein domain specific binding, identical protein binding, ubiquitin protein ligase binding, and organic cyclic compound binding, etc (Figure 3C). Moreover, cellular components (CCs) analysis showed that the significant terms mainly included cytoplasmic part, membrane-bounded organelle, mitochondrion, intracellular organelle lumen, organelle lumen, membrane-enclosed lumen, cytoplasm and nucleoplasm, etc (Figure 3D).

To further elucidate the potential mechanisms of FMNT and CS against colon cancer, KEGG pathway enrichment analysis of those 147 key targets was conducted. KEGG pathway annotation showed that 91 and 89 targets were involved in the signal transduction and cancer, respectively (Figure 4A). The top 20 KEGG pathway enrichments with a p-value <0.05 were displayed in Figure 4B. The significant pathways mainly included hepatitis C, pathways in cancer, hepatitis B, MAPK signaling pathway, prostate cancer, PI3K-Akt signaling pathway, toxoplasmosis and apoptosis, *etc.* It further showed that 42 and 46 targets were involved in the MAPK (ko04010) and PI3K-Akt (ko04151) signaling pathways, respectively (Figure 4C). The MAPK signaling pathway is essential in regulating many cellular processes including cell differentiation, cell stress response, cell division, metabolism, cell proliferation, motility and apoptosis. The role of the MAPK pathway in various diseases, including cancer, has been widely studied and well recognized (Haigis et al., 2008; Ahearn et al., 2011). As shown in Supplementary Figure 1, FMNT and CS could modulate multiple signaling molecules and pathways to suppress cancer proliferation, promote apoptosis, and inhibit angiogenesis. The key targets of the MAPK signaling pathway mainly include MAPK1, MAPK3, EGFR, AKT1, TP53, MYC, FOS, and MAPK8 (Supplementary Figure S1A). The PI3K-Akt signaling pathway is another crucial intracellular signal transduction pathway that closely regulate cell growth, migration, metabolism, proliferation and angiogenesis [28]. The PI3K-Akt is also a crucial signaling pathway contributing to initiation and development of various cancers (Noorolyai et al., 2019; Pompura and Dominguez-Villar, 2018). The key targets of the PI3K-Akt signaling pathway mainly include AKT1, HSP90AA1, HSP90AB1, TP53, PTEN, MYC, EGFR, and RELA (Supplementary Figure S1B). Hence, the potential mechanisms associated with the MAPK and PI3K-Akt signaling pathways were further verified using experimental validation coupled with molecular docking.

3.4 HQ, FMNT and CS significantly inhibited the viability of HT29 and Caco2 cells

MTT assay was performed to detect the effects of HQ, FMNT and CS on the viability of HT29 and Caco2 cells. It was found that

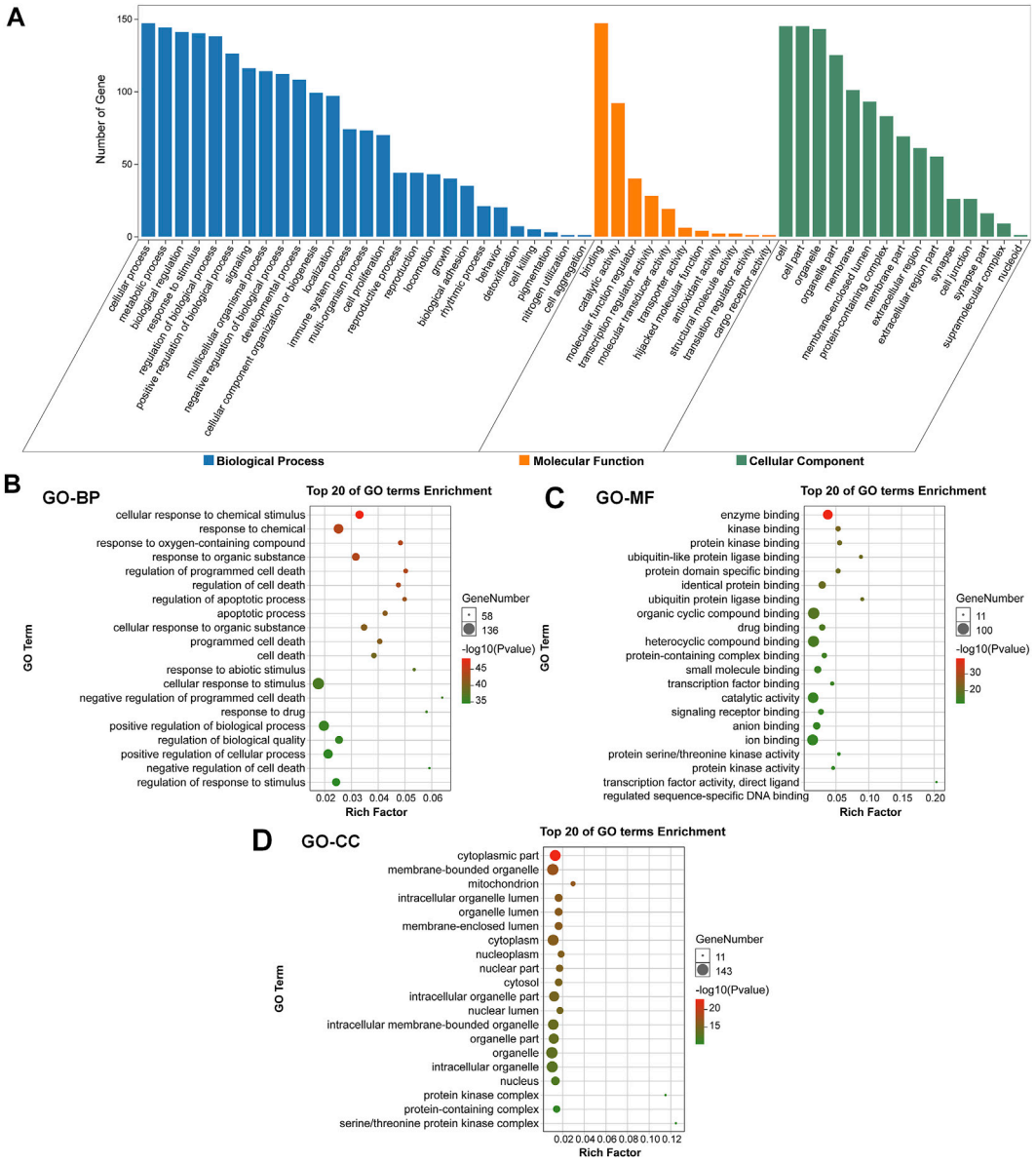

FIGURE 3
GO enrichment analysis of the key targets of FMNT and CS against colon cancer **(A)** The number of genes involved in the biological process (BP), molecular function (MF) and cellular component (CC) **(B)** GO-BP enrichment analysis of the 147 key targets **(C)** GO-MF enrichment analysis of the 147 key targets **(D)** GO-CC enrichment analysis of the 147 key targets. The top 20 enriched GO terms are displayed, and only terms with $p < 0.05$ were selected for analysis.

treatment with HQ at 3.125–100 mg/mL for 48 h significantly suppressed the viability of HT29 and Caco2 cells in a dose-dependent manner (Figures 5A, B, $p < 0.001$). The IC50 value of HQ in HT29 and Caco2 cells after treatment was 26.67 and 25.31 mg/mL, respectively. After treating cells with FMNT and CS at 3.125–200 μM for 48 h, cell viabilities were also significantly suppressed in a dose-dependent manner (Figures 5C–F, $p < 0.05$ or $p < 0.001$). 5-FU, which was used a positive control, also produced significant inhibition toward the viability of HT29 and Caco2 cells as expected ($p < 0.001$). Accordingly, three concentrations of 25, 50, and 100 mg/mL for HQ, and three concentrations of 25, 50, and 100 μM for FMNT or CS, and a duration of 48 h treatment were selected to conduct the following experiments.

3.5 HQ, FMNT and CS significantly inhibited the proliferation of HT29 and Caco2 cells

EdU assay was used to further evaluate the effects of HQ, FMNT and CS on the proliferation of HT29 and Caco2 cells. As shown in Figures 6A, B, treatment with HQ at 25, 50, and 100 mg/mL for 48 h significantly decreased EdU positive cells in a dose-dependent manner over the control ($p < 0.05$ or $p < 0.001$), indicating that HQ could significantly suppressed the proliferation of HT29 and Caco2 cells. The number of EdU positive cells in the FMNT or CS treated groups were also significantly reduced in a dose-dependent manner (Figures 6C–F, $p < 0.05$, $p < 0.01$ or $p < 0.001$), indicating that both FMNT and CS significantly suppressed the proliferation

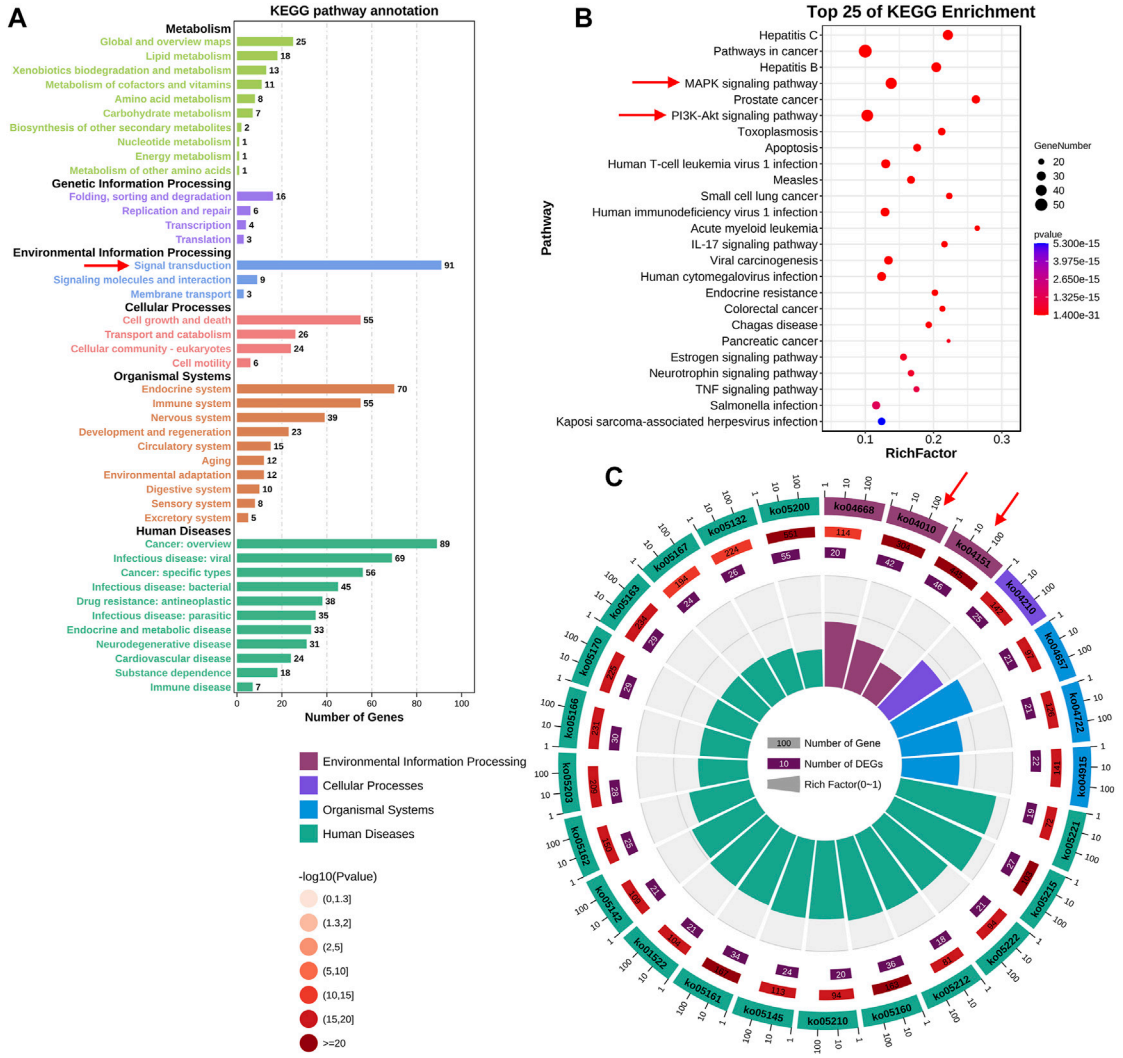

FIGURE 4
KEGG enrichment analysis of the key targets of FMNT and CS against colon cancer **(A)** The number of genes involved in the KEGG enrichment annotation **(B)** KEGG enrichment analysis of the 147 key targets. The top 25 enriched KEGG pathways are displayed, and only terms with $p < 0.05$ were selected for analysis **(C)** The number of genes and rich factors of the top 25 enriched KEGG pathways.

of HT29 and Caco2 cells. 5-FU, as a positive control, markedly inhibited the proliferation of HT29 and Caco2 cells as expected ($p < 0.001$).

3.6 HQ, FMNT and CS significantly induced apoptosis of HT29 and Caco2 cells

An Annexin V-FITC/PI staining assay was performed to evaluate whether HQ, FMNT and CS could induce apoptosis of HT29 and Caco2 cells. Treatment with HQ at 25, 50, and 100 mg/mL for 48 h significantly induced the apoptosis rate of HT29 and Caco2 cells in a dose-dependent manner (Figure 7A, $p < 0.001$). Apoptosis rate was also dose-dependently increased in HT29 and Caco2 cells exposed to FMNT (Figure 7B, $p < 0.01$ or $p < 0.001$) or CS (Figure 7C, $p < 0.001$) at 10, 20, and 40 μM for 48 h.

3.7 HQ, FMNT and CS significantly suppressed the migration of HT29 and Caco2 cells

Wound healing assay was used to evaluate the effects of HQ, FMNT and CS on the migration of HT29 and Caco2 cells. As shown in Figures 8A, B, treatment with HQ at 25, 50, and 100 mg/mL for 12–48 h significantly suppressed the migration ratio of HT29 and Caco2 cells dose-dependently over the control ($p < 0.05$, $p < 0.01$ or $p < 0.001$). Incubation of FMNT and CS at 10, 20, and 40 μM also exhibited significant inhibitory effects on the migration of HT29 and Caco2 cells (Figures 8C–F, $p < 0.05$, $p < 0.01$ or $p < 0.001$).

E-cadherin, N-cadherin, and Vimentin are critical epithelial–mesenchymal transformation (EMT)-related proteins, which that modulate cell migration and tumor invasiveness. E-cadherin is notably downregulated while N-cadherin and Vimentin are upregulated during EMT [30]. Hence, the

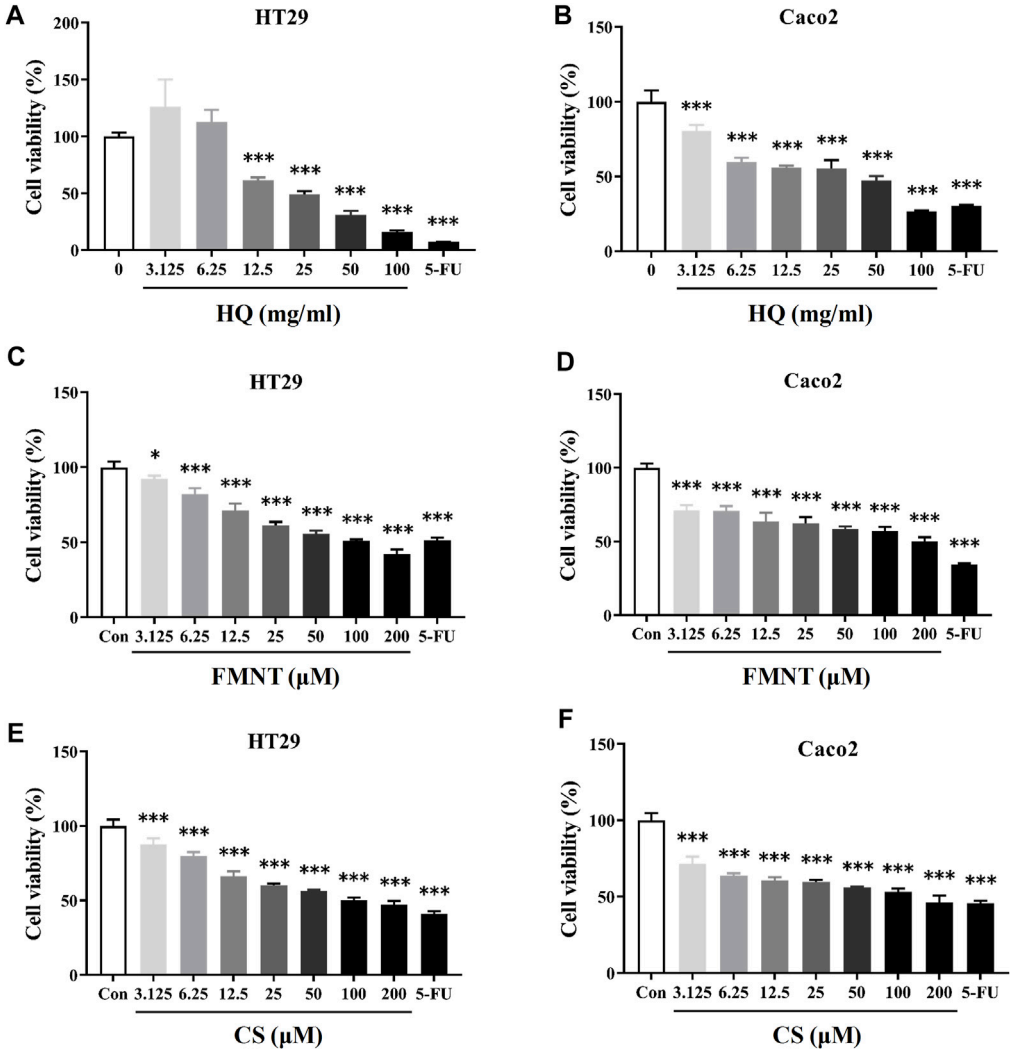

FIGURE 5
HQ, FMNT and CS significantly inhibited the viability of HT29 and Caco2 cells. The cytotoxicity of HQ (3.125–100 mg/mL, 48 h) **(A and B)**, FMNT (3.125–200 μM, 48 h) **(C and D)** and CS (3.125–200 μM, 48 h) **(E and F)** toward HT29 and Caco2 cells, respectively. 5-FU was used as a positive control for inhibition of cell viability. The data represent the mean ± SD (n = 3). *p < 0.05 and ***p < 0.001 compared with the control group.

intracellular protein levels of E-cadherin, N-cadherin, and Vimentin were further determined. As shown in Figure 9A, exposure to HQ at 25, 50, and 100 mg/mL for 48 h significantly upregulated the E-cadherin protein levels, while dose-dependently downregulated the protein levels of N-cadherin and Vimentin over the control (p < 0.05, p < 0.01, or p < 0.001). It was observed that incubation of FMNT and CS at 10, 20, and 40 μM for 48 h also strikingly increased the E-cadherin protein levels, while decreased the protein levels of N-cadherin and Vimentin in a dose-dependent manner (Figures 9B, C, p < 0.05, p < 0.01, or p < 0.001). Moreover, the results of immunofluorescence assay further revealed the expression of intracellular E-cadherin, N-cadherin, and Vimentin with the same treatment. Of note, the fluorescence intensity of E-cadherin was markedly enhanced, while the fluorescence intensity of N-cadherin and Vimentin was notably decreased in the cells exposed to HQ, FMNT and CS over the control cells (Figure 10).

3.8 HQ, FMNT and CS significantly inhibited the ERK1/2 and PI3K-Akt signaling pathways

Western blot analysis was further performed to understand the roles of ERK1/2 and PI3K-Akt signaling in mediating the inhibitory effects of HQ, FMNT and CS against colon cancer. Compared with the control cells, exposure to HQ at 25, 50, and 100 mg/mL for 48 h strikingly downregulated the p-ERK1/2 expression in a dose-dependent manner (Figure 11A, p < 0.01, or p < 0.001), while did not notably alter the total ERK1/2 expression. Thus, p-ERK1/2/ERK1/2 ratio was significantly decreased in the cells exposed to HQ than that in the control cells (Figure 11A, p < 0.01, or p < 0.001). The treatment of HQ at high dose also slightly downregulated the p-AKT expression without marked change in total Akt expression. Similarly, Western blot analysis demonstrated a decreased p-ERK1/2 expression in the cells exposed to FMNT or CS (Figures 11B, C,

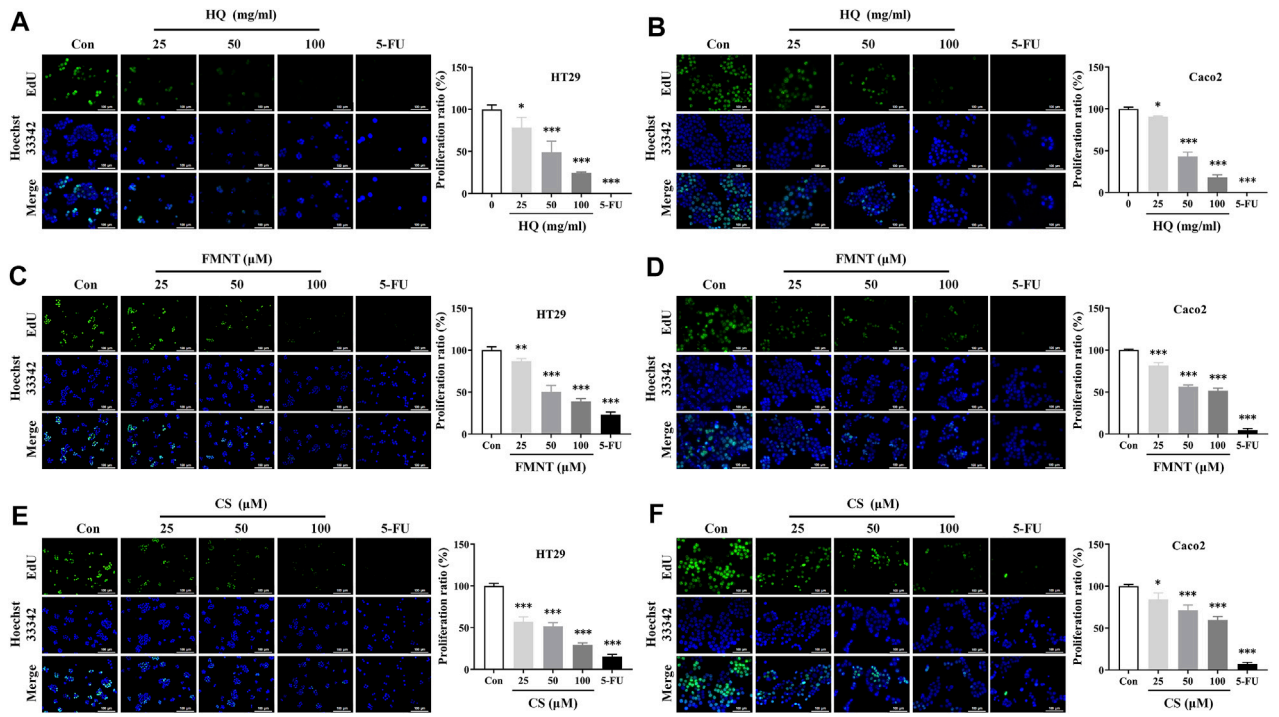

FIGURE 6
HQ, FMNT and CS significantly inhibited the proliferation of HT29 and Caco2 cells. The effects of HQ (25, 50 and 100 mg/mL, 48 h) **(A and B)**, FMNT (25, 50 and 100 μM, 48 h) **(C and D)** and CS (25, 50 and 100 μM, 48 h) **(E and F)** on the proliferation of HT29 and Caco2 cells, respectively. 5-FU was used as a positive control for inhibition of cell proliferation. The data represent the mean ± SD (n = 3). *p < 0.05, **p < 0.01 and ***p < 0.001 compared with the control group.

$p < 0.05$ or $p < 0.001$). Thus, FMNT and CS treatment significantly decreased the p-ERK1/2/ERK1/2 ratio compared with the control cells (Figures 11B, C, $p < 0.01$, or $p < 0.001$). The same treatment of FMNT and CS at their high doses also slightly downregulated the p-Akt protein levels, while did not notably alter the total Akt expression (Figures 11B, C).

Person correlation analysis showed that the inactivation of HQ, FMNT and CS on ERK1/2 signaling pathway was closely related to their inhibitory effects against colon cancer. It was observed that HQ-induced decrease in ratio of p-ERK1/2/ERK1/2 was positively related to inhibition of cell viability, proliferation, and migration, while were negatively related to promotion of the cell apoptosis (Supplementary Figure S2, $p < 0.001$). Similarity, a strong positive correlation was found between the decrease in p-ERK1/2/ERK1/2 ratio and inhibition of cell viability, proliferation, and migration by FMNT and CS. Conversely, a significant negative correlation was observed between the decreased p-ERK1/2/ERK1/2 ratio and promotion of the cell apoptosis by FMNT and CS (Supplementary Figures S3, S4, $p < 0.001$).

3.9 FMNT and CS showed strong binding affinity for the core targets of EGFR/RAS/RAF/MEK/ERK pathway

Overactivation of the RAS/RAF/MEK/ERK signaling pathway is associated with the carcinogenesis and progression of numerous cancers (Zhang et al., 2019; Zhu et al., 2020). Epidermal growth factor receptor (EGFR), a typical receptor tyrosine kinase, is activated by binding with ligands and takes part in cell differentiation, proliferation, migration, and apoptosis *via* activating the subsequent intracellular signaling pathways (Zhang et al., 2019). RAS/RAF/MEK/ERK is one of the most key EGFR downstream signaling pathways (Zhang et al., 2019). Thus, EGFR/RAS/RAF/MEK/ERK pathway is an essential target in clinical cancer therapy. Development of inhibitors of this pathway is considered as promising strategy for the prevention and treatment of numerous cancers (Supplementary Figure S5). Hence, molecular docking study was further conducted to explore the binding affinity of FMNT and CS with EGFR/RAS/RAF/MEK/ERK pathway. The pattern diagram of molecular docking was shown in Figure 12. Protein residues Glu738 and Asp831 in EGFR formed hydrogen bonds with FMNT and CS, respectively (Figures 12A, B). FMNT could bind to the protein residue Lys483, forming one single hydrogen bond (Figure 12C), while CS could bind to the protein residues Cys532 and Lys483 in BRAF through hydrogen bonds (Figure 12D). Protein residues Met146 and Gly144 in MEK1 formed hydrogen bonds with FMNT (Figure 12E), while only residue Met146 in MEK1 and CS bonded to each other through one single hydrogen bond (Figure 12F). FMNT could interact with the residue Met150 (Figure 12G), while CS could interact with the residues Met150 and Asn199 in MEK2 through hydrogen bonds (Figure 12H). Both FMNT and CS could interact with the residue Met125 in ERK1through hydrogen bonds (Figures 12I, J). CS could also interact with the residue Asp184 in ERK1 (Figure 12J). Protein residues Lys52 and Glu107 in ERK2 formed one single hydrogen bond with FMNT and CS, respectively (Figures 12K, L). The docking scores for FMNT and CS with the six crystal structures were showed in

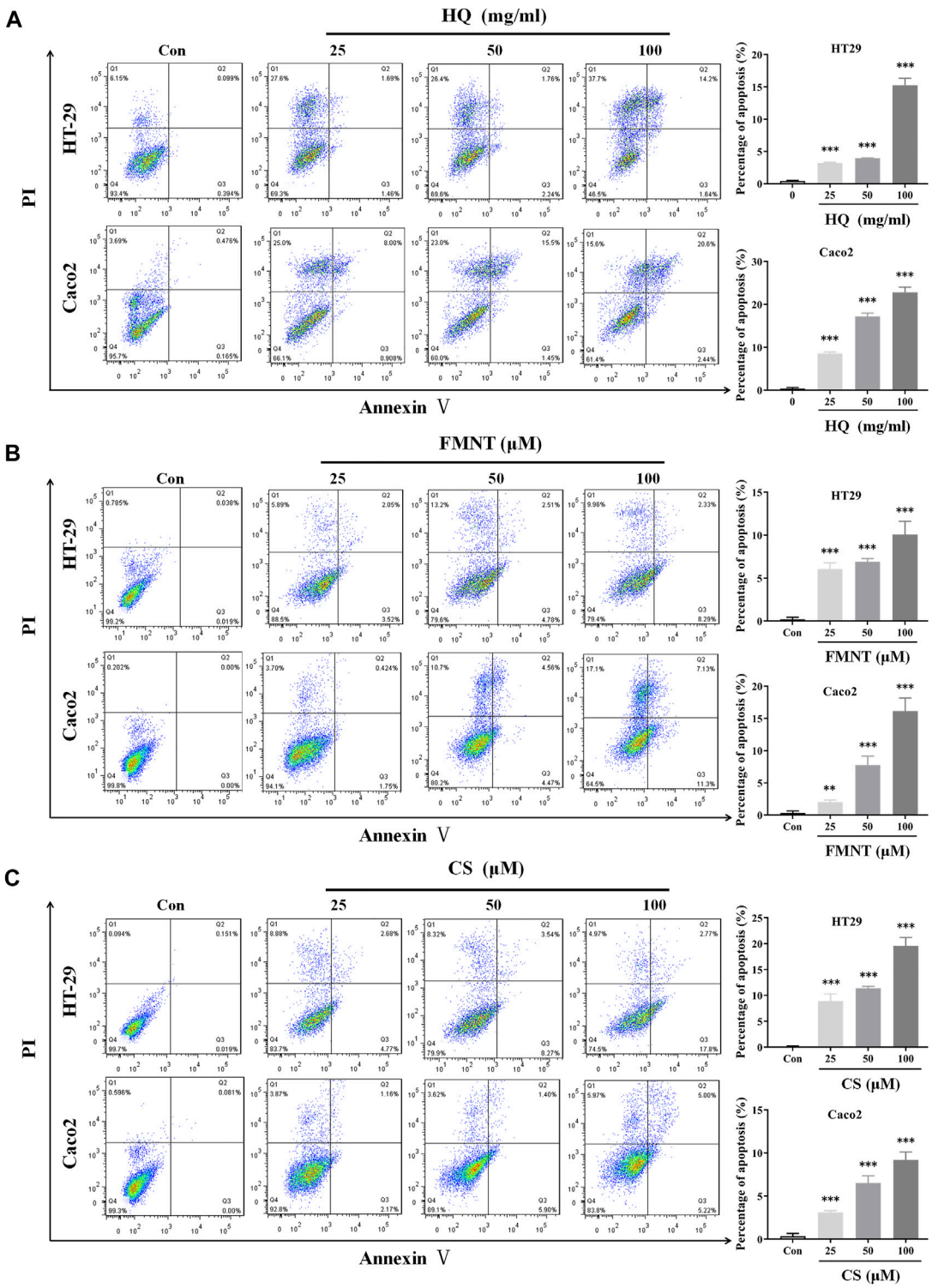

FIGURE 7
HQ, FMNT and CS significantly induced apoptosis of HT29 and Caco2 cells. The effects of HQ (25, 50 and 100 mg/mL, 48 h) **(A)**, FMNT (25, 50 and 100 μM, 48 h) **(B)** and CS (25, 50 and 100 μM, 48 h) **(C)** on the apoptosis of HT29 and Caco2 cells. The data represent the mean ± SD (n = 3). $^{**}p < 0.01$ and $^{***}p < 0.001$ compared with the control group.

Table 1. The bond strength of hydrogen bonds represents the binding affinity between ligand compounds and receptor molecules, and when the docking score is lower, the binding affinity is stronger. An affinity <−7 indicates strong binding activity (Trott and Olson, 2010). Thus, the results revealed that FMNT and CS have a strong binding affinity for the key targets of EGFR/RAS/RAF/MEK/ERK pathway, and the binding affinity of CS with the targets was stronger than that of FMNT to the same targets.

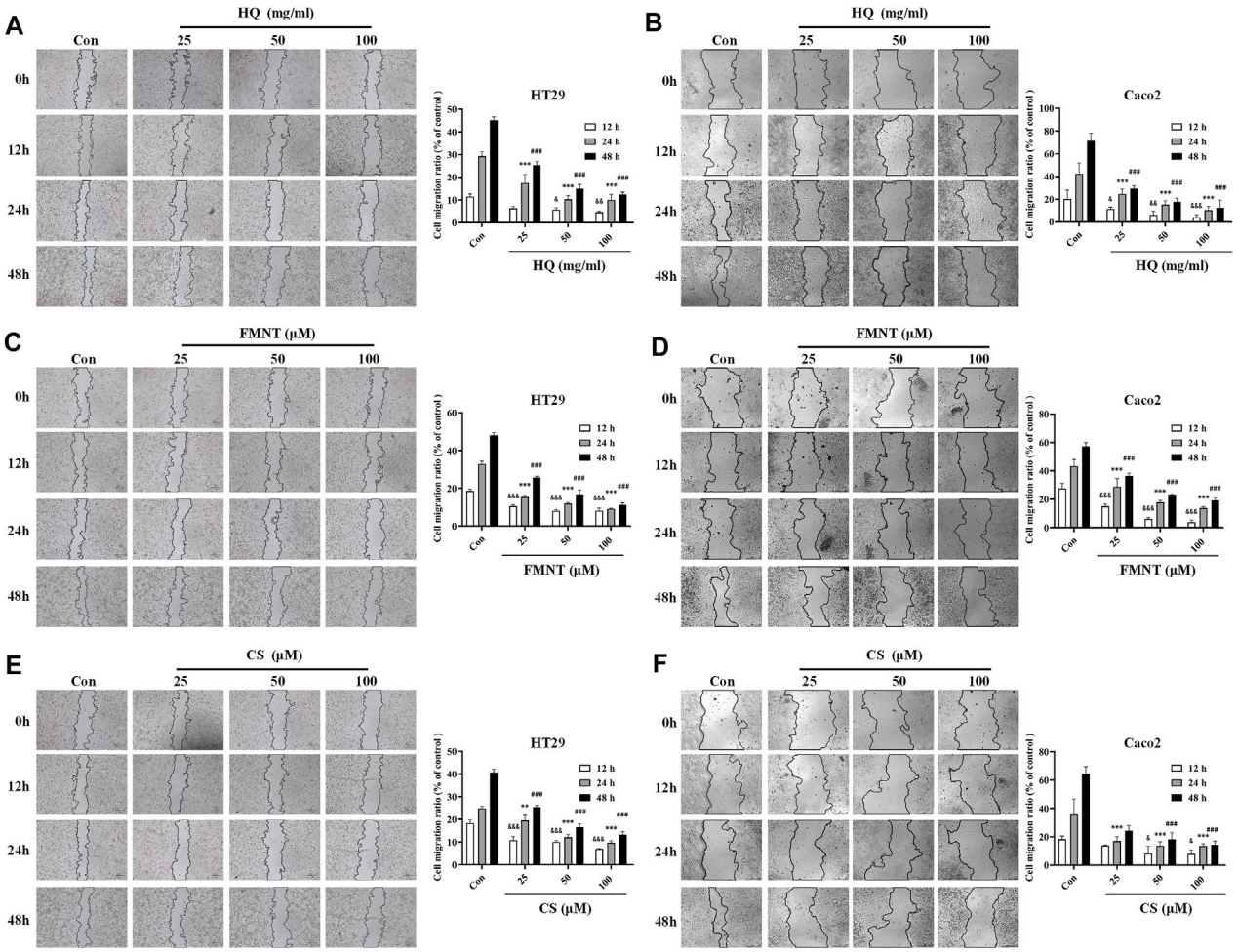

FIGURE 8
HQ, FMNT and CS significantly suppressed the migration of HT29 and Caco2 cells. The effects of HQ (25, 50 and 100 mg/mL) **(A and B)**, FMNT (25, 50 and 100 μM) **(C and D)** and CS (25, 50 and 100 μM) **(E and F)** on the migration of HT29 and Caco2 cells for 12, 24 and 48 h, respectively. The data represent the mean ± SD ($n = 3$). $^{\&}p < 0.05$, $^{\&\&}p < 0.01$ and $^{\&\&\&}p < 0.001$ compared with the control group for 12 h incubation. $^{***}p < 0.001$ compared with the control group for 24 h incubation. $^{\#}p < 0.05$, $^{\#\#}p < 0.01$ and $^{\#\#\#}p < 0.001$ compared with the control group for 48 h incubation.

4 Discussion

Worldwide, colon cancer is the third most frequent malignant disease with high morbidity, recurrence and mortality (Ferlay et al., 2019; Kong et al., 2020). Despite advances in surgery, chemotherapy, radiotherapy and immunotherapy, the prognosis in colon cancer patients remains poor and the recurrence rate is still high (Kong et al., 2020). What is more, long-term use of these therapies will easily produce undesirable side effects and toxicologically unsafe consequences (Kong et al., 2020). CHMs have played an indispensable role in healthcare throughout Chinese history, and have also been increasingly used worldwide for prevention and treatment of various diseases. Substantial evidence exists that CHMs are effective and safe as alternative remedies for patients with colon cancer. However, the applications of many CHMs in the clinical treatment of colon cancer is also greatly restricted because of their multiple ingredients and different mechanisms of action (Yan et al., 2017; Guo et al., 2019). Hence, it is urgent and necessary to fully elucidate the effects and molecular mechanisms to promote the applications of CHMs for healthcare all over the world.

In recent years, network pharmacology has been increasingly applied to expand our knowledge pertaining to the multiple targets and mechanisms of CHMs in the clinical treatment of various diseases, including numerous cancers (Li and Zhang, 2013; Hao da and Xiao, 2014). Network pharmacology, a new discipline which integrates network biology and polypharmacology approaches, is able to reveal drug properties and interactions with multiple protein targets. Hence, network pharmacology can provide beneficial information for studying the modulation of various complex biological, physiological, and pathological systems (Berger and Iyengar, 2009; Li and Zhang, 2013; Hao da and Xiao, 2014). Currently, network pharmacology has been frequently used as a powerful tool to elucidate the complex and holistic mechanisms of CHMs (Li and Zhang, 2013; Hao da and Xiao, 2014). Therefore, we first screened the potential targets of HQ and its bioactive ingredients FMNT and CS against colon cancer, as well as investigated the mechanism using network pharmacology analysis. 147 potential targets of FMNT and CS in the suppression of colon cancer were obtained (Figure 2). 19 core targets were further screened and analyzed. It was apparent that the 19 key targets, included AKT1,

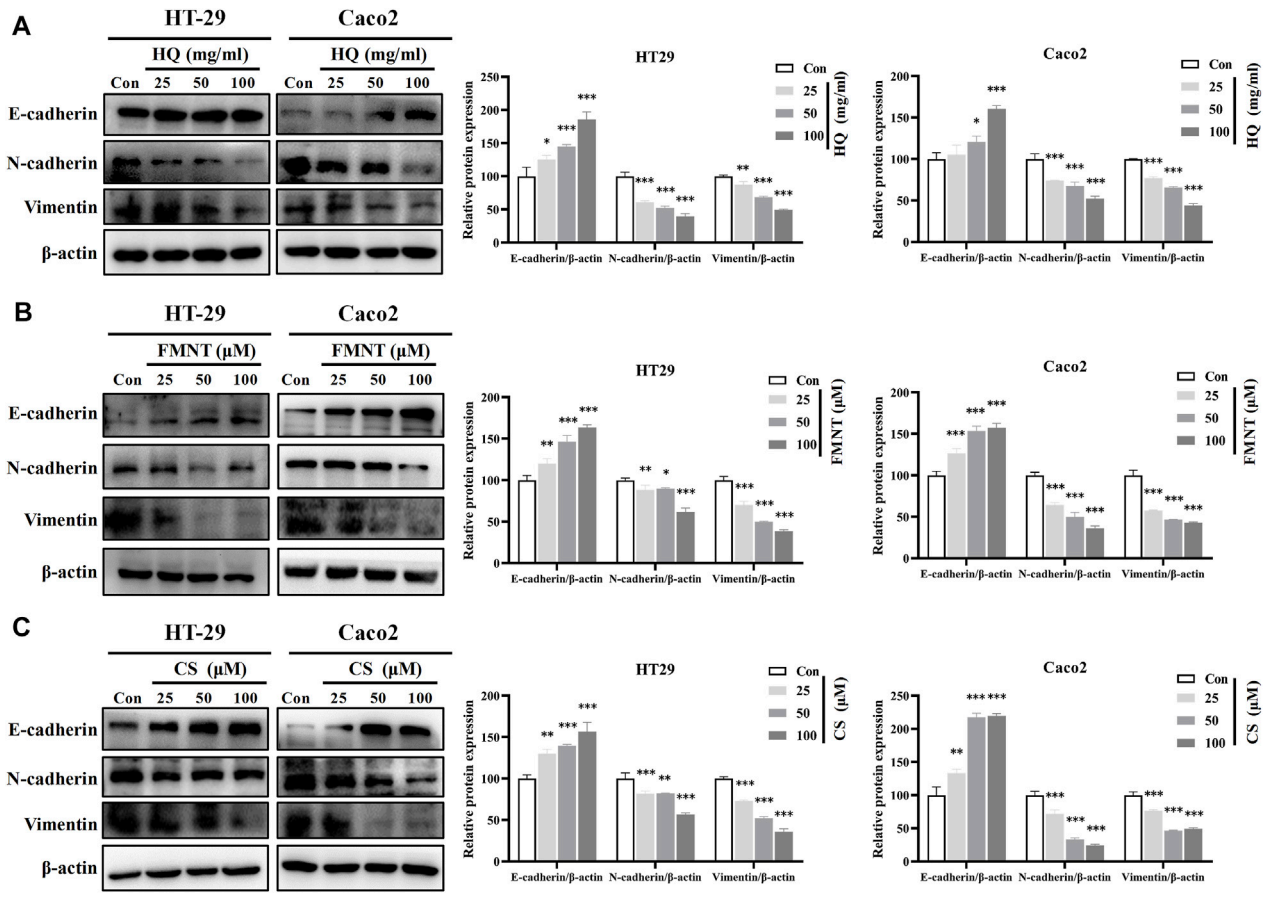

FIGURE 9
HQ, FMNT and CS significantly upregulated E-cadherin protein levels, and downregulated N-cadherin and Vimentin protein levels in HT29 and Caco2 cells. The protein levels of E-cadherin, N-cadherin, and Vimentin in HT29 and Caco2 cells were detected after treatment with HQ (25, 50 and 100 mg/mL, 48 h) **(A)**, FMNT (25, 50 and 100 μM, 48 h) **(B)** or CS (25, 50 and 100 μM, 48 h) **(C)**, respectively. The data represent the mean ± SD (n = 3). $^{**}p < 0.01$ and $^{***}p < 0.001$ compared with the control group.

TP53, MAPK3, EGFR, HSP90AA1, ESR1, MYC, CASP3, TNF, JUN, PTEN, MAPK1, FOS, RELA, FN1, PTGS2, HSP90AB1, MAPK8 and PPARG, were closely involved in cell proliferation, differentiation, migration, and apoptosis. Next, GO enrichment analysis proposed that FMNT and CS could exhibit inhibitory activity against colon cancer by simultaneously activating various BPs, CCs, and MFs (Figure 3). KEGG pathway enrichment further indicated that multiple pathways including pathways in cancer, MAPK and PI3K-Akt signaling pathways could be associated with the inhibitory effects of FMNT and CS against colon cancer (Figure 4). Accordingly, we next conducted experimental validation to elucidate the mechanism of HQ, FMNT and CS against colon cancer.

Previous studies showed that HQ and its isoflavonoids have pharmacological effects against colon cancer. HQ can not only inhibit the proliferation, cause cell cycle arrest and promote apoptosis of colon cancer cells, but also inhibit the migration of colon cancer cells (Tseng et al., 2016; Tan et al., 2019). HQ could effectively inhibit the tumors of human colon cancer cells grafted into nude mice without obvious unsafe consequences (Tseng et al., 2016), which demonstrated that HQ might be a potential chemopreventive drug for therapy colon cancer. The study of HQ in controlling angiogenesis revealed that HQ exerted anti-tumor activity in colon cancer cells *via* modulation of mTOR and COX-2 signaling, which together reduced VEGF expression to suppress angiogenesis in human CRC cell and tumor xenograft (Auyeung et al., 2016). FMNT was also proven to downregulate the expression of key pro-angiogenic factors such as VEGF and matrix metalloproteinases in colon cancer cells, and to inhibit angiogenesis and tumor cell invasion, thereby supporting its use in advanced and metastatic colon therapies (Auyeung et al., 2012). In addition to FMNT, CS could notably inhibited proliferation and induced apoptosis of colon cancer cells through regulating multiple signaling, including ERβ/MiR-95, ERβ/miR-17, IGF-1R and PI3K-Akt signaling pathways (Chen et al., 2015b; Zhao et al., 2016), which indicates that CS serves as an attractive chemotherapeutic agent against colon cancer. The results from this study demonstrated that HQ, FMNT and CS could effectively inhibit the viability and proliferation, as well as promote apoptosis of HT29 and Caco2 cells (Figures 5–7), suggesting that FMNT and CS could be the beneficial ingredients responsible for the therapeutic efficacy of HQ in the suppression of colon cancer.

Growing evidence suggests that invasion and metastasis are the fundamental reason of colon cancer treatment failure and the leading cause of death in colon cancer patients (Wen et al., 2022). Suppression of invasion and metastasis is of great

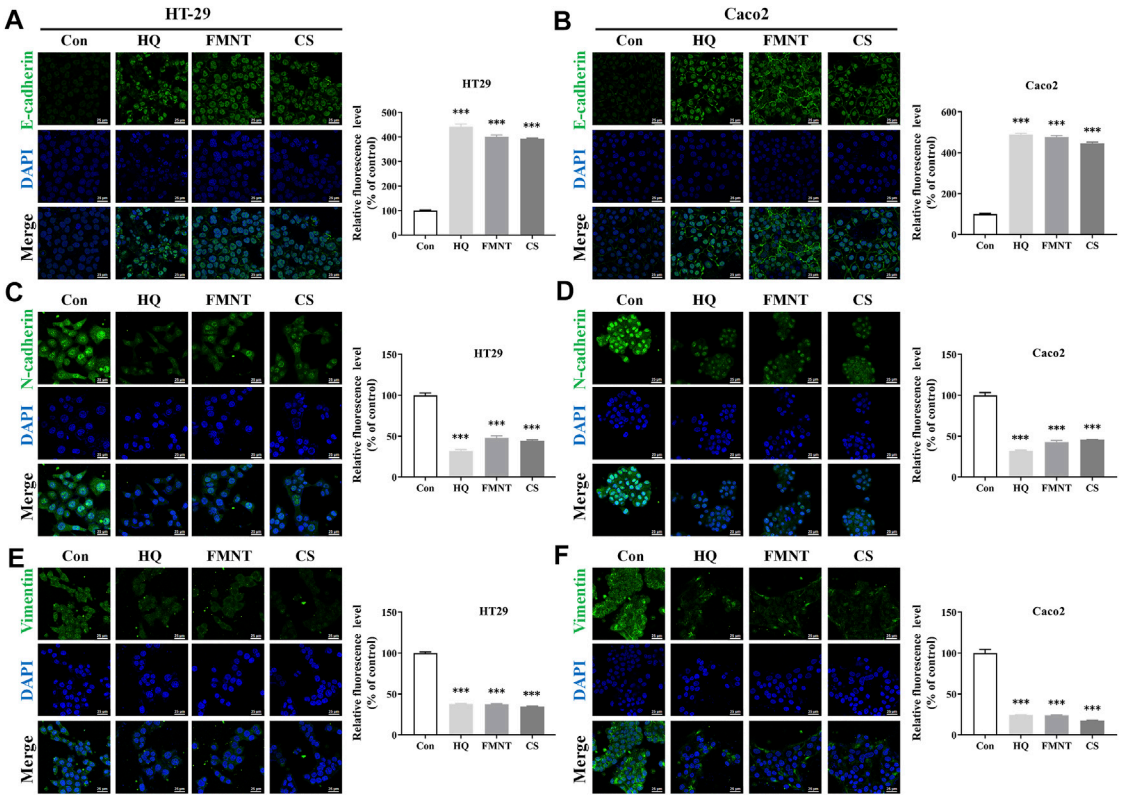

FIGURE 10
HQ, FMNT and CS significantly increased the fluorescence intensity of E-cadherin **(A, B)**, and decreased the fluorescence intensity of N-cadherin **(C, D)** and Vimentin **(E, F)** in HT29 and Caco2 cells. The fluorescence intensity of E-cadherin, N-cadherin, and Vimentin in HT29 and Caco2 cells were detected after treatment with HQ (100 mg/mL, 48 h), FMNT (100 μM, 48 h) or CS (100 μM, 48 h), respectively. The data represent the mean ± SD (n = 3). ***p < 0.001 compared with the control group.

therapeutic interest in counteracting chemoresistance in patients with colon cancer. The proliferation of tumor cells was the basis of tumor invasion and metastasis (Yang et al., 2019). This current study showed that HQ, FMNT and CS could dose-dependently inhibit the proliferation of colon cancer cells (Figure 6). Thus, the wound healing assay was conducted to further confirm the impact of HQ, FMNT and CS on the metastasis of colon cancer cells. It was found that HQ, FMNT and CS could significantly suppress the migration of colon cancer cells in dose- and time-dependent manners (Figure 8), indicating that HQ, FMNT and CS could inhibit the metastasis of colon cancer cells. It is well-known that E-cadherin, N-cadherin, and Vimentin are critical EMT-related proteins, which play pivotal roles in modulation of cell migration and tumor invasiveness (Hazan et al., 2000). E-cadherin, a calcium-dependent cell-cell adhesion molecule, takes part in epithelial cell behavior, tissue formation, and cancer suppression (van Roy and Berx, 2008). N-cadherin, which serves as an indicator of ongoing EMT, is closely associated with the development of diverse cancers (Loh et al., 2019). Vimentin, as a typical marker for EMT, is overexpressed in various epithelial cancers and correlates well with accelerated tumor growth, invasion, and poor prognosis (Satelli and Li, 2011). During EMT, N-cadherin and Vimentin are upregulated while E-cadherin is downregulated. Hence, the expression of intracellular E-cadherin, N-cadherin, and Vimentin were further determined. It was found that HQ, FMNT and CS could strikingly upregulate the E-cadherin protein levels, while simultaneously downregulated the protein levels of N-cadherin and Vimentin in a dose-dependent manner (Figure 9). In addition, immunofluorescence assay revealed that the fluorescence intensity of E-cadherin was markedly increased, while the fluorescence intensity of N-cadherin and Vimentin was notably decreased (Figure 10). These data further indicate that HQ, FMNT and CS could effectively suppress colon cancer by inhibiting the metastasis of colon cancer cells.

In this study, the network pharmacological study found that the MAPK and PI3K-Akt signaling pathways were two important pathways for HQ in treating colon cancer. MAPK signaling pathway has a crucial role in cell proliferation, differentiation, migration, and apoptosis, including phosphorylation of ERK1/2, P38, and JNK (Haigis et al., 2008; Ahearn et al., 2011). ERK1/2, one of the best-characterized members of MAPK family, mediates a wide range of cellular responses like gene expression, metabolism, motility, cell survival and death (Wang et al., 2022). Substantial evidence exists that the phosphorylation of ERK1/2 could increase cell proliferation and cause an anti-apoptotic effect, thereby promoting the progression of tumor invasion and metastasis (Lebedev et al., 2022; Wang et al., 2022). Conversely, suppression of ERK1/2 could effectively block many other extracellular signals that promote cell growth and movement, ultimately suppressing tumor invasion and metastasis (Lebedev et al., 2022; Wang et al., 2022). Hence, identification of small molecules that can inhibit ERK1/2 activity may be a useful

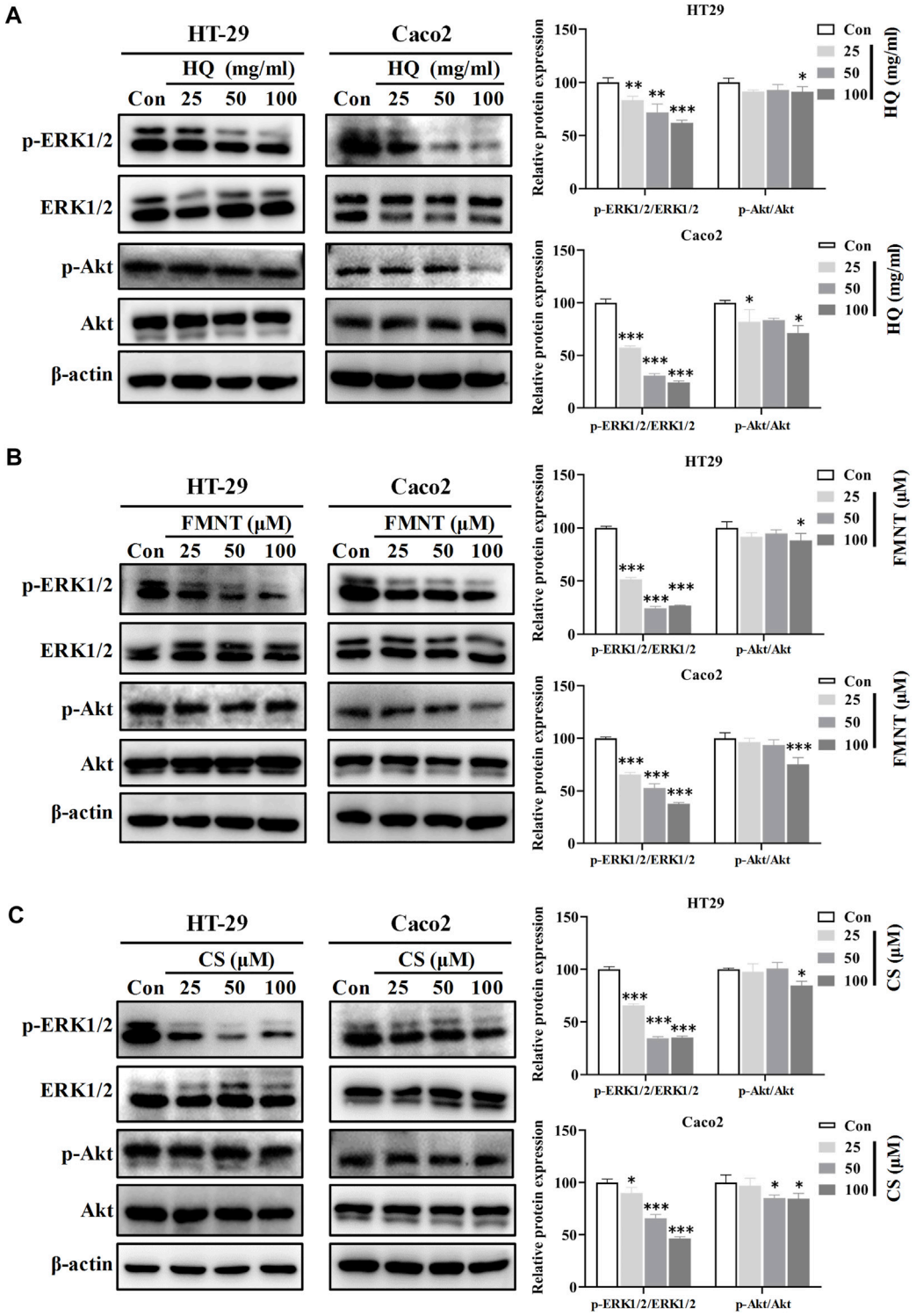

FIGURE 11
HQ, FMNT and CS significantly inhibited the ERK1/2 and PI3K-AKT signaling pathways. The protein levels of p-Erk1/2, ERK1/2, p-AKT and AKT in HT29 and Caco2 cells were detected after treatment with HQ (25, 50 and 100 mg/mL, 48 h) **(A)**, FMNT (25, 50 and 100 μM, 48 h) **(B)** or CS (25, 50 and 100 μM, 48 h) **(C)**, respectively. The data represent the mean ± SD (n = 3). *$p < 0.05$, **$p < 0.01$ and ***$p < 0.001$ compared with the control group.

pharmacological strategy for the clinical treatment of numerous cancers (Lebedev et al., 2022; Wang et al., 2022). In addition to ERK1/2, the PI3K-Akt signaling pathway also takes part in a variety of cellular activities, including cell growth, metabolism, motility, proliferation, survival, and apoptosis (Porta et al., 2014). Aberrant activation of the PI3K-Akt pathway promotes the growth and proliferation of tumor cells in various types of human cancers (Huang and Hung, 2009; Porta et al., 2014). Knockout or

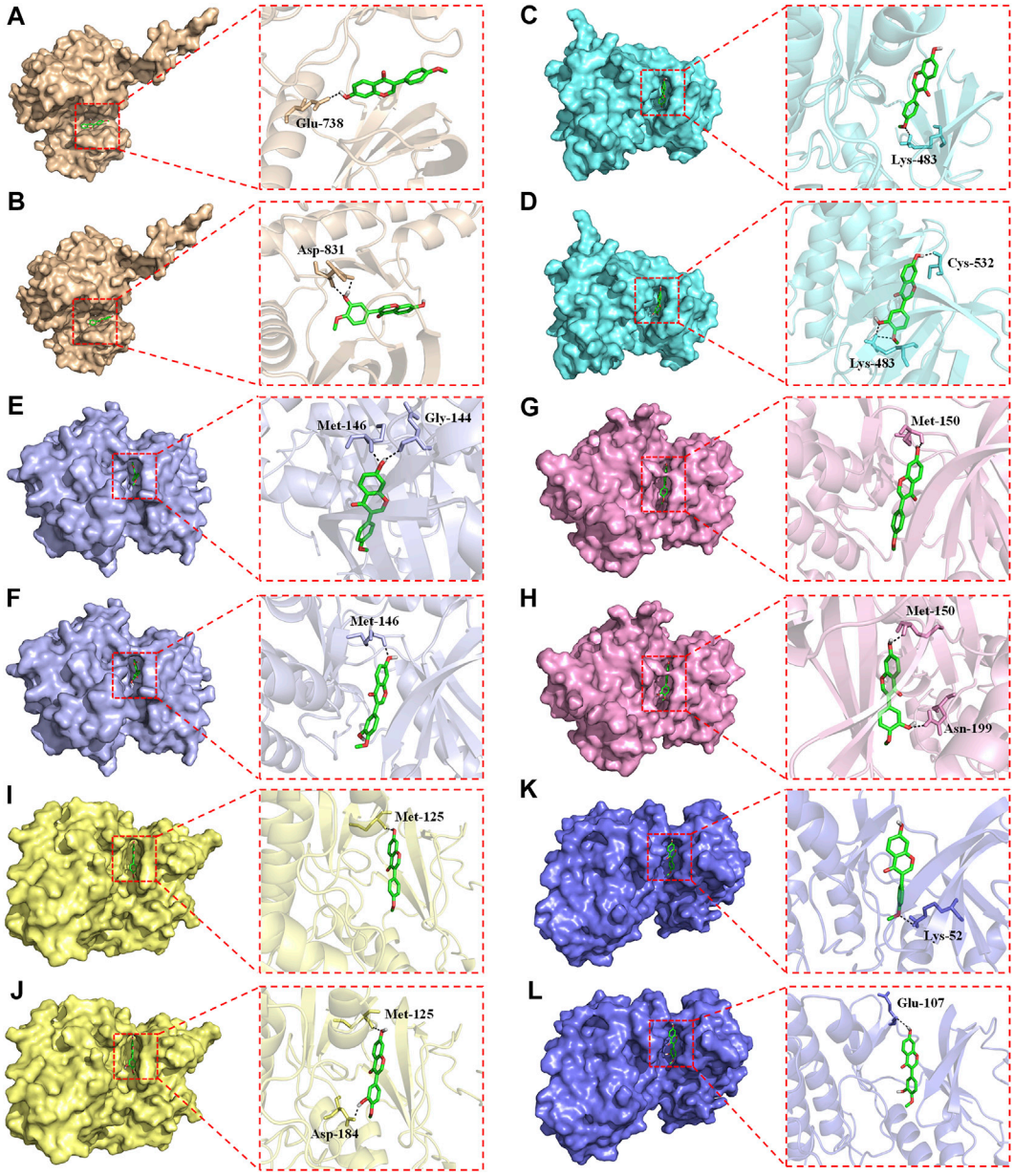

FIGURE 12
Pattern diagrams of molecular docking. FMNT-EGFR **(A)**. CS-EGFR **(B)**. FMNT-BRAF **(C)**. CS-BRAF **(D)**. FMNT-MEK1 **(E)**. CS-MEK1 **(F)**. FMNT-MEK2 **(G)**. CS-MEK2 **(H)**. FMNT-ERK1 **(I)**. CS-ERK1 **(J)**. FMNT-ERK2 **(K)**. CS-ERK2 **(L)**.

suppression of PI3K-Akt pathway has been an attractive strategy to effectively inhibit tumor growth and invasiveness (Cheng et al., 2005). The data of this study displayed that HQ, FMNT and CS significantly decreased the intracellular p-ERK1/2 expression in a dose-dependent manner, while did not notably alter the total ERK1/2 expression (Figure 11). The same treatment of HQ, FMNT and CS at their high doses also slightly downregulated the intracellular p-AKT expression without marked alteration in total Akt expression (Figure 11). Person correlation analysis revealed that HQ, FMNT and CS-induced decrease in p-ERK1/2/ERK1/2 ratio was positively related to their inhibition of cell viability, proliferation, and migration, while were negatively related to their promotion of the cell apoptosis (Supplementary Figures S2-S4). These results suggested that HQ, FMNT and CS could manifest remarkable inhibitory activity against colon cancer mainly *via* reducing the phosphorylation of ERK1/2 to inhibit the ERK1/2 pathway. This suppression of colon cancer by HQ, FMNT and CS was also partially mediated *via* inactivation of the PI3K-Akt signaling pathway. Finally, to validate the potential mechanism of HQ, FMNT and CS against colon cancer, molecular docking was further performed to explore the binding affinity of FMNT and CS with upstream molecules of ERK1/2 pathway. As protein-serine/threonine kinases, ERK1 and ERK2 participate in the RAS/ARF/MEK/ERK signal transduction cascade that play a crucial role in the modulation of a large variety of cellular activities including cell adhesion, metabolism, cell survival, cell migration, cell cycle

progression, proliferation, differentiation and transcription (Roskoski, 2012). Overactivation of the RAS/ARF/MEK/ERK signaling is correlated with the carcinogenesis and progression of numerous cancers (Zhang et al., 2019; Zhu et al., 2020). Epidermal growth factor receptor (EGFR), a typical receptor tyrosine kinase, is activated by binding with ligands and takes part in cell survival, proliferation, migration, differentiation, and apoptosis *via* activating the subsequent intracellular signaling pathways (Zhang et al., 2019). RAS/ARF/MEK/ERK is one of the most key EGFR downstream signaling pathways (Zhang et al., 2019). Development of inhibitors that target EGFR/RAS/ARF/MEK/ERK pathway is considered an effective and promising strategy for the clinical treatment of numerous cancers (Supplementary Figures S5). The pattern diagram of molecular docking showed that different amino acid residues in the crystal structures of EGFR, RAS, ARF, MEK or ERK formed hydrogen bonds with FMNT and CS, respectively (Figure 12). The bond strength of hydrogen bonds represents the binding affinity between ligand compounds and receptor molecules, and when the docking score is lower, the binding affinity is stronger. An affinity <−7 suggests strong binding activity (Trott and Olson, 2010). The results of molecular docking study indicate that FMNT and CS have a strong binding affinity for the key targets of EGFR/RAS/ARF/MEK/ERK pathway, and the binding affinity of CS with the targets was stronger than that of FMNT to the same targets (Table 1). These finding indicated that the mechanism of the HQ, FMNT and CS against colon cancer might be due to suppression of the ERK1/2 pathway through potent inhibition of its upstream molecules. Further studies are needed to determine the exact mechanism(s) of the regulation of HQ, FMNT and CS on the ERK1/2 signaling pathway. Further animal experimental research on the inhibitory effects of HQ, FMNT and CS against colon cancer needs to be continued.

5 Conclusion

This study investigated the effects and mechanism of HQ and its bioactive ingredients FMNT and CS against colon cancer using network pharmacology analysis coupled with experimental validation and molecular docking. The findings suggested that the HQ exerted good therapeutic effects against colon cancer by mainly inhibiting the ERK1/2 signaling pathway. FMNT and CS were two bioactive ingredients responsible for the inhibitory effects of HQ against colon cancer. The current study expands our knowledge pertaining to the effects and mechanism of HQ against colon cancer, and suggests that FMNT and CS will hopefully serve as prospective compounds for colon cancer treatment.

Data availability statement

The original contributions presented in the study are included in the article/Supplementary Material, further inquiries can be directed to the corresponding authors.

Author contributions

JW and XY conceived and designed the experiments; YH, WZ, DT, HC and GZ performed the experiments. XT, YZ, WG and YW helped on the data collection and analysis; JW, XY and YH wrote and revised the manuscript.

Funding

This research was funded by the grants of Science and Technology Projects in Guangzhou (202201011393, 202102021196), Project of Traditional Chinese Medicine Bureau of Guangdong Province (20211111, 20231234, 20201201), Key-Area Research and Development Program of Guangdong Province (2020B1111100004), Guangdong Basic and Applied Basic Research Foundation (2020B1515130005), and First Class Undergraduate Major Construction Project of High Level University (2022JXA010).

Conflict of interest

The authors declare that the research was conducted in the absence of any commercial or financial relationships that could be construed as a potential conflict of interest.

Publisher's note

Supplementary material

The Supplementary Material for this article can be found online at: https://www.frontiersin.org/articles/10.3389/fphar.2023.1111912/full#supplementary-material

References

Ahearn, I. M., Haigis, K., Bar-Sagi, D., and Philips, M. R. (2011). Regulating the regulator: Post-translational modification of RAS. *Nat. Rev. Mol. Cell Biol.* 13, 39–51. doi:10.1038/nrm3255

Amberger, J. S., Bocchini, C. A., Schiettecatte, F., Scott, A. F., and Hamosh, A. (2015). OMIM.org: Online Mendelian Inheritance in Man (OMIM®), an online catalog of human genes and genetic disorders. *Nucleic Acids Res.* 43, D789–D798. doi:10.1093/nar/gku1205

An, L., Lin, Y., Li, L., Kong, M., Lou, Y., Wu, J., et al. (2020). Integrating network pharmacology and experimental validation to investigate the effects and mechanism of Astragalus flavonoids against hepatic fibrosis. *Front. Pharmacol.* 11, 618262. doi:10.3389/fphar.2020.618262

Ashburner, M., Ball, C. A., Blake, J. A., Botstein, D., Butler, H., Cherry, J. M., et al. (2000). Gene ontology: Tool for the unification of biology. The gene Ontology consortium. *Nat. Genet.* 25, 25–29. doi:10.1038/75556

Auyeung, K. K., Han, Q. B., and Ko, J. K. (2016). Astragalus membranaceus: A review of its protection against inflammation and gastrointestinal cancers. *Am. J. Chin. Med.* 44, 1–22. doi:10.1142/S0192415X16500014

Auyeung, K. K., Law, P. C., and Ko, J. K. (2012). Novel anti-angiogenic effects of formononetin in human colon cancer cells and tumor xenograft. *Oncol. Rep.* 28, 2188–2194. doi:10.3892/or.2012.2056

Berger, S. I., and Iyengar, R. (2009). Network analyses in systems pharmacology. *Bioinformatics* 25, 2466–2472. doi:10.1093/bioinformatics/btp465

Cappell, M. S. (2008). Pathophysiology, clinical presentation, and management of colon cancer. *Gastroenterol. Clin. North Am.* 37, 1–24. doi:10.1016/j.gtc.2007.12.002

Chen, J., Li, C., Zhu, Y., Sun, L., Sun, H., Liu, Y., et al. (2015a). Integrating GO and KEGG terms to characterize and predict acute myeloid leukemia-related genes. *Hematology* 20, 336–342. doi:10.1179/1607845414Y.0000000209

Chen, J., Zhao, X., Li, X., and Wu, Y. (2015b). Calycosin induces apoptosis by the regulation of ERβ/miR-17 signaling pathway in human colorectal cancer cells. *Food Funct.* 6, 3091–3097. doi:10.1039/c5fo00374a

Cheng, J. Q., Lindsley, C. W., Cheng, G. Z., Yang, H., and Nicosia, S. V. (2005). The Akt/PKB pathway: Molecular target for cancer drug discovery. *Oncogene* 24, 7482–7492. doi:10.1038/sj.onc.1209088

Fagunwa, I. O., Loughrey, M. B., and Coleman, H. G. (2017). Alcohol, smoking and the risk of premalignant and malignant colorectal neoplasms. *Best. Pract. Res. Clin. Gastroenterol.* 31, 561–568. doi:10.1016/j.bpg.2017.09.012

Ferlay, J., Colombet, M., Soerjomataram, I., Mathers, C., Parkin, D. M., Piñeros, M., et al. (2019). Estimating the global cancer incidence and mortality in 2018: GLOBOCAN sources and methods. *Int. J. Cancer.* 144, 1941–1953. doi:10.1002/ijc.31937

Gan, D., Xu, X., Chen, D., Feng, P., and Xu, Z. (2019). Network pharmacology-based pharmacological mechanism of the Chinese medicine rhizoma drynariae against osteoporosis. *Med. Sci. Monit.* 25, 5700–5716. doi:10.12659/MSM.915170

Gong, G., Zheng, Y., Yang, Y., Sui, Y., and Wen, Z. (2021). Pharmaceutical values of calycosin: One type of flavonoid isolated from Astragalus. *Evid. Based Complement. Altern. Med.* 2021, 9952578. doi:10.1155/2021/9952578

Guo, Z., Lou, Y., Kong, M., Luo, Q., Liu, Z., and Wu, J. (2019). A systematic review of phytochemistry, pharmacology and pharmacokinetics on astragali radix: Implications for astragali radix as a personalized medicine. *Int. J. Mol. Sci.* 20, 1463. doi:10.3390/ijms20061463

Haigis, K. M., Kendall, K. R., Wang, Y., Cheung, A., Haigis, M. C., Glickman, J. N., et al. (2008). Differential effects of oncogenic K-Ras and N-Ras on proliferation, differentiation and tumor progression in the colon. *Nat. Genet.* 40, 600–608. doi:10.1038/ng.115

Hao da, C., and Xiao, P. G. (2014). Network pharmacology: A rosetta stone for traditional Chinese medicine. *Drug Dev. Res.* 75, 299–312. doi:10.1002/ddr.21214

Hazan, R. B., Phillips, G. R., Qiao, R. F., Norton, L., and Aaronson, S. A. (2000). Exogenous expression of N-cadherin in breast cancer cells induces cell migration, invasion, and metastasis. *J. Cell Biol.* 148, 779–790. doi:10.1083/jcb.148.4.779

Hopkins, A. L. (2007). Network pharmacology. *Nat. Biotechnol.* 25, 1110–1111. doi:10.1038/nbt1007-1110

Huang, W. C., and Hung, M. C. (2009). Induction of Akt activity by chemotherapy confers acquired resistance. *J. Formos. Med. Assoc.* 108, 180–194. doi:10.1016/S0929-6646(09)60051-6

Kong, M. Y., Li, L. Y., Lou, Y. M., Chi, H. Y., and Wu, J. J. (2020). Chinese herbal medicines for prevention and treatment of colorectal cancer: From molecular mechanisms to potential clinical applications. *J. Integr. Med.* 18, 369–384. doi:10.1016/j.joim.2020.07.005

Lebedev, T. D., Khabusheva, E. R., Mareeva, S. R., Ivanenko, K. A., Morozov, A. V., Spirin, P. V., et al. (2022). Identification of cell type-specific correlations between ERK activity and cell viability upon treatment with ERK1/2 inhibitors. *J. Biol. Chem.* 102226, 102226. doi:10.1016/j.jbc.2022.102226

Li, M., Han, B., Zhao, H., Xu, C., Xu, D., Sieniawska, E., et al. (2022). Biological active ingredients of Astragali Radix and its mechanisms in treating cardiovascular and cerebrovascular diseases. *Phytomedicine* 98, 153918. doi:10.1016/j.phymed.2021.153918

Li, S., and Zhang, B. (2013). Traditional Chinese medicine network pharmacology: Theory, methodology and application. *Chin. J. Nat. Med.* 11, 110–120. doi:10.1016/S1875-5364(13)60037-0

Loh, C. Y., Chai, J. Y., Tang, T. F., Wong, W. F., Sethi, G., Shanmugam, M. K., et al. (2019). The E-cadherin and N-cadherin switch in epithelial-to-mesenchymal transition: Signaling, therapeutic implications, and challenges. *Cells* 8, 1118. *Cells*. doi:10.3390/cells8101118

Lou, Y., Guo, Z., Zhu, Y., Zhang, G., Wang, Y., Qi, X., et al. (2019). Astragali radix and its main bioactive compounds activate the Nrf2-mediated signaling pathway to induce P-glycoprotein and breast cancer resistance protein. *J. Ethnopharmacol.* 228, 82–91. doi:10.1016/j.jep.2018.09.026

Noorolyai, S., Shajari, N., Baghbani, E., Sadreddini, S., and Baradaran, B. (2019). The relation between PI3K/AKT signalling pathway and cancer. *Gene* 698, 120–128. doi:10.1016/j.gene.2019.02.076

Pompura, S. L., and Dominguez-Villar, M. (2018). The PI3K/AKT signaling pathway in regulatory T-cell development, stability, and function. *J. Leukoc. Biol.* 103, 1065–1076. doi:10.1002/JLB.2MIR0817-349R

Porta, C., Paglino, C., and Mosca, A. (2014). Targeting PI3K/Akt/mTOR signaling in cancer. *Front. Oncol.* 4, 64. doi:10.3389/fonc.2014.00064

Roskoski, R., Jr. (2012). ERK1/2 MAP kinases: Structure, function, and regulation. *Pharmacol. Res.* 66, 105–143. doi:10.1016/j.phrs.2012.04.005

Ruan, X., Du, P., Zhao, K., Huang, J., Xia, H., Dai, D., et al. (2020). Mechanism of Dayuanyin in the treatment of coronavirus disease 2019 based on network pharmacology and molecular docking. *Chin. Med.* 15, 62. doi:10.1186/s13020-020-00346-6

Satelli, A., and Li, S. (2011). Vimentin in cancer and its potential as a molecular target for cancer therapy. *Cell. Mol. Life Sci.* 68, 3033–3046. doi:10.1007/s00018-011-0735-1

Shi, J., Zheng, L., Lin, Z., Hou, C., Liu, W., Yan, T., et al. (2015). Study of pharmacokinetic profiles and characteristics of active components and their metabolites in rat plasma following oral administration of the water extract of Astragali radix using UPLC-MS/MS. *J. Ethnopharmacol.* 169, 183–194. doi:10.1016/j.jep.2015.04.019

Tan, X., Xian, W., Li, X., Chen, Y., Geng, J., Wang, Q., et al. (2022). Mechanisms of Quercetin against atrial fibrillation explored by network pharmacology combined with molecular docking and experimental validation. *Sci. Rep.* 12, 9777. doi:10.1038/s41598-022-13911-w

Tan, X., Xu, M., Liu, F., Xu, M., Yao, Y., and Tang, D. (2019). Antimetastasis effect of Astragalus membranaceus-curcuma zedoaria via β-catenin mediated CXCR4 and EMT signaling pathway in HCT116. *Evid. Based Complement. Altern. Med.* 2019, 9692350. doi:10.1155/2019/9692350

Trott, O., and Olson, A. J. (2010). AutoDock Vina: Improving the speed and accuracy of docking with a new scoring function, efficient optimization, and multithreading. *J. Comput. Chem.* 31, 455–461. doi:10.1002/jcc.21334

Tseng, A., Yang, C. H., Chen, C. H., Chen, C. H., Hsu, S. L., Lee, M. H., et al. (2016). An *in vivo* molecular response analysis of colorectal cancer treated with Astragalus membranaceus extract. *Oncol. Rep.* 35, 659–668. doi:10.3892/or.2015.4441

van Roy, F., and Berx, G. (2008). The cell-cell adhesion molecule E-cadherin. *Cell. Mol. Life. Sci.* 65 (23), 3756–3788. doi:10.1007/s00018-008-8281-1

Wang, H., Chi, L., Yu, F., Dai, H., Si, X., Gao, C., et al. (2022). The overview of Mitogen-activated extracellular signal-regulated kinase (MEK)-based dual inhibitor in the treatment of cancers. *Bioorg. Med. Chem.* 70, 116922. doi:10.1016/j.bmc.2022.116922

Wen, Y., Zhang, X., Li, X., Tian, L., Shen, S., Ma, J., et al. (2022). Histone deacetylase (HDAC) 11 inhibits matrix metalloproteinase (MMP) 3 expression to suppress colorectal cancer metastasis. *J. Cancer.* 13, 1923–1932. doi:10.7150/jca.66914

Wu, J., Kong, M., Lou, Y., Li, L., Yang, C., Xu, H., et al. (2020). Simultaneous activation of erk1/2 and Akt signaling is critical for formononetin-induced promotion of endothelial function. *Front. Pharmacol.* 11, 608518. doi:10.3389/fphar.2020.608518

Xu, D., Wang, X., Huang, D., Chen, B., Lin, X., Liu, A., et al. (2022). Disclosing targets and pharmacological mechanisms of total bioflavonoids extracted from Selaginella doederleinii against non-small cell lung cancer by combination of network pharmacology and proteomics. *J. Ethnopharmacol.* 286, 114836. doi:10.1016/j.jep.2021.114836

Yan, Z., Lai, Z., and Lin, J. (2017). Anticancer properties of traditional Chinese medicine. *Comb. Chem. High. Throughput Screen* 20, 423–429. doi:10.2174/1386207320666170116141818

Yang, L., Zhao, L., Zeng, T., Chen, H., Shao, J., Yang, S., et al. (2019). Mechanisms underlying therapeutic effects of traditional Chinese medicine on gastric cancer. *Cancer Manag. Res.* 11, 8407–8418. doi:10.2147/CMAR.S218214

Ye, L., Jia, Y., Ji, K. E., Sanders, A. J., Xue, K., Ji, J., et al. (2015). Traditional Chinese medicine in the prevention and treatment of cancer and cancer metastasis. *Oncol. Lett.* 10, 1240–1250. doi:10.3892/ol.2015.3459

Zhang, J., Song, Y., Liang, Y., Zou, H., Zuo, P., Yan, M., et al. (2019). Cucurbitacin IIa interferes with EGFR-MAPK signaling pathway leads to proliferation inhibition in A549 cells. *Food Chem. Toxicol.* 132, 110654. doi:10.1016/j.fct.2019.110654

Zhao, X., Li, X., Ren, Q., Tian, J., and Chen, J. (2016). Calycosin induces apoptosis in colorectal cancer cells, through modulating the ERβ/MiR-95 and IGF-1R, PI3K/Akt signaling pathways. *Gene* 591, 123–128. doi:10.1016/j.gene.2016.07.012

Zhu, J., Li, C., Yang, H., Guo, X., Huang, T., and Han, W. (2020). Computational study on the effect of inactivating/activating mutations on the inhibition of MEK1 by trametinib. *Int. J. Mol. Sci.* 21, 2167. doi:10.3390/ijms21062167

frontiers | Frontiers in Pharmacology

TYPE Systematic Review
PUBLISHED 23 January 2023
DOI 10.3389/fphar.2023.1074506

OPEN ACCESS

EDITED BY
Mitesh Patel,
Parul University, India

REVIEWED BY
Jun Wang,
Hefei University, China
Mandava Venkata Basaveswara Rao,
Krishna University, India

*CORRESPONDENCE
Yanfeng Liu,
liuyaf8888@sina.com

†These authors contributed equally to this work and share first authorship

SPECIALTY SECTION
This article was submitted to Pharmacology of Anti-Cancer Drugs, a section of the journal Frontiers in Pharmacology

RECEIVED 19 October 2022
ACCEPTED 09 January 2023
PUBLISHED 23 January 2023

CITATION
Deng N, Qiao M, Li Y, Liang F, Li J and Liu Y (2023), Anticancer effects of licochalcones: A review of the mechanisms.
Front. Pharmacol. 14:1074506.
doi: 10.3389/fphar.2023.1074506

Anticancer effects of licochalcones: A review of the mechanisms

Nan Deng[1†], Mingming Qiao[2†], Ying Li[1], Fengyan Liang[1], Jingjing Li[1] and Yanfeng Liu[1*]

[1]Dongzhimen Hospital, Beijing University of Chinese Medicine, Beijing, China, [2]Chongqing Institute for Food and Drug Control, Chongqing, China

Cancer is a disease with a high fatality rate representing a serious threat to human health. Researchers have tried to identify effective anticancer drugs. Licorice is a widely used traditional Chinese medicine with various pharmacological properties, and licorice-derived flavonoids include licochalcones like licochalcone A, licochalcone B, licochalcone C, licochalcone D, licochalcone E, and licochalcone H. By regulating the expression in multiple signaling pathways such as the EGFR/ERK, PI3K/Akt/mTOR, p38/JNK, JAK2/STAT3, MEK/ERK, Wnt/β-catenin, and MKK4/JNK pathways, and their downstream proteins, licochalcones can activate the mitochondrial apoptosis pathway and death receptor pathway, promote autophagy-related protein expression, inhibit the expression of cell cycle proteins and angiogenesis factors, regulate autophagy and apoptosis, and inhibit the proliferation, migration, and invasion of cancer cells. Among the licochalcones, the largest number of studies examined licochalcone A, far more than other licochalcones. Licochalcone A not only has prominent anticancer effects but also can be used to inhibit the efflux of antineoplastic drugs from cancer cells. Moreover, derivatives of licochalcone A exhibit strong antitumor effects. Currently, most results of the anticancer effects of licochalcones are derived from cell experiments. Thus, more clinical studies are needed to confirm the antineoplastic effects of licochalcones.

KEYWORDS

anti-cancer, mechanism, licochalcone, licochalcone A, autophagy, apoptosis, cell cycle

1 Introduction

Cancer seriously affects human health, and in the 21st century, it is expected to become the main cause of death in every country/region (Bray et al., 2018; Keshavarz-Fathi and Rezaei, 2021). Licorice is a widely used traditional Chinese medicine with a variety of pharmacological properties including anti-inflammatory, antioxidant, antidiabetic, anti-asthmatic, and anticancer activities. The pharmacological effects are related to the flavonoids it contains, among which licochalcones have considerable antitumor activity (Hosseinzadeh and Nassiri-Asl, 2015; Pia et al., 2019).

This review systematically reviewed the evidence on the anticancer effects of licochalcones. Licochalcones in licorice comprise licochalcone A (LA), licochalcone B (LB), licochalcone C (LC), licochalcone D (LD), licochalcone E (LE), and licochalcone H (LH) (Figure 1). These licochalcones can activate the mitochondrial apoptosis pathway and the death receptor pathway, promote autophagy-related protein expression, inhibit cell cycle protein expression, and regulate cancer migration-related protein expression *via* multiple signaling pathways, including EGFR/ERK, PI3K/Akt/mTOR, p38/JNK, JAK2/STAT3, MEK/ERK, Wnt/

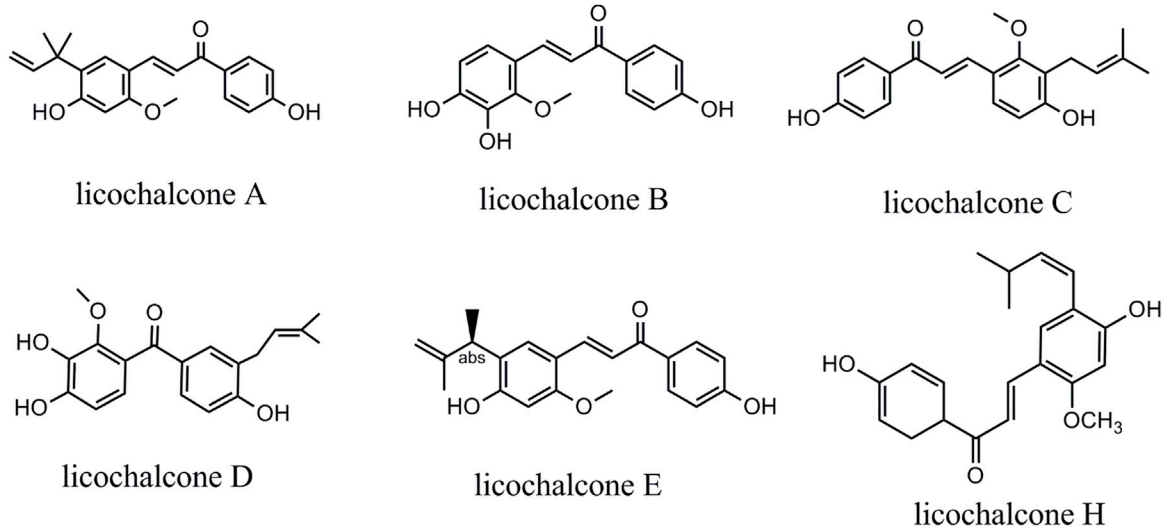

FIGURE 1
Chemical structure of licochalcones.

β-catenin, and MKK4/JNK signaling pathways. Via these mechanisms, licochalcones can induce autophagy and apoptosis in cancer cells, as well as inhibit cancer cell proliferation, migration, and invasion. In tumor tissues, LA can also inhibit angiogenesis and the cellular efflux of anticancer drugs. At present, the antineoplastic effects of LA are most prominent. Various LA derivatives exhibit stronger antitumor effects than LA, and exploring the anticancer mechanisms of these licochalcone derivatives may be a focus of future studies. As most of the licochalcone-induced effects have been examined in cell experiments, more clinical studies are needed to confirm the antitumor effects of licochalcones in the future. Thus, this paper systematically reviewed the literature regarding licochalcone-induced anticancer effects with a focus on LA to provide an overview of the current knowledge and guide further basic and clinical research.

2 Anticancer effects of licochalcones on tumor cells

2.1 Lung cancer

Epidemiological studies have shown that approximately 18 million people are diagnosed with lung cancer each year, and 16 million of them die from this disease (Chen et al., 2014; Hirsch et al., 2017). Licochalcones can induce apoptosis and autophagy, and they inhibit the proliferation, migration, and invasion of lung cancer cells (Keshavarz-Fathi and Rezaei, 2021).

2.1.1 Induction of autophagy

LC3-II is considered to be a characteristic protein of the autophagy process. LA (10–15 μM) can induce autophagy in A549 and H1299 lung cancer cells by increasing the LC3-II/LC3-I ratio, as well as the levels of the autophagy-related proteins ATG5, ATG7, and P62. LA-induced increases in CHOP expression also promote autophagy (Tang et al., 2016; Lin et al., 2019a). Furthermore, LA-induced autophagy in lung cancer cells is associated with the induction of endoplasmic reticulum stress. LA (10 μM) enhances the expression of miR-144-3p, causes unfolded protein response, and triggers autophagy by promoting the accumulation and expression of ATG1, ATG3, ATG6, and ATG16 *via* activation of the PERK/ATF4/CHOP signaling pathway (Chen et al., 2018).

2.1.2 Induction of apoptosis

Activation of the mitochondrial apoptosis pathway is closely related to mitochondrial dysfunction. LA (2.5–25 μM) inhibited ATP production and caused mitochondrial dysfunction in H1299 and H322 lung cancer cells by inhibiting hypoxia-induced HIF-1α accumulation and the expression of target genes *GLUT1* and *PDK1*, which induced activation of the mitochondrial apoptosis pathway and apoptosis of cancer cells (Park et al., 2021). LA (10–15 μM) can activate the mitochondrial apoptosis pathway and induce apoptosis in H460 and A549 lung cancer cells by decreasing the levels of Bcl-xL and Bcl-2 while increasing the levels of Bad, Bax, cleaved PARP, and caspase-3 (Tang et al., 2016; Qiu et al., 2017; Lin et al., 2019a). In addition, the survivin protein inhibits caspase-3 activity and prevents cancer cell apoptosis. LA (5–50 μM) downregulated the expression of survivin by inhibiting the EGFR signaling pathway and its downstream kinases ERK1/2 and AKT in H3255, HCC827, H1975, and A549 lung cancer cells (Gao et al., 2021). LB (5–15 μM) inhibited the EGFR and MET signaling pathways and induced mitochondrial dysfunction and endoplasmic reticulum stress in HCC827 lung cancer cells, which induced the loss of MMP, release of cytochrome c, and increased expression of caspases (Oh et al., 2019a).

2.1.3 Cell cycle block

By inhibiting the expression of MDM2, cyclin B1, CDC2, and CDC25C, LA (10–15 μM) led to cell cycle arrest of H460 and A549 lung cancer cells at the G2/M phase (Qiu et al., 2017; Lin et al., 2019a). Heng et al. found that decreases in the proliferation of lung cancer cells by LA were related to the inhibition of the

Wnt/β-catenin signaling pathway (Heng and Cheah, 2021). LB (5–15 μM) caused cell cycle arrest of HCC827 lung cancer cells at the G2/M phase by decreasing the expression of cyclinB1 and CDC2 proteins while increasing p27 expression (Oh et al., 2019a).

2.1.4 Inhibition of migration and invasion

LA (2–20 μM) inhibited the AKT signaling pathway and the expression of the downstream transcription factor Sp1, which reduced the levels of MMP-1 and MMP-3 and inhibited the migration and invasion of A549 and H460 lung cancer cells (Huang et al., 2014).

2.1.5 Activation of the immune system

PD-L1 is a key immune checkpoint, and reducing the production of PD-L1 can play a role in immunotherapy. LA (10–50 μM) inhibited the expression of PD-L1 and thereby induced the production of reactive oxygen species (ROS) in A549 lung cancer cells, which inhibited the phosphorylation of 4EBP1, activated the PERK/eIF2α pathway, and ultimately induced apoptosis in cancer cells (Yuan et al., 2021).

2.2 Liver cancer

Licochalcones can induce apoptosis and inhibit the proliferation, migration, and invasion of hepatocellular carcinoma cells (Keshavarz-Fathi and Rezaei, 2021).

2.2.1 Induction of apoptosis

By inhibiting the PI3K/Akt/mTOR signaling pathway, LA (5–20 μM) activated the mitochondrial apoptosis pathway and promoted the expression of Bax, Bad, and caspase-3, thereby inducing apoptosis in HepG2 cells (Wu et al., 2019). In addition, LA (1–50 μM) induced endoplasmic reticulum stress in HepG2 cells by inducing phosphorylation of VEGFR2, c-Met receptor, and PLCγ1 and enhancing the cytosolic Ca^{2+} release from the endoplasmic reticulum, which subsequently induced ROS accumulation, the expression of CHOP, as well as caspase-4, -9, and -3, and ultimately cell apoptosis (Choi et al., 2014). Wang et al. found that the production and accumulation of intracellular ROS also activate the mitochondrial apoptosis pathway and increased the expression of Bad, Bax, Bak, PUMA, and caspase-3. The production of intracellular ROS in HepG2 cells is involved in the LA-induced (5–50 μM) downregulation of PDK1 and rubicon by activating the ULK1/Atg13 signaling pathway and increasing the expression of TSC1/2, PRAS40, CTMP, and PP2A. Moreover, LA activates the death receptor pathway and caspase cascade by increasing the expression of DR3, DR5, and Fas. LA also decreases the expression of the survival factor PKCε, p70S6K, and Akt. Through these effects, LA (30–70 μM) finally induces apoptosis in HepG2 cells (Niu et al., 2018; Wang et al., 2018). LA (70 μM) can induce apoptosis of HepG2 cells by regulating the MAPK and FoxO signaling pathways (Wang et al., 2021). Likewise, LB (10–120 μM) induces apoptosis in HepG2 cells by activating the extrinsic apoptotic pathway (i.e., increasing the expression of TNFR1, Fas, Fas-L, caspase-8, JUN, and Fos) and mitochondrial apoptosis pathway (i.e., increasing the expression of Bak, caspase-9, and caspase-3) (Wang et al., 2019). LB (120 μM) can promote the apoptosis of HepG2 cells by regulating microRNAs (miRNAs) including miR-29b-3p and miR-96-5p (Wang and Wang, 2021). By inhibiting the expression of EGFR and MET, promoting the accumulation of intracellular ROS, activating the mitochondrial apoptosis pathway, increasing the expression of Bid, Bad, and cleaved PARP, and reducing the expression of Bcl-xL and Mcl-1, LD (5–20 μM) induced apoptosis in HCC827 cells (Oh et al., 2020).

2.2.2 Cell cycle block

LA (30–70 μM) blocked the cell cycle of HepG2 cells at the G2/M transition by increasing the expression of Weel, P21, and JNK1 while decreasing the expression of survivin, cyclin B1, cyclin D1, and CDK1. Further research showed the observed effects were related to the inhibition of the p38/JNK/ERK signaling pathway (Chen et al., 2017; Wang et al., 2018). By decreasing the expression of CDK1, cyclin B1, CHK2, CDC14B, and CDC7 and increasing the expression of p21, LB (10–120 μM) caused the cell cycle arrest of HepG2 cells at the G2/M phase (Wang et al., 2019). LB (10–20 μM) blocked the cell cycle of HepG2 and Huh7 cells at the G2/M phase *via* increased p27 expression and decreased cyclin B1 and Cdc2 levels (Zhang et al., 2022). By decreasing the expression levels of cyclin B1 and CDC2 and increasing those of p21 and p27, LD (5–20 μM) induced a cell cycle arrest of HCC827 cells at the G2/M phase (Oh et al., 2020).

2.2.3 Inhibition of migration and invasion

By downregulating the expression of uPA and MMP9 through inhibition of the MKK4/JNK and NF-κB signaling pathways, LA (5–20 μM) inhibited the migration and invasion of HA22T/VGH and SK-Hep-1 cells (Tsai et al., 2014; Wu et al., 2018a).

2.3 Breast cancer

Research has shown that licochalcones can induce apoptosis and autophagy and inhibit the proliferation, migration, invasion, and angiogenesis of breast cancer cells (Keshavarz-Fathi and Rezaei, 2021).

2.3.1 Induction of autophagy

LA (5–50 μM) can inhibit the PI3K/Akt/mTOR signaling pathway, which increases the expression of LC3-II protein and ultimately induces autophagy in MCF-7 cells (Xue et al., 2018).

2.3.2 Induction of apoptosis

By inhibiting the PI3K/Akt/mTOR signaling pathway, LA (5–50 μM) activated the mitochondrial apoptosis pathway, reduced the expression of Bcl-2, and promoted the expression of Bax and caspase-3, thereby inducing the apoptosis in MCF-7 cells (Huang et al., 2019). By decreasing the mitochondrial membrane potential and inducing ROS production, LA (5–50 μM) upregulated the expression of Bid, Bad and cleaved PARP, downregulated the expression of Bcl-2 and Bcl-xL, and induced the apoptosis in MCF-7 and MDA-MB-231 cells. The authors suggested that these effects were related to the inhibition of Sp1 (Kang et al., 2017a). Via increases in the level of acylcarnitine and inhibition of prostaglandin reductase 1 expression, LA (1–100 μM) caused respiratory dysfunction in HCC38 TNBC cells and thus induced cancer cells apoptosis (Roberts et al., 2017). LB (10–50 μM) induced apoptosis in MCF-7 cells by increasing the expression of Bid, Bad, cleaved PARP, and caspase-3 while decreasing the expression of Bcl-2 (Yu et al., 2016).

2.3.3 Cell cycle block

By downregulating the expression of Sp1, LA inhibited the proliferation of MCF-7 and MDA-MB-231 cells *via* increases in the expression of the proteins p21 and p27 and decreases in the expression of Mcl-1 and survivin (Kang et al., 2017a). LA (5–15 μg/mL) also blocked the cell cycle of MCF-7 cells at the G1 phase *via* reduced cyclin D1 expression (Bortolotto et al., 2017). By reducing the expression of cyclin D1 and increasing the expression of p21, LA (5–50 μM) led to cell cycle arrest of MCF-7 cells at the G0/G1 phase (Huang et al., 2019). The overexpression of PRMT6 in human breast cancer is related to tumorigenesis (Cheng and Bedford, 2011), and LA (10–100 μM) caused the cell cycle arrest of MCF-7 cells at the G2/M phase by inhibiting PRMT6 expression and subsequently p53 expression (Gong et al., 2020). By downregulating the expression levels of cyclin A, CDK2, and CDC25A and increasing the level of p21, LB (10–50 μM) induced the cell cycle arrest of MCF-7 cells at the S phase (Yu et al., 2016). By decreasing the expression of CDK4, CDK2, cyclin A, and cyclin D1, LE (7–14 mg/kg) inhibited the proliferation of MDA-MB 231 cells in mice (Kwon et al., 2013).

2.3.4 Inhibition of migration and invasion

LA (5–40 μM) inhibited the migration and invasion of MDA-MB-231 cells by suppressing the expression of E-cadherin and vimentin *via* inhibition of the p38 MAPK and AKT signaling pathways (Huang et al., 2019). By decreasing the expression of uPA and MMP-9, LE (7–14 mg/kg) inhibited the migration and invasion of MDA-MB 231 cells in mice (Kwon et al., 2013).

2.3.5 Inhibition of angiogenesis

Via downregulation of VEGF-A, LE (7–14 mg/kg) inhibited angiogenesis in cancer tissue in a xenograft mouse model using MDA-MB 231 breast cancer cells (Kwon et al., 2013).

2.4 Oral carcinoma

Head and neck cancer is the seventh most common cancer in the world, and almost half of the tumors are oral carcinomas. Oral squamous cell carcinoma is the most common form of oral cancer, with a poor prognosis and high mortality (Vitorio et al., 2020). Licochalcones can induce apoptosis and inhibit the proliferation, migration, and invasion of oral carcinoma cells (Keshavarz-Fathi and Rezaei, 2021).

2.4.1 Induction of apoptosis

By activating the mitochondrial apoptosis pathway and increasing the expression of Bax, Bid, cleaved PARP, and caspase-3, LA (10–40 μM) induced apoptosis in HN22 and HSC4 cells (Cho et al., 2014). Similarly, by activating the mitochondrial apoptosis pathway and the caspase cascade, LA (5–100 μg/mL) induced apoptosis in SCC-25 cells (Zeng et al., 2014). In addition to its effects on the mitochondrial apoptosis pathway, LA (IC_{50} = 50 μM) activated the FasL-mediated death receptor pathway and upregulated the caspase-8 and -3 levels in KB cells (Kim et al., 2014). In pharyngeal squamous carcinoma FaDu cells, LA (10–100 μM) activated the death receptor pathway by increasing the expression of TRAIL *via* stimulation of the ERK1/2 and p38 MAPK signaling pathways. Moreover, the activation of the ERK1/2 and p38 MAPK signaling pathways upregulated the p53 expression, thereby increasing the levels of Bad, Bax, caspase-3, -8, and -9, as well as the release of cytochrome c (Yang et al., 2014; Park et al., 2015). LB (10–30 μM) can also activate the death receptor pathway (i.e., increased expression of DR 4 and DR5) and induce endoplasmic reticulum stress (i.e., increased CHOP expression) in HN22 and HSC4 cells, which causes mitochondrial membrane depolarization, upregulates the expression of Bax, cleaved PARP, and caspase-3, and downregulates the expression of survivin, Bcl-xL, and Mcl-1 (Oh et al., 2016). By inhibiting the JAK2/STAT3 signaling pathway leading to activation of the death receptor pathway (i.e., increased expression of DR4 and DR5), endoplasmic reticulum stress (i.e., elevated ROS and CHOP levels), and mitochondrial apoptosis pathway (i.e., upregulated expression of p21, Bax, Bid, Apaf-1, and cleaved PARP; downregulated expression of Bcl-2, Mcl-1, and survivin), LC (10–50 μM) and LD (10–30 μM) induced apoptosis in HN22 and HSC4 cells (Oh et al., 2018; Seo et al., 2019). LD (12.5–50 μg/mL) induced apoptosis in pharyngeal squamous carcinoma FaDu cells by increasing Fas-L, p53, Bax, Bid, and caspase-3 expression while decreasing the expression of Bcl-2 by activating the death receptor and mitochondrial apoptosis pathways (Yu et al., 2017). LH (10–30 μM) induced apoptosis in HSC2 and HSC3 cells by downregulating the expression of Bcl-2 and Bcl-xL and upregulating the expression of Bax and Bad *via* inhibition of Matr3 expression (Nho et al., 2019). LH (5–20 μM) can also induce apoptosis in HN22 and HSC4 cells by activating the death receptor pathway, endoplasmic reticulum stress, and mitochondrial apoptosis pathway *via* inhibition of the JAK/STAT3 signaling pathway (Oh et al., 2019b).

2.4.2 Cell cycle block

LA (5–100 μg/mL) led to cell cycle arrest of SCC-25 cells at the S and G2/M phases (Zeng et al., 2014). Further research showed that LA (10–40 μM) inhibited the proliferation of HN22 and HSC4 cells by inhibiting Sp1 expression and regulating its downstream proteins including p27, p21, and cyclin D1 (Cho et al., 2014). Both LB and LD (10–30 μM) can induce G1 phase arrest in HN22 and HSC4 cells by increasing the p21 and p27 levels and decreasing the level of cyclin D1 (Oh et al., 2016; Seo et al., 2019). Likewise, LH (5–20 μM) induced G1 phase arrest in HN22 and HSC4 cells by increasing the p21 and p27 levels and decreasing the level of cyclin D1 *via* inhibition of the JAK/STAT3 signaling pathway (Oh et al., 2019b).

2.4.3 Inhibition of migration and invasion

LA (25–100 μM) inhibited the migration and invasion of SCC4 and CAL-27 cells by downregulating the IGF-1, MMP-2, and MMP-9 levels *via* inhibition of the PI3K/AKT signaling pathway (Hao et al., 2019). LA (25–100 μg/mL) can also inhibit the migration and invasion of SCC-25 cells by decreasing MMP-2 expression while increasing the levels of TIMP and E-cadherin (Shen et al., 2014).

2.5 Esophageal cancer

Esophageal cancer belongs to the head and neck cancers and is the sixth leading cause of cancer-related death. Its incidence rate increases every year (Zhang et al., 2021). Licochalcones can induce apoptosis and inhibit proliferation in esophageal cancer cells (Keshavarz-Fathi and Rezaei, 2021).

2.5.1 Induction of apoptosis

LB (5–20 μM) induced apoptosis in KYSE-450 and KYSE-510 cells by inhibiting the JAK2/STAT3 signaling pathway and decreasing the expression of Mcl-1 (Song et al., 2020). Via inhibition of the JNK/p38 MAPK signaling pathway, LC (10–50 μM) induced endoplasmic reticulum stress (i.e., increased GRP78 and CHOP expression) and activated the mitochondrial apoptosis pathway in various esophageal squamous carcinoma cells, including KYSE-30, KYSE-70, KYSE-410, KYSE-450, and KYSE-510 cells (Kwak et al., 2020a). LH (5–20 μM) induced the apoptosis in KYSE-30 and KYSE-450 cells by activating the death receptor pathway, mitochondrial apoptosis pathway, and endoplasmic reticulum stress *via* increased DR4, DR5, CHOP, p21, Bax, Bid, Apaf-1, and cleaved PARP expression, stimulated ROS production, and decreased expression of Bcl-2, Mcl-1, and survivin (Kwak et al., 2020b).

2.5.2 Cell cycle block

LB (5–20 μM) induced G2/M phase cell cycle arrest in KYSE-450 and KYSE-510 cells (Song et al., 2020). LH (5–20 μM) blocked the cell cycle of KYSE-30 and KYSE-450 cells at the G2/M phase by downregulating CDC2 and cyclin B1 expression and upregulating p21 and p27 (Kwak et al., 2020b).

2.6 Gastric cancer

Stomach cancer is the fifth most commonly diagnosed cancer and the third leading cause of cancer death (Bray et al., 2018). Research has shown that licochalcones can induce apoptosis and inhibit proliferation in gastric cancer cells (Keshavarz-Fathi and Rezaei, 2021).

2.6.1 Induction of apoptosis

By activating the ERK, JNK, and p38 MAPK signaling pathways and inhibiting the PI3K/AKT signaling pathway, LA (20–100 μM) promoted the intracellular ROS generation and stimulated both the mitochondrial apoptosis pathway and caspase cascade in BGC-823 cells (Hao et al., 2015). Via activation of the mitochondrial apoptosis pathway, induction of Bax, Bad, cleaved PARP, caspase-3, -8, and -9 expression, and decrease in Bcl-2 expression, LA induced the apoptosis in five gastric cell lines including GES-1, MKN-28, SGC7901, AGS, and MKN-45 cells. The respective IC_{50} values of LA were 92.7, 42.0, 40.8, 41.1, and 40.7 μM (Xiao et al., 2011; Lin et al., 2017). Moreover, the inhibitory effect of LA (10–50 μM) on the AKT signaling pathway can downregulate the expression of hexokinase 2A and inhibit glycolysis, thereby inducing apoptosis of MKN45 and SGC7901 cells (Wu et al., 2018b).

2.6.2 Cell cycle block

By increasing retinoblastoma expression and decreasing cyclin A, cyclin B, and MDM2 expression, LA (5–50 μM) caused the cell cycle arrest of MKN-28, AGS, and MKN-45 cells at the G2/M transition (Xiao et al., 2011; Lin et al., 2017).

2.7 Colon cancer

Globally, colon cancer is the second most common cancer in women and the third most common cancer in men with slightly increased case numbers in men (O'Keefe, 2016). Licochalcones can induce apoptosis and inhibit proliferation in colon cancer cells (Keshavarz-Fathi and Rezaei, 2021).

2.7.1 Induction of apoptosis

LA (10–40 μM) can enhance the production of intracellular ROS by inhibiting the expression of thioredoxin reductase-1, which activates the mitochondrial apoptosis pathway and induces apoptosis in HCT-116 cells (Wu et al., 2020).

2.7.2 Cell cycle block

LA(IC_{50} = 7 and 8.8 μM, respectively) can prevent the hypoxia-induced proliferation of SW480 and SW620 cells by inhibiting the TrkB/AKT signaling pathway (Arita et al., 2020). LA (5–25 μmol/L) blocked the cell cycle of HCT116 cells at the G1 phase by increasing the level of p21 *via* inhibition of the JNK1 signaling pathway (Yao et al., 2014).

2.8 Bladder cancer

Bladder cancer is the 10th most common form of cancer worldwide (Bray et al., 2018). Research has shown that licochalcones can induce apoptosis of bladder cancer cells, inhibit their proliferation, and activate the immune system (Keshavarz-Fathi and Rezaei, 2021).

2.8.1 Induction of apoptosis

By increasing intracellular Ca^{2+} and ROS levels, decreasing mitochondrial membrane potential, upregulating Apaf-1, caspase-9, caspase-3, and cleaved PARP levels, and elevating the Bax/Bcl-2 ratio, LA (10–80 μM) induced T24 cells apoptosis (Yang et al., 2016; Hong et al., 2019). LB (40–80 μM) induced apoptosis in T24 and EJ cells *via* decreases in Bcl-2 and survivin expression and enhanced expression of Bax, cleaved PARP, and caspase-3 (Yuan et al., 2014). LC (10–50 μM) induced apoptosis in T24 cells by decreasing Bcl-2, Bcl-w, and Bcl-xL expression levels while increasing Bax and Bim expression levels (Wang et al., 2015).

2.8.2 Cell cycle block

By downregulating cyclin A, cyclin B1, and Wee1 expression and upregulating the expression of the cyclin-dependent kinase inhibitor p21WAF1/CIP1, LA (10–60 μM) blocked the cell cycle of T24 cells at the G2/M phase (Jiang et al., 2014; Hong et al., 2019). Via decreases in CDK1, CDK2, CDC25A, and CDC25B expression, LB (40–80 μM) led to cell cycle arrest of T24 and EJ cells at the S phase (Yuan et al., 2014).

2.8.3 Activation of the immune system

In C3H/HeN mice carrying UM-UC-3 cells, LA (40 mg/kg) enhanced the activity of cytotoxic T lymphocytes and increased the number of $CD4^+$ $CD25^+$ Foxp3+ regulatory T cells. This suggests that LA can be used to treat bladder cancer by modulating the immune response (Zhang et al., 2016).

2.9 Cervical and ovarian cancer

In women, the incidence and mortality rates of cervical and ovarian cancers are lower than those of breast, colorectal, and lung

cancers (Bray et al., 2018). Licochalcones can induce autophagy and apoptosis and inhibit the proliferation of cervical and ovarian cancer cells (Keshavarz-Fathi and Rezaei, 2021).

2.9.1 Induction of autophagy

LA (10–50 μM) induced autophagy in SiHa and HeLa cervical cells by increasing the levels of LC3-II, Beclin1, ATG5, ATG7, and ATG12 through inhibition of the PI3K/Akt/mTOR signaling pathway (Tsai et al., 2015).

2.9.2 Induction of apoptosis

By inhibiting the PI3K/Akt/mTOR signaling pathway, LA (10–50 μM) also induced apoptosis in SiHa, HeLa, CaSki, and C33A cervical cells *via* upregulation of caspase-3, caspase-9, and cleaved PARP levels and downregulation of Bcl-2 levels (Tsai et al., 2015). In addition, LA (25–50 μM) induces apoptosis in HeLa cells by increasing the expression of TRAIL-R2 (Szliszka et al., 2012). Via induction of ROS production, loss of mitochondrial transmembrane potential, cytochrome c release, increases in Bid and Bax levels, decreases in survivin, Bcl-2, and p53 levels, and activation of the caspase cascade, LA (5–25 μM) induced also the apoptosis in OVCAR-3 and SK-OV-3 ovarian cancer cells (Lee et al., 2012; Kim et al., 2013).

2.9.2 Cell cycle block

LA (IC_{50} = 10.7 μM) prevented the hypoxia-induced proliferation of HeLa S3 cells by inhibiting the TrkB/AKT signaling pathway (Arita et al., 2020).

2.10 Glioma

Glioma is one of the most common primary malignancies of the adult central nervous system (Chen et al., 2021). Licochalcones can induce apoptosis and inhibit the proliferation, migration, and invasion of gliomas (Keshavarz-Fathi and Rezaei, 2021).

2.10.1 Induction of apoptosis

By reducing the mitochondrial membrane potential and the production of ATP, LA (2–12.5 μM) induced mitochondrial fragmentation and caspase-3, -8, and -9 expression in glioma stem cells including GS-Y01, GS-Y03, U87GS, GS-NCC01, and A172GS cells (Kuramoto et al., 2017).

2.10.2 Cell cycle block

By reducing the cyclin A, cyclin B1, cyclin E1, CDK1, CDK2, and CDK4 expression levels, LA (5–40 μM) induced the cell cycle arrest of glioma U87 cells at the G2/M phase (Lu et al., 2018).

2.10.3 Inhibition of migration and invasion

By downregulating ADAM9 expression through inhibited activation of the MEK/ERK signaling pathway, LA (10–50 μM) prevented the migration and invasion of human gliomas including M059K, U-251 MG, and GBM8901 cells (Huang et al., 2018).

2.11 Sarcomas

Sarcomas are a rare, heterogeneous group of malignant tumors of the bone or soft tissue (Walczak and Irwin, 2013). Research has shown that licochalcones can induce autophagy and apoptosis and inhibit the proliferation, migration, and invasion of sarcomas (Keshavarz-Fathi and Rezaei, 2021).

2.11.1 Induction of autophagy

LA (5–20 μmol/L) induced autophagy in A375 and B16 cells by increasing the expression of LC3-II, Beclin1, ATG5, and p62 *via* activation of the miR-142-3p/Rheb/mTOR signaling pathway (Zhang et al., 2020). By upregulating the LC3A/B-II level, LA (10–40 μM) induced autophagy in osteosarcoma HOS cells (Shen et al., 2019). By suppressing the PI3K/AKT/mTOR pathway, LB (5–20 μM) increased the expression of ARPs (ATG7, Beclin1) and promoted the p62 and LC3B decomposition turnover in MG-63 and U2OS cells, thereby inducing autophagy (Huang and Jin, 2022).

2.11.2 Induction of apoptosis

By activating the miR-142-3p/Rheb/mTOR signaling pathway, LA (5–20 μmol/L) activated the caspase cascade and induced apoptosis in A375 and B16 cells (Chen et al., 2019; Zhang et al., 2020). In addition, by activating the extrinsic (i.e., upregulation of CHOP, DR4, and DR5 expression) and intrinsic (i.e., inhibition of Sp1 expression) apoptosis pathways, LA (5–20 μM) induced mitochondrial dysfunction, endoplasmic reticulum stress, and ultimately apoptosis in A375 melanoma cells (Kang et al., 2017b). Via increases in caspase-8, caspase-3, and cleaved PARP expression levels and decreases in Bcl-2, XIAP, and survivin expression levels, LA (10–40 μM) induced apoptosis in HOS cells (Shen et al., 2019). By activating the p38 MAPK signaling pathway, increasing the expression of Bax, cleaved PARP, caspase-3, -8, and -9, and decreasing the expression of Bcl-2, LA (20–100 μM) induced apoptosis in osteosarcoma 143B cells (Lin et al., 2019b). Via activation of the death receptor pathway (i.e., increased DR4 and DR5 expression), endoplasmic reticulum stress (i.e., increased CHOP expression), and mitochondrial apoptosis pathway (i.e., increased Bax and cleaved PARP expression and decreased Bcl-xL, Mcl-1, survivin, and Bcl-2 expression), LA (10–40 μM) induced apoptosis in malignant pleural mesothelioma MSTO-211H and H28 cells (Kim et al., 2015). Moreover, LD (20–80 μmol/L) induced the apoptosis in A375 cells by causing a loss in mitochondrial membrane potential, increasing ROS production and Bax, caspase-9, and caspase-3 expression, and downregulating the expression of Bcl-2 (Si et al., 2018).

2.11.3 Cell cycle block

LA (10–40 μM) induced the cell cycle arrest of HOS cells at the G2/M transition by decreasing the levels of CDC2 and CDC25C *via* activation of the ATM/Chk2 checkpoint pathway (Shen et al., 2019). Moreover, LA (10–40 μM) blocked the cell cycle of MSTO-211H and H28 cells at the G1 phase by inhibiting cyclin D1 expression (Kim et al., 2015). LA (5–20 μM) also led to cell cycle arrest of HT-1080 cells at the G2 phase by decreasing the levels of CDK1 and CDK2 *via* inhibition of R132C-mutant isocitrate dehydrogenase 1 (Hu et al., 2020). Furthermore, LA (IC_{50} = 10.7 μM) inhibited hypoxia-induced proliferation of the neuroblastoma cell lines SK-N-SH, TGW, and GOTO by inhibiting the TrkB/AKT signaling pathway (Arita et al., 2020).

2.11.4 Inhibition of migration and invasion

By decreasing the expression of MMP-2 and MMP-9, LD (20–80 μmol/L) inhibited the migration and invasion of A375 cells (Si et al., 2018).

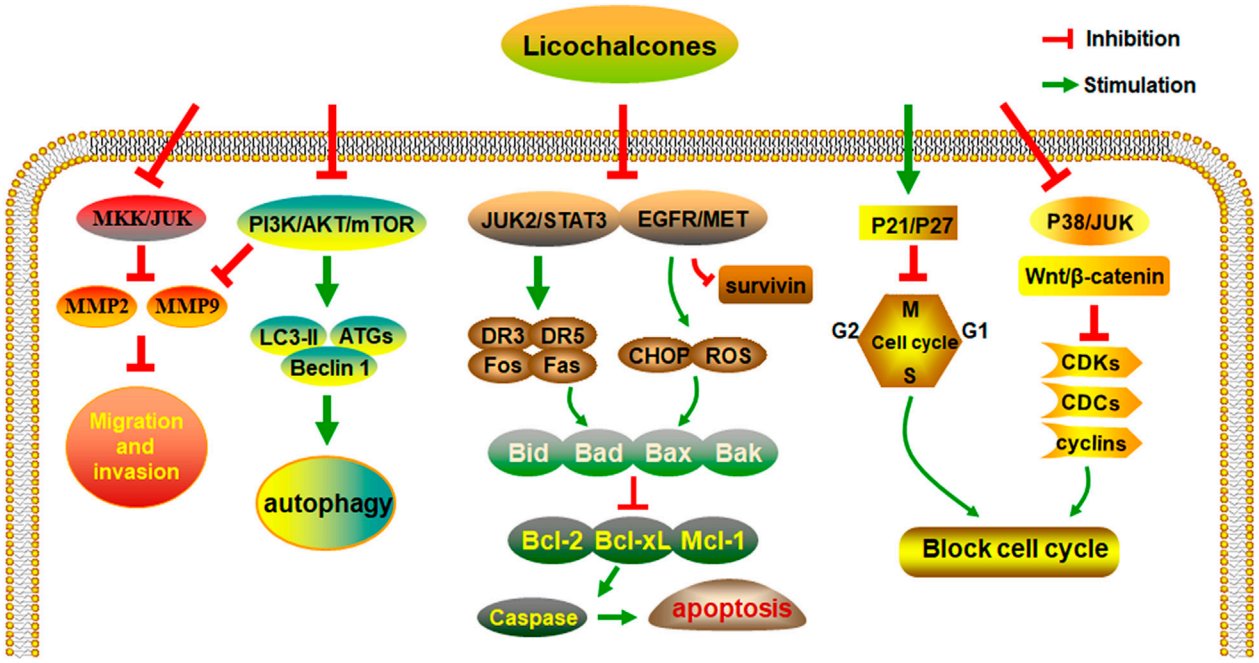

FIGURE 2
The anti-cancer activities and molecular mechanisms of licochalcones.

3 Inhibition of the efflux of anticancer drugs

BCRP is an ATP-binding cassette transporter that has an important influence on the metabolism of anticancer drugs. Inhibition of BCRP expression can promote increased intestinal (re)uptake of antineoplastic drugs and decrease their hepatic metabolization, thereby enhancing their bioavailability. In addition to BCRP functions in normal tissues, the overexpression of this transporter in tumors causes multidrug resistance to anticancer drugs such as mitoxantrone, flavonol, and methotrexate (Steinbach et al., 2002; Volk et al., 2002; Tamaki et al., 2010). By reducing the expression of BCRP, LA (10–100 μM) reduced the BCRP-mediated efflux of doxorubicin and temozolomide in BCRP-MDCKII cells. Molecular docking analyses showed that Pi-Pi stacked interactions and potential Pi-Alkyl interactions play important roles (Fan et al., 2019). P-glycoprotein is also an important efflux protein, which mediates the drug resistance of a variety of cancer cells. LA (50–100 μM) reversed the resi stance of KB/MDR1 cells to vinblastine by inhibiting the activity of P-glycoprotein (Nabekura et al., 2015). By inhibiting c-Met overexpression, LA (Chen et al., 2014; Choi et al., 2014; Huang et al., 2014; Tang et al., 2016; Hirsch et al., 2017; Qiu et al., 2017; Chen et al., 2018; Niu et al., 2018; Wang et al., 2018; Lin et al., 2019a; Oh et al., 2019a; Wu et al., 2019; Gao et al., 2021; Heng and Cheah, 2021; Park et al., 2021; Yuan et al., 2021) decreased the activity of HCC827 and PC-9 cells and decreased gefitinib resistance in non-small cell lung cancer cells (Han et al., 2022). For H1975 gefitinib-resistant non-small cell lung cancer cells, LA (10–100 μM) reduced their drug resistance by decreasing Hsp90 activity through binding to the N-terminal ATP binding site of Hsp90 (Seo, 2013).

4 Review and speculation of the structure-activity relationship

Chalcones are widely recognized as privileged structures, families of molecules featuring scaffolds that upon appropriate decoration can lead to a large spectrum of diverse biological effects. Rossi et al. inserted substituents with different electronic and steric properties into ring B, and altered their positions on the aromatic core, resulting a new range of derivatives. These derivatives induced a remarkable block in G2/M phases, earlier and higher than LA (Rossi et al., 2022). Additionally, approximating to paclitaxel, a series of derivatives of LA (benzimidazole-2-substituted phenyl or pyridine-propylenone) showed significantly better anti-proliferative activity against HCT116, MCF-7 and HepG2 cells than 5-fluorouracil (Wu et al., 2016). Studies have shown that various synthetic LA derivatives are more cytotoxic to cancer cells than naturally occurring licochalcones. Bromo-retrochalcone and trifluoromethyl-retrochalcone can be used as antineoplastic drugs for pleural mesothelioma and oral squamous cell carcinoma with stronger anticancer activity than LA (Yoon et al., 2018). A derivative of LA (LA-linked thiazole-imidazopyridine) has greater antitumor activity than etoposide in MCF-7 and MDA MB-231 breast cancer cells, A549 lung cancer cells, and DU-145 prostate cancer cells (Suma et al., 2020). This indicates that structural modifications of licochalcones to increase their anticancer efficacy are promising.

5 Conclusion

Studies have shown that licochalcones have a wide range of anticancer activities, such as in gastric, lung, colon, breast, liver, and bladder cancer. Among all licochalcones, LA has the most

substantial antitumor effect. Although LA does not have such effects on all types of cancers, it still shows great potential for anticancer treatment. After analyzing and collating the literature, we conclude that the regulation of multiple signaling pathways by licochalcones including the EGFR/ERK, PI3K/Akt/mTOR, p38/JNK, JAK2/STAT3, MEK/ERK, Wnt/β-catenin, and MKK4/JNK signaling pathways is the key to their antineoplastic effects (Figure 2).

Among the examined licochalcones, LA not only has antineoplastic effects but also can be used to reduce drug efflux from cancer cells and reduce adverse reactions caused by other antitumor drugs (Herbrechter et al., 2015). Therefore, we believe that the use of LA as an adjunct to anticancer drugs holds great promise. Although licochalcones have demonstrated their value as antitumor drugs, most of these studies are in the cell experiment stage. More clinical studies are needed to confirm the antineoplastic effects of licochalcones. Moreover, except for LA, studies of other licochalcones regarding their anticancer potential are insufficient, making it necessary to further explore the antitumor mechanisms of other licochalcones.

Data availability statement

The original contributions presented in the study are included in the article/Supplementary Material, further inquiries can be directed to the corresponding author.

Author contributions

ND and MQ contributed equally to this article, participated in the study designed and drafted the manuscript. YL, FL, and JL contributed in manuscript modification. YL oversaw the study. All authors read and approved the final manuscript.

Funding

This work was supported by National Natural Science Foundation of China (No. 8227151783).

Conflict of interest

The authors declare that the research was conducted in the absence of any commercial or financial relationships that could be construed as a potential conflict of interest.

Publisher's note

Supplementary material

The Supplementary Material for this article can be found online at: https://www.frontiersin.org/articles/10.3389/fphar.2023.1074506/full#supplementary-material

References

Arita, M., Koike, J., Yoshikawa, N., Kondo, M., and Hemmi, H. (2020). Licochalcone A inhibits bdnf and TrkB gene expression and hypoxic growth of human tumor cell lines. *Int. J. Mol. Sci.* 21 (2), 506. doi:10.3390/ijms21020506

Bortolotto, L. F., Barbosa, F. R., Silva, G., Bitencourt, T. A., Beleboni, R. O., Baek, S. J., et al. (2017). Cytotoxicity of trans-chalcone and licochalcone A against breast cancer cells is due to apoptosis induction and cell cycle arrest. *Biomed. Pharmacother.* 85, 425–433. doi:10.1016/j.biopha.2016.11.047

Bray, F., Ferlay, J., Soerjomataram, I., Siegel, R., Torre, L., and Jemal, A. (2018). Global cancer statistics 2018: GLOBOCAN estimates of incidence and mortality worldwide for 36 cancers in 185 countries. *CA a cancer J. Clin.* 68 (6), 394–424. doi:10.3322/caac.21492

Chen, G., Ma, Y., Jiang, Z., Feng, Y., Han, Y., Tang, Y., et al. (2018). Lico A causes er stress and apoptosis via up-regulating miR-144-3p in human lung cancer cell line H292. *Front. Pharmacol.* 9, 837. doi:10.3389/fphar.2018.00837

Chen, R., Lin, K., Chen, M., and Lu, W. (2019). Licochalcone A inhibits melanoma cell growth and migration via arresting cell cycle and suppressing Akt phosphorylation. *Febs Open Bio* 9, 328.

Chen, X., Liu, Z., Meng, R., Shi, C., and Guo, N. (2017). Antioxidative and anticancer properties of Licochalcone A from licorice. *J. Ethnopharmacol.* 198, 331–337. doi:10.1016/j.jep.2017.01.028

Chen, X. J., Guo, G. C., Lu, Y. L., Wang, S. S., Zhang, Y., and Huang, Q. (2021). Mechanisms and functions of long non-coding RNAs in glioma [Review]. *Oncol. Rep.* 45 (4), 9. doi:10.3892/or.2021.7960

Chen, Z., Fillmore, C. M., Hammerman, P. S., Kim, C. F., and Wong, K. K. (2014). Non-small-cell lung cancers: A heterogeneous set of diseases. *Nat. Rev. Cancer* 14 (8), 535–546. doi:10.1038/nrc3775

Cheng, D., and Bedford, M. T. (2011). Xenoestrogens regulate the activity of arginine methyltransferases. *Chembiochem a Eur. J. Chem. Biol.* 12 (2), 323–329. doi:10.1002/cbic.201000522

Cho, J. J., Chae, J. I., Yoon, G., Kim, K. H., Cho, J. H., Cho, S. S., et al. (2014). Licochalcone A, a natural chalconoid isolated from Glycyrrhiza inflata root, induces apoptosis via Sp1 and Sp1 regulatory proteins in oral squamous cell carcinoma. *Int. J. Oncol.* 45 (2), 667–674. doi:10.3892/ijo.2014.2461

Choi, A. Y., Choi, J. H., Hwang, K. Y., Jeong, Y. J., Choe, W., Yoon, K. S., et al. (2014). Licochalcone A induces apoptosis through endoplasmic reticulum stress via a phospholipase Cγ1-Ca(2+)-and reactive oxygen species-dependent pathway in HepG2 human hepatocellular carcinoma cells. *Apoptosis* 19 (4), 682–697. doi:10.1007/s10495-013-0955-y

Fan, X., Bai, J., Zhao, S., Hu, M., Sun, Y., Wang, B., et al. (2019). Evaluation of inhibitory effects of flavonoids on breast cancer resistance protein (BCRP): From library screening to biological evaluation to structure-activity relationship. *Toxicol. vitro* 61, 104642. doi:10.1016/j.tiv.2019.104642

Gao, F., Li, M., Yu, X., Liu, W., Zhou, L., and Li, W. (2021). Licochalcone A inhibits EGFR signalling and translationally suppresses survivin expression in human cancer cells. *J. Cell. Mol. Med.* 25 (2), 813–826. doi:10.1111/jcmm.16135

Gong, S., Maegawa, S., Yang, Y., Gopalakrishnan, V., Zheng, G., and Cheng, D. (2020). Licochalcone A is a natural selective inhibitor of arginine methyltransferase 6. *Biochem. J.* 478, 389–406. doi:10.1042/bcj20200411

Han, S., Li, X., Gan, Y., and Li, W. (2022). Licochalcone A promotes the ubiquitination of c-met to abrogate gefitinib resistance. *Biomed. Res. Int.* 2022, 5687832. doi:10.1155/2022/5687832

Hao, W. J., Yuan, X., Yu, L., Gao, C. X., Sun, X. L., Wang, D., et al. (2015). Licochalcone A-induced human gastric cancer BGC-823 cells apoptosis by regulating ROS-mediated MAPKs and PI3K/AKT signaling pathways. *Sci. Rep.* 5, 10336. doi:10.1038/srep10336

Hao, Y., Zhang, C., Sun, Y., and Xu, H. (2019). Licochalcone A inhibits cell proliferation, migration, and invasion through regulating the PI3K/AKT signaling pathway in oral squamous cell carcinoma. *OncoTargets Ther.* 12, 4427–4435. doi:10.2147/ott.s201728

Heng, W. S., and Cheah, S. C. (2021). Identification of phytochemical-based β-catenin nuclear localization inhibitor in NSCLC: Differential targeting population from member of isothiocyanates. *Molecules* 26 (2), 224. doi:10.3390/molecules25010224

Herbrechter, R., Ziemba, P. M., Hoffmann, K. M., Hatt, H., Werner, M., and Gisselmann, G. (2015). Identification of Glycyrrhiza as the rikkunshito constituent

with the highest antagonistic potential on heterologously expressed 5-HT3A receptors due to the action of flavonoids. *Front. Pharmacol.* 6, 130. doi:10.3389/fphar.2015.00130

Hirsch, F. R., Scagliotti, G. V., Mulshine, J. L., Kwon, R., Curran, W. J., Wu, Y. L., et al. (2017). Lung cancer: Current therapies and new targeted treatments. *Lancet* 389 (10066), 299–311. doi:10.1016/s0140-6736(16)30958-8

Hong, S. H., Cha, H. J., Hwang-Bo, H., Kim, M. Y., Kim, S. Y., Ji, S. Y., et al. (2019). Anti-proliferative and pro-apoptotic effects of licochalcone A through ROS-mediated cell cycle arrest and apoptosis in human bladder cancer cells. *Int. J. Mol. Sci.* 20 (15), 3820. doi:10.3390/ijms20153820

Hosseinzadeh, H., and Nassiri-Asl, M. (2015). Pharmacological effects of Glycyrrhiza spp. and its bioactive constituents: Update and review. *Phytotherapy Res. PTR* 29 (12), 1868–1886. doi:10.1002/ptr.5487

Hu, C., Zuo, Y., Liu, J., Xu, H., Liao, W., Dang, Y., et al. (2020). Licochalcone A suppresses the proliferation of sarcoma HT-1080 cells, as a selective R132C mutant IDH1 inhibitor. *Bioorg. Med. Chem. Lett.* 30 (2), 126825. doi:10.1016/j.bmcl.2019.126825

Huang, C. F., Yang, S. F., Chiou, H. L., Hsu, W. H., Hsu, J. C., Liu, C. J., et al. (2018). Licochalcone A inhibits the invasive potential of human glioma cells by targeting the MEK/ERK and ADAM9 signaling pathways. *Food & Funct.* 9 (12), 6196–6204. doi:10.1039/c8fo01643g

Huang, H. C., Tsai, L. L., Tsai, J. P., Hsieh, S. C., Yang, S. F., Hsueh, J. T., et al. (2014). Licochalcone A inhibits the migration and invasion of human lung cancer cells via inactivation of the Akt signaling pathway with downregulation of MMP-1/-3 expression. *Tumour Biol.* 35 (12), 12139–12149. doi:10.1007/s13277-014-2519-3

Huang, W. C., Su, H. H., Fang, L. W., Wu, S. J., and Liou, C. J. (2019). Licochalcone A inhibits cellular motility by suppressing E-cadherin and MAPK signaling in breast cancer. *Cells* 8 (3), 218. doi:10.3390/cells8030218

Huang, Z., and Jin, G. (2022). Licochalcone B induced apoptosis and autophagy in osteosarcoma tumor cells via the inactivation of PI3K/AKT/mTOR pathway. *Biol. Pharm. Bull.* 45 (6), 730–737. doi:10.1248/bpb.b21-00991

Jiang, J., Yuan, X., Zhao, H., Yan, X., Sun, X., and Zheng, Q. (2014). Licochalcone A inhibiting proliferation of bladder cancer T24 cells by inducing reactive oxygen species production. *Bio-medical Mater. Eng.* 24 (1), 1019–1025. doi:10.3233/bme-130899

Kang, T. H., Seo, J. H., Oh, H., Yoon, G., Chae, J. I., and Shim, J. H. (2017). Licochalcone A suppresses specificity protein 1 as a novel target in human breast cancer cells. *J. Cell. Biochem.* 118 (12), 4652–4663. doi:10.1002/jcb.26131

Kang, T. H., Yoon, G., Kang, I. A., Oh, H. N., Chae, J. I., and Shim, J. H. (2017). Natural compound licochalcone B induced extrinsic and intrinsic apoptosis in human skin melanoma (A375) and squamous cell carcinoma (A431) cells. *Phytotherapy Res.* 31 (12), 1858–1867. doi:10.1002/ptr.5928

Keshavarz-Fathi, M., and Rezaei, N. (2021). Cancer immunoprevention: Current status and future directions. *Archivum Immunol. Ther. Exp.* 69 (1), 3. doi:10.1007/s00005-021-00604-x

Kim, J-S., Park, M-R., Lee, S-Y., Kim, D. K., Moon, S-M., Kim, C. S., et al. (2014). Licochalcone A induces apoptosis in KB human oral cancer cells via a caspase-dependent FasL signaling pathway. *Oncol. Rep.* 31 (2), 755–762. doi:10.3892/or.2013.2929

Kim, K. H., Yoon, G., Cho, J. J., Cho, J. H., Cho, Y. S., Chae, J. I., et al. (2015). Licochalcone A induces apoptosis in malignant pleural mesothelioma through downregulation of Sp1 and subsequent activation of mitochondria-related apoptotic pathway. *Int. J. Oncol.* 46 (3), 1385–1392. doi:10.3892/ijo.2015.2839

Kim, Y. J., Jung, E. B., Myung, S. C., Kim, W., and Lee, C. S. (2013). Licochalcone A enhances geldanamycin-induced apoptosis through reactive oxygen species-mediated caspase activation. *Pharmacology* 92, 49–59. doi:10.1159/000351846

Kuramoto, K., Suzuki, S., Sakaki, H., Takeda, H., Sanomachi, T., Seino, S., et al. (2017). Licochalcone A specifically induces cell death in glioma stem cells via mitochondrial dysfunction. *FEBS* 7 (6), 835–844. doi:10.1002/2211-5463.12226

Kwak, A. W., Cho, S. S., Yoon, G., Oh, H. N., Lee, M. H., Chae, J. I., et al. (2020). Licochalcone H synthesized by modifying structure of licochalcone C extracted from Glycyrrhiza inflata induces apoptosis of esophageal squamous cell carcinoma cells. *Cell Biochem. biophysics* 78 (1), 65–76. doi:10.1007/s12013-019-00892-3

Kwak, A. W., Choi, J. S., Liu, K., Lee, M. H., Jeon, Y. J., Cho, S. S., et al. (2020). Licochalcone C induces cell cycle G1 arrest and apoptosis in human esophageal squamous carcinoma cells by activation of the ROS/MAPK signaling pathway. *J. Chemother.* 32. 132–143. doi:10.1080/1120009X.2020.1721175

Kwon, S. J., Park, S. Y., Kwon, G. T., Lee, K. W., Kang, Y. H., Choi, M. S., et al. (2013). Licochalcone E present in licorice suppresses lung metastasis in the 4T1 mammary orthotopic cancer model. *Cancer Prev. Res.* 6 (6), 603–613. doi:10.1158/1940-6207.capr-13-0012

Lee, C. S., Kwak, S. W., Kim, Y. J., Lee, S. A., Park, E. S., Myung, S. C., et al. (2012). Guanylate cyclase activator YC-1 potentiates apoptotic effect of licochalcone A on human epithelial ovarian carcinoma cells via activation of death receptor and mitochondrial pathways. *Eur. J. Pharmacol.* 683, 54–62. doi:10.1016/j.ejphar.2012.03.024

Lin, R. C., Yang, S. F., Chiou, H. L., Hsieh, S. C., Wen, S. H., Lu, K. H., et al. (2019). Licochalcone A-induced apoptosis through the activation of p38MAPK pathway mediated mitochondrial pathways of apoptosis in human osteosarcoma cells *in vitro* and *in vivo*. *Cells* 8 (11), 1441. doi:10.3390/cells8111441

Lin, X., Tian, L., Wang, L., Li, W., Xu, Q., and Xiao, X. (2017). Antitumor effects and the underlying mechanism of licochalcone A combined with 5-fluorouracil in gastric cancer cells. *Oncol. Lett.* 13 (3), 1695–1701. doi:10.3892/ol.2017.5614

Lin, Y. J., Liang, W. M., Chen, C. J., Tsang, H., Chiou, J. S., Liu, X., et al. (2019). Network analysis and mechanisms of action of Chinese herb-related natural compounds in lung cancer cells. *Phytomedicine* 58, 152893. doi:10.1016/j.phymed.2019.152893

Lu, W. J., Wu, G. J., Chen, R. J., Chang, C. C., Lien, L. M., Chiu, C. C., et al. (2018). Licochalcone A attenuates glioma cell growth *in vitro* and *in vivo* through cell cycle arrest. *Food & Funct.* 9 (8), 4500–4507. doi:10.1039/c8fo00728d

Nabekura, T., Hiroi, T., Kawasaki, T., and Uwai, Y. (2015). Effects of natural nuclear factor-kappa B inhibitors on anticancer drug efflux transporter human P-glycoprotein. *Biomed. Pharmacother.* 70, 140–145. doi:10.1016/j.biopha.2015.01.007

Nho, S. H., Yoon, G., Seo, J. H., Oh, H. N., Cho, S. S., Kim, H., et al. (2019). Licochalcone H induces the apoptosis of human oral squamous cell carcinoma cells via regulation of matrin 3. *Oncol. Rep.* 41 (1), 333–340. doi:10.3892/or.2018.6784

Niu, Q., Zhao, W., Wang, J., Li, C., Yan, T., Lv, W., et al. (2018). LicA induces autophagy through ULK1/Atg13 and ROS pathway in human hepatocellular carcinoma cells. *Int. J. Mol. Med.* 41 (5), 2601–2608. doi:10.3892/ijmm.2018.3499

O'Keefe, S. J. D. (2016). Diet, microorganisms and their metabolites, and colon cancer. *Nat. Rev. Gastroenterol. Hepatol.* 13 (12), 691–706. doi:10.1038/nrgastro.2016.165

Oh, H., Yoon, G., Shin, J. C., Park, S. M., Cho, S. S., Cho, J. H., et al. (2016). Licochalcone B induces apoptosis of human oral squamous cell carcinoma through the extrinsic- and intrinsic-signaling pathways. *Int. J. Oncol.* 48 (4), 1749–1757. doi:10.3892/ijo.2016.3365

Oh, H. N., Lee, M. H., Kim, E., Kwak, A. W., Yoon, G., Cho, S. S., et al. (2020). Licochalcone D induces ROS-dependent apoptosis in gefitinib-sensitive or resistant lung cancer cells by targeting EGFR and MET. *Biomolecules* 10 (2), 297. doi:10.3390/biom10020297

Oh, H. N., Lee, M. H., Kim, E., Yoon, G., Chae, J. I., and Shim, J. H. (2019). Licochalcone B inhibits growth and induces apoptosis of human non-small-cell lung cancer cells by dual targeting of EGFR and MET. *Phytomedicine Int. J. phytotherapy Phytopharm.* 63, 153014. doi:10.1016/j.phymed.2019.153014

Oh, H. N., Oh, K. B., Lee, M. H., Seo, J. H., Kim, E., Yoon, G., et al. (2019). JAK2 regulation by licochalcone H inhibits the cell growth and induces apoptosis in oral squamous cell carcinoma. *Phytomedicine* 52, 60–69. doi:10.1016/j.phymed.2018.09.180

Oh, H. N., Seo, J. H., Lee, M. H., Kim, C., Kim, E., Yoon, G., et al. (2018). Licochalcone C induced apoptosis in human oral squamous cell carcinoma cells by regulation of the JAK2/STAT3 signaling pathway. *J. Cell. Biochem.* 119 (12), 10118–10130. doi:10.1002/jcb.27349

Park, M. K., Ji, J., Haam, K., Han, T. H., Lim, S., Kang, M. J., et al. (2021). Licochalcone A inhibits hypoxia-inducible factor-1α accumulation by suppressing mitochondrial respiration in hypoxic cancer cells. *Biomed. Pharmacother.* 133, 111082. doi:10.1016/j.biopha.2020.111082

Park, M. R., Kim, S. G., Cho, I. A., Oh, D., Kang, K. R., Lee, S. Y., et al. (2015). Licochalcone-A induces intrinsic and extrinsic apoptosis via ERK1/2 and p38 phosphorylation-mediated TRAIL expression in head and neck squamous carcinoma FaDu cells. *Food Chem. Toxicol.* 77, 34–43. doi:10.1016/j.fct.2014.12.013

Pia, G. D. M., Sara, F., Mario, F., and Lorenza, S. (20192019). Biological effects of licochalcones. *Mini-Reviews Med. Chem.* 19 (8), 647–656. doi:10.2174/1389557518666180601095420

Qiu, C., Zhang, T., Zhang, W., Zhou, L., Yu, B., Wang, W., et al. (2017). Licochalcone A inhibits the proliferation of human lung cancer cell lines A549 and H460 by inducing G2/M cell cycle arrest and er stress. *Int. J. Mol. Sci.* 18 (8), 1761. doi:10.3390/ijms18081761

Roberts, L. S., Yan, P., Bateman, L. A., and Nomura, D. K. (2017). Mapping novel metabolic nodes targeted by anti-cancer drugs that impair triple-negative breast cancer pathogenicity. *ACS Chem. Biol.* 12 (4), 1133–1140. doi:10.1021/acschembio.6b01159

Rossi, M., Cappadone, C., Picone, G., Bisi, A., Farruggia, G., Belluti, F., et al. (2022). Natural-like chalcones with antitumor activity on human MG63 osteosarcoma cells. *Molecules* 27 (12), 3751. doi:10.3390/molecules27123751

Seo, J. H., Choi, H. W., Oh, H. N., Lee, M. H., Kim, E., Yoon, G., et al. (2019). Licochalcone D directly targets JAK2 to induced apoptosis in human oral squamous cell carcinoma. *J. Cell. physiology* 234 (2), 1780–1793. doi:10.1002/jcp.27050

Seo, Y. H. (2013). Discovery of licochalcone A as a natural product inhibitor of Hsp90 and its effect on gefitinib resistance in non-small cell lung cancer (nsclc). *Bull. Korean Chem. Soc.* 34 (6), 1917–1920. doi:10.5012/bkcs.2013.34.6.1917

Shen, H., Zeng, G., Tang, G., Cai, X., Bi, L., Huang, C., et al. (2014). Antimetastatic effects of licochalcone A on oral cancer via regulating metastasis-associated proteases. *Tumour Biol.* 35 (8), 7467–7474. doi:10.1007/s13277-014-1985-y

Shen, T. S., Hsu, Y. K., Huang, Y. F., Chen, H. Y., Hsieh, C. P., and Chen, C. L. (2019). Licochalcone A suppresses the proliferation of osteosarcoma cells through autophagy and ATM-chk2 activation. *Molecules* 24 (13), 2435. doi:10.3390/molecules24132435

Si, L., Yan, X., Hao, W., Ma, X., Ren, H., Ren, B., et al. (2018). Licochalcone D induces apoptosis and inhibits migration and invasion in human melanoma A375 cells. *Oncol. Rep.* 39 (5), 2160–2170. doi:10.3892/or.2018.6329

Song, M., Yoon, G., Choi, J. S., Kim, E., Liu, X., Oh, H. N., et al. (2020). Janus kinase 2 inhibition by Licochalcone B suppresses esophageal squamous cell carcinoma growth. *Phytotherapy Res.* 34 (8), 2032–2043. doi:10.1002/ptr.6661

Steinbach, D., Sell, W., Voigt, A., Hermann, J., Zintl, F., Sauerbrey, A., et al. (2002). BCRP gene expression is associated with a poor response to remission induction therapy in childhood acute myeloid leukemia. *Leukemia* 16 (8), 1443–1447. doi:10.1038/sj.leu.2402541

Suma, V. R., Sreenivasulu, R., Rao, M., Subramanyam, M., Ahsan, M. J., Alluri, R., et al. (2020). Design, synthesis, and biological evaluation of chalcone-linked thiazole-imidazopyridine derivatives as anticancer agents. *Med. Chem. Res.* 29 (9), 1643–1654. doi:10.1007/s00044-020-02590-9

Szliszka, E., Jaworska, D., Ksek, M., Czuba, Z., and Król, W. (2012). Targeting death receptor TRAIL-R2 by chalcones for TRAIL-induced apoptosis in cancer cells. *Int. J. Mol. Sci.* 13 (11), 15343–15359. doi:10.3390/ijms131115343

Tamaki, H., Satoh, H., Hori, S., Ohtani, H., and Sawada, Y. (2010). Inhibitory effects of herbal extracts on breast cancer resistance protein (BCRP) and structure-inhibitory potency relationship of isoflavonoids. *Drug metabolism Pharmacokinet.* 25 (2), 170–179. doi:10.2133/dmpk.25.170

Tang, Z. H., Chen, X., Wang, Z. Y., Chai, K., Wang, Y. F., Xu, X. H., et al. (2016). Induction of C/EBP homologous protein-mediated apoptosis and autophagy by licochalcone A in non-small cell lung cancer cells. *Sci. Rep.* 6, 26241. doi:10.1038/srep26241

Tsai, J. P., Hsiao, P. C., Yang, S. F., Hsieh, S. C., Bau, D. T., Ling, C. L., et al. (2014). Licochalcone A suppresses migration and invasion of human hepatocellular carcinoma cells through downregulation of MKK4/JNK via NF-κB mediated urokinase plasminogen activator expression. *PloS one* 9 (1), e86537. doi:10.1371/journal.pone.0086537

Tsai, J. P., Lee, C. H., Ying, T. H., Lin, C. L., Lin, C. L., Hsueh, J. T., et al. (2015). Licochalcone A induces autophagy through PI3K/Akt/mTOR inactivation and autophagy suppression enhances Licochalcone A-induced apoptosis of human cervical cancer cells. *Oncotarget* 6 (30), 28851–28866. doi:10.18632/oncotarget.4767

Vitorio, J. G., Duarte-Andrade, F. F., Pereira, T. D. F., Fonseca, F. P., Amorim, L. S. D., Martins-Chaves, R. R., et al. (2020). Metabolic landscape of oral squamous cell carcinoma. *Metabolomics* 16 (10), 105. doi:10.1007/s11306-020-01727-6

Volk, E. L., Farley, K. M., Wu, Y., Li, F., Robey, R. W., and Schneider, E. (2002). Overexpression of wild-type breast cancer resistance protein mediates methotrexate resistance. *Cancer Res.* 62 (17), 5035–5040.

Walczak, B. E., and Irwin, R. B. (2013). Sarcoma chemotherapy. *J. Am. Acad. Orthop. Surg.* 21 (8), 480–491. doi:10.5435/jaaos-21-08-480

Wang, J., Liao, A. M., Thakur, K., Zhang, J. G., Huang, J. H., and Wei, Z. J. (2019). Licochalcone B extracted from Glycyrrhiza uralensis fisch induces apoptotic effects in human hepatoma cell HepG2. *J. Agric. food Chem.* 67 (12), 3341–3353. doi:10.1021/acs.jafc.9b00324

Wang, J., and Wang, C. Y. (2021). Integrated miRNA and mRNA omics reveal the anti-cancerous mechanism of licochalcone B on human hepatoma cell HepG2. *Food Chem. Toxicol.* 150, 112096. doi:10.1016/j.fct.2021.112096

Wang, J., Wei, B., Thakur, K., Wang, C. Y., Li, K. X., and Wei, Z. J. (2021). Transcriptome analysis reveals the anti-cancerous mechanism of licochalcone A on human hepatoma cell HepG2. *Front. Nutr.* 8, 807574. doi:10.3389/fnut.2021.807574

Wang, J., Zhang, Y. S., Thakur, K., Hussain, S. S., Zhang, J. G., Xiao, G. R., et al. (2018). Licochalcone A from licorice root, an inhibitor of human hepatoma cell growth via induction of cell apoptosis and cell cycle arrest. *Food Chem. Toxicol.* 120, 407–417. doi:10.1016/j.fct.2018.07.044

Wang, P., Yuan, X., Wang, Y., Zhao, H., Sun, X., and Zheng, Q. (2015). Licochalcone C induces apoptosis via B-cell lymphoma 2 family proteins in T24 cells. *Mol. Med. Rep.* 12 (5), 7623–7628. doi:10.3892/mmr.2015.4346

Wu, J., Zhang, X. X., Wang, Y. H., Sun, Q. M., Chen, M., Liu, S. L., et al. (2018). Licochalcone A suppresses hexokinase 2-mediated tumor glycolysis in gastric cancer via downregulation of the Akt signaling pathway. *Oncol. Rep.* 39 (3), 1181–1190. doi:10.3892/or.2017.6155

Wu, L. T., Jiang, Z., Shen, J. J., Yi, H., Zhan, Y. C., Sha, M. Q., et al. (2016). Design, synthesis and biological evaluation of novel benzimidazole-2-substituted phenyl or pyridine propyl ketene derivatives as antitumour agents. *Eur. J. Med. Chem.* 114, 328–336. doi:10.1016/j.ejmech.2016.03.029

Wu, M. H., Chiu, Y. F., Wu, W. J., Wu, P. L., Lin, C. Y., Lin, C. L., et al. (2018). Synergistic antimetastatic effect of cotreatment with licochalcone A and sorafenib on human hepatocellular carcinoma cells through the inactivation of MKK4/JNK and uPA expression. *Environ. Toxicol.* 33 (12), 1237–1244. doi:10.1002/tox.22630

Wu, P., Yu, T., Wu, J., and Chen, J. (2020). Licochalcone a induces ROS-mediated apoptosis through TrxR1 inactivation in colorectal cancer cells. *BioMed Res. Int.* 2020, 5875074. doi:10.1155/2020/5875074

Wu, R., Li, X-Y., Wang, W-H., Cai, F-F., Chen, X-L., Yang, M-D., et al. (2019). Network pharmacology-based study on the mechanism of bushen-jianpi decoction in liver cancer treatment. *Evidence-Based Complementary Altern. Med.* 2019, 1–13. doi:10.1155/2019/3242989

Xiao, X. Y., Hao, M., Yang, X. Y., Ba, Q., Li, M., Ni, S. J., et al. (2011). Licochalcone A inhibits growth of gastric cancer cells by arresting cell cycle progression and inducing apoptosis. *Cancer Lett.* 302 (1), 69–75. doi:10.1016/j.canlet.2010.12.016

Xue, L., Zhang, W. J., Fan, Q. X., and Wang, L. X. (2018). Licochalcone A inhibits PI3K/Akt/mTOR signaling pathway activation and promotes autophagy in breast cancer cells. *Oncol. Lett.* 15 (2), 1869–1873. doi:10.3892/ol.2017.7451

Yang, P., Tuo, L., Wu, Q., and Cao, X. (2014). Licochalcone-A sensitizes human esophageal carcinoma cells to TRAIL-mediated apoptosis by proteasomal degradation of XIAP. *Hepato-gastroenterology* 61 (133), 1229–1234.

Yang, X., Jiang, J., Yang, X., Han, J., and Zheng, Q. (2016). Licochalcone A induces T24 bladder cancer cell apoptosis by increasing intracellular calcium levels. *Mol. Med. Rep.* 14 (1), 911–919. doi:10.3892/mmr.2016.5334

Yao, K., Chen, H., Lee, M. H., Li, H., Ma, W., Peng, C., et al. (2014). Licochalcone A, a natural inhibitor of c-Jun N-terminal kinase 1. *Cancer Prev. Res.* 7 (1), 139–149. doi:10.1158/1940-6207.capr-13-0117

Yoon, G., Cheon, S. H., Shim, J. H., and Cho, S. S. (2018). Design and evaluation of licochalcone a derivatives as anticancer agents. *Nat. Product. Commun.* 13, 1934578X1801300–689. doi:10.1177/1934578x1801300609

Yu, L., Ma, J., Han, J., Wang, B., Chen, X., Gao, C., et al. (2016). Licochalcone B arrests cell cycle progression and induces apoptosis in human breast cancer MCF-7 cells. *Recent Pat. anti-cancer drug Discov.* 11 (4), 444–452. doi:10.2174/1574892811666160906091405

Yu, S. J., Cho, I. A., Kang, K. R., Jung, Y. R., Cho, S. S., Yoon, G., et al. (2017). Licochalcone-E induces caspase-dependent death of human pharyngeal squamous carcinoma cells through the extrinsic and intrinsic apoptotic signaling pathways. *Oncol. Lett.* 13 (5), 3662–3668. doi:10.3892/ol.2017.5865

Yuan, L. W., Jiang, X. M., Xu, Y. L., Huang, M. Y., Chen, Y. C., Yu, W. B., et al. (20212021). Licochalcone A inhibits interferon-gamma-induced programmed death-ligand 1 in lung cancer cells. *Phytomedicine* 80, 153394. doi:10.1016/j.phymed.2020.153394

Yuan, X., Li, T., Xiao, E., Zhao, H., Li, Y., Fu, S., et al. (2014). Licochalcone B inhibits growth of bladder cancer cells by arresting cell cycle progression and inducing apoptosis. *Food Chem. Toxicol.* 65, 242–251. doi:10.1016/j.fct.2013.12.030

Zeng, G., Shen, H., Yang, Y., Cai, X., and Xun, W. (2014). Licochalcone A as a potent antitumor agent suppresses growth of human oral cancer SCC-25 cells *in vitro* via caspase-3 dependent pathways. *Tumour Biol.* 35 (7), 6549–6555. doi:10.1007/s13277-014-1877-1

Zhang, J. J., Wu, H. D., and Wang, R. Y. (2021). Metabolic syndrome and esophageal cancer risk: A systematic review and meta-analysis. *Diabetology Metabolic Syndrome* 13 (1), 8. doi:10.1186/s13098-021-00627-6

Zhang, Y., Gao, M., Chen, L., Zhou, L., Bian, S., and Lv, Y. (2020). Licochalcone A restrains microphthalmia-associated transcription factor expression and growth by activating autophagy in melanoma cells via miR-142-3p/Rheb/mTOR pathway. *Phytotherapy Res.* 34 (2), 349–358. doi:10.1002/ptr.6525

Zhang, Y. Y., Feng, P. P., Wang, H. F., Zhang, H., Liang, T., Hao, X. S., et al. (2022). Licochalcone B induces DNA damage, cell cycle arrest, apoptosis, and enhances TRAIL sensitivity in hepatocellular carcinoma cells. *Chemico-biological Interact.* 365, 110076. doi:10.1016/j.cbi.2022.110076

Zhang, Y. Y., Huang, C. T., Liu, S. M., Wang, B., Guo, J., Bai, J. Q., et al. (2016). Licochalcone A exerts antitumor activity in bladder cancer cell lines and mice models. *Trop. J. Pharm. Res.* 15, 1151–1157. doi:10.4314/tjpr.v15i6.6

frontiers | Frontiers in Pharmacology

TYPE Review
PUBLISHED 20 March 2023
DOI 10.3389/fphar.2023.1154034

OPEN ACCESS

EDITED BY
Visweswara Rao Pasupuleti,
REVA University, India

REVIEWED BY
Nida Mubin,
Aligarh Muslim University, India
Jhalak Singhal,
Jawaharlal Nehru University, India

*CORRESPONDENCE
Fahad Khan,
fahadkhan.bio@niet.co.in
Mohd Saeed,
mo.saeed@uoh.edu.sa

SPECIALTY SECTION
This article was submitted to Pharmacology of Anti-Cancer Drugs, a section of the journal Frontiers in Pharmacology

RECEIVED 30 January 2023
ACCEPTED 02 March 2023
PUBLISHED 20 March 2023

CITATION
Pandey P, Khan F, Alshammari N, Saeed A, Aqil F and Saeed M (2023), Updates on the anticancer potential of garlic organosulfur compounds and their nanoformulations: Plant therapeutics in cancer management.
Front. Pharmacol. 14:1154034.
doi: 10.3389/fphar.2023.1154034

Updates on the anticancer potential of garlic organosulfur compounds and their nanoformulations: Plant therapeutics in cancer management

Pratibha Pandey[1], Fahad Khan[1]*, Nawaf Alshammari[2,3], Amir Saeed[4,3], Farrukh Aqil[5] and Mohd Saeed[2,3]*

[1]Department of Biotechnology, Noida Institute of Engineering and Technology, Noida, Uttar Pradesh, India, [2]Department of Biology, College of Sciences, University of Hail, Hail, Saudi Arabia, [3]Molecular Diagnostics and Personalized Therapeutics Unit, University of Hail, Hail, Saudi Arabia, [4]Department of Medical Laboratory Sciences, College of Applied Medical Sciences, University of Hail, Hail, Saudi Arabia, [5]Department of Medicine and Brown Cancer Center, University of Louisville, Louisville, KY, United States

Garlic (*Allium sativum* L.) possesses numerous pharmacological potential, including antibacterial, antiarthritic, antithrombotic, anticancer, hypoglycemic, and hypolipidemic effects. The anti-cancer action of garlic is likely the best researched of the many advantageous pharmacological effects, and its use offers significant protection against the risk of developing cancer. A few active metabolites of garlic have been reported to be essential in the destruction of malignant cells due to their multi-targeted activities and lack of significant toxicity. The bioactive compounds in garlic having anticancer properties include diallyl trisulfide, allicin, allyl mercaptan diallyl disulfide, and diallyl sulphide. Different garlic-derived constituents and their nanoformulations have been tested for their effects against various cancers including skin, ovarian, prostate, gastric, breast, and lung, colorectal, liver, oral, and pancreatic cancer. The objective of this review is to summarize the antitumor activity and associated mechanisms of the organosulfur compounds of garlic in breast carcinoma. Breast cancer continues to have a significant impact on the total number of cancer deaths worldwide. Global measures are required to reduce its growing burden, particularly in developing nations where incidence is increasing quickly and fatality rates are still high. It has been demonstrated that garlic extract, its bioactive compounds, and their use in nanoformulations can prevent breast cancer in all of its stages, including initiation, promotion, and progression. Additionally, these bioactive compounds affect cell signaling for cell cycle arrest and survival along with lipid peroxidation, nitric oxide synthase activity, epidermal growth factor receptor, nuclear factor kappa B (NF-κB), and protein kinase C in breast carcinoma. Hence, this review deciphers the anticancer potential of garlic components and its nanoformulations against several breast cancer thereby projecting it as a potent drug candidate for efficient breast cancer management.

KEYWORDS

garlic, plant therapeutics, cancer, nanoformulations, organosulfur compounds, drug delivery, molecular mechanism

1 Introduction

Natural remedies have been used extensively to cure human illnesses since ancient times, and they are now being used as a key resource in drug development studies. The best hope for cancer patients is either early diagnosis or surgical tumor removal followed by radiation therapy and chemotherapy. Nevertheless, cancer continues to be one of the major cause of mortality across the globe and demands an urgent need for developing effective ways to combat morbidity and mortality along with high economic costs (Newman and Cragg, 2012; George et al., 2021). In-depth research on phytochemicals has shown that they have anticarcinogenic properties, which affect cancer initiation, proliferation, and progression *via* regulating numerous pathways, such as differentiation, cell proliferation, apoptosis, invasion, angiogenesis, metastasis, and migration (Basmadjian et al., 2014; Ranjan et al., 2019). *Allium sativum* L., also recognized as garlic, is a member of the Alliaceae family. The term Alliaceae comes from the Celtic word "all," which means strong and nature's gift to mankind. The bulbs of garlic range in color from white to pink having a pungent scent and fragrant flavor (Takagi, 2020). The therapeutic and preventive properties of garlic against numerous cancers have been assessed by several epidemiologic, preclinical, and clinical investigations. *Allium sativum* extracts have been shown to have numerous biological properties including antiviral, antiprotozoal, antibacterial, anti-inflammatory, antifungal, and antioxidant activities (El-Saber Batiha et al., 2020). The anti-cancerous potential of garlic has been validated by many preclinical studies using human cancer cells, including those of the lung, mouth, stomach, pancreas, ovary, endometrium, breast, prostate, and bone cancer (Dorant et al., 1993; Tanaka et al., 2006). Further, laboratory experimentation has demonstrated that chemical components reported in garlic can repair DNA damage, induce cancer cell growth arrest, and reduce inflammatory responses.

Nanotechnology aims to improve the ability of drugs to effectively treat cancer by ensuring that they are delivered to the right target at the right times. Recently, nanotechnology-based delivery approaches have drawn wider attention as a potential solution to issues related with drug solubility and bioavailability, toxicity, and distribution. Novel approaches incorporating the therapeutic characteristics of garlic extracts and their constituents, either alone or in nanoparticle formulations, may thus result in more efficient and effective anticancer activity (Charron et al., 2015; Mandal et al., 2019; Zhang et al., 2020). Nanobiotechnology has gained attention in the last 20 years as a field of study that has influenced the development of new medications. Due to their low volume/surface ratio and several advanced and novel physiochemical properties, such as color, solubility, strength, toxicity, magnetic, optical, and thermodynamics, nanomaterial, the topic of our investigation, differ significantly from their macro scale counterparts in terms of capabilities. Mechanism associated with nanoparticles biogenesis include reduction of metallic ions of numerous biomolecules found in living things. The manufacture of vast amounts of well-defined, contaminant-free nanoparticles with defined size and morphology is made possible by nanoparticle biogenesis, which also lessens the environmental impact of biological synthesis. Recent nanotechnological advancements demonstrated the synthesis of nanoparticles utilizing the potential of microorganisms and plant based materials (tissue and extracts) including garlic constituents.

Garlic and its derived components potentially reduced the progression of tumor in animal model and suppressed cancer cell growth. In conventional medicine, *A. sativum* L. is used to prevent, and treat a number of malignancies, including cancers of blood, breast, prostate, ovarian, and gastrointestine. Major active phytoconstituents of *A. sativum* include diallyl thiosulfinate, methyl allyl trisulfide, diallyl tetrasulfide, S-allyl cysteine sulfoxide, dipropyl sulfide, dially trisulfide, 3-vinyl-4H-1,2-dithiin, allyl methane sulfinate, diallyl disulfide, dipropyl disulfide, allyl methyl thiosulfinate, S-methyl cysteinesulfoxide, 3-vinyl-6H-1,2-dithiin, dimethyl disulfide, dimethyl sulfide, methylpropyl disulfide, S-propyl cysteine sulfoxide, 3-vinyl-6H-1,3-dithiin, and, methyl methane sulfinate. Garlic derivatives including diallyl disulfide, are found to be highly effective in suppressing the growth of breast cancer cells. Mechanisms behind this growth suppression include the activation of metabolizing enzymes for carcinogen detoxification, inhibition of reactive oxygen species (ROS) generation and DNA adduct formation, control of the cell cycle, and apoptosis induction. Thus, we have focused our review on deciphering the anticancer potential of garlic against breast cancer in order to elucidate the potent drug candidate for effective management of breast cancer.

Breast cancer is one of the most common neoplasm in women worldwide, in both industrialized and developing nations. The invasion and proliferation of breast cancer have been lessened by using available therapies such as chemotherapy, hormone and radiation therapy, and/or surgery. Scientists are looking for more effective treatments for breast cancer, such as natural chemicals, as the majority of chemotherapeutic medications are linked to drug resistance, cancer relapse, and adverse effects. Apoptosis is induced and metastasis is inhibited by specific natural molecules, substances originating from living things, which inhibit cancer progression. These bioactive molecules have displayed significant efficacy in advanced stage of several cancers including breast cancer with increased survival rate and reduced morbidity (Noel et al., 2020; Sung et al., 2021). Here, we also review organosulfur compounds that have been shown in numerous studies to have anti-cancer properties against breast cancer cells. These organosulfur compounds encourage cell death, prevent breast cancer formation, and slow the growth of cancerous cells. There are very limited reviews discussing the potential anticancer efficacy of new formulations of garlic extracts and their constituents in breast cancer. In-depth descriptions of how garlic, its bioactive components, and its nanoformulations work against various malignancies are provided in this review, which also considers the potential for turning these substances into medications that fight cancer.

2 Major active constituents of *Allium sativum* L

The anticancer potential of numerous sulfur-containing compounds and other bioactive constituents of garlic has been extensively studied. Garlic has high concentrations of zinc,

TABLE 1 Phytoconstituents of garlic (Data retrieved from SWISS ADME software).

Major active constituents	Full form	Chemical structure	Pubchem ID	GI absorption	BBB permeant
γ-glutamyl-S-allyl-L-cysteine	gamma-L-glutamyl-[(S)-allyl]-L-cysteine	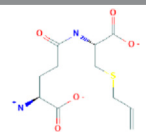	91,820,320	Low	No
Alliin	S-allyl-L-cysteine sulfoxide	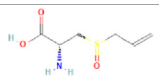	9,576,089	High	No
Allicin	S-allyl prop-2-ene-1-sulfinothioate	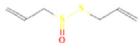	65,036	High	Yes
DATS	Diallyl trisulfide		16,315	High	Yes
DADS	Diallyl disulfide		16,590	High	Yes
DAS	Diallyl sulfide		11,617	High	Yes
AMS	Allyl methyl sulfide		66,282	High	Yes
Thiacremonone	2,4-Dihydroxy-2,5-dimethylthiophen-3(2H)-one	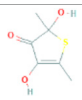	539,170	High	No
Ajoene	(E)-Ajoene	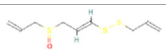	5386591	High	No
SAMC	S-allyl mercapto cysteine	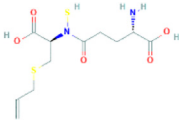	129847556	Low	No
FO	N-trans-feruloyloctopamine	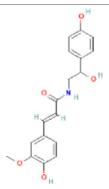	24096391	High	No
MSeC	Se-methyl-L-selenocysteine		147,004	High	No
SAC	S-allyl-L-cysteine	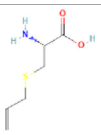	9793905	High	No
SBC	S-benzyl-cysteine	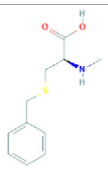	13817365	High	No

(Continued on following page)

TABLE 1 (*Continued*) **Phytoconstituents of garlic (Data retrieved from SWISS ADME software).**

Major active constituents	Full form	Chemical structure	Pubchem ID	GI absorption	BBB permeant
SPRC	S-propargyl-cysteine	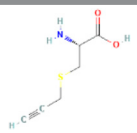	22789047	High	No

potassium, sulfur, phosphorus, and a moderate level of selenium, magnesium, calcium, iron, sodium, manganese, and vitamins (A, B and C). In recent years numerous bioactive compounds have been identified in garlic including polyphenols, flavanols, flavonoids, saponins, tannins, sulfur-containing compounds (such as alliin, ajoene, allicin, DATS, allylpropyl disulfide, S-allylcysteine (SAC), vinyldithiins, poly-saccharides, enzymes (including myrosinase, allinase, and peroxidase) and other com-pounds including phellandrene, *ß*-phellandrene, linalool, geraniol, and citral (Ansary et al., 2020). Table 1 summarizes the best reported phytoconstituents of garlic that have displayed significant anticancer potential. Allicin is the main sulfur containing active compound, and it produces a large number of allyl sulfur compounds that are oil-soluble and have anticancer properties (Bat-Chen et al., 2010; Chen et al., 2016; Zou et al., 2016; Dhanarasu, 2017). Two different non-volatile organosulfur compounds, L-cysteine sulfoxides and γ-glutamyl-L-cysteine peptides (having γ-glutamyl-S-allyl-L-cysteine), are present in whole, intact garlic cloves. When raw garlic cloves are crushed, mashed, or chewed, an enzyme called alliinase is created. The enzyme alliinase breaks down the amino acid allicin into 2-propenesulfenic acid, releasing pyruvic acid and ammonia in the process. At room temperature, 2-propenesulfenic acid is highly reactive and unstable. Two molecules of 2-propenesulfenic acid spontaneously interact to form allicin and eliminate water (Shukla and Kalra, 2007; Omar and Al-Wabel, 2010; Yun et al., 2014). Diallyl trisulfide (DATS), diallyl disulfide (DADS), allyl methyl sulphide (AMS), and diallyl sulphide (DAS) are some of the organosulfur compounds that are produced when allicin breaks down and are soluble in fat (Shang et al., 2019). It additionally yields ajoene when fermented with organic solvents. To create S-allyl mercapto cysteine (SAMC), allicin can interact with L-cysteine in the body. It was discovered that the skin of garlic contained FO (N-trans-feruloyloctopamine), a hydroxycinnamic acid derivative (Viswanathan et al., 2014; Wu et al., 2015). Natural organoselenium compounds named MSeC (Se-methyl-L-selenocysteine), a derivative of S-methyl cysteine, have been reported in garlic. The dipeptide glutamyl-S-allyl-L-cysteine, which is water soluble, is reported as peptide-glutamyl-L-cysteine. During formation of aged garlic extracts, SAC and SAMC (water-soluble organosulfur compounds) are produced from glutamyl-S-allyl-L-cysteine after prolonged fermentation of crushed garlic in an aqueous solution (Block et al., 1996; Block, 1997). From aged garlic extract, S-benzyl-cysteine (SBC), a structural analog of SAC that is water soluble, was isolated and studied. S-propargyl-cysteine (SPRC) is a derivative of SAC, an H_2S donor has been prepared from garlic extract (Rose et al., 2005; Rose et al., 2019).

3 Anti-cancer efficacy of garlic extracts and their nanoformulations in breast carcinoma

The most common neoplasm in women worldwide, in both industrialized and developing nations, is breast cancer. Over 2 million new cases of female breast cancer are anticipated, along with 684,996 cancer-related fatalities worldwide in 2020. Among women, it is the primary cause of cancer and the most frequently diagnosed type. The invasion and proliferation of breast cancer have been lessened by using available therapeutics such as chemotherapy, hormone therapy, radiation therapy, and surgery. Lipodox™, Doxil™ (pegylated liposomal doxorubicin), and Abraxane™ (nanoparticulate albumin-based paclitaxel therapeutic) have been clinically utilized as a potent component of current combinatorial chemotherapies against triple negative breast cancer over conventional drug therapies. Myocet liposomal™ (non-pegylated liposome) has been approved for its usage in triple negative breast cancer along with vinorelbine or cyclophosphamide. Taxol™ (carrier free paclitaxel solution) with Cremophor EL has also got approval for its usage triple negative breast cancer (Ghanbari-Movahed et al., 2021; Ghosh et al., 2021; Miguel et al., 2022). However, these therapies still associated with life threatening toxicities.

Garlic is recognized to have potent anticancer efficacy due to the presence of several organic and sulfur components. These compounds affect multiple stages of cancer cell proliferation, development, growth, migration, invasion, and metastasis by interfering with cell cycle regulation, inhibiting cell signaling pathways, apoptosis induction, autophagy, and antioxidant potential (Shang et al., 2019; Zhang et al., 2020; De Greef et al., 2021). The sulfur compounds in garlic are both fat- and water-soluble and demonstrate anticancer effects by reducing oxidative stress, metabolizing carcinogens, and boosting immune response (Miroddi et al., 2011; Lan et al., 2013). The therapeutic potential of garlic nanoformulations was higher than that of the photo component alone. For instance, allicin nanoparticles showed a stronger anti-angiogenesis impact than allicin by itself (Shafeeque and Hashim, 2018). In addition to providing targeted drug delivery, the use of NDDSs for drug delivery can in-crease the bioavailability of medications that are poorly water-soluble, allow for the co-delivery of several medications, prevent drug toxicity in normal cells, and extend the duration of therapeutic activity. In order to show their potential anticancer actions, nanoformulations have been used to deliver parent chemicals directly to the crucial locations of the malignant tissues. Nanoscale materials are used as carriers for delivering medications to their sites of action in NDDSs, which is a

rapidly evolving field of science. ROS and cytotoxicity investigation revealed enhanced antitumor potential of DADS when incorporated with solid lipid nanoparticles in comparison to DADS-free drug in breast cancer cells (Nkrumah-Elie et al., 2012). The anticancer potential of key constituents of garlic extracts, and their nanoformulations should therefore be thoroughly studied. The growth of MCF-7 human breast cancer cells was inhibited by an aqueous preparation of allicin and garlic powder. Growth arrest of cancer cells in G2/M or G0/G1 phase of cell cycle were reported in conjunction with growth inhibition. The growth-inhibitory impact of allicin was closely related to the reduction in intracellular glutathione (GSH) levels in both MCF-7 (luminal-A) and HCC-70 (triple-negative) breast cancer cells (Hirsch et al., 2000; Chen et al., 2016; Rosas-González et al., 2020). While both alliin and allicin reduced cell viability of MCF-7 (luminal-A) and HCC-70 (triple-negative) breast cancer cells, allicin showed more pronounced cytotoxicity and antiproliferative activity in both cells by lowering mitochondrial membrane potential, apoptotic induction, and enhanced expression level of various caspases. Additionally, it increased the expression level of proapoptotic proteins (p21, Noxa, and Bak) while downregulated the expression level of Bcl-xL antiapoptotic protein (Tsubura et al., 2011; Milczarek, 2020; Fatima et al., 2021; Catanzaro et al., 2022). In contrast to allicin, alliin caused senescence in both MCF-7 (luminal-A) and HCC-70 (triple-negative) breast cancer cells in a dose dependent manner (Farhat et al., 2021).

Oil-soluble components from garlic, namely, DAS, DADS, and DATS, significantly reduced the proliferation of CMT-13 (canine mammary tumor) cells in comparison to water soluble organosulfur compounds. While DATS was cytotoxic, DAS and DADS were cytostatic. The cancer-suppressing potency was enhanced with an increase in intracellular GSH levels in addition to the number of sulfur atoms (Sundaram and Milner, 1993; Nakagawa et al., 2001; Lei et al., 2008). DADS also showed cytotoxicity toward the MCF-7 (ER-positive human breast cancer) cells, T47D (differentiated epithelial sub strain), KPL-1 (created from the malignant effusion of a breast cancer patient), MDA-MB-231 and MKL-F (ER-negative) human breast cancer cells (Altonsy et al., 2012; Na et al., 2012; Hahm et al., 2021). In MDA-MB-231 cells, it resulted in cell cycle arrest (sub-G1 phase) and apoptotic induction. This was accompanied by modulations in the expression levels of numerous proteins such as Bax, Bcl-xL, and caspase-3.

DADS presented significant cytotoxicity against MCF-7 cancer cells *via* apoptosis induction, increased PARP and caspase-3 cleavages, activated SAPK/JNK/p38 pathways and suppressed extracellular ERK/MAPK cell signaling pathways (Lei et al., 2008; Jun et al., 2009). Diallyl trisulfide (DATS) treatment significantly increased growth arrest at the G2/M phase in both MCF-7 and MDA-MB-231cells when compared to control cells, which is consistent with the RNA seq findings. In addition, DATS administration dramatically elevated the Ser10 phosphorylation of histone H3 (mitotic marker) in both breast cancer cells. However, DADS did not affect SLIT/ROBO signaling in breast cancer cells (Huang et al., 2015). Annexin V/propidium iodide (PI) staining in DATS-treated MCF-7 cells indicated apoptotic cell death with an increased growth arrest at G0/G1 phase. In MCF-7 cells, DATS triggered the Bcl-2 (anti-apoptotic protein) phosphorylation and the proteolytic cleavage of PARP (poly ADP-ribose polymerase). MCF-7 cells treated with SP600125 (JNK inhibitor) or transiently transfected with dominant-negative JNK experienced a reduction in DATS-induced apoptosis and increased ROS generation. N-acetyl-l-cysteine prevented DATS-induced apoptosis and JNK activation. Additionally, DATS-treated MCF-7 cells demonstrated enhanced AP-1 DNA binding activity, which was suppressed by NAC and the JNK inhibitor. The cells treated with c-jun siRNA were resistant to proteolytic PARP cleavage in DATS treated cancer cells. Female Balb/c mice given 5 mol/kg DATS orally were unable to generate human MCF-7 cell tumor xenografts (Nkrumah-Elie et al., 2012). Altonsy et al. (Altonsy et al., 2012) corroborated these findings and reported that DADS inhibited the growth of MCF-7 carcinoma cells *via* cell cycle arrest at sub-G0 phase and apoptotic induction. Additionally, DADS promoted H4 histone hyperacetylation by inducing phosphatidylserine translocation to modulate Bax, Bcl-xL, Bcl-2, and Bcl-W protein expression levels and caspase-3 activation. Another study reported DADS cytotoxicity toward MCF-7 cells with reduced cell proliferation and apoptosis induction *via* intrinsic signaling pathways associated with upregulated protein (Bax, Bad, and caspases) expression levels and downregulated Bcl-2 protein expression levels (Xiao et al., 2014). DADS treatment further resulted in reduced cell growth of several human triple-negative breast cancer cells (MDA-MB-231, BT-549, and MDA-MB-468) *via* regulating *ß*-catenin signaling pathway. Increased expression of Bax, caspase-3, and caspase-9, as well as decreased levels of Bcl-2, matrix metallo-proteinase-9 (MMP-9), and *ß*-catenin siRNA, were associated with the induction of apoptosis and inhibition of cell proliferation (Malki et al., 2009; Nkrumah-Elie et al., 2012; Li et al., 2018). MDA-MB-231 cells treated with DADS had higher levels of miR-34a expression. The SRC/Ras/ERK signaling pathway was finally blocked by further suppression of SRC expression (Cao et al., 2014). In MCF-10A cells (typical human mammary epithelial cells), DATS reduced the ability of benzo [a]pyrene to cause cancer by preventing cell division, causing cell cycle arrest at the G2/M phase, and inhibiting the production of ROS and DNA damage (Kiesel and Stan, 2017).

DATS treatment induced cell cycle arrest (G2/M phase) and apoptosis, which drastically reduced MCF-7 cell viability and not affected the MCF-12A normal human breast epithelial cells. Enhanced translocation of p53 from the cytoplasm into the nucleus was associated with the activation of apoptosis, along-with upregulation of the Bax and p53 protein expression levels. Akt and Bcl-2 protein expression levels were further inhibited, whereas FAS and cyclin D1 protein expression levels were elevated (Liu et al., 2017). Cancer stem cells (CSCs) from the MCF-7 and SUM159 cell lines of two human breast cancers were used to create tumor spheres, however, DATS blocked this by lowering the levels of numerous proteins CD44, ALDH1A1, Nanog, and Oct4. Apoptosis was found to inhibit cell proliferation *via* modulating Bax, caspases, cyclin D1, Bcl-2, caspases and proliferating cell nuclear antigen (PCNA) expression levels. Further it has been shown that DATS inhibited the aberrant cell signaling pathway associated with carcinogenesis such as Wnt/β-catenin (regulator of breast CSCs). Exposure of DATS in breast cancer cells has enhanced c-Myc and GSK-3β expression levels while downregulated the expression levels of

phospho-glycogen synthase kinase-3β (p-GSK-3β), and ß-catenin (Johnston, 2010).

Kim and colleagues noted downregulation of numerous cell components including that Forkhead transcription factor Forkhead box Q1 (FoxQ1) protein, Dachshund homolog 1 (DACH1) and aldehyde dehydrogenase 1 (ALDH1) in DATS-mediated CSC suppression. Trx-1 expression and Trx-1 reductase enzyme activity were decreased by DATS in breast cancer cells (MDA-MB-231, ZR-75–1, Hs578T, and MCF-7) (Malla et al., 2021). The cysteine residues in thioredoxin-1 (redox-active disulfide/dithiol) containing 12kD protein, are converted to an oxidized disulfide bond (intra-molecular Trx-1-S2) configuration through a chemical process. Trx-1, which is released by tumor cells, speeds up the growth of tumors and reduces patient survival. Trx1 overexpression in tumor cells caused the JNK/p38 signaling pathway-associated apoptosis signal-regulating kinase 1 (ASK1) expression to be suppressed, which in turn suppressed apoptosis. Another study revealed DATS mediated growth inhibition of MDA-MB-231, MCF10A-H-Ras, and MCF-7 breast cancer cells by reducing secretases expression levels such as ADAM-17 and ADAM-10 (a disintegrin and metalloprotease-10), that are linked to the activated Notch signaling pathway. Additionally, it inhibited Jagged-2 and Jagged-1 (Notch ligands) associated with activated Notch signaling pathway (Kim et al., 2016).

DATS reduced transforming growth factor-β1 (TGF-β1) and thromboxane B2 (TXB2) production *via* blocking platelet activation and aggregation (by platelet-activating factor), and hence resulted in inhibition of platelet-mediated hematogenous metastasis of MDA-MB-231 cells (Hahm and Singh, 2014; Liu et al., 2015; Li et al., 2020). DATS suppressed ER-protein levels, a novel target of the drug in two potent breast cancer cells, MCF-7 and T47D. Along with reduced nuclear ER-protein levels and inhibition of ER-mRNA, the expression levels of cyclin D1 and pS2 were also downregulated. DATS treatment also resulted in downregulation of overexpressed Peptidyl-prolyl cis-trans isomerase (Pin1), which further restrained the activity of ERE2e1b-luciferase reporter (Sigounas et al., 1997). By suppressing mRNA expression levels of Bcl-2, cyclin D1, Bcl-xL, MMP-2, and vascular endothelial growth factor (VEGF) in MDA-MB-231 and MCF-7 breast cancer cells, DATS intervention significantly reduced leptin-induced cell proliferation, clonogenic cell viability, invasion and migration potential. DATS also displayed a strong antimetastatic effect by reducing MMP-2/9 expression levels in triple-negative breast cancer cells (HS 578t and MDA-MB-231 cells) and ultimately blocked both the NF-κB and ERK/MAPK signaling pathway (Ip et al., 1992; Zhang et al., 2014). In MCF-7 cells, DATS treatment induced ROS mediated apoptosis and subsequent activation of AP-1 and JNK, together with enhanced ROS accumulation (Cao et al., 2014).

Another *in vivo* study reported reduced STAT3 expression levels in DATS treated breast cancer xenografts in mice. Further, DATS treatment decreased the incidences of breast cancers in xenografted MDA-MB-231 tumor models *via* reducing MMP-2 and -9 expression levels (Wei et al., 2017; Liu et al., 2018; Vijayakumar et al., 2019). DATS (natural histone deacetylase inhibitor) treatment prevented the MDA-MB-231 hypoxia-inducing cell metastasis in embryonic zebrafish tumor model *via* blocking the HIF-1 transcriptional activity. Furthermore, it reduced EMT-related proteins (Slug, MMP-2 and Snail), VEGF-A and L1CAM protein expression levels. In female ACI rats (an inbred line derived from a cross between Copenhagen and August strains), DAS reduced the concentrations of diethylstilbestrol (DES)-induced lipid hydroperoxides (Selvan et al., 2018).

SAMC, a stable organosulfur derivative from garlic, displayed potent anti-proliferative properties against MCF-7 breast cancer cells (Sigounas et al., 1997). MCF-7 and MDA-MB-231 cells displayed potent growth inhibition after SAMC treatment due to increased p21 and p53 expression levels, induction of apoptosis, cell cycle arrest (G0/G1 phase), increased caspase-9, and caspase-3 expression levels in relation to the mitochondrial apoptotic pathway, reduced Bcl-xL and Bcl-2 expression levels. SAC dramatically slowed the development of MDA-MB-231 breast carcinoma cells in a dose and time dependent manner. Increased E-cadherin expression and decreased MMP-2 expression levels in MDA-MB-231 cells after SAC therapy imply that cell proliferation, adhesion, and invasion are inhibited, which helps to prevent metastasis.

Using a rat model of DMBA-induced mammary tumors, it is shown that the use of garlic powder successfully inhibited the growth of tumors and validated the fact that DADS has been more active than AMS and DAS. According to Schaffer et al., supplementation with garlic powder, SAC, and DADS reduced the incidence of mammary cancer in rats, hence preventing the development of mammary carcinogenesis brought on by N-methyl-N-nitrosourea (MNU) (Schaffer et al., 1996; Petrovic et al., 2018; Xiong et al., 2018). 67NR breast cancer cell, which was implanted in mammary pads of BALB/c mice, demonstrated anticancer activity by being inhibited by garlic extract. Additionally, by reducing the DMBA-DNA interaction to lower the incidence of mammary tumors, in the long run, garlic powder prevented DMBA-induced mammary cancer tumors in rats. Among the numerous organosulfur compounds, garlic compounds that are oil-soluble have been shown in rodents to have stronger anticancer action than those that are water-soluble. DMBA, 2-amino-1-methyl-6-phenylimidazo [4,5-b] pyridine (PhIP) and MNU induced mammary cancer in rats were significantly inhibited by DADS (Zhang et al., 2014). After subcutaneous injection of MCF-7 and MDA-MB-231 cells in nude mice xenograft tumor models were created that showed anticancer and antiproliferative behavior from DADS. DADS treatment lead to the activation of tristetraprolin expression and significant downregulation of MMP-9 protein and urokinase-type plasminogen activator expression (Nakagawa et al., 2001). DADS demonstrated reduced growth proliferation by reducing initial tumor weight in female nude mice (with orthotopic transplantation, KPL-1), resulting in growth inhibition in human breast cancer cells (*in vitro* and *in vivo*) (Yi and Su, 2013; Kim et al., 2020). Table 2 summarizes the mechanism of garlic and its constituents by which they slow anticancer activity against breast cancer cells.

Despite strong anticancer activity of various garlic derived plant therapeutics, these compounds suffer from oral bioavailability and off target toxicity. Therefore, several nanoformulations have been tried to improve the bioavailability of these compounds. Garlic extracts contain anticancer chemicals can combine to generate nano-conjugates that can help stop the spread of cancer cells. When administered at a concentration of 100 g/mL, garlic clove extract-mediated silver nanoparticles (G-AgNPs) displayed

TABLE 2 Anticancer effects of garlic constituents on breast cancer.

Components of garlic	Mechanism of action	References
DATS	• DATS treatment induced apoptosis in MCF-7 cells with Bax (pro-apoptotic protein) and p53 induction and offered a potent strategy for breast cancer management	Hahm and Singh (2014)
	• Apoptotic induction *via* reducing peptidyl-prolyl cis–trans isomerase (Pin1) protein expression level in T47D and MCF-7 cells	Liu et al. (2015)
	• Inhibited metastasis and MMP2/9 activity of TNBC cells *via* down-regulating transcriptional activities of ERK/MAPK and NF-κB signaling pathways	Kim et al. (2016)
	• Inhibition of leptin induced oncogenic signaling in MCF-7 and MDA-MB-231 *via* reducing STAT3 protein expression	Liu et al. (2018)
	• Inhibited the Trx-1 expression and enzymatic activity of Trx reductase in breast cancer cells	Wei et al. (2017)
	• Inhibited HIF-1α transcriptional activity and hypoxia-induced hematogenous metastasis in a dose-dependent manner in MDA-MB-231 cells. Induced ROS production and apoptotic cell death in MCF-7 and MDA-MB-231 breast cancer cells	Chandra-Kuntal et al. (2013)
SAMC (aged garlic)	Displayed growth inhibitory potential in MCF-7 breast cancer cells	Sigounas et al. (1997)
DADS	DADS alienated the efficacy of linoleic acid (breast cancer cell stimulator) and synergized the efficacy of eicosapentaenoic acid (breast cancer cell suppressor) in MDA-MB-231 cells thereby projecting it as a strong modulator of breast cancer cell proliferation	Nakagawa et al. (2001)
Diallyl disulfide	Prevented mammary cancer growth in female rats	Ip et al. (1992)
Ajoene	Induced growth arrest and apoptosis *via* targeting protein folding in the endoplasmic reticulum of in MDA-MB-231 cancer cells	Kaschula et al. (2016)

cytotoxic action against the MCF-7 cell line. Additionally, it affected the nucleus morphology of MCF-7 cells, causing cell clumping and membrane instability (Menon et al., 2012). G-AgNPs did not cause any toxicity or mortality in neonates of *Corylus cornuta*. In a different study, garlic extract-mediated silver nanoparticles (Ag-S2) caused cytotoxicity in the MCF-7 cancer cell line by reducing cell viability in a concentration-dependent manner (Ahamed et al., 2022). Nevertheless, MCF-7 cells were not toxicated by the gold nanoparticles (G-AuNPs) produced by garlic extract. Superparamagnetic hematite nanoparticles made from garlic extract were synthesized, and their cytotoxicity against the breast cancer MCF-7 cell line was examined. The findings imply that at an IC_{50} of 346.25 mg/mL, the cell proliferation was inhibited in a dose responsive manner (Talluri et al., 2017). Even ZnO-reduced graphene oxide nanocomposites (ZnO-RGO NCs) made from the extract of garlic cloves showed increased cytotoxicity against MCF-7 cells (Kim et al., 2020). DADS nanoparticles (solid lipid) demonstrated higher cytotoxicity than DADS alone against MCF-7 carcinoma cells by inducing apoptosis (*via* intrinsic signaling pathway) associated with elevated expression levels of Bax, Bad, caspase-3, and caspase-9, and decreased protein expression level of Bcl-2 (Lee et al., 2015). Figure 1 presents a proposed pathway for garlic induced apoptosis in breast cancer.

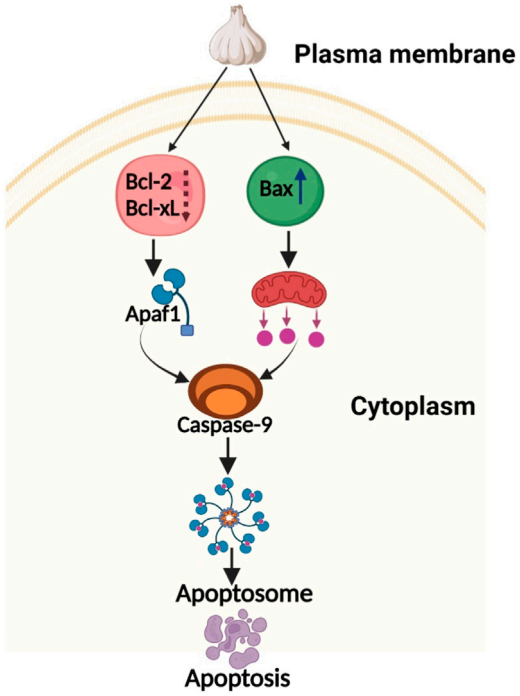

FIGURE 1
Proposed pathway for garlic induced apoptosis in breast cancer.

4 Clinical trials of garlic products and constituents in breast cancer

Five grams of crushed garlic (raw) enhanced the expression of several genes, including the proto-oncogene c-Jun, the aryl hydrocarbon receptor, nuclear translocator, HIF-1A (hypoxia-inducible factor 1A), oncostatin M (OSM), and the viral oncogene homolog (V-rel avian reticuloendotheliosis) in a clinical investigation involving 17 volunteers. These findings indicated that garlic components are multifaceted and comprise activation of genes associated with immunity, xenobiotic

metabolism, and apoptosis in humans and Mono Mac six cells. (Charron et al., 2015). Similar findings were made in clinical research that involved 20 cancer patients and found that raw garlic and allicin had cytotoxic effects against a variety of cancer types (Bespalov et al., 2004). Garlic supplements were reported beneficial in the management of breast cancer (benign) patients, where they resulted in the suppression of breast fibromatosis. Furthermore, garlic intake also reduced docetaxel removal in patients having CYP3A5*1A allele (Zuniga et al., 2019). Garlic consumption can be increased to promote health, according to a randomized controlled trial of breast cancer survivors (Ishikawa et al., 2006). A dose of four capsules per day for 12 weeks of aged garlic extract (AGE) treatment significantly enhanced number of natural killer (NK) cells and its activity in patients with advanced lung, colon, pancreatic and liver cancer. Each capsule included 500 mg of AGE, 11 mg of sucrose fatty acid ester and 727 mg of crystalline cellulose. Respective doses were ceased after 12 weeks, with a follow-up after further 12 weeks to monitor the number of NK cells and its activity (Tanaka et al., 2006). Additionally, aged garlic extract inhibited cell growth and minimized the occurrence of human colorectal adenoma *via* modulating numerous cell signaling path-ways (Millen et al., 2007). Raw garlic consumption (five pyramid doses per day) for a duration of 12 months, with a follow-up after 12 months, was found to lessen the risk of colorectal adenoma in a randomized controlled trial on 57,560 patients (Ma et al., 2012).

Long-term garlic supplementation was further associated with reduced risk of mortality in patients with stomach cancer. For a period of 7 years, a dosage of 200 mg of aged garlic extract and 1 mg of steam-distilled garlic oil was administered twice daily. In this randomized intervention study, 3,365 participants were used to investigate the incidence and mortality of stomach cancer using a 2 2 factorial design. Follow-up period is initially 7.3 years, and it is later extended to 22.3 years (Li et al., 2019; Guo et al., 2020). Garlic supplementation had more pronounced protective impact on gastric cancer prevention when combined with abstinence from alcohol. This randomized clinical trial found a relationship between smoking and an increased risk of gastric cancer incidence and death. After a follow-up period of 22.3 years, more pronounced anti cancerous effect was reported after garlic supplementation in gastric cancer when the individuals abstained from alcohol (You et al., 2001). Garlic formulations slowed the evolution of pre-cancerous gastric lesion, and examinations of serum samples further demonstrated that participants in the participating treatment groups had significantly greater S-allyl cysteine (SAC) doses (Zhang et al., 2008). Allicin was injected into the lesion site of individuals with gastric cancer *via* a gastroscopy in a different study that involved a randomized controlled trial with 80 participants. The medication was given to the patient 48 h before surgery.

Laboratory testing of the gastric cancer tissue removed after gastrectomy demonstrated that allicin had the ability to impede cancer cell proliferation *via* apoptotic induction, cell cycle arrest (at G0/G1 phase) and modulated Bax and Fas (upregulated), Bcl-2 (downregulated) expression levels (Gatt et al., 2015). Allin and allicin, two garlic constituents, have been shown to protect patients against the side effects of chemotherapy (including febrile neutropenia). This was frequently seen in chemotherapy patients with hematological malignancies. Patients who participated in a 101-patient randomized controlled experiment received two doses of 450 mg of allicin and allin daily. The patients were monitored daily until the neutropenia was resolved by incessant monitoring of complete blood count (CBC) (Tilli et al., 2003). In another clinical trial, aqueous garlic extract showed preventive properties against prostate carcinoma by increasing flow and frequency of urine. Despite the fact that the follow-up period was unreported, the trial was carried out on 27 patients (daily dose of 1 mL/kg body weight) for 30 days. A study using 21 patients found that the active ingredient in garlic, ajoene, had anticancer properties against skin cancer. The tumor size was reduced after topical application of 0.4% ajoene cream (400 mg ajoene, 0.3 ml sorbitonoleate and 0.3 ml polysorbate 80 in 100 ml 1% of carbomeric gel) as shown by activated apoptotic pathways and modulated Bcl-2 expression levels (Shashikant et al., 1985).

Evaluation of dietary supplements and medications used for health purposes requires documentation of their efficacy and safety. The ways of processing garlic can influence its effectiveness and safety. However, there is no recommended everyday garlic in-take, the German Commission E monograph from 1988 advised that a per day intake of 12 cloves (or about 4 g) of garlic is good for human health. Fresh garlic, garlic oil, garlic powder, and AGE are the four main categories into which commercially produced garlic preparations fall. Even though garlic has been reported safe when used as a complementary (or condiment) agent, safety concerns still need to be addressed. There are three things to keep in mind when using garlic: a) allicin remains one of the key irritant in raw garlic; b) oil-soluble OSCs reported to be more toxic in comparison to water-soluble OSCs and c) toxicity associated with OSCs becomes much less harmful over time. When allicin was administered directly into the intestinal tract of rats, the intestinal linings were harmed and the gut flora was altered using enteric-coated garlic products. The mucosal epithelial membrane may become damaged by fresh garlic (Amagase et al., 2001; Macan et al., 2006). A number of studies, including those for teratogenicity, mutagenicity, acute and subacute toxicity, and chronic toxicity, have shown that AGE is relatively safe. Recent clinical trials demonstrated that, when used as a supplemental drug, AGE was safe for patients receiving warfarin therapy (Song and Milner, 2001). Because there are so many different garlic preparations available, the medicinal consequences are also diverse, suggesting that some preparations could have negative effects. A monograph that outlines the process and requirements for AGE has been created by the U.S. Pharmacopoeia and other organizations. Garlic preparations should be consumed while considering their potential side effects, metabolism, drug-synergistic interactions, interference with vital enzymes, and impact on normal microflora. Consumers could make better decisions if labels included recommendations based on laboratory and clinical findings. Additionally, the anticancer properties of uncrushed garlic will be reduced when heated in the microwave or oven (Nakagawa et al., 2001; Mondal et al., 2022). Garlic has been shown to have anticancer properties by obstructing various phases of carcinogenesis. The nutritional or chemopreventive benefits of garlic, however, go far beyond the idea that it has therapeutic effects against cancer. To investigate the novel properties of garlic, more carefully planned experiments and trials are needed. (Hirsch et al., 2000).

5 Conclusion

Garlic contains bioactive substances that have substantial anticarcinogenic effects *via* a number of pathways, including cell cycle arrest, apoptosis, and stimulation of the angiogenic cascade. The nutritional and therapeutic benefits of garlic have been well-known. Among the numerous phytoconstituents of garlic, certain compounds, including SAC, allicin, DAS, SAMC, DATS, and DADS have strong anti-cancer activity. Derivatives of garlic and their nanoformulations resulted in altered expression levels of numerous re-ported genes associated with the regulation of several important signaling pathways, including the JNK, Akt/PI3K, p38, MAPK, EMT, Wnt, p53, ERK1/2, NF-κB, Nrf2, STAT3 and Chk1/cyclin B1 in human breast carcinoma. In a variety of preclinical cancer models, bioactive constituents of garlic and their nanoformulations decreased the cell proliferation, adhesion, apoptosis evasion, migration, invasion, and metastasis of several cancer types. While several signaling pathways have been targeted by various researchers for investigating the mechanism behind the anticancer efficacy of garlic phytocomponents, additional research is still required to fully comprehend these molecular targets of garlic and their derivatives inside diverse organ systems. Paucity of well-studied, potent clinical studies and thorough safety assessment, despite promising preclinical research on the anticancer potential of garlic components, increases the desire for additional clinical research. The nanoformulations of garlic demonstrated some efficient delivery methods with enhanced bioavailability. The efficacy of nanoparticles formulations of garlic constituents in the treatment of breast cancer was higher than compounds alone. However, more investigations are still needed to decipher the therapeutic potential of garlic components *via* utilizing crucial targets of cell signaling pathways for better management of human breast cancer in addition to well-controlled clinical investigations. Altogether, in this review, we have demonstrated the anticancer potential of garlic phytoconstituents and its nanoformulations as beneficial nutraceuticals and pharmaceuticals for the efficient management of human breast cancer.

Author contributions

Conceptualization, PP, FK, FA, and MS; writing—original draft preparation, PP and FK; writing—review and editing, MS, FA, NA, and AS; visualization, MS, NA, and AS; supervision, MS, NA, and AS; project administration, MS, NA, and AS All authors have read and agreed to the published version of the manuscript.

Funding

This research has been funded by Scientific Research Deanship at University of Hail - Saudi Arabia through project number MDR-22 030.

Conflict of interest

The authors declare that the research was conducted in the absence of any commercial or financial relationships that could be construed as a potential conflict of interest.

Publisher's note

All claims expressed in this article are solely those of the authors and do not necessarily represent those of their affiliated organizations, or those of the publisher, the editors and the reviewers. Any product that may be evaluated in this article, or claim that may be made by its manufacturer, is not guaranteed or endorsed by the publisher.

Supplementary material

The Supplementary Material for this article can be found online at: https://www.frontiersin.org/articles/10.3389/fphar.2023.1154034/full#supplementary-material

References

Ahamed, M., Akhtar, M. J., Khan, M. M., and Alhadlaq, H. A. (2022). Facile green synthesis of ZnO-RGO nanocomposites with enhanced anticancer efficacy. *Methods* 199, 28–36. doi:10.1016/j.ymeth.2021.04.020

Altonsy, M. O., Habib, T. N., and Andrews, S. C. (2012). Diallyl disulfide-induced apoptosis in a breast-cancer cell line (MCF-7) may be caused by inhibition of histone deacetylation. *Nutr. cancer* 64 (8), 1251–1260. doi:10.1080/01635581.2012.721156

Amagase, H., Petesch, B. L., Matsuura, H., Kasuga, S., and Itakura, Y. (2001). Intake of garlic and its bioactive components. *J. Nutr.* 131 (3), 955S–962S. doi:10.1093/jn/131.3.955S

Ansary, J., Forbes-Hernández, T. Y., Gil, E., Cianciosi, D., Zhang, J., Elexpuru-Zabaleta, M., et al. (2020). Potential health benefit of garlic based on human intervention studies: A brief overview. *Antioxidants* 9 (7), 619. doi:10.3390/antiox9070619

Basmadjian, C., Zhao, Q., Bentouhami, E., Djehal, A., Nebigil, C. G., Johnson, R. A., et al. (2014). Cancer wars: Natural products strike back. *Front. Chem.* 2, 20. doi:10.3389/fchem.2014.00020

Bat-Chen, W., Golan, T., Peri, I., Ludmer, Z., and Schwartz, B. (2010). Allicin purified from fresh garlic cloves induces apoptosis in colon cancer cells via Nrf2. *Nutr. cancer* 62 (7), 947–957. doi:10.1080/01635581.2010.509837

Bespalov, V. G., Niu, B., Ivanova, O. A., Krzhivitskiĭ, P. I., Semiglazov, V. F., Aleksandrov, V. A., et al. (2004). Study of an antioxidant dietary supplement" Karinat" in patients with benign breast disease. *Vopr. Onkol.* 50 (4), 467–472.

Block, E., Cai, X. J., Uden, P. C., Zhang, X., Quimby, B. D., and Sullivan, J. J. (1996). Allium chemistry: Natural abundance of organoselenium compounds from garlic, onion and related plants and in human garlic breath. *Pure Appl. Chem.* 68 (4), 937–944. doi:10.1351/pac199668040937

Block, E. (1997). "Organoselenium and organosulfur phytochemicals from genus allium plants (onion, garlic): Relevance for cancer protection," in *Food factors for cancer prevention* (Tokyo: Springer), 215–221.

Cao, M., Hou, D., Liang, H., Gong, F., Wang, Y., Yan, X., et al. (2014). miR-150 promotes the proliferation and migration of lung cancer cells by targeting SRC kinase signalling inhibitor 1. *Eur. J. cancer* 50 (5), 1013–1024. doi:10.1016/j.ejca.2013.12.024

Catanzaro, E., Canistro, D., Pellicioni, V., Vivarelli, F., and Fimognari, C. (2022). Anticancer potential of allicin: A review. *Pharmacol. Res.* 177, 106118. doi:10.1016/j.phrs.2022.106118

Chandra-Kuntal, K., Lee, J., and Singh, S. V. (2013). Critical role for reactive oxygen species in apoptosis induction and cell migration inhibition by diallyl trisulfide, a cancer chemopreventive component of garlic. *Breast cancer Res. Treat.* 138 (1), 69–79. doi:10.1007/s10549-013-2440-2

Charron, C. S., Dawson, H. D., Albaugh, G. P., Solverson, P. M., Vinyard, B. T., Solano-Aguilar, G. I., et al. (2015). A single meal containing raw, crushed garlic influences expression of immunity- and cancer-related genes in whole blood of humans. *J. Nutr.* 145 (11), 2448–2455. doi:10.3945/jn.115.215392

Chen, F., Li, H., Wang, Y., Gao, M., Cheng, Y., Liu, D., et al. (2016). Inhibition of allicin in Eca109 and EC9706 cells via G2/M phase arrest and mitochondrial apoptosis pathway. *J. Funct. Foods* 25, 523–536. doi:10.1016/j.jff.2016.06.027

De Greef, D., Barton, E. M., Sandberg, E. N., Croley, C. R., Pumarol, J., Wong, T. L., et al. (2021). Anticancer potential of garlic and its bioactive constituents: A systematic and comprehensive review. *Seminars cancer Biol.* 73, 219–264. doi:10.1016/j.semcancer.2020.11.020

Dhanarasu, S. (2017). Protective role of allicin (diallyl thiosulfinate) on cell surface glycoconjugate moieties in 7, 12-dimethylbenz (a) anthracene-induced oral carcinogenesis. *Trop. J. Pharm. Res.* 16 (8), 1797–1804. doi:10.4314/tjpr.v16i8.7

Dorant, E., van den Brandt, P. A., Goldbohm, R. A., Hermus, R. J., and Sturmans, F. (1993). Garlic and its significance for the prevention of cancer in humans: A critical view. *Br. J. cancer* 67 (3), 424–429. doi:10.1038/bjc.1993.82

El-Saber Batiha, G., Magdy Beshbishy, A., Wasef, G. L., Elewa, Y. H., Al-Sagan, A. A., Abd El-Hack, M. E., et al.(2020). Chemical constituents and pharmacological activities of garlic (allium sativum L.): A review. *Nutrients* 12 (3), 872. doi:10.3390/nu12030872

Farhat, Z., Hershberger, P. A., Freudenheim, J. L., Mammen, M. J., Hageman Blair, R., Aga, D. S., et al. (2021). Types of garlic and their anticancer and antioxidant activity: A review of the epidemiologic and experimental evidence. *Eur. J. Nutr.* 60 (7), 3585–3609. doi:10.1007/s00394-021-02482-7

Fatima, N., Baqri, S. S. R., Alsulimani, A., Fagoonee, S., Slama, P., Kesari, K. K., et al. (2021). Phytochemicals from Indian ethnomedicines: Promising prospects for the management of oxidative stress and cancer. *Antioxidants* 10 (10), 1606. doi:10.3390/antiox10101606

Gatt, M. E., Strahilevitz, J., Sharon, N., Lavie, D., Goldschmidt, N., Kalish, Y., et al. (2015). A randomized controlled study to determine the efficacy of garlic compounds in patients with hematological malignancies at risk for chemotherapy-related febrile neutropenia. *Integr. Cancer Ther.* 14 (5), 428–435. doi:10.1177/1534735415588928

George, B. P., Chandran, R., and Abrahamse, H. (2021). Role of phytochemicals in cancer chemoprevention: Insights. *Antioxidants* 10 (9), 1455. doi:10.3390/antiox10091455

Ghanbari-Movahed, M., Kaceli, T., Mondal, A., Farzaei, M. H., and Bishayee, A. (2021). Recent advances in improved anticancer efficacies of camptothecin nano-formulations: A systematic review. *Biomedicines* 9 (5), 480. doi:10.3390/biomedicines9050480

Ghosh, S., Javia, A., Shetty, S., Bardoliwala, D., Maiti, K., Banerjee, S., et al. (2021). Triple negative breast cancer and non-small cell lung cancer: Clinical challenges and nano-formulation approaches. *J. Control. Release* 337, 27–58. doi:10.1016/j.jconrel.2021.07.014

Guo, Y., Li, Z. X., Zhang, J. Y., Ma, J. L., Zhang, L., Zhang, Y., et al. (2020). Association between lifestyle factors, vitamin and garlic supplementation, and gastric cancer outcomes: A secondary analysis of a randomized clinical trial. *JAMA Netw. open* 3 (6), e206628. doi:10.1001/jamanetworkopen.2020.6628

Hahm, E. R., and Singh, S. V. (2014). Diallyl trisulfide inhibits estrogen receptor-α activity in human breast cancer cells. *Breast cancer Res. Treat.* 144 (1), 47–57. doi:10.1007/s10549-014-2841-x

Hahm, E. R., Kim, S. H., Mathan, S. V., Singh, R. P., and Singh, S. V. (2021). Mechanistic targets of diallyl trisulfide in human breast cancer cells identified by RNA-seq analysis. *J. Cancer Prev.* 26 (2), 128–136. doi:10.15430/JCP.2021.26.2.128

Hirsch, K., Danilenko, M., Giat, J., Miron, T., Rabinkov, A., Wilchek, M., et al. (2000). Effect of purified allicin, the major ingredient offreshly crushed garlic, on cancer cell proliferation. *Nutr. cancer* 38 (2), 245–254. doi:10.1207/S15327914NC382_14

Huang, J., Yang, B., Xiang, T., Peng, W., Qiu, Z., Wan, J., et al. (2015). Diallyl disulfide inhibits growth and metastatic potential of human triple-negative breast cancer cells through inactivation of the β-catenin signaling pathway. *Mol. Nutr. food Res.* 59 (6), 1063–1075. doi:10.1002/mnfr.201400668

Ip, C., Lisk, D. J., and Stoewsand, G. S. (1992). Mammary cancer prevention by regular garlic and selenium-enriched garlic. *Nutr. Cancer* 17, 279. doi:10.1080/01635589209514197

Ishikawa, H., Saeki, T., Otani, T., Suzuki, T., Shimozuma, K., Nishino, H., et al. (2006). Aged garlic extract prevents a decline of NK cell number and activity in patients with advanced cancer. *J. Nutr.* 136 (3), 816S–820S. doi:10.1093/jn/136.3.816S

Johnston, S. R. (2010). New strategies in estrogen receptor–positive breast cancer. *Clin. Cancer Res.* 16 (7), 1979–1987. doi:10.1158/1078-0432.CCR-09-1823

Jun, Z., Suzuki, M., Xiao, J., Wen, J., Talbot, S. G., Li, G. C., et al. (2009). Comparative effects of natural and synthetic diallyl disulfide on apoptosis of human breast-cancer MCF-7 cells. *Biotechnol. Appl. Biochem.* 52 (2), 113–119. doi:10.1042/BA20070242

Kaschula, C. H., Hunter, R., Cotton, J., Tuveri, R., Ngarande, E., Dzobo, K., et al. (2016). The garlic compound ajoene targets protein folding in the endoplasmic reticulum of cancer cells. *Mol. Carcinog.* 55 (8), 1213–1228. doi:10.1002/mc.22364

Kiesel, V. A., and Stan, S. D. (2017). Diallyl trisulfide, a chemopreventive agent from Allium vegetables, inhibits alpha-secretases in breast cancer cells. *Biochem. biophysical Res. Commun.* 484 (4), 833–838. doi:10.1016/j.bbrc.2017.01.184

Kim, S. H., Kaschula, C. H., Priedigkeit, N., Lee, A. V., and Singh, S. V. (2016). Forkhead box Q1 is a novel target of breast cancer stem cell inhibition by diallyl trisulfide. *J. Biol. Chem.* 291 (26), 13495–13508. doi:10.1074/jbc.M116.715219

Kim, S. H., Hahm, E. R., Singh, K. B., and Singh, S. V. (2020). Diallyl trisulfide inhibits leptin-induced oncogenic signaling in human breast cancer cells but fails to prevent chemically-induced luminal-type cancer in rats. *J. cancer Prev.* 25 (1), 1–12. doi:10.15430/JCP.2020.25.1.1

Lan, X. Y., Sun, H. Y., Liu, J. J., Lin, Y., Zhu, Z. Y., Han, X., et al. (2013). Effects of garlic oil on pancreatic cancer cells. *Asian Pac. J. Cancer Prev.* 14 (10), 5905–5910. doi:10.7314/apjcp.2013.14.10.5905

Lee, G. Y., Lee, J. J., and Lee, S. M. (2015). Antioxidant and anticoagulant status were improved by personalized dietary intervention based on biochemical and clinical parameters in cancer patients. *Nutr. cancer* 67 (7), 1083–1092. doi:10.1080/01635581.2015.1073754

Lei, X. Y., Yao, S. Q., Zu, X. Y., Huang, Z. X., Liu, L. J., Zhong, M., et al. (2008). Apoptosis induced by diallyl disulfide in human breast cancer cell line MCF-7. *Acta Pharmacol. Sin.* 29 (10), 1233–1239. doi:10.1111/j.1745-7254.2008.00851.x

Li, X., Meng, Y., Xie, C., Zhu, J., Wang, X., Li, Y., et al. (2018). Diallyl Trisulfide inhibits breast cancer stem cells via suppression of Wnt/β-catenin pathway. *J. Cell. Biochem.* 119 (5), 4134–4141. doi:10.1002/jcb.26613

Li, W. Q., Zhang, J. Y., Ma, J. L., Li, Z. X., Zhang, L., Zhang, Y., et al. (2019). Effects of *Helicobacter pylori* treatment and vitamin and garlic supplementation on gastric cancer incidence and mortality: Follow-up of a randomized intervention trial. *bmj* 366, l5016. doi:10.1136/bmj.l5016

Li, H., Xu, F., Gao, G., Gao, X., Wu, B., Zheng, C., et al. (2020). Hydrogen sulfide and its donors: Novel antitumor and antimetastatic therapies for triple-negative breast cancer. *Redox Biol.* 34, 101564. doi:10.1016/j.redox.2020.101564

Liu, Y., Zhu, P., Wang, Y., Wei, Z., Tao, L., Zhu, Z., et al. (2015). Antimetastatic therapies of the polysulfide diallyl trisulfide against triple-negative breast cancer (TNBC) via suppressing MMP2/9 by blocking NF-κB and ERK/MAPK signaling pathways. *PloS one* 10 (4), e0123781. doi:10.1371/journal.pone.0123781

Liu, Y., Zhao, Y., Wang, Y., Zhu, P., Wei, Z., Wang, S., et al. (2017). Suppressive role of diallyl trisulfide in the activated platelet-mediated hematogenous metastasis of MDA-MB-231 human breast cancer cellsfide in the activated platelet-mediated hematogenous metastasis of MDA-MB-231 human breast cancer cells. *Int. J. Mol. Med.* 39 (6), 1516–1524. doi:10.3892/ijmm.2017.2953

Liu, Y., Zhao, Y., Wei, Z., Tao, L., Sheng, X., Wang, S., et al. (2018). Targeting thioredoxin system with an organosulfur compound, diallyl trisulfide (DATS), attenuates progression and metastasis of triple-negative breast cancer (TNBC). *Cell. Physiology Biochem.* 50 (5), 1945–1963. doi:10.1159/000494874

Ma, J. L., Zhang, L., Brown, L. M., Li, J. Y., Shen, L., Pan, K. F., et al. (2012). Fifteen-year effects of *Helicobacter pylori*, garlic, and vitamin treatments on gastric cancer incidence and mortality. *J. Natl. Cancer Inst.* 104 (6), 488–492. doi:10.1093/jnci/djs003

Macan, H., Uykimpang, R., Alconcel, M., Takasu, J., Razon, R., Amagase, H., et al. (2006). Aged garlic extract may be safe for patients on warfarin therapy. *J. Nutr.* 136 (3), 793S–795S. doi:10.1093/jn/136.3.793S

Malki, A., El-Saadani, M., and Sultan, A. S. (2009). Garlic constituent diallyl trisulfide induced apoptosis in MCF7 human breast cancer cells. *Cancer Biol. Ther.* 8 (22), 2175–2185. doi:10.4161/cbt.8.22.9882

Malla, R., Marni, R., Chakraborty, A., and Kamal, M. A. (2021). Diallyl disulfide and diallyl trisulfide in garlic as novel therapeutic agents to overcome drug resistance in breast cancer. *J. Pharm. Analysis* 12, 221–231. doi:10.1016/j.jpha.2021.11.004

Mandal, S. K., Das, A., Dey, S., Sahoo, U., Bose, S., Bose, A., et al. (2019). Bioactivities of Allicin and related organosulfur compounds from garlic: Overview of the literature since 2010. *Egypt. J. Chem.* 62, 0–11. Special Issue (Part 1) Innovation in Chemistry). doi:10.21608/ejchem.2019.15787.1954

Menon, D., Basanth, A., Retnakumari, A., Manzoor, K., and Nair, S. V. (2012). Green synthesis of biocompatible gold nanocrystals with tunable surface plasmon resonance using garlic phytochemicals. *J. Biomed. Nanotechnol.* 8 (6), 901–911. doi:10.1166/jbn.2012.1455

Miguel, R. D. A., Hirata, A. S., Jimenez, P. C., Lopes, L. B., and Costa-Lotufo, L. V. (2022). Beyond formulation: Contributions of nanotechnology for translation of anticancer natural products into new drugs. *Pharmaceutics* 14 (8), 1722. doi:10.3390/pharmaceutics14081722

Milczarek, M. (2020). The premature senescence in breast cancer treatment strategy. *Cancers* 12 (7), 1815. doi:10.3390/cancers12071815

Millen, A. E., Subar, A. F., Graubard, B. I., Peters, U., Hayes, R. B., and Weissfeld, J. L. (2007). Fruit and vegetable intake and prevalence of colorectal adenoma in a cancer screening trial. *Am. J. Clin. Nutr.* 86 (6), 1754–1764. doi:10.1093/ajcn/86.6.1754

Miroddi, M., Calapai, F., and Calapai, G. (2011). Potential beneficial effects of garlic in oncohematology. *Mini Rev. Med. Chem.* 11 (6), 461–472. doi:10.2174/138955711795843293

Mondal, A., Banerjee, S., Bose, S., Mazumder, S., Haber, R. A., Farzaei, M. H., et al. (2022). Garlic constituents for cancer prevention and therapy: From phytochemistry to novel formulations. *Pharmacol. Res.* 175, 105837. doi:10.1016/j.phrs.2021.105837

Na, H. K., Kim, E. H., Choi, M. A., Park, J. M., Kim, D. H., and Surh, Y. J. (2012). Diallyl trisulfide induces apoptosis in human breast cancer cells through ROS-mediated activation of JNK and AP-1. *Biochem. Pharmacol.* 84 (10), 1241–1250. doi:10.1016/j.bcp.2012.08.024

Nakagawa, H., Tsuta, K., Kiuchi, K., Senzaki, H., Tanaka, K., Hioki, K., et al. (2001). Growth inhibitory effects of diallyl disulfide on human breast cancer cell lines. *Carcinogenesis* 22 (6), 891–897. doi:10.1093/carcin/22.6.891

Newman, D. J., and Cragg, G. M. (2012). Natural products as sources of new drugs over the 30 years from 1981 to 2010. *J. Nat. Prod.* 75 (3), 311–335. doi:10.1021/np200906s

Nkrumah-Elie, Y. M., Reuben, J. S., Hudson, A., Taka, E., Badisa, R., Ardley, T., et al. (2012). Diallyl trisulfide as an inhibitor of benzo pyrene-induced precancerous carcinogenesis in MCF-10A cells. *Food Chem. Toxicol.* 50 (7), 2524–2530. doi:10.1016/j.fct.2012.04.010

Noel, B., Singh, S. K., Lillard, J. W., Jr, and Singh, R. (2020). Role of natural compounds in preventing and treating breast cancer. *Front. Biosci. Sch. Ed.* 3 (12), 137–160. doi:10.2741/S544

Omar, S. H., and Al-Wabel, N. A. (2010). Organosulfur compounds and possible mechanism of garlic in cancer. *Saudi Pharm. J.* 18 (1), 51–58. doi:10.1016/j.jsps.2009.12.007

Petrovic, V., Nepal, A., Olaisen, C., Bachke, S., Hira, J., Søgaard, C. K., et al. (2018). Anti-cancer potential of homemade fresh garlic extract is related to increased endoplasmic reticulum stress. *Nutrients* 10 (4), 450. doi:10.3390/nu10040450

Ranjan, A., Ramachandran, S., Gupta, N., Kaushik, I., Wright, S., Srivastava, S., et al. (2019). Role of phytochemicals in cancer prevention. *Int. J. Mol. Sci.* 20 (20), 4981. doi:10.3390/ijms20204981

Rosas-González, V. C., Téllez-Bañuelos, M. C., Hernández-Flores, G., Bravo-Cuellar, A., Aguilar-Lemarroy, A., Jave-Suárez, L. F., et al. (2020). Differential effects of alliin and allicin on apoptosis and senescence in luminal A and triple-negative breast cancer: Caspase, ΔΨm, and pro-apoptotic gene involvement. *Fundam. Clin. Pharmacol.* 34 (6), 671–686. doi:10.1111/fcp.12559

Rose, P., Whiteman, M., Moore, P. K., and Zhu, Y. Z. (2005). Bioactive S-alk (en) yl cysteine sulfoxide metabolites in the genus allium: The chemistry of potential therapeutic agents. *Nat. Product. Rep.* 22 (3), 351–368. doi:10.1039/b417639c

Rose, P., Moore, P. K., Whiteman, M., and Zhu, Y. Z. (2019). An appraisal of developments in allium sulfur chemistry: Expanding the pharmacopeia of garlic. *Molecules* 24, 4006. doi:10.3390/molecules24214006

Schaffer, E. M., Liu, J. Z., Green, J., Dangler, C. A., and Milner, J. A. (1996). Garlic and associated allyl sulfur components inhibit N-methyl-N-nitrosourea induced rat mammary carcinogenesis. *Cancer Lett.* 102 (1-2), 199–204. doi:10.1016/0304-3835(96)04160-2

Selvan, D. A., Mahendiran, D., Kumar, R. S., Rahiman, A. K., and Kalilur RahimAn, A. (2018). Garlic, green tea and turmeric extracts-mediated green synthesis of silver nanoparticles: Phytochemical, antioxidant and *in vitro* cytotoxicity studies. *J. Photochem. Photobiol. B: Biol.* 180, 243–252. doi:10.1016/j.jphotobiol.2018.02.014

Shafeeque, K., and Hashim, K. M. (2018). Comparative anti-angiogenesis study between allicin nanoparticle and normal allicin from garlic (*Allium sativum* Linn). *Eur. J. Exp. Biol.* 8, 27. doi:10.21767/2248-9215.100068

Shang, A., Cao, S. Y., Xu, X. Y., Gan, R. Y., Tang, G. Y., Corke, H., et al. (2019). Bioactive compounds and biological functions of garlic (*Allium sativum* L.). *Foods* 8 (7), 246. doi:10.3390/foods8070246

Shashikant, K. N., Basappa, S. C., and Sreenivasamurthy, V. (1985). Allicin concentration in the gut of rats and its influence on the microflora. *J. food Sci. Technol.* 22 (6), 440–442.

Shukla, Y., and Kalra, N. (2007). Cancer chemoprevention with garlic and its constituents. *Cancer Lett.* 247 (2), 167–181. doi:10.1016/j.canlet.2006.05.009

Sigounas, G., Hooker, J., Anagnostou, A., and Steiner, M. (1997). S-allylmercaptocysteine inhibits cell proliferation and reduces the viability of erythroleukemia, breast, and prostate cancer cell lines. *Nutr. Cancer* 27, 186. doi:10.1080/01635589709514523

Song, K., and Milner, J. A. (2001). The influence of heating on the anticancer properties of garlic. *J. Nutr.* 131 (3), 1054S–1057S. doi:10.1093/jn/131.3.1054S

Sundaram, S. G., and Milner, J. A. (1993). Impact of organosulfur compounds in garlic on canine mammary tumor cells in culture. *Cancer Lett.* 74 (1-2), 85–90. doi:10.1016/0304-3835(93)90048-e

Sung, H., Ferlay, J., Siegel, R. L., Laversanne, M., Soerjomataram, I., Jemal, A., et al. (2021). Global cancer statistics 2020: GLOBOCAN estimates of incidence and mortality worldwide for 36 cancers in 185 countries. *CA: a cancer J. Clin.* 71 (3), 209–249. doi:10.3322/caac.21660

Takagi, H. (2020). "Garlic *Allium sativum* L," in *Onions and allied crops* (United States: CRC Press), 109–146.

Talluri, S. V., Kuppusamy, G., Karri, V. V. S. R., Yamjala, K., Wadhwani, A., Madhunapantula, S. V., et al. (2017). Application of quality-by-design approach to optimize diallyl disulfide-loaded solid lipid nanoparticles. *Artif. Cells, Nanomedicine, Biotechnol.* 45 (3), 474–488. doi:10.3109/21691401.2016.1173046

Tanaka, S., Haruma, K., Yoshihara, M., Kajiyama, G., Kira, K., Amagase, H., et al. (2006). Aged garlic extract has potential suppressive effect on colorectal adenomas in humans. *J. Nutr.* 136 (3), 821S–826S. doi:10.1093/jn/136.3.821S

Tilli, C. M. L. J., Stavast-Kooy, A. J. W., Vuerstaek, J. D. D., Thissen, M. R. T. M., Krekels, G. A. M., Ramaekers, F. C. S., et al. (2003). The garlic-derived organosulfur component ajoene decreases basal cell carcinoma tumor size by inducing apoptosis. *Archives dermatological Res.* 295 (3), 117–123. doi:10.1007/s00403-003-0404-9

Tsubura, A., Lai, Y. C., Kuwata, M., Uehara, N., and Yoshizawa, K. (2011). Anticancer effects of garlic and garlic-derived compounds for breast cancer control. *Anti-Cancer Agents Med. Chem. Former. Curr. Med. Chemistry-Anti-Cancer Agents)* 11 (3), 249–253. doi:10.2174/187152011795347441

Vijayakumar, S., Malaikozhundan, B., Saravanakumar, K., Durán-Lara, E. F., Wang, M. H., and Vaseeharan, B. (2019). Garlic clove extract assisted silver nanoparticle–Antibacterial, antibiofilm, antihelminthic, anti-inflammatory, anticancer and ecotoxicity assessment. *J. Photochem. Photobiol. B: Biol.* 198, 111558. doi:10.1016/j.jphotobiol.2019.111558

Viswanathan, V., Phadatare, A. G., and Mukne, A. (2014). Antimycobacterial and antibacterial activity of *Allium sativum* bulbs. *Indian J. Pharm. Sci.* 76 (3), 256–261.

Wei, Z., Shan, Y., Tao, L., Liu, Y., Zhu, Z., Liu, Z., et al. (2017). Diallyl trisulfides, a natural histone deacetylase inhibitor, attenuate HIF-1α synthesis, and decreases breast cancer metastasis. *Mol. Carcinog.* 56 (10), 2317–2331. doi:10.1002/mc.22686

Wu, Y., Wu, Z. R., Chen, P., Deng, W. R., Wang, Y. Q., Li, H. Y., et al. (2015). Effect of the tyrosinase inhibitor (S)-N-trans-feruloyloctopamine from garlic skin on tyrosinase gene expression and melanine accumulation in melanoma cells. *Bioorg. Med. Chem. Lett.* 25 (7), 1476–1478. doi:10.1016/j.bmcl.2015.02.028

Xiao, X., Chen, B., Liu, X., Liu, P., Zheng, G., Ye, F., et al. (2014). Diallyl disulfide suppresses SRC/Ras/ERK signaling-mediated proliferation and metastasis in human breast cancer by up-regulating miR-34a. *PLoS One* 9 (11), e112720. doi:10.1371/journal.pone.0112720

Xiong, T., Liu, X. W., Huang, X. L., Xu, X. F., Xie, W. Q., Zhang, S. J., et al. (2018). Tristetraprolin: A novel target of diallyl disulfide that inhibits the progression of breast cancer. *Oncol. Lett.* 15 (5), 7817–7827. doi:10.3892/ol.2018.8299

Yi, L., and Su, Q. (2013). Molecular mechanisms for the anti-cancer effects of diallyl disulfide. *Food Chem. Toxicol.* 57, 362–370. doi:10.1016/j.fct.2013.04.001

You, W. C., Chang, Y. S., Heinrich, J., Ma, J. L., Liu, W. D., Zhang, L., et al. (2001). An intervention trial to inhibit the progression of precancerous gastric lesions: Compliance, serum micronutrients and S-allyl cysteine levels, and toxicity. *Eur. J. cancer Prev.* 10 (3), 257–263. doi:10.1097/00008469-200106000-00009

Yun, H. M., Ban, J. O., Park, K. R., Lee, C. K., Jeong, H. S., Han, S. B., et al. (2014). Potential therapeutic effects of functionally active compounds isolated from garlic. *Pharmacol. Ther.* 142 (2), 183–195. doi:10.1016/j.pharmthera.2013.12.005

Zhang, Z. D., Li, Y., and Jiao, Z. K. (2008). Effect of local application of allicinvia gastroscopy on cell proliferation and apoptosis of progressive gastric carcinoma. *Zhongguo Zhong xi yi jie he za zhi Zhongguo Zhongxiyi Jiehe Zazhi= Chin. J. Integr. Traditional West. Med.* 28 (2), 108–110.

Zhang, H., Wang, K., Lin, G., and Zhao, Z. (2014). Antitumor mechanisms of S-allyl mercaptocysteine for breast cancer therapy. *BMC complementary Altern. Med.* 14 (1), 270–312. doi:10.1186/1472-6882-14-270

Zhang, Y., Liu, X., Ruan, J., Zhuang, X., Zhang, X., and Li, Z. (2020). Phytochemicals of garlic: Promising candidates for cancer therapy. *Biomed. Pharmacother.* 123, 109730. doi:10.1016/j.biopha.2019.109730

Zou, X., Liang, J., Sun, J., Hu, X., Lei, L., Wu, D., et al. (2016). Allicin sensitizes hepatocellular cancer cells to anti-tumor activity of 5-fluorouracil through ROS-mediated mitochondrial pathway. *J. Pharmacol. Sci.* 131 (4), 233–240. doi:10.1016/j.jphs.2016.04.017

Zuniga, K. E., Parma, D. L., Muñoz, E., Spaniol, M., Wargovich, M., and Ramirez, A. G. (2019). Dietary intervention among breast cancer survivors increased adherence to a Mediterranean-style, anti-inflammatory dietary pattern: The Rx for Better Breast Health Randomized Controlled Trial. *Breast cancer Res. Treat.* 173 (1), 145–154. doi:10.1007/s10549-018-4982-9

frontiers | Frontiers in Pharmacology

TYPE Review
PUBLISHED 17 April 2023
DOI 10.3389/fphar.2023.1160616

OPEN ACCESS

EDITED BY
Mohd Adnan,
University of Hail, Saudi Arabia

REVIEWED BY
Ashun Chaudhary,
Central University of Himachal Pradesh, India
Mounir Tilaoui,
Waterford Institute of Technology, Ireland
Salman Ahmed,
University of Karachi, Pakistan

*CORRESPONDENCE
Daniela Calina,
calinadaniela@gmail.com
Javad Sharifi-Rad,
javad.sharifirad@gmail.com
Basem Al-Omari,
basem.alomari@ku.ac.ae

RECEIVED 07 February 2023
ACCEPTED 05 April 2023
PUBLISHED 17 April 2023

CITATION
Rajkovic J, Novakovic R, Grujic-Milanovic J, Ydyrys A, Ablaikhanova N, Calina D, Sharifi-Rad J and Al-Omari B (2023), An updated pharmacological insight into calotropin as a potential therapeutic agent in cancer. *Front. Pharmacol.* 14:1160616. doi: 10.3389/fphar.2023.1160616

An updated pharmacological insight into calotropin as a potential therapeutic agent in cancer

Jovana Rajkovic[1], Radmila Novakovic[1], Jelica Grujic-Milanovic[2], Alibek Ydyrys[3], Nurzhanat Ablaikhanova[4], Daniela Calina[5]*, Javad Sharifi-Rad[6]* and Basem Al-Omari[7]*

[1]Institute for Pharmacology, Clinical Pharmacology and Toxicology, Faculty of Medicine, University of Belgrade, Belgrade, Serbia, [2]Institute for Medical Research, National Institute of the Republic of Serbia, University of Belgrade, Belgrade, Serbia, [3]Biomedical Research Centre, Al-Farabi Kazakh National University, Almaty, Kazakhstan, [4]Department of Biophysics, Biomedicine and Neuroscience, Al-Farabi Kazakh National University, Almaty, Kazakhstan, [5]Department of Clinical Pharmacy, University of Medicine and Pharmacy of Craiova, Craiova, Romania, [6]Facultad de Medicina, Universidad del Azuay, Cuenca, Ecuador, [7]Department of Epidemiology and Population Health, College of Medicine and Health Sciences, Khalifa University, Abu Dhabi, United Arab Emirates

Calotropin is a pharmacologically active compound isolated from milkweed plants like *Calotropis procera, Calotropis gigantea,* and *Asclepias currasavica* that belong to the Asclepiadaceae family. All of these plants are recognised as medical traditional plants used in Asian countries. Calotropin is identified as a highly potent cardenolide that has a similar chemical structure to cardiac glycosides (such as digoxin and digitoxin). During the last few years, cytotoxic and antitumor effects of cardenolides glycosides have been reported more frequently. Among cardenolides, calotropin is identified as the most promising agent. In this updated and comprehensive review, we aimed to analyze and discuss the specific mechanisms and molecular targets of calotropin in cancer treatment to open new perspectives for the adjuvant treatment of different types of cancer. The effects of calotropin on cancer have been extensively studied in preclinical pharmacological studies *in vitro* using cancer cell lines and *in vivo* in experimental animal models that have targeted antitumor mechanisms and anticancer signaling pathways. The analyzed information from the specialized literature was obtained from scientific databases until December 2022, mainly from PubMed/MedLine, Google Scholar, Scopus, Web of Science, and Science Direct databases using specific MeSH search terms. The results of our analysis demonstrate that calotropin can be a potential chemotherapeutic/chemopreventive adjunctive agent in cancer pharmacotherapeutic management.

KEYWORDS
calotropin, anticancer, molecular targets, signaling pathways, apoptosis, cytotoxicity

1 Introduction

Cancer is a process that occurs in different cells of the body, resulting from acquiring genetic and epigenetic changes in them, which leads to uncontrolled cell growth (Lee and Kim, 2022; GBD 2019 Colorectal Cancer Collaborators, 2022). In tumor formation increased attendance of reactive oxygen species (ROS) is involved because they activate various

oncogenic signaling pathways, induce mutation of DNA, and induce immune escape, which, together with the microenvironment, angiogenesis, often lead to metastasis (Mitroi et al., 2019; Tsoukalas et al., 2019; Nakamura and Takada, 2021; Scheau et al., 2021) Cancer drug treatments differ depending on the type and stage of the tumor (Buga et al., 2019). Due to the heterogeneity of cancers and their responses to treatment, major efforts are being made to improve existing therapeutic protocols or to find new adequate therapeutics (Ianoși et al., 2019; Iordache et al., 2019) In light of this, is still actual to explore natural products to develop the final anticancer drug entity, which has fewer side effects, is low-cost, and has better application. Numerous studies have reported that many plant species and their bioactive compounds have anti-cancer properties (Khan et al., 2022). The cytotoxic effects of different plant extracts are well known and many compounds isolated from the plants are being detailed and evaluated for anticancer activities in different *in vitro* and *in vivo* models. Solowey et al. (2014) investigated 17 whole plant extracts on ten different human cancer cells. The efficacy of cell death in tumor cells varied depending on the content of multiple molecules with antitumor activities but was often aligned with ethnobotanical sources of historical use (Solowey et al., 2014). Calotropin belongs to the cardenolides, which is a class of cardiac glycosides (Mo et al., 2016) (Supplementary File S1). Cardiac glycosides are prominent in the treatment of cardiovascular diseases treat as congestive heart failure in humans (Silva et al., 2018), but also as a poison in the African dart arrow (Agrawal et al., 2012). The main and first established mechanism of action of cardenolides such as calotropin was the inhibition of the sodium-potassium exchanger, Na^+/K^+-ATPase. This enzyme allows the active transport of Na^+ and K^+ ions through the cell membrane. It was observed that calotropin has a more perceptible impact on the myocardium compared to it on skeletal muscles, as myocytes have more active Na^+/K^+-ATPase (Koch et al., 2020). As consequence, this can allow for higher cardiac output by the cardiac muscles but can also lead to arrhythmia (Hoyer et al., 2011). In the upcoming years after calotropin isolation, many studies have been dedicated to its crystal and molecular structure, and new methods of isolation. In recent years, researchers have conducted numerous studies on the anticancer effects of calotropin. One of the reasons is the fact that cardenolides target the enzyme Na^+/K^+-ATPase and lead to dysregulation of the sodium-potassium ion gradients and disrupt the membrane potential (Vila Petroff et al., 2003). Others have sought to exhibit *in vitro* cytotoxic and cytotoxic effects of the cardiac glycosides against lung cancer (Ibrahim et al., 2014; Kim et al., 2016), and leukemia (Nakano et al., 2020). In preclinical models of the STK11 mutant lung cancer cells, the cardiac glycosides directly inhibit ATP function. Clinical-relevant doses of cardenolide inhibit cell proliferation and migration of these tumor cells (Kim et al., 2016). In leukemia, overexpression of MYC protein initiates proliferation and blocks cell differentiation, thus treatment of these cells with cardiac glycoside leads to inhibition of the MYC pathway (Da Costa et al., 2018). Pederson et al. (2020) reported that cardenolide display potency against two triple-negative breast cancer (TNBC) cells BT-549 and Hs578T cells. A similar study was done by Zhou et al. (2019) about the anticancer activity of colorectal cancer cells. Today, despite considerable efforts to find adequate anticancer therapy, cancer remains one of the leading causes of death worldwide (Nakamura and Takada, 2021). The use of traditional chemotherapy and radiation therapy in combination with surgery, and/or immunotherapies, and hormone therapy sometimes do not give satisfactory results, and therefore use of targeted therapies has become more common in recent times (Nakamura and Takada, 2021). The current review represents an update of the anticancer mechanisms, molecular targets, and signaling pathways of calotropin, a natural bioactive compound of current interest in the pharmacotherapeutic management of cancer.

2 Review methodology

To get a comprehensive overview of the most recent data on anticancer molecular mechanisms of calotropin, the following specialized databases were searched, such as PubMed/MedLine, Google Scholar, Scopus, Web of Science, and Science Direct using the following terms MeSH alone or in combination: "Antineoplastic Agents," "Phytogenic/pharmacology," "Apoptosis/drug effects," "Calotropis/chemistry," "Calotropis/metabolism," "Cardenolides/chemistry", "Cardenolides/isolation and purification", "Cardenolides/pharmacology", "Cell Line, Tumor, Cell Proliferation/drug effects", "Reactive Oxygen Species/metabolism", "Humans", "Signal Transduction/drug effects", "Reactive Oxygen Species/metabolism". This study included articles published in English that proved the anticancer molecular mechanisms of calotropin. Pharmacological studies that did not specify anticancer mechanisms and specific signaling pathways, doses used in the experiment, and *in silico* studies without evidence from preclinical pharmacological studies were excluded. The most important data were summarized in tables and figures. The taxonomy of plant species was validated according to World Flora Online and the chemical structures according to PubChem (WFO, 2021; PubChem, 2022).

3 Natural sources, traditional and current uses

Calotropin (also known as Pecilocerin A, Pekilocerin A) primarily was isolated from *Calotropis procera* (Ait) R. Br., *Calotropis gigantea* (L.) R. Br (Cg) and *Asclepias subulata*, the plants belonging to the family Asclepiadaceae (Agrawal et al., 2012; Kadiyala et al., 2013; Rascón Valenzuela et al., 2015a). Plants from the family *Asclepiadoideae,* have been found in Africa, Asia, Europe, Australia, South America, and the tropics of North America. *Calotropis sp*. is common in Africa and Asia and widely distributed throughout India, Sri Lanka, Nepal, Maldives, South China and Malaysia, and Pakistan (Kadiyala et al., 2013). Other species of this family such as *Asclepias sp*., mostly known as the desert plants, are native to America (Rascón Valenzuela et al., 2015b). The mentioned species of the family *Asclepiadoideae* have been since ancient times part of traditional medicine for the treatment of various diseases related to the central nervous system, skin diseases, digestive system, respiratory system, reproductive system pain, and cancer (Rascón Valenzuela et al., 2015a). Different parts of these plants have been used since antiquity

as a galenical in traditional medicine. Calotropin is isolated from latex, leaves, and root bark from plants (Kadiyala et al., 2013). Accidental poisoning is common in animals who have ingested milkweed. Interestingly, some insects species, the pyrgomorphid grasshopper *P. bufonius* and caterpillar of monarch butterflies eat milkweeds of the plants family *Asclepiadoideae* and stored calotropin as a defense mechanism against predators and parasites (Agrawal et al., 2012). Phytochemical studies of plants from family *Asclepiadoideae* have revealed the presence of several types of compounds such as cardenolide, pregnane glycosides, secopregnane glycosides, triterpenoids, steroidal glycosides (Elgamal et al., 1999). A native plant of the family *Asclepiadaceae* is distributed in the tropical and subtropical regions of the planet. In some of these regions, the dependence on traditional plant-based medicines persists until today, especially if you keep in mind that many parts of this plant are useable. In the past, these plants have been popular to cure several human diseases such as fever, asthma, rheumatism, indigestion, diarrhoea, and dysentery (Al-Taweel et al., 2017). Despite long evidence of using traditional plants that contain calotpropin as a part of folk medicine, its antitumor and cytotoxic effects have been examined just recently in a controlled laboratory condition. The first evidence of the cytotoxic effect of calotropin may be found in an article written by Kupchan et al. (1964) dated 1964. An alcoholic extract of *Asclepias curassavica* was tested on *in vitro* cells cultured from human carcinoma of the nasopharynx and the observed cytotoxic activity was attributed to calotropin isolated from that extract. The flower and leaf are widely used parts of *Calotropis procera (Cp)*. The leaf extract of *Cp* possessed a powerful antiulcer activity by to the reduction gastric acid secretion, as well as augmenting the mucosal defensive factors and inhibiting lipid peroxide levels (Al-Taweel et al., 2017). In a previous study, it has been shown that extracts from all parts of these plants have a variety of biological activities (Huang et al., 2018; Mutiah et al., 2018). The pharmaceutical potential of extracts gained from the bark and leaves of plant *Cp* showed notable antibacterial potential against different bacterial strains (Sharma et al., 2015; Pattnaik et al., 2017). The ethanol extract of the *Cp* in a dosage of 500 mg/kg induced significant antipyretic and analgesic activity in mice (Mossa et al., 1991). The study of Magalhães et al. (2010) reported that among five extracts, ethyl acetate and acetone extract of *Cp* displayed higher cytotoxic potential against two different tumor cells: colon (HCT-8) and melanoma (B-16) cells. The same authors also reported that those extracts induced a significant reduction in tumor weight as well as the growth of the sarcoma tumor in mice. Several previous studies of the biological activities of *Cp* have shown anti-inflammatory (Kumar et al., 2015; Kumar et al., 2022), and antifungal activity (Al-Rowaily et al., 2020; Freitas et al., 2020) were shown.

4 Therapeutic activity, cellular and molecular mechanisms of calotropin in various types of cancer

4.1 Brain cancer

A recent study investigated several types of cardiac glycosides isolated from *Calotropis gigantea* and showed that calotropin had the most pronounced cytotoxicity on A172 and U251 glioblastoma cell lines, and confirmed a possible anticancer mechanism that includes G2/M phase cell arrest (He et al., 2021). Another evidence that calotropin may have cytotoxic effects on cancer cell lines derives from its capability to inhibit the enzyme Na^+/K^+-ATPase. Na^+/K^+-ATPase is an important transmembrane protein found in all mammalian cells with the main role in cell ion homeostasis. A potential target for anticancer therapy contributes to its role in signal transduction, and overexpression, as well as in ion homeostasis, in severe neoplasms (Bejček et al., 2021). In research that was done by Meneses-Sagrero et al. (2022) anticancer effects of calotropin were analysed using commercial brain porcine Na^+/K^+-ATPase. Calotropin showed dose-response inhibitory effects on Na^+/K^+-ATPase activity (IC_{50} = 0.27 ± 0.06 μM). The IC_{50} value was by a previous study where was observed that calotropin has the same IC_{50} value on porcine cerebral cortex Na^+/K^+-ATPase activity (Agrawal et al., 2021). This value of IC_{50} of calotropin is very similar to other well-known cardenolides like ouabain and digoxin which indicated the great inhibitory potential of calotropin on Na^+/K^+-ATPase. Also, kinetic analysis on Na^+/K^+-ATPase activity showed that the nature of this inhibition is non-competitive (Meneses-Sagrero et al., 2022).

4.2 Breast cancer

Breast cancer occurs when normal cells in the breast change and grow out of control and it occurs with a frequency of 13% in the global population, and TNBC represents 10%–20% of all breast cancers (Yao et al., 2017). More than a decade ago six TNBC subtypes of breast cancer cells have been identified based on tumor gene expression analyses, one of them being BT-549 cells (Pederson et al., 2020). Nine cardenolides from *Calotropis gigantea* exhibited selective cytotoxic activities on TNBC, but calotropin was notably more selective for BT-549 cells (Pederson et al., 2020). Regarding human triple-negative breast cancers (TNBC) cell lines were shown effects of calotropin different IC_{50} values and selectivity across different human TNBC cell lines (Pederson et al., 2020). Calotropin was more selective for BT-459 cells (IC_{50} = 0.03 ± 0.002 μM) and Hs578T cells (IC_{50} = 0.06 ± 0.01 μM) compared to MDA-MB-231 (IC_{50} value was 0.44 ± 0.08 μM). The results suggested that BT-459 cells are more sensitive to calotropin due to increases in intracellular Ca^{2+} levels, leading to cell death at lower concentrations than is required in other human TNBC cell lines. Another evidence that calotropin may have cytotoxic effects on cancer cell lines derives from its capability to inhibit the enzyme Na+/K + -ATPase viz altering through key transmembrane cellular protein homeostasis. The possible explanation of the different effects of calotropin in the different human triple-negative breast cancer cell lines may derive from the expression of different Na^+/K^+-ATPase isoforms and ↑Na^+/Ca^{2+} exchanger (NCX) isoforms. It has been shown that α1 Na^+/K^+-ATPase isoform is more resistant to inhibition by some cardiac glycosides, and at the same time, its expression was lowest in BT-459 cells. However, in another cell line Hs578T the expression of α1 Na^+/K^+-ATPase isoform was intermediate. Related to another hypothesis with Na^+/Ca^{2+} exchanger isoforms, it was observed that the mRNA of NCX1 isoform was significantly higher in BT-459 and Hs578T

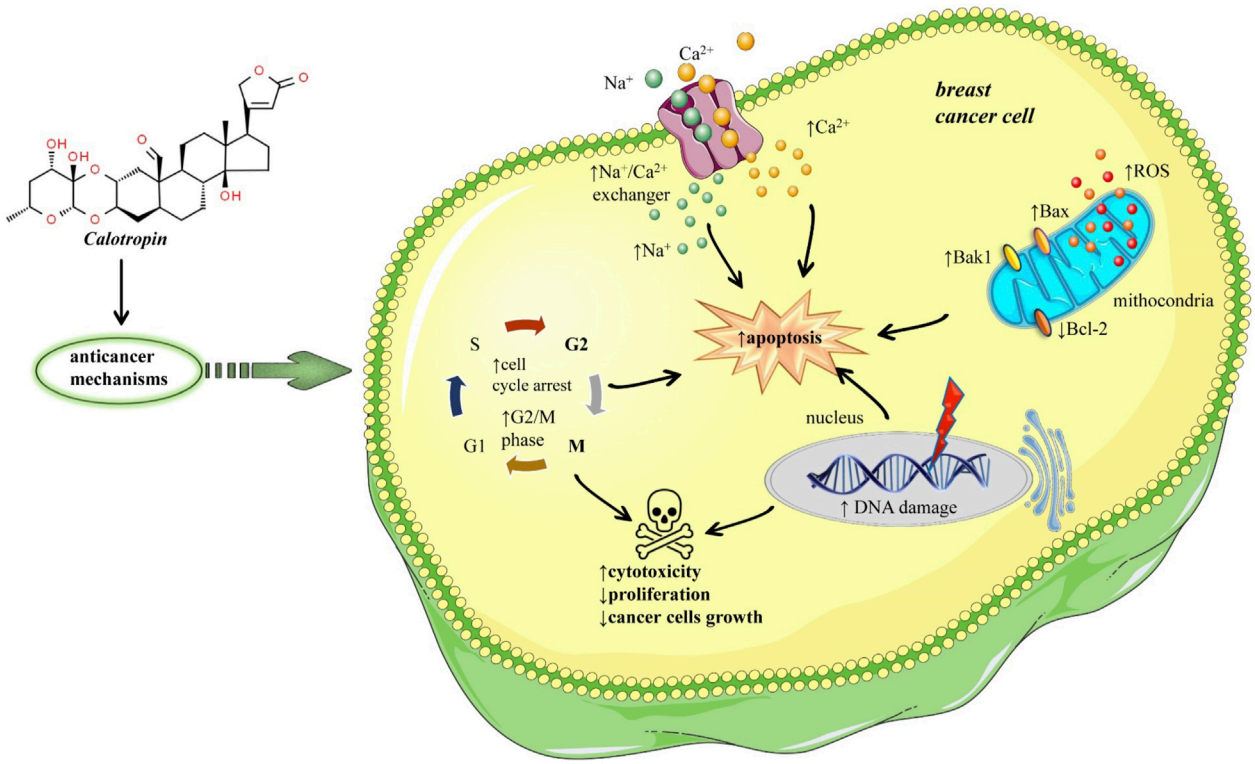

FIGURE 1
Potential mechanisms of anticancer effects of calotropin in breast malignant tumor. Calotropin inhibits Ca2+ efflux via the Na+/Ca2+ exchanger, increasing intracellular Na+ and Ca2+, triggering apoptosis. Calotropin also induces apoptosis and cell death in tumour cells by disintegrating DNA and arresting the cell cycle in the G2/M phase. It also increases Bax/Bak1 expression and significantly reduces Bcl-2 expression, so this Bax/Bcl-2 ratio plays an important role in determining apoptosis. Symbols: ↑increase, ↓decrease.

compared to the other human triple-negative breast cancer cell lines. Thus, the high mRNA expression of NCX1 may predict sensitivity to calotropin. The breast cancer BT-549 cells were treated with different doses of calotropin, 150 nM and 500 nM. The results showed that both doses of calotropin inhibit the efflux of Ca^{2+} via the Na^{+}/Ca^{2+} exchanger. A major consequence of this inhibition is increased intracellular Na^{+}, leading to increased Ca^{2+} entry and elevated concentrations of intracellular Ca^{2+}. Cancer cells with defects in this signalling pathway might be particularly vulnerable, as an increase in intracellular Ca^{2+} triggers apoptosis (Vila Petroff et al., 2003) (Figure 1). Calotropin also induces apoptosis in breast cancer MCF-7 cell lines, by modulating the phosphatidylserine gene, DNA disintegration, and G2/cell cycle arrest. Also, this treatment increased the expression of Bax/Bak1 and significantly reduced Bcl-2 expression, so this ratio of Bax/Bcl-2 plays an important role in determining apoptosis (Kharat and Kharat, 2019) (Figure 1).

4.3 Lung cancer

One of the most common types of human cancer is non-small cell lung cancer (NSCLC) which is characterized by invasion, migration, rapid growth, and reoccurrence (Guo et al., 2022). *In vitro* studies on NSCLC showed that treatment with calotropin promoted apoptosis by increasing the expression of pro-apoptosis genes: *caspase-3, caspase-8*, and apoptotic protease activating factor-1 (Apaf-1) and downregulated expression of anti-apoptotic proteins: p53, B-cell lymphoma (Bcl 2) and Bclw (Paesmans et al., 2015). On the same calotropin treatment of cancer cells activates the TGF-β/ERK signaling pathway, by decreasing the expression of TGF-β and ERK½, and downregulating phosphorylation of ERK½ (Paesmans et al., 2015). *In vivo* assay on NSCLC-bearing mice showed that calotropin treatment markedly inhibited tumor growth, increased the number of apoptotic cells, and significantly promoted apoptosis markers: caspase-3 and caspase-8. Long-term observation has shown that this treatment significantly prolonged the survival of these mice (Paesmans et al., 2015) (Figure 2).

Epithelial-mesenchymal transition (EMT) involves changes in the intracellular cytoskeleton and extracellular matrix. After EMT, cells lost polarization, acquire an elongated morphology, and possess strong intercellular adhesion and polarity, which can be attributed to the reorganization of the actin cytoskeleton as well as increased expression of vimentin or keratin (Grände et al., 2002). EMT is a complex which can be activated by different inflammatory stimuli like TGF-β growth factor, cytotoxic T-lymphocyte–associated antigen 4 (CTLA-4), hypoxia, or extracellular matrix components (Grände et al., 2002). CTLA-4 is a multifactorial protein with an important role in the communication process in cells, was significant downregulation in NSCLC cells after calotropin administration led

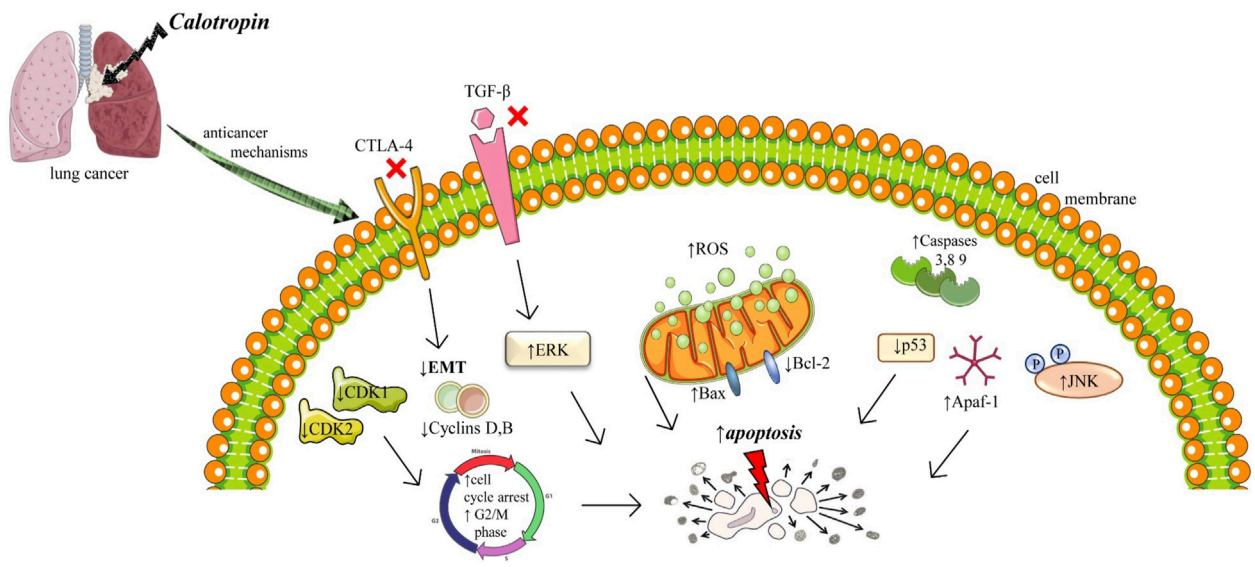

FIGURE 2
Illustrative scheme with cytotoxic mechanisms of Calotropin in lung cancer. Abbreviations and symbols: ↑ increase, ↓decrease, Epithelial-mesenchymal transition (EMT), Reactive oxygen species (ROS), mitogen-activated protein (MAP) kinases and cJun NH2-terminal kinase (JNK), transforming growth factor β (TGF-β), cytotoxic T-lymphocyte–associated antigen 4 (CTLA-4).

to tumor inhibition. Also, calotropin inhibited the protein expression levels of TGF-β, an essential factor in carcinogenesis (Tian et al., 2018). Therefore, calotropin administration regulated apoptosis, inhibited tumor growth, and prolonged survival in NSCLC cells via the TGF-β/ERK signaling pathway (Tian et al., 2018).

Another research compared calotropin inhibitory and pro-apoptotic activity on two types of NSCLC cell lines: cisplatin-induced resistant NSCLC cell line (A549/CDDP) and its parent's cells lung adenocarcinoma A549 (Mo et al., 2016). Interestingly, while A549/CDDP was significantly inhibited by calotropin in a concentration-dependent manner (IC_{50} 0.33 ± 0.06 μM at 48 h), the same inhibitory effect on A549 was weak (IC_{50} 38.46 ± 1.16 μM at 48 h). Furthermore, while cell cycle arrest in the G2/M phase and an increased number of cells in the apoptotic phase were observed in A549/CDDP after treatment with calotropin, the same effects lack in A549. After the treatment with calotropin the expression of CDK1, CDK2, cyclin A, and cyclin B was significantly downregulated in A549/CDDP cell line, while p21 and p53 protein levels were increased. The same as in the previously mentioned research, the expression levels of the precursor forms of Cap- 3, Cap-8, and Cap-9 were downregulated and their active forms were upregulated. Also, the increased intracellular levels of ROS were observed in the same cell lines, as well as changes in mitochondrial membrane potential and poly (ADP-ribose) polymerase (PARP) after treatment with calotropin (in a dose of 0.5 and 1.0 μM) compared to a control group. The levels of anti-apoptotic protein Bcl-2 were decreased and pro-apoptotic Bax protein levels were increased in a concentration-dependent manner in the treatment group. All of the previously mentioned results were not observed after the treatment of calotropin on the A549 cell line. In A549/CDDP cell line treatment with calotropin was correlated with increased phosphorylation of JNK (which has an essential role in signalling pathways of apoptosis), while this was not observed in the A549 cell line. There is no provided explanation of the differences in the effects of calotropin on these 2 cell lines (Mo et al., 2016).

The anticancer activity of calotropin on A549 cells through caspase-dependent apoptosis activated by extrinsic pathway was obtained in research done by Rascón-Valenzuela et al. (2016) and colleagues. A recent study (Rascón Valenzuela et al., 2015a) indicated that the IC_{50} values of calotropin on the same cell line are 0.0013 μM, while antiproliferative activity was confirmed on another two cancer cell lines LS 180 (human colorectal adenocarcinoma cell line) and PC-3 (human prostate cancer cell line) with IC_{50} values 0.06 and 0.41 μM, respectively. Also, the cytotoxic effects of calotropin on lung adenocarcinoma A549 cells were confirmed in the research done by Sweidan et al. (2021). Interestingly, they compared the effects of calotropin on human fibroblast cell lines as normal cells and the toxicity of calotropin was lower which indicated that calotropin is more selective to cancer cells compared to normal cells. The same observation on human normal cells was reported by Rascón-Valenzuela et al. (2015). The *in vitro* growth inhibitory activity of calotropin was tested on A549 cells, PC-3, and U373 (glioblastoma cell line) by Ibrahim and colleagues, and the same value of IC_{50} (0.005 μM) was reported for all 3 cell lines (Ibrahim et al., 2014).

Comprehensive research on the anticancer effects of calotropin was done by Tian et al. (2018). They used bronchioalveolar carcinoma H358 cells treated with calotropin (0.50 mg/mL) for 24 h, 48 h, and 72 h based on the subject of analysis to investigate the inhibitory effects of calotropin on the growth and aggressiveness of cancer cells. Also, *in vivo* study was performed using 80 specific pathogen-free female nude (6–8 weeks old, weight 30–35 g) mice. All of them were subcutaneously injected with H358 cells and after that divided into 2 groups. In the treatment group, mice were intravenously injected with calotropin (5.0 mg/kg)

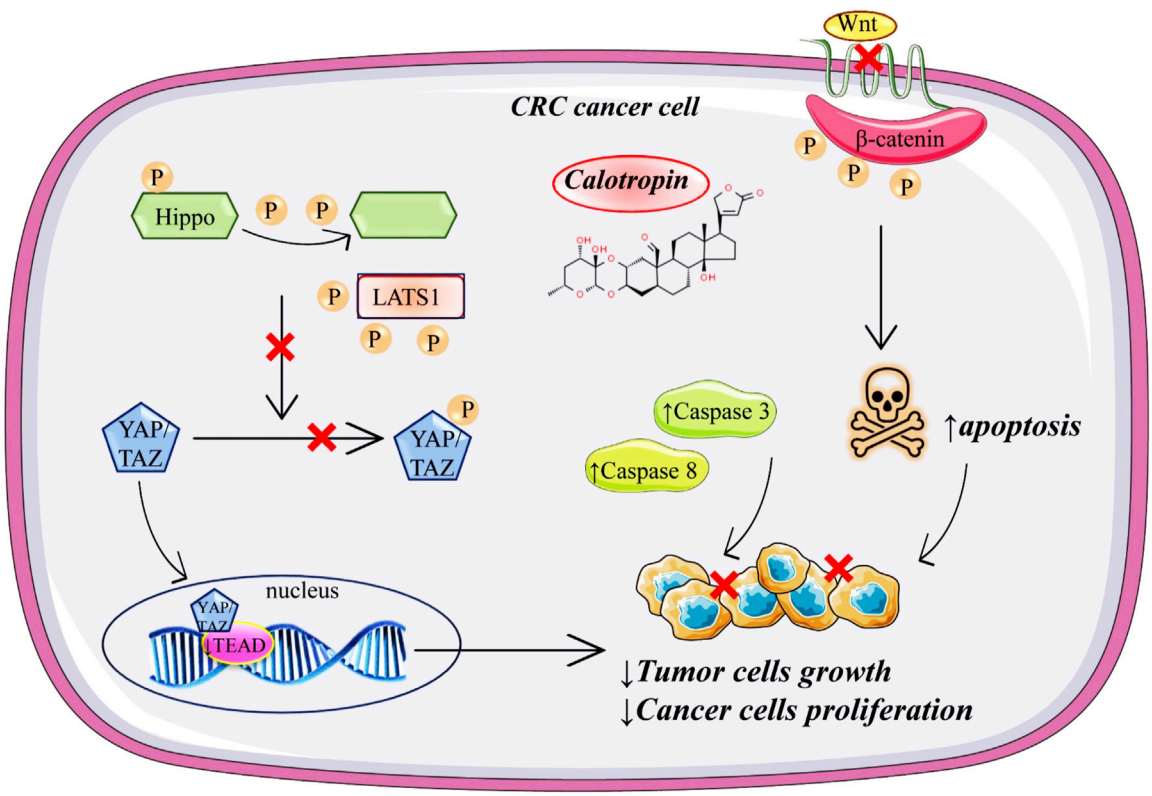

FIGURE 3
Schematic representation of anticancer mechanisms of calotropin in colorectal cancer.

every day for 7 days, while PBS injections were used as the control. Related to *in vitro* experiments on H358 cells it was observed that calotropin suppressed cell growth in a time-dependent manner (after 72 h treatment). The cell proliferation was arrested at the G2/M phase. Also, calotropin inhibited protein level expression of cyclins (cyclin-dependent kinases: CDK1 and CDK2), fibronectin, vimentin and E-cadherin. The migration and invasion were inhibited after treatment with calotropin. Analysis of calotropin effects on H358 cells apoptosis showed that apoptosis was promoted. There was increased pro-apoptosis gene expression of caspase-3 (Cap-3), caspase-8 (Cap-8), and Apaf-1, while anti-apoptosis protein expression levels of p53, Bcl-2, and Bsl-w were decreased. Also, calotropin promoted Cyt-c and JNK protein expression levels. Additional effects of calotropin indicated that its treatment of H358 cells decreased the CTLA-4 (T-lymphocyte-associated-protein 4) protein expression (CTLA-4 protein is a checkpoint receptor that downregulates T cell activation), and inhibited the TGF-β protein expression levels and phosphorylation and protein expression levels of ERK1/2, indicated that probably TGF-β/ERK signalling pathway is included in calotropin-mediated apoptosis.

4.4 Digestive cancers

4.4.1 Liver cancer

One of the most aggressive cancers with a poor prognosis is liver cancer, the most common type being hepatocellular carcinoma (HCC). The anticancer activity of calotropin in HCC was linked to the suppression of fatty acid levels by a decrease in inflammatory cytokines and adipocyte shrinkage, as can be seen in a different model of liver carcinogenesis (Zhang et al., 2020). During the early phase of hepatocarcinogenesis, inflammatory and parenchymal cells release large amounts of IL-6 and TNF-α which is responsible for the release of TGF-β1. The elevated level of inflammatory cytokines triggers mitogen-activated protein (MAP) kinases and cJun NH2-terminal kinase (JNK), which is implicated in the progression of liver fibrosis and deposition of collagen. Calotropin treatment decreases IL-6 and TNF-α expression, implying that the inflammatory process suppresses and slows the progression of carcinogenesis (Pan et al., 2018). Also, the IC_{50} value of calotropin was reported on the human hepatocarcinoma cell line (HepG2) and Raji cells (human B lymphoblastoid cell line), and values were 0.04 and 0.02 μM, respectively, which confirmed its cytotoxic effect on tumor cell lines (Li et al., 2009).

Recently, the pro-apoptotic effects of calotropin were confirmed on HepG2 and human colorectal adenocarcinoma cells (Caco-2) (Martucciello et al., 2022).

4.4.2 Colorectal cancer

Colorectal cancer (CRC) is a malignant neoplasm that develops in the colon and rectum, and its symptoms can be extremely varied; in its early stages, CRC is asymptomatic and is detected through screening examinations (2022). Calotropin markedly suppresses the proliferation of colorectal cancer cells by the Hippo pathway through the activity of

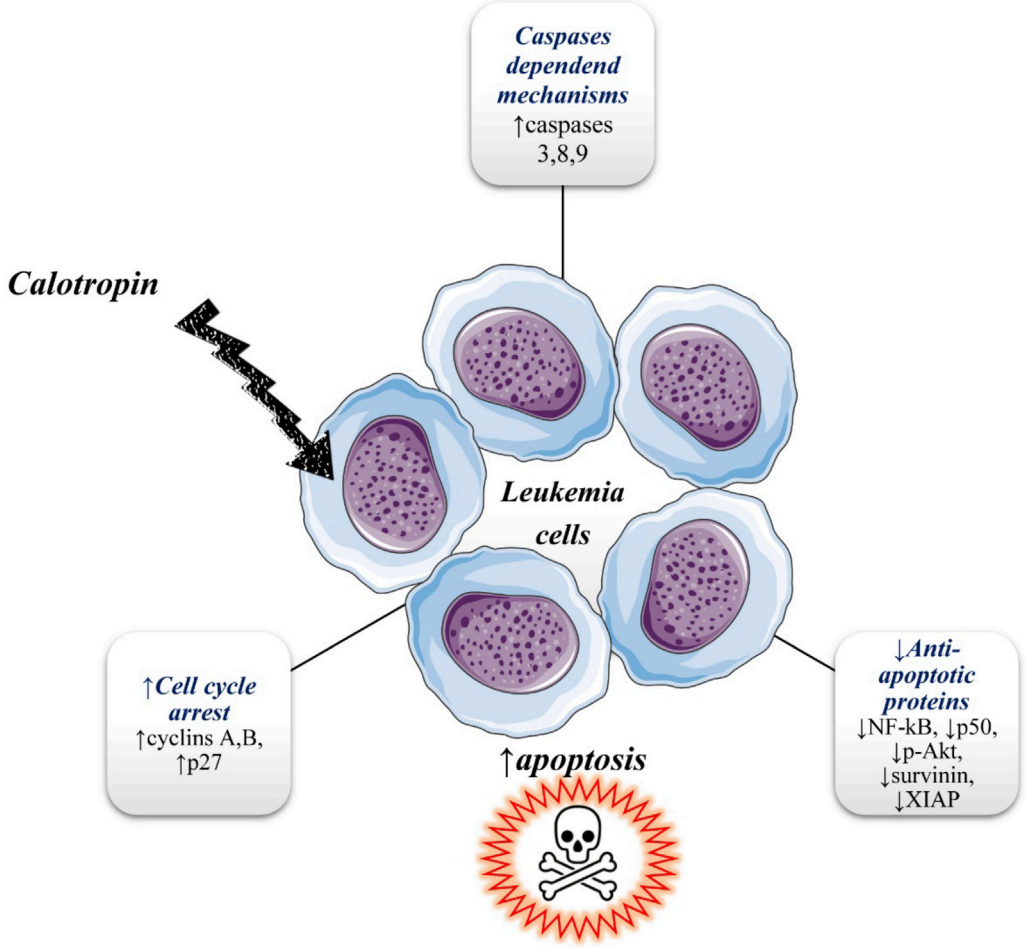

FIGURE 4
Illustrative diagram with anti-leukemic mechanisms of calotropin. Symbols: ↑increase, ↓decrease.

YAP (Zhou et al., 2019). Since the Hippo pathway is a highly complex signaling network with >30 components, dysregulation of the Hippo pathway components often leads to aberrant cell growth and tumor formation (Meng et al., 2016). Treatment with calotropin induces YAP dephosphorylation in colorectal cancer cells. Dephosphorylation of YAP, after calotropin treatment, induced its translocation into the nucleus of the colorectal cancer cells. After nuclear localization, YAP interacts with the transcription factors of the TEAD family (Figure 3). Downregulation of the TEAD target gene, after administration of calotropin decrease the expansion of progenitor cells, and tissue overgrowth. Together, these data showed that calotropin inhibits tumor growth in colorectal cancer cells (Meng et al., 2016) (Figure 3). When *in vivo* experiments of a 25-day short-term observation period were analysed it was suggested that injection of calotropin inhibited tumor growth. In the treatment group, the number of apoptotic cells and lymphocyte infiltration was increased. In excised tumors from the treatment group expression levels of Casp-3 and Casp-8 were increased. Besides the fact that the administration of calotropin has significantly inhibited tumor growth, after the 120-day observation period the prolonged mice survival was noted as well.

In another research done by Zhou et al. (2019), it was indicated that calotropin may inhibit tumor growth. The *in vitro* study was done on two types of human colorectal cancer cell lines HT-29 and HCT116, treated with calotropin for 24 h. Increased concentrations of calotropin (0.2–10 μM) inhibit proliferation in a dose-dependent manner in both cancer cell lines. Also, calotropin promoted dephosphorylation of YAP (Yes-associated protein) and induced its nuclear localization in colorectal cancer cells, therefore supporting the hypothesis that the Hippo signalling pathway is included in calotropin-induced inhibition of cell proliferation. Additionally, calotropin treatment shortened the half-life of LATS1 (large tumor suppressor 1) protein, the main kinase in the Hippo pathway that phosphorylates YAP. Calotropin probably promotes LATS1 degradation through the ubiquitination/proteasome pathway. Another part of the study was *in vivo* performed with BALB/c immunodeficient nude mice injected with HT-29 cells (6–8 weeks old). Mice were divided into two groups, the treatment group where calotropin was intravenously administered once every 2 days for 3 weeks, and the control group was treated in the same way during the same period with DMSO as a vehicle. It has been shown that the tumor obtained from the calotropin-treatment group was reduced in volume and weight. Another research on colon cancer cells (SW480 colon adenocarcinoma cell line) marked calotropin as an anticancer agent which inhibits the Wnt signalling pathway by decreasing nuclear and cytosolic located β-catenin in a dose-

TABLE 1 Summarized data obtained from preclinical pharmacological studies regarding calotropin anticancer activity.

Cancer type	Experimental model	Molecular mechanisms/ signaling pathways	Results	Ref
Brain cancer	*in vitro* A172, U251 glioblastoma cells	↑cell arrest in G2/M phase ↓Na^+/K^+-ATPase	↑cytotoxicity IC_{50} = 0.27 ± 0.06 μM	He et al. (2021)
Breast cancer	*in vitro* BT-549, Hs578T MDA-MB-231 TNBC cells	↑intracellular Ca^{2+} ↓Na^+/K^+-ATPase ↓NCX1 ↑intracellular Ca^{2+}	↑cytotoxicity ↑ apoptosis IC_{50} = 0.03 ± 0.002 μM for BT-459 IC_{50} = 0.06 ± 0.01 μM for Hs578T IC_{50} = 0.44 ± 0.08 μM for MDA-MB-231	Pederson et al. (2020)
	in vitro BT-549 cells	↓Na^+/K^+-ATPase ↑intracellular Ca^{2+}	↑ apoptosis IC_{50} = 150–500 nM	Vila Petroff et al. (2003)
	in vitro MCF-7 cells	↑DNA disintegration ↑G2/M cell cycle arrest ↑Bax/Bak1, ↓Bcl-2	↑ apoptosis IC_{50} = 40 μg/mL	Kharat and Kharat (2019)
Lung cancer	*in vitro* non-small cell lung cancer NSCLC cells *in vivo* NSCLC-bearing mice	↑ caspases 3,8; ↑Apaf-1 ↓p53, ↓Bcl2, ↓Bclw ↑TGF-β/ERK	↑ apoptosis ↓tumor growth ↑apoptotic cells ↑survival of mice	Paesmans et al. (2015)
	in vitro NSCLC cells	↑TGF-β/ERK	↓tumor growth ↓carcinogenesis	Tian et al. (2018)
	in vitro A549/CDDP cells A549 cells	↑cycle arrest in the G2/M phase ↓CDK1, ↓CDK2 ↓cyclin A, B ↑p2, ↑p53, ↓Cap- 3, 8, 9 ↑ROS, ↑PARP, ↓Bcl-2, ↑Bax, ↑JNK	↑ apoptosis IC_{50} = 0.33 ± 0.06 μM for A549/CDDP cells IC_{50} = 38.46 ± 1.16 μM for A549 cells	Mo et al. (2016)
	in vitro A549 cells	↑caspases	↑ apoptosis IC_{50} = 0.0013 μM	Rascón-Valenzuela et al. (2016)
	in vitro bronchioalveolar carcinoma H358 cells *in vivo* mice injected with H358 cells	↑G2/M cell cycle arrest ↓CDK1, ↓CDK2, ↓fibronectin, ↓vimentin, ↓E-cadherin ↑caspases ↓p53, ↓Bcl-2, ↓Bsl-w ↓CTLA-4, ↓TGF-β/ERK	↓cancer cells growth Dose = 5.0 mg/kg ↑ apoptosis IC_{50} = 0.50 mg/mL	Tian et al. (2018)
Liver cancer	*in vitro* hepatocarcinoma HepG2 cells	↓IL-6, ↓TNF-α ↓TGF-β1, ↓JNK	↑cytotoxicity anti-inflammatory, ↓carcinogenesis IC_{50} = 0.04–0.02 μM	Li et al. (2009)
Colorectal cancer	*in vitro* CRC cells *in vivo* mice with CRC	↓Hippo pathway ↑YAP dephosphorylation ↓TEAD ↑Cap-3, 8	↓proliferation ↑apoptosis ↑lymphocyte infiltration ↓ cancer cells growth ↓tumor formation ↑mice survival	Meng et al. (2016)
	in vitro HT-29, HCT116 cells *in vivo* BALB/c immunodeficient nude mice injected with HT-29 cells	↑YAP dephosphorylation ↓Hippo ↓LATS1	↓cell proliferation ↓tumor growth ↓ tumor volume and weight IC_{50} = 0.2–10 μM	Zhou et al. (2019)
	in vitro SW480 cells	↓Wnt, ↓β-catenin ↓CK1α, ↑mRNA	↑apoptosis IC_{50} = 5.2 nM	Park et al. (2014)

(Continued on following page)

TABLE 1 (*Continued*) Summarized data obtained from preclinical pharmacological studies regarding calotropin anticancer activity.

Cancer type	Experimental model	Molecular mechanisms/ signaling pathways	Results	Ref
Leukemia	*in vitro* human chronic myeloid leukemia K562 cells human acute myeloid leukemia HL 60 cells	↑cell arrest in G2/M phase ↓cyclin A, B ↑Cap-3, 8,9, ↑p27 ↓NFκB/p50, ↓p-Akt ↓survivin ↓XIAP	↓ cancer cells growth ↑apoptosis IC_{50} = 0.01–20 μg/mL	Wang et al. (2009)
	in vitro adult T-cell leukemia/lymphoma ATL cells	↑cell arrest in G2/M phase	↑apoptosis	Nakano et al. (2020)

Abbreviations and symbols: ↑upregulated, ↓downregulated, B-cell lymphoma (Bcl 2), cisplatin-induced resistant NSCLC cell line (A549/CDDP), Yes-associated protein (YAP), large tumor suppressor 1 protein (LAST1), casein kinase 1α (CK1α), caspase (Cap), apoptotic protease activating factor-1 (Apaf-1), Na^+-Ca^{2+} exchanger (NCX), bcl-2-like protein 4 (Bax), interleukin (IL), X-linked inhibitor of apoptosis protein (XIAP), transforming growth factor β (TGF-β), Nuclear factor kappa-light-chain-enhancer of activated B cells (NF-κB).

dependent manner and leading to degradation of β-catenin by increasing the phosphorylation of β-catenin through casein kinase 1α (CK1α) (Park et al., 2014). Additionally, they concluded that calotropin increased mRNA and protein levels of CK1α. Further, since the Wnt signalling pathway is recognised as a regulator of the early and late stages of apoptosis, the early signs of apoptosis on the SW480 colon cancer cell line were observed after calotropin (5.2 nM) exposure for 24 h.

4.5 Leukemia

The observation that the anticancer effects of calotropin are probably mediated in a caspase-dependent manner was for the first time reported on human chronic myeloid leukemia K562 cells in research done by Wang et al. (2009). In the same research, calotropin treatment showed that the human acute myeloid leukemia HL 60 cells were more sensitive to cytotoxicity than K562 cells (K562 cells are the model system for the study of resistance to chemotherapy). The growth of cells was inhibited in a time and dose-dependent manner (0.01–20 μg/mL) in the G2/M phase with observed downregulation of cyclins, cyclin A, and cyclin B, and upregulation of p27 in K562 cells. It was suggested that calotropin may induce apoptosis through the caspase-dependent mechanism because in a dose-dependent manner was observed increases in the activity of Casp-3, Caps 8, and Casp-9 after calotropin treatment. Also, in a dose-dependent manner treatment with calotropin inhibit the expression of anti-apoptotic proteins and inhibitors of apoptotic proteins including NF-κB, p50, p-Akt and survivin, and XIAP (Figure 4). Calotropin is considered a potential agent for the treatment of adult T-cell leukemia/lymphoma (ATL). Nakano et al. (2020) showed that calotropin stopped the proliferation of MT-1 and MT-2 cells at the G2/M phase and promote apoptosis. At the same time, lower toxicity of calotropin was expressed toward normal PB-MNCs (peripheral blood mononuclear cells) compared to human T-cell leukemia virus type I infected T-cell lines (HTLV-I). MT-1 was derived from leukemia cells of peripheral blood from a patient with ATL, while the MT-2 cell line was derived from normal human cord leukocytes of the healthy donor which were co-cultivated with leukemia cells from an ATL patient (Yoshida et al., 1982). Table 1

5 Calotropin synergistic effects with chemotherapeutic agents

Standard treatments currently involve chemotherapy with or without surgical resection but there are still certain limitations. Using traditional plant extracts as an alternative therapeutic strategy is subject to much research. Standard chemotherapy is associated with drug resistance and the occurrence of systemic adverse effects on different organs that limit its utility Therefore, to overcome these barriers and achieve better therapeutic success, there are recommendations in some studies of a combination regimen of traditional chemotherapeutic and medicinal plant extracts (Sawong et al., 2022). In recent years, the role of cardenolides as a potential anticancer agent was revealed and has emerged as a possible adjunctive therapy to anticancer therapeutics. Sawong et al. (2022) have shown in a recent study that a combination of low-concentration doxorubicin and calotropin-induced apoptosis is accompanied by suppressed ATP production in HepG2 cells. After this treatment, the production of ATP was reduced, which was associated with the inhibition of glucose intake. Hepatocellular carcinoma cells switch to the glycolysis pathway, but they cannot neutralize ATP deficit so it induced apoptotic cell death in cancer cells. The rate of colorectal cancer is about 4.3% for men and 4.0% for women (https://www.wcrf.org/cancer-trends/colorectal-cancer-statistics/accessed September 2022), so only during 2020, there were more than 1. 9 million of new cases (https://www.wcrf.org/cancer-trends/colorectal-cancer-statistics/accessed September 2022) (2022). The combination of low concentrations of 5-FU and calotropin in comparison to a high dose of 5-FU reduced cell viability and abolish resistance to this conventional chemotherapeutic in HCT116 colorectal cancer cells. The same treatment significantly reduced the cellular ATP levels and increase ROS levels in HCT116 cells (Winitchaikul et al., 2021). Additionally, the increased intracellular concentration of ROS triggers autophagy and induced apoptotic cell death suppressing the activity of antioxidative enzymes (Scherz-Shouval et al., 2019). The level of the expression of autophagy-related genes could be reduced or even completely absent in cancer cells after calotropin treatment (Pederson et al., 2020).

6 Limitations

The therapeutic limitations and clinical pitfalls of calotropin as an anticancer agent are represented by insufficient data on adverse and toxic effects in humans. Very few cases have reported some digestive, hepatotoxic adverse effects and only one case with severe cardiotoxicity (Iyadurai et al., 2020). Other important limitations are the lack of clinical studies of calotropin in cancer, and the lack of *in vivo* studies of calotropin in experimental animal models for all cancers. As a result, these studies are needed in the future to confirm its anti-cancer therapeutic potential. Translational pharmacological studies are also needed to establish effective therapeutic doses in humans.

7 Conclusion

Traditional medicine from the Middle East, India, and China has a long period of usage, development and impact on the later evolvement of a great number of approved drugs and supplements. Until today this traditional medicine has been recognized as one of the most diverse with daily consumption by a huge number of their citizens. Despite their long-term usage, for most of the traditionally used plants, the full mechanism of action has not been discovered yet. However, modern medicine in the last few decades turns to reveal its true impact on health improvement and to confirm its mechanism of action. Finding the critical molecules in these traditionally used plants has a further influence on the development of modern drugs approved by different regulatory bodies across the world. Studies have shown that calotropin has cytotoxic and antitumor effects, the most representative effects being on breast, colon, lung and leukemia cancers. The main limitation of calotropin is represented by the fact its anticancer activity has been confirmed *in vitro*, while there is a lack of *in vivo* evidence, which is especially noted regarding human clinical studies; there are no available clinical trials where calotropin was investigated. Increasing interest in the anticancer effects of calotropin and numerous evidences of its activity on cancer cell lines puts calotropin on the pedestal of cancer research. Additionally, the encouraging evidence that the cytotoxic effects of calotropin can be avoided on normal cell lines makes it a promising agent for further research. There is not a lot of evidence of anticancer activity for chemicals obtained from plant-like there are for calotropin. However, it is evident that *in vivo* experiments on animals are still deficient, and that should be the next step in calotropin research.

Author contributions

Conceptualization and design were performed by JS-R; validation, investigation, data curation, and writing were performed by JR, RN, JG-M AY, and NA; review and editing were performed by DC, JS-R, and BA-O; supervision DC, JS-R, and BA-O; All the authors contributed equally, read and approved the final manuscript. All authors contribute equally, and have read and agreed to the published version of the manuscript.

Conflict of interest

The authors declare that the research was conducted in the absence of any commercial or financial relationships that could be construed as a potential conflict of interest.

Publisher's note

All claims expressed in this article are solely those of the authors and do not necessarily represent those of their affiliated organizations, or those of the publisher, the editors and the reviewers. Any product that may be evaluated in this article, or claim that may be made by its manufacturer, is not guaranteed or endorsed by the publisher.

Supplementary material

The Supplementary Material for this article can be found online at: https://www.frontiersin.org/articles/10.3389/fphar.2023.1160616/full#supplementary-material

References

Agrawal, A. A., Böröczky, K., Haribal, M., Hastings, A. P., White, R. A., Jiang, R. W., et al. (2021). Cardenolides, toxicity, and the costs of sequestration in the coevolutionary interaction between monarchs and milkweeds. *Proc. Natl. Acad. Sci. U. S. A.* 118, e2024463118. doi:10.1073/pnas.2024463118

Agrawal, A. A., Petschenka, G., Bingham, R. A., Weber, M. G., and Rasmann, S. (2012). Toxic cardenolides: Chemical ecology and coevolution of specialized plant-herbivore interactions. *New Phytol.* 194, 28–45. doi:10.1111/j.1469-8137.2011.04049.x

Al-Rowaily, S. L., Abd-ElgawadAssaeed, A. M., Elgamal, A. M., Gendy, A., Mohamed, T. A., et al. (2020). Essential oil of *Calotropis procera*: Comparative chemical profiles, antimicrobial activity, and allelopathic potential on weeds. *Molecules* 25, 5203. doi:10.3390/molecules25215203

Al-Taweel, A. M., Perveen, S., Fawzy, G. A., Rehman, A. U., Khan, A., Mehmood, R., et al. (2017). Evaluation of antiulcer and cytotoxic potential of the leaf, flower, and fruit extracts of *Calotropis procera* and isolation of a new lignan glycoside. *Evid. Based Complement. Altern. Med.* 2017, 8086791. doi:10.1155/2017/8086791

Bejček, J., Spiwok, V., Kmoníčková, E., and Rimpelová, S. (2021). Na(+)/K(+)-ATPase revisited: On its mechanism of action, role in cancer, and activity modulation. *Molecules* 26, 1905. doi:10.3390/molecules26071905

Buga, A. M., Docea, A. O., Albu, C., Malin, R. D., Branisteanu, D. E., Ianosi, G., et al. (2019). Molecular and cellular stratagem of brain metastases associated with melanoma. *Oncol. Lett.* 17, 4170–4175. doi:10.3892/ol.2019.9933

Da Costa, E. M., Armaos, G., Mcinnes, G., Beaudry, A., Moquin-Beaudry, G., Bertrand-Lehouillier, V., et al. (2018). Targeting MYC overexpressing leukemia with cardiac glycoside proscillaridin through downregulation of histone acetyltransferases. bioRxiv.

Elgamal, M. H. A., Hanna, A. G., Morsy, N. A. M., Duddeck, H., Simon, A., Gáti, T., et al. (1999). Complete and signal assignments of 5α-cardenolides isolated from *Calotropis procera* R. BR. *J. Mol. Struct.* 477, 201–208. doi:10.1016/s0022-2860(98)00615-2

Freitas, C. D. T., Silva, R. O., Ramos, M. V., Porfírio, C., Farias, D. F., Sousa, J. S., et al. (2020). Identification, characterization, and antifungal activity of cysteine peptidases from *Calotropis procera* latex. *Phytochemistry* 169, 112163. doi:10.1016/j.phytochem.2019.112163

GBD 2019 Colorectal Cancer Collaborators (2022). Global, regional, and national burden of colorectal cancer and its risk factors, 1990-2019: A systematic analysis for the global burden of disease study 2019. *Lancet Gastroenterol. Hepatol.* 7, 627–647. doi:10.1016/S2468-1253(22)00044-9

Grände, M., Franzen, A., Karlsson, J. O., Ericson, L. E., Heldin, N. E., and Nilsson, M. (2002). Transforming growth factor-beta and epidermal growth factor synergistically stimulate epithelial to mesenchymal transition (EMT) through a MEK-dependent mechanism in primary cultured pig thyrocytes. *J. Cell. Sci.* 115, 4227–4236. doi:10.1242/jcs.00091

Guo, Q., Liu, L., Chen, Z., Fan, Y., Zhou, Y., Yuan, Z., et al. (2022). Current treatments for non-small cell lung cancer. *Front. Oncol.* 12, 945102. doi:10.3389/fonc.2022.945102

He, Y. L., Yang, H. Y., Huang, P. Z., Feng, W. J., and Gao, K. (2021). Cytotoxic cardenolides from *Calotropis gigantea*. *Phytochemistry* 192, 112951. doi:10.1016/j.phytochem.2021.112951

Hoyer, K., Song, Y., Wang, D., Phan, D., Balschi, J., Ingwall, J. S., et al. (2011). Reducing the late sodium current improves cardiac function during sodium pump inhibition by ouabain. *J. Pharmacol. Exp. Ther.* 337, 513–523. doi:10.1124/jpet.110.176776

Huang, Y. H., Lei, J., Yi, G. H., Huang, F. Y., Li, Y. N., Wang, C. C., et al. (2018). Coroglaucigenin induces senescence and autophagy in colorectal cancer cells. *Cell. Prolif.* 51, e12451. doi:10.1111/cpr.12451

Ianoşi, S. L., Batani, A., Ilie, M. A., Tampa, M., Georgescu, S. R., Zurac, S., et al. (2019). Non-invasive imaging techniques for the *in vivo* diagnosis of Bowen's disease: Three case reports. *Oncol. Lett.* 17, 4094–4101. doi:10.3892/ol.2019.10079

Ibrahim, S. R., Mohamed, G. A., Shaala, L. A., Moreno, L., Banuls, Y., Kiss, R., et al. (2014). Proceraside A, a new cardiac glycoside from the root barks of Calotropis procera with *in vitro* anticancer effects. *Nat. Prod. Res.* 28, 1322–1327. doi:10.1080/14786419.2014.901323

Iordache, A. M., Docea, A. O., Buga, A. M., Mitrut, R., Albulescu, D., Zlatian, O., et al. (2019). The incidence of skin lesions in contrast media-induced chemical hypersensitivity. *Exp. Ther. Med.* 17, 1113–1124. doi:10.3892/etm.2018.7056

Iyadurai, R., Gunasekaran, K., Jose, A., and Pitchaimuthu, K. (2020). Calotropis poisoning with severe cardiac toxicity A case report. *J. Fam. Med. Prim. Care* 9, 4444–4447. doi:10.4103/jfmpc.jfmpc_783_20

Kadiyala, M., Ponnusankar, S., and Elango, K. (2013). *Calotropis gigantiea* (L.) R. Br (apocynaceae): A phytochemical and pharmacological review. *J. Ethnopharmacol.* 150, 32–50. doi:10.1016/j.jep.2013.08.045

Khan, M. I., Bouyahya, A., Hachlafi, N. E. L., Menyiy, N. E., Akram, M., Sultana, S., et al. (2022). Anticancer properties of medicinal plants and their bioactive compounds against breast cancer: A review on recent investigations. *Environ. Sci. Pollut. Res. Int.* 29, 24411–24444. doi:10.1007/s11356-021-17795-7

Kharat, K. R., and Kharat, A. S. (2019). The *Calotropis gigantea* methanolic extract induces apoptosis in human breast carcinoma cells. *Iran. J. Med. Sci.* 44, 483–492. doi:10.30476/ijms.2019.44966

Kim, N., Yim, H. Y., He, N., Lee, C. J., Kim, J. H., Choi, J. S., et al. (2016). Cardiac glycosides display selective efficacy for STK11 mutant lung cancer. *Sci. Rep.* 6, 29721. doi:10.1038/srep29721

Koch, V., Nieger, M., and Bräse, S. (2020). Towards the synthesis of calotropin and related cardenolides from 3-epiandrosterone: A-Ring related modifications. *Org. Chem. Front.* 7, 2670–2681. doi:10.1039/d0qo00269k

Kumar, V. L., Guruprasad, B., Chaudhary, P., Fatmi, S. M., Oliveira, R. S., and Ramos, M. V. (2015). Protective effect of proteins derived from *Calotropis procera* latex against acute inflammation in rat. *Auton. Autacoid Pharmacol.* 35, 1–8. doi:10.1111/aap.12022

Kumar, V. L., Verma, S., and Das, P. (2022). Anti-inflammatory and antioxidant effect of methanol extract of latex of *Calotropis procera* in rat model of colorectal cancer. *J. Ethnopharmacol.* 296, 115503. doi:10.1016/j.jep.2022.115503

Kupchan, S. M., Knox, J. R., Kelsey, J. E., and Saenzrenauld, J. A. (1964). CALOTROPIN, a cytotoxic principle isolated from *Asclepias curassavica* L. *Science* 146, 1685–1686. doi:10.1126/science.146.3652.1685

Lee, J. E., and Kim, M. Y. (2022). Cancer epigenetics: Past, present and future. *Semin. Cancer Biol.* 83, 4–14. doi:10.1016/j.semcancer.2021.03.025

Li, J. Z., Qing, C., Chen, C. X., Hao, X. J., and Liu, H. Y. (2009). Cytotoxicity of cardenolides and cardenolide glycosides from *Asclepias curassavica*. *Bioorg Med. Chem. Lett.* 19, 1956–1959. doi:10.1016/j.bmcl.2009.02.045

Magalhães, H. I., Ferreira, P. M., Moura, E. S., Torres, M. R., Alves, A. P., Pessoa, O. D., et al. (2010). *In vitro* and *in vivo* antiproliferative activity of *Calotropis procera* stem extracts. *Acad Bras Cienc* 82, 407–416. doi:10.1590/s0001-37652010000200017

Martucciello, S., Paolella, G., Romanelli, A. M., Sposito, S., Meola, L., Cerulli, A., et al. (2022). Pro-apoptotic and pro-autophagic properties of cardenolides from aerial parts of *Pergularia tomentosa*. *Molecules* 27, 4874. doi:10.3390/molecules27154874

Meneses-Sagrero, S. E., Rascón-Valenzuela, L. A., García-Ramos, J. C., Vilegas, W., Arvizu-Flores, A. A., Sotelo-Mundo, R. R., et al. (2022). Calotropin and corotoxigenin 3-O-glucopyranoside from the desert milkweed *Asclepias subulata* inhibit the Na(+)/K(+)-ATPase activity. *PeerJ* 10, e13524. doi:10.7717/peerj.13524

Meng, Z., Moroishi, T., and Guan, K. L. (2016). Mechanisms of Hippo pathway regulation. *Genes. Dev.* 30, 1–17. doi:10.1101/gad.274027.115

Mitroi, M., Albulescu, D., Capitanescu, A., Docea, A. O., Musat, G., Mitroi, G., et al. (2019). Differences in the distribution of CD20, CD3, CD34 and CD45RO in nasal mucosa and polyps from patients with chronic rhinosinusitis. *Mol. Med. Rep.* 19, 2792–2800. doi:10.3892/mmr.2019.9932

Mo, E. P., Zhang, R. R., Xu, J., Zhang, H., Wang, X. X., Tan, Q. T., et al. (2016). Calotropin from *Asclepias curasavica* induces cell cycle arrest and apoptosis in cisplatin-resistant lung cancer cells. *Biochem. Biophys. Res. Commun.* 478, 710–715. doi:10.1016/j.bbrc.2016.08.011

Mossa, J. S., Tariq, M., Mohsin, A., Ageel, A. M., Al-Yahya, M. A., Al-Said, M. S., et al. (1991). Pharmacological studies on aerial parts of *Calotropis procera*. *Am. J. Chin. Med.* 19, 223–231. doi:10.1142/S0192415X91000302

Mutiah, R., Widyawaruyanti, A., and Sukardiman, S. (2018). Calotroposid A: A glycosides terpenoids from *Calotropis gigantea* induces apoptosis of colon cancer WiDr cells through cell cycle arrest G2/M and caspase 8 expression. *Asian Pac J. Cancer Prev.* 19, 1457–1464. doi:10.22034/APJCP.2018.19.6.1457

Nakamura, H., and Takada, K. (2021). Reactive oxygen species in cancer: Current findings and future directions. *Cancer Sci.* 112, 3945–3952. doi:10.1111/cas.15068

Nakano, D., Ishitsuka, K., Takashima, M., Arima, R., Satou, A., Tsuchihashi, R., et al. (2020). Screening of promising chemotherapeutic candidates from plants against human adult T-cell leukemia/lymphoma (VI): Cardenolides from *Asclepias curassavica*. *Biol. Pharm. Bull.* 43, 1609–1614. doi:10.1248/bpb.b20-00465

Paesmans, M., Grigoriu, B., Ocak, S., Roelandts, M., Lafitte, J. J., Holbrechts, S., et al. (2015). Systematic qualitative review of randomised trials conducted in nonsmall cell lung cancer with a noninferiority or equivalence design. *Eur. Respir. J.* 45, 511–524. doi:10.1183/09031936.00092814

Pan, L. C., Xiao, H. Y., Yin, W. J., and Lin, Z. (2018). Correlation between HSD17B4 expression in rat liver cancer tissues and inflammation or proliferation. *Eur. Rev. Med. Pharmacol. Sci.* 22, 3386–3393. doi:10.26355/eurrev_201806_15160

Park, H. Y., Toume, K., Arai, M. A., Sadhu, S. K., Ahmed, F., and Ishibashi, M. (2014). Calotropin: A cardenolide from *Calotropis gigantea* that inhibits Wnt signaling by increasing casein kinase 1α in colon cancer cells. *Chembiochem* 15, 872–878. doi:10.1002/cbic.201300786

Pattnaik, P. K., Kar, D., Chhatoi, H., Shahbazi, S., Ghosh, G., and Kuanar, A. (2017). Chemometric profile and antimicrobial activities of leaf extract of *Calotropis procera* and *Calotropis gigantea*. *Nat. Prod. Res.* 31, 1954–1957. doi:10.1080/14786419.2016.1266349

Pederson, P. J., Cai, S., Carver, C., Powell, D. R., Risinger, A. L., Grkovic, T., et al. (2020). Triple-negative breast cancer cells exhibit differential sensitivity to cardenolides from *Calotropis gigantea*. *J. Nat. Prod.* 83, 2269–2280. doi:10.1021/acs.jnatprod.0c00423

PubChem (2022). PubChem. Available: https://pubchem.ncbi.nlm.nih.gov/.

Rascón-Valenzuela, L. A., Jiménez Estrada, M., Velázquez Contreras, C. A., Garibay Escobar, A., Medina Juárez, L. A., Gámez Meza, N., et al. (2015b). Antiproliferative and apoptotic activities of extracts of *Asclepias subulata*. *Pharm. Biol.* 53, 1741–1751. doi:10.3109/13880209.2015.1005752

Rascón-Valenzuela, L. A., Velázquez, C., Garibay-Escobar, A., Vilegas, W., Medina-Juárez, L. A., Gámez-Meza, N., et al. (2016). Apoptotic activities of cardenolide glycosides from *Asclepias subulata*. *J. Ethnopharmacol.* 193, 303–311. doi:10.1016/j.jep.2016.08.022

Rascón-Valenzuela, L., Velázquez, C., Garibay-Escobar, A., Medina-Juárez, L. A., Vilegas, W., and Robles-Zepeda, R. E. (2015a). Antiproliferative activity of cardenolide glycosides from *Asclepias subulata*. *J. Ethnopharmacol.* 171, 280–286. doi:10.1016/j.jep.2015.05.057

Sawong, S., Pekthong, D., Suknoppakit, P., Winitchaikul, T., Kaewkong, W., Somran, J., et al. (2022). Calotropis gigantea stem bark extracts inhibit liver cancer induced by diethylnitrosamine. *Sci. Rep.* 12, 12151. doi:10.1038/s41598-022-16321-0

Scheau, C., Caruntu, C., Badarau, I. A., Scheau, A. E., Docea, A. O., Calina, D., et al. (2021). Cannabinoids and inflammations of the gut-lung-skin barrier. *J. Pers. Med.* 11, 494. doi:10.3390/jpm11060494

Scherz-Shouval, R., Shvets, E., Fass, E., Shorer, H., Gil, L., and Elazar, Z. (2019). Reactive oxygen species are essential for autophagy and specifically regulate the activity of Atg4. *Embo J.* 38, e101812. doi:10.15252/embj.2019101812

Sharma, M., Tandon, S., Aggarwal, V., Bhat, K. G., Kappadi, D., Chandrashekhar, P., et al. (2015). Evaluation of antibacterial activity of *Calotropis gigentica* against *Streptococcus mutans* and *Lactobacillus acidophilus*: An *in vitro* comparative study. *J. Conserv. Dent.* 18, 457–460. doi:10.4103/0972-0707.168809

Silva, I. T., Munkert, J., Nolte, E., Schneider, N. F. Z., Rocha, S. C., Ramos, A. C. P., et al. (2018). Cytotoxicity of AMANTADIG – A semisynthetic digitoxigenin derivative – Alone and in combination with docetaxel in human hormone-refractory prostate cancer cells and its effect on Na+/K+-ATPase inhibition. *Biomed. Pharmacother.* 107, 464–474. doi:10.1016/j.biopha.2018.08.028

Solowey, E., Lichtenstein, M., Sallon, S., Paavilainen, H., Solowey, E., and Lorberboum-Galski, H. (2014). Evaluating medicinal plants for anticancer activity. *ScientificWorldJournal* 2014, 721402. doi:10.1155/2014/721402

Sweidan, N., Esawi, E., Ismail, M., and Alshaer, W. (2021). Anticancer Cardenolides from the aerial parts of *Calortopis procera*. *Z Naturforsch C J. Biosci.* 76, 243–250. doi:10.1515/znc-2020-0281

Tian, L., Xie, X. H., and Zhu, Z. H. (2018). Calotropin regulates the apoptosis of non-small cell cancer by regulating the cytotoxic T-lymphocyte associated antigen 4-mediated TGF-β/ERK signaling pathway. *Mol. Med. Rep.* 17, 7683–7691. doi:10.3892/mmr.2018.8853

Tsoukalas, D., Fragkiadaki, P., Docea, A. O., Alegakis, A. K., Sarandi, E., Vakonaki, E., et al. (2019). Association of nutraceutical supplements with longer telomere length. *Int. J. Mol. Med.* 44, 218–226. doi:10.3892/ijmm.2019.4191

Vila Petroff, M. G., Palomeque, J., and Mattiazzi, A. R. (2003). Na(+)-Ca2+ exchange function underlying contraction frequency inotropy in the cat myocardium. *J. Physiol.* 550, 801–817. doi:10.1113/jphysiol.2003.044321

Wang, S. C., Lu, M. C., Chen, H. L., Tseng, H. I., Ke, Y. Y., Wu, Y. C., et al. (2009). Cytotoxicity of calotropin is through caspase activation and downregulation of anti-apoptotic proteins in K562 cells. *Cell. Biol. Int.* 33, 1230–1236. doi:10.1016/j.cellbi.2009.08.013

WFO (2021). WFO the World Flora online. Available: http://www.worldfloraonline.org/.

Winitchaikul, T., Sawong, S., Surangkul, D., Srikummool, M., Somran, J., Pekthong, D., et al. (2021). *Calotropis gigantea* stem bark extract induced apoptosis related to ROS and ATP production in colon cancer cells. *PLoS One* 16, e0254392. doi:10.1371/journal.pone.0254392

Yao, H., He, G., Yan, S., Chen, C., Song, L., Rosol, T. J., et al. (2017). Triple-negative breast cancer: Is there a treatment on the horizon? *Oncotarget* 8, 1913–1924. doi:10.18632/oncotarget.12284

Yoshida, M., Miyoshi, I., and Hinuma, Y. (1982). A retrovirus from human leukemia cell lines: Its isolation, characterization, and implication in human adult T-cell leukemia (ATL). *Princess Takamatsu Symp.* 12, 285–294.

Zhang, X., Cao, L., Ji, B., Li, L., Qi, Z., and Ding, S. (2020). Endurance training but not high-intensity interval training reduces liver carcinogenesis in mice with hepatocellular carcinogen diethylnitrosamine. *Exp. Gerontol.* 133, 110853. doi:10.1016/j.exger.2020.110853

Zhou, L., Cai, L., Guo, Y., Zhang, H., Wang, P., Yi, G., et al. (2019). Calotropin activates YAP through downregulation of LATS1 in colorectal cancer cells. *Onco Targets Ther.* 12, 4047–4054. doi:10.2147/OTT.S200873

frontiers | Frontiers in Oncology

TYPE Original Research
PUBLISHED 17 April 2023
DOI 10.3389/fonc.2023.1143664

OPEN ACCESS

EDITED BY
Mitesh Patel,
Parul University, India

REVIEWED BY
Man-Tat Lau,
Children's Medical Research Institute, Australia
Mounir Tilaoui,
Waterford Institute of Technology, Ireland

*CORRESPONDENCE
Yucui Dong
dongyucui521@yeah.net
Xiao Zhu
xzhu@ytu.edu.cn

SPECIALTY SECTION
This article was submitted to Pharmacology of Anti-Cancer Drugs, a section of the journal Frontiers in Oncology

RECEIVED 13 January 2023
ACCEPTED 04 April 2023
PUBLISHED 17 April 2023

CITATION
Zhang X, Zhao L, Xiao J, Wang Y, Li Y, Zhu C, Zhang H, Zhang Y, Zhu X and Dong Y (2023) 5-Demethylnobiletin mediates cell cycle arrest and apoptosis *via* the ERK1/2/AKT/STAT3 signaling pathways in glioblastoma cells. *Front. Oncol.* 13:1143664. doi: 10.3389/fonc.2023.1143664

5-Demethylnobiletin mediates cell cycle arrest and apoptosis *via* the ERK1/2/AKT/STAT3 signaling pathways in glioblastoma cells

Xuehua Zhang[1], Leilei Zhao[1], Jinlong Xiao[1], Yudi Wang[1], Yunmeng Li[1], Chaoqun Zhu[2], He Zhang[3], Yurui Zhang[1], Xiao Zhu[2]* and Yucui Dong[1]*

[1]Department of Immunology, Binzhou Medical University, Yantai, China, [2]School of Computer and Control Engineering, Yantai University, Yantai, China, [3]Department of Immunology, Qiqihar Medical University, Qiqihar, China

5-Demethylnobiletin is the active ingredient in citrus polymethoxyflavones that could inhibit the proliferation of several tumor cells. However, the anti-tumor effect of 5-Demethylnobiletin on glioblastoma and the underlying molecular mechanisms are remains unknown. In our study, 5-Demethylnobiletin markedly inhibited the viability, migration and invasion of glioblastoma U87-MG, A172 and U251 cells. Further research revealed that 5-Demethylnobiletin induces cell cycle arrest at the G0/G1 phase in glioblastoma cells by downregulating Cyclin D1 and CDK6 expression levels. Furthermore, 5-Demethylnobiletin significantly induced glioblastoma cells apoptosis by upregulating the protein levels of Bax and downregulating the protein level of Bcl-2, subsequently increasing the expression of cleaved caspase-3 and cleaved caspase-9. Mechanically, 5-Demethylnobiletin trigged G0/G1 phase arrest and apoptosis by inhibiting the ERK1/2, AKT and STAT3 signaling pathway. Furthermore, 5-Demethylnobiletin inhibition of U87-MG cell growth was reproducible *in vivo* model. Therefore, 5-Demethylnobiletin is a promising bioactive agent that might be used as glioblastoma treatment drug.

KEYWORDS

glioblastoma, 5-Demethylnobiletin, cell cycle arrest, cell apoptosis, ERK1/2, AKT, STAT3

1 Introduction

Glioblastoma (GBM) is the most common, lethal, and aggressive adult central nervous system (CNS) primary malignant brain tumor (1). The traditional treatment of standard for patients with GBM consists of maximum surgical excision followed by concurrent chemotherapy and radiotherapy (2). Unfortunately, the traditional treatment methods are not ideal, the recurrence rate is high as well as the emergence of tumor resistance. After treatment, the median survival time for GBM patients is 15 months, with a 5-year survival

rate of less than 5% (3). Therefore, it is essential to discover novel drugs and identify new therapeutic strategies to enhance GBM therapy.

Polymethoxyflavones (PMFs) are a class of highly methoxylated flavonoids unique to citrus plants, and they are gaining increasing attention due to their diverse biological activities (4–6). Nobiletin and tangeretin are the main PMFs in citrus peels (7). Previous research has shown that nobiletin has potent anti-leukemic characteristics and has the potential for chemoprevention (8, 9). 5-Demethylnobiletin (5-DMN) is one of the promising nobiletin derivatives, the most plentiful demethylated PMF, which is mainly generated during long-term storage by autohydrolysis of nobiletin in citrus peel. 5-DMN has plenty of biological properties, including anticancer, anti-inflammatory, antioxidant and neuroprotective (7, 10). Interestingly enough, 5-DMN inhibited the growth of various tumor cells more effectively than nobiletin (11). Recent research has demonstrated that 5-DMN has anticancer effects in human leukemia (12), colon (13) and lung cancer (14). Chen et al. (6) discovered that 5-DMN could increase the synthesis of polymerized tubulin and cause cell cycle arrest in the G2/M phase by activating JNK signal in lung cancer cells. In acute myeloid leukemia, 5-DMN inhibited cell proliferation and induced apoptosis by affecting the NF-κB signaling pathway (15). Furthermore, 5-DMN treatment of colon cancer cell line HCT116 cells increased the apoptosis rate of the cells by activating the caspase cascade reaction (16). However, there was no evidence that 5-DMN inhibited GBM cell growth specifically by modulating cell cycle and apoptosis-related signaling pathways. In addition, studies have shown that 5-DMN not only promoted neurocytogenesis and neurogenesis, but also negatively regulated acetylcholinesterase (AChE) activity (17). This means that 5-DMN could through the blood-brain barrier and could be used in the treatment of neurodegenerative diseases and cholinergic abnormalities (18, 19), and may have a pharmacological advantage in the treatment of intracranial tumors.

In our study, the antitumor effects and potential mechanisms underlying the impact of 5-DMN on GBM were investigated for the first time both *in vitro* and *in vivo*. We elucidated that 5-DMN promoted G0/G1 phase arrest and apoptosis in glioblastoma cells by restraining the ERK1/2, AKT and STAT3 signaling pathways. The results of our study will help to evaluate the potential applications of 5-DMN as a clinical agent for glioblastoma.

2 Materials and methods

2.1 Ethical statement

All animal experiments protocols were designed in strict accordance with the guidelines and approved by the Animal Experiment Ethics Committee of Binzhou Medical University.

2.2 Cell culture and reagents

Human glioblastoma cell lines, including U87-MG, A172 and U251 were obtained from the American Type Culture Collection (ATCC) (Manassas, VA, USA). Cells were grown in Dulbecco's Modified Eagle's Medium (DMEM, Gibco) with 10% fetal bovine serum (FBS; Vistech) and 1% penicillin/streptomycin (Beyotime, Shanghai, China) at 37°C incubator with 5% CO_2. 5-Demethylnobiletin was obtained from Selleck (Shanghai, China) and stored in dimethyl sulfoxide (DMSO) at the appropriate concentration of 10 mM. The inhibitors were purchased from Sigma-Aldrich (StLouis, MO, USA), which were kept at optimal concentrations in DMSO.

2.3 MTT assays

When cells reached the logarithmic growth phase, they were digested with 0.25% trypsin and adjusted to a density of 6×10^4 cells/ml and 100 μL cell suspension was added to a 96-well plate. The GBM cells were treated for 48 h with 5-DMN at various doses (0, 6.25, 12.5, 25, 50, 100 μM) after cell adhesion. Each well received 20 μL of MTT reagent (0.5 mg/mL, Sigma-Aldrich) and the cells were incubated for 4 h. The supernatant was discarded, and 150 μL of DMSO was added. After 3 times of shaking plate, the absorbance at 490 nm was measured using a microplate reader (DMI3000, Leica, Germany) to determine the cell viability rate.

2.4 Live/dead co-staining by Calcein-AM and PI

Different doses of 5-DMN (0, 12.5, 25, 50 μM) or inhibitors were applied after cells attained 80% confluence in a 6-well plate. After 48 h treatment, the Calcein AM/Propidium Iodide (PI) staining kit (Solarbio, Beijing, China) was used to stain the cells. Incubation for 0.5 h at 37°C, PBS was used to wash the cells and representative photograph were captured using Confocal laser scanning microscopy (Carl Zeiss AG, Jena, Germany).

2.5 Migration assays

Wound healing experiments were used to measure cell migratory ability. When GBM cells reached the appropriate density, and confluent cells were wounded with a 10-μL pipette tip before being incubated with 5-DMN for 48 h. Six visual fields were randomly selected to observe and quantify the wound closure rate at different time points under the microscope.

2.6 Invasion assays

Transwell chambers (Corning, New York, USA) were precoated with Matrigel (BD Biosciences) in a 24-well plate. The serum-starved cells were diluted with serum-free DMEM medium to a density of 1×10^6 cells/ml and 100 μL cell suspension was added to the upper chamber. The lower well contains 600 μL DMEM supplemented with 5% FBS. When GBM cells had adhered to the well, the lower chamber medium was changed to drug-medium

containing 5-DMN of 25 or 50 μM and then incubation for 48 h. The GBM cells on the lower surface were fixed and stained with 1% crystal violet (Sigma-Aldrich). Cell invasion rates were quantified in six randomly selected fields and images of the cells were captured at 20 × magnification.

2.7 Cell cycle analysis

GBM cells were incubated with four concentrations of 5-DMN for 48 h before being collected, fixed with 70% pre-cooled ethanol and incubated additional 12 h at 4 °C. Cell precipitation were rinsed twice with PBS, RNase and PI were added for DNA staining, and the fluorescence intensity was measured by Flow cytometry (Beckman Coulter, Inc., Brea, CA, USA). The Modfit software (Scribpps Research, La Jolla, CA, USA) was used to analyze the percentage of cells in each phase of the cell cycle.

2.8 Cell apoptosis assays

The flow cytometer was used to analyze cell apoptosis using the Annexin V-FITC Apoptosis Assay Kit (Beyotime). GBM cells at the logarithmic growth stage were seeded in 6-well plate before being treated with 5-DMN (0, 12.5, 25, 50 μM) for 48 h. After the cells were collected, loading buffer in moderation was added for suspended cells, followed by 5 μL Annexin V-FITC and 5 μL PI incubation and prepared within 1 h.

2.9 Western blotting

Cell protein was harvested using cell lysis buffer (Solarbio) and protein concentration was measured using the BSA protein kit (Solarbio). Protein samples of 30 μg were taken from each lane for 10% sodium dodecyl sulfate-polyacrylamide gel electrophoresis (SDS-PAGE). The proteins were transferred to PVDF membranes, which were incubated with primary antibody at 4 °C overnight. All antibodies were purchased from Cell Signaling Technology (CST, Danvers, MA, USA): anti-Cyclin D1 (1:1000, cat no. 55506), anti-CDK6 (1:1000, cat no. 13331), anti-Bcl-2 (1:1000, cat no. 15071), anti-Bax (1:1000, cat no. 89477), anti-caspase-3 (1:1000, cat no. 9662), anti-cleaved caspase-3 (1:1000, cat no. 9661), anti-caspase-9 (1:1000, cat no. 9508), anti-cleaved caspase-9 (1:1000, cat no. 9509), p-ERK1/2 (1:2000, cat no. 4370), ERK (1:1000, cat no. 4695), p-AKT (1:2000, cat no. 4060), AKT (1:1000, cat no. 4685), p-STAT3 (1:2000, cat no. 9145), STAT3 (1:1000, cat no. 9139) and β-actin (1:1000, cat no. 4970). After being three times washed in TBST, PVDF membrane was incubated with HRP-conjugated second antibody at room temperature for 2 h. Enhanced chemiluminescence (ECL, Thermo Fisher Scientific, Shanghai, China) was used to visualize the immunocomplexes, and gray-scale values for each band were determined using Image J software.

2.10 *In vivo* antitumor activity study

BALB/c female nude mice aged 4-week-old were purchased from SiPeiFu (SPF Biotechnology Co., Ltd, Beijing) and lived in a germfree environment with constant temperature and humidity, suitable for food and water. All mice were slowly injected subcutaneously with U87-MG cells (5×10^6 cells/100 μL) under the armpit of the right forelimb. When the tumors reached 3-4mm in diameter, these nude mice were divided into 5-DMN and control groups, and administered an intraperitoneal (i. p.) injection of 5% DMSO + 40% PEG300 (Selleck) + 5% Tween 80 (Selleck) + 50% water (control) or 5-DMN 3 mg/kg that was dissolved in DMSO, PEG300, Tween 80 and water (5:40:5:50 v/v). Mice were given treatment every other day using 100 μL total volumes. Tumor volumes were assessed every two days and were calculated as $0.5 \times \text{length} \times \text{width}^2$. The mice were sacrificed under adequate anesthesia 21 days after treatment.

2.11 Statistical analyses

The experiments data was expressed as the mean ± standard deviation (mean ± SD). All statistical analyses were performed with the SPSS version 23.0 software, and graphics were created with the GraphPad Prism 8 program (GraphPad Software, San Diego, CA). The data from two groups were compared using a two-tailed Student's t-test or a two-way ANOVA. $^*p < 0.05$; $^{**}p < 0.01$; $^{***}p < 0.001$ were considered statistically significant differences.

3 Results

3.1 5-DMN inhibits the viability, migration and invasion ability of GBM cells *in vitro*

To explore the impact of 5-DMN on glioblastoma *in vitro*, U87-MG, A172 and U251 cells were treated with 5-DMN for 48 h at set concentrations. The cell activity data revealed that 5-DMN administration greatly inhibited the proliferation of U87-MG, A172, and U251 cells (Figure 1A). Similar procedures were implemented to assess the cell activity on normal human brain astrocyte cell lines (HA1800) and human embryonic kidney (HEK293T) cell lines. The results showed that 5-DMN had no significant cytotoxic activity on HA1800 and HEK293T cell in the concentration range of 0 - 100 μM for 48 h (Figure S1A). To determine cell viability more intuitively, a living/dead assay was conducted. Calcein-AM/PI was employed to stain living with green and dead cells with red. The results indicated that the green fluorescence of living cells reduced dramatically, while the red fluorescence increased significantly accompanied the increase of 5-DMN concentration, which further verified the outstanding cytotoxicity of 5-DMN (Figure 1B).

The poor prognosis of GBM patients was related to the motility and metastasis ability of the tumor cells. Therefore, migration and invasion experiments were conducted after different concentration

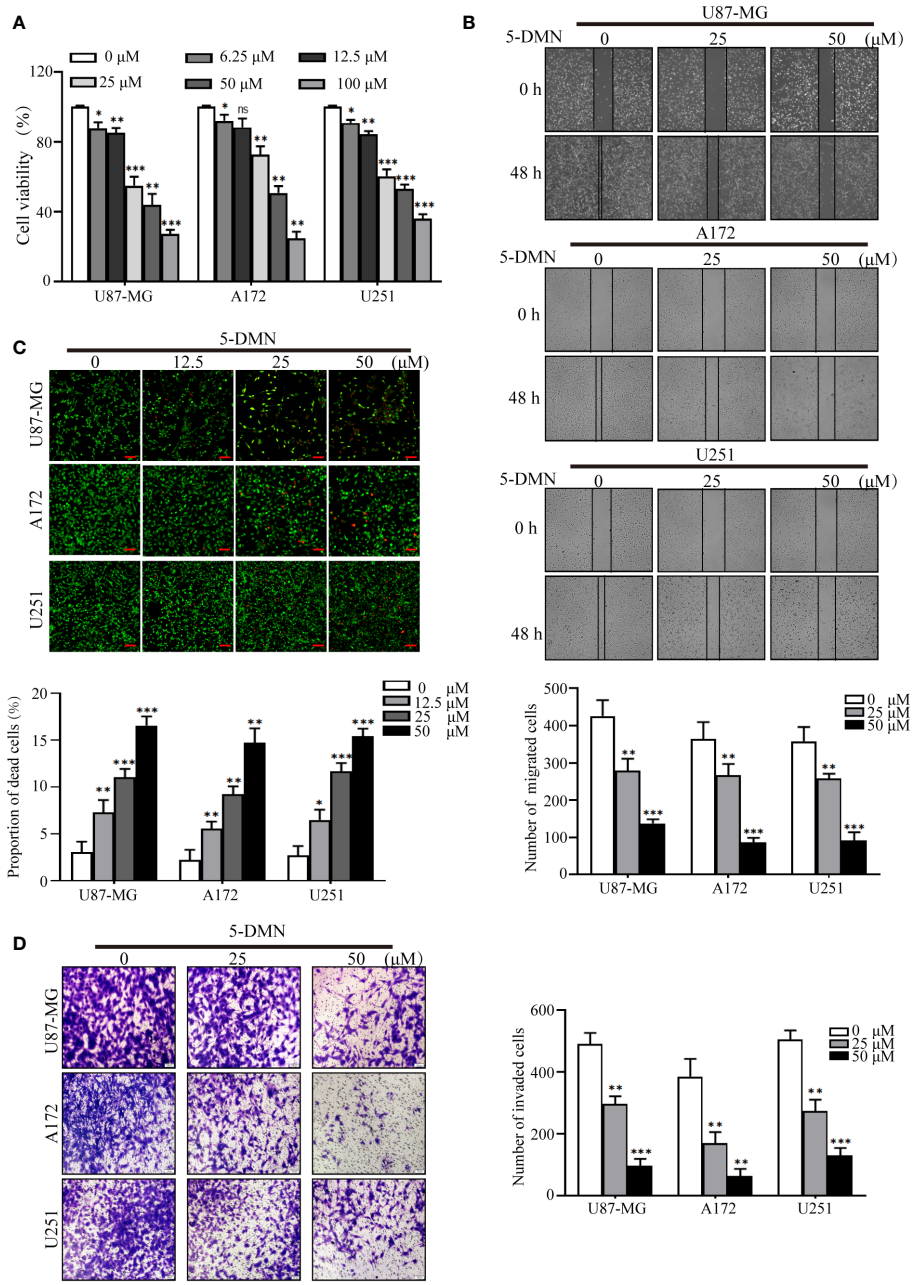

FIGURE 1
Inhibitory effects of 5-DMN on the viability, migration and invasion of GBM cells. **(A)** Cell viability was determined using the MTT assay after cultured U87-MG, A172, and U251 cells were incubated with various doses of 5-DMN for 48 h. **(B)** The merged image of live cells (green) and dead cells (red) in GBM cells treated with different concentrations of 5-DMN. Scale bar = 100 μm. **(C)** Wound healing assays were used to determine the migration ability of U87-MG, A172, and U251 cells after 48 h of incubation with 5-DMN (0, 25, 50 μM). **(D)** The invasion ability of GBM cells treated with or without 5-DMN (25, 50 μM) for 48 h was detected by transwell assays. Values are the means ± SD of three independent experiments. *p<0.05, **p<0.01, ***p<0.001 vs. cells in the untreated control group. ns, no significance.

5-DMN (25 μM, 50 μM) was added to U87-MG, A172 and U251 cells. As shown in Figures 1C, D, GBM cells migration and invasion in the 5-DMN treatment group was considerably reduced in a dose-dependent manner. In addition, to further evaluate the cytotoxicity on GBM cells of 5-DMN compared with Temozolomide (TMZ), which is the first-line chemotherapeutic drug for patients with GBM, U87-MG, A172 and U251 cells were treated with TMZ for 48 h. As shown in Figure S1B, in treatments with the same drug concentration, the cytotoxic effect of TMZ was not obvious in the three GBM cells compared with 5-DMN, suggesting a higher anti-cancer efficacy of 5-DMN in GBM cells. Furthermore, wound healing experiment was conducted after different concentration TMZ (25 μM, 50 μM) was added to GBM cells for 48 h, the results showed that U87-MG, A172 and U251 cells migration was

not significantly reduced in the TMZ treatment group (Figure S1C). In conclusion, our results demonstrated that 5-DMN had the potential to inhibit GBM cells malignant biological behavior *in vitro*.

3.2 5-DMN induces G0/G1 phase cycle arrest in GBM cells

To investigate whether 5-DMN-induced decrease in GBM cell viability was related to cell cycle arrest, flow cytometry was used to analyze cell cycle distribution after a 48-h treatment with 5-DMN. Figure 2A showed that the percentages of 5-DMN treated cells in the G0/G1 phase was considerably higher than that the control group. To further explained the mechanism that 5-DMN mediated cell cycle arrest, the expression of G0/G1 phase related proteins was evaluated in U87-MG, A172 and U251 cells, respectively. The activity of Cyclin D1 and CDK are required for G1 phase progression of the cell cycle and G1/S transition (20). Western blotting analysis demonstrated that Cyclin D1 and CDK6 expression was considerably reduced in 5-DMN-treated GBM cells compared with the control group (Figure 2B). The aforementioned data showed that 5-DMN induced G0/G1 phase cell cycle arrest by regulating the expression of Cyclin D1 and CDK6.

3.3 5-DMN induces apoptosis in GBM cells

To further investigate whether the inhibitory activity of 5-DMN-induced cell proliferation was associated with apoptosis, Annexin V-FITC/PI double staining was used to evaluate the apoptotic rate of cells treated with 5-DMN for 48 h. As shown in Figure 3A, the apoptotic cells were significantly increased in U87-MG, A172 and U251 cells with the increase of 5-DMN concentration. Then, the expression of signaling proteins related to apoptosis was tested by western blotting in these cells. We found that the protein levels of Bax, cleaved caspase-3, -9 was remarkedly elevated, while the expression of Bcl-2, caspase-3, -9 was inhibited in 5-DMN-treated cells (Figure 3B). In conclusion, these results demonstrated that 5-DMN effectively induced GBM cells apoptosis.

3.4 5-DMN inhibits the ERK1/2, AKT and STAT3 signaling pathways in GBM cells

ERK1/2, PI3K/AKT and STAT3 signaling are classical oncogenic signaling pathways that have been reported in GBM (21, 22). To tested whether 5-DMN had the inhibitory effect on these signal molecules, we treated GBM cells with 5-DMN at four different concentrations. Western blotting analysis showed that the phosphorylation of ERK1/2, AKT and STAT3 in 5-DMN treated

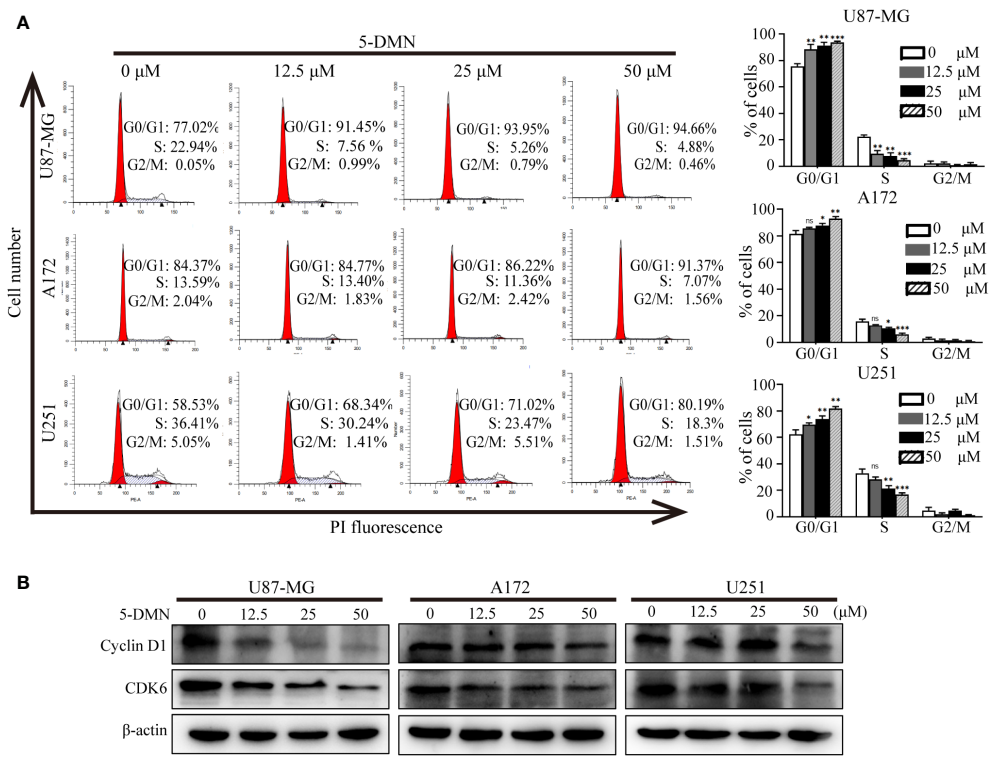

FIGURE 2
5-DMN induces cell cycle arrest at the G0/G1 phase in GBM cells. **(A)** The cell cycle distribution of U87-MG, A172, and U251 cells treated with different concentrations of 5-DMN was determined using flow cytometry. The histograms indicated the distribution of cell cycle from three separate experiments. **(B)** Levels of Cyclin D1 and CDK6 proteins in 5-DMN-treated GBM cells were detected by western blotting. The loading control was β-actin. *p<0.05, **p<0.01, ***p<0.001. ns, no significance.

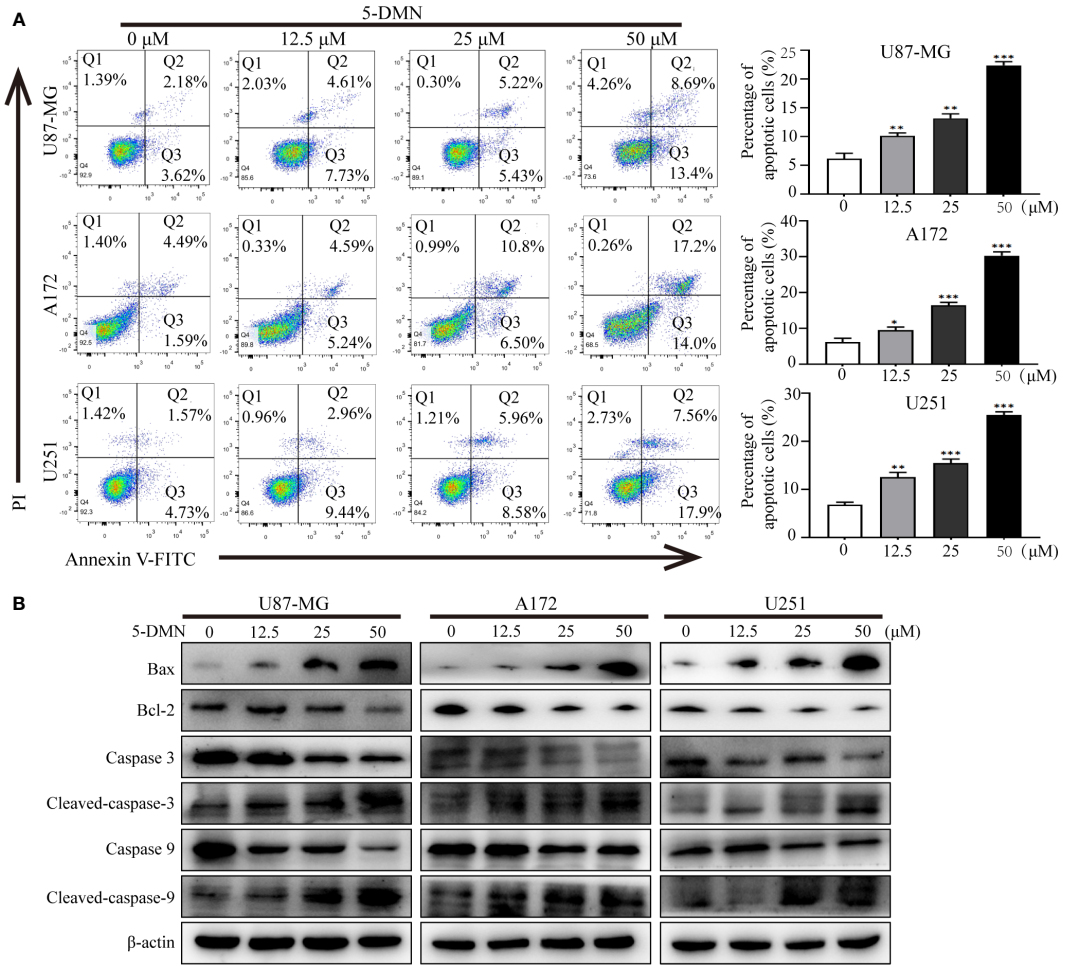

FIGURE 3
5-DMN induces GBM cells apoptosis. **(A)** The apoptotic rate of U87-MG, A172, and U251 cells after 5-DMN treatment was determined using double staining with Annexin V-FITC/PI. The histograms showed the percentage of apoptosis in three separate experiments. **(B)** Western blotting analysis of the expression of Bcl-2, Bax and caspase-3/9. The loading control was β-actin. *p<0.05, **p<0.01, ***p<0.001 vs. the untreated group cells.

cells were considerably lower than the control group (Figures 4A, B). These data indicated that 5-DMN could inhibit the ERK1/2, PI3K/AKT and STAT3 signal pathway in GBM cells.

3.5 Cell cycle arrest and apoptosis are mediated by the inhibition of the ERK1/2, AKT and STAT3 signaling pathway

To determine whether 5-DMN induced cell viability, cell cycle arrest and apoptosis were related to ERK1/2, AKT or STAT3 signaling pathways, the MEK inhibitor U0126, PI3K inhibitor LY294002 and STAT3 inhibitor WP1066 were used for further investigation in U87-MG cells. Figure 5A showed that the number of PI-positive cells in the U0126, LY294002 and WP1066 groups were obviously higher than the control group. Interestingly, a higher number of PI-positive cells were observed when combination of these inhibitors and 5-DMN than for 5-DMN treatment. Flow cytometric analysis also demonstrated that U0126, LY294002 and WP1066 significantly increased G0/G1 phase arrest induced by 5-DMN (Figure 5B). The same results were obtained by using flow cytometry to detect the apoptotic rate in 5-DMN or combination different inhibitors treated U87-MG cells (Figure 6A). These results indicated that in the process of G0/G1 phase arrest and cell death, ERK1/2, AKT and STAT3 signaling were suppressed by 5-DMN. Western blotting revealed that U0126, LY294002 and WP1066 further enhanced the inhibition of 5-DMN on the expression of cyclin-related proteins (Cyclin D1 and CDK6) and the promotion on the expression of pro-apoptosis-related proteins (caspase-3 and -9) (Figure 6B). In summary, 5-DMN induced G0/G1 phase arrest and triggered apoptosis by blocking the ERK1/2, AKT and STAT3 signaling pathways in GBM cells.

3.6 5-DMN inhibits the proliferation of GBM cells *in vivo*

To further assess the cytotoxicity of 5-DMN *in vivo*, U87-MG cells (5×10^6 cells/100 μL) were implanted into BALB/c nude mice *via* slowly injection. When the tumor grew to a diameter of 3-4 mm,

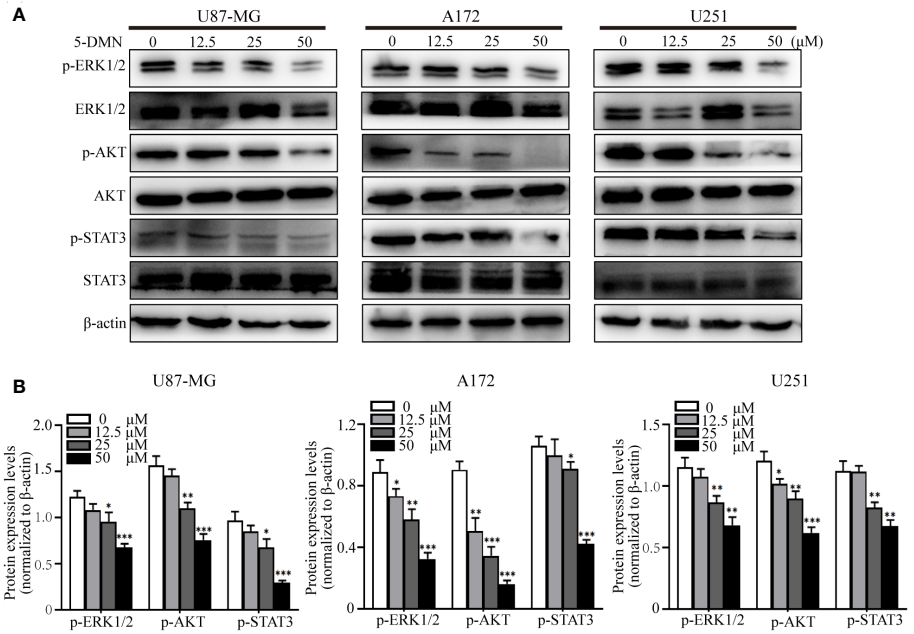

FIGURE 4
5-DMN inhibits the ERK1/2, AKT and STAT3 pathways in GBM cells. Cultured U87-MG, A172 and U251 cells were incubated with or without 50 μM 5-DMN for 48 h. **(A)** Western blotting analysis of the expression of p-ERK1/2, ERK1/2, p-AKT, AKT, p-STAT3 and STAT3. **(B)** The relative protein levels of p-ERK1/2, p-AKT and p-STAT3 in 5-DMN-treated GBM cells were analyzed. The protein levels in the untreated group were used to standardize the relative protein ratio. *p<0.05, **p<0.01, ***p<0.001 vs. cells in the untreated group.

nude mice were randomly assigned to the control and 5-DMN groups, and then injected intraperitoneally every other day. After nine times of administration, the tumor growth curve results showed that 5-DMN (3 mg/kg) effectively inhibited the tumor growth compared with the control group (Figure 7A). During treatment, the weight of nude mice was monitored before each injection, and the results demonstrated that 5-DMN treatment had no influence on body weight (Figure 7B). Tumors were separated and tumor weights were also measured (Figures 7C, D). The tumor weight of the animals in 5-DMN group was 0.135 ± 0.027 g, significantly less than that of 0.317 ± 0.043 g in the control group. The aforementioned results suggested 5-DMN treatment group could delay tumor growth compared with the control group. During the tumorigenesis period, there was no mice death in the treatment group or the control group. To evaluate the drug toxicity of 5-DMN on mice at the therapeutic dose, the weights of body and organs weights were also measured when tumors were removed. As shown in Figures 7E, F, the results demonstrated there were no statistical different between 5-DMN and control groups. Therefore, the results showed that 5-DMN, which might have limited toxicity *in vivo*, could significantly inhibited the growth of GBM xenograft.

4 Discussion

Glioblastoma (GBM) is the most common primary malignant brain tumor with the characteristics of high recurrence rate, high mortality and the median survival of less than one year (23). Although 5-DMN has been implicated in the inhibition of cell proliferation in some cancers (12–14, 24), the underlying molecular mechanism which 5-DMN inhibits glioblastoma progression remains unclear. According to our findings, 5-DMN decreased the growth of GBM cell lines both *in vitro* and *in vivo*. This inhibition of 5-DMN was associated with cell cycle arrest and enhanced apoptosis. Furthermore, we also observed that 5-DMN has the capacity to prevent GBM cell migration and invasion. The underlying mechanisms of 5-DMN action in GBM cells may be influenced by the inhibitory effect of 5-DMN on the ERK1/2, PI3K/AKT and STAT3 signaling pathway.

Recent research have indicated that 5-DMN induced cytotoxicity in a variety types of cancer cells; however, the pharmacokinetics of 5-DMN differ in different tissues, which may lead to different antitumor effects (18). In *in vitro* studies, 5-DMN significantly decreased cancer cell line viability, including HCT116, THP1, CL1-5 and CL13, which IC50 values were 13.5 μM, 32.3 μM, 12.8 μM and 21.8 μM, respectively (6, 15, 16). Our results showed that 5-DMN exhibited different cytotoxicity in U87-MG, A172 and U251 cells. A172 and U251 cells treated with 5-DMN for 48 h had a similar IC50 values (50 μM) whereas the IC50 values in U87-MG cells were 33.5 μM. In addition, the high death rates and low cure rates of cancer are due in large part to the highly aggressive nature of tumor cells (25). Our study showed that 5-DMN could inhibit the migratory and invasive potential of cultured three different GBM cells.

The G1/S phase checkpoint is the first important restriction point in the cell division cycle (26). Cyclin-dependent kinases (CDKs) belongs to the serine/threonine protein kinase family, which regulate cell division and transcription (27). Unrestricted cell cycle progression and rapid growth caused by abnormal CDK4/

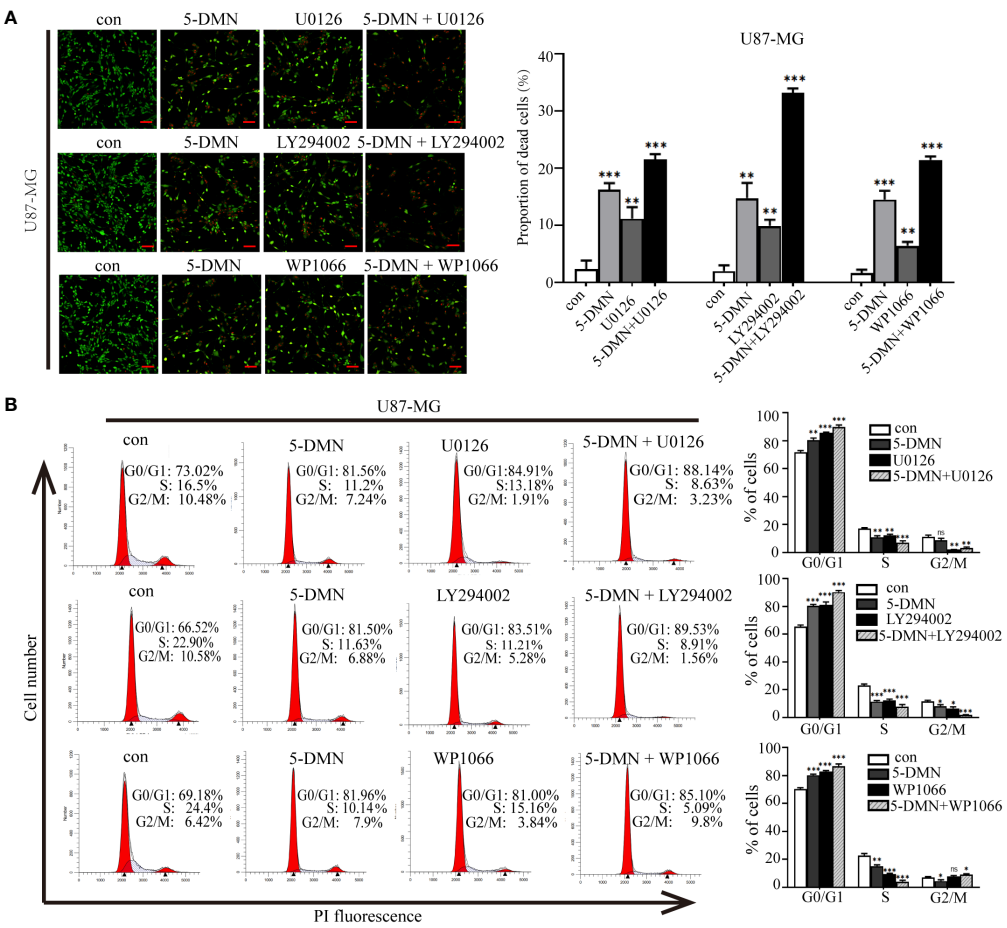

FIGURE 5
Roles of ERK1/2, AKT and STAT3 signaling in cell viability and G0/G1 phase arrest triggered by 5-DMN. **(A)** Live/dead staining assay of U87-MG cells after 5-DMN (50 μM) with or without the U0126 (15 μM), LY294002 (15 μM) and WP1066 (10 μM) for 48 h. **(B)** U87-MG cells were treated 5-DMN with or without the inhibitors and cell cycle distribution was determined. *p<0.05, **p<0.01, ***p<0.001 vs. cells in the control group. ns, no significance.

6 signaling have been confirmed as glioma progression markers (28). Cyclin D1, a D-type cyclin protein, is an important regulator of cell cycle progression. Recent research found that Cyclin D1 expression was significantly higher in GBM tissues, predicting poor outcomes (29). Cyclin D1/CDK4 (CDK6) form complexes and then responsible for early G1 regulation (30). 5-DMN was discovered to block cell cycles in both the G0/G1 and G2/M phases of HCT116 ($p53^{+/+}$), while in THP-1 and lung cancer cells, 5-DMN induced S- and G2/M phase arrest respectively (6, 8, 15, 31). Our results demonstrated that 5-DMN enhanced the percentage of G0/G1 phase in three GBM cells. A further western blotting analysis showed that 5-DMN was able to significantly downregulate the protein level of Cyclin D1 and CDK6 in concentration-dependent manner in GBM cells. Therefore, 5-DMN is a natural Cyclin D1 and CDKs inhibitor that suppress GBM tumorigenesis by inducting G0/G1 phase arrest. In addition, p21 and p27 are endogenous inhibitors of Cyclin/CDK and prevent the G1 transition to S by binding to the complex (32, 33). Whether p21 and p27 participate in the inhibition of 5-DMN-induced glioma cell proliferation remains to be further tested.

Apoptosis is programmed cell death that plays a critical role in the pathogenesis of GBM. Mitochondria-mediated caspase cascade activation is intimately associated with apoptosis, can be initiated by many stimuli (34). Members of the Bcl-2 family are generally considered to be located in the mitochondrial outer model and act as important regulators to regulate apoptosis (35). The Bcl-2 family is separated into two groups: One group contains anti-apoptotic proteins such as Bcl-2, while another group contains pro-apoptotic proteins such as Bax. The balance between these two proteins influences whether or not tumor cells undergo apoptosis (36, 37). Increasing evidence revealed that 5-DMN is a powerful apoptosis inducer in AML cell and non-small-cell lung carcinoma cells (6, 15). Consistent with previous research, GBM cell apoptosis related proteins were also changed after 5-DMN treatment, including caspase-9 and caspase-3 activation; the Bcl-2 was down-regulated, while the Bax was up-regulated. Therefore, 5-DMN can induce apoptosis of GBM cells through mitochondrial signaling pathway.

Inflammation is a stress response that is closely associated with the development of cancer (38). Previous study reported that 5-DMN reduced the expression of inflammation-related cytokines IL-1β, IL-6 and TNF-α by inhibiting the expression of p-JAK2 and p-STAT3 (39). Another study demonstrated that 5-DMN could reduce CCl4-induced fibrotic liver and regulate inflammatory responses in liver tissue *via* blocking the MAPK pathway (40). As

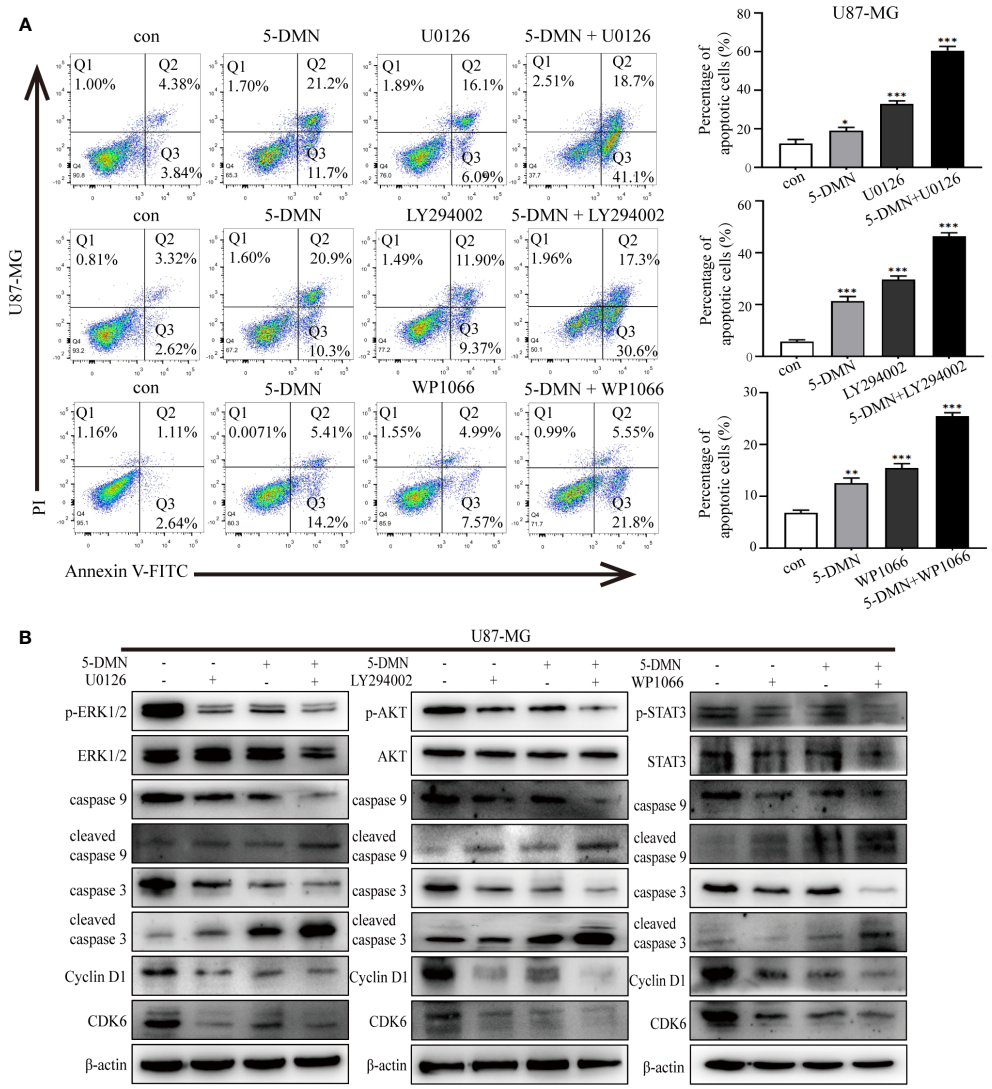

FIGURE 6
The ERK1/2, AKT and STAT3 signaling pathways influence the effects of 5-DMN on cell apoptosis, cycle and apoptosis-related proteins. **(A)** The apoptotic rate of U87-MG cells was determined using Annexin V-FITC/PI double staining after 5-DMN treatment with or without inhibitor. **(B)** Western blotting detected cell cycle proteins and apoptosis-related proteins levels in 5-DMN-treated U87-MG cells with or without pathway inhibitors. *p<0.05, **p<0.01, ***p<0.001 vs. cells in the control group.

we know, the JAK2/STAT3 and MAPK pathways also are classic crucial oncogenic signaling pathway, but whether 5-DMN regulates these two pathways in tumors has not been reported. Our study found that 5-DMN could significantly reduce the levels of p-ERK1/2 and p-STAT3 in a concentration-dependent manner in GBM cells. Furthermore, the inhibition of the ERK1/2 and STAT3 pathway by application U0126 and WP1066 could increase cell apoptosis and the number of cells blocked in G0/G1 phase. PI3K/AKT signaling not only regulates cell proliferation, but it also plays a role in tumor cell apoptosis (41). The PI3K/AKT pathway is also abnormally activated in GBM, as evidenced by abnormally elevated phosphorylation levels (42, 43). Although previous research found that the PI3K/AKT pathway was not required for autophagy in response to 5-DMN (6), our data showed that 5-DMN reduced the expression of p-AKT. Surprisingly, the PI3K/AKT pathway was also involved in the regulation of cell cycle arrest and apoptosis produced by 5-DMN. In summary, the above evidence indicated that 5-DMN promoted cell cycle arrest and apoptosis *via* inhibition of the ERK1/2, PI3K/AKT, and STAT3 signaling pathways.

Chen and Tan et al. reported that 5-DMN inhibited the growth of CL1-5 cells using murine ectopic xenografts models of lung cancer (6, 44). Our *in vivo* data demonstrated that the i.p. injection of 5-DMN at doses of 3 mg/kg, could greatly decrease tumor development in the nude mice transplantation model of GBM. Moreover, the body and organ weight data demonstrated that the nude mice treated with 5-DMN grow normally, which may imply that 5-DMN has low toxicity and less impact side effects *in vivo*. This may serve as a reminder that 5-DMN is a potentially effective anti-GBM drug, and we will investigate its toxicity in future experiments.

However, there are some limitations in our study. Although treatment with 5-DMN significantly decreased cell malignant

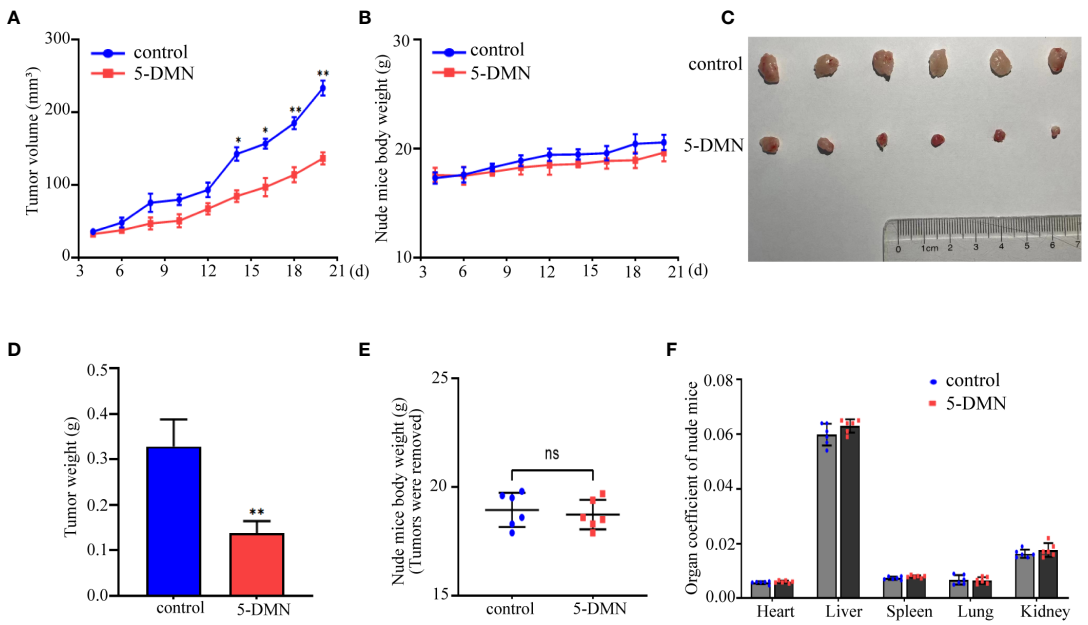

FIGURE 7
The antitumor effect of 5-DMN in BALB/c nude mice tumor model. **(A)** The volumes of tumor were evaluated at the indicated number of days after animals were treatment with 5-DMN. **(B)** The body weight changes of 5-DMN-treated group or control group mice. **(C)** Photograph of tumor tissues isolated from killed nude mice. **(D)** Quantification of tumor weight. Body weights **(E)** and organs weights **(F)** of nude mice were measured after tumors were resection. *p<0.05, **p<0.01 vs. cells in the untreated group. n= 6. ns, no significance.

behavior and promoted cell apoptosis, this phenomenon was only validated in three human GBM cell lines and subcutaneous tumor models. Further study will be required to better characterize this function. In conclusion, this study demonstrated that 5-DMN could inhibit cell proliferation, induce apoptosis in GBM cells *in vitro* and *in vivo* and effectively arrest the cell cycle in G0/G1 phase, probably by deactivating the ERK1/2, PI3K/AKT and STAT3 signaling pathways. According to the findings of this study, 5-DMN might be utilized as a potential drug for GBM treatment.

Data availability statement

The original contributions presented in the study are included in the article/Supplementary Material. Further inquiries can be directed to the corresponding authors.

Ethics statement

The animal study was reviewed and approved by the Animal Experiment Ethics Committee of Binzhou Medical University.

Author contributions

XZhang analyzed and interpreted the experiments and wrote the manuscript. LZ and JX designed and analyzed the experiments. YW, YL and CZ performed cell cycle, western blotting analyses and the subcutaneous model *in vivo* assays. HZ and YZ performed the cell culture and cell behavior experiments. XZhu and YD assisted with data analysis and manuscript preparation. YD revised and approved the final version of the manuscript. All authors contributed to the article and approved the submitted version.

Funding

This work was supported by the Shandong Provincial Natural Science Foundation of China (ZR2021MH036 to Y-C D); the National Natural Science Foundation of China (61902094 to XZ (Xiao Zhu)); the Science and Technology Program of Binzhou Medical University (50012304325 to Y-C D).

Conflict of interest

The authors declare that the research was conducted in the absence of any commercial or financial relationships that could be construed as a potential conflict of interest.

Publisher's note

All claims expressed in this article are solely those of the authors and do not necessarily represent those of their affiliated organizations, or those of the publisher, the editors and the reviewers. Any product that may be evaluated in this article, or

claim that may be made by its manufacturer, is not guaranteed or endorsed by the publisher.

Supplementary material

The Supplementary Material for this article can be found online at: https://www.frontiersin.org/articles/10.3389/fonc.2023.1143664/full#supplementary-material

SUPPLEMENTARY FIGURE 1
The inhibitory effect of 5-DMN on normal cells viability and TMZ on GBM cells. **(A)** Cell viability of normal human brain astrocyte HA1800 and HEK293T cells after being treated with different concentrations of 5-DMN for 48 h. **(B)** Cell viability was determined using the MTT assay after cultured U87-MG, A172, and U251 cells were incubated with various doses (0, 6.25, 12.5, 25, 50, 100 μM) of TMZ for 48 h. **(C)** Wound healing assays were used to determine the migration ability of GBM cells after 48 h of incubation with TMZ (0, 25, 50 μM). Values are the means ± SD of three independent experiments. *p<0.05, **p<0.01, ***p<0.001 vs. cells in the untreated control group.

References

1. Huang B, Li X, Li Y, Zhang J, Zong Z, Zhang H. Current immunotherapies for glioblastoma multiforme. *Front Immunol* (2020) 11:603911. doi: 10.3389/fimmu.2020.603911

2. Stupp R, Mason WP, van den Bent MJ, Weller M, Fisher B, Taphoorn MJ, et al. Radiotherapy plus concomitant and adjuvant temozolomide for glioblastoma. *N Engl J Med* (2005) 352(10):987–96. doi: 10.1056/NEJMoa043330

3. Davis ME. Epidemiology and overview of gliomas. *Semin Oncol Nurs* (2018) 34 (5):420–9. doi: 10.1016/j.soncn.2018.10.001

4. Lai CS, Li S, Miyauchi Y, Suzawa M, Ho CT, Pan MH. Potent anti-cancer effects of citrus peel flavonoids in human prostate xenograft tumors. *Food Funct* (2013) 4 (6):944–9. doi: 10.1039/c3fo60037h

5. Arivazhagan L, Sorimuthu Pillai S. Tangeretin, a citrus pentamethoxyflavone, exerts cytostatic effect *via* p53/p21 up-regulation and suppresses metastasis in 7,12-dimethylbenz(alpha)anthracene-induced rat mammary carcinoma. *J Nutr Biochem* (2014) 25(11):1140–53. doi: 10.1016/j.jnutbio.2014.06.007

6. Chen YK, Wang HC, Ho CT, Chen HY, Li S, Chan HL, et al. 5-demethylnobiletin promotes the formation of polymerized tubulin, leads to G2/M phase arrest and induces autophagy *via* JNK activation in human lung cancer cells. *J Nutr Biochem* (2015) 26(5):484–504. doi: 10.1016/j.jnutbio.2014.12.003

7. Zhang M, Pan Y, Dong Q, Tang X, Xin Y, Yin B, et al. Development of organogel-based emulsions to enhance the loading and bioaccessibility of 5-demethylnobiletin. *Food Res Int* (2021) 148:110592. doi: 10.1016/j.foodres.2021.110592

8. Goh JXH, Tan LT, Goh JK, Chan KG, Pusparajah P, Lee LH, et al. Nobiletin and derivatives: functional compounds from citrus fruit peel for colon cancer chemoprevention. *Cancers* (2019) 11(6):867. doi: 10.3390/cancers11060867

9. Chen PY, Chen YT, Gao WY, Wu MJ, Yen JH. Nobiletin down-regulates c-KIT gene expression and exerts antileukemic effects on human acute myeloid leukemia cells. *J Agric Food Chem* (2018) 66(51):13423–34. doi: 10.1021/acs.jafc.8b05680

10. Zhang M, Zhu J, Zhang X, Zhao DG, Ma YY, Li D, et al. Aged citrus peel (chenpi) extract causes dynamic alteration of colonic microbiota in high-fat diet induced obese mice. *Food Funct* (2020) 11(3):2667–78. doi: 10.1039/c9fo02907a

11. Kowalska K, Olejnik A, Rychlik J, Grajek W. Cranberries (Oxycoccus quadripetalus) inhibit adipogenesis and lipogenesis in 3T3-L1 cells. *Food Chem* (2014) 148:246–52. doi: 10.1016/j.foodchem.2013.10.032

12. Li S, Pan MH, Lai CS, Lo CY, Dushenkov S, Ho CT. Isolation and syntheses of polymethoxyflavones and hydroxylated polymethoxyflavones as inhibitors of HL-60 cell lines. *Bioorg Med Chem* (2007) 15(10):3381–9. doi: 10.1016/j.bmc.2007.03.021

13. Qiu P, Dong P, Guan H, Li S, Ho CT, Pan MH, et al. Inhibitory effects of 5-hydroxy polymethoxyflavones on colon cancer cells. *Mol Nutr Food Res* (2010) 54 Suppl 2:S244–52. doi: 10.1002/mnfr.200900605

14. Xiao H, Yang CS, Li S, Jin H, Ho CT, Patel T. Monodemethylated polymethoxyflavones from sweet orange (Citrus sinensis) peel inhibit growth of human lung cancer cells by apoptosis. *Mol Nutr Food Res* (2009) 53(3):398–406. doi: 10.1002/mnfr.200800057

15. Chen PY, Wang CY, Tsao EC, Chen YT, Wu MJ, Ho CT, et al. 5-demethylnobiletin inhibits cell proliferation, downregulates ID1 expression, modulates the NF-kappaB/TNF-alpha pathway and exerts antileukemic effects in AML cells. *Int J Mol Sci* (2022) 23(13):7392. doi: 10.3390/ijms23137392

16. Song M, Lan Y, Wu X, Han Y, Wang M, Zheng J, et al. The chemopreventive effect of 5-demethylnobiletin, a unique citrus flavonoid, on colitis-driven colorectal carcinogenesis in mice is associated with its colonic metabolites. *Food Funct* (2020) 11 (6):4940–52. doi: 10.1039/d0fo00616e

17. Trivedi S, Maurya P, Sammi SR, Gupta MM, Pandey R. 5-desmethylnobiletin augments synaptic ACh levels and nicotinic ACh receptor activity: a potential candidate for alleviation of cholinergic dysfunction. *Neurosci Lett* (2017) 657:84–90. doi: 10.1016/j.neulet.2017.08.010

18. Ding H, You Q, Li D, Liu Y. 5-demethylnobiletin: insights into its pharmacological activity, mechanisms, pharmacokinetics and toxicity. *Phytomedicine* (2022) 104:154285. doi: 10.1016/j.phymed.2022.154285

19. Chiu SP, Wu MJ, Chen PY, Ho YR, Tai MH, Ho CT, et al. Neurotrophic action of 5-hydroxylated polymethoxyflavones: 5-demethylnobiletin and gardenin a stimulate neuritogenesis in PC12 cells. *J Agric Food Chem* (2013) 61(39):9453–63. doi: 10.1021/jf4024678

20. Yeh ES, Means AR. PIN1, the cell cycle and cancer. *Nat Rev Cancer* (2007) 7 (5):381–8. doi: 10.1038/nrc2107

21. Xie B, Zhang L, Hu W, Fan M, Jiang N, Duan Y, et al. Dual blockage of STAT3 and ERK1/2 eliminates radioresistant GBM cells. *Redox Biol* (2019) 24:101189. doi: 10.1016/j.redox.2019.101189

22. Shahcheraghi SH, Tchokonte-Nana V, Lotfi M, Lotfi M, Ghorbani A, Sadeghnia HR. Wnt/beta-catenin and PI3K/Akt/mTOR signaling pathways in glioblastoma: two main targets for drug design: a review. *Curr Pharm Des* (2020) 26(15):1729–41. doi: 10.2174/1381612826666200131100630

23. Wang Z, Guo X, Gao L, Wang Y, Ma W, Xing B. Glioblastoma cell differentiation trajectory predicts the immunotherapy response and overall survival of patients. *Aging* (2020) 12(18):18297–321. doi: 10.18632/aging.103695

24. Sergeev IN, Ho CT, Li S, Colby J, Dushenkov S. Apoptosis-inducing activity of hydroxylated polymethoxyflavones and polymethoxyflavones from orange peel in human breast cancer cells. *Mol Nutr Food Res* (2007) 51(12):1478–84. doi: 10.1002/mnfr.200700136

25. Medikonda R, Dunn G, Rahman M, Fecci P, Lim M. A review of glioblastoma immunotherapy. *J Neurooncol* (2021) 151(1):41–53. doi: 10.1007/s11060-020-03448-1

26. Chen J, Ouyang Y, Cao L, Zhu W, Zhou Y, Zhou Y, et al. Diazepam inhibits proliferation of human glioblastoma cells through triggering a G0/G1 cell cycle arrest. *J Neurosurg Anesthesiol* (2013) 25(3):285–91. doi: 10.1097/ANA.0b013e31828bac6a

27. Tadesse S, Yu M, Kumarasiri M, Le BT, Wang S. Targeting CDK6 in cancer: state of the art and new insights. *Cell Cycle* (2015) 14(20):3220–30. doi: 10.1080/15384101.2015.1084445

28. Schroder LB, McDonald KL. CDK4/6 inhibitor PD0332991 in glioblastoma treatment: does it have a future? *Front Oncol* (2015) 5:259. doi: 10.3389/fonc.2015.00259

29. Sun T, Xu YJ, Jiang SY, Xu Z, Cao BY, Sethi G, et al. Suppression of the USP10/CCND1 axis induces glioblastoma cell apoptosis. *Acta Pharmacol Sin* (2021) 42 (8):1338–46. doi: 10.1038/s41401-020-00551-x

30. Bhattacharya K, Bag AK, Tripathi R, Samanta SK, Pal BC, Shaha C, et al. Mahanine, a novel mitochondrial complex-III inhibitor induces G0/G1 arrest through redox alteration-mediated DNA damage response and regresses glioblastoma multiforme. *Am J Cancer Res* (2014) 19(4):629–47.

31. Qiu P, Guan H, Dong P, Li S, Ho CT, Pan MH, et al. The p53-, bax- and p21-dependent inhibition of colon cancer cell growth by 5-hydroxy polymethoxyflavones. *Mol Nutr Food Res* (2011) 55(4):613–22. doi: 10.1002/mnfr.201000269

32. Brandts CH, Bilanges B, Hare G, McCormick F, Stokoe D. Phosphorylation-independent stabilization of p27kip1 by the phosphoinositide 3-kinase pathway in glioblastoma cells. *J Biol Chem* (2005) 280(3):2012–9. doi: 10.1074/jbc.M408348200

33. Gartel AL, Radhakrishnan SK. Lost in transcription: p21 repression, mechanisms, and consequences. *Cancer Res* (2005) 65(10):3980–5. doi: 10.1158/0008-5472.CAN-04-3995

34. Pan Z, Zhang X, Yu P, Chen X, Lu P, Li M, et al. Cinobufagin induces cell cycle arrest at the G2/M phase and promotes apoptosis in malignant melanoma cells. *Front Oncol* (2019) 9:853. doi: 10.3389/fonc.2019.00853

35. Kale J, Osterlund EJ, Andrews DW. BCL-2 family proteins: changing partners in the dance towards death. *Cell Death Differ* (2018) 25(1):65–80. doi: 10.1038/cdd.2017.186

36. Maes ME, Schlamp CL, Nickells RW. BAX to basics: how the BCL2 gene family controls the death of retinal ganglion cells. *Prog Retin Eye Res* (2017) 57:1–25. doi: 10.1016/j.preteyeres.2017.01.002

37. Strasser A, Vaux DL. Viewing BCL2 and cell death control from an evolutionary perspective. *Cell Death Differ* (2018) 25(1):13–20. doi: 10.1038/cdd.2017.145

38. Singh R, Mishra MK, Aggarwal H. Inflammation, immunity, and cancer. *Mediators Inflammation* (2017) 2017:6027305. doi: 10.1155/2017/6027305

39. Wang Y, Zang W, Ji S, Cao J, Sun C. Three polymethoxyflavones purified from ougan (Citrus reticulata cv. suavissima) inhibited LPS-induced NO elevation in the neuroglia BV-2 cell line *via* the JAK2/STAT3 pathway. *Nutrients* (2019) 11(4):791. doi: 10.3390/nu11040791

40. Chang SN, Kim SH, Dey DK, Park SM, Nasif O, Bajpai VK, et al. 5-O-Demethylnobiletin alleviates CCl4-induced acute liver injury by equilibrating ROS-mediated apoptosis and autophagy induction. *Int J Mol Sci* (2021) 22(3):1083. doi: 10.3390/ijms22031083

41. Lu L, Chen G, Yang J, Ma Z, Yang Y, Hu Y, et al. Bone marrow mesenchymal stem cells suppress growth and promote the apoptosis of glioma U251 cells through downregulation of the PI3K/AKT signaling pathway. *BioMed Pharmacother* (2019) 112:108625. doi: 10.1016/j.biopha.2019.108625

42. Tong L, Li J, Li Q, Wang X, Medikonda R, Zhao T, et al. ACT001 reduces the expression of PD-L1 by inhibiting the phosphorylation of STAT3 in glioblastoma. *Theranostics* (2020) 10(13):5943–56. doi: 10.7150/thno.41498

43. Barzegar Behrooz A, Talaie Z, Jusheghani F, Łos MJ, Klonisch T, Ghavami S. Wnt and PI3K/Akt/mTOR survival pathways as therapeutic targets in glioblastoma. *Int J Mol Sci* (2022) 23(3):1353. doi: 10.3390/ijms23031353

44. Tan KT, Li S, Li YR, Cheng SL, Lin SH, Tung YT. Synergistic anticancer effect of a combination of paclitaxel and 5-demethylnobiletin against lung cancer cell line *In Vitro* and *In Vivo*. *Appl Biochem Biotechnol* (2019) 187(4):1328–43. doi: 10.1007/s12010-018-2869-1

frontiers | Frontiers in Pharmacology

TYPE Original Research
PUBLISHED 27 April 2023
DOI 10.3389/fphar.2023.1096001

OPEN ACCESS

EDITED BY
Guangying Qi,
Affiliated Hospital of Guilin Medical University, China

REVIEWED BY
Shih-Min Hsia,
Taipei Medical University, Taiwan
Guolin Tan,
Central South University, China

*CORRESPONDENCE
Guodong Zheng,
gd200237@126.com
Yi Cai,
yicaisysu@163.com
Depo Yang,
lssydp@mail.sysu.edu.cn

†These authors have contributed equally to this work and share first authorship

‡These authors share last authorship

RECEIVED 11 November 2022
ACCEPTED 07 April 2023
PUBLISHED 27 April 2023

CITATION
Yang W, Liang Y, Liu Y, Chen B, Wang K, Chen X, Yu Z, Yang D, Cai Y and Zheng G (2023), The molecular mechanism for inhibiting the growth of nasopharyngeal carcinoma cells using polymethoxyflavonoids purified from pericarp of *Citrus reticulata* 'Chachi' via HSCCC.
Front. Pharmacol. 14:1096001.
doi: 10.3389/fphar.2023.1096001

The molecular mechanism for inhibiting the growth of nasopharyngeal carcinoma cells using polymethoxyflavonoids purified from pericarp of *Citrus reticulata* 'Chachi' via HSCCC

Wanling Yang[1†], Yiyao Liang[1†], Yujie Liu[1†], Baizhong Chen[2], Kanghui Wang[1], Xiaojing Chen[1], Zhiqian Yu[1], Depo Yang[3*‡], Yi Cai[1*‡] and Guodong Zheng[1*‡]

[1]Guangzhou Municipal and Guangdong Provincial Key Laboratory of Molecular Target and Clinical Pharmacology, The NMPA and State Key Laboratory of Respiratory Disease, School of Pharmaceutical Sciences and the Fifth Affiliated Hospital, Guangzhou Medical University, Guangzhou, China, [2]Guangdong Xinbaotang Biological Technology Co., Ltd., Jiangmen, China, [3]School of Pharmaceutical Sciences, Sun Yat-sen University, Guangzhou, China

Polymethoxyflavonoids (PMFs), the main bioactive compounds naturally occurring in the pericarp of *Citrus reticulata* 'Chachi' (CRCP), possess significant antitumor action. However, the action of PMFs in nasopharyngeal carcinoma (NPC) is currently unknown. The present research study was conducted to investigate the inhibitory mechanisms of PMFs from CRCP on NPC growth *in vivo* and *in vitro*. In our research, we used high-speed counter-current chromatography (HSCCC) to separate four PMFs (nobiletin (NOB), 3,5,6,7,8,3′,4′-heptamethoxyflavone (HMF), tangeretin (TGN), and 5-hydroxy-6,7,8,3′,4′-pentamethoxyflavone (5-HPMF)) from CRCP. CCK-8 assay was used to preliminarily screen cell viability following exposure to the four PMFs. Colony formation, Hoechst-33258 staining, transwell, and wound scratch assays were performed to assess the anti-proliferation, invasion, migration, and apoptosis-inducing effects of HMF on NPC cells. NPC tumors in xenograft tumor transplantation experiments were also established to explore the effect of HMF (100 and 150 mg/kg/day) on NPC. The histopathological changes in the treated rats were observed by H&E staining and Ki-67 detection by immunohistochemical techniques. The expressions of P70S6K, p-P70S6K, S6, p-S6, COX-2, p53, and p-p53 were measured by Western blot. The four PMFs were obtained with high purity (>95.0%). The results of the preliminary screening by CCK-8 assay suggested that HMF had the strongest inhibitory effect on NPC cell growth. The results of the colony formation, Hoechst-33258 staining, transwell, and wound scratch assays indicated that HMF had significant anti-proliferation, invasion, migration, and apoptosis-inducing ability in NPC cells. Moreover, HMF

Abbreviations: AMPK, AMP-activated protein kinase; CRCP, *Citrus reticulata* 'Chachi' pericarp; FBS, fetal bovine serum; HSCCC, high-speed counter-current chromatography; HMF, 3,5,6,7,8,3′,4′-heptamethoxyflavone; NOB, nobiletin; NPC, nasopharyngeal carcinoma; PBS, phosphate-buffered saline; IMRT, intensity-modulated radiotherapy; PMFs, polymethoxyflavonoids; PE, petroleum ether; TGN, tangeretin; 5-HPMF, 5-hydroxy-6,7,8,3′,4′-pentamethoxyflavone.

suppressed NPC tumor growth in xenograft tumor transplantation experiments. Further investigation suggested that HMF regulated NPC cells proliferation, apoptosis, migration, and invasion by activating AMPK-dependent signaling pathways. In conclusion, HMF-induced AMPK activation inhibited NPC cell growth, invasion, and metastatic potency by downregulating the activation of the mTOR signaling pathway and COX-2 protein levels, as well as enhancing the p53 phosphorylation level. Our study provides a crucial experimental basis for the clinical treatment of NPC, as well as the development and utilization of PMFs from CRCP.

KEYWORDS

Citrus reticulata 'Chachi' pericarp, high-speed counter-current chromatography, polymethoxyflavonoids, proliferation, AMPK signaling pathway

1 Introduction

Nasopharyngeal carcinoma (NPC), emerging from the nasopharyngeal epithelium, is especially common in East and Southeast Asia (Lee et al., 2019). The delayed treatment and worse prognosis occur mainly due to the hidden early clinical symptoms. Intensity-modulated radiotherapy (IMRT) is considered ideal for the local treatment of NPC for its dose protection on organs around the nasopharynx, whereas distant metastases also occur in some patients treated with IMRT; these tumor cells develop resistance to chemotherapy and radiotherapy in the later period of treatment (Perri et al., 2019). Collectively, metastasis, relapse, resistance to chemotherapy, and side effects are urgent clinical problems in NPC treatment. Hence, developing naturally efficient and low-toxicity drugs as NPC therapeutics is of urgent need (Wang C Y et al., 2020).

Based on the Chinese Pharmacopoeia (2020 edition), *Citrus reticulata* 'Chachi', a major cultivar of *Citrus reticulata* Blanco, is planted and harvested in Xinhui region, Guangdong Province in China (Pharmacopoeia, 2020). Polymethoxyflavonoids (PMFs) naturally occurring in citrus have been identified as the main bioactive non-volatile constituents in the pericarpium of *Citrus reticulata* 'Chachi' (CRCP), mainly including nobiletin (NOB), 3,5,6,7,8,3′,4′-heptamethoxyflavone (HMF), tangeretin (TGN), and 5-hydroxy-6,7,8,3′,4′-pentamethoxyflavone (5-HPMF) (Kong et al., 2020; Nair et al., 2018). Emerging studies have reported that PMFs strongly inhibit tumor cell proliferation (Shi et al., 2013). For instance, TGN has proliferation inhibitory and apoptosis induction effects in three gastric cancer cell lines (AGS, SGC-7901, and BGC-823) (Wang Y et al., 2020). Moreover, 5-HPMF led to apoptosis induction and cell cycle block in HCT116 colon cancer cells (Qiu et al., 2011). We also previously demonstrated the growth inhibition and apoptosis induction of nobiletin in NPC cells (Zheng et al., 2019). Nevertheless, the mechanism of action of PMFs in CRCP on NPC is unknown and worth exploring in further studies.

AMP-activated protein kinase (AMPK) is capable of regulating cell metabolism in eukaryotic cells and is crucial for maintaining energy homeostasis in the human body (Tokunaga et al., 2019). AMPK activation elicited the inhibition of malignant tumor occurrence and development by inhibiting tumor cell proliferation, migration, and invasion and inducing apoptosis. For instance, the AMPK activator (Acadesine, AICAR) inhibited the proliferation and induced apoptosis in HepG2/C3A, Huh-7, and SK-HEP-1 hepatoma cells (Ferretti et al., 2016). In contrast, the effect of apoptosis-inducing ginsenoside metabolites on non-small cell lung cancer cells A549 and H1975 could be reversed by AMPK inhibition (Li et al., 2019). Moreover, metformin-induced AMPK activation inhibited the proliferation and induced apoptosis of NPC C666-1 cells, suggesting that AMPK is a potential target for NPC therapy (Zhao et al., 2011).

In the present study, the high-speed counter-current chromatography (HSCCC) method was established for the isolation and preparation of four PMF monomeric components from CRCP for the first time. Cell counting kit-8 (CCK-8) assays were used to further screen the four monomeric compounds for their proliferation-inhibiting effects on NPC cells. Moreover, colony formation, Hoechst-33258 staining, transwell, and wound scratch assays were performed to examine the anti-proliferation, invasion, migration, and apoptosis-inducing abilities following HMF treatment of NPC cells. The xenograft NPC-tumor transplantation experiments were constructed *in vivo*, and H&E staining and Ki-67 detection by immunohistochemical technique were performed to observe histopathological changes to investigate the anti-NPC effect of HMF (100 and 150 mg/kg/day). In addition, the molecular mechanism of the PMF components in regulating the apoptotic, migratory, and invasive effects of NPC cells in combination with the AMPK-mTOR signaling pathway was explored.

2 Materials and methods

2.1 Herbal medicine

The *Citrus reticulata* "Chachi" pericarp (CRCP), purchased from Xinbaotang Biological Technology Co., Ltd. (Jiangmen, Guangdong, China) in January 2018, was identified by Prof. Guodong Zheng. Meanwhile, the CRCP samples were stored at the Pharmacognosy Laboratory of Guangzhou Medical University.

2.2 Chemicals and reagents

Chromatographical acetonitrile was bought from Thermo Fisher Scientific (China). Analytical-grade petroleum ether (PE), methanol,

and ethyl acetate were bought from Honeywell (USA). Ultrapure water was obtained from a Milli-Q system (Millipore, USA). The other chemicals were analysis-grade chemicals.

RPMI 1640 medium and fetal bovine serum (FBS) were purchased from Gibco (Logan, UT, USA). Cell counting kit 8 (CCK-8) was bought from DOJINDO (Japan). Antibodies (including β-actin, p-AMPK, AMPK, p-S6, S6, p-P70S6K, P70S6K, p-p53, p53, and COX-2) were purchased from Cell Signaling Technology (USA); Compound C (an AMPK inhibitor) was bought from Santa Cruz Biotech (USA). Matrix basement membrane was purchased from Corning Co., Ltd. (USA). The apoptosis-Hoechst Staining Kit was purchased from Beyotime Biotechnology Co., Ltd. (Shanghai, China). Crystal violet reagent was purchased from Damao (Tianjin, China). Ki-67 was purchased from Wuhan Servicebio Technology Co., Ltd. The four PMFs obtained from CRCP were used in DMSO and were stored at −20°C and diluted for use.

2.3 Simultaneous purification of four PMFs from CRCP by HSCCC

2.3.1 Enrichment of PMFs from CRCP

The CRCP was pulverized into powder and passed through a 20-mesh sieve (1 kg). The powder samples were then extracted four times by PE solvent heat reflux extraction. The parameters (liquid to solid ratio) were 4:1, 3:1, 3:1, and 3:1, with an extraction time of 1 h, respectively. The aforementioned four extracting solutions were merged for rotatory evaporation until deposition occurred. The residues were weighed accurately after drying and kept at 4°C.

The HPLC-PDA method for the aforementioned PE extracts was performed on the Dikma Diamonsil C_{18} column (250 mm × 4.6 mm i.d., 5 μm). The elution system was composed of 50% water (phase A) and 50% acetonitrile (phase B). The flow velocity was 1 mL·min^{-1}, and the injection sample load was 10 μL. All samples were verified at 330 nm and 25°C after filtering through a 0.22-μm membrane.

2.3.2 Purification and identification of four PMFs from CRCP

A solvent system including petroleum ether–ethyl acetate–methanol–water (1:0.8:0.9:1, v/v/v/v) was chosen for further HSCCC purification of PMFs by comparing the partition coefficient ($K = A_1/A_2$) values by the peak areas of the PMFs by HPLC-PDA (A_1 and A_2) and the peak shape in HSCCC. In each HSCCC separation, the column was first filled with the upper (stationary) phase, and then the rotary was set at 1,000 rpm. The other apparatus was set as follows: column temperature 35°C and detection wavelength 330 nm. The bottom (mobile) phase was then pumped into the column at a flow rate of 2.0 mL·min^{-1}. When the two phases reached hydrodynamic equilibrium, the PE extract deposit (200 mg) was dissolved in the bottom phase solution (10 mL) for injection. All effluent was detected at a wavelength of 330 nm, and sample fractions (3 mL of each test tube) were gathered for further analysis and other research.

The sample fractions were dissolved in trichloro-deuterio-methane to identify compounds by ^{1}H-NMR, ^{13}C-NMR, and ESI-MS. The purity analyses were performed by the normalization method of the peak area. The HPLC-PDA method was performed as described in Section 2.3.1.

2.4 Cell culture

CNE-2 and 5-8F cells were cultured in RPMI 1640 with certain percentages of FBS in an incubator (air to CO_2 ratio 95:5) at 37°C. Replacement of the medium was performed every other day. As the cells reached 80%–90% confluency, trypsin was added to digest cells for the proper time, and then the cells were subcultured. Before treatment with PMFs purified from CRCP, the cells were incubated in RPMI 1640 containing free FBS for 12 h.

2.5 Cell viability

CNE-2 and 5-8F cells were cultured in 96-well cell plates (5×10^3/well). Next, 100 μL of RPMI 1640 medium (10% FBS) was added to 96-well cell plates, and the plates were incubated in 5% CO_2, at 37°C for 24 h. Replacement of the FBS-free medium was carried out for 12 h on cells before treatment with HMF. Each well was supplied with CCK-8 liquid (10 μL) for 1 h. The absorbance measurement was performed on a Multi-Volume Spectrophotometer system (BioTek Instruments, Inc., USA) at 450nm.

2.6 Colony formation assay

CNE-2 and 5-8F cells were inoculated into six-well cell plates (800/well). RPMI 1640 medium containing 10% FBS (2 mL) was added and incubated in a cell incubator (5% CO_2, 37°C) for 24 h to allow the cells to completely adhere to the wall. Then, the cells were incubated with media containing HMF at different concentrations (10 μM, 25 μM, and 50 μM), respectively. The incubation medium was changed every 2 days while maintaining the original drug concentrations. After 14 days, colonies with >50 cells stained with crystal violet (0.5%) at room temperature, were counted on a stereomicroscope after 1 h. Relative clone-forming efficiency (%) = (number of cell colonies with more than 50 cells in the administration group/ number of cell colonies with cells more critical than 50 in the control group) × 100%.

2.7 Hoechst-33258 staining

CNE-2 and 5-8F cells were plated at 9×10^4/well into 12-well plates supplemented with 1 mL of medium (10% FBS) and incubated at 37°C overnight. Next, 4% paraformaldehyde (500 μL/well) was used to fix the cells at room temperature for 10 min after treatment with HMF (10 μM, 25 μM, 50 μM) for 24 h. Then, 500 μL of Hoechst-33258 (Beyotime, China) was added to stain the cells for 5 min at room temperature in the dark, washing twice with PBS. A liquor of 50 μL anti-fluorescence sealing was

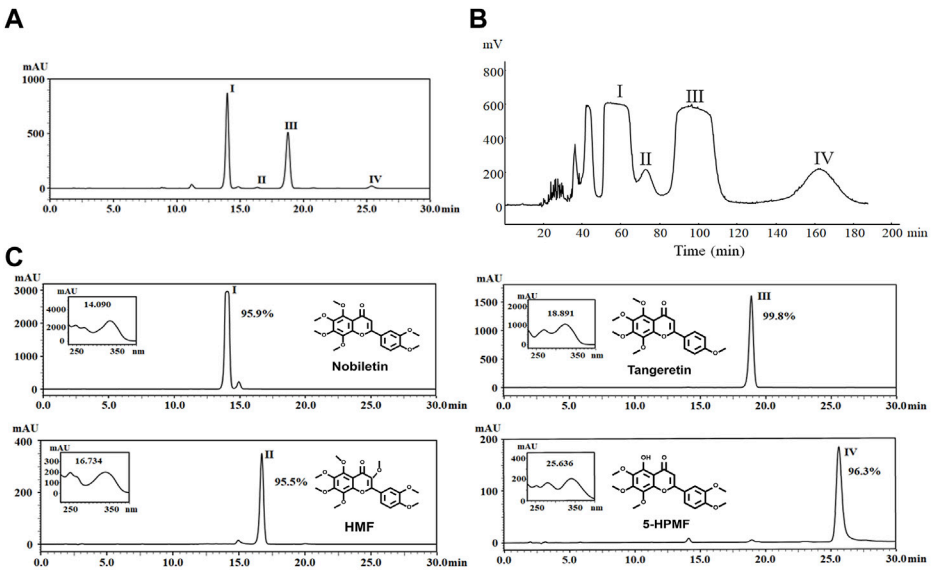

FIGURE 1
(A) HPLC chromatogram of nobiletin (I), HMF (II), tangeretin (III), and 5-HPMF (IV) purified from a PE deposit of CRCP at 330 nm. **(B)** Chromatogram of HSCCC separation for components (I–IV) at 330 nm and a flow rate of 2 mL·min^{-1}. Fractions (I–IV) were collected from the effluent. **(C)** Identification and purity analysis of fractions (I–IV) by ESI-MS, ^{1}H-NMR, ^{13}C-NMR, and HPLC-PDA.

added to prevent fluorescence quenching. A fluorescence microscope was used to observe and image apoptotic morphological features (chromatin condensation and nuclear fragmentation) (20×).

2.8 Wound scratch healing

CNE-2 and 5-8F cells were inoculated into six-well plates (3×10^5/well) supplemented with medium for 24 h. Semblable straight scratches were made on monolayers in each well with sterile pipette tips, which were then washed twice with 1 mL PBS. An inverted microscope (10×) was used to take representative pictures at 0 h. After that, the wounds were treated with HMF (10 μM, 25 μM, and 50 μM) for 24 h, respectively, and then the same scratch position at 0 h was photographed. ImageJ software was used to measure and analyze the areas between the edges of the wounds. Mobility (%) = (0 h blank area → 24 h blank area)/0 h blank area × 100%.

2.9 Transwell migration assay

Matrix glue (50 mg/L) was diluted with RPMI 1640 medium without serum (v/v, 1:8). A matrix glue dilution (45 μL) was appended to the upper transwell chamber. An incubator (5% CO_2) at 37°C was used to incubate for 2 h. The excess medium was removed after forming. CNE-2 and 5-8F cell suspensions incubated with HMF (10 μM, 25 μM, 50 μM) were spread in Matrigel plate wells with serum-free RPMI 1640 medium (2.5×10^6 cells/well). The lower well was supplied with 600 μL of complete medium (RPMI 1640 and 10% FBS) to stimulate cell migration. The cells were incubated for 24 h and those that had not migrated through the Matrigel plate wells were wiped off with swabs. A total of 1 mL of paraformaldehyde (4%) was applied to fix the cells in the bottom chamber for 30 min. Pictures of the cells were taken under the microscope (10×) and counted in ImageJ software after staining with 1 mL of 1% crystal violet at room temperature for 1 h.

2.10 Western blot analysis

The expression levels of AMPK-dependent signaling pathway proteins (P70S6K, p-P70S6K, S6, p-S6, COX-2, p53, and p-p53) were examined by Western blot analysis. Cells (CNE-2 and 5-8F) were inoculated into six-well plates (2×10^6/well), incubated with HMF (10 μM, 25 μM, and 50 μM) for 48 h, and then lysed with RIPA buffer with an added inhibitor cocktail of protease and phosphatase. The BCA assay method was used to measure protein concentrations. Appropriate quantities of protein samples (20 μg) were subjected to polyacrylamide gel electrophoresis and transferred to PVDF membranes. The membranes were then incubated with 5% skim milk for 1 h at room temperature and then incubated with the primary antibodies (p-AMPK, AMPK, p-P70S6K, P70S6K, p-S6, S6, COX-2, p-p53, and p53) at 4°C overnight before washing three times with TBST. Then, the membranes were incubated with an appropriate peroxidase-conjugated secondary antibody (1:1,500) at room temperature for 1 h. Finally, enhancement of the immunoreactivity signals was detected by a chemiluminescence system. The relative density of the target bands was statistically analyzed using Quantity One analysis software. β-Actin was used for protein level normalization.

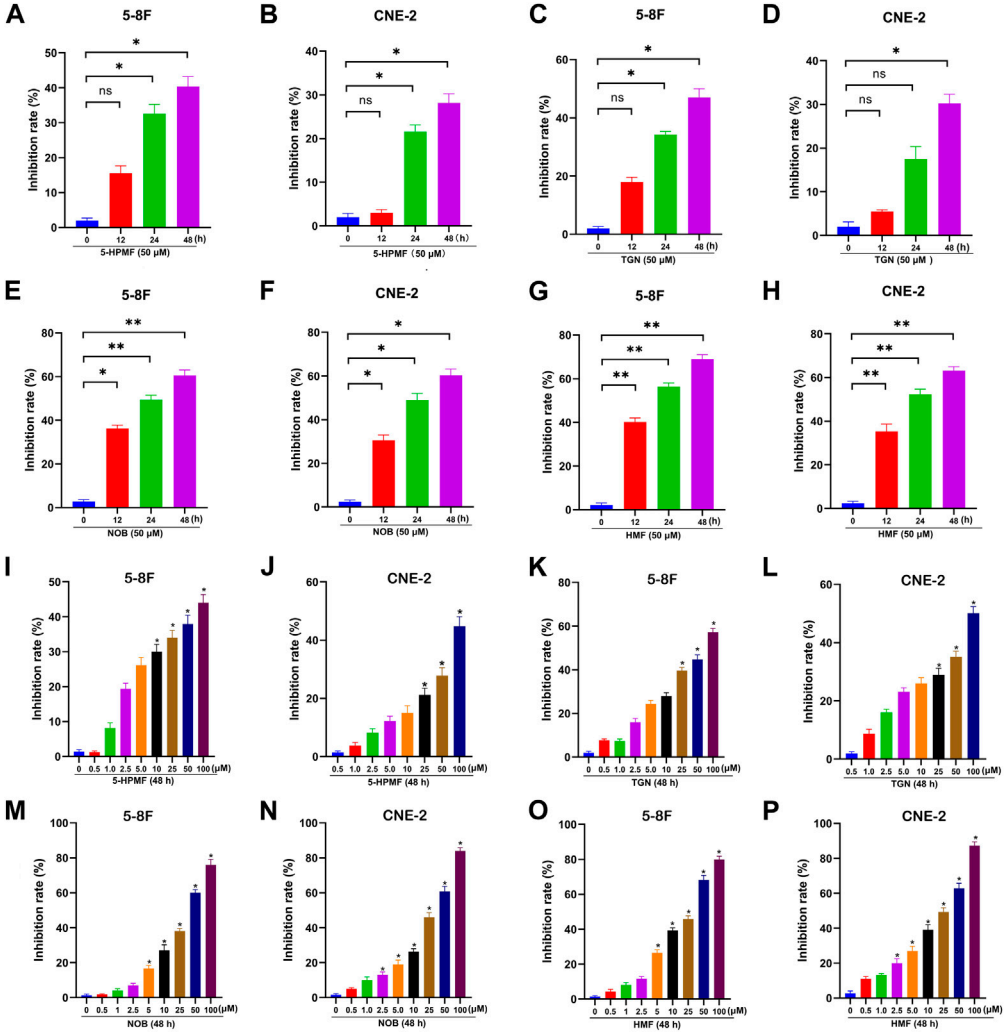

FIGURE 2
Anti-proliferation effects of the four PMFs (5-HPMF, TGN, NOB, and HMF) in human nasopharyngeal carcinoma cells. **(A–H)** 5-8F and CNE-2 cell lines were incubated with the four PMFs (50 μM) for 12 h, 24 h, and 48 h, respectively. **(I–P)** 5-8F and CNE-2 cell lines were incubated with different concentrations (0, 0.5, 1, 2.5, 5, 10, 25, 50, and 100 μM) of the four PMFs for 48 h. Cell viability was examined by CCK-8 assay. All data were described as the mean ± SD of three independent and repeated experiments. Compared to the control group (0 μM): $*p < 0.05$; $**p < 0.01$; ns, not significant.

2.11 Construction of the transplanted tumor model *in vivo*

2.11.1 Construction of nude mice tumor-bearing model

Thirty male nude mice (6 weeks old, 18–22 g) were bought from Guangzhou Jingwei Biological Co., Ltd. (Guangdong, China). The environment is under specific pathogen-free conditions between 22°C and 28°C and give free access to food and water. CNE-2 (1.5×10^6 cells) were suspended in PBS and Matrigel matrix solution (1:1, v/v) and subcutaneously injected into the axilla of the right forelimb of the nude mice. When the mean tumor volume reached approximately 100 mm^3, the mice were randomly and equally divided into three groups (n = 10), and administered oral HMF (100 and 150 mg/kg/day) for 14 days, respectively. At the same time, the normal control (NC) group was administered 0.5% CMC-Na. The weights of the mice were recorded daily, and the tumor volume was weighed on the scales and measured with a ruler. The curve of changes was plotted. The tumor volume was calculated as the long diameter length × short diameter^2 × 0.5.

2.11.2 Hematoxylin and eosin (H&E) staining

H&E staining was performed as previously described (Zhang et al., 2018). The nude-mouse transplanted tumor was removed and weighed. Then, the tumor tissue was stored in a 4% paraformaldehyde solution to maintain cell morphology and

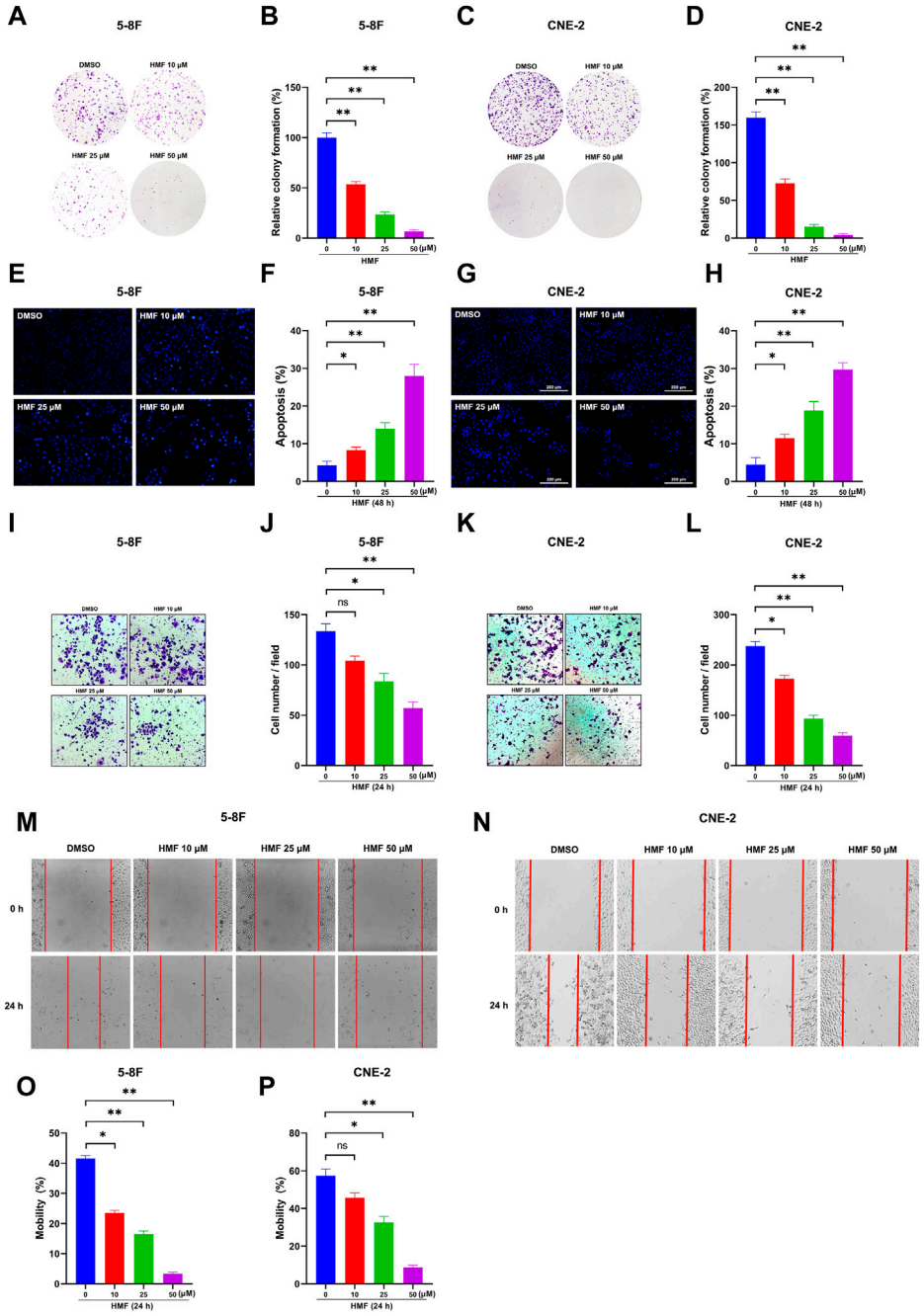

FIGURE 3
HMF induces NPC cell apoptosis and inhibits migration and invasion. **(A,C)** The indicated numbers of cells were incubated in six-well dishes and treated with HMF (0, 10, 25, and 50 μM). After 7 days, the colonies were stained with 0.5% crystal violet. **(B,D)** The number of colonies containing ≥50 cells and the relative colony formation were counted under a microscope to quantify the proliferation. **(E,G)** 5-8F and CNE-2 cells were stained with Hoechst-33258 after incubation with different concentrations (0, 10, 25, and 50 μM) of HMF. The morphological changes were analyzed using a fluorescence microscope (20×). **(F,H)** Apoptosis (%) of 5-8F and CNE-2 cells treated with HMF (0, 10, 25, and 50 μM) for 24 h. **(I,K)** Representative images of transwell-migration assays of 5-8F and CNE-2 cells treated with HMF (0, 10, 25, and 50 μM) for 24 h (10×). **(J,L)** Quantification of cell migration expressed by cell counting. **(M,N)** Representative images of scratch assays performed in 5-8F and CNE-2 cells with HMF treatment (0, 10, 25, and 50 μM) for 24 h (10×). **(O,P)** Mobility (%) was measured 24 h after the cells were scratched. All data are described as the mean ± SD of three independent and repeated experiments. Compared to the control group (0 μM): $*p < 0.05$; $**p < 0.01$; ns, not significant.

structure for >24 h. The tumor tissues were then embedded in paraffin, cut into slices (8 μm), and stained with H&E. The stained slices were scanned under a light microscope (Olympus, Japan) to evaluate tumor damage.

2.11.3 Immunohistochemistry (IHC)

The tissue sections were first dewaxed and hydrated. Antigen retrieval of Ki-67 was performed with a steamer with citrate buffer, pH 7, for 32 min. The tissue sections were then incubated

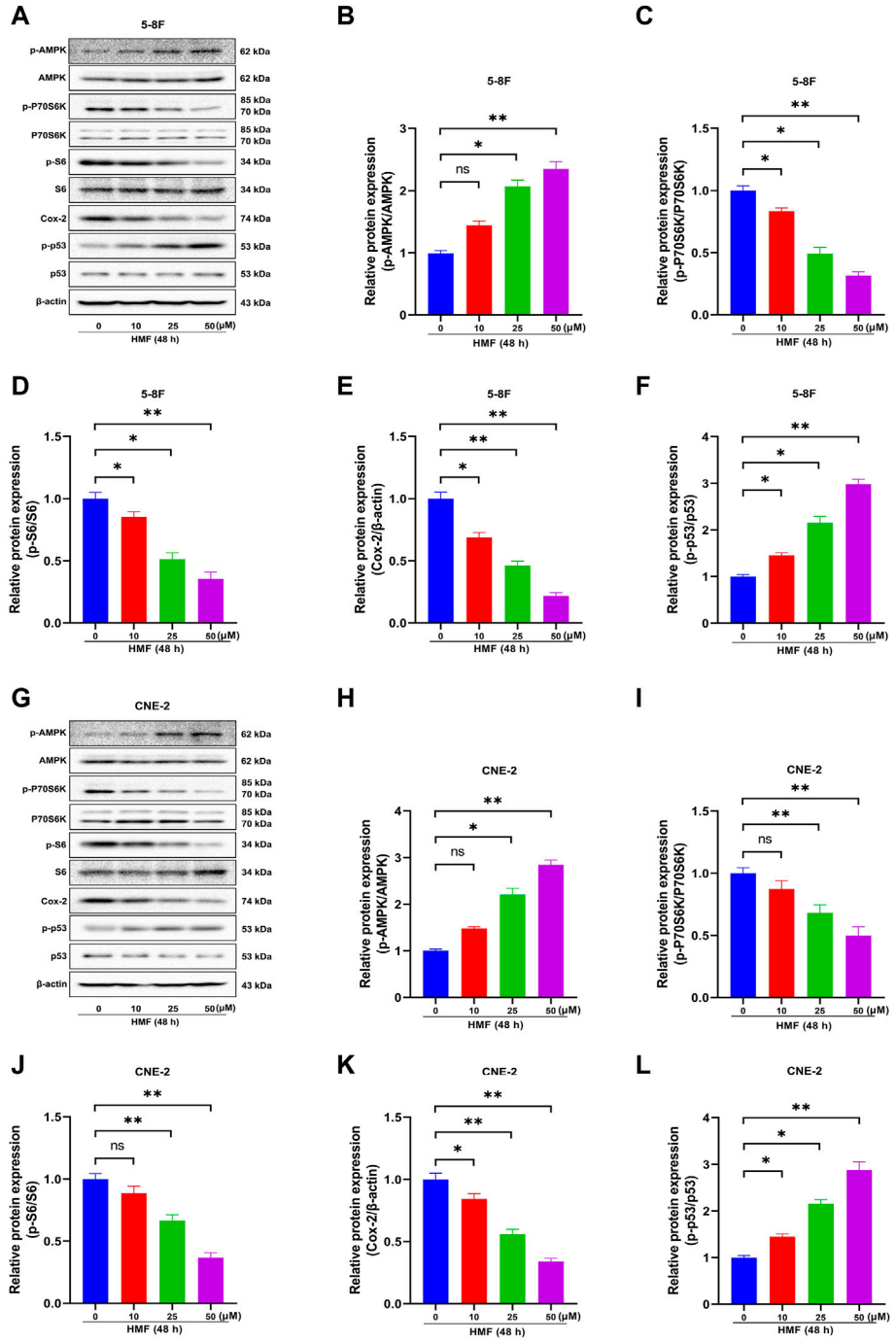

FIGURE 4
Effect of HMF on 5-8F and CNE-2 human nasopharyngeal carcinoma cells through the AMPK signaling pathway. **(A,G)** 5-8F and CNE-2 cell lysates treated with HMF (0, 10, 25, and 50 μM) assessed by Western blot analysis with antibodies against p-AMPK, AMPK, p-P70S6K, P70S6K, p-S6, S6, COX-2, p-p53, and p53. β-Actin served as the loading control. **(B–D)** and **(H–J)** Quantification of phosphorylation expression levels of key AMPK-mTOR pathway molecules (p-AMPK/AMPK, p-P70S6K/P70S6K, and p-S6/S6) in two NPC cells lines. **(E,K)** Quantification of COX-2 expression levels. **(F,L)** Quantification of p53 phosphorylation levels. All data are described as the mean ± SD of three independent and repeated experiments. Compared to the control group (0 μM): $*p < 0.05$, $**p < 0.01$; ns, no significance.

with primary polyclonal mouse monoclonal antibodies against Ki-67. Biotinylated goat anti-mouse IgG and IgM (200 mg·ml^{-1}) were used as secondary antibodies. The I-ViewTM DAB Detection Kit was used for endogenous peroxidase blocking, followed by an ethanol gradient for rehydration. Neutral gum was used to seal the slices. Finally, the slices were inspected via a microscope. Ki-67 cells were considered positive when the cells were stained brownish yellow.

2.12 Statistical analysis

All experimental data were described as means ± standard deviation (mean ± SD), and each experiment was repeated three times (n = 3). Data analyses were performed on one-way ANOVA LSD statistics using SPSS 16.0 software. The significance of the differences was indicated as $^{*}p < 0.05$ and $^{**}p < 0.01$.

3 Results

3.1 Four PMFs purified via HSCCC from PE deposits in CRCP

Approximately 1 mg of petroleum ether extract enriched from CRCP was dissolved in 10 mL of methanol, from which four compounds (I–IV) were detected by the HPLC-PDA method (Figure 1A). These included 325 mg of Compound I, 67 mg of Compound II, 249 mg of Compound III, and 90 mg of Compound IV, which were obtained after separation by HSCCC (Figure 1B). The purity examination was analyzed by HPLC-PDA and calculated using the peak area normalization method, which suggested that these compounds reached 95.0% purity (95.9%, 95.5%, 99.8%, and 96.3% for Compounds I–IV), respectively. ESI-MS, ^{1}H-NMR, and ^{13}C-NMR analyses were further performed to identify the structures of the four purified PMFs (5-HPMF, TGN, NOB, and HMF) (Figure 1C).

3.2 Effects of the four PMFs on the viability of 5-8F and CNE-2 cell lines

To evaluate the anti-NPC effects of the four PMFs (5-HPMF, TGN, NOB, and HMF), the cell viability of two NPC cell lines treated with various concentrations of monomeric PMFs (0, 0.5, 1, 2.5, 5, 10, 25, 50, and 100 μM) for 48 h and treated with monomeric PMFs (50 μM) for 12 h, 24 h, and 48 h, respectively, was analyzed by CCK-8 assay. As indicated in Figure 2, the four PMFs (5-HPMF, TGN, NOB, and HMF) could inhibit the proliferation of 5-8F and CNE-2 cells lines in time- and dose-dependent manners ($^{*}p < 0.05$ and $^{**}p < 0.01$). The IC_{50} values of 5-HPMF and TGN in the two NPC cell lines exceeded >50 μM. The IC_{50} values of NOB were 36.579 ± 0.659 μM (CNE-2) and 37.256 ± 0.365 μM (5-8F cells), respectively. HMF showed the strongest cytotoxicity, with IC_{50} values of 36.273 ± 0.502 μM (CNE-2) and 31.786 ± 0.841 μM (5-8F cells). Thus, HMF was selected for further research on its anti-NPC effects.

3.3 HMF inhibits proliferation and induces apoptosis in 5-8F and CNE-2 cell lines

Based on the aforementioned results, we focused on the anti-NPC effects of HMF in further studies. As Figures 3A–D show, the number of cell colonies containing ≥50 cells and the relative colony formation were significantly decreased in cells treated with HMF (10, 25, 50 μM) compared to the control group after 7 days. These findings further indicated that HMF suppressed 5-8F and CNE-2 cell proliferation. To simultaneously explore the anti-apoptotic effects of HMF on NPC cell lines, we performed Hoechst-33258 staining and examined the samples on a fluorescence microscope. The morphological changes of 5-8F and CNE-2 cell lines treated with HMF (10, 25, and 50 μM) were observed on a fluorescence microscope (20×). Compared with the control group, 5-8F and CNE-2 cells in the HMF group showed condensation of nuclear chromatin staining, atomic shrinkage, and other apoptosis phenomena. The apoptosis rate of the HMF group was remarkably higher than that in the control group ($^{*}p < 0.05$ and $^{**}p < 0.01$). Among them, the apoptotic effect of high-dose HMF (50 μM) groups was the strongest (Figures 3E–H). These results indicated that HMF significantly induced growth inhibition and apoptosis in NPC cell lines (5-8F and CNE-2).

3.4 HMF inhibits invasion and migration of 5-8F and CNE-2 cell lines

To determine the effect of HMF on the migration and invasion of CNE-2 and 5-8F cells, wound-healing and transwell-migration assays were performed. As shown in Figures 3I–L, the HMF dose dependently inhibited the invasion of CNE-2 and 5-8F cells. The wound healing levels calculated at two time points (0 h and 24 h) showed remarkably weaker cell migration ability in HMF groups (10, 25, and 50 μM) compared to the control groups in the two NPC cell lines (Figures 3M–P) ($^{*}p < 0.05$, $^{**}p < 0.01$). These results demonstrated that HMF dose-dependently inhibited the invasion and migration of NPC cells (5-8F and CNE-2).

3.5 HMF regulates the AMPK-dependent signaling pathway in NPC cells

AMPK is a crucial regulator of cellular energy metabolism. AMPK activation participates in the body's metabolic and energy regulation by regulating multiple related pathways, accounting for apoptosis and proliferation inhibition in cancer cells. The protein levels of p-AMPK, AMPK, p-P70S6K, P70S6K, p-S6, S6, COX-2, p-p53, and p53 in two NPC cell lines were detected by Western blot to explore the effects of the AMPK signal cascade on HMF-induced NPC cell apoptosis and proliferation inhibition. As shown in Figures 4A–F, in 5-8F cells, the HMF treatment group (25 and 50 μM) showed significantly upregulated protein levels of phosphorylated AMPK (p-AMPK/AMPK). At the same time, phosphorylated P70S6K and S6 (p-P70S6K/P70S6K and p-S6/S6) levels were dose-dependently and significantly reduced. These results suggested that HMF could inhibit the AMPK-mTOR signaling pathway in 5-8F cells. Moreover, the protein levels of COX-2 were downregulated in the HMF group compared to the control group, suggesting that HMF induced the activation of the AMPK/COX-2 signaling pathway in both cell lines. Meanwhile, compared to the control group, the HMF treatment group showed significantly upregulated p-p53/p53, indicating that HMF inhibited NPC cell growth and proliferation through the AMPK/p53 signaling pathway ($^{*}p < 0.05$ and $^{**}p < 0.01$). We also showed that HMF inhibited the AMPK-dependent pathway in NPC CNE-2 cells (Figures 4G–L).

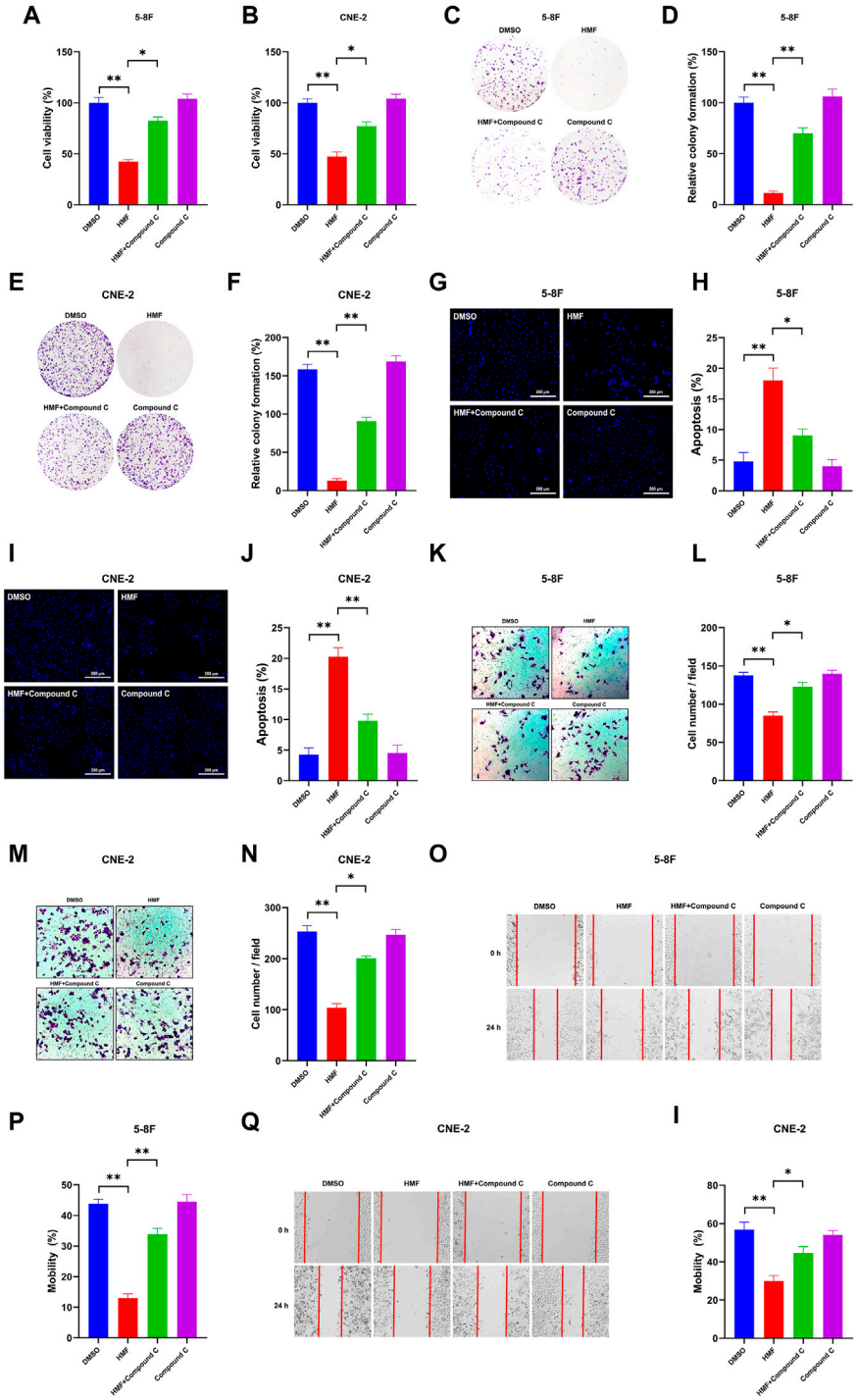

FIGURE 5
Effects of AMPK on proliferation, apoptosis, and metastasis through regulation of the AMPK-dependent signal pathway in two NPC cell lines. After high-dose HMF (50 μM) co-treated with Compound C (AMPK inhibitor) for 24 h. **(A,B)** The cell viability was determined by CCK-8 assay. **(C–F)** The colonies were stained with 0.5% crystal violet, and the colony numbers were quantified. **(G,I)** Assessment of the morphological changes in each treatment group using a fluorescence microscope (20×). **(H,J)** Apoptosis (%) in each group. **(K–N)** Representative images of transwell migration assays (10×) and quantification of cell migration expressed by cell counting. **(O–I)** Representative images of the scratch assay (10×) and mobility (%)24 h after the cells were scratched. All data are described as the mean ± SD of three independent and repeated experiments. Compared to the control group (0 μM): $*p < 0.05$; $**p < 0.01$; ns, not significant.

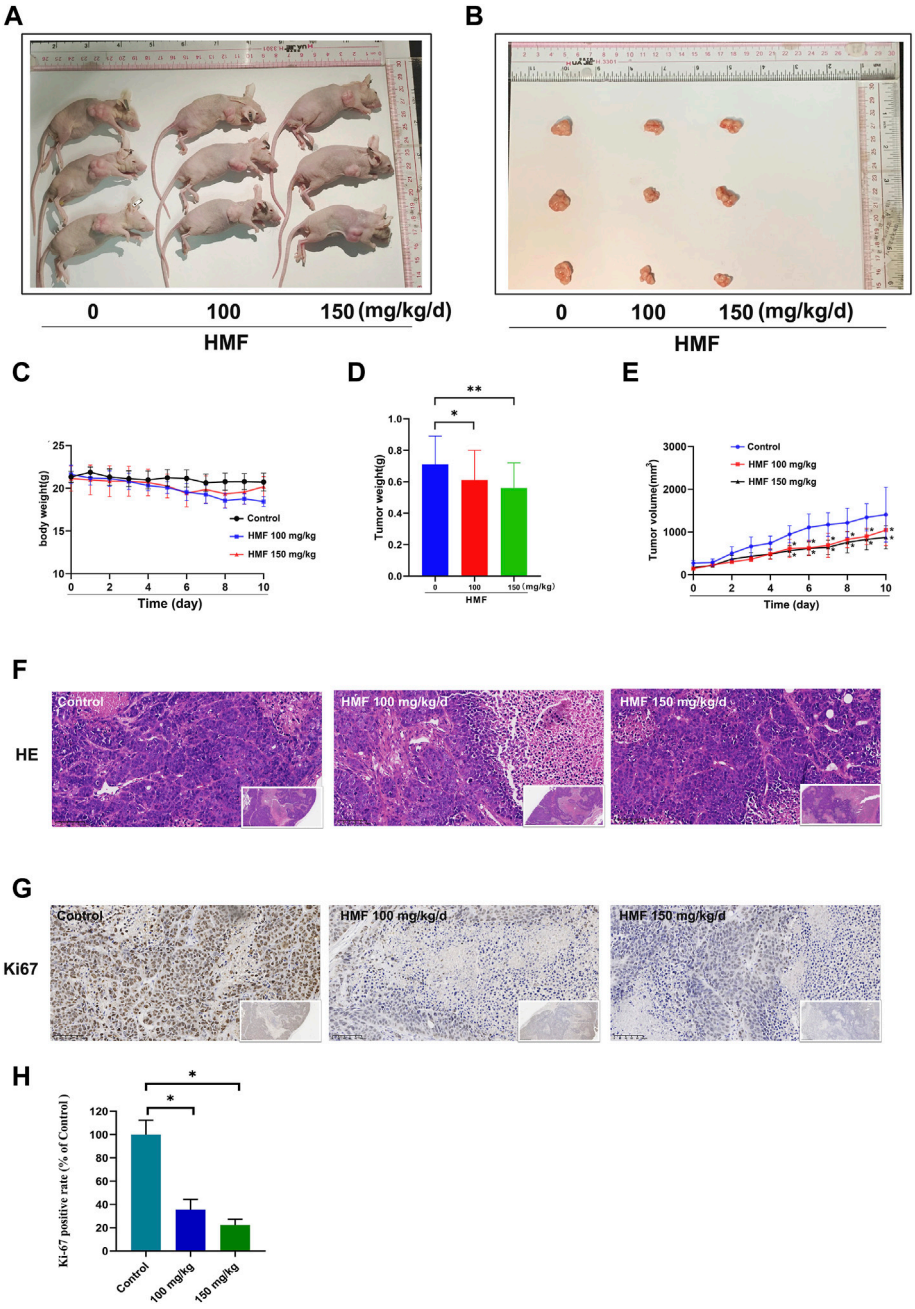

FIGURE 6
HMF inhibits NPC tumor growth and promotes tumor cell death in nude mice. **(A,B)** NPC tumors of nude mice. **(C)** Daily body weight variation in tumor-bearing nude mice in the control and HMF treatment groups. **(D)** Weight and **(E)** volume changes of implanted tumors for 10 days. **(F)** H&E staining of tumor tissues from each treatment group (400×). **(G)** Ki-67 staining was conducted to detect NPC cell proliferation. **(H)** Quantified analysis of Ki-67 positivity rate (%) and AMPK expression (%). All data are described as the mean ± SD of three independent and repeated experiments. Compared to the control group (0 μM): $*p < 0.05$; $**p < 0.01$; ns, not significant.

3.6 HMF inhibits proliferation and induces apoptosis by regulating the AMPK-dependent signal pathway in NPC cells

To further confirm whether the AMPK-dependent pathway participates in the effect of HMF on NPC cells, we co-administered an AMPK inhibitor (Compound C) and HMF in two NPC cell lines. As shown in Figures 5A, B, HMF inhibited the proliferation of 5-8F and CNE-2 cells; however, pretreatment with compound C reversed the HMF-induced inhibition of proliferation. Similarly, the relative colony formation was significantly increased in the Compound C/HMF group compared to the group administered HMF alone (Figures 5C–F). Moreover, we also showed that Compound C pretreatment reversed the HMF-induced apoptosis in 5-8F and CNE-2 cells (Figures 5G–J) ($*p < 0.05$ and $**p < 0.01$). These results indicated that HMF

inhibited the proliferation and induced the apoptosis of NPC cell lines through the AMPK-dependent pathway.

3.7 HMF inhibits invasion and migration by regulating the AMPK-dependent signal pathway in NPC cells

Compound C was co-administered with HMF in 5-8F and CNE-2 cells to confirm whether HMF was involved in regulating the invasion and migration of NPC cell lines via the AMPK-related pathway. Compound C was co-administered with HMF in 5-8F and CNE-2 cells. As shown in Figures 5K–N, HMF could inhibit 5-8F and CNE-2 cell invasion, which was ameliorated by pretreatment with Compound C. Similarly, HMF also could inhibit migration of CNE-2 and 5-8F cells, while pretreatment with Compound C reversed this HMF-induced migration inhibition (Figures 5O–I) ($^*p < 0.05$ and $^{**}p < 0.01$). These results showed that HMF inhibited invasion and migration by activating AMPK-dependent signaling pathways in NPC cells.

3.8 HMF inhibits NPC cell growth *in vivo*

A CNE-2 cell-transplanted xenograft tumor model in nude mice was performed to assess the anti-tumor action of HMF. The nude mice were split at random into three groups and were administrated HMF (100 and 150 mg/kg/day). After 14 days of implantation and HMF treatment, the tumor volumes and weights were measured after the dissection of the nude mice. As shown in Figures 6A–E, the tumor sizes in the HMF-treated mice were smaller than those in the control mice ($^*p < 0.05$, $^{**}p < 0.01$); however, no remarkable change in body weight was observed (Figure 6C). H&E staining showed that nude mice administered HMF treatment had worse tumor tissue necrosis than those of the control group. The tumor cells in the control group showed evident nucleolus and large nuclei that were arranged densely. In contrast, a loose arrangement was observed in the HMF-treated groups (Figure 6F). The Ki-67 assay revealed that compared to the control group, HMF treatment inhibited tumor cell proliferation (Figures 6G, H) ($^*p < 0.05$). These results indicated that HMF inhibited NPC cell growth *in vivo*.

4 Discussion

HSCCC, unlike the traditional chromatographic column and adsorbent resin, is a continuous liquid–liquid partitioning chromatography with the advantages of a reduced analysis running time, no irreversible adsorption, and a high loading amount. HSCCC has been successfully used for the separation of many natural products due to its flexible two-phase solvent system (Yang et al., 2020; Li et al., 2022). In the present study, four PMFs were successfully isolated and purified from CRCP in large quantities by petroleum ether heated reflux and HSCCC. These compounds were identified as NOB (325 mg), HMF (67 mg), TGN (249 mg), and 5-HPMF (90 mg) by ESI-MS, ^{1}H-NMR, and ^{13}C-NMR, and all purities were >95.0% by HPLC-PDA method. Hence, HSCCC is an ideal method for efficiently purifying large amounts of PMFs from CRCP. The valorization of PMFs is beneficial to provide a material basis for follow-up research on anti-NPC.

PMFs have been a research focus for their significant and broad pharmacological activities, such as anti-atherosclerosis, anti-inflammatory, and anti-tumor effects (Kong et al., 2020). For instance, TGN inhibits G1/S division and breast cancer cell metastasis by up-regulating p53/P21 and inhibiting matrix metalloproteinase-2 (MMP-2), MMP-9, and vascular endothelial growth factor, respectively (Arivazhagan and Sorimuthu, 2014). We previously reported inhibition of the proliferation and induction of apoptosis in NPC C666-1 cells by nobiletin (Zheng et al., 2019). However, systematic studies on PMF action in NPC are lacking. The present study compared the inhibitory effects of four PMFs (5-HPMF, TGN, NOB, and HMF) on NPC cells by CCK-8 assay. The results showed that the four PMFs inhibited the proliferation of 5-8F and CNE-2 cells in time- and dose-dependent manners. The inhibition effect based on IC_{50} was in the following order: HMF>NOB>TGN>5-HPMF. HMF showed the strongest cytotoxicity, with IC_{50} values of 36.273 ± 0.502 μM (CNE-2) and 31.786 ± 0.841 μM (5-8F). Further studies demonstrated the inhibitory effects of HMF on the proliferation, migration, and invasion and induction of apoptosis in NPC cell lines (CNE-2 and 5-8F). More importantly, HMF (100 and 150 mg/kg/day) could singly inhibit NPC growth *in vivo*.

PMFs attached with more methoxy group show stronger anti-tumor ability since the lower polarity contributes to cancer cell penetration (Gao et al., 2018; Kim and Lim, 2020). 3,5,6,7,8,3′,4′-Heptamethoxyflavone (HMF) contains 2-phenyl chromogenic ketone as the basic parent nucleus and C-3, C-5, C-6, C-7, C-8, C-3′, and C-4′ attached with -OCH_3, which indicate its lower polarity and planar structure.

Emerging studies have focused on the neuroprotective and antidepressant effect of HMF (Sawamoto et al., 2017). For instance, HMF showed neuroprotection against brain ischemia by inducing BDNF production and anti-inflammatory actions (Okuyama et al., 2014; Okuyama et al., 2015) and demonstrated an immunomodulatory function for the reduction of interleukin-4 expression in CD3/CD28-stimulated spleen cells in mice (Nakajima et al., 2016). However, its anti-tumor activity rarely has been mentioned, and the molecular mechanism for the anti-tumor effects of HMF remains unclear.

AMPK, an evolutionarily highly conserved serine/threonine protein kinase, functions to maintain and regulate the dynamic balance of cell energy by participating in glucose and lipid metabolism, in which it serves as an important physiological and pathological energy receptor in eukaryotic cells. Previous studies demonstrated that AMPK affects tumor cell growth in the following AMPK-dependent pathways. First, AMPK inhibits tumor cell proliferation and protein synthesis by negatively regulating mTOR-dependent signaling pathways. Ribosomal protein S6 kinase, 70 kDa (P70S6K) is one of the main downstream effectors of the AMPK-mTOR signal pathway. In general, mTOR phosphorylates S6K, which in turn phosphorylates the S6 protein of the 40S ribosomal subunit, regulating the initiation of translation, mRNA processing, and cell growth. Malignant tumor cells require large amounts of energy for proliferation. AMPK is activated when energy is depleted, accounting for the inactivation of mTOR and

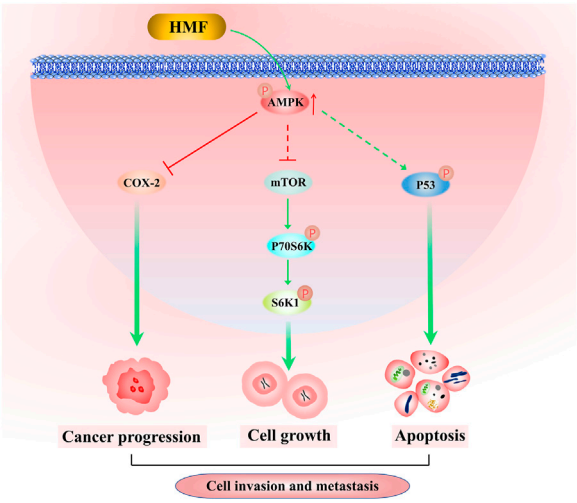

FIGURE 7
Molecular mechanism by which HFM inhibits nasopharyngeal carcinoma cell growth. HMF-induced AMPK activation inhibits NPC cell growth, invasion, and metastatic potency via downregulation of the activation of the mTOR signaling pathway and COX-2 protein levels, as well as enhancement of p53 phosphorylation.

tumor cell growth inhibition. Briefly, AMPK activation regulates tumor cell growth, invasion, and metastasis, whereas the specific action of AMPK on the metastatic potency of NPC cells remains unknown (Zhou et al., 2017). In our study, following HMF treatment, the protein expression levels of p-AMPK, which promotes cell death, and the protein levels of the phosphorylated form of P70S6K and S6 were remarkably inhibited in 5-8F and CNE-2 cells. This observation is consistent with those of previous studies which reported that the AMPK and mTOR pathways might interact in inhibiting the proliferation and inducing the apoptosis of cancer cells, such as colorectal cancer (Dutta et al., 2022), breast cancer (Li et al., 2021), and lung cancer (Song et al., 2021). For instance, the volatile components of frankincense, pine needle, and geranium inhibited the activity, proliferation, migration, and invasion and induced apoptosis of McF-7 human breast cancer cells. In the present study, we found that HMF significantly upregulated AMPK phosphorylation and decreased the protein level of p-P70S6K and S6 in CNE-2 and 5-8F cells, suggesting that HMF induced the activation of an AMPK-mTOR signaling pathway.

AMPK is a critical factor in regulating cellular energy metabolism by promoting ATP production and energy metabolism (Thirupathi and Chang, 2019). The AMPK/COX-2 pathway is also involved in regulating tumor cell growth, migration, and invasion. Cyclooxygenase-2 (COX-2), an inducible central enzyme of prostaglandin biosynthesis, is stimulated by growth factors, inflammatory mediators, and carcinogenic agents; thus, it is also considered an anticancer target, as it is highly expressed in tumor tissues and participates in tumor occurrence and development. MMP-2, which functions to degrade cellular basement membranes, is necessary for malignant tumor cells to penetrate multiple basement membrane barriers around tissues, blood vessels, nerves, and muscles in the process of metastasis. The invasive and metastatic ability of cancer cells occurs due to the metabolites of the cyclooxygenase (COX) and lipoxygenase pathways (PGF2-α and 5-HPETE). Therefore, COX-2 inhibition reduces MMP-2 production, which, in turn, inhibits tumor invasion and metastasis (Reich and Martin, 1996). Highly activated AMPK inhibits the extracellular signal-regulated kinase (ERK) and COX signaling pathways, thereby reducing melanoma metastasis (Kim et al., 2012). Moreover, COX-2 inhibitors affect the apoptosis susceptibility of solid tumors, which is closely related to prognosis. The AMPK/COX-2 signaling pathway is also involved in apoptosis induced by natural products, such as curcumin, quercetin (Lee et al., 2009), and green tea catechin (Park et al., 2009) in colon cancer cells. Our research found that compared to the control group, the HMF treatment group upregulated the p-AMPK/AMPK protein level and downregulated the COX-2 protein level. Combining with the results of Hoechst-33258 staining to detect the level of cell apoptosis, transwell assays to examine cell migration, and wound scratch healing assays to measure invasion ability, HMF may inhibit NPC cell growth through the AMPK/COX-2 signaling pathway.

Previous studies demonstrated that AMPK induced apoptosis by regulating p53-dependent signaling pathways. p53, the most commonly mutated gene in cancer, is considered a tumor suppressor under metabolic stress. Deletion or mutation of p53 leads to uncontrolled cell growth, apoptosis inhibition, chemotherapy resistance, and promotion of tumor formation (Liu et al., 2011). When energy is scarce in the body, AMPK phosphorylates p53 to limit cell growth and save energy. Hence, increased AMPK activity promotes p53 transcription and inhibits cancer cell growth rates. Hemistepsin A could inhibit HCC cell proliferation and induce G0/G1 cell cycle arrest and mitochondrial-related apoptosis by activating AMPK/p53 pathways in the human hepatoma Huh7 cell line (Baek et al., 2020). Analogously, α-lipoic acid inhibits cell proliferation, adhesion, invasion, and colony formation in the human HT29 and mouse MCA38 colon cancer cell lines via the AMPK/p53 signaling pathway (Park et al., 2015). In the present study, after HMF treatment, the expression levels of p-p53/p53 and p-AMPK/AMPK on CNE-2 and 5-8F in the HMF group were significantly increased compared to those in the control group. Synthesizing the aforementioned results of apoptosis indicators, we concluded that HMF might mediate the AMPK/p53 signaling pathway to regulate apoptosis and exert an anti-NPC effect.

While multiple studies have reported that the upregulation of AMPK could inhibit cancer cell growth, few studies have focused on the inhibitory effect of AMPK-activated drugs on NPC cells (Xia et al., 2021; Liu et al., 2022). Previous studies reported that metformin and some plant-derived products, including curcumol, lupeol, resveratrol, and andrographolide, inhibited NPC cell growth by AMPK activation. Metformin, a synthetic biguanide, is used for the treatment of type II diabetes and induces both AMPK-dependent and AMPK-independent genes/pathways, accounting for its inhibitory effects on cancer cell growth (An and He, 2016; Safe et al., 2018). For instance, metformin inhibited C666-1 cell proliferation by decreasing cyclin D1 levels and inducing G1 cell cycle arrest, which may be involved in the AMPK-mediated inhibition of mTORC1 signaling (Zhao et al., 2011). Among the aforementioned natural AMPK-activated drugs, curcumol, lupeol, and andrographolide are terpenoid compounds with low polarity. Curcumol-induced autophagy and apoptosis through the activation of the AMPK/mTOR pathway in CNE-2 cells (Wang et al., 2021). Analogously, andrographolide suppressed the proliferation and induced the apoptosis of C666-1 cells through regulation of the LKB1/AMPK/mTOR signal pathway (Wu et al., 2018). Lupeol

modulated apoptosis, ferroptosis, and inflammation in CNE1 nasopharyngeal carcinoma cells through the AMPK/NF-κB pathway (Zhou et al., 2022). Resveratrol, a natural non-flavonoid phenolic compound found in red grapes, inhibited proliferation and induced apoptosis in the C666-1 nasopharyngeal carcinoma cell line via AMPK activation (Cai et al., 2015). PMFs attached with more methoxy group show stronger anti-tumor effects since their lower polarity contributes to the penetration of cancer cells. In our study, HMF belonged to PMFs attached with seven methoxy groups, indicating its low polarity and plan structure. HMF-induced AMPK activation inhibited the growth, invasion, and metastatic potency of NPC cells by downregulating mTOR signaling pathway activation and COX-2 protein levels, as well as enhancing p53 phosphorylation.

In conclusion, the results of this study demonstrated for the first time that HMF purified from CRCP significantly inhibited the proliferation and induced apoptosis of NPC cells (CNE-2 and 5-8F) and also inhibited NPC cell migration and invasion. The results of the tumor transplantation experiment in nude mice confirmed the inhibitory effect of HMF on NPC cell growth *in vivo*. Further investigation revealed that HMF appeared to act via AMPK-dependent signaling pathways involved in NPC cell growth, migration, and invasion inhibition (Figure 7). These findings provide a preliminary experimental basis for treating NPC and the development and utilization of PMFs in CRCP.

Data availability statement

The original contributions presented in the study are included in the article/Supplementary Material. Further inquiries can be directed to the corresponding authors.

Ethics statement

The animal study was reviewed and approved by the Ethics Committee of Guangzhou Medical University.

Author contributions

WY, YiL, and YuL: conceptualization, visualization, investigation, and writing—original draft. BC: methodology, software, and data curation. KW: software and data curation. XC: software and data curation. ZY: software and data curation. GZ, YC, and DY: methodology, software, data curation, validation, supervision, and writing—review and editing. All authors agree to be accountable for all aspects of the work, ensuring its integrity and accuracy.

Funding

The Undergraduate Teaching Quality and Teaching Reform Project Construction Project of Guangdong Province in 2022 (YJGH [2023] No. 4), the Guangdong Basic and Applied Basic Research Foundation (no. 2021A1515220188), College-enterprise cooperation and Double-hundred Project Typical Case in 2022 (GXH [2023] no.45), the Medical Science and Technology Research Foundation of Guangdong Province (no. A2022063), open research funds from The Sixth Affiliated Hospital of Guangzhou Medical University, Qingyuan People's Hospital (no. 202201-205), the 2022 Student Innovation Ability Improvement Program of Guangzhou Medical University (no. gydf [2022]66).

Conflict of interest

Author BC was employed by Guangdong Xinbaotang Biological Technology Co., Ltd.

The remaining authors declare that the research was conducted in the absence of any commercial or financial relationships that could be construed as a potential conflict of interest.

Publisher's note

References

An, H., and He, L. (2016). Current understanding of metformin effect on the control of hyperglycemia in diabetes. *J. Endocrinol.* 228 (3), R97–R106. doi:10.1530/JOE-15-0447

Arivazhagan, L., and Sorimuthu, P. S. (2014). Tangeretin, a citrus pentamethoxyflavone, exerts cytostatic effect via p53/p21 up-regulation and suppresses metastasis in 7,12-dimethylbenz(α)anthracene-induced rat mammary carcinoma. *J. Nutr. Biochem.* 25 (11), 1140–1153. doi:10.1016/j.jnutbio.2014.06.007

Baek, S. Y., Hwang, U. W., Suk, H. Y., and Kim, Y. W. (2020). Hemistepsin A inhibits cell proliferation and induces G0/G1-phase arrest, cellular senescence and apoptosis via the AMPK and p53/p21 signals in human hepatocellular carcinoma. *Biomolecules* 10 (5), 713–728. doi:10.3390/biom10050713

Cai, Y., Zhao, L., Qin, Y., Zhang, M., and He, Y. (2015). Resveratrol inhibits proliferation and induces apoptosis of nasopharyngeal carcinoma cell line C666-1 through AMPK activation. *Pharmazie* 70 (6), 399–403. doi:10.1691/ph.2015.4815

Dutta, N., Pemmaraju, D. B., Ghosh, S., Ali, A., Mondal, A., and Majumder, C. (2022). Alkaloid-rich fraction of Ervatamia coronaria sensitizes colorectal cancer through modulating AMPK and mTOR signalling pathways. *J. Ethnopharmacol.* 283, 114666. doi:10.1016/j.jep.2021.114666

Ferretti, A. C., Tonucci, F. M., Hidalgo, F., Almada, E., Larocca, M. C., and Favre, C. (2016). AMPK and PKA interaction in the regulation of survival of liver cancer cells subjected to glucose starvation. *Oncotarget* 7 (14), 17815–17828. doi:10.18632/oncotarget.7404

Gao, Z., Gao, W., Zeng, S. L., Li, P., and Liu, E. H. (2018). Chemical structures, bioactivities and molecular mechanisms of citrus polymethoxyflavones. *J. Funct. Foods* 40, 498–509. doi:10.1016/j.jff.2017.11.036

Kim, D. S., and Lim, S. B. (2020). Semi-continuous subcritical water extraction of flavonoids from citrus unshiu peel: Their antioxidant and enzyme inhibitory activities. *Antioxidants-Basel* 9 (5), 360. doi:10.3390/antiox9050360

Kim, H. S., Kim, M. J., Kim, E. J., Yang, Y., Lee, M. S., and Lim, J. S. (2012). Berberine-induced AMPK activation inhibits the metastatic potential of melanoma cells via reduction of ERK activity and COX-2 protein expression. *Biochem. Pharmacol.* 83 (3), 385–394. doi:10.1016/j.bcp.2011.11.008

Kong, F., Ding, Z., Zhang, K., Duan, W., Qin, Y., and Su, Z. (2020). Optimization of extraction flavonoids from Exocarpium Citri Grandis and evaluation its hypoglycemic and hypolipidemic activities. *J. Ethnopharmacol.* 262, 113178–113185. doi:10.1016/j.jep.2020.113178

Lee, H. M., Okuda, K. S., González, F. E., and Patel, V. (2019). Current perspectives on nasopharyngeal carcinoma. *Adv. Exp. Med. Biol.* 1164, 11–34. doi:10.1007/978-3-030-22254-3_2

Lee, Y. K., Park, S. Y., Kim, Y. M., Lee, W. S., and Park, O. J. (2009). AMP kinase/cyclooxygenase-2 pathway regulates proliferation and apoptosis of cancer cells treated with quercetin. *Exp. Mol. Med.* 41 (3), 201–207. doi:10.3858/emm.2009.41.3.023

Li, C., Dong, Y., Wang, L., Xu, G., Yang, Q., Tang, X., et al. (2019). Ginsenoside metabolite compound K induces apoptosis and autophagy in non-small cell lung cancer cells via AMPK-mTOR and JNK pathways. *Biochem. Cell Biol.* 97 (4), 406–414. doi:10.1139/bcb-2018-0226

Li, L., Zhao, J., Yang, T., and Sun, B. (2022). High-speed countercurrent chromatography as an efficient technique for large separation of plant polyphenols: A review. *Food Res. Int.* 153, 110956. doi:10.1016/j.foodres.2022.110956

Li, Z., Li, C., Wu, Q., Tu, Y., Wang, C., and Yu, X. (2021). MEDAG enhances breast cancer progression and reduces epirubicin sensitivity through the AKT/AMPK/mTOR pathway. *Cell Death Dis.* 12 (1), 97. doi:10.1038/s41419-020-03340-w

Liu, J., Lin, Y., Yang, H., Deng, Q., Chen, G., and He, J. (2011). The expression of p33(ING1), p53, and autophagy-related gene Beclin1 in patients with non-small cell lung cancer. *Tumour Biol.* 32 (6), 1113–1121. doi:10.1007/s13277-011-0211-4

Liu, T., Li, Y., Sun, J., Tian, G., and Shi, Z. (2022). Gitogenin suppresses lung cancer progression by inducing apoptosis and autophagy initiation through the activation of AMPK signaling. *Int. Immunopharmacol.* 111, 108806. doi:10.1016/j.intimp.2022.108806

Nakajima, M., Ogawa, M., Amakura, Y., Yoshimura, M., Okuyama, S., and Furukawa, Y. (2016). 3,5,6,7,8,3',4'-Heptamethoxyflavone reduces interleukin-4 production in the spleen cells of mice. *Biomed. Res-Tokyo* 37 (2), 95–99. doi:10.2220/biomedres.37.95

Okuyama, S., Miyoshi, K., Tsumura, Y., Amakura, Y., Yoshimura, M., and Yoshida, T. (2015). 3,5,6,7,8,3',4'-heptamethoxyflavone, a citrus polymethoxylated flavone, attenuates inflammation in the mouse hippocampus. *Brain Sci.* 5 (2), 118–129. doi:10.3390/brainsci5020118

Okuyama, S., Morita, M., Miyoshi, K., Nishigawa, Y., Kaji, M., and Sawamoto, A. (2014). 3,5,6,7,8,3',4'-Heptamethoxyflavone, a citrus flavonoid, on protection against memory impairment and neuronal cell death in a global cerebral ischemia mouse model. *Neurochem. Int.* 70, 30–38. doi:10.1016/j.neuint.2014.03.008

Park, I. J., Lee, Y. K., Hwang, J. T., Kwon, D. Y., Ha, J., and Park, O. J. (2009). Green tea catechin controls apoptosis in colon cancer cells by attenuation of H2O2-stimulated COX-2 expression via the AMPK signaling pathway at low-dose H2O2. *Ann. N. Y. Acad. Sci.* 1171, 538–544. doi:10.1111/j.1749-6632.2009.04698.x

Park, S., Choi, S. K., Choi, Y., and Moon, H. S. (2015). AMPK/p53 Axis is essential for α-lipoic acid-regulated metastasis in human and mouse colon cancer cells. *J. Invest. Med.* 63 (7), 882–885. doi:10.1097/JIM.0000000000000233

Perri, F., Della, V. S. G., Caponigro, F., Ionna, F., Longo, F., and Buonopane, S. (2019). Management of recurrent nasopharyngeal carcinoma: Current perspectives. *Oncotargets Ther.* 12, 1583–1591. doi:10.2147/OTT.S188148

Pharmacopoeia, C. O. N. (2020). *The Pharmacopoeia of the People's Republic of China*. China: China Medical Science and Technology Press.

Qiu, P., Guan, H., Dong, P., Li, S., Ho, C. T., and Pan, M. H. (2011). The p53-Bax- and p21-dependent inhibition of colon cancer cell growth by 5-hydroxy polymethoxyflavones. *Mol. Nutr. Food Res.* 55 (4), 613–622. doi:10.1002/mnfr.201000269

Reich, R., and Martin, G. R. (1996). Identification of arachidonic acid pathways required for the invasive and metastatic activity of malignant tumor cells. *Prostaglandins* 51 (1), 1–17. doi:10.1016/0090-6980(95)00154-9

Safe, S., Nair, V., and Karki, K. (2018). Metformin-induced anticancer activities: Recent insights. *Biol. Chem.* 399 (4), 321–335. doi:10.1515/hsz-2017-0271

Sawamoto, A., Okuyama, S., Amakura, Y., Yoshimura, M., Yamada, T., and Yokogoshi, H. (2017). 3,5,6,7,8,3',4'-Heptamethoxyflavone ameliorates depressive-like behavior and hippocampal neurochemical changes in chronic unpredictable mild stressed mice by regulating the brain-derived neurotrophic factor: Requirement for ERK activation. *Int. J. Mol. Sci.* 18 (10), 2133. doi:10.3390/ijms18102133

Shi, M. D., Liao, Y. C., Shih, Y. W., and Tsai, L. Y. (2013). Nobiletin attenuates metastasis via both ERK and PI3K/Akt pathways in HGF-treated liver cancer HepG2 cells. *Phytomedicine* 20 (8-9), 743–752. doi:10.1016/j.phymed.2013.02.004

Song, G., Fang, J., Shang, C., Li, Y., Zhu, Y., and Xiu, Z. (2021). Ad-apoptin inhibits glycolysis, migration and invasion in lung cancer cells targeting AMPK/mTOR signaling pathway. *Exp. Cell Res.* 409 (2), 112926–112935. doi:10.1016/j.yexcr.2021.112926

Thirupathi, A., and Chang, Y. Z. (2019). Role of AMPK and its molecular intermediates in subjugating cancer survival mechanism. *Life Sci.* 227, 30–38. doi:10.1016/j.lfs.2019.04.039

Tokunaga, R., Cao, S., Naseem, M., Battaglin, F., Lo, J. H., and Arai, H. (2019). AMPK variant, a candidate of novel predictor for chemotherapy in metastatic colorectal cancer: A meta-analysis using tribe, maverick and FIRE3. *Int. J. Cancer* 145 (8), 2082–2090. doi:10.1002/ijc.32261

Wang, C. Y., Wang, T. C., Liang, W. M., Hung, C. H., Chiou, J. S., and Chen, C. J. (2020). Effect of Chinese herbal medicine therapy on overall and cancer related mortality in patients with advanced nasopharyngeal carcinoma in taiwan. *Front. Pharmacol.* 11, 607413. doi:10.3389/fphar.2020.607413

Wang, J., Liu, G., Li, X., Huangfu, M., Liu, Y., and Li, X. (2021). Curcumol simultaneously induces both apoptosis and autophagy in human nasopharyngeal carcinoma cells. *Phytother. Res.* 35 (12), 7004–7017. doi:10.1002/ptr.7321

Wang, Y., Chen, Y., Zhang, H., Chen, J., Cao, J., and Chen, Q. (2020). Polymethoxyflavones from citrus inhibited gastric cancer cell proliferation through inducing apoptosis by upregulating RARβ, both *in vitro* and *in vivo*. *Food Chem. Toxicol.* 146, 111811–111821. doi:10.1016/j.fct.2020.111811

Wu, B., Chen, X., Zhou, Y., Hu, P., Wu, D., and Zheng, G. (2018). Andrographolide inhibits proliferation and induces apoptosis of nasopharyngeal carcinoma cell line C666-1 through LKB1-AMPK-dependent signaling pathways. *Pharmazie* 73 (10), 594–597. doi:10.1691/ph.2018/8583

Xia, Y. C., Zha, J. H., Sang, Y. H., Yin, H., Xu, G. Q., and Zhen, J. (2021). AMPK activation by ASP4132 inhibits non-small cell lung cancer cell growth. *Cell Death Dis.* 12 (4), 365–378. doi:10.1038/s41419-021-03655-2

Yang, Y., Khan, B. M., Zhang, X., Zhao, Y., Cheong, K. L., and Liu, Y. (2020). Advances in separation and purification of bioactive polysaccharides through high-speed counter-current chromatography. *J. Chromatogr. Sci.* 58 (10), 992–1000. doi:10.1093/chromsci/bmaa063

Zhang, Z., Qu, J., Zheng, C., Zhang, P., Zhou, W., and Cui, W. (2018). Nrf2 antioxidant pathway suppresses Numb-mediated epithelial-mesenchymal transition during pulmonary fibrosis. *Cell Death Dis.* 9 (2), 83–94. doi:10.1038/s41419-017-0198-x

Zhao, L., Wen, Z. H., Jia, C. H., Li, M., Luo, S. Q., and Bai, X. C. (2011). Metformin induces G1 cell cycle arrest and inhibits cell proliferation in nasopharyngeal carcinoma cells. *Anat. Rec.* 294 (8), 1337–1343. doi:10.1002/ar.21283

Zheng, G. D., Hu, P. J., Chao, Y. X., Zhou, Y., Yang, X. J., and Chen, B. Z. (2019). Nobiletin induces growth inhibition and apoptosis in human nasopharyngeal carcinoma C666-1 cells through regulating PARP-2/SIRT1/AMPK signaling pathway. *Food Sci. Nutr.* 7 (3), 1104–1112. doi:10.1002/fsn3.953

Zhou, J. C., Wu, B., Zhang, J. J., and Zhang, W. (2022). Lupeol triggers oxidative stress, ferroptosis, apoptosis and restrains inflammation in nasopharyngeal carcinoma via AMPK/NF-κB pathway. *Immunopharm Immunot* 44 (4), 621–631. doi:10.1080/08923973.2022.2072328

Zhou, M., Shen, S., Zhao, X., and Gong, X. (2017). Luteoloside induces G(0)/G(1) arrest and pro-death autophagy through the ROS-mediated AKT/mTOR/p70S6K signalling pathway in human non-small cell lung cancer cell lines. *Biochem. Bioph Res. Co.* 494 (1-2), 263–269. doi:10.1016/j.bbrc.2017.10.042

frontiers | Frontiers in Pharmacology

TYPE Original Research
PUBLISHED 31 May 2023
DOI 10.3389/fphar.2023.1174867

OPEN ACCESS

EDITED BY
Mitesh Patel,
Parul University, India

REVIEWED BY
Patrick Valere Tsouh Fokou,
The University of Bamenda, Cameroon
Lauve Rachel Yamthe Tchokouaha,
Institut de Recherches Médicales et d'Etudes des Plantes Médicinales,
Cameroon

*CORRESPONDENCE
Harish R. Darasaguppe,
harish.dr@icmr.gov.in
Basanagouda M. Patil,
bmpatil59@hotmail.com
Subarna Roy,
roys@icmr.gov.in

RECEIVED 27 February 2023
ACCEPTED 12 May 2023
PUBLISHED 31 May 2023

CITATION
Patil PP, Kumar P, Khanal P, Patil VS, Darasaguppe HR, Bhandare VV, Bhatkande A, Shukla S, Joshi RK, Patil BM and Roy S (2023), Computational and experimental pharmacology to decode the efficacy of *Theobroma cacao* L. against doxorubicin-induced organ toxicity in EAC-mediated solid tumor-induced mice.
Front. Pharmacol. 14:1174867.
doi: 10.3389/fphar.2023.1174867

Computational and experimental pharmacology to decode the efficacy of *Theobroma cacao* L. against doxorubicin-induced organ toxicity in EAC-mediated solid tumor-induced mice

Priyanka P. Patil[1,2], Pranjal Kumar[3], Pukar Khanal [2], Vishal S. Patil [1,2], Harish R. Darasaguppe[1]*, Vishwambhar Vishnu Bhandare[1], Arati Bhatkande[1], Sudhanshu Shukla[3], Rajesh K. Joshi[1], Basanagouda M. Patil[4]* and Subarna Roy[1]*

[1]Indian Council of Medical Research- National Institute of Traditional Medicine, Belagavi, Karnataka, India, [2]Department of Pharmacology and Toxicology, KLE College of Pharmacy Belagavi, KLE Academy of Higher Education and Research (KAHER), Belagavi, Karnataka, India, [3]Department of Biosciences and Bioengineering, Indian Institute of Technology Dharwad, Dharwad, Karnataka, India, [4]PRES's Pravara Rural College of Pharmacy Pravaranagar, Loni, Maharashtra, India

Background and objective: Doxorubicin is extensively utilized chemotherapeutic drug, and it causes damage to the heart, liver, and kidneys through oxidative stress. *Theobroma cacao* L (cocoa) is reported to possess protective effects against several chemical-induced organ damages and also acts as an anticancer agent. The study aimed to determine whether the administration of cocoa bean extract reduces doxorubicin-induced organ damage in mice with Ehrlich ascites carcinoma (EAC) without compromising doxorubicin efficacy.

Methodology: Multiple *in vitro* methods such as cell proliferation, colony formation, chemo-sensitivity, and scratch assay were carried out on cancer as well as normal cell lines to document the effect of cocoa extract (COE) on cellular physiology, followed by *in vivo* mouse survival analysis, and the organ-protective effect of COE on DOX-treated animals with EAC-induced solid tumors was then investigated. *In silico* studies were conducted on cocoa compounds with lipoxygenase and xanthine oxidase to provide possible molecular explanations for the experimental observations.

Results: *In vitro* studies revealed potent selective cytotoxicity of COE on cancer cells compared to normal. Interestingly, COE enhanced DOX potency when used in combination. The *in vivo* results revealed reduction in EAC and DOX-induced toxicities in mice treated with COE, which also improved the mouse survival time; percentage of lifespan; antioxidant defense system; renal, hepatic, and cardiac function biomarkers; and also oxidative stress markers. COE reduced DOX-induced histopathological alterations. Through molecular docking and MD simulations, we observed chlorogenic acid and 8′8 methylenebiscatechin, present in cocoa, to have the highest binding affinity with lipoxygenase and

xanthine oxidase, which lends support to their potential in ameliorating oxidative stress.

Conclusion: The COE reduced DOX-induced organ damage in the EAC-induced tumor model and exhibited powerful anticancer and antioxidant effects. Therefore, COE might be useful as an adjuvant nutritional supplement in cancer therapy.

KEYWORDS

cocoa, cytotoxicity, doxorubicin, organ toxicity, oxidative stress

Introduction

Doxorubicin is an anthracycline antibiotic that has been indicated to deal with malignancy associated with vital organs with topoisomerase II inhibition, which cleaves the DNA of tumor cells (Thorn et al., 2011). Although doxorubicin is a potent cytotoxic agent in cancer chemotherapy, its utilization is limited due to its unwanted adverse effects, including myelosuppression, cardiomyopathy, and damage to other vital organs due to the free radicals produced by the doxorubicin metabolite (van der Zanden et al., 2021). In this regard, it is important to identify the agent to deal with the doxorubicin metabolite-activated reactive oxygen species (ROS) system without affecting the therapeutic action of doxorubicin. Cardiotoxicity caused by doxorubicin can be acute and manifest during or 2 to 3 days after administration. Acute cardiotoxicity occurs in about 11% of cases. There are substantially fewer cases of persistent doxorubicin cardiotoxicity, with an estimated incidence of 1.7%. For the majority of the time, it becomes evident after 30 days of administration of the last dose, although it can also happen 6–10 years afterward. Dosage is a major factor in doxorubicin cardiomyopathy incidence. When doxorubicin is administered at doses of 500–550 mg/m^2, 551–600 mg/m^2, and greater than 600 mg/m^2, the incidence is around 4%, 18%, and 36%, respectively (Tri and Wilkins, 1978).

Previously, several reports have explained that medicinal plants possess a broad biological spectrum due to the presence of many secondary metabolites, which may act on multiple pathways involved in disease pathogenesis. In this regard, one can think to conceptualize the broad pharmacological spectral activity in managing cancer by "neutralization of the ROS system and enhancement of the pharmacological threshold of established chemotherapeutic agents," which may be achieved by utilizing traditional medicines as they are rich in bioactive principles for multiple pharmacological activities with broad biological processes (Atanasov et al., 2021).

Theobroma cacao L. nibs (family Sterculiaceae), native to Central America, have been reported to contain multiple secondary metabolites (flavonoids, polyphenols, and alkaloids) and are also indicated for multiple pharmacological activities, *viz*., anti-inflammatory, anti-cancer, cardioprotective, nephroprotective, and hepatoprotective, including anti-oxidant properties (Zięba et al., 2019; Cura et al., 2021; Fanton et al., 2021; Sun et al., 2021). Due to these pharmacological properties, it can be hypothesized that nibs of *Theobroma cacao* may neutralize the doxorubicin-metabolite-mediated ROS system and have a protective effect on the heart, liver, and kidneys in the chemotherapy involving doxorubicin. In addition, it may also amplify the effect of doxorubicin as *T. cacao* itself possesses anti-cancer properties.

Hence, the present study aimed to investigate the effect of *T. cacao* nibs' hydroalcoholic extract (COE) supplementation over doxorubicin-induced organ toxicities in solid tumor models and cell line models *in vitro* and also assess the anticancer efficacies of COE alone or in combination with doxorubicin.

Materials and methods

Plant collection, authentication, and extract preparation

Cocoa nibs were collected from Sirsi (14°.34′38.7984 N, 74°.58′21.288 E), India; authenticated at ICMR-NITM Belagavi, and deposited in the herbarium (voucher number RMRC-1392). The freshly collected nibs were washed under running water, chopped, and dried under shade; turned into a coarse powder; defatted with petroleum ether; macerated (1 week) in a closed container using ethanol 80% v/v; filtered, concentrated, and lyophilized; and stored in an airtight container for further use (Ruzaidi et al., 2005).

In vitro assays

Cell culture and maintenance

All the *in vitro* studies were carried out on the A549, Ehrlich's ascites carcinoma, and Chinese hamster ovary (CHO) cell lines. All the cell lines were procured from the National Center for Cell Sciences (NCCS), Pune. A549 cells were grown in Ham's F12K media (AL1065-500 mL), while EAC and CHO cell lines were grown in Dulbecco's modified Eagle's medium (DMEM, D6429-500 mL), each supplemented with fetal bovine serum (Gibco: 10270–106; 10% v/v), penicillin (100 U/mL), and streptomycin (100 μg/mL) (penicillin–streptomycin, Sigma: P4333-100 ML). All the cells were cultured at 37°C and 5% CO_2 in a humidified incubator.

Chemo-sensitivity assay

All three cell lines were used for chemo-sensitivity assay using various concentrations of COE (2.5 μg/mL to 2560 μg/mL), doxorubicin (0.125 μg/mL to 128 μg/mL), and a combination of both (1.25–1280 μg/mL COE + 0.0625–64 μg/mL doxorubicin) for 48 h, and cell viability was assayed using MTT (as explained in cell proliferation assay in the following section). The data were normalized and plotted.

Cell proliferation assay

All three cell lines were utilized for the cell proliferation assay (Kumar et al., 2019). Briefly, cells were treated with doxorubicin (1 μg/mL), COE (40 μg/mL), and a combination of doxorubicin

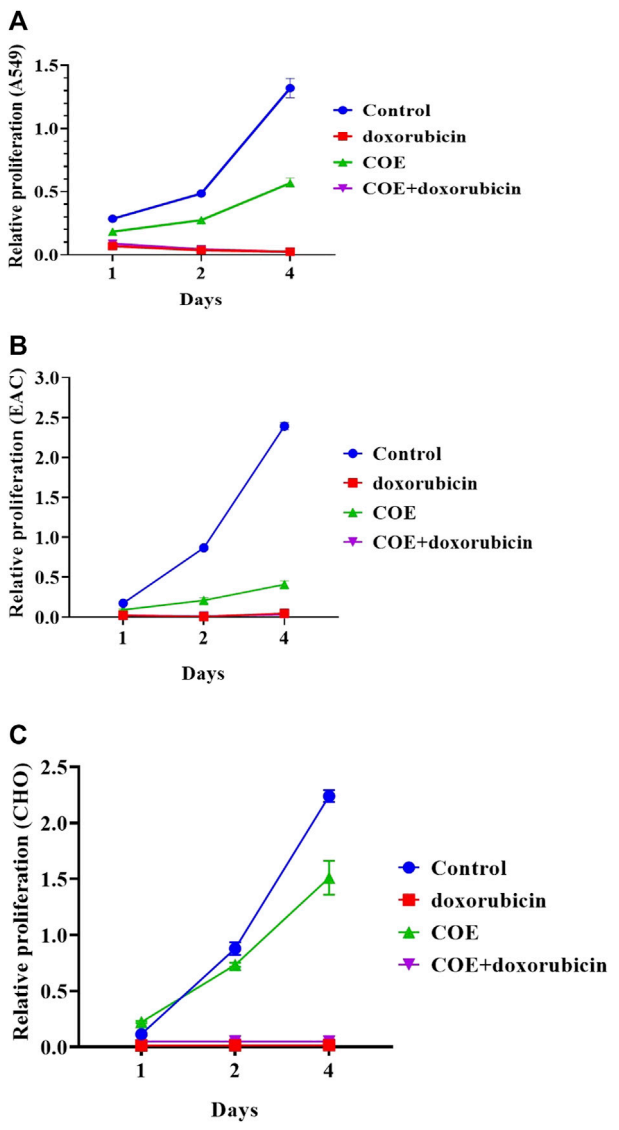

FIGURE 1
Effect of doxorubicin and COE treatment on relative cell proliferation in **(A)** A549, **(B)** EAC, and **(C)** CHO cell lines.

(0.5 μg/mL) with COE (20 μg/mL) along with control (DMSO) for 48 h. Later, cells were detached using a trypsin–EDTA solution, collected, counted, and plated for all the assays. For the cell proliferation assay, 2000 cells per well were seeded in a 96-well plate (in triplicate). MTT (Sigma: M5655-1G) was added after 24, 48, and 96 h of seeding (for triplicate samples) for each treatment group, and after 4 h of incubation at 37°C, absorbance was recorded at 570 nm. The data were normalized and plotted.

Colony formation assay

The colony formation assay was performed similarly to the cell proliferation assay, except for the seeding density, i.e., 200 cells per well were seeded in a 24-well plate in duplicate and cultured for 2 weeks. Colonies with at least 50 cells were counted and plotted, and an image was captured and presented (Kumar et al., 2019).

Scratch assay

For the scratch assay, 0.2×10^6 cells per well were seeded in a 24-well plate. Cells were treated with the aforementioned concentration of test samples, and the migration was analyzed by measuring the scratch size over various time points. The data were normalized as per the scratch size at 0 hours and plotted (Kumar et al., 2019).

In vivo pharmacology

Ethical clearance and animal procurement

The experiment was performed after obtaining ethical clearance from the IAEC at ICMR-NITM, Belagavi for the use of laboratory animals (approval number: IAEC/ICMR-NITM BGM/2019/3). Healthy female Balb/c mice (22–25 g) were procured from a registered CPCSEA supplier and maintained at 23°C ± 2°C temperature, 50% ± 5% humidity, and a 12/12 h light-dark cycle. Animals had ad libitum access to food and water throughout the experiment.

Tumor cell transplantation and grouping of animals

The Ehrlich ascites carcinoma cells-carrying donor mice were obtained from *Invivo* biosciences, Bangalore, India, and were maintained and propagated by serial intraperitoneal transplantation (1×10^6 cells) into healthy mice in an aseptic environment and propagated for 14 d. Ehrlich ascites carcinoma cells were received from donor mice and suspended in sterile saline. A viable number of cells (~2×10^6 cells) were injected subcutaneously into the thigh region of the right hind limb (Gothoskar and Ranadive, 1971; Elsherbiny et al., 2016).

In the present study, a total of 80 animals were randomly divided into five groups (n = 16), of which group 1 served as normal (n = 16) and the rest were induced tumors by injecting EAC cells (2×10^6) (suspended in 0.2 mL saline/mice) subcutaneously. The tumor size of all EAC-inoculated mice crossing the 50 mm^3 limit was considered day 0 (11th day after implantation), and treatment was initiated. Tumor size was measured using a Vernier caliper every week and calculated using the following equation as mentioned by Schirner et al. (1998).

$$\textit{Tumor volume} = \textit{Longest diameter X Shortest width X } 0.5$$

The study included the animals grouping as *Normal*: vehicle (2% gum acacia OD); *EAC*: vehicle (2% gum acacia *p. o.*, OD); *DOX*: EAC + doxorubicin 4.91 mg/kg, *i. p.*, *q. w.*; *COE200*: EAC + Cocoa 200 mg/kg, *p. o.*, OD; and *COE200+ DOX*: EAC + doxorubicin 4.91 mg/kg, *i. p.*, *q. w.* + cocoa 200 mg/kg, *p. o.*, OD.

The treatment was carried out for 21 days, and six animals from each group were randomly separated. Blood was collected by the retro-orbital route separately for hematological and biochemical analysis. Furthermore, animals were euthanized with an overdose of ketamine to collect the tumor mass and vital organs (heart, liver, and kidneys) for antioxidant and histopathological studies. However, the rest of the animals (n = 10 per group) were kept for survival analysis for up to 60 days. The mean survival time was calculated as explained by Elsherbiny et al. (2016) as follows:

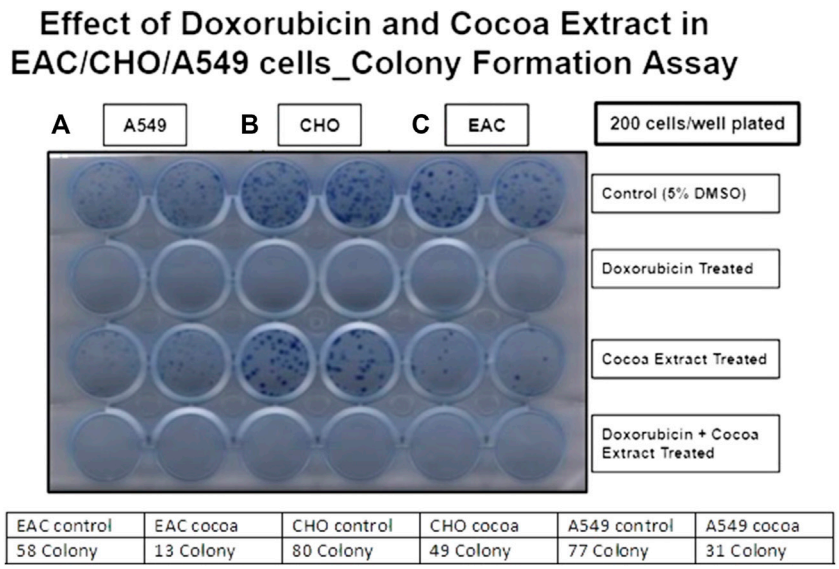

FIGURE 2
Effect of doxorubicin and COE treatment on colony formation in **(A)** A549, **(B)** CHO, and **(C)** EAC cell lines.

$$\mathrm{MST} = \frac{\Sigma\, Survival\ time\ (days)\ of\ each\ mouse \in a\ group}{Total\ number\ of\ mice}.$$

$$Increased\ life\ span\,(\%) = \frac{MST\ of\ treated\ mice}{MST\ of\ the\ cancer\ control\ group} X100.$$

Measurements and methods

As mentioned previously, body weight and tumor size were measured once a week. A total of six animals from each group were selected randomly, and blood, vital organs, and tumor mass were collected as previously mentioned. Furthermore, we evaluated multiple biochemical parameters, i.e., creatinine kinase-MB, lactate dehydrogenase, aspartate aminotransferase (AST), alanine aminotransferase (ALT), alkaline phosphatase (ALP), creatinine, and urea using commercially available kits (Biosystems) using a semi-automated analyzer (A15 Biosystems). In addition, we evaluated the anti-oxidant biomarkers, i.e., catalase (Claiborn, A., 1985), SOD (Misra and Fridovich, 1972), GSH (Sedlak and Lindsay, 1968), and LPO (Ohkawa et al., 1979). The hematological parameters such as complete blood counts (RBC, WBC, and platelets), mean corpuscular volume (MCV), mean corpuscular hemoglobin concentration, % Hb mean corpuscular hemoglobin, mean cell hemoglobin concentration, and packed cell volume were measured using an automatic hematology analyzer (Erba H560).

For histopathological analysis, the tissue was sectioned, and the samples (heart, liver, kidney, and tumor) were fixed in formalin (10%) and stained using hematoxylin and eosin. The samples were observed under a light microscope (Olympus BH-2, Olympus, Tokyo, Japan).

Molecular modeling studies

The anticancer agent doxorubicin induces hepatic and renal toxicity, mainly due to oxidative stress. Our experimental study showed that cacao extracts have significant potential in reducing the oxidative stress triggered by doxorubicin. Therefore, to gain detailed structural insights into this mechanism, we proposed screening phytocompounds from *T. cacao* against two important enzymes: lipoxygenase (LOX) and xanthine oxidase (XO), which are the key players in producing oxidative stress (Chung et al., 1997; Czapski et al., 2012; Kostić et al., 2015).

In this study, phytocompounds from *T. cacao* were selected, and their structures (in SDF format) were retrieved from the PubChem small-molecular databases. The virtual screening was performed using an automated POAP pipeline based on the AutoDock Vina interface (Samdani and Vetrivel, 2018; Patil et al., 2022). The structures of all the ligands were converted to 3D format and subjected to energy minimization for 5000 steps using the default LigPrep parameters in the POAP pipeline. The structures of receptors (LOX: 1N8Q and XO: 3AM9) have been prepared by removing water molecules and other heteroatoms that were used to obtain the crystal structures. The missing loop regions in the structures were built using the modeler interface in Chimera 1.15. We used the CastP tool to predict the largest and best possible binding pocket in both receptors, namely, LOX and XO. The parameters used for the virtual screening of phytochemicals against LOX and XO were selected from earlier similar studies (Patil et al., 2022b). The docked conformations obtained were ranked by the binding energy values, the intermolecular interactions were analyzed using Chimera, and publication-quality figures were generated in PyMOL. The best identified docked complex of phytocompounds for each of the receptors, i.e., LOX and XO, was further subjected to all-atom MD simulation in an explicit solvent. The chlorogenic acid (CHL) and 8,8-methylenebiscatechin (MBC) formed much more stable complexes with the least binding energy (−6.4 kcal/mol

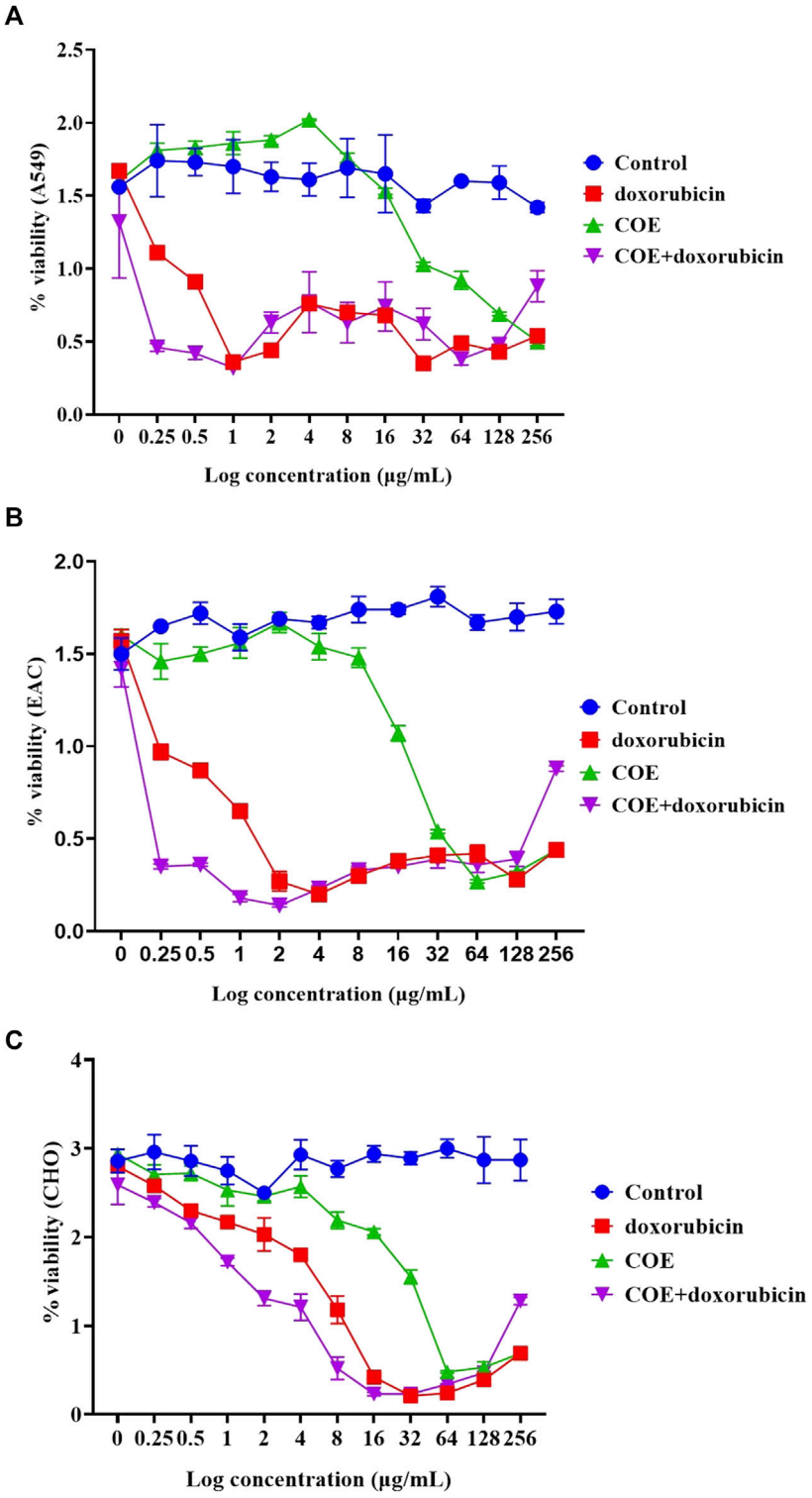

FIGURE 3
Effect of doxorubicin and COE treatment on chemo-sensitivity assays in **(A)** A549, **(B)** EAC, and **(C)** CHO cell lines.

and −11.3 kcal/mol, respectively) and expressed stable non-bonded interactions at the conserved binding site region. Therefore, we have considered these two complexes, namely, LOX-CHL and XO-MBC, for further molecular dynamics simulations. To investigate the structural stability of LOX-CHL and XO-MBC complexes, we used all atom-explicit MD

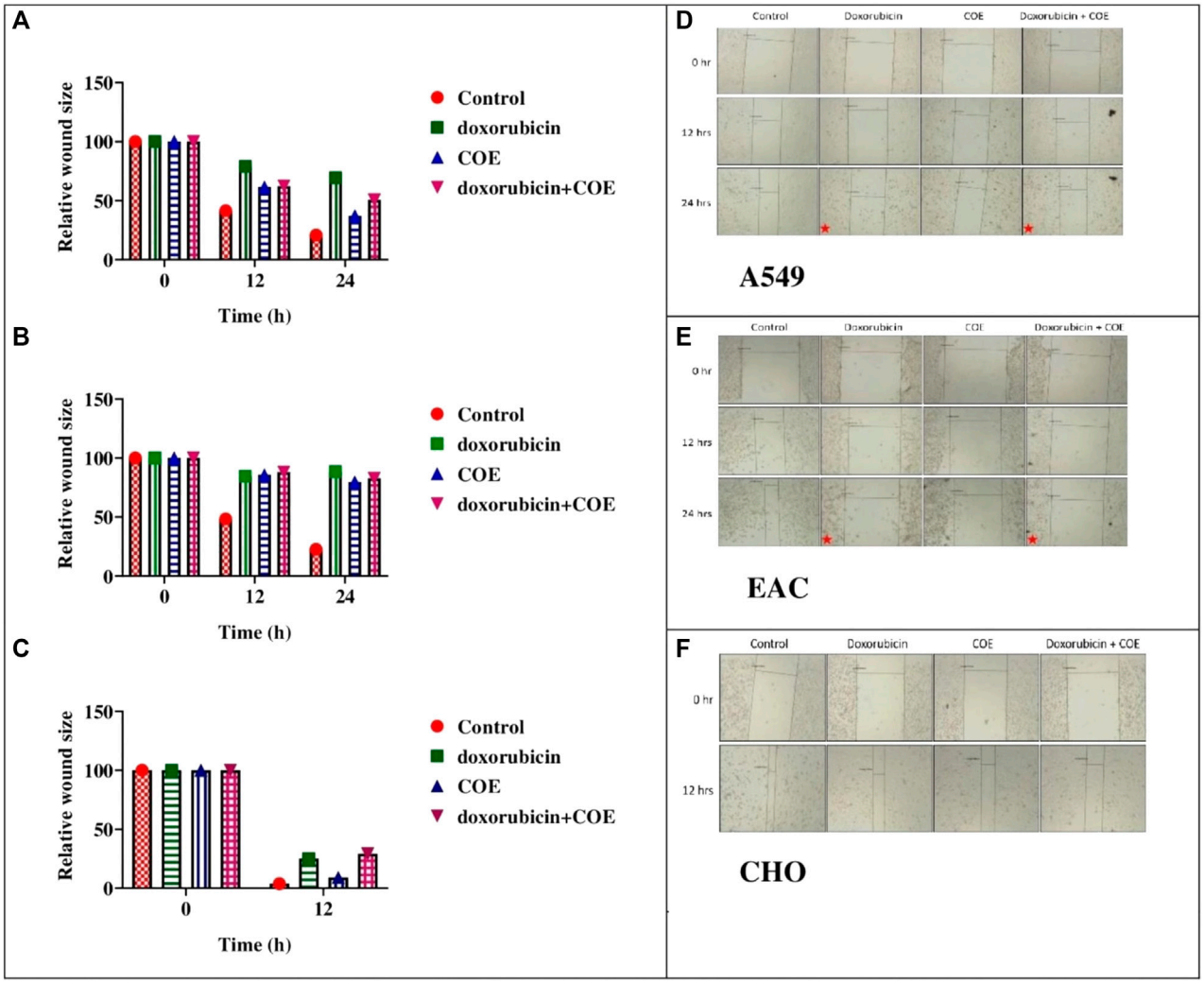

FIGURE 4
Effect of doxorubicin and COE treatment on relative scratch in **(A)** A549, **(B)** EAC, and **(C)** CHO cell lines and effect of doxorubicin and COE treatment on relative scratch in **(D)** A549, **(E)** EAC, and **(F)** CHO cell lines. Represents cell under cell death.

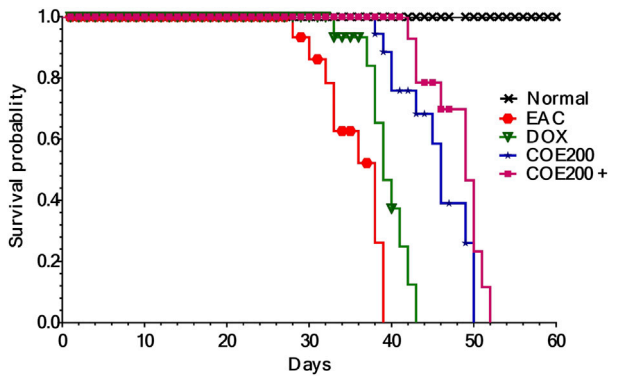

FIGURE 5
Kaplan–Meier survival curve for COE- and doxorubicin-treated groups. There was a significant difference ($p < 0.001$) in Mantel–Cox log-rank between the groups.

simulation methods using the GROMACS 2021.5 software package. The partial charges of both ligands MBC and CHL were generated using the antechamber module of AmberTools18. The Amber ff99SBildn force field was used to build the topology files. The complexes were solvated in a cuboidal box (10Å) with the TIP3P water model using periodic boundary conditions, and charges over the systems were neutralized by adding the required number of counterions such as Na+/Cl-. The topology and coordinate files for both these complexes were generated and converted to a Gromacs-compatible file format using ParmEd. The prepared systems were subjected to energy minimization using the steepest descent method, followed by a conjugate gradient. Systems were equilibrated using canonical NVT and isothermic–isobaric NPT ensembles for a period of 1 ns. The unrestrained production MD run was further continued for 100 ns, and trajectories were recorded every 2 fs. The parameters used to perform MD simulations were adopted from earlier similar studies (Khanal et al., 2022). The

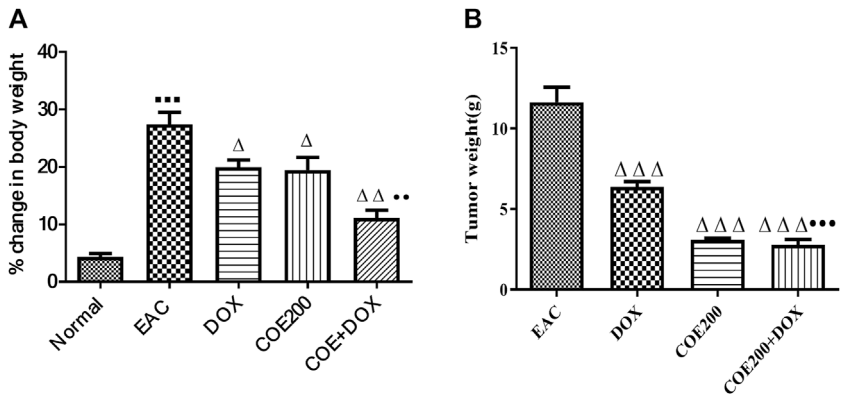

FIGURE 6
Effect of COE on **(A)** percentage change in body weight and **(B)** tumor weight (g) in solid Ehrlich tumor-bearing mice after 21 days of treatment. All values are expressed as the mean ± SEM (n = 6). One-way analysis of variance (ANOVA) followed by Tukey's test; $p < 0.001$, compared with normal; $^{\Delta}p < 0.05$ and $^{\Delta\Delta\Delta}p < 0.001$, compared with EAC; $^{\bullet\bullet}p < 0.01$ compared with DOX.

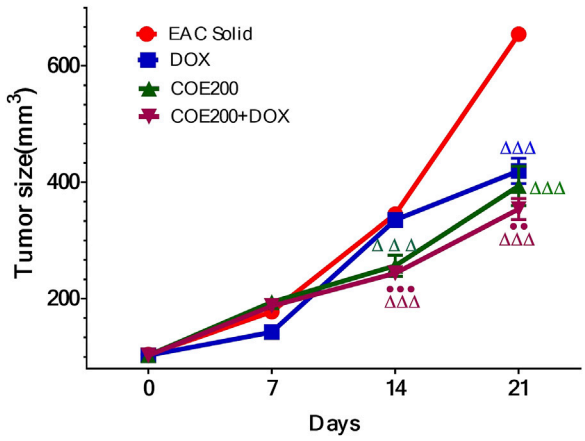

FIGURE 7
Tumor volume (mm^3) in solid Ehrlich tumor-bearing mice. All values are expressed as a mean ± SEM (n = 6). One-way analysis of variance (ANOVA) followed by Tukey's test; $p < 0.001$, compared with normal; $^{\Delta}p < 0.05$ and $^{\Delta\Delta\Delta}p < 0.001$, compared with EAC; $^{\bullet\bullet}p < 0.01$ compared with DOX.

trajectories obtained were analyzed for structural stability and their intermolecular interactions, followed by reimaging the PBC conditions. The inbuilt Gromacs tools like gmxrms, gms rmsf, and gmx gyrate were used to analyze structural stability, and other required tools were used for specific analysis wherever required, such as CPPTRAJ and LigPlus. The plots were generated using Grace 5.1.25.

Statistical analysis

Data were expressed as mean ± SEM. The mean difference between groups was analyzed using one-way ANOVA followed by Tukey's post-hoc test with GraphPad Prism *ver*. 5. The difference in mean of the group was considered to be significant if $p < 0.05$.

Results

In vitro assays

We examined the effect of COE on cellular physiology, such as cell proliferation and colony formation assays. In a cell proliferation assay, COE-treated cells showed reduced viability compared to the control in all three cell lines (A549, EAC, and CHO). However, the treatment with the chemotherapeutic drug, doxorubicin, was more effective than the COE-independent treatment. As expected, COE co-treatment with doxorubicin was more potent than COE-independent treatment. However, the effectiveness of COE and doxorubicin co-treatment was in a similar pattern compared to that of doxorubicin-independent treatment (Figure 1). Similarly, the colony formation assay resulted in reduced colony formation capability on COE treatment compared to control (the number of colonies was much higher in control vs. COE treatment for A549 (77 vs. 31), EAC (58 vs. 13), and CHO (80 vs. 49) cells). However, the treatment of doxorubicin alone or in combination with COE resulted in complete inhibition of colony formation capability, which is due to the lethal effect of doxorubicin (Figure 2).

Similarly, the chemo-sensitivity assay showed that there was a similar run in percentage viability in the control group. In COE and doxorubicin-independent treatments, there was a decrease in the percentage viability in A549, EAC, and CHO cell lines. However, it was observed that doxorubicin alone was more potent than COE-independent treatment. In addition, within the lower concentration of doxorubicin and COE treatments, the percentage viability was reduced in all the cell lines compared to the rest of the treatments, i.e., A549 (log concentration ~0.5 μg/mL), EAC (log concentration ~2 μg/mL), and CHO (log concentration ~8 μg/mL) (Figure 3).

The scratch assay was performed to evaluate the effect of COE on migration. In A549, EAC, and CHO cell lines, the generated scratch size (at 0 h) started decreasing gradually over time in the control group. However, doxorubicin treatment led to cell death and resulted in a relatively higher scratch size at 12 and 24 h compared to the control. Interestingly, the COE treatment showed higher scratch size, i.e., a reduction in migration with time compared to the control.

TABLE 1 Effect of doxorubicin and COE treatment on hematological parameters.

Groups	Normal	EAC	DOX	COE 200	COE 200+ DOX
Hb (% g)	13.83 ± 0.68	9.20 ± 0.15■■■	7.90 ± 0.18	11.33 ± 0.13▲▲	10.77 ± 0.20●●●
WBCs (cell/cmm)	27.21 ± 2.10	51.02 ± 1.50■■■	25.56 ± 1.70▲▲▲	33.91 ± 0.10▲▲▲	29.77 ± 1.40▲▲▲
RBC million (cell/cmm)	8.79 ± 0.20	5.00 ± 0.20■■■	4.23 ± 0.20	7.40 ± 0.00▲▲▲	6.03 ± 0.20▲●●●
Platelet count (cell/cmm)	1030.00 ± 20.90	789.00 ± 20.00■■■	645.60 ± 16.20▲▲	1007.00 ± 23.80▲▲▲	870.40 ± 35.60●●●
PCV (%)	54.78 ± 1.40	27.37 ± 2.20■■■	32.23 ± 1.00	36.97 ± 0.70▲▲▲	39.63 ± 0.40▲▲▲●●
MCV (fL)	51.52 ± 0.80	52.40 ± 0.20	51.43 ± 0.30	50.37 ± 0.06▲	51.37 ± 0.20
MCHC (gm/dL)	31.75 ± 0.70	24.12 ± 0.70■■■	31.18 ± 0.3▲▲▲	32.03 ± 0.40▲▲▲	32.05 ± 0.50▲▲▲
Lymphocytes (%)	74.50 ± 0.60	11.67 ± 1.05■■■	19.67 ± 0.60▲▲▲	32.00 ± 1.00▲▲▲	44.50 ± 1.50▲▲▲●●●
Neutrophils (%)	21.83 ± 0.80	80.83 ± 1.60■■■	63.00 ± 0.40▲▲▲	59.83 ± 0.90▲▲▲	54.17 ± 1.70▲▲▲●●●
Eosinophils (%)	0.66 ± 0.20	2.50 ± 0.20■■■	1.50 ± 0.20▲	1.80 ± 0.10	1.30 ± 0.20▲▲
Monocytes (%)	0.30 ± 0.20	5.16 ± 0.70■■■	2.50 ± 0.40▲▲	3.16 ± 0.10▲	2.16 ± 0.40▲▲
MCH(pg)	16.45 ± 0.20	17.90 ± 0.10■■	17.10 ± 0.20	15.52 ± 0.30▲▲▲	15.77 ± 0.30▲▲▲●

All values are expressed as a mean ± SEM (n = 6). One-way analysis of variance (ANOVA) followed by Tukey's test. ■■ $p < 0.01$.
■■■ $p < 0.001$, compared with normal.
▲ $p < 0.05$.
▲▲ $p < 0.01$.
▲▲▲ $p < 0.001$, compared with EAC.
●● $p < 0.01$.
●●● $p < 0.001$ compared with DOX.

TABLE 2 Effect of COE treatment on cardiac, Hepatic, and kidney biomarkers.

Groups	Normal	EAC	DOX	COE200	COE200+ DOX
CK-MB(U/L)	170.2 ± 1.6	251.5 ± 2.4 ■■■	360 ± 2.6▲▲▲	236.8 ± 1.5▲▲	255.5 ± 3.2●●●
LDH(U/L)	1955 ± 14.6	4268 ± 22.5■■■	5264 ± 20.8▲▲▲	2654 ± 15.5▲▲▲	4176 ± 18.3▲●●●
AST(U/L)	217.7 ± 16.3	620.3 ± 21.2■■■	898.7 ± 25.4▲▲▲	512.2 ± 17.2▲▲	547.7 ± 7.9 ▲▲ ●●●
ALT(U/L)	75.5 ± 2.2	150.7 ± 2.9■■■	234.8 ± 5.8▲▲▲	80 ± 6.7▲▲▲	124.5 ± 1.4▲▲●●●
ALP(U/L)	20.83 ± 0.4	37.83 ± 2.6■■■	46.67 ± 1.0▲▲	29.33 ± 1.1▲▲	39.5 ± 2.0●
Creatinine (mgs %)	0.125 ± 0.0	0.28 ± 0.0■■■	0.32 ± 0.0▲	0.23 ± 0.0▲▲	0.2383 ± 0.0▲●●●
BUN (mgs %)	30.83 ± 0.9	77.33 ± 0.9■■■	87.67 ± 1.6▲▲▲	55.67 ± 0.9▲▲▲	70.17 ± 1.64▲▲●●●

All values are expressed as a mean ± SEM (n = 6). One-way analysis of variance (ANOVA) followed by Tukey's test ■■■ $p < 0.001$, compared with normal.
▲ $p < 0.05$.
▲▲ $p < 0.01$.
▲▲▲ $p < 0.001$, compared with EAC.
● $p < 0.05$.
●● $p < 0.01$.
●●● $p < 0.001$, compared with DOX.

COE co-treatment with a lower doxorubicin concentration showed a greater reduction in migration (Figure 4A). The CHO cell line scratch closure was much faster than that of the other two cell lines, which allowed us to collect data for up to 12 h only (Figure 4B).

In vivo pharmacology

Effect of COE treatment on survival

There was no death observed in the normal group throughout the study. However, deaths were observed from the 28th to the 39th day in the EAC group. Furthermore, treatment with COE and doxorubicin has shown an increased lifespan, and it was maximal within the COE200+ DOX group (Figure 5). The log-rank (Mantel–Cox) test reflected the increased lifespan of COE-treated animals in combination with doxorubicin compared to the rest of the animals with $\chi 2 = 185.8$ and Df = 4.

Effect of COE on body weight, tumor weight, and tumor size

There was a significant increase in percentage change in body weight ($p < 0.001$) within EAC compared to normal, which was significantly reversed in all treatment groups (Figure 6). In addition, the combined action of COE and doxorubicin significantly

TABLE 3 Effect of administration of COE on doxorubicin-induced depletion of LPO, GSH, SOD, and CAT levels in heart, liver, and kidney tissues of mice.

Tissue	Treatment	LPO (nano-moles/mg of protein)	GSH (μMol/mg protein)	SOD (units/mg of protein)	CAT(units/mg of protein)
Heart	**Normal**	50.77 ± 1.7	26.29 ± 3.1	196.1 ± 2.7	0.57 ± 0.05
	EAC	177.3 ± 4.1 ■■■	17.51 ± 1.1 ■■	76.87 ± 3.7 ■■■	0.39 ± 0.02 ■■
	DOX	229 ± 3.08 ▲▲▲	14.99 ± 0.7	77.07 ± 5.9	0.31 ± 0.02
	COE200	148.3 ± 3.3 ▲▲▲	25.56 ± 1.05 ▲	111.5 ± 7.2 ▲▲	0.55 ± 0.01 ▲
	COE200+ DOX	163.6 ± 1.9 ▲●●●	22.75 ± 0.8 ●	105.4 ± 9.0 ▲●	0.49 ± 0.02 ●●
Liver	**Normal**	86.5 1 ± 6.5	164.2 ± 3.4	192.6 ± 11.2	0.5 ± 0.06
	EAC	165.8 ± 7.1 ■■■	91.47 ± 4.9 ■■■	127.8 ± 15.4 ■■	0.2 ± 0.02 ■■
	DOX	212 ± 7.6 ▲▲▲	88.39 ± 2	124.8 ± 9.3	0.1 ± 0.03
	COE200	105.8 ± 4.1 ▲▲▲	149.5 ± 9 ▲▲▲	181.9 ± 3.4 ▲	0.4 ± 0.03 ▲
	COE200+ DOX	168.5 ± 3.4 ●●●	131.7 ± 3.3 ▲▲▲●●●	176.2 ± 7.6 ▲●	0.3 ± 0.05
Kidney	**Normal**	252.9 ± 6.7	29.7 ± 2.4	46 ± 3.7	0.79 ± 0.02
	EAC	526.9 ± 18.9 ■■■	13.03 ± 1.6 ■■■	22.5 ± 2 ■■■	0.38 ± 0.01 ■■■
	DOX	483.1 ± 15.2 ▲▲▲	12.2 ± 0.4	14.9 ± 0.3	0.16 ± 0.01 ▲▲▲
	COE200	238 ± 13.2 ▲▲▲	26.2 ± 1.7 ▲▲▲	36.81 ± 2.8 ▲▲	0.60 ± 0.03 ▲▲▲
	COE200+ DOX	303.3 ± 11.9 ▲▲▲	20.41 ± 0.8 ▲▲▲●●●	21.7 ± 0.9	0.42 ± 0.0 ●●●

All values are expressed as a mean ± SEM (n = 6). One-way analysis of variance (ANOVA) followed by Tukey's test.
■■■ $p < 0.001$, compared with normal.
▲ $p < 0.05$.
▲▲ $p < 0.01$.
▲▲▲ $p < 0.001$, compared with EAC.
● $p < 0.05$.
●● $p < 0.01$.
●●● $p < 0.001$, compared with DOX. LPO, lipid peroxidation; GSH, glutathione; SOD, superoxide dismutase; CAT: catalase.

decreased the change in body weight compared to doxorubicin alone (Figure 6). In addition, there was a significant decrease ($p < 0.001$) in tumor weight with doxorubicin and COE-independent and combination treatment. Furthermore, the combined action of COE and doxorubicin significantly decreased tumor weight compared to the DOX group. Likewise, there was a significant decrease ($p < 0.001$) in the progression of tumor size observed from the 14th day of treatment in COE treatment groups. Furthermore, on the 21st day, there was a significant decrease ($p < 0.001$) in tumor size in all treatment groups compared to EAC, although the combination group showed a significant reduction ($p < 0.01$) in tumor size compared to the independent DOX group (Figure 7).

Effect on hematological parameters

There was a significant decrease in hemoglobin ($p < 0.001$) in EAC (9.2% ± 0.15%) compared to normal (13.83% ± 0.68%), which was significantly increased ($p < 0.01$) with COE-independent treatment. A further decrease in hemoglobin in the DOX group (7.9% ± 0.18%) was observed, which was significantly increased in the combination group (10.77% ± 0.20%) compared to DOX. Furthermore, there was a significant increase ($p < 0.001$) in WBC count (51.02 ± 1.5 cell/cm) in EAC compared to normal (27.21 ± 2.1 cell/cm), which was significantly decreased ($p < 0.001$) in all treatment groups compared to EAC (Table 1). In addition, there was a significant decrease in RBC and platelet count in EAC ($p < 0.001$). These cell counts were further decreased after doxorubicin treatment. The reduction in the cell count was reversed in the COE treatment groups. There was a significant decrease ($p < 0.001$) in PCV, MCHC, and lymphocytes compared to normal, which were observed to be significantly improved ($p < 0.005$–0.001) with doxorubicin and COE treatment, independent and in combination. In contrast, there was a significant increase ($p < 0.001$) in neutrophil, eosinophils, monocytes, and MCH ($p < 0.01$) within EAC compared with normal, which was ameliorated with independent or combination of doxorubicin and COE (Table 1).

Effect of COE on cardiac, hepatic, and kidney biomarkers

In the present study, we observed a significant increase ($p < 0.001$) in CK-MB, LDH, ALT, AST, ALP, creatinine, and BUN levels within the EAC groups. Furthermore, these biomarkers were significantly increased ($p < 0.05$–0.001) in the DOX group. In contrast, these markers were significantly ($p < 0.05$–0.001) ameliorated in the COE group. Likewise, in the combination treatment group, significant decreases in these parameters were observed when compared to the DOX group (Table 2).

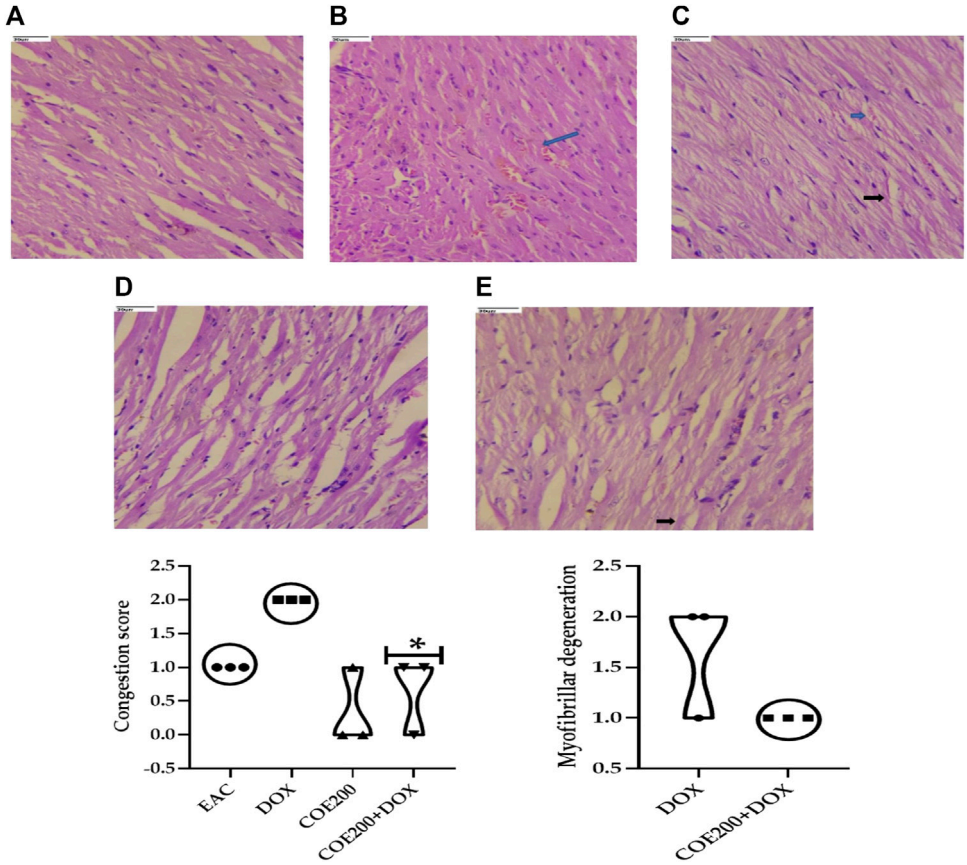

FIGURE 8
Effect of COE in cardiac histology. Photograph of the heart section of different treatment groups stained with hematoxylin and eosin. Plates at ×40 magnification. **(A)** Normal, **(B)** EAC, **(C)** DOX, **(D)** COE, and **(E)** COE + DOX. EAC group **(B)** showing congestion (blue arrow) and myofibrillar degeneration (black arrow). All values are expressed as mean ± SEM (n = 3), one-way analysis of variance (ANOVA) followed by Tukey's test ● $p < 0.05$, compared with DOX.

Effect of COE on antioxidant biomarkers

There was a significant increase in the LPO level ($p < 0.001$) in the heart, liver, and kidney within EAC animals compared to normal, which was significantly reversed with COE treatment. Furthermore, there was a significant increase in LPO ($p < 0.001$) in the DOX group compared to the EAC group, which was reversed with combination treatment. Similarly, there was a significant decrease ($p < 0.01, 0.001$) in cardiac, hepatic, and kidney GSH, SOD, and CAT activities compared to normal. Doxorubicin-independent treatment had no significant influence over GSH, SOD, and CAT activities in the heart, liver, and kidney. However, COE treatment groups significantly ameliorated ($p <$ 0.05–0.001) their GSH, SOD, and CAT activity in the heart, liver, and kidney compared to the EAC group. In addition, the combined action of COE with doxorubicin significantly ($p < 0.05$–0.001) influenced GSH level, SOD, and CAT activity in the heart, liver, and kidney (Table 3).

Effect of COE on cardiac, hepatic, kidney, and solid tumor histology

Normal architecture was observed in the heart, liver, and kidney tissue in the normal group of animals. Furthermore, in the EAC group, congestion and myofibrillar degeneration were noted in cardiac tissues (Figure 8). Venous and sinusoidal congestion, Kupffer cell hyperplasia, spotty necrosis, apoptosis, inflammation, and hepatocellular dysplasia were noted within hepatic tissues (Figure 9), while tubular and glomerular congestion, glomerular atrophy, tubular cell swelling, inflammation, widening of the Bowman space, and cytoplasmic vacuoles were observed in kidney tissues (Figure 10). In addition, these variables were traced in the EAC group, which were markedly increased with doxorubicin-independent treatment. Furthermore, these histopathological changes were mitigated in COE-treated groups. We also observed the tumor tissue and saw a maximum number of cords and nests of tumor cells, congestion, angiogenesis, hemorrhage, invading muscle infiltration, fibrosis, necrosis, anaplasia, and mitotic activity in the EAC group compared to the rest of the interventions (Figure 11).

In silico study

Molecular modeling studies

About 27 previously reported phytocompounds in cacao were collated (Patil et al., 2022b). The successful docking of these 27 phytocompounds to both the receptors LOX and XO has been

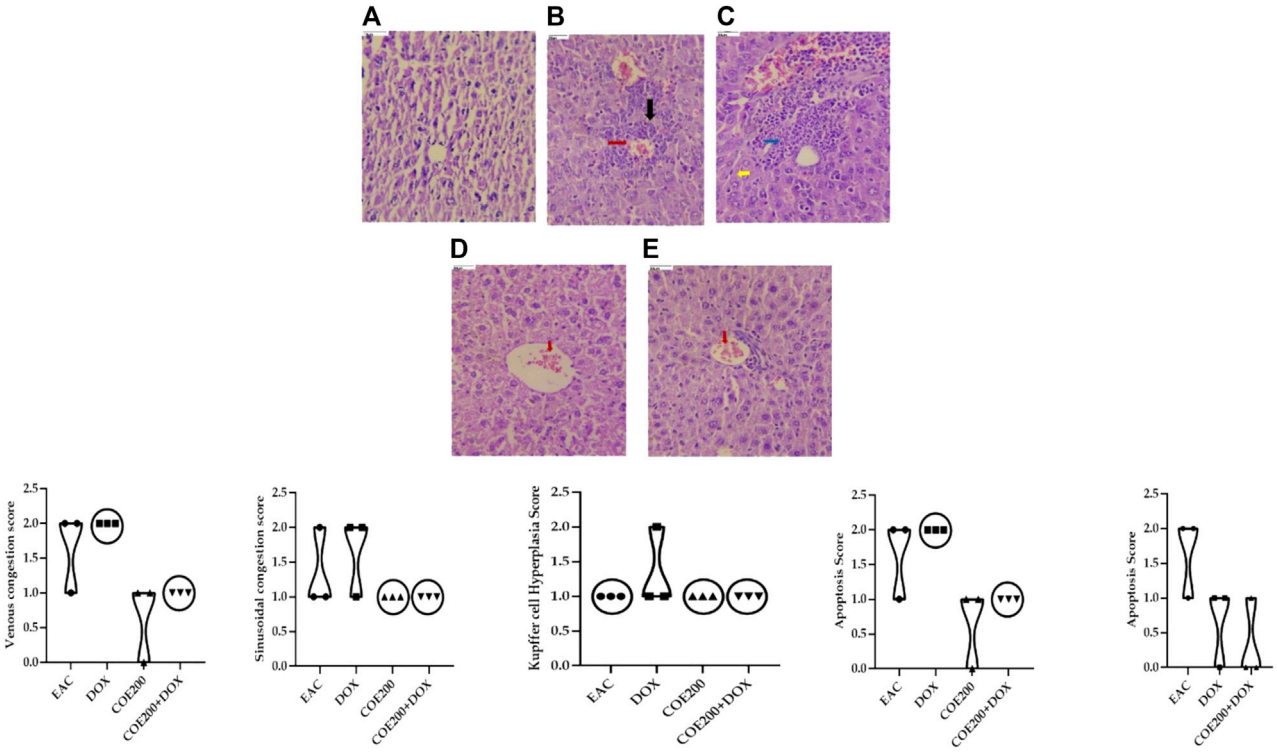

FIGURE 9
Effect of COE in hepatic histology. Photograph of liver section of different treatment groups stained with hematoxylin and eosin. Plates at ×40 magnification. **(A)** Normal, **(B)** EAC, **(C)** DOX, **(D)** COE, and **(E)** COE + DOX. EAC and DOX groups are showing venous and sinusoidal congestion (red and blue), Kupffer cell hyperplasia (yellow), apoptosis, and spotty necrosis (black). All values are expressed as a mean ± SEM (n = 3), one-way analysis of variance (ANOVA) followed by Tukey's test.

performed using the POAP pipeline to the binding site determined by CastP. It has been observed that the 27 compounds docked to the LOX and XO bind to the binding pocket with varying binding affinity. We also observed that some of the phytocompounds bound to the LOX do not favor the binding site interactions and show higher binding energy (+ve binding energy value). The binding energy value of the phytocompounds bound to LOX ranged from −6.4 kcal/mol to + 38.5 kcal/mol, while phytocompounds bound to XO ranged from −6.2 kcal/mol to −11.3 kcal/mol. Careful analysis of the docked complexes revealed that large-sized compounds having a higher molecular weight failed to occupy the specified binding pocket in the LOX structure, and hence do not form stable interactions. We have now considered top-screened compounds, namely, chlorogenic acid (binding energy = −6.4 kcal/mol) and 8′8 methylenebiscatechin (binding energy = −11.3 kcal/mol) bound to LOX and XO, respectively, for further MD simulation studies. For simplicity, chlorogenic acid and 8′8 methylenebiscatechin are hereafter referred to as CHL and MBC, respectively. The orientation of the docked pose of complexes LOX–CHL and XO–MBC is shown in Figures 12A, B. The significant intermolecular non-bonded interactions stabilizing the complexes LOX–CHL and XO–MBC are shown in Table 4.

The structural stability of the complexes LOX–CHL and XO–MBC for the period of 100 ns has been investigated by analyzing parameters such as RMSD, RMSF, Rg, and SASA. The average RMSD values for complexes LOX–CHL and XO–MBC have been recorded as 1.8 Å and 3.2 Å, respectively (Supplementary Figure S1A). Both trajectories reached an equilibrated state after 40 ns of simulation. The LOX–CHL and XO–MBC complexes show very stable dynamics and conserved binding pocket interactions during the 100 ns of simulation (refer Supplementary Figures S1 and S2). The probability of RMSD distribution has been analyzed to gain more confidence in the convergence of the MD simulation trajectory (Supplementary Figure S2) The probability distribution plot showed a higher probability (0.9) for both the complexes LOX–CHL and XO–MBC for fewer RMSD values (1.8 Å and 3.25 Å, respectively), indicating the trajectories are well-converged (refer Supplementary Figure S2). The Rg values represent the compactness of both complexes and reveal the stable dynamics throughout the simulation (Supplementary Figure S1B). Similar stable dynamics have also been expressed by the SASA values representing the compact folding and showed no exposure of the binding pocket region to the solvent (Supplementary Figure S1B). The maximum number of H-bonding interactions formed by the complexes LOX–CHL and XO–MBC were 6 and 11, respectively (Supplementary Figure S1D). The RMSF values show the least residual fluctuations (<1.5 Å) at the active site residues and the surrounding region of the binding pocket in both complexes (Supplementary Figures S3A and S3B). In XO, the C-terminal flexible loop, where native secondary structure folds are lacking,

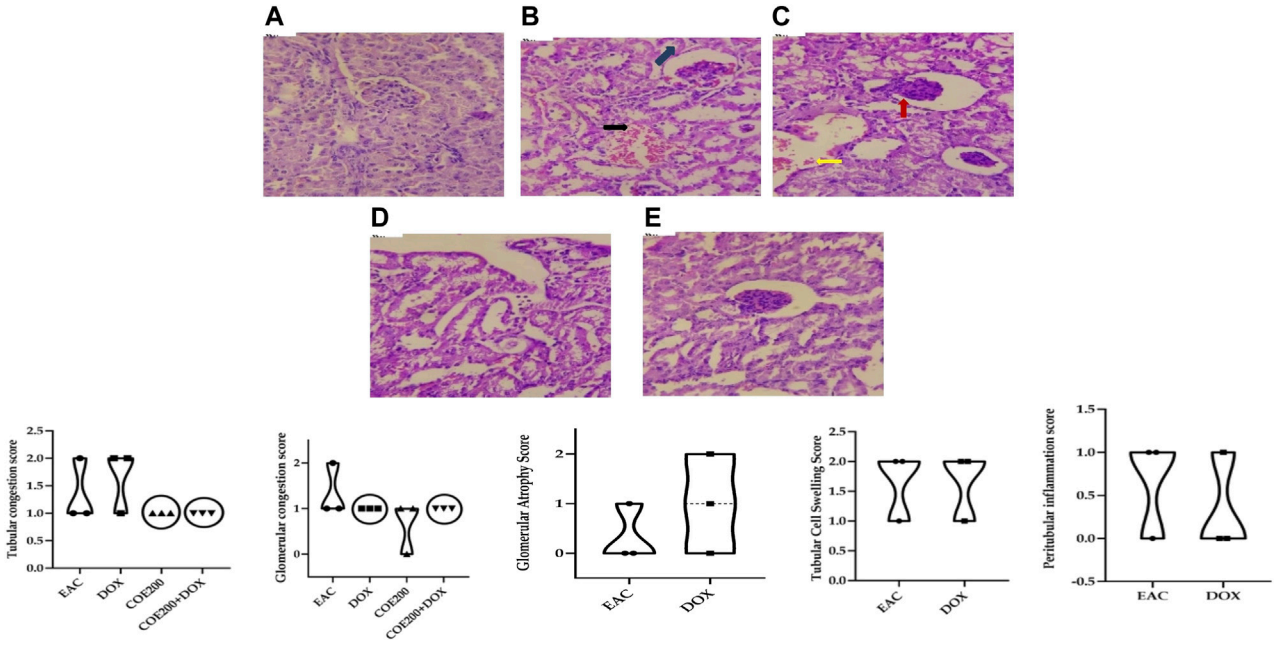

FIGURE 10
Effect of COE in kidney histology. Photograph of the kidney section of different treatment groups stained with hematoxylin and eosin. Plates at ×40 magnification. **(A)** Normal, **(B)** EAC, **(C)** DOX, **(D)** COE, **(E)** COE + DOX. EAC and DOX groups are showing tubular (black) and glomerular (blue) congestion, inflammation, glomerular atrophy (red), and tubular cell swelling (yellow). All values are expressed as a mean ± SEM (n = 3), one-way analysis of variance (ANOVA) followed by Tukey's test.

represents maximum RMSF values (>6 Å). In LOX, the N-terminal loop region showed higher residual fluctuations up to 5 Å (Supplementary Figure S3A). The minimum distance and the total number of all contacts are plotted for both complexes to provide detailed insights into their inter-molecular interactions (Figures 13A, B).

The minimum distance plotted for LOX–CHL shows an increase in the distance of 2.4 Å; furthermore, it decreases to 1.5 after 80 ns, while XO–MBC shows a consistent minimum distance of 1.6 Å throughout the simulation period.

The free energy landscape has been explored for both the complexes, of which complex XO–MBC showed the least energy state conformations were clustered in one group in the free energy landscape, while the other complex LOX–CHL showed three minimums over the free energy landscape, representing conformational diversity exhibited by the LOX upon binding of CHL. Supplementary Figures S4A and S4B represent the free energy landscape for both the complexes in 2D and 3D, respectively. Further concerted motion in complexes LOX–CHL (Figure 14A) and XO–MBC (Figure 14B) has been analyzed for representative frames from the stable trajectories, and it reveals the strong self-correlation for the individual residues (diagonal line shown in red) with itself, and binding pocket residues also express the positive correlation with moderate amplitude. Overall, the amplitude of the negative correlation was decreased in the complex XO–MBC when compared to LOX–CHL (Figures 14A, B).

Discussion

The results obtained during our study clearly demonstrated that COE alone or in combination with doxorubicin exerted better antitumor activity than doxorubicin alone, as evidenced by the improved survival time and tumor regression. *In vitro* assays provide the physiological environment to examine several cellular activities. *In vitro* studies showed that COE alone has a role in the reduction of the cell proliferation rate, colony formation capability, and migratory potential in EAC as well as human cancer cell lines (A549). COE has demonstrated stronger anticancer action on cancer cells than on healthy cells. In addition, COE enhanced the potency of doxorubicin when used in combination with a lower concentration (of doxorubicin) in the inhibition of cancer cell proliferation, migration, and cell cycle arrest. In this assay, the 1:1 ratio of DOX and cocoa (50% of each) in the combination group was selected to evaluate the potential therapeutic benefits of DOX at a lower concentration when used in combination with cocoa. Furthermore, it also has the added advantage of preventing possible undesirable effects when combining the two substances at higher concentration. The scratch assay results suggest that COE might have a role in the inhibition of epithelial–mesenchymal transition (EMT), the first step of metastasis. The induction of the EMT process leads to resistance toward chemotherapeutic drugs (Shibue and Weinberg, 2017). The EMT induction may reduce the cell proliferation rate and increase the expression of proteins responsible for inhibiting apoptosis as well as the expression of

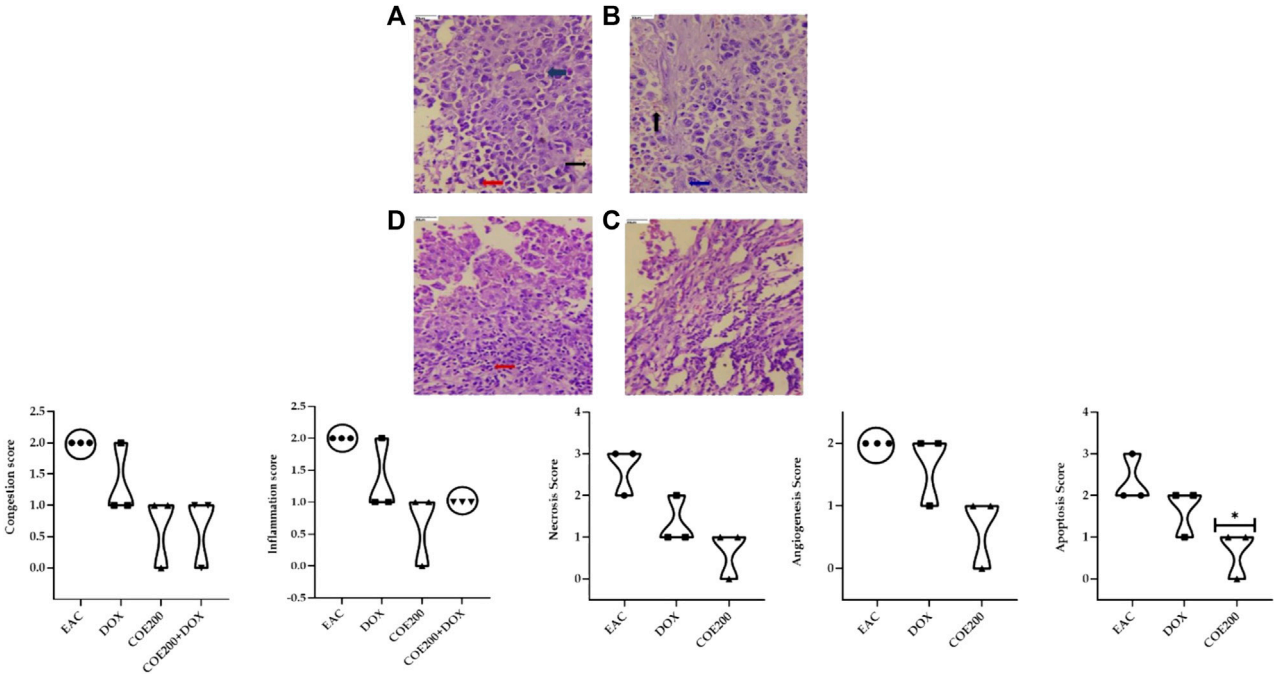

FIGURE 11
Effect of COE on tumor histology. Photograph of the tumor section of different treatment groups stained with hematoxylin and eosin. Plates at ×40 magnification. **(A)** EAC, **(B)** DOX, **(C)** COE, and **(D)** COE + DOX. EAC and DOX groups are showing congestion (black), inflammation (blue), hemorrhage, angiogenesis, apoptosis, and necrosis (red). All values are expressed as a mean ± SEM (n = 3). One-way analysis of variance (ANOVA) followed by Tukey's test ▲ $p < 0.05$ compared with EAC.

transporter-related proteins to efflux drugs (Shibue and Weinberg, 2017). The COE might be involved in the modulation of EMT initiation. Some anti-proliferative agents have already been designed to inhibit EMT initiation (Thiery and Sleeman, 2006). The natural product COE can be used as an alternative anti-proliferative agent. The COE may be involved in the modulation of signaling processes and may provide a better delivery system for chemotherapeutic drugs such as doxorubicin. However, further experimental validation will be needed to confirm our hypothesis.

Furthermore, COE markedly reduced the doxorubicin-induced cytotoxicities in cardiac, hepatic, and nephritic tissues in the EAC-induced solid tumor mouse model. The cell protective nature of COE toward cardiac myocytes, hepatocytes, and nephrons, manifested through histological and biochemical investigation, could be through the termination of Fenton and redox reactions, as there were ameliorated enzymatic and non-enzymatic antioxidant biomarkers.

Further combinatorial therapy of COE with doxorubicin in tumor-bearing mice showed an increase in survival time by 1.20 fold compared to the DOX group. Within 21 days of treatment, we observed a significant decrease in tumor size in doxorubicin- and COE-treated animals; the outcome was further effective with combined treatment, which was evidenced via the assessment of tumor size. This decrease in tumor size with combined treatment could be the outcome of the synergetic effect, which might be due to the anti-cancer potency of COE (Martin et al., 2013). Moreover, there was a significant increase in the percentage change in body weight in the EAC group, which pointedly declined with the combined and independent action of both agents. In addition, there was no significant difference between the percentage change in body weight in the doxorubicin- and COE-treated groups. However, the percentage change in body weight was significantly lower in combination than in the DOX group, suggesting COE's synergetic effect with doxorubicin. In addition, this decrease in percentage change in body weight supports the outcome of controlling tumor size with each intervention. Likewise, we observed a significant reduction in tumor weight with doxorubicin and COE-independent and combination action over tumor weight; a significant reduction in tumor weight in combination vs. DOX points toward a synergistic effect. Furthermore, the anti-tumor effect of COE reflected in our study is the auxiliary outcome, conveyed via a significant increase in lifespan.

In chemotherapy, doxorubicin has a major role in dealing with many cancers. However, it produces severe toxic effects on hematological parameters, which is one of the limiting factors in implementing doxorubicin chemotherapy (Ogura, 2001). In this regard, one can contemplate if any natural products with antioxidant potency could ameliorate the hematological parameters over synthetic chemotherapeutic agents, including doxorubicin. Herein, we observed significant amelioration of multiple hematological parameters with the combined action of COE with doxorubicin vs. DOX. Previously, it was reported that doxorubicin metabolites disturb hematological function, which could be a doxorubicin-activated ROS system (Afsar et al., 2017). In addition, ROS has a direct impact on Hb, RBC, WBC, platelets,

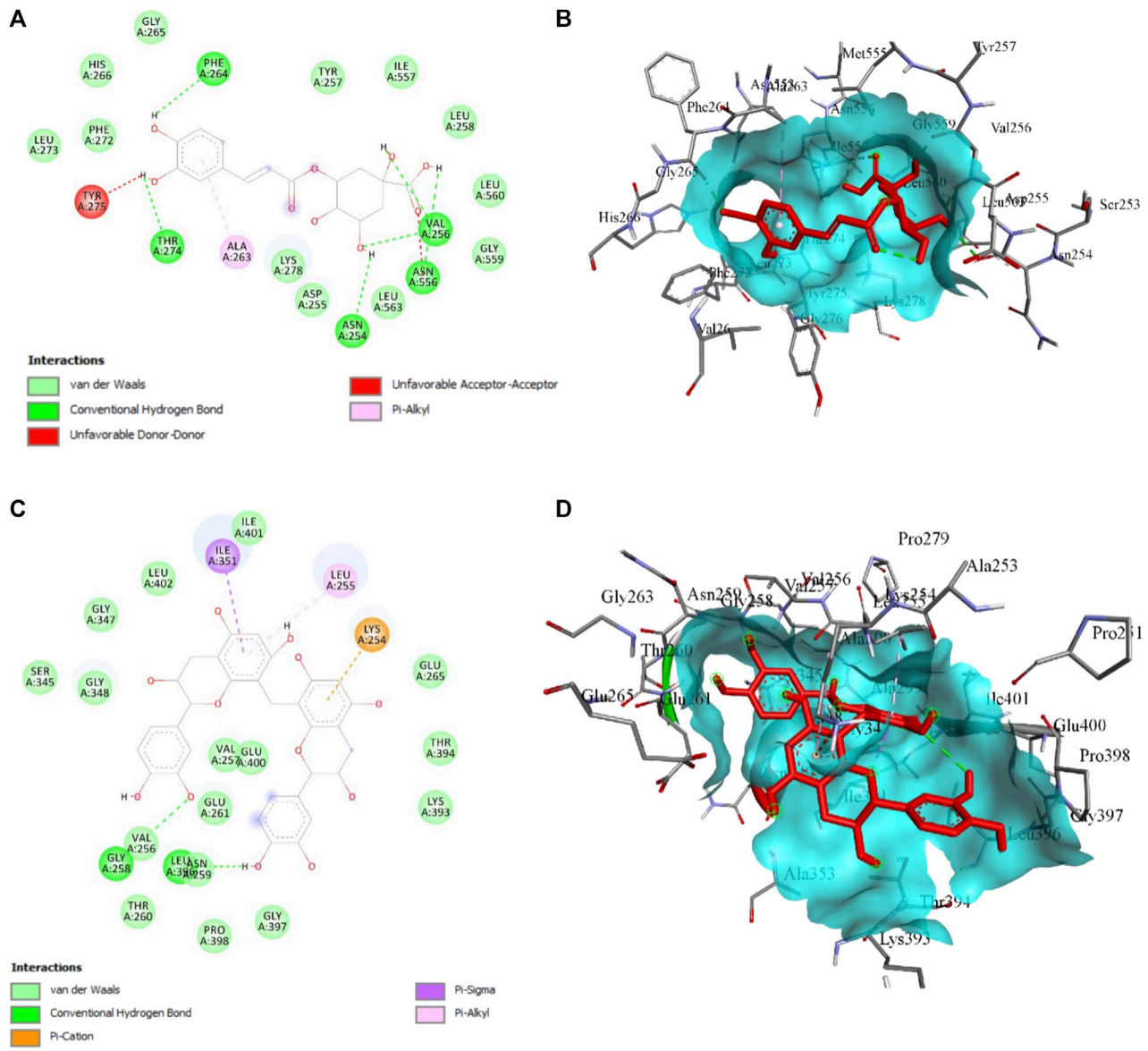

FIGURE 12
(A) 2D and **(B)** 3D presentation for the interaction of CHL with LOX, **(C)** 2D and **(B)** 3D presentation for the interaction of MBC with XO. The green bond represents the H-bond interaction, the red bond represents unfavorable interaction due to steric hindrance, and the rest represent hydrophobic interaction.

and other hematological parameters, which directly affects cellular apoptosis due to compromising immunity, affecting the transport of nutrition and oxygen (Gwozdzinski et al., 2021). Previously, COE extract was reported for its potent antioxidant activity due to the presence of phenolic bioactives and flavonoids (catechin, epicatechin, and procyanidins) (Lamuela-Raventós et al., 2001; Massee et al., 2015); this may trigger scavenging free radicals and terminate redox and Fenton reactions within the ROS system, which could have driven the ameliorated hematological parameters.

In cancer chemotherapy, organ toxicity is one of the major complications, and it affects the homeostatic function, which is most commonly reported in doxorubicin therapy (Mitry and Edwards, 2016; Santos and Goldenberg, 2018). Therefore, we quantified multiple parameters like CK-MB, LDH, AST, ALT, ALP, creatinine, and BUN in different treatment groups. We found that these biomarkers were significantly increased in treatment with doxorubicin alone compared to EAC, indicating chemotherapy-induced organ toxicities. Likewise, free radical generation during doxorubicin therapy causes significant damage to the myocardium, resulting in increased membrane permeability and release of CPK-MB and LDH enzymes. Doxorubicin treatment showed a 1.43-fold and 1.23-fold increase in CPK_MB and LDH enzymes, respectively, compared to EAC treatment. In addition, the liver and kidney showed an increased AST level by 1.44 folds, ALT by 1.55 folds, creatinine by 1.14 folds, and BUN by 1.13 folds compared to that of EAC. Interestingly, these parameters were

TABLE 4 Crucial intermolecular non-bonded interactions stabilizing LOX–CHL and XO–MBC complexes during MD simulation.

Complex	Conformation	Interactions	Type	Distance	Angle
LOX–CHL	Initial	B:UNL850:HO1–A:ASN556:OD1	Conventional hydrogen bond	2.91137	112.244
		B:UNL850:HO3–A:ARG252:O	Conventional hydrogen bond	2.41292	121.391
		A:LYS278:HE3–B:UNL850:O1	Carbon hydrogen bond	2.86753	129.811
		A:LEU560:HA–B:UNL850:O5	Carbon hydrogen bond	3.03038	110.953
		A:ASN254:HA–B:UNL850	Pi-sigma	2.74586	
		A:SER253:C,O; ASN254:N - B:UNL850	Amide-Pi stacked	4.39367	
	Final	B:UNL850:HO1–A:GLU197:OE1	Conventional hydrogen bond	1.47963	178.887
		B:UNL850:HO4–A:ASN556:O	Conventional hydrogen bond	2.92387	109.221
		A:GLY559:HA3–B:UNL850:O3	Carbon hydrogen bond	2.67742	127.64
		B:UNL850–A:LEU258	Pi-alkyl	5.41188	
XO–MBC	Initial	A:LYS247:HZ2–B:UNL1330:O4	Conventional hydrogen bond	1.91825	159.485
		A:LEU255:HN–B:UNL1330:O10	Conventional hydrogen bond	2.78719	153.983
		A:ILE351:HN–B:UNL1330:O9	Conventional hydrogen bond	3.02736	157.068
		A:SER353:HN–B:UNL1330:O7	Conventional hydrogen bond	2.31487	153.78
		A:ASN359:HD21–B:UNL1330:O7	Conventional hydrogen bond	2.00375	139.321
		B:UNL1330:HO3–A:GLY396:O	Conventional hydrogen bond	1.96909	133.105
		B:UNL1330:HO5–A:GLY347:O	Conventional hydrogen bond	1.71796	151.971
		B:UNL1330:HO6–A:ASN359:OD1	Conventional hydrogen bond	1.93259	138.227
		A:GLU252:HA–B:UNL1330:O11	Carbon hydrogen bond	2.89095	
		A:LYS254:HA–B:UNL1330:O10	Carbon hydrogen bond	2.46619	
		A:PRO397:HA–B:UNL1330:O3	Carbon hydrogen bond	2.6411	
		B:UNL1330:HC1–A:PRO251:O	Carbon hydrogen bond	2.71201	
		B:UNL1330:HO1–B:UNL1330	Pi-donor hydrogen bond	2.77657	
		B:UNL1330–A:ILE351	Alkyl	5.08421	
		B:UNL1330:C29–A:ILE351	Alkyl	4.4021	
		B:UNL1330–A:LEU395	Pi-alkyl		
	final	A:ILE350:HN–B:UNL1330:O9	Conventional hydrogen bond	1.91771	148.298
		A:ILE351:HN–B:UNL1330:O9	Conventional hydrogen bond	2.70033	170.438
		A:SER353:HN–B:UNL1330:O7	Conventional hydrogen bond	2.73856	157.904
		B:UNL1330:HO1–B:UNL1330:O	Conventional hydrogen bond	1.91953	164.544
		B:UNL1330:HO3–A:LEU395:O	Conventional hydrogen bond	1.93889	96.437
		B:UNL1330:HO4–A:LEU255:O	Conventional hydrogen bond	1.63738	168.378
		B:UNL1330:HO5–A:GLY347:O	Conventional hydrogen bond	1.88205	131.813
		B:UNL1330:HO8–A:ASN349:OD1	Conventional hydrogen bond	1.82011	
		B:UNL1330:HO8–A:ASN349:O	Conventional hydrogen bond	2.96447	
		B:UNL1330:HO9–A:GLU252:O	Conventional hydrogen bond	1.59684	
		A:PRO397:HA–B:UNL1330:O4	Carbon hydrogen bond	2.78821	
		A:LYS254:NZ–B:UNL1330	Pi-cation	4.3856	

(Continued on following page)

TABLE 4 (*Continued*) **Crucial intermolecular non-bonded interactions stabilizing LOX–CHL and XO–MBC complexes during MD simulation.**

Complex	Conformation	Interactions	Type	Distance	Angle
		A:PHE273–B:UNL1330	Pi–Pi T-shaped	4.92736	
		B:UNL1330–A:ILE351	Alkyl	5.26081	
		B:UNL1330–A:LEU395	Pi-Alkyl	5.46509	
		B:UNL1330–A:LYS254			

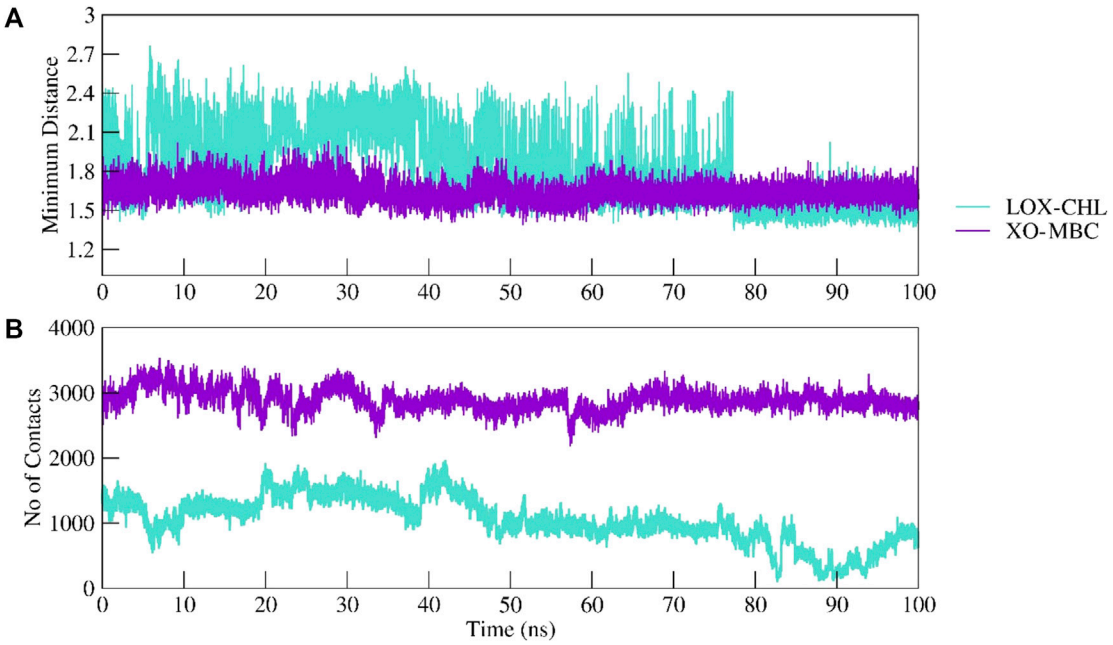

FIGURE 13
Intermolecular interactions between LOX–CHL and XO–MBC. Complexes were investigated by calculating the minimum distance between the protein and ligand group **(A)** and maximum number of total non-bonded contacts formed are shown **(B)**.

markedly reversed in a combinatorial regimen of COE along with doxorubicin, which showed better activity of COE in the protection of vital organs in chemotherapy. This protective action of cocoa is owing to its defense against oxidative stress induced during chemotherapy. Cocoa in the form of dark chocolate high in flavonoids may be a good strategy for reducing cardiovascular risk by having beneficial effects in inhibiting platelet aggregation, lowering blood pressure, reducing dyslipidemia, and lowering plasma glucose levels (Zięba et al., 2019). Reactive oxygen species, which are generated during drug biotransformation processes, can bind and react with cellular components in the liver to cause liver damage and thereby impair liver function (Cichoż-Lach and Michalak, 2014). Antioxidants present in cocoa increase nitric oxide levels and have hepatoprotective potential (Asiedu-Gyekye et al., 2016). A similar trend was observed when antioxidant biomarkers were monitored. The elevated levels of LPO and decreased GSH, SOD, CAT, and total thiol levels in the DOX group compared to the EAC group were substantially reversed in all COE-treated groups, augmenting its effectiveness in organ protection. Similar findings were reported previously for the potency of COE in the neutralization of the ROS system generated via various stress responses that could have been ameliorated, as evidenced by multiple investigations into regulating the homeostatic functions of various organs (S. Noori et al., 2008).

Lipoxygenase and xanthine oxidase are involved in the generation of oxidative stress (Chung et al., 1997; Wisastra and Dekker, 2014), which is observed in various pathogenic conditions, including cancer, and contributes to tissue injury (Pizzino et al., 2017). In the present study, we observed the amelioration of various oxidative stress biomarkers in multiple organs after COE co-treatment with doxorubicin. Moreover, our previous studies also support the efficacy of COE in ameliorating oxidative stress and cancer progression (Patil et al., 2022b; 2022a). Emmanuel et al. reported that cocoa leaf polyphenolic-rich extract inhibited xanthine oxidase due to the flavonoids and phenolic acids present in the extract (Irondi et al., 2017). In addition, catechin and its derivatives are reported to inhibit xanthine oxidase (catechin 303.95 μM, uncompetitive; epicatechin 20.48 μM, mixed; epigallocatechin 10.66 μM, mixed; epicatechin gallate 2.86 μM, mixed; and epigallocatechin gallate

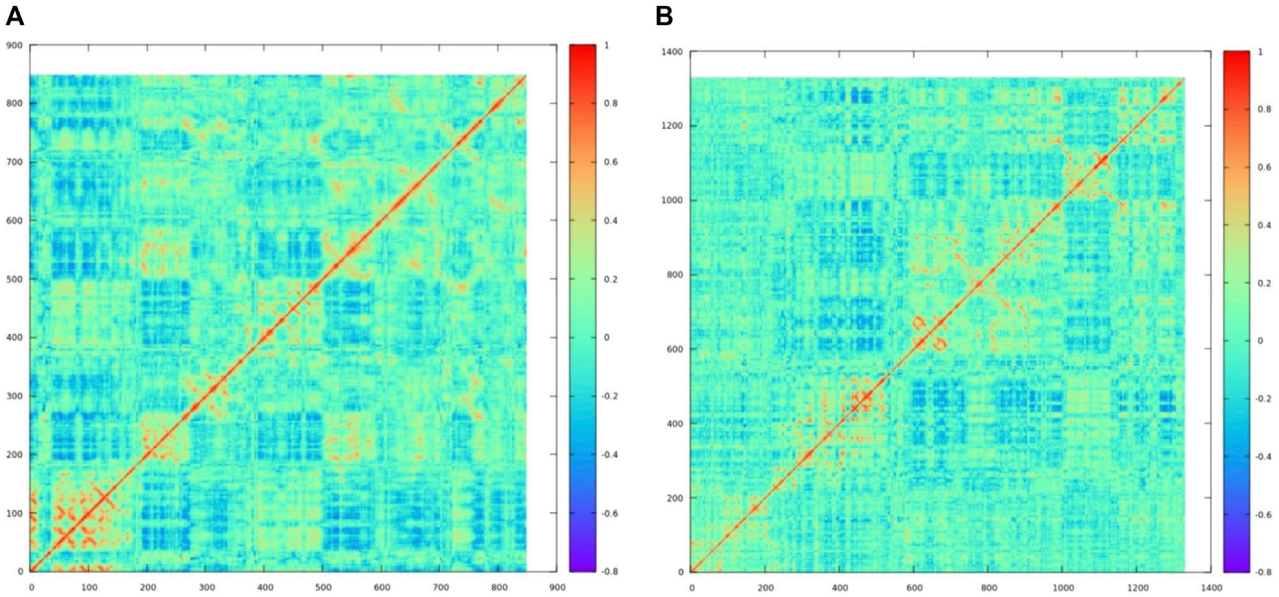

FIGURE 14
The dynamic cross-correlation matrix reveals concerted motion in the complexes **(A)** LOX–CHL and **(B)** XO–MBC. The red color represents the positive correlation, the blue color represents the negative correction, and the cyan color (zero value) represents no correlation.

0.76 μM, competitive inhibition. Collectively, cocoa flavonoids not only have antioxidant effects but also inhibit lipoxygenase activities (Schewe et al., 2002). Human LOX5 and LTA4 synthase activities are inhibited by (−)-epicatechin, and its low-molecular-weight procyanidins from cocoa products have a purported anti-inflammatory effect (Schewe et al., 2002). Previous studies showed CHL as a potent LOX inhibitor with an IC_{50} of 0.32 mg/mL and 61.27 μmol/L. In addition, based on the molecular docking and MD simulations, we observed chlorogenic acid and 8′8 methylenebiscatechin to have the highest binding affinity with lipoxygenase and xanthine oxidase to support their potential in ameliorating oxidative stress, which is also supported by the previous reports of the anti-oxidant properties of chlorogenic acid (Xu et al., 2012) and catechins (Bernatoniene and Kopustinskiene, 2018).

The roles of the aforementioned markers were further supported by the results of histopathological examination. There was a significant increase in the congestion score and myofibrillar degeneration in the EAC solid tumor model, which was further increased with doxorubicin treatment. Similar findings of cardiotoxicity were reported by Reddy et al. (2012), in which the authors demonstrated the efficacy of the cocoa extract as a cardioprotective agent in the EAC solid tumor model. Furthermore, in the EAC and DOX groups, we traced a remarkable increase in spotty necrosis, apoptosis, inflammation, hepatocellular dysplasia, venous and sinusoidal congestion, and Kupffer cell hyperplasia in hepatic tissues (Reddy et al., 2012). However, in COE 200, regeneration of cells was noted; this compromised tissue damage. These results summarize the effect of COE on doxorubicin-induced organ toxicity. Similarly, EAC- and DOX-exposed groups pointed toward tubular and glomerular congestion, glomerular atrophy, tubular cell swelling, inflammation, widening Bowman space, and cytoplasmic vacuoles, which were ameliorated via COE treatment, whether independent or in combination with doxorubicin. Furthermore, the observed cytotoxicity was also confirmed by histopathological devastation of the tumor mass, reduced tumor growth, decreased mitotic pattern, increased necrosis, and the occurrence of apoptotic nuclei via COE treatment.

Conclusion

This study not only demonstrated the protective effect of COE against doxorubicin-induced organ toxicities (heart, liver, and kidney) but also indicated synergistic potential with the anticancer activity of doxorubicin. Furthermore, our study demonstrated the efficacy of COE to neutralize the free radicals generated by doxorubicin; maintain cell integrity, along with inherent anti-cancer properties; and prolong the survival time of EAC mice. Overall, COE exhibits promising nutraceutical properties toward cardioprotective, hepatoprotective, and nephroprotective effects when supplemented with doxorubicin. Further confirmatory studies at the clinical level are needed to establish COE as a health supplement in cancer patients undergoing doxorubicin-based chemotherapy.

Data availability statement

The original contributions presented in the study are included in the article/Supplementary Materials; further inquiries can be directed to the corresponding authors.

Ethics statement

The animal study obtained ethical clearance from IAEC at ICMR-NITM, Belagavi for the use of laboratory animals (approval number: IAEC/ICMR-NITM BGM/2019/3).

Author contributions

PP: experimentation, methodology, investigation, formal analysis, and writing—original draft. PKu: performed cell culture experiments, formal analysis, and writing—review and editing. PKh: formal analysis and writing—review and editing. VP and VB: *in silico* experimentation, formal analysis, and writing—review and editing. AB: assisted in experimentation. HD: data curation, visualization, review, supervision, funding acquisition, and writing—review and editing. SS: supervised *in vitro* studies and analysis. RJ: review and editing. BP: methodology, supervision, validation, data curation, and writing—review and editing. SR: conceptualization, methodology, supervision, data curation, project administration, funding acquisition, and writing—review and editing. All authors contributed to the article and approved the submitted version.

Funding

The work was supported by the Indian Council of Medical Research-National Institute of Traditional Medicine (ICMR-NITM), Belagavi, Karnataka, India (Intramural funds).

Acknowledgments

The authors gratefully acknowledge the ICMR-National Institute of Traditional Medicine, Belagavi, for providing resources. PP thanks the College of Pharmacy, Belagavi, KLE Academy of Higher Education and Research (KAHER), Belagavi, and Indian Institute of Technology, Dharwad, for their support. PP thanks the Directorate of Minorities, Govt. of Karnataka, for awarding fellowship for Ph.D. program (Grant No. CR-27/2018-19).

Conflict of interest

The authors declare that the research was conducted in the absence of any commercial or financial relationships that could be construed as a potential conflict of interest.

Publisher's note

All claims expressed in this article are solely those of the authors and do not necessarily represent those of their affiliated organizations, or those of the publisher, the editors, and the reviewers. Any product that may be evaluated in this article, or claim that may be made by its manufacturer, is not guaranteed or endorsed by the publisher.

Supplementary material

The Supplementary Material for this article can be found online at: https://www.frontiersin.org/articles/10.3389/fphar.2023.1174867/full#supplementary-material

References

Afsar, T., Razak, S., Batoo, K. M., and Khan, M. R. (2017). *Acacia hydaspica* R. Parker prevents doxorubicin-induced cardiac injury by attenuation of oxidative stress and structural Cardiomyocyte alterations in rats. *BMC Complement. Altern. Med.* 17, 554. doi:10.1186/s12906-017-2061-0

Asiedu-Gyekye, I. J., Edem Kukuia, K. K., Seidu, A. M., Antwi-Boasiako, C., N'guessan, B. B., Frimpong-Manso, S., et al. (2016). Unsweetened natural cocoa powder has the potential to attenuate high dose artemether-lumefantrine-induced hepatotoxicity in non-malarious Guinea pigs. *Evid. Based Complement. Altern. Med.* 2016, 7387286–7387311. doi:10.1155/2016/7387286

Atanasov, A. G., Zotchev, S. B., Dirsch, V. M., and Supuran, C. T. (2021). Natural products in drug discovery: Advances and opportunities. *Nat. Rev. Drug Discov.* 20 (3), 200–216. doi:10.1038/s41573-020-00114-z

Bernatoniene, J., and Kopustinskiene, D. (2018). The role of catechins in cellular responses to oxidative stress. *Molecules* 23, 965. doi:10.3390/molecules23040965

Cichoż-Lach, H., and Michalak, A. (2014). Oxidative stress as a crucial factor in liver diseases. *World J. Gastroenterol.* 20 (25), 8082.

Chung, H. Y., Baek, B. S., Song, S. H., Kim, M. S., Huh, J. I., Shim, K. H., et al. (1997). Xanthine dehydrogenase/xanthine oxidase and oxidative stress. *AGE* 20, 127–140. doi:10.1007/s11357-997-0012-2

Claiborn, A. (1985). *CRC hand book of methods for oxygen radical research*. Boca Raton, Florida, USA: CRC Press.

Cura, J. K., Basilio, A., and Llagas, Ma. C. D. L. (2021). Antidiabetic, anti-inflammatory and cytotoxic potential of Theobroma cacao Linn. husk aqueous extracts. *Clin. Phytoscience* 7, 94. doi:10.1186/s40816-021-00320-1

Czapski, G. A., Czubowicz, K., and Strosznajder, R. P. (2012). Evaluation of the antioxidative properties of lipoxygenase inhibitors. *Pharmacol. Rep.* 64, 1179–1188. doi:10.1016/S1734-1140(12)70914-3

Elsherbiny, N. M., Younis, N. N., Shaheen, M. A., and Elseweidy, M. M. (2016). The synergistic effect between vanillin and doxorubicin in ehrlich ascites carcinoma solid tumor and MCF-7 human breast cancer cell line. *Pathol. - Res. Pract.* 212, 767–777. doi:10.1016/j.prp.2016.06.004

Fanton, S., Cardozo, L. F. M. F., Combet, E., Shiels, P. G., Stenvinkel, P., Vieira, I. O., et al. (2021). The sweet side of dark chocolate for chronic kidney disease patients. *Clin. Nutr.* 40, 15–26. doi:10.1016/j.clnu.2020.06.039

Gothoskar, S. V., and Ranadive, K. J. (1971). Anticancer screening of SAN-AB: An extract of marking nut, semecarpus anacardium. *Indian J. Exp. Biol.* 9, 372–375.

Gwozdzinski, K., Pieniazek, A., and Gwozdzinski, L. (2021). Reactive oxygen species and their involvement in red blood cell damage in chronic kidney disease. *Oxid. Med. Cell. Longev.* 2021, 6639199–6639219. doi:10.1155/2021/6639199

Irondi, E. A., Olanrewaju, S., Oboh, G., Olasupo, F., and Boligon, A. A. (2017). Inhibitory potential of cocoa leaves polyphenolics-rich extract on xanthine oxidase and angiotensin 1-converting enzyme. *J. Biol. Act. Prod. Nat.* 7, 39–51. doi:10.1080/22311866.2017.1293564

Khanal, P., Patil, V. S., Bhandare, V. V., Patil, P. P., Patil, B. M., Dwivedi, P. S., et al. (2022). Systems and in vitro pharmacology profiling of diosgenin against breast cancer. *Front. Pharmacol.* 13.

Kostić, D. A., Dimitrijević, D. S., Stojanović, G. S., Palić, I. R., Đorđević, A. S., and Ickovski, J. D. (2015). Xanthine oxidase: Isolation, assays of activity, and inhibition. *J. Chem.* 2015, 1–8. doi:10.1155/2015/294858

Kumar, P., Khadirnaikar, S., and Shukla, S. K. (2019). PILAR1, a novel prognostic LncRNA, reveals the presence of a unique subtype of lung adenocarcinoma patients with KEAP1 mutations. *Gene* 691, 167–175. doi:10.1016/j.gene.2018.12.060

Lamuela-Raventós, R. M., Andrés-Lacueva, C., Permanyer, J., and Izquierdo-Pulido, M. (2001). More antioxidants in cocoa. *J. Nutr.* 131, 834–835. doi:10.1093/jn/131.3.834

Martin, M. A., Goya, L., and Ramos, S. (2013). Potential for preventive effects of cocoa and cocoa polyphenols in cancer. *Food Chem. Toxicol.* 56, 336–351. doi:10.1016/j.fct.2013.02.020

Massee, L. A., Ried, K., Pase, M., Travica, N., Yoganathan, J., Scholey, A., et al. (2015). The acute and sub-chronic effects of cocoa flavanols on mood, cognitive and cardiovascular health in young healthy adults: A randomized, controlled trial. *Front. Pharmacol.* 6, 93. doi:10.3389/fphar.2015.00093

Misra, H. P., and Fridovich, I. (1972). The role of superoxide anion in the autoxidation of epinephrine and a simple assay for superoxide dismutase. *J. Biol. Chem.* 247, 3170–3175. doi:10.1016/s0021-9258(19)45228-9

Mitry, M. A., and Edwards, J. G. (2016). Doxorubicin induced heart failure: Phenotype and molecular mechanisms. *IJC Heart Vasc.* 10, 17–24. doi:10.1016/j.ijcha.2015.11.004

Noori, S., Nasir, K., and Mahboob, T. (2008). Effects of cocoa powder on oxidant/antioxidant status in liver, heart and kidney tissues of rats. *J. Anim. Plant Sci.* 19 (4), 174–178.

Ogura, M. (2001). Adriamycin (doxorubicin). *Gan Kagaku Ryoho* 28, 1331–1338.

Ohkawa, H., Ohishi, N., and Yagi, K. (1979). Assay for lipid peroxides in animal tissues by thiobarbituric acid reaction. *Anal. Biochem.* 95, 351–358. doi:10.1016/0003-2697(79)90738-3

Patil, P. P., Khanal, P., Patil, V. S., Charla, R., Harish, D. R., Patil, B. M., et al. (2022a). Effect of theobroma cacao L. On the efficacy and toxicity of doxorubicin in mice bearing ehrlich ascites carcinoma. *Antioxidants* 11, 1094. doi:10.3390/antiox11061094

Patil, P. P., Patil, V. S., Khanal, P., Darasaguppe, H. R., Charla, R., Bhatkande, A., et al. (2022b). Network pharmacology and *in vitro* testing of *Theobroma cacao* extract's antioxidative activity and its effects on cancer cell survival. *PLOS ONE* 17, e0259757. doi:10.1371/journal.pone.0259757

Patil, V. S., Harish, D. R., Vetrivel, U., Deshpande, S. H., Khanal, P., Hegde, H. V., et al. (2022c). Pharmacoinformatics analysis reveals flavonoids and diterpenoids from *Andrographis paniculata* and *Thespesia populnea* to target hepatocellular carcinoma induced by hepatitis B virus. *Appl. Sci.* 12, 10691. doi:10.3390/app122110691

Pizzino, G., Irrera, N., Cucinotta, M., Pallio, G., Mannino, F., Arcoraci, V., et al. (2017). Oxidative stress: Harms and benefits for human health. *Oxid. Med. Cell. Longev.* 2017, 8416763–8416813. doi:10.1155/2017/8416763

Reddy, Ag., Anjaneyulu, Y., Shivakumar, P., and Rani, M. (2012). A study on the toxic effects of doxorubicin on the histology of certain organs. *Toxicol. Int.* 19, 241–244. doi:10.4103/0971-6580.103656

Ruzaidi, A., Amin, I., Nawalyah, A. G., Hamid, M., and Faizul, H. A. (2005). The effect of Malaysian cocoa extract on glucose levels and lipid profiles in diabetic rats. *J. Ethnopharmacol.* 98, 55–60. doi:10.1016/j.jep.2004.12.018

Samdani, A., and Vetrivel, U. (2018). Poap: A gnu parallel based multithreaded pipeline of open babel and AutoDock suite for boosted high throughput virtual screening. *Comput. Biol. Chem.* 74, 39–48. doi:10.1016/j.compbiolchem.2018.02.012

Santos, D. S. D., and Goldenberg, R. C. (2018). "Doxorubicin-induced cardiotoxicity: From mechanisms to development of efficient therapy," in *Cardiotoxicity*. Editor W. Tan (London, United Kingdom: IntechOpen). doi:10.5772/intechopen.79588

Schewe, T., Kühn, H., and Sies, H. (2002). Flavonoids of cocoa inhibit recombinant human 5-lipoxygenase. *J. Nutr.* 132, 1825–1829. doi:10.1093/jn/132.7.1825

Schirner, M., Hoffmann, J., Menrad, A., and Schneider, M. R. (1998). Antiangiogenic chemotherapeutic agents: Characterization in comparison to their tumor growth inhibition in human renal cell carcinoma models. *Clin. Cancer Res.* 4, 1331–1336. Available at: http://clincancerres.aacrjournals.org/content/4/5/1331.abstract.

Sedlak, J., and Lindsay, R. H. (1968). Estimation of total, protein-bound, and nonprotein sulfhydryl groups in tissue with Ellman's reagent. *Anal. Biochem.* 25, 192–205. doi:10.1016/0003-2697(68)90092-4

Shibue, T., and Weinberg, R. A. (2017). EMT, CSCs, and drug resistance: The mechanistic link and clinical implications. *Nat. Rev. Clin. Oncol.* 14, 611–629. doi:10.1038/nrclinonc.2017.44

Sun, M., Gu, Y., Glisan, S. L., and Lambert, J. D. (2021). Dietary cocoa ameliorates non-alcoholic fatty liver disease and increases markers of antioxidant response and mitochondrial biogenesis in high fat-fed mice. *J. Nutr. Biochem.* 92, 108618. doi:10.1016/j.jnutbio.2021.108618

Thiery, J. P., and Sleeman, J. P. (2006). Complex networks orchestrate epithelial–mesenchymal transitions. *Nat. Rev. Mol. Cell. Biol.* 7, 131–142. doi:10.1038/nrm1835

Thorn, C. F., Oshiro, C., Marsh, S., Hernandez-Boussard, T., McLeod, H., Klein, T. E., et al. (2011). Doxorubicin pathways: Pharmacodynamics and adverse effects. *Pharmacogenet. Genomics* 21, 440–446. doi:10.1097/FPC.0b013e32833ffb56

Tri, T. B., and Wilkins, J. (1978). Doxorubicin cardiomyopathy. *Ann. Intern. Med.* 89 (1), 137.

van der Zanden, S. Y., Qiao, X., and Neefjes, J. (2021). New insights into the activities and toxicities of the old anticancer drug doxorubicin. *FEBS J.* 288, 6095–6111. doi:10.1111/febs.15583

Wisastra, R., and Dekker, F. (2014). Inflammation, cancer and oxidative lipoxygenase activity are intimately linked. *Cancers* 6, 1500–1521. doi:10.3390/cancers6031500

Xu, J. G., Hu, Q. P., and Liu, Y. (2012). Antioxidant and DNA-protective activities of chlorogenic acid isomers. *J. Agric. Food Chem.* 60, 11625–11630. doi:10.1021/jf303771s

Zięba, K., Makarewicz-Wujec, M., and Kozłowska-Wojciechowska, M. (2019). Cardioprotective mechanisms of cocoa. *J. Am. Coll. Nutr.* 38, 564–575. doi:10.1080/07315724.2018.1557087

frontiers | Frontiers in Oncology

TYPE Review
PUBLISHED 16 June 2023
DOI 10.3389/fonc.2023.1168321

Check for updates

OPEN ACCESS

EDITED BY
Visweswara Rao Pasupuleti,
Reva University, India

REVIEWED BY
Frederick E. Williams,
University of Toledo, United States
Yongping Bao,
University of East Anglia, United Kingdom

*CORRESPONDENCE
Ahmad Faizal Abdull Razis
madfaizal@upm.edu.my
Daniela Calina
calinadaniela@gmail.com
Javad Sharifi-Rad
javad.sharifirad@gmail.com

RECEIVED 17 February 2023
ACCEPTED 16 May 2023
PUBLISHED 16 June 2023

CITATION
Asif Ali M, Khan N, Kaleem N, Ahmad W, Alharethi SH, Alharbi B, Alhassan HH, Al-Enazi MM, Razis AFA, Modu B, Calina D and Sharifi-Rad J (2023) Anticancer properties of sulforaphane: current insights at the molecular level. *Front. Oncol.* 13:1168321. doi: 10.3389/fonc.2023.1168321

Anticancer properties of sulforaphane: current insights at the molecular level

Muhammad Asif Ali[1], Noohela Khan[2], Nabeeha Kaleem[1], Waqas Ahmad[1], Salem Hussain Alharethi[3], Bandar Alharbi[4], Hassan H. Alhassan[5], Maher M. Al-Enazi[6], Ahmad Faizal Abdull Razis[7,8]*, Babagana Modu[8,9], Daniela Calina[10]* and Javad Sharifi-Rad[11]*

[1]Department of Food Science and Human Nutrition, University of Veterinary & Animal Sciences, Lahore, Pakistan, [2]Department of Nutrition Sciences, Rashid Latif Medical College, Lahore, Pakistan, [3]Department of Biological Science, College of Arts and Science, Najran University, Najran, Saudi Arabia, [4]Department of Medical Laboratory Science, College of Applied Medical Sciences, University of Ha'il, Hail, Saudi Arabia, [5]Department of Clinical Laboratory Science, College of Applied medical Sciences, Jouf University, Sakaka, Saudi Arabia, [6]Department of Medical Laboratory Sciences, College of Applied Medical Sciences in Al-Kharj, Prince Sattam Bin Abdulaziz University, Al-Kharj, Saudi Arabia, [7]Department of Food Science, Faculty of Food Science and Technology, Universiti Putra Malaysia, Serdang, Selangor, Malaysia, [8]Natural Medicines and Products Research Laboratory, Institute of Bioscience, Universiti Putra Malaysia, Serdang, Selangor, Malaysia, [9]Department of Biochemistry, Faculty of Science, University of Maiduguri, Maiduguri, Borno, Nigeria, [10]Department of Clinical Pharmacy, University of Medicine and Pharmacy of Craiova, Craiova, Romania, [11]Facultad de Medicina, Universidad del Azuay, Cuenca, Ecuador

Sulforaphane (SFN) is an isothiocyanate with multiple biomedical applications. Sulforaphane can be extracted from the plants of the genus *Brassica*. However, broccoli sprouts are the chief source of sulforaphane and are 20 to 50 times richer than mature broccoli as they contain 1,153 mg/100 g. SFN is a secondary metabolite that is produced as a result of the hydrolysis of glucoraphanin (a glucosinolate) by the enzyme myrosinase. This review paper aims to summarize and understand the mechanisms behind the anticancer potential of sulforaphane. The data was collected by searching PubMed/MedLine, Scopus, Web of Science, and Google Scholar. This paper concludes that sulforaphane provides cancer protection through the alteration of various epigenetic and non-epigenetic pathways. It is a potent anticancer phytochemical that is safe to consume with minimal side effects. However, there is still a need for further research regarding SFN and the development of a standard dose.

KEYWORDS

sulforaphane, isothiocyanate, anticancer mechanisms, cytotoxicity, apoptosis

1 Introduction

Cancer is one of the most prevalent and fatal diseases throughout the globe. As per the World Health Organization, in 2020, cancer is the sole reason for the death of more than 10 million individuals (1). For the treatment of cancer, various medical treatments are applied, including chemotherapies and radiotherapies. Besides their potential benefits, such treatments also impose detrimental effects on various organs of the body (2). The consumption of phytochemicals must be incorporated into our diet to benefit from their anticancer properties. Since the beginning, cruciferous vegetables are known for their anticancer properties. Unfortunately, these are never ingested in sufficient amounts that can alter the health biomarkers. Cruciferous vegetables are rich in several nutrients and bioactive components, especially isothiocyanates that provide various health benefits (3). The isothiocyanates are the hydrolytic metabolites of glucosinolates, and examples include allyl isothiocyanate (AITC), benzyl isothiocyanate (BITC), phenethyl isothiocyanate (PEITC), and sulforaphane (SFN) (4, 5). The most important biological active isothiocyanate is sulforaphane, or simply SFN, which is potent in providing numerous health benefits by modulating epigenetic and non-epigenetic mechanisms. It did not receive much attention until 1992, even though it was first identified and isolated in 1959 (6). This updated review aimed to summarize and highlight the mechanisms behind the anticancer potential of sulforaphane.

2 Review methodology

This comprehensive review aims to provide updated information on the anticancer mechanisms of sulforaphane. The most relevant and recent data regarding the anticancer activity of sulforaphane were obtained through an online search of the following scientific databases—PubMed/MedLine, Scopus, Web of Science, and Google Scholar—using the next MeSH terms: "Brassica/chemistry", "Chemoprevention", "Isothiocyanates/metabolism", "Isothiocyanates/pharmacology", "Isothiocyanates/therapeutic use", "Neoplasms/drug therapy", "Neoplasms/prevention & control", "Biological Products/therapeutic use". The chemical structure has been validated using Pubchem and the taxonomy of the plant according to WorldFloraOnline (7, 8). The most representative data regarding the anticancer activities of sulforaphane are summarized in a schematic diagram and tables.

3 Bioavailability of sulforaphane and applications of nanotechnologies in improving its bioactivity

The dietary sources of SFN include mainly the plants (especially cruciferous vegetables) of the genus *Brassica* such as broccoli, brussels sprouts, kale, and cauliflower (3). As per a recent review, broccoli sprouts are the chief source of sulforaphane and are 20 to 50 times richer than mature broccoli as they contain 1,153 mg/100 g, whereas the concentration of SFN in mature broccoli is 44–171 mg/100 g. Sulforaphane is significantly effective as it is readily available in blood because of its high bioavailability (80%). The higher bioavailability is due to its lighter molecular weight in comparison to other polyphenols (6, 9). Recently, the trend of nanoencapsulation of various bioactive components to gain maximum benefits is increased. Since the last century, a lot of progress has been made in the field of nanotechnology. Advancement in research has made it possible for the development of polymeric biodegradable nanoparticles for better results and controlled/targeted delivery of drugs. Longhai Piao et al. likewise worked on the nanoencapsulation of sulforaphane using a triblock copolymer PCL-PEG-PCL, *i.e.*, poly(caprolactone)-poly(ethylene glycol)-poly(caprolactone). The results revealed that the PCL-PEG-PCL-encapsulated SFN enhanced the cancer cell apoptosis more efficiently than the free sulforaphane in the *in vitro* trial. Additionally, the study validated that the SFN encapsulation with triblock copolymer was safe and can be used for effective and targeted sulforaphane delivery to cancerous cells (10). A study on the effect of basil seed gum-encapsulated broccoli sprout extract disclosed that encapsulation helped in the controlled release of sulforaphane, which is more effective in the treatment of cancer than free sulforaphane. Furthermore, the data also revealed that the release of SFN from the micelles was more in intestinal-stimulated conditions compared to the gastric-stimulated condition (11). Similarly, the results of an investigation conducted by Lucía Yepes-Molina et al. showed that the encapsulated sulforaphane had more stability. Additionally, in the *in vitro* trial, the investigators discovered that the SFN-rich membrane vesicles were potent in reducing the inflammatory markers on HL-60 cell linings. Another group of investigators worked on the encapsulation of sulforaphane in broccoli membrane vesicles (BM vesicles). The study evaluated the capability and potential of encapsulated sulforaphane on SK-MEL-28 (melanoma) cell linings. The *in vitro* analysis revealed that BM vesicles containing SFN had high absorption and metabolism in cancerous cells. Furthermore, encapsulated sulforaphane efficiently reduced cancer and its markers (12).

4 Phytochemistry of sulforaphane and its derivatives

Sulforaphane is chemically a product of a 4-(methylsulfonyl) butyl group that is attached to a nitrogen atom (6, 13, 14). SFN is a secondary metabolite produced as a result of the hydrolysis of glucoraphanin (a glucosinolate) by the enzyme myrosinase (6, 9, 15). Because sulforaphane has gained a lot of attention due to its potential against numerous diseases, especially cancer, scientists are interested in developing its derivatives which could be an important discovery in the world of medicine for cancer treatment. The group

of Prachi Heda et al. had made some progress in this regard by synthesizing sulforaphane derivatives including SFN-glutathione, SFN-cysteine-glycine, SFN-cysteine, SFN-N-acetylcysteine, PEITC, and sulforaphane. Out of all these SFN derivatives, phenethyl isothiocyanate was found to be the most effective due to its high bioavailability, gastric absorption, and blood–brain barrier permeability. PEITC was involved in the inhibition of human S-adenosylmethionine decarboxylase (a lyase), p38alpha (a transferase), heme-oxygenase 1 (an oxidoreductase), and human cytochrome P450 (an oxidoreductase) activation. Furthermore, the downregulation of these enzymes exhibited a reduction in cancerous cell proliferation and angiogenesis and other cancer-progressing mechanisms (16). A review paper also unveiled the similar anticancer properties of sulforaphane and its derivatives, including sulforaphane and phenethyl isothiocyanate (17). Another *in vitro* study also disclosed that benzyl sulforaphane (a derivative of SFN) is more efficient in preventing and treating liver carcinoma by restraining the Akt/MAPK pathways and triggering the Nrf2/ARE signaling pathways (18). Similarly, Kun Hu et al. derived a series of SFN derivatives and evaluated the potential of these derivatives in an *in vitro* study on five different cell linings isolated from liver hepatocellular carcinoma (HepG2), human breast adenocarcinoma (MCF-7), human lung adenocarcinoma (A549), human neuroblastoma (SH-SY5Y), and human colon cancer (HCT-116). The data revealed that the sulforaphane derivative synthesized by introducing the benzyl group at the side chain of sulforaphane (benzyl sulforaphane) showed enhanced anticancer activity than any other derivative and SFN itself. The benzyl derivative of sulforaphane triggered cell cycle arrest apoptosis and Nrf2 activation more efficiently than SFN (19).

5 Anticancer mechanisms of sulforaphane

5.1 Cellular and molecular implications

Since the discovery of sulforaphane, many scientific studies outlining its health benefits have been published; it is a biologically active phytochemical that has many biological properties, such as anti-inflammatory, anticancer, cardioprotective, antioxidative, cytoprotective, DNA protective, and antimicrobial properties. Additionally, it is also a potent immune booster and detoxifier (9, 14). Table 1 presents all the beneficial effects of sulforaphane proven in various research articles. Although SFN shows various properties, the most important property is its potential against cancer. SFN protects against cancer by inhibiting cancer cell proliferation, arresting the cell cycle, and enhancing the process of apoptosis (24–26). Sulforaphane provides cancer protection via the alteration of several epigenetic and non-epigenetic mechanisms; this was demonstrated in the case of many types of cancer. Sulforaphane stalls the activity of the enzyme histone deacetylase (HDAC) in cancerous cells. The inhibition of histone deacetylase is important in cancer prevention as it enhances several mechanisms such as apoptosis and cell cycle arrest (50–54). Furthermore, SFN also halts histone phosphorylation by enhancing the phosphatases, especially PP1β and PP2α (25, 55, 56). The epigenetic modulation of sulforaphane on breast cancer was assessed in another study. The results disclosed that there was a significant reduction in histone deacetylase activity and the cell proliferation marker (Ki-67) (57). Another study revealed that SFN downgraded processes like cell proliferation, the activity of histone deacetylase, and cell growth.

TABLE 1 Summary of sulforaphane biological activities.

Bioactivity	Mechanism	Reference
Anti-inflammatory	↓proinflammatory markers, ↓NF- kB	(20–23)
Anticancer	↑cell cycle arrest, ↓metastases, ↓angiogenesis ↑apoptosis, ↑Nrf2	(24–26)
	Protects the DNA, ↑ histone deacetylase	(27–30)
	↑Nrf2 antioxidant signaling cascade	(29, 31–34)
Antioxidant	↑antioxidant defense, ↑GSH	(22, 35, 36)
Cardioprotective	↓oxidative stress ↑TRxRS, ↑GR, ↑GSTs, ↑NQO1	(36–38)
Cytoprotective	The antioxidative potential of sulforaphane enhanced the production and activity of cytoprotective proteins to help protect the cell lining ↑cellular defense mechanisms, ↑detoxification, ↑redox reactions, ↑Nrf2	(32, 33)
Immunostimulant	Immune booster, ↑NK cell activity	(22)
Antimicrobial	↓growth of various gram-positive and gram-negative bacteria by preventing pyocyanin production, biofilm formation, and quorum sensing highly effective against *Helicobacter pylori*	(39–42)
Anti-carcinogenesis	Nrf2 and TrxRs have a dual role in cancer by protecting against oxidative stress. However, overactivation can promote tumor growth and may cause chemoresistance. Therefore, sulforaphane dosage must be selected carefully	(43–49)

↑, increase; ↓, decrease; Nrf2, nuclear transcription factor; TRxRS, thioredoxin reductase; GSH, glutathione; GR, glutathione reductase; GSTs, glutathione-S transferase; NADPH, nicotinamide adenine dinucleotide phosphate; NQO1, NAD(P)H quinone oxidoreductase; NK cells, natural killer cells.

Furthermore, it reduced the expression of various receptors such as estrogen receptor-α and human epidermal growth factor receptor-2 in cancerous cell lining (58) (Figure 1).

DNA methyl transferases (DNMTs) are a family of enzymes that catalyze the transfer of the methyl group to the DNA. The suppression of these enzymes enhances the process of apoptosis and cell cycle arrest. SNF actively downregulates the function of DNMTs (especially DNMT1 and DNMT3B) and protects against cancer (25, 54, 59, 60) (Figure 1). Noncoding RNA is a molecule that does not need to be translated into protein to perform its functions. There are several different types of ncRNA, but miRNA (microRNA) and lncRNA (long noncoding RNA) are of great importance. These ncRNAs are usually involved in the regulation of numerous cell functions such as apoptosis, proliferation, and differentiation. The upregulation or downregulation of ncRNA plays a vital role in controlling the progression of cancer. Sulforaphane is one of those bioactive components that can suppress the growth of cancerous cells by regulating these ncRNAs. Various studies validated that SFN exhibits anticancer properties by halting as well as by enhancing the expression of a wide range of miRNAs and lncRNAs (25, 60–63). A study conducted by Scott R. Baier et al. likewise unveiled the off-target effects of SFN. The results were in favor of the hypothesis, *i.e.*, SFN not only targets the cancer suppressor genes but also stimulates the transcriptional activity of long terminal repeats. The study also confirmed that the consumption of broccoli sprouts causes the inhibition of histone acetylation (64) (Figure 1).

Nuclear factor erythroid 2-related factor 2 (Nrf2) is a transcription factor that regulates the cellular defense mechanism (65). The activation of Nrf2 channels the cascade of antioxidants and exerts the anticancer effect by causing a reduction in cell transformation and development. SFN decreases cancer proliferation by enhancing the expression of Nrf2. Additionally, sulforaphane suppresses the expression of NF-$_{\kappa}$B that ultimately downregulates the inflammatory markers (25, 29, 31–34, 66, 67). The group of Julie E. Bauman studied the chemopreventive potential of sulforaphane by using preclinical models. The results of an *in vitro* model revealed that sulforaphane enhances the activation of Nrf2 signaling in normal mucosal epithelial cells and head and neck squamous cell carcinoma cell lines. The SFN extract was found to be highly effective in blocking the activity of inactivation of an oncogenic factor pSTAT3. However, in the outcomes of the *in vivo* model, SFN notably decreased the size and incidence of 4-nitroquinoline-1-oxide (a carcinogen) which induced oral cancer in mice (68). Several studies confirmed that sulforaphane provides cancer protection by inhibiting the proliferation of cancerous cells and downgrading the process of angiogenesis. To investigate this potential, Prayag et al. conducted an *in vitro* study. The results disclosed that sulforaphane notably increased the antioxidant cascade and enhanced the activity of natural cell killers by increasing the expression of MHC class I chain-related proteins A and B (69).

5.2 The hormetic effect of sulforaphane

Hormesis is a phenomenon characterized by a biphasic dose or concentration–response, where low doses or concentrations of a compound can stimulate a beneficial effect, while high doses or concentrations can lead to inhibitory effects (70).

This means that, at low doses, a compound may have a stimulatory effect, while at high doses, it may have an inhibitory effect. The review of Calabrese et al. explained this hormetic effect of sulforaphane and revealed that SFN induces hormetic dose responses in studies through the upregulation of the Nrf2/ARE pathway. This biphasic response is well integrated, concentration dependent, and specific to targeted cell types. The hormetic response of sulforaphane can decrease the incidence and severity of various human-related pathologies, and it has also been found to be involved in the enhancement of stem cell proliferation. Similar

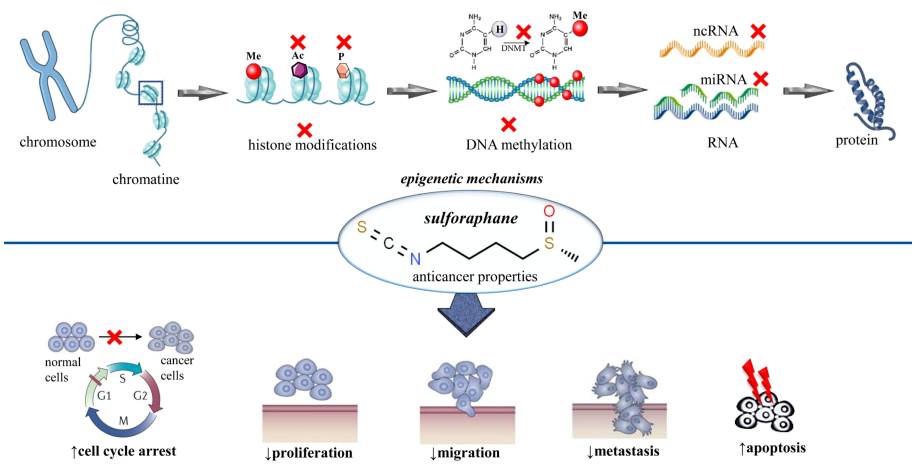

FIGURE 1
Summarized scheme regarding epigenetic modifications of sulforaphane in cancer. At the cellular level, sulforaphane shows anticancer activity by altering the epigenetic mechanisms. These epigenetic mechanisms involve histone acetylation, histone phosphorylation, DNA methylation, and modulation of noncoding RNAs. x, inhibition; Ac, acetylation; P, phosphorylation; Me, methylation; DNA, deoxyribonucleic acid; RNA, ribonucleic acid; DNMT, DNA methyltransferase.

hormesis-based chemoprotection has been reported with other dietary supplements such as curcumin, ginkgo biloba, ginseng, green tea, and resveratrol. The activation of the Nrf2 (nuclear factor erythroid-derived 2)/ARE (antioxidant response elements) pathway is likely a principal and underlying mechanism of hormesis, which can limit age-related damage, numerous disease processes progression, and induction of toxicities due to chemicals and radiations (70).

6 Synergic anticancer effect of sulforaphane in combination with other chemotherapeutic agents

Sulforaphane can also be used with conventional cancer treatments to achieve an enhanced effect. The group of Małgorzata Milczarek shed light on the development of new combinations by conducting an *in vitro* study. The data unveiled that the combination of sulforaphane and fluorouracil is more effective in enhancing the process of apoptosis than fluorouracil alone. In the *in vitro* analysis, it was confirmed that combination arrests the cancerous cell cycle in the S-phase in the colon cell linings, especially HT-29 and Caco-2 (71). Similarly, the combination of sulforaphane with gefitinib (a potent drug used for the treatment of lung cancer) also showed a marked increase in the inhibition of cell proliferation and expression of numerous factors in comparison to both agents alone (72). Recently, another study disclosed that a combinatory regimen of SFN with allyl isothiocyanate is more effective in cancer prevention compared to a single treatment. The synergism between these two compounds enhanced the arrest of the cell cycle and the programmed cell death. In addition to this, the investigators found that the combined therapy also caused an increase in the downregulation of cell migration (73). Similarly, another research supported the notion that both luteolin and SFN together provide enhanced anti-inflammatory properties than alone. The dose-dependent inhibition of NO by sulforaphane was 51% and by luteolin was 46%, respectively. However, the combined therapy demonstrated inhibited nitric oxide production by 56%, proving that the combination led to an increase in the reduction of inflammatory markers, especially the decrease in nitric oxide production (74).

7 Clinical studies

Broccoli is rich in glucoraphanin which is a precursor of sulforaphane. To study the effect of sulforaphane, a randomized control trial on the prevention of prostate cancer was designed by a group of investigators. The study showed that sulforaphane significantly reduced the progression of prostate cancer and disease severity after the broccoli soup intervention for at least 1 year by altering the gene expression (75). Melanoma is a form of skin cancer that originates from melanocytes (pigment-producing cells). Several studies inferred that the presence of atypical nevi is one of the key risk factors for melanoma. Therefore, in melanoma patients, Shawn Tahata et al. explored the effect of the oral administration of broccoli sprout extract at three different dose levels (50, 100, and 200 μmol). The study inferred that sulforaphane significantly reduced the levels of proinflammatory cytokines in plasma and increased the tumor suppressor decorin in tissues, thus preventing the risk of melanoma (76). Another randomized double-blinded study disclosed that sulforaphane is highly effective in reducing serum prostate-specific antigen (PSA) levels. Serum PSA levels are usually high in men suffering from prostate cancer after radical prostatectomy. The study inferred that the administration of 60 mg SFN in the form of a tablet significantly reduced the PSA progression after at least 3 months of treatment (77). A recent study suggested that sulforaphane is highly beneficial in preventing ulcerative disease by inhibiting the growth of *Helicobacter pylori*. As per the group of Akinori Yanaka, the consumption of broccoli sprouts consecutively for 2 months can downgrade the colonization of the bacterium. This poses a cancer-preventive effect because of the reduction in oxidative stress caused by *H. pylori* (78). Additionally, several ongoing and completed clinical trials aim to investigate the chemoprotective and preventive effects of sulforaphane. The investigations also revealed that sulforaphane can help prevent and reduce the risk of cancer via modulating the gene expression by downregulating and upregulating various pathways in cells. However, there is still a need for further investigation on the sulforaphane cancer protective/preventive potential and mechanisms (57, 79–84). Table 2 shows a summary of the representative data regarding the clinical studies with sulphoraphane.

8 Safety data

Conventional chemotherapeutic drugs such as paclitaxel, fluorouracil, tamoxifen, and raloxifene are a few commonly used chemo-preventive medications; but, besides their beneficial effect, such chemotherapy also poses several harmful effects (85). For this reason, over the past few years, the use of traditional medicinal plants for the treatment of various diseases has caught the attention of scientists. Medicinal plants are rich in bioactive components and phytochemicals and protect against many diseases without causing detrimental effects on the body's organs. Such plants are highly advantageous for the innovation of numerous drugs with enormous benefits and lower undesirable effects. Isothiocyanates, especially sulforaphane, are highly effective against cancer and have been used as a medicine in China for thousands of years (86–88). Numerous studies proved that SFN can be used at various doses and in combination with other compounds without showing toxicity. A randomized controlled trial was designed to assess the safety and therapeutic effect of sulforaphane-rich drinks on thyroid hormonal status and thyroid autoimmune status. The results of the 12-week study concluded that the beverage containing on average of 40 μmol of SFN and 600 μmol of glucoraphanin per day was safe to consume (89).

TABLE 2 Clinical studies with sulphoraphane.

Study subjects	Type of study	Country	Enrolled subjects	Type of intervention	Status/ phase	Objectives/main findings	Refs
Men on active surveillance for prostate cancer	Randomized control trial	United Kingdom	199 patients	Glucoraphanin-rich broccoli soup for 12 months	Completed	SFN significantly reduced the progression of prostate cancer and disease severity after the broccoli soup intervention for at least 1 year by altering the gene expression	(75)
Melanoma patients with multiple atypical nevi	Randomized control trial	United States of America	17 patients	Broccoli sprout extract at three different dose levels (50, 100, and 200 µmol) for 28 days	Completed	SFN prevented the risk of melanoma by reducing plasma proinflammatory cytokines and by enhancing the tumor suppressor decorin in tissues	(76)
Men with biochemical recurrence after radical prostatectomy	Double-blinded, randomized, placebo-controlled multicenter trial	France	78 patients	60 mg of oral sulforaphane (two tablets comprising of 10-mg sulforaphane each for three times a day) for 6 months	Completed	SFN is highly effective in reducing the serum PSA levels	(77)
Helicobacter pylori-positive volunteers	Randomized control trial	Japan	50 participants	70 g/day of glucoraphanin-rich 3-day-old germinated broccoli sprouts (Broccoli Super Sprout) for 8 weeks	Completed	The consumption of broccoli sprouts consecutively for 2 months can downgrade the colonization of *Helicobacter pylori* and provide a cancer-preventive effect due to the reduction in oxidative stress caused by *H. pylori*	(78)
Former smokers	Randomized clinical trial	United States of America	67 participants	Four tablets of sulforaphane two times per day (each dose comprising of 120 µmol of sulforaphane)	Active, not recruiting	The study aims to investigate that SFN can improve, maintain, or worsen the condition of former smokers who are at a high risk of developing cancer due to their smoking habit. Furthermore, the study also seeks to examine the potential of sulforaphane in reversing the changes in lung cells that are associated with cancer development	(84)
Men with recurrent prostate cancer	Phase II clinical trial	United States of America	20 patients	Sulforaphane-rich extracts (200 µmol/daily) for 20 weeks	Completed	The investigation revealed that using the SFN extract did not result in significant PSA declines in most of the patients with recurrent prostate cancer. Despite this, the treatment was found to be safe and had some positive effects on PSADT modulation. However, there is still a need for further investigation	(79)
Men scheduled for a prostate biopsy aged ≥21 years	Double-blind, randomized controlled trial	United States of America	98 participants	Sulforaphane-rich broccoli sprout extract capsules twice a day for 4 weeks (each capsule consists of 200 µmol of sulforaphane)	Completed	The supplementation of broccoli sprout extract is correlated with the modulation of gene expression. The study also disclosed that there was no significant difference in HDAC activity and the biomarkers of prostate cancer	(83)
Female patients of age greater than 18 years diagnosed with DCIS on core or incisional/excisional biopsy scheduled for definitive surgery	Phase II double-blind, randomized clinical trial	United States of America	34 participants	100 µmols of sulforaphane from broccoli sprout dissolved in 150 ml mango juice once a day for 14 days	Completed	The investigators aim to study the effect of the intervention on breast cancer-related factors. Furthermore, the investigators want to determine the potential of SFN in the enhancement of protective enzyme levels in breast tissue and the acceptability of the treatment among participants	(81)

(Continued)

TABLE 2 Continued

Study subjects	Type of study	Country	Enrolled subjects	Type of intervention	Status/ phase	Objectives/main findings	Refs
Male patients of age 18–80 years scheduled for template biopsy of the prostate as part of routine investigation or staging for prostate cancer	Double-blind, randomized clinical trial	United Kingdom	40 participants	1. Two Allin capsules once a day for 4 weeks 2. Sulforaphane capsules once a day for 4 weeks	Completed	The study aims to investigate the relationship between the ingestion of allin, sulforaphane, and prostate metabolism.	(82)
Male patients between 40 and 75 years old with low- or intermediate-grade prostate cancer have a PSA level <20 ng/ml and have chosen radical prostatectomy, brachytherapy, or active surveillance as their main treatment	Randomized clinical trial	United States	45 participants	Sulforaphane-rich broccoli sprout extract (100 mol of sulforaphane, every other day for 5 weeks)	Completed	The investigation revealed the changes in phase II enzyme expression, levels of blood F2 isoprostane, levels of prostate tissue 8-hydroxy-2'-deoxyguanosine (8OHdG), levels of serum DHT (dihydrotestosterone) and testosterone, and levels of serum 3-alpha-diol gluconate (3α-DG)	(80)
Women with abnormal mammogram findings were scheduled for breast biopsies	Double-blind, randomized controlled trial	United States of America	54 participants	250 mg of a broccoli seed extract containing glucoraphanin as precursor to sulforaphane	Completed	The study disclosed that glucoraphanin supplementation for 2–8 weeks does not cause any adverse effects but may not be sufficient for producing changes in breast tissue tumor biomarkers. Future studies employing larger sample sizes should evaluate alternative dosing and duration regimens to inform dietary SFN strategies in breast cancer chemoprevention	(57)

9 Conclusion

Natural bioactive compounds currently have numerous applications in cancer chemotherapy. Furthermore, the vast spectrum of natural compounds provides important compounds for therapeutic refinement through molecular modifications. Many anticancer compounds are either natural products or substances derived from natural products. The conjugation of toxic natural products with monoclonal antibodies or with macromolecular carriers can lead to more precisely targeted therapies. As only a small percentage of higher plants have been systematically investigated, research on natural compounds as chemotherapeutic agents arouses further interest as well as multidisciplinary scientific collaborations. The results of preclinical studies showed that sulforaphane provides cancer protection through the alteration of various epigenetic and non-epigenetic pathways. The therapeutic limitations of the use of sulforaphane in cancer are represented by the complete lack of knowledge of the potential anticancer effects at the cellular level and the effects on the immune system, the lack of translational studies to establish the effective doses in humans, and the interactions with conventional chemotherapy medication. However, considering everything together, the results of preclinical and clinical studies point to new therapeutic perspectives towards the possible development of new sulforaphane-based anticancer drugs.

Author contributions

All authors made a significant contribution to the work reported, whether that is in the conception, study design, execution, acquisition of data, analysis, and interpretation, or in all these areas, that is, revising or critically reviewing the article; giving final approval of the version to be published; agreeing on the journal to which the article has been submitted; and confirming to be accountable for all aspects of the work. All authors have read and agreed to the published version of the manuscript.

Conflict of interest

The authors declare that the research was conducted in the absence of any commercial or financial relationships that could be construed as a potential conflict of interest.

Publisher's note

References

1. Sung H, Ferlay J, Siegel RL, Laversanne M, Soerjomataram I, Jemal A, et al. Global cancer statistics 2020: globocan estimates of incidence and mortality worldwide for 36 cancers in 185 countries. *Ca: A Cancer J For Clin* (2021) 71:209–49. doi: 10.3322/caac.21660

2. GBD 2019 Colorectal Cancer Collaborators. Global, regional, and national burden of colorectal cancer and its risk factors 1990-2019: a systematic analysis for the global burden of disease study 2019. *Lancet Gastroenterol Hepatol* (2022) 7(7):627–47. doi: 10.1016/S2468-1253(22)00044-9

3. Houghton CA, Fassett RG, Coombes JS. Sulforaphane: translational research from laboratory bench to clinic. *Nutr Rev* (2013) 71:709–26. doi: 10.1111/nure.12060

4. Fofaria NM, Ranjan A, Kim S-H, Srivastava SK. Mechanisms of the anticancer effects of isothiocyanates. In: *The enzymes*. Elsevier (2015).

5. Jaiswal AK. *Nutritional composition and antioxidant properties of fruits and vegetables*. Academic Press (2020).

6. Kamal MM, Akter S, Lin C-N, Nazzal S. Sulforaphane as an anticancer molecule: mechanisms of action, synergistic effects, enhancement of drug safety, and delivery systems. *Arch Of Pharmacal Res* (2020) 43:371–84. doi: 10.1007/s12272-020-01225-2

7. WFO. *Wfo the world flora online* (2021). Available at: http://www.worldfloraonline.org/.

8. PubChem. *Pubchem* (2022). Available at: https://pubchem.ncbi.nlm.nih.gov/.

9. Houghton CA. Sulforaphane: its "coming of age" as a clinically relevant nutraceutical in the prevention and treatment of chronic disease. *Oxid Med Cell Longevity* (2019) 2019. doi: 10.1155/2019/2716870

10. Kheiri Manjili H, Sharafi A, Attari E, Danafar H. Pharmacokinetics and *In vitro* and *In vivo* delivery of sulforaphane by pcl–Peg–Pcl copolymeric-based micelles. *Artif Cells Nanomed And Biotechnol* (2017) 45:1728–39. doi: 10.1080/21691401.2017.1282501

11. Azarashkan Z, Farahani S, Abedinia A, Akbarmivehie M, Motamedzadegan A, Heidarbeigi J, Hayaloğlu AA. Co-encapsulation of broccoli sprout extract nanoliposomes into basil seed gum: effects on in vitro antioxidant, antibacterial and anti-Listeria activities in ricotta cheese. *Int J Food Microbiol* (2022) 376:109761. doi: 10.1016/j.ijfoodmicro.2022.109761

12. Yepes-Molina L, Carvajal M. Nanoencapsulation of sulforaphane in broccoli membrane vesicles and their *In vitro* antiproliferative activity. *Pharm Biol* (2021) 59:1488–502. doi: 10.1080/13880209.2021.1992450

13. Yagishita Y, Uruno A, Yamamoto M. *Molecular nutrition and diabetes*. Elsevier Inc (2016).

14. de Oliveira MR. Sulforaphane and its modulation of brain redox status: the mitochondria as a target. In: *Oxidative stress and dietary antioxidants in neurological diseases*. Elsevier (2020).

15. Parker JK. Introduction to aroma compounds in foods. In: *Flavour development, analysis and perception in food and beverages*. Elsevier (2015).

16. Heda P, Ravishankar S, Shankar A, Chaganti S, Rajan D, Parekh R, et al. Identifying promising anticancer sulforaphane derivatives using QSAR, docking, and ADME studies. *J Student Res* (2021) 10. doi: 10.47611/jsrhs.v10i4.2247

17. Kaboli PJ, Khoshkbejari MA, Mohammadi M, Abiri A, Mokhtarian R, Vazifemand R, et al. Targets and mechanisms of sulforaphane derivatives obtained from cruciferous plants with special focus on breast cancer–contradictory effects and future perspectives. *Biomed Pharmacother* (2020) 121:109635. doi: 10.1016/j.biopha.2019.109635

18. Ren J, Yuan L, Wang Y, Chen G, Hu K. Benzyl sulforaphane is superior to sulforaphane in inhibiting the Akt/Mapk and activating the Nrf2/Are signalling pathways in Hepg2 cells. *J Pharm And Pharmacol* (2018) 70:1643–53. doi: 10.1111/jphp.13015

19. Hu K, Qi Y-J, Zhao J, Jiang H-F, Chen X, Ren J. Synthesis and biological evaluation of sulforaphane derivatives as potential antitumor agents. *Eur J medicinal Chem* (2013) 64:529–39. doi: 10.1016/j.ejmech.2013.03.045

20. Heiss E, Herhaus C, Klimo K, Bartsch H, Gerhäuser C. Nuclear factor κB is a molecular target for sulforaphane-mediated anti-inflammatory mechanisms. *J Biol Chem* (2001) 276:32008–15. doi: 10.1074/jbc.M104794200

21. Ritz SA, Wan J, Diaz-Sanchez D. Sulforaphane-stimulated phase ii enzyme induction inhibits cytokine production by airway epithelial cells stimulated with diesel extract. *Am J Physiology-Lung Cell And Physiol* (2007) 292:L33–9. doi: 10.1152/ajplung.00170.2006

22. Zhang Y, Tang L. Discovery and development of sulforaphane as a cancer chemopreventive phytochemical 1. *Acta Pharmacologica Sin* (2007) 28:1343–54. doi: 10.1111/j.1745-7254.2007.00679.x

23. Mangla B, Javed S, Sultan MH, Kumar P, Kohli K, Najmi A, et al. Sulforaphane: a review of its therapeutic potentials, advances in its nanodelivery, recent patents, and clinical trials. *Phytother Res* (2021) 35:5440–58. doi: 10.1002/ptr.7176

24. Lenzi M, Fimognari C, Hrelia P. Sulforaphane as a promising molecule for fighting cancer. *Cancer Treat Res* (2014) 159:207–23. doi: 10.1007/978-3-642-38007-5_12

25. Su X, Jiang X, Meng L, Dong X, Shen Y, Xin Y. Anticancer activity of sulforaphane: the epigenetic mechanisms and the Nrf2 signaling pathway. *Oxid Med And Cell Longevity* (2018) 2018. doi: 10.1155/2018/5438179

26. Pradhan N, Kar S, Parbin S, Sengupta D, Deb M, Das L, et al. Epigenetic dietary interventions for prevention of cancer. In: *Epigenetics of cancer prevention*. Elsevier (2019).

27. Myzak MC, Karplus PA, Chung F-L, Dashwood RH. A novel mechanism of chemoprotection by sulforaphane: inhibition of histone deacetylase. *Cancer Res* (2004) 64:5767–74. doi: 10.1158/0008-5472.CAN-04-1326

28. Myzak MC, Hardin K, Wang R, Dashwood RH, Ho E. Sulforaphane inhibits histone deacetylase activity in bph-1, lncap and pc-3 prostate epithelial cells. *Carcinogenesis* (2006) 27:811–9. doi: 10.1093/carcin/bgi265

29. Dickinson SE, Rusche JJ, Bec SL, Horn DJ, Janda J, Rim SH, et al. The effect of sulforaphane on histone deacetylase activity in keratinocytes: differences between *in vitro* and *in vivo* analyses. *Mol Carcinogenesis* (2015) 54:1513–20. doi: 10.1002/mc.22224

30. Ganai SA. Histone deacetylase inhibitor sulforaphane: the phytochemical with vibrant activity against prostate cancer. *Biomed Pharmacother* (2016) 81:250–7. doi: 10.1016/j.biopha.2016.04.022

31. Morimitsu Y, Nakagawa Y, Hayashi K, Fujii H, Kumagai T, Nakamura Y, et al. A sulforaphane analogue that potently activates the Nrf2-dependent detoxification pathway. *J Of Biol Chem* (2002) 277:3456–63. doi: 10.1074/jbc.M110244200

32. Guerrero-Beltrán CE, Calderón-Oliver M, Pedraza-Chaverri J, Chirino YI. Protective effect of sulforaphane against oxidative stress: recent advances. *Exp Toxicologic Pathol* (2012) 64:503–8. doi: 10.1016/j.etp.2010.11.005

33. Houghton CA, Fassett RG, Coombes JS. Sulforaphane and other nutrigenomic Nrf2 activators: can the clinician's expectation be matched by the reality? *Oxid Med Cell Longevity* (2016) 2016. doi: 10.1155/2016/7857186

34. Uddin MS, Al Mamun A, Jakaria M, Thangapandiyan S, Ahmad J, Rahman MA, et al. Emerging promise of sulforaphane-mediated Nrf2 signaling cascade against neurological disorders. *Sci Total Environ* (2020) 707:135624. doi: 10.1016/j.scitotenv.2019.135624

35. Lee Y-J, Lee S-H. Sulforaphane induces antioxidative and antiproliferative responses by generating reactive oxygen species in human bronchial epithelial beas-2b cells. *J Korean Med Sci* (2011) 26:1474–82. doi: 10.3346/jkms.2011.26.11.1474

36. Mukherjee S, Gangopadhyay H, Das DK. Retraction: broccoli: a unique vegetable that protects mammalian hearts through the redox cycling of the thioredoxin superfamily. *J Agric And Food Chem* (2012) 60:2768–8. doi: 10.1021/jf3008585

37. Mukherjee S, Gangopadhyay H, Das DK. Broccoli: a unique vegetable that protects mammalian hearts through the redox cycling of the thioredoxin superfamily. *J Agric And Food Chem* (2008) 56:609–17. doi: 10.1021/jf0728146

38. Angeloni C, Leoncini E, Malaguti M, Angelini S, Hrelia P, Hrelia S. Modulation of phase II enzymes by sulforaphane: implications for its cardioprotective potential. *J Agric Food Chem* (2009) 57:5615–22. doi: 10.1021/jf900549c

39. Devi JR, Thangam EB. Studies on antioxidant and antimicrobial activities of purified sulforaphane from brassica oleraceae var. rubra. *J Pharm Res* (2012) 5:3582–4. doi: 10.7314/apjcp.2012.13.5.2095

40. Romeo L, Iori R, Rollin P, Bramanti P, Mazzon E. Isothiocyanates: an overview of their antimicrobial activity against human infections. *Molecules* (2018) 23:624. doi: 10.3390/molecules23030624

41. Abukhabta S, Khalil Ghawi S, Karatzas KA, Charalampopoulos D, Mcdougall G, Allwood JW, et al. Sulforaphane-enriched extracts from glucoraphanin-rich broccoli exert antimicrobial activity against gut pathogens *in vitro* and innovative cooking methods increase *in vivo* intestinal delivery of sulforaphane. *Eur J Nutr* (2021) 60:1263–76. doi: 10.1007/s00394-020-02322-0

42. Janczewski Ł. Sulforaphane and its bifunctional analogs: synthesis and biological activity. *Molecules* (2022) 27:1750. doi: 10.3390/molecules27051750

43. Arner ES, Holmgren A. The thioredoxin system in cancer. In: *Seminars in cancer biology*. Elsevier (2006). p. 420–6.

44. Lau A, Villeneuve NF, Sun Z, Wong PK, Zhang DD. Dual roles of Nrf2 in cancer. *Pharmacol Res* (2008) 58:262–70. doi: 10.1016/j.phrs.2008.09.003

45. Li C, Thompson MA, Tamayo AT, Zuo Z, Lee J, Vega F, et al. Over-expression of thioredoxin-1 mediates growth, survival, and chemoresistance and is a druggable target in diffuse Large b-cell lymphoma. *Oncotarget* (2012) 3:314–26. doi: 10.18632/oncotarget.463

46. Gonzalez-Donquiles C, Alonso-Molero J, Fernandez-Villa T, Vilorio-Marqués L, Molina A, Martín V. The NRF2 transcription factor plays a dual role in colorectal cancer: a systematic review. *PloS One* (2017) 12:e0177549. doi: 10.1371/journal.pone.0177549

47. Bian M, Fan R, Zhao S, Liu W. Targeting the thioredoxin system as a strategy for cancer therapy. *J Medicinal Chem* (2019) 62:7309–21. doi: 10.1021/acs.jmedchem.8b01595

48. Jia J-J, Geng W-S, Wang Z-Q, Chen L, Zeng X-S. The role of thioredoxin system in cancer: strategy for cancer therapy. *Cancer Chemother Pharmacol* (2019) 84:453–70. doi: 10.1007/s00280-019-03869-4

49. Kumar H, Kumar RM, Bhattacharjee D, Somanna P, Jain V. Role of Nrf2 signaling cascade in breast cancer: strategies and treatment. *Front Pharmacol* (2022) 13:720076. doi: 10.3389/fphar.2022.720076

50. Ho E, Clarke JD, Dashwood RH. Dietary sulforaphane, a histone deacetylase inhibitor for cancer prevention. *J Nutr* (2009) 139:2393–6. doi: 10.3945/jn.109.113332

51. Kim H-J, Bae S-C. Histone deacetylase inhibitors: molecular mechanisms of action and clinical trials as anti-cancer drugs. *Am J Trans Res* (2011) 3:166.

52. Atwell LL, Beaver LM, Shannon J, Williams DE, Dashwood RH, Ho E. Epigenetic regulation by sulforaphane: opportunities for breast and prostate cancer chemoprevention. *Curr Pharmacol Rep* (2015) 1:102–11. doi: 10.1007/s40495-014-0002-x

53. Jiang L-L, Zhou S-J, Zhang X-M, Chen H-Q, Liu W. Sulforaphane suppresses *In vitro* and *In vivo* lung tumorigenesis through downregulation of hdac activity. *Biomed Pharmacother* (2016) 78:74–80. doi: 10.1016/j.biopha.2015.11.007

54. Dos Santos PWDS, Machado ART, De Grandis RA, Ribeiro DL, Tuttis K, Morselli M, et al. Transcriptome and DNA methylation changes modulated by sulforaphane induce cell cycle arrest, apoptosis, DNA damage, and suppression of proliferation in human liver cancer cells. *Food Chem Toxicol* (2020) 136:111047. doi: 10.1016/j.fct.2019.111047

55. Most D, Ferguson L, Harris RA. Molecular basis of alcoholism. In: *Handbook of clinical neurology* (2014).

56. Abbaoui B, Telu KH, Lucas CR, Thomas-Ahner JM, Schwartz SJ, Clinton SK, et al. The impact of cruciferous vegetable isothiocyanates on histone acetylation and histone phosphorylation in bladder cancer. *J Proteomics* (2017) 156:94–103. doi: 10.1016/j.jprot.2017.01.013

57. Atwell LL, Zhang Z, Mori M, Farris PE, Vetto JT, Naik AM, et al. Sulforaphane bioavailability and chemopreventive activity in women scheduled for breast biopsy. *Cancer Prev Res* (2015) 8:1184–91. doi: 10.1158/1940-6207.CAPR-15-0119

58. Pledgie-Tracy A, Sobolewski MD, Davidson NE. Sulforaphane induces cell type–specific apoptosis in human breast cancer cell lines. *Mol Cancer Ther* (2007) 6:1013–21. doi: 10.1158/1535-7163.MCT-06-0494

59. Pop S, Enciu AM, Tarcomnicu I, Gille E, Tanase C. Phytochemicals in cancer prevention: modulating epigenetic alterations of dna methylation. *Phytochem Rev* (2019) 18:1005–24. doi: 10.1007/s11101-019-09627-x

60. Hyun TK. A recent overview on sulforaphane as a dietary epigenetic modulator. *EXCLI J* (2020) 19:131–4. doi: 10.17179/excli2019-2039

61. Mattick JS, Makunin IV. Non-coding rna. *Hum Mol Genet* (2006) 15:R17–29. doi: 10.1093/hmg/ddl046

62. Rafiei H, Ashrafizadeh M, Ahmadi Z. Micrornas as novel targets of sulforaphane in cancer therapy: the beginning of a new tale? *Phytother Res* (2020) 34:721–8. doi: 10.1002/ptr.6572

63. Kalhori MR, Khodayari H, Khodayari S, Vesovic M, Jackson G, Farzaei MH, et al. Regulation of long non-coding rnas by plant secondary metabolites: a novel anticancer therapeutic approach. *Cancers* (2021) 13:1274. doi: 10.3390/cancers13061274

64. Baier SR, Zbasnik R, Schlegel V, Zempleni J. Off-target effects of sulforaphane include the derepression of long terminal repeats through histone acetylation events. *J Nutr Biochem* (2014) 25:665–8. doi: 10.1016/j.jnutbio.2014.02.007

65. Sharifi-Rad J, Seidel V, Izabela M, Monserrat-Mequida M, Sureda A, Ormazabal V, et al. Phenolic compounds as Nrf2 inhibitors: potential applications in cancer therapy. *Cell Commun Signal* (2023) 21:89. doi: 10.1186/s12964-023-01109-0

66. Mao L, Yang T, Li X, Lei X, Sun Y, Zhao Y, et al. Protective effects of sulforaphane in experimental vascular cognitive impairment: contribution of the Nrf2 pathway. *J Of Cereb Blood Flow Metab* (2019) 39:352–66. doi: 10.1177/0271678X18764083

67. Esfandyari S, Aleyasin A, Noroozi Z, Taheri M, Khodarahmian M, Eslami M, et al. The protective effect of sulforaphane against oxidative stress through activation of Nrf2/ARE pathway in human granulosa cells. *Cell J (Yakhteh)* (2021) 23:692. doi: 10.22074/cellj.2021.7393

68. Bauman JE, Zang Y, Sen M, Li C, Wang L, Egner PA, et al. Prevention of carcinogen-induced oral cancer by sulforaphane. *Cancer Prev Res* (2016) 9:547–57. doi: 10.1158/1940-6207.CAPR-15-0290

69. Amin PJ, Shankar BS. Sulforaphane induces ROS mediated induction of NKG2D ligands in human cancer cell lines and enhances susceptibility to NK cell mediated lysis. *Life Sci* (2015) 126:19–27. doi: 10.1016/j.lfs.2015.01.026

70. Calabrese EJ, Kozumbo WJ. The phytoprotective agent sulforaphane prevents inflammatory degenerative diseases and age-related pathologies via Nrf2-mediated hormesis. *Pharmacol Res* (2021) 163:105283. doi: 10.1016/j.phrs.2020.105283

71. Milczarek M, Mielczarek L, Lubelska K, Dąbrowska A, Chilmonczyk Z, Matosiuk D, et al. *In vitro* evaluation of sulforaphane and a natural analog as potent inducers of 5-fluorouracil anticancer activity. *Molecules* (2018) 23:3040. doi: 10.3390/molecules23113040

72. Wang F, Wang W, Li J, Zhang J, Wang X, Wang M. Sulforaphane reverses gefitinib tolerance in human lung cancer cells via modulation of sonic hedgehog signaling. *Oncol Lett* (2018) 15:109–14. doi: 10.3892/ol.2017.7293

73. Rakariyatham K, Yang X, Gao Z, Song M, Han Y, Chen X, et al. Synergistic chemopreventive effect of allyl isothiocyanate and sulforaphane on non-small cell lung carcinoma cells. *Food Funct* (2019) 10:893–902. doi: 10.1039/C8FO01914B

74. Rakariyatham K, Wu X, Tang Z, Han Y, Wang Q, Xiao H. Synergism between luteolin and sulforaphane in anti-inflammation. *Food Funct* (2018) 9:5115–23. doi: 10.1039/C8FO01352G

75. Traka MH, Melchini A, Coode-Bate J, Al Kadhi O, Saha S, Defernez M, et al. Transcriptional changes in prostate of men on active surveillance after a 12-Mo glucoraphanin-rich broccoli intervention–results from the effect of sulforaphane on prostate cancer prevention (Escape) randomized controlled trial. *Am J Of Clin Nutr* (2019) 109:1133–44. doi: 10.1093/ajcn/nqz012

76. Tahata S, Singh SV, Lin Y, Hahm E-R, Beumer JH, Christner SM, et al. Evaluation of biodistribution of sulforaphane after administration of oral broccoli sprout extract in melanoma patients with multiple atypical nevievaluation of sulforaphane in patients with atypical nevi. *Cancer Prev Res* (2018) 11:429–38. doi: 10.1158/1940-6207.CAPR-17-0268

77. Cipolla BG, Mandron E, Lefort JM, Coadou Y, Della Negra E, Corbel L, et al. Effect of sulforaphane in men with biochemical recurrence after radical prostatectomy. *Cancer Prev Res* (2015) 8:712–9. doi: 10.1158/1940-6207.CAPR-14-0459

78. Yanaka A, Fahey JW, Fukumoto A, Nakayama M, Inoue S, Zhang S, et al. Dietary sulforaphane-rich broccoli sprouts reduce colonization and attenuate gastritis in helicobacter pylori–infected mice and humans. *Cancer Prev Res* (2009) 2:353–60. doi: 10.1158/1940-6207.CAPR-08-0192

79. Alumkal JJ, Slottke R, Schwartzman J, Cherala G, Munar M, Graff JN, et al. A phase II study of sulforaphane-rich broccoli sprout extracts in men with recurrent prostate cancer. *Investigational New Drugs* (2015) 33:480–9. doi: 10.1007/s10637-014-0189-z

80. ClinicalTrials.gov. *Effects of sulforaphane on normal prostate tissue (PHASE)* (2016). Available at: https://clinicaltrials.gov/ct2/show/study/NCT00946309?term=sulforaphane&cond=cancer&draw=2&rank=10 (Accessed 30 April 2023).

81. ClinicalTrials.gov. *Study to evaluate the effect of sulforaphane in broccoli sprout extract on breast tissue* (2018). Available at: https://clinicaltrials.gov/ct2/show/study/NCT00982319?term=sulforaphane&cond=cancer&draw=2&rank=7 (Accessed 30 April 2023).

82. ClinicalTrials.gov. *Accumulation of dietary bioactives and prostate cancer (ADaPT)* (2020). Available at: https://clinicaltrials.gov/ct2/show/study/NCT04046653?term=sulforaphane&cond=cancer&draw=2&rank=9 (Accessed 30 April 2023).

83. Zhang Z, Garzotto M, Davis EW, Mori M, Stoller WA, Farris PE, et al. Sulforaphane bioavailability and chemopreventive activity in men presenting for biopsy of the prostate gland: a randomized controlled trial. *Nutr And Cancer* (2020) 72:74–87. doi: 10.1080/01635581.2019.1619783

84. Yuan J. Randomized clinical trial of lung cancer chemoprevention with sulforaphane in former smokers. *US Natl Library Of Med: Bethesda Md USA* (2022).

85. Watanabe T, Oba T, Tanimoto K, Shibata T, Kamijo S, Ito KI. Tamoxifen resistance alters sensitivity to 5-fluorouracil in a subset of estrogen receptor-positive breast cancer. *PloS One* (2021) 16:E0252822. doi: 10.1371/journal.pone.0252822

86. Li M, Gao J, Tang Y, Liu M, Wu S, Qu K, et al. Traditional herbal medicine-derived sulforaphene lfs-01 reverses colitis in mice by selectively altering the gut microbiota and promoting intestinal gamma-delta T cells. *Front Pharmacol* (2018) 8:959. doi: 10.3389/fphar.2017.00959

87. Wang H, Wang F, Wu S, Liu Z, Li T, Mao L, et al. Traditional herbal medicine-derived sulforaphene promotes mitophagic cell death in lymphoma cells through Crm1-mediated P62/Sqstm1 accumulation and ampk activation. *Chemico-Biological Interact* (2018) 281:11–23. doi: 10.1016/j.cbi.2017.12.017

88. Wu G, Yan Y, Zhou Y, Duan Y, Zeng S, Wang X, et al. Sulforaphane: expected to become a novel antitumor compound. *Oncol Res* (2020) 28:439. doi: 10.3727/096504020X15828892654385

89. Chartoumpekis DV, Ziros PG, Chen J-G, Groopman JD, Kensler TW, Sykiotis GP. Broccoli sprout beverage is safe for thyroid hormonal and autoimmune status: results of a 12-week randomized trial. *Food Chem Toxicol* (2019) 126:1–6. doi: 10.1016/j.fct.2019.02.004

frontiers | Frontiers in Pharmacology

TYPE Original Research
PUBLISHED 28 June 2023
DOI 10.3389/fphar.2023.1206981

OPEN ACCESS

EDITED BY
Mitesh Patel,
Parul University, India

REVIEWED BY
Pukar Khanal,
KLE College of Pharmacy, India
Rohit Kumar Tiwari,
Sharda School of Allied Health Sciences, India

*CORRESPONDENCE
Ahmed Alafnan,
a.alafnan@uoh.edu.sa

RECEIVED 16 April 2023
ACCEPTED 13 June 2023
PUBLISHED 28 June 2023

CITATION
Alafnan A, Khalifa NE, Hussain T and Osman ME (2023), Cucurbitacin-B instigates intrinsic apoptosis and modulates Notch signaling in androgen-dependent prostate cancer LNCaP cells. *Front. Pharmacol.* 14:1206981.
doi: 10.3389/fphar.2023.1206981

Cucurbitacin-B instigates intrinsic apoptosis and modulates Notch signaling in androgen-dependent prostate cancer LNCaP cells

Ahmed Alafnan[1]*, Nasrin E. Khalifa[2,3], Talib Hussain[1] and Mhdia Elhadi Osman[4]

[1]Department of Pharmacology and Toxicology, College of Pharmacy, University of Ha'il, Ha'il, Saudi Arabia, [2]Department of Pharmaceutics, College of Pharmacy, University of Ha'il, Ha'il, Saudi Arabia, [3]Department of Pharmaceutics, Faculty of Pharmacy, University of Khartoum, Khartoum, Sudan, [4]Department of Clinical Pharmacy, College of Pharmacy, University of Ha'il, Ha'il, Saudi Arabia

Introduction: Among numerous triterpenoids of the Cucurbitaceae family, Cucurbitacin-B (Cur-B) is being explored for its pharmacological attributes. Reports from previous studies have explicitly shown that Cur-B possesses substantial anticancer effects. The present report focuses on exploring the anticancer attributes of Cur-B against androgen-dependent PCa LNCaP cells.

Methods: LNCaP cells were exposed to commercially available purified Cur-B at varying concentrations that were selected as 5, 10, 15, 20, and 25 μM for some time of 24 h to perform various experimental studies.

Results: Cytotoxicity evaluation revealed that Cur-B impeded the LNCaP cell's viability at 5 μM (p <0.05) which increased considerably at a concentration of 25 μM (p <0.001). Cur-B was also efficacious in inducing the changes within nuclear morphology followed by a concomitant increase in the activities of key caspases including caspase-3, -8, and -9 intriguingly in a dose-dependent trend. Cur-B treatment not only resulted in the augmentation of intracellular ROS levels within LNCaP cells at 5 μM (p <0.05) but also in-creased significantly at 25 μM concentration (p <0.001). Elevation in the ROS levels was also found to be correlated with dissipated mitochondrial membrane potential ($\Delta\Psi m$) which culminated in the onset of significant apoptosis at 25 μM concentration (p <0.001). Cur-B exposure also resulted in the downregulation of cyclin D1, cyclin-dependent kinase 4 (CDK4) followed by amplified levels of $p21^{Cip1}$ mRNA. Importantly, exposure of Cur-B competently reduced the expression of the Notch signaling cascade which may be the plausible cause behind Cur-B-instigated apoptotic cell death and cell cycle arrest in LNCaP cells.

Discussion: These observations thus, explicitly indicated that Cur-B could be plausibly further explored as potent therapeutics against androgen-dependent PCa.

KEYWORDS

anti-cancer, apoptosis, cell cycle, cucurbitacin-B, Notch signaling

1 Introduction

Prostate cancer (PCa) is a debilitating malignancy within the male population globally. As per the recently available statistics, 1,414,259 male individuals were diagnosed positive for PCa by the end of the year 2020. Indeed, PCa contributed to 7.3% of the total 19,292,789 cases of positively diagnosed different cancers. Moreover, PCa was also responsible for 375,304 confirmed deaths globally by the end of the year 2020 (Bilal, et al., 2022). Usually, the onset of the disease in males happens during 60–70 years of age, which significantly increases both the mortality and morbidity of PCa (Alafnan, et al., 2021). The Notch signaling pathway serves as an important development pathway that modulates the onset and progression followed by metastasis of PCa (Leong and Gao, 2008). Previously, Notch signaling was reviewed to modulate the tumorigenicity of PCa stem cells and is thus involved in regulating the proliferation of oncogenes along with the development of chemotherapeutic resistance (Mourkioti, et al., 2022). Indeed, hyperactivated Notch signaling has been the hallmark of PCa observed in both clinical and preclinical models (Shou, et al., 2001; Mourkioti, et al., 2022).

Furthermore, Notch signaling was also shown to play an important role in imparting resistance toward enzalutamide within PCa cells that were found to be ameliorated by using Notch signaling inhibitors (Farah, et al., 2019). Exhaustive research over the last several decades has provided the impetus for a better understanding of some very important pathophysiological and their associated mechanisms in PCa. This has further contributed to elucidating various interventions (including surgical and/or radiological interventions usually coupled with chemotherapeutics) followed by androgen ablation therapies. Although effective, the efficiencies of these interventions are primarily dependent on the stage of PCa, thereby compelling the need for further exploration of new interventions against PCa. The present typical protocol for clinical management of prostate cancer mostly relies on the use of drugs like docetaxel, which have already been reported to cause a side effect on the health of individuals by affecting the microtubules and destabilizing them (Mukhtar, et al., 2014). Docetaxel has also been associated with various research studies to prompt resistance due to the instantaneous efflux of the therapeutic drug caused by mutations in the microtubules (Hwang, 2012).

In addition to it, another key drawback due to the utilization of standard chemotherapeutics is their related ill effects, which appallingly have an unconstructive impact on blood cells along with cells of the mouth and digestive tract and even hair follicles (Altun and Sonkaya, 2018). Among diverse recognized fruit and vegetable crops, Cucurbitaceae is one of the major families, which has almost 125 genera besides 960 species. The members of this family have been identified as a component of prehistoric medical and culinary traditions. Interestingly, they have also been considered a key component of folk medicines that are formerly mentioned in Ayurveda for their medicinal benefits (Olarewaju, et al., 2021). Quite a few members of the Cucurbitaceae family have already been mentioned for the treatment of various diseases. The chemical composition of cucurbitacins is referred to as triterpenoid adjoined by a base nuclear frame as 19-(10″9)-abeo-5α-lanostane that is responsible for carrying oxygen atoms at different positions (Kaushik, et al., 2015). A recent study has documented the antitumor effect of cucurbitacin compound and its derivative against human breast cancer cells like MCF-7 and MDA-MB 231 (Varela, et al., 2022). Cucurbitacin B (Cur-B) is a predominantly distributed natural compound. It primarily belongs to the families Cucurbitaceae and Cruciferae and has been shown in a range of plants, such as *Cucumis melo*, *Cucurbita andreana*, *Ecballium elaterium*, *Wilbrandia ebracteata*, and *Trichosanthes cucumerina* (Cai, et al., 2015). An accrued number of reports have demonstrated the multiple pharmacological activities, such as anti-inflammatory, antioxidant, antiviral, hypoglycemic, hepatoprotective, neuroprotective, and anti-cancer effects, which mainly contribute to the treatment and management of various ailments, namely, inflammatory diseases, neurodegenerative diseases, diabetes mellitus, and cancers (Chen, et al., 2008). It is worth noting that Cur-B is the most abundant and active form of cucurbitacin, and as a result, it has garnered substantial attention from researchers across the globe as compared to the other classes of cucurbitacin (Sallam, et al., 2018).

Nevertheless, the mechanistic approach to the anti-cancerous potential of Cur-B and its probable role in the modulation of the Notch signaling cascade remains unfamiliar in the case of androgen-dependent human PCa LNCaP cells. Therefore, we hypothesized this study to examine that Cur-B mediates anti-cancer effects through the modulation of Notch signaling components against human PCa LNCaP cells.

2 Materials and methods

2.1 Materials

Cucurbitacin-B (SKU: PHL82226) and inhibitors of respective caspases, propidium iodide (PI), DCFH-DA, and Hoechst-33342 dye were commercially procured from Sigma-Aldrich (St. Louis, Missouri, USA). The caspase-specific kits used in the study were procured from BioVision, Waltham, Massachusetts, United States. Materials required for tissue culture including Ham's F12K media, FBS along with antibiotic–antimycotic solution, SYBR Green kit (DyNAmo ColorFlash), and Verso cDNA Synthesis Kit were obtained from Thermo Fisher Scientific, Waltham, Massachusetts, USA. MTT dye along with the total RNA purification kit was obtained from HiMedia Labs, Pune, India.

2.2 Cell culture

Human-derived androgen-dependent prostate adenocarcinoma LNCaP cells were obtained from the National Centre for Cell Science, Pune, India. LNCaP cells were allowed to proliferate under standard tissue culture conditions at 37 °C along with 5% CO_2. The RPMI-1640 media supplemented with a cocktail of 1% antibiotic–antimycotic and 10% FBS was used during the study. The passage number of the LNCaP cells used in the present study was five. All the imaging reported in the present study was accomplished using FLoid Imaging Station (Thermo Fisher Scientific, United States).

2.3 Methods

2.3.1 Cur-B-mediated cytotoxicity

The evaluation of cytotoxicity of Cur-B at varied concentrations on LNCaP cells (androgen-sensitive prostate adenocarcinoma) was performed through the MTT assay, with a slightly modified protocol (Marignol, et al., 2013). Approximately 5×10^3 cells per well were given treatment of Cur-B at the concentration of 5, 10, 15, 20, and 25 μM for a time period of 24 h, incubated in a humidified environment. After incubation, the media of each well were removed, and MTT dye was added to it (5 mg/mL; 10 μL) and was further left for 4 h. The formazan crystals were dissolved in 100 μL DMSO, and the absorbance of treated and untreated groups was documented at 570 nm with the help of a spectrophotometer. The cellular viability of LNCaP cells was estimated as percentage (%) in comparison with the control LNCaP cells.

Cellular viability % = (absorbance of treated LNCaP cells)/(absorbance of untreated LNCaP control cells) × 100.

2.3.2 Morphological attributes of PCa cells

Cur-B-treated PCa cells were observed for modifications in their morphology in comparison with untreated cells. Nearly 5×10^3 cells/well were subjected to the treatment of Cur-B at previously mentioned concentrations and left for 24 h. Finally, morphological modifications in different groups of PCa LNCaP cells were examined in the bright light of FLoid Imaging Station.

2.3.3 Effects on nuclear morphology

The apoptotic efficacy of Cur-B was evaluated on LNCaP cells, and the treated cells were examined qualitatively through DAPI (Tiwari, et al., 2021). LNCaP cells were seeded approximately 5×10^3 cells/well. Cells were afterward exposed to the previously mentioned Cur-B concentrations, followed by an incubation of 24 h. Subsequently, the LNCaP cells were washed using chilled PBS. Thereafter, chilled methanol was used for fixing the LNCaP cells approximately for 10 min. Finally, these were then permeabilized using a mixture of 3% paraformaldehyde (PFA) and Triton X-100 (0.25%) and consequently stained with DAPI. The LNCaP cells were observed, and photomicrographs were captured at an excitation : emission ratio of 390/40 nm : 446/33 nm, respectively.

2.3.4 Onset of apoptosis

For the assessment of Cur-B in instigating the apoptosis induction in LNCaP cells, PI staining was performed along with the quantification through ImageJ software (NIH, USA). Approximately 5×10^3 cells per well were exposed to the treatment of Cur-B at previously mentioned concentrations and left for 24 h. The PI staining fluorescence was further recorded at an excitation: emission wavelength of 586/15 nm: 646/68 nm, respectively, and further quantified though ImageJ software.

2.3.5 Estimation of caspase/s activities

Commercially accessible caspase-8, -9, and -3 colorimetric kits were acquired and utilized to exhibit the activities of stated caspases in androgen-sensitive LNCaP cells as per the supplier's instructions. After Cur-B treatment (aforementioned concentrations), 3×10^6 LNCaP cells were lysed using 0.05 mL chilled lysis buffer along with 10 min incubation on ice. The lysate was subjected to centrifugation at 4 °C, 10,000 rpm for 1 min, and the supernatant was collected. Thereafter, 0.05 mL lysate of treatment and control cells well supplemented with 0.05 mL reaction buffer. Subsequently, each well was further supplemented with DEVD-pNA (4 mM) and incubated for approximately 10 min; last, the absorbance of each well was recorded at 405 nm. Percentage enhancement within the activities of the different caspases was further pre-meditated by comparing the alterations with that of untreated LNCaP cells.

2.3.6 Effects of caspase inhibitors

Cytotoxicity instigated by Cur-B on LNCaP cells was further investigated through using inhibitors for caspase-8, -9, and -3. LNCaP cells were at first treated for approximately 2 h with ZIETD-FMK, Z-LEHD-FMK, and Z-DEVD-FMK (50 μM each; inhibitors for caspase-8, -9, and -3, respectively). Afterward, the cells were retreated with Cur-B at aforementioned concentrations and incubated for another 24 h. Finally, the viable percentage of Cur-B-treated LNCaP cells was quantified following the procedure described previously in MTT-mediated estimation of viable LNCaP cells.

2.3.7 Estimation of mitochondrial membrane potential (ΔΨm)

ΔΨm of Cur-B treated LNCaP cells was examined using commercially accessible kit using the supplier's protocol. The fluorescence intensity was assessed approximately 30 min after addition to the Mito-NIR dye and assay buffer-B at excitation/emission 640/680 nm, respectively, through a microplate reader.

2.3.8 ROS estimation

The elevation of ROS production after the Cur-B treatment within the androgen-sensitive LNCaP cells was assessed qualitatively with the help of DCFH-DA stain as described earlier (Ahmad, et al., 2021). Approximately 5×10^3 cells per well were supplemented with Cur-B at aforementioned concentrations (5–25 μM) followed by 12 h of incubation. After incubation, the media from every well was removed, cells were stained using DCFH-DA (10 μM) and incubated in the dark for 30 min; last, the cells were washed carefully and visualized, and photomicrographs were captured under the green channel fluorescence microscope.

2.3.9 Real-time qPCR analysis

For evaluating the alterations within the genes like CDK4, $p21^{Cipl}$, cyclin D1, Bax, Bad, Bcl2, Notch1 , Hes1, and Jagged1, LNCaP cells (1×10^6 cells/well) were transferred and left to adhere for the night under optimum tissue culture environment. After overnight adherence, these cells were given treatment with the previously stated Cur-B concentration for 24 h before their total RNA was extracted. The extracted RNA was further used to synthesize cDNA, and then the qRT-PCR-based analysis was performed using the SYBR Green qPCR Kit as per the supplier's manual. Comparative CT method was employed for analyzing the variations in the expression of stated genes with GAPDH as the control gene. The primers used were the same as reported previously as demonstrated in Table 1 (Ahmad, et al., 2022; Alafnan, et al., 2022).

2.3.10 Statistical evaluation

Data characterize the mean ± SEM of separate experiments (n = 3), where each experiment was performed at least thrice. Statistical

TABLE 1 List of forward and reverse sequences of primers used in the study.

Target gene	Forward (5′–3′) sequence	Reverse (3′–5′) sequence
CDK4	CCATCAGCACAGTTCGTGAGGT	TCAGTTCGGGATGTGGCACAGA
$p21^{Cip1}$	AGGTGGACCTGGAGACTCTCAG	TCCTCTTGGAGAAGATCAGCCG
Cyclin D1	CTTCCTCTCCAAAATGCCAG	AGAGATGGAAGGGGGAAAGA
Bax	TCAGGATGCGTCCACCAAGAAG	TGTGTCCACGGCGGCAATCATC
Bad	CCAACCTCTGGGCAGCACAGC	TTTGCCGCATCTGCGTTGCTGT
Bcl2	ATCGCCCTGTGGATGACTGAGT	GCCAGGAGAAATCAAACAGAGGC
GAPDH	CGACCACTTTGTCAAGCTCA	CCCCTCTTCAAGGGGTCTAC
Hes1	GGAAATGACAGTGAAGCACCTCC	GAAGCGGGTCACCTCGTTCATG
Notch1	CTGGTCAGGGAAATCGTG	TGGGCAGTGGCAGATGTAG
Jagged1	TGCTACAACCGTGCCAGTGACT	TCAGGTGTGTCGTTGGAAGCCA

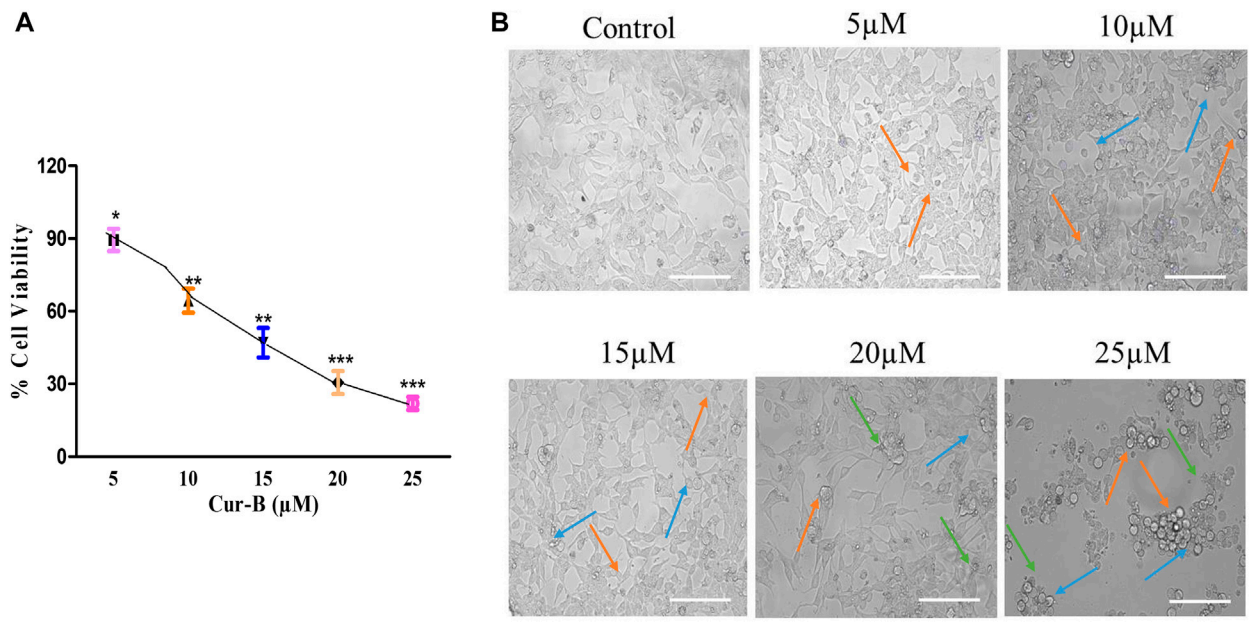

FIGURE 1
(A) Percent (%) cell viability of LnCap cells after treatment with various doses of Cur-B and **(B)** Alterations in morphology of LnCap cells upon treatment with different doses of Cur-B for 24 h as compared to the control. Scale bar = 100 μm.

significances in between the formulated groups were estimated using one-way ANOVA.

3 Results

3.1 Cur-B suppressed the proliferation of androgen-dependent PCa LNCaP cells

The cytotoxicity assay was performed by treating LNCaP cells with different doses of Cur-B (5, 10, 15, 20, and 25 μM) for 24 h. IC50 of Cur-B against LNCaP cells was found to be 10.71 ± 1.08 μM (Figure 1A). It was demonstrated that the treatment of Cur-B substantially inhibited the proliferation of PCa cells (Figure 1B), which was found to 89.46% ± 3.75%, 64.42% ± 4.05%, 47.06% ± 4.97%, 30.59% ± 3.85%, and 21.92% ± 2.21% as compared to the vehicle or control at the suggested doses of 5, 10, 15, 20, and 25 μM of Cur-B, respectively. Thus, these findings concluded that Cur-B suppressed the proliferation rate of PCa cells in a dose-dependent manner.

3.2 Cur-B altered the morphology of androgen-dependent PCa LNCaP cells

To investigate whether the suppression of cell proliferation and occurrence of cell death are due to the treatment of Cur-B, LNCaP

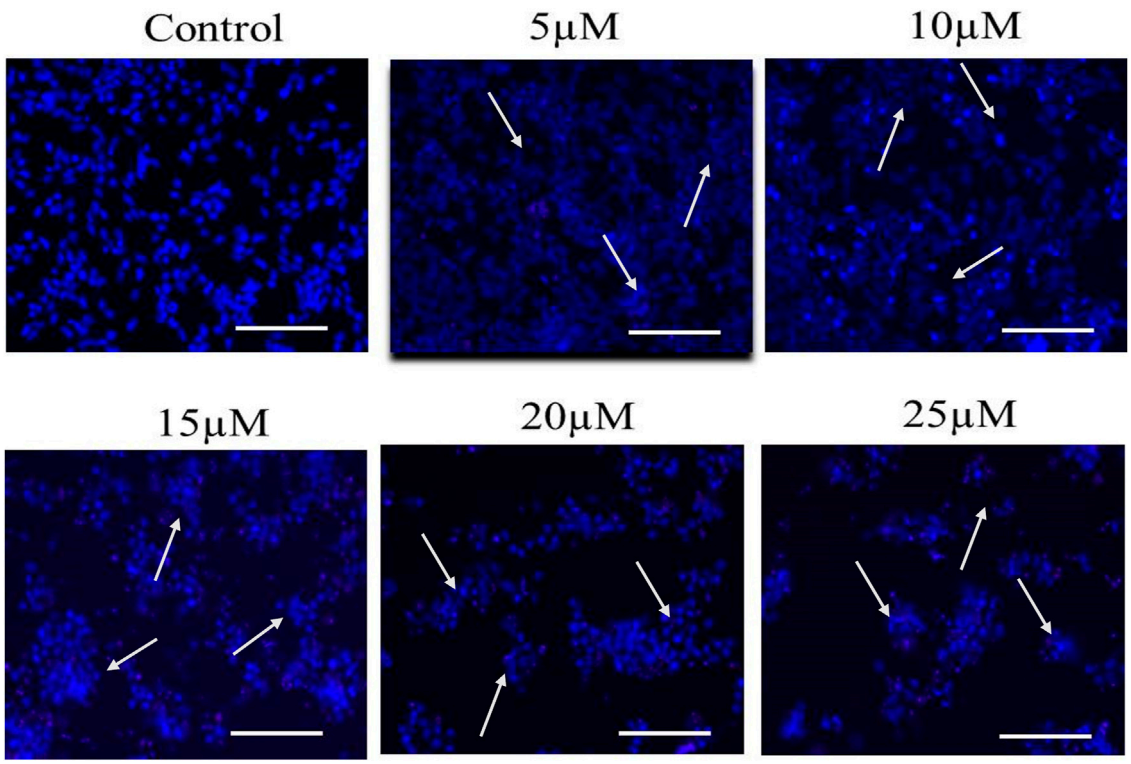

FIGURE 2
Cur-B mediates nuclear condensation and fragmentation in LNCaP PCa cells after staining with DAPI. White arrows indicate the nuclear condensation in LNCaP cells. Scale bar = 100 μm.

cells were examined under a phase contrast microscope. It was observed that treatment with increasing doses of Cur-B reduced the number of adherent cells and enhanced the number of floating PCa cells. Phase contrast micrographs revealed that a considerable number of cells underwent various morphological alterations, such as cell swelling, rounding up of cells, and disintegration of plasma, as shown in Figure 1C, substantiating Cur-B-mediated antiproliferative effects in androgen-dependent PCa cells, whereas vehicle or control cells exhibited unaltered flattened morphology.

3.3 Cur-B induced fragmentation and condensation in androgen-dependent LNCaP cells

Multiple morphological alterations are found linked with the cells undergoing apoptosis such as the rounding up of cells that shrunk and lost communication with neighboring cells. However, there are some highly sensitive cells that even get removed from the surface of the plates. To evaluate nuclear condensation and fragmentation induced by Cur-B in LNCaP, cells were cultured with Cur-B for 24 h. The cells were stained with DAPI after treatment with Cur-B for 24 h and studied by fluorescence microscopy. It was evident that the treated PCa cells exhibited substantial condensation and fragmentation, which are peculiar attributes of apoptosis as compared to the vehicle or control, which demonstrated the exact round nuclei with diffuse blue fluorescence (Figure 2).

3.4 Cur-B instigated apoptosis in androgen-dependent PCa cells

Cur-B instigated apoptosis within LNCaP cells and was measured by PI staining through a fluorescence microscope. As shown in the fluorescence micrographs of Figure 3, apoptotic cells were distinguished by augmented red fluorescence suggesting the formation of apoptotic bodies in Cur-B-treated LNCaP cells. Indeed, due to the presence of intact nuclei in vehicle or control cells, they were defined by the presence of diffuse red fluorescence. Furthermore, Cur-B-induced apoptosis was quantified in LNCaP cells. As observed in Figure 3, a dose-dependent increase in apoptotic cells exhibiting bright red fluorescence was observed in comparison with the control. Thus, our results suggested that Cur-B-induced morphological alterations in a dose-dependent manner in the nucleus eventually lead to apoptosis.

3.5 Cur-B treatment increases caspase activation

To investigate, the underlying mechanism in Cur-B-induced apoptosis is due to the activation of caspases in PCa cells. As shown in Figure 4A, there was a substantial induction of caspase activities within PCa cells upon treatment with increasing doses of Cur-B (5, 10, 15, 20, and 25 μM) for 24 h. The percentage (%) increase in the activities of caspase-8 and -9 was found to be

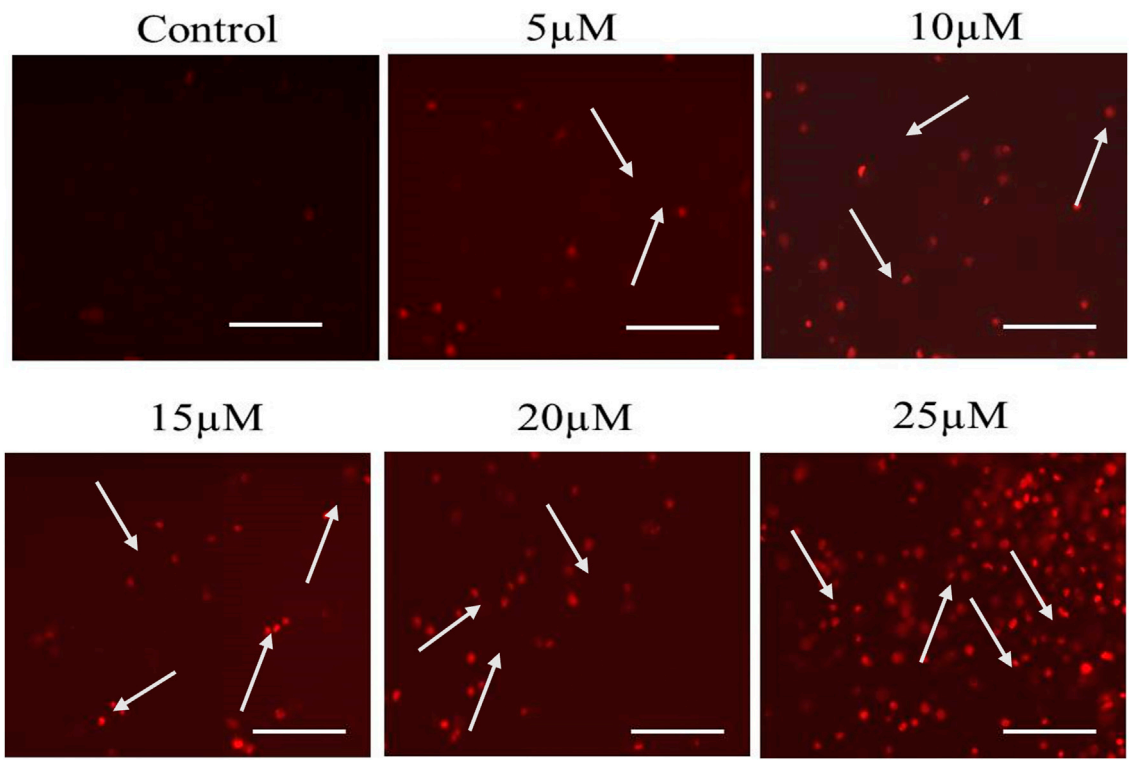

FIGURE 3
Cur-B mediated the instigation of apoptosis within LNCaP cells as evaluated through PI staining. White arrows indicate the apoptotic nuclei of Cur-B-treated LNCaP cells. Scale bar 100 μm. Significance among different dosage groups were determined using one-way ANOVA followed by Dunnett's post-test, where * represents $p < 0.05$, ** $p < 0.01$, and *** $p < 0.001$ (GraphPad Prism, Ver. 5).

19.87% ± 3.45%, 32.43% ± 4.19%, 52.72% ± 3.53%, 77.37% ± 3.57%, and 99.26% ± 4.96%; 29.65% ± 3.54%, 53.73% ± 3.40%, 83.58% ± 3.45%, 114.51% ± 2.36%, and 123.68% ± 3.64% in comparison with control, at the indicated doses of 5, 10, 15, 20, and 25 μM of Cur-B, respectively (Figure 4A). In addition, enhancement in caspase-3 activity was found to be 35.87% ± 3.45%, 54.43% ± 4.54%, 79.72% ± 4.72%, 123.96% ± 3.36%, and 173.68 ± 5.12, respectively. Thus, these findings concluded the involvement of both extrinsic and intrinsic pathways of apoptosis in Cur-B-treated PCa cells.

3.6 Attenuation of Cur-B-mediated apoptosis

To subsequently affirm the involvement of caspase activation in Cur-B-mediated apoptosis in LNCaP cells, the MTT assay was performed in prostate cells pre-treated with caspase-8, -9, and -3 inhibitors (Z-IETD-FMK, Z-LEHD-FMK, and Z-DEVD-FMK, respectively) for 2 h followed by treatment with different doses of Cur-B for another 24 h (Figures 4B–D). It was witnessed that preliminary treatment with caspase inhibitors completely attenuated the apoptosis induced by Cur-B in PCa cells suggesting that caspase activation is tightly linked to apoptosis induction in LNCaP cells.

3.7 Cur-B impeded ΔΨm

The loss in mitochondrial viability is an established mediator of apoptosis. The alteration within ΔΨm indicates the initiation of apoptotic cell death through the intrinsic pathway. As explicitly seen in Figure 5, Cur-B exposure succeeded in reducing Mito-NIR-mediated fluorescence, clearly outlining the efficacy of Cur-B in altering the ΔΨm in LNCaP cells comparatively with untreated control. Intriguingly, the ΔΨm reduction in LNCaP cells was directly proportional with the Cur-B concentration.

3.8 Cur-B increased intracellular ROS

To delineate the mode of action in Cur-B, we therefore assessed the levels of intracellular ROS in Cur-B treated and untreated PCa cells by the DCFH-DA staining method. It was observed that the aggregation of DCHF-DA in treated cells indicated that Cur-B elevated the ROS generation in LNCaP cells (Figure 6A). Furthermore, the quantitative assessment of ROS generation was performed to validate the aforementioned results. As observed, in LNCaP cells, the intracellular level of ROS was enhanced by 41.71% ± 5.48%, 59.01% ± 4.59%, 79.42% ± 3.62%, 122.88% ± 4.66%, and 150.86% ± 4.94% in C33A cells at the indicated doses of

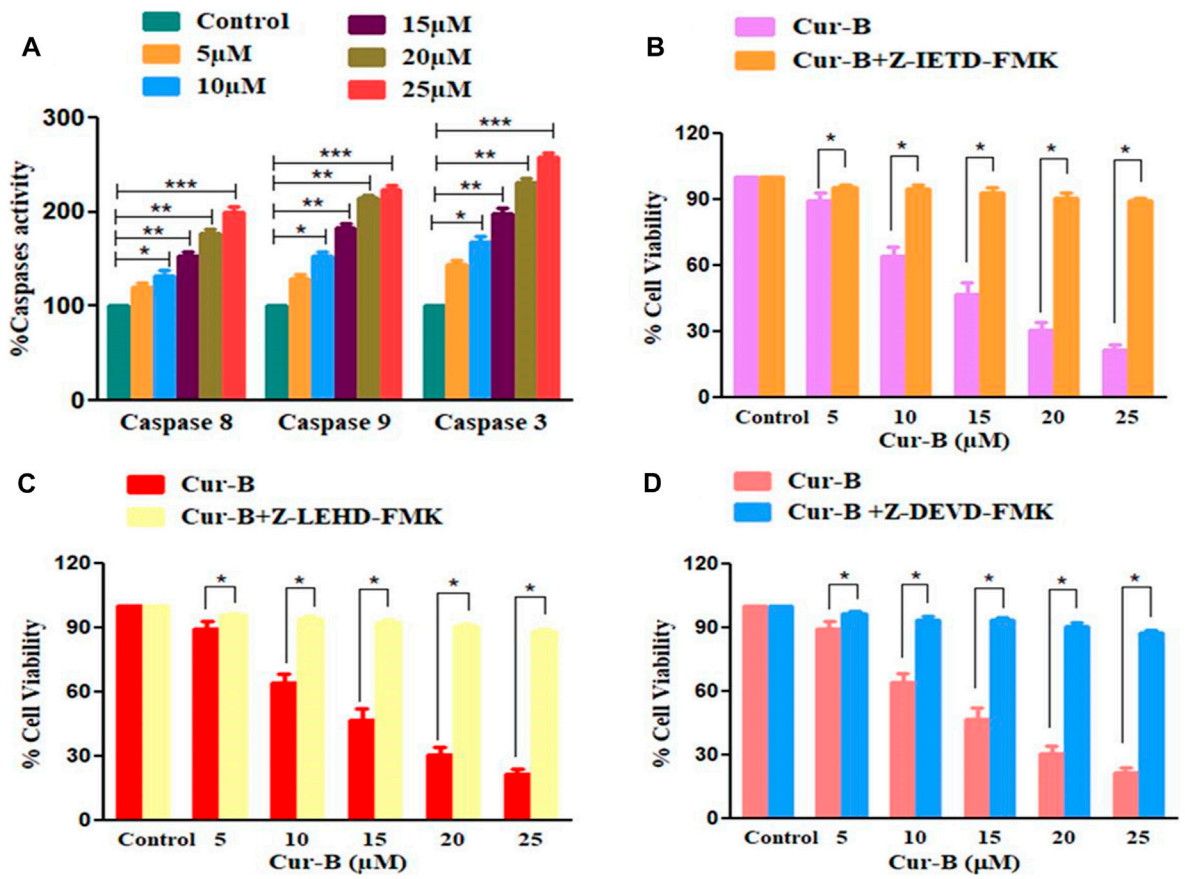

FIGURE 4
(A) Effect of Cur-B on the activation of caspase-8, -9, and -3 and **(B–D)** cytotoxic effects of Cur-B against the caspase inhibitor pre-treated LNCaP cells. Significance among different dosage groups were determined using one-way ANOVA followed by Dunnett's post-test and by two-tailed Paired Student's *t*-test as applicable, where * represents $p < 0.05$, ** $p < 0.01$, and *** $p < 0.001$ (GraphPad Prism, Ver. 5).

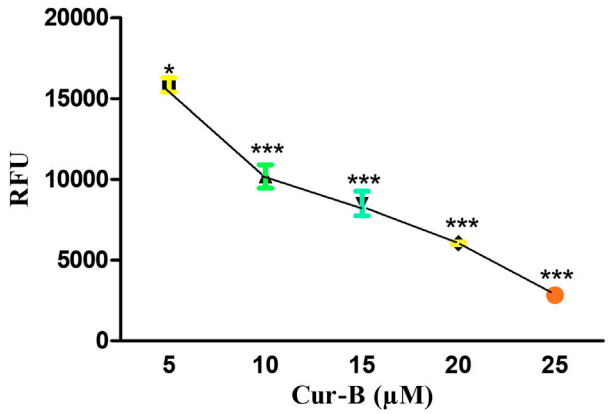

FIGURE 5
Cur-B mediates the decrease in NIR fluorescence in LnCap cells as compared to the control after staining with Mito-NIR dye indicating depolarized mitochondria. Scale bar 100 μm.

5, 10, 15, 20, and 25 μM Cur-B, respectively (Figure 6B). Therefore, these results suggested that Cur-B elevated the production of ROS in PCa cells in a dose-proportional trend.

3.9 Cur-B modulated the expression of key gene mRNA in androgen-dependent LNCaP cells

Real-time PCR analysis was performed to assess the effects of Cur-B on the gene expression of key genes of the cell cycle in LNCaP PCa cells. As shown in Figure 7, treatment with increasing doses of Cur-B decreased the mRNA expression of cyclinD1 and CDK4 to 0.85 ± 0.04, 0.76 ± 0.05, 0.52 ± 0.02, and 0.31 ± 0.04 folds; 0.93 ± 0.02, 0.76 ± 0.04, 0.57 ± 0.05, and 0.31 ± 0.03 folds, respectively, as compared with the control. In addition, the mRNA expression of $p21^{Cip1}$ was augmented by 1.34 ± 0.06, 1.54 ± 0.05, 1.76 ± 0.03, and 2.09 ± 0.05 folds, as compared to the control. Thus, it is suggested that Cur-B significantly modulated the expression level of cell cycle-related genes in PCa cells.

3.10 Cur-B modulated the mRNA expression of pro- and anti-apoptotic proteins

To investigate the effect of Cur-B on the expression of apoptotic and anti-apoptotic markers in androgen-dependent LNCaP PCa cells, qPCR was performed. It was found that the treatment, with

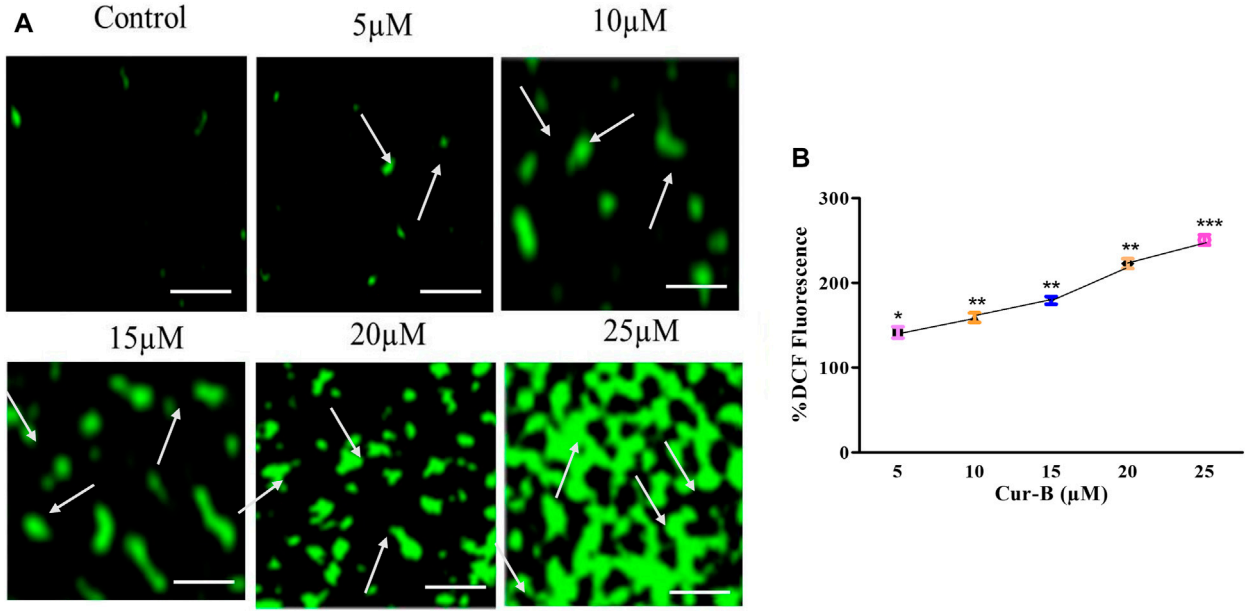

FIGURE 6
(A) Qualitative and **(B)** quantitative assessment of ROS levels within LnCap cells after treatment with various concentrations of Cur-B as compared to the control. Scale bar = 100 μμm.

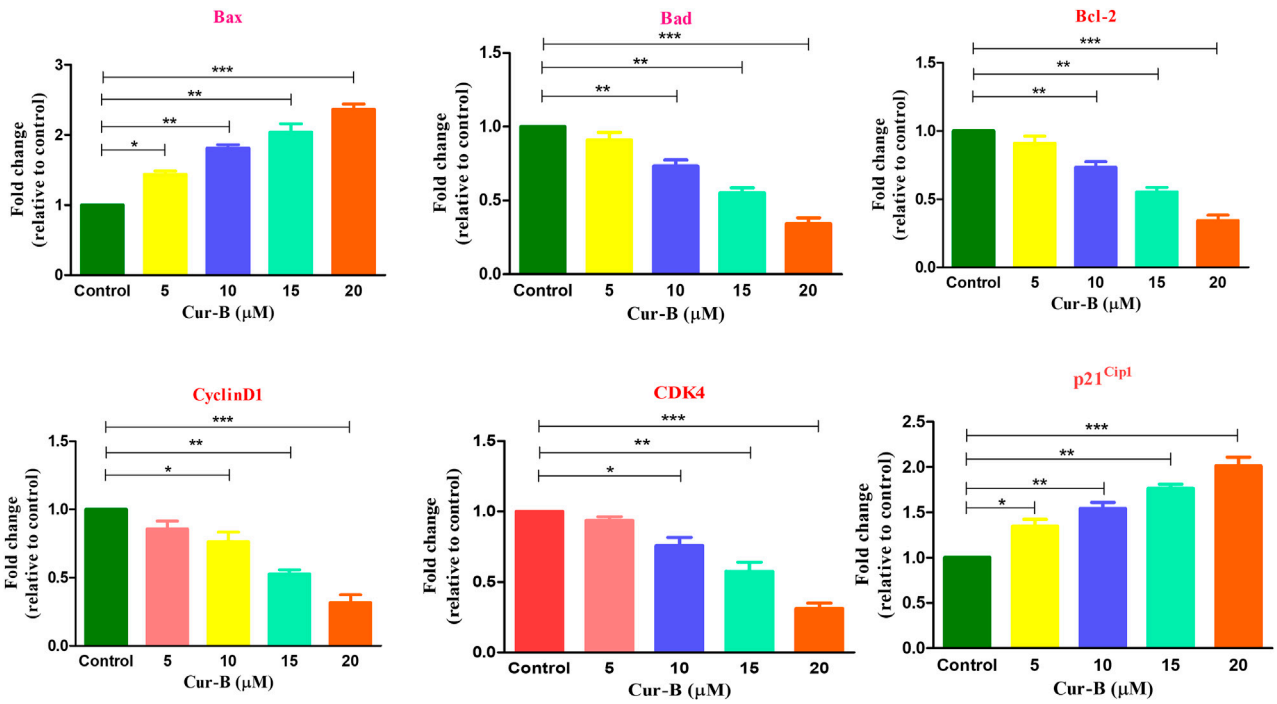

FIGURE 7
Effect of Cur-B in the modulation of apoptotic and cell cycle genes mRNA expression in LNCaP PCa cells. Significance among different dosage groups were determined using one-way ANOVA followed by Dunnett's post-test where * represents $p < 0.05$, ** $p < 0.01$, and *** $p < 0.001$ (GraphPad Prism, Ver. 5).

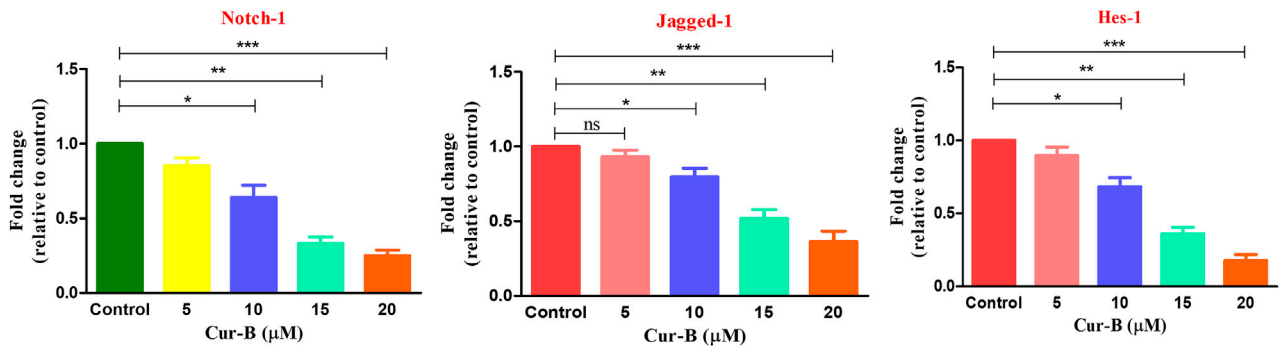

FIGURE 8
Effect of Cur-B on the key components of the Notch signaling pathway in LNCaP PCa cells. Significance among different dosage groups were determined using one-way ANOVA followed by Dunnett's post-test, where * represents $p < 0.05$, ** $p < 0.$, and *** $p < 0.001$ (GraphPad Prism, Ver. 5).

increasing concentrations of Cur-B (5, 10, 15, and 20 μM), declined in the gene expression of the anti-apoptotic marker, namely, Bcl2 by 0.91 ± 0.04, 0.73 ± 0.03, 0.55 ± 0.02, and 0.34 ± 0.03 folds. On the other hand, Cur-B treatment augmented the mRNA expression of Bax and Bad by 1.43 ± 0.03, 1.81 ± 0.04, 2.04 ± 0.09, and 2.36 ± 0.06 folds; and 1.32 ± 0.03, 1.53 ± 0.06, 1.79 ± 0.04, and 1.97 ± 0.05 folds, respectively, after 24-h treatment (Figure 7).

3.11 Cur-B mediates the downregulation of Notch signaling pathway in LNCaP cells

To decipher the underlying molecular mechanism of Cur-B-mediated apoptosis in androgen-dependent LNCaP cells, its efficacy on modulating the key components of the Notch signaling cascade was studied. We examined the effect of Cur-B on Notch-1, its ligand Jagged-1, and its downstream target Hes-1 in LNCaP cells. As demonstrated in Figure 8, Cur-B reduced the mRNA expression of Notch-1 mRNA within LNCaP cells in a dose-proportional manner. The increasing doses of Cur-B declined the expression of Notch-1 by 0.85 ± 0.04, 0.64 ± 0.06, 0.33 ± 0.03, and 0.25 ± 0.03 folds, as compared to the vehicle or control (Figure 8). Additionally, we also studied the effect of Cur-B on the expression of Jagged-1 (ligand of Notch-1) and Hes-1 (downstream target). It was found that Cur-B reduced the expression of Jagged-1 by 0.83 ± 0.03, 0.76 ± 0.07, 0.50 ± 0.04, and 0.26 ± 0.05 folds, whereas this reduction for Hes-1 was found to be 0.89 ± 0.03, 0.73 ± 0.03, 0.49 ± 0.05, and 0.21 ± 0.04 folds, as compared to the vehicle or control in PCa cells (Figure 8).

4 Discussion

Due to delayed diagnosis and inadequacy in the therapeutic strategies, PCa still remains the prime cause of cancer-associated demises in men (Dong, et al., 2019). It has been established that multiple dietary phytochemicals have been explored for their chemo-preventive potential and their capability to suppress the growth and proliferation rate, metastasis, invasion, and angiogenesis without incurring deleterious aftereffects. Thus, they could be a plausible adjunct in declining both the occurrence and mortality of cancer by obstructing, reversing, and delaying the process of tumorigenesis (Ranjan, et al., 2019). For decades, cucurbitacins which are also called tetracyclic triterpenes frequently found in the Cucurbitaceae family are used as complementary medicine (Budisan, et al., 2017). They hold the potential to be employed as plausible bioactive agents for suppressing the progression of cancer, and also, these compounds contain various structural modifications for anticipatory chemotherapeutic modalities. Henceforth, we studied and explored the mechanistic action and potential utility of Cur-B in PCa cells with the urge of finding a new and potent anticancer candidate. In the present investigation, we have demonstrated that Cur-B exhibited an anticancer effect, enhanced the generation of intracellular ROS, and apoptosis induction via downregulating Notch signaling pathways in PCa cells.

First, we demonstrated that treatment with Cur-B significantly suppressed the growth and proliferation of LNCaP PCa cells in a dose-proportional manner as assessed by the MTT assay. Thereafter, phase contrast microscopy has revealed that treatment of Cur-B has substantially altered the morphology of LNCaP cells by detaching them from the surface of flasks, rounding up of cells, and cellular constriction, which indicated Cur-B-mediated cytotoxicity in PCa cells.

Earlier investigations have suggested that various chemotherapeutic candidates suppress cellular proliferation by inducing apoptosis (Chen, et al., 2012). It is very well-known that chromatin condensation and fragmentation are the chief characteristics of apoptosis, which are associated with cell rounding, the decline in the volume of cells, and the formation of apoptotic bodies (Wong, 2011). Our results of DAPI staining suggested that Cur-B instigated apoptosis in androgen-dependent LNCaP cells. Furthermore, our results of PI staining also support the aforementioned results, where apoptotic nuclei stained with PI in LNCaP cells indicated that Cur-B induced apoptosis in PCa cells.

During apoptosis caspases (proteolytic enzymes) are activated from their inactive proenzymes form to their active form, which eventually leads to cleavage at specific aspartate sites. However, caspase-8 and -9 are initiators which undergo autocatalytic

activation and mediate the procession of executioner-caspase-3 (Shi, 2004). It was observed that the treatment of Cur-B mediates the dose-dependent activation of caspase-8, -9, and -3, which indicated that Cur-B mediates apoptosis induction via both extrinsic and intrinsic apoptotic pathways in human PCa cells. Moreover, Cur-B-induced cytotoxicity in LNCaP cells was substantially decreased and reduced by caspase-8, -9, and -3 inhibitors, thereby implicating the critical contribution of caspase-8, -9, and -3 during Cur-B-induced apoptosis. Thus, it is can be reasonably concluded that Cur-B might induce apoptosis in LNCaP cells via both caspase-dependent and independent pathways.

An upsurge in oxidative stress via the elevation of intracellular ROS levels is anticipated to modulate cellular homeostasis resulting in a decrease in the dissipation of mitochondrial membrane potential and DNA damage, eventually leading to apoptosis (Guo, et al., 2013). Moreover, DCHF-DA fluorescence staining substantiated that Cur-B mediates the augmentation of intracellular ROS in LNCaP cells. In addition, the quantitative evaluation of the intracellular ROS level was in support of microscopy and thus concluded that Cur-B induces ROS-mediated apoptosis in LNCaP cells.

Mitochondria are the chief cellular sites for the production of ROS which results in the loss of mitochondrial membrane potential leading to cytochrome c release (Zorov, et al., 2014). Our findings revealed that Cur-B treatment decreases the NIR fluorescence, which was indicative of mitochondrial depolarization in Mito-NIR dye-stained LNCaP PCa cells. Thus, Cur-B treatment effectively altered the mitochondrial membrane potential with increasing doses of Cur-B in PCa cells.

Various phases of cell cycle progression in cancer cells are positively regulated by cyclin-dependent kinases (CDKs) and negatively regulated by CDK inhibitors (CDKIs) (Shi, 2004). Our qPCR analysis revealed that treatment of Cur-B modulated the gene expression of cyclin D1, CDK4, and p21 in prostate cancer cells. Furthermore, Bcl-2 family members are also known as the regulators of apoptosis. Both pro- and anti-apoptotic proteins act in coordination to maintain the homeostatic balance within the cells (Moin, et al., 2021). Cur-B treatment significantly elevated the mRNA expressions of Bax and Bad and deflated the levels of Bcl-2 expression in LNCaP PCa cells.

Hyperactivated Notch signaling is found to be associated with various carcinomas of the breast, brain, cervical, lung, colon, head, and neck, renal cell carcinoma, acute myeloid, Hodgkin and large cell lymphomas, and pancreatic cancer (Singh, et al., 2019). However, Notch-1 is reportedly found to be overexpressed in prostate cancer cells (Guo, et al., 2011). Therefore, in the present investigation, our findings revealed that Cur-B obstructed the Notch signaling pathway in PCa cells. It was observed that gene expression studies have shown that Cur-B downregulated Notch signaling via the inhibition of Notch-1 and its ligand Jagged-1 within treated PCa cells along with the suppression of Hes-1, its downstream target. It is essential to target Notch as it may have chemo-preventive and anti-cancer effects, which could lead to decreased incidences of disease and ameliorated survival rate of patients. Although there are multiple drug candidates or therapeutic agents in the process to accomplish this goal, the Notch signaling pathway is often found to be hyperactivated in solid tumors and regulates cell fate decisions and maintains cancer stem cells. Additionally, the enhanced expression of Notch pathway components is clinically linked with poorer prognosis in various types of cancer. As a consequence, targeting Notch may have chemopreventive and anti-cancer effects, leading to decreased incidences of diseases and improved survival. However, various researchers are paying more attention in developing such therapeutic agents to achieve this goal. Utilizing the potential of naturally derived agents to target the Notch pathway offers the potential advantage of low toxicity to normal tissue. There are various terpenoids, such as glycyrrhizin, carvacrol, and andrographolide, which modulate Notch pathway components in a context-dependent manner. A recent study showed that the inhibitory effect of carvacrol on the cell cycle is associated with the downregulation of cyclinD1 and CDK4 and the upregulation of suppressor protein p21 in androgen-independent PC-3 human prostate cancer. Additionally, carvacrol blocked Notch-1 and Jagged-1 protein expression, resulting in the inhibition of the Notch signaling pathway (Khan et al., 2019). In addition, andrographolide is a lactone diterpenoid that constraints the growth of SW-480 cells through the inhibition of the Notch signaling pathway (Khan et al., 2021). Furthermore, glycyrrhizin, a triterpenoid, suppressed the growth of cervical cancer cells via targeting the key components of the Notch signaling pathway (Ahmad et al., 2022). Thus, terpenoids modulate Notch signaling in several types of cancer and concurrently decrease *in vitro* cell viability and *in vivo* tumor growth, suggesting a potential role for their clinical use to target Notch pathway components, either alone or in combination with current therapeutic agents.

Consequently, various scientists have switched their focus toward dietary natural compounds for targeting the Notch signaling cascade in cancer (Kiesel and Stan, 2022). Therefore, our present study strengthened the inhibitory role of Cur-B against the development and progression of PCa via the induction of apoptosis and alteration of the Notch signaling cascade. Furthermore, there are some shortcomings in utilizing Cur-B as an effective anticancer drug in which it exerts non-selective toxicity which indicates its toxic nature toward normal cells. However, under conditions of a reasonable dose and administration time, Cur-B exhibits no toxicity to experimental cells and animals. Various pharmacokinetic studies have demonstrated that Cur-B can be absorbed and cleared *in vivo* and is broadly distributed in internal organs in huge amounts with a high tissue to plasma ratio; however, its oral bioavailability is low (Dai et al., 2023).

5 Conclusion

To summarize, our report revealed that Cur-B holds a propitious apoptotic and anticancer potential against the androgen-dependent LNCaP cell line *in vitro*. Our results concluded that Cur-B suppressed the growth of PCa cells, which is associated with apoptosis induction, caspase activation, ROS generation, dissipation of mitochondrial membrane potential, and modulation of genes associated with apoptosis and cell cycle arrest. Thus, our data affirmed the plausible potential of Cur-B as an alternative and complementary medicine for the treatment of PCa.

Data availability statement

The raw data supporting the conclusion of this article will be made available by the authors, without undue reservation.

Author contributions

Conceptualization, AA; methodology, NK; software, TH and NK; validation, AA and TH; formal analysis, MO; investigation, TH and MO; resources, AA; data curation, TH; writing—original draft preparation, AA and TH; writing—review and editing, NK and MO; visualization, TH; supervision, AA; project administration, AA; funding acquisition, AA. All authors contributed to the article and approved the submitted version.

Funding

This research has been funded by Deputy for Research and Innovation, Ministry of Education through Initiative of Institutional Funding at University of Ha'il—Saudi Arabia through project number IFP-22 112.

Conflict of interest

The authors declare that the research was conducted in the absence of any commercial or financial relationships that could be construed as a potential conflict of interest.

Publisher's note

All claims expressed in this article are solely those of the authors and do not necessarily represent those of their affiliated organizations, or those of the publisher, the editors, and the reviewers. Any product that may be evaluated in this article, or claim that may be made by its manufacturer, is not guaranteed or endorsed by the publisher.

Supplementary material

The Supplementary Material for this article can be found online at: https://www.frontiersin.org/articles/10.3389/fphar.2023.1206981/full#supplementary-material

References

Ahmad, A., Tiwari, R. K., Almeleebia, T. M., Al Fayi, M. S., Alshahrani, M. Y., Ahmad, I., et al. (2021). Swertia chirayita suppresses the growth of non-small cell lung cancer A549 cells and concomitantly induces apoptosis via downregulation of JAK1/STAT3 pathway. *Saudi J. Biol. Sci.* 28 (11), 6279–6288. doi:10.1016/j.sjbs.2021.06.085

Ahmad, A., Tiwari, R. K., Saeed, M., Ahmad, I., and Ansari, I. A. (2022). Glycyrrhizin mediates downregulation of notch pathway resulting in initiation of apoptosis and disruption in the cell cycle progression in cervical cancer cells. *Nutr. cancer* 74 (2), 622–639. doi:10.1080/01635581.2021.1895234

Alafnan, A., Alamri, A., Hussain, T., and Rizvi, S. M. D. (2022). Cucurbitacin-B exerts anticancer effects through instigation of apoptosis and cell cycle arrest within human prostate cancer PC3 cells via downregulating JAK/STAT signaling cascade. *Pharm. (Basel).* 15 (10), 1229. doi:10.3390/ph15101229

Alafnan, A., Hussain, T., Rizvi, S. M. D., Moin, A., and Alamri, A. (2021). Prostate apoptotic induction and NFκB suppression by dammarolic acid: Mechanistic insight into onco-therapeutic action of an aglycone asiaticoside. *Curr. Issues Mol. Biol.* 43 (2), 932–940. doi:10.3390/cimb43020066

Altun, İ., and Sonkaya, A. (2018). The most common side effects experienced by patients were receiving first cycle of chemotherapy. *Iran. J. Public Health* 47 (8), 1218–1219.

Bilal, M., Javaid, A., Amjad, F., Youssif, T. A., and Afzal, S. (2022). An overview of prostate cancer (PCa) diagnosis: Potential role of miRNAs. *Transl. Oncol.* 26, 101542. doi:10.1016/j.tranon.2022.101542

Budisan, L., Gulei, D., Zanoaga, O. M., Irimie, A. I., Sergiu, C., Braicu, C., et al. (2017). Dietary intervention by phytochemicals and their role in modulating coding and non-coding genes in cancer. *Int. J. Mol. Sci.* 18 (6), 1178. doi:10.3390/ijms18061178

Cai, Y., Fang, X., He, C., Li, P., Xiao, F., Wang, Y., et al. (2015). Cucurbitacins: A systematic review of the phytochemistry and anticancer activity. *Am. J. Chin. Med.* 43 (7), 1331–1350. doi:10.1142/S0192415X15500755

Chen, J. C., Zhang, G. H., Zhang, Z. Q., Qiu, M. H., Zheng, Y. T., Yang, L. M., et al. (2008). Octanorcucurbitane and cucurbitane triterpenoids from the tubers of Hemsleya endecaphylla with HIV-1 inhibitory activity. *J. Nat. Prod.* 71 (1), 153–155. doi:10.1021/np0704396

Chen, X., Bao, J., Guo, J., Ding, Q., Lu, J., Huang, M., et al. (2012). Biological activities and potential molecular targets of cucurbitacins: A focus on cancer. *Anticancer Drugs* 23 (8), 777–787. doi:10.1097/CAD.0b013e3283541384

Dai, S., Wang, C., Zhao, X., Ma, C., Fu, K., Liu, Y., et al. (2023). Cucurbitacin B: A review of its pharmacology, toxicity, and pharmacokinetics. *Pharmacol. Res.* 187, 106587. doi:10.1016/j.phrs.2022.106587

Dong, L., Zieren, R. C., Xue, W., de Reijke, T. M., and Pienta, K. J. (2019). Metastatic prostate cancer remains incurable, why? *Asian J. Urol.* 6 (1), 26–41. doi:10.1016/j.ajur.2018.11.005

Farah, E., Li, C., Cheng, L., Kong, Y., Lanman, N. A., Pascuzzi, P., et al. (2019). NOTCH signaling is activated in and contributes to resistance in enzalutamide-resistant prostate cancer cells. *J. Biol. Chem.* 294 (21), 8543–8554. doi:10.1074/jbc.RA118.006983

Guo, C., Sun, L., Chen, X., and Zhang, D. (2013). Oxidative stress, mitochondrial damage and neurodegenerative diseases. *Neural Regen. Res.* 8 (21), 2003–2014. doi:10.3969/j.issn.1673-5374.2013.21.009

Guo, S., Liu, M., and Gonzalez-Perez, R. R. (2011). Role of Notch and its oncogenic signaling crosstalk in breast cancer. *Biochim. Biophys. Acta* 1815 (2), 197–213. doi:10.1016/j.bbcan.2010.12.002

Hwang, C. (2012). Overcoming docetaxel resistance in prostate cancer: A perspective review. *Ther. Adv. Med. Oncol.* 4 (6), 329–340. doi:10.1177/1758834012449685

Kaushik, U., Aeri, V., and Mir, S. R. (2015). Cucurbitacins - an insight into medicinal leads from nature. *Pharmacogn. Rev.* 9 (17), 12–18. doi:10.4103/0973-7847.156314

Khan, F., Singh, V. K., Saeed, M., Kausar, M. A., and Ansari, I. A. (2019). Carvacrol induced program cell death and cell cycle arrest in androgen-independent human prostate cancer cells via inhibition of notch signaling. *Anti-cancer agents Med. Chem.* 19 (13), 1588–1608. doi:10.2174/1871520619666190731152942

Khan, I., Mahfooz, S., Saeed, M., Ahmad, I., and Ansari, I. A. (2021). Andrographolide inhibits proliferation of colon cancer SW-480 cells via downregulating notch signaling pathway. *Anti-cancer agents Med. Chem.* 21 (4), 487–497. doi:10.2174/1871520620666200717143109

Kiesel, V. A., and Stan, S. D. (2022). Modulation of notch signaling pathway by bioactive dietary agents. *Int. J. Mol. Sci.* 23 (7), 3532. doi:10.3390/ijms23073532

Leong, K. G., and Gao, W. Q. (2008). The Notch pathway in prostate development and cancer. *Differentiation* 76 (6), 699–716. doi:10.1111/j.1432-0436.2008.00288.x

Marignol, L., Rivera-Figueroa, K., Lynch, T., and Hollywood, D. (2013). Hypoxia, notch signalling, and prostate cancer. *Nat. Rev. Urol.* 10 (7), 405–413. doi:10.1038/nrurol.2013.110

Moin, A., Wani, S. U. D., Osmani, R. A., Abu Lila, A. S., Khafagy, E. S., Arab, H. H., et al. (2021). Formulation, characterization, and cellular toxicity assessment of tamoxifen-loaded silk fibroin nanoparticles in breast cancer. *Drug Deliv.* 28 (1), 1626–1636. doi:10.1080/10717544.2021.1958106

Mourkioti, I., Angelopoulou, A., Belogiannis, K., Lagopati, N., Potamianos, S., Kyrodimos, E., et al. (2022). Interplay of developmental hippo-notch signaling pathways with the DNA damage response in prostate cancer. *Cells* 11 (15), 2449. doi:10.3390/cells11152449

Mukhtar, E., Adhami, V. M., and Mukhtar, H. (2014). Targeting microtubules by natural agents for cancer therapy. *Mol. Cancer Ther.* 13 (2), 275–284. doi:10.1158/1535-7163.MCT-13-0791

Olarewaju, O. O., Fajinmi, O. O., Arthur, G. D., Coopoosamy, R. M., and Naidoo, K. K. (2021). Food and medicinal relevance of Cucurbitaceae species in Eastern and Southern Africa. *Bull. Natl. Res. Cent.* 45, 208–215. doi:10.1186/s42269-021-00659-y

Ranjan, A., Ramachandran, S., Gupta, N., Kaushik, I., Wright, S., Srivastava, S., et al. (2019). Role of phytochemicals in cancer prevention. *Int. J. Mol. Sci.* 20 (20), 4981. doi:10.3390/ijms20204981

Sallam, A. M., Esmat, A., and Abdel-Naim, A. B. (2018). Cucurbitacin-B attenuates CCl4 -induced hepatic fibrosis in mice through inhibition of STAT-3. *Chem. Biol. Drug Des.* 91 (4), 933–941. doi:10.1111/cbdd.13160

Shi, Y. (2004). Caspase activation, inhibition, and reactivation: A mechanistic view. *Protein Sci.* 13 (8), 1979–1987. doi:10.1110/ps.04789804

Shou, J., Ross, S., Koeppen, H., de Sauvage, F. J., and Gao, W. Q. (2001). Dynamics of notch expression during murine prostate development and tumorigenesis. *Cancer Res.* 61 (19), 7291–7297.

Singh, R., Letai, A., and Sarosiek, K. (2019). Regulation of apoptosis in health and disease: The balancing act of BCL-2 family proteins. *Nat. Rev. Mol. Cell Biol.* 20 (3), 175–193. doi:10.1038/s41580-018-0089-8

Tiwari, R. K., Singh, S., Gupta, C. L., Pandey, P., Singh, V. K., Sayyed, U., et al. (2021). Repolarization of glioblastoma macrophage cells using non-agonistic dectin-1 ligand encapsulating TLR-9 agonist: Plausible role in regenerative medicine against brain tumor. *Int. J. Neurosci.* 131 (6), 591–598. doi:10.1080/00207454.2020.1750393

Varela, C., Melim, C., Neves, B. G., Sharifi-Rad, J., Calina, D., Mamurova, A., et al. (2022). Cucurbitacins as potential anticancer agents: New insights on molecular mechanisms. *J. Transl. Med.* 20 (1), 630. doi:10.1186/s12967-022-03828-3

Wong, R. S. (2011). Apoptosis in cancer: From pathogenesis to treatment. *J. Exp. Clin. Cancer Res.* 30 (1), 87. doi:10.1186/1756-9966-30-87

Zorov, D. B., Juhaszova, M., and Sollott, S. J. (2014). Mitochondrial reactive oxygen species (ROS) and ROS-induced ROS release. *Physiol. Rev.* 94 (3), 909–950. doi:10.1152/physrev.00026.2013

frontiers | Frontiers in Pharmacology

TYPE Review
PUBLISHED 03 August 2023
DOI 10.3389/fphar.2023.1187181

OPEN ACCESS

EDITED BY
Mitesh Patel,
Parul University, India

REVIEWED BY
Husain Yar Khan,
Wayne State University, United States
Arezoo Rajabian,
Mashhad University of Medical Sciences, Iran

*CORRESPONDENCE
Praveen Dhyani,
praveendhyani86@gmail.com
Ahmad Faizal Abdull Razis,
madfaizal@upm.edu.my
Monica Butnariu,
monicabutnariu@yahoo.com
Javad Sharifi-Rad,
javad.sharifirad@gmail.com

RECEIVED 15 March 2023
ACCEPTED 21 July 2023
PUBLISHED 03 August 2023

CITATION
Trivedi VL, Soni R, Dhyani P, Sati P, Tejada S, Sureda A, Setzer WN, Faizal Abdull Razis A, Modu B, Butnariu M and Sharifi-Rad J (2023), Anti-cancer properties of boswellic acids: mechanism of action as anti-cancerous agent. *Front. Pharmacol.* 14:1187181. doi: 10.3389/fphar.2023.1187181

Anti-cancer properties of boswellic acids: mechanism of action as anti-cancerous agent

Vijay Laxmi Trivedi[1], Ruchi Soni[2], Praveen Dhyani[3]*, Priyanka Sati[4], Silvia Tejada[5,6,7], Antoni Sureda[5,6,8], William N. Setzer[9,10], Ahmad Faizal Abdull Razis[11,12]*, Babagana Modu[12,13], Monica Butnariu[14]* and Javad Sharifi-Rad[15]*

[1]High Altitude Plant Physiology Research Centre (HAPPRC), HNB. Garhwal University (A Central University), Srinagar Garhwal, Uttarakhand, India, [2]Regional Centre for Organic and Natural Farming, Ghaziabad, Uttar Pradesh, India, [3]Institute for Integrated Natural Sciences, University of Koblenz, Koblenz, Germany, [4]Department of Biotechnology, Kumaun University, Bhimtal, Uttarakhand, India, [5]Laboratory of Neurophysiology, Department of Biology, University of the Balearic Islands, Palma de Mallorca, Spain, [6]Health Research Institute of Balearic Islands (IdISBa), Palma de Mallorca, Spain, [7]CIBER Fisiopatología de la Obesidad y Nutrición (CIBEROBN), Instituto de Salud Carlos III (ISCIII), Madrid, Spain, [8]Research Group in Community Nutrition and Oxidative Stress, University of the Balearic Islands—IUNICS, Palma de Mallorca, Spain, [9]Aromatic Plant Research Center, Lehi, UT, United States, [10]Department of Chemistry, University of Alabama in Huntsville, Huntsville, AL, United States, [11]Department of Food Science, Faculty of Food Science and Technology, Universiti Putra Malaysia, Selangor, Malaysia, [12]Natural Medicines and Products Research Laboratory, Institute of Bioscience, Universiti Putra Malaysia, Selangor, Malaysia, [13]Department of Biochemistry, Faculty of Science, University of Maiduguri, Maiduguri, Nigeria, [14]University of Life Sciences "King Mihai I" From Timisoara, Timis, Romania, [15]Facultad de Medicina, Universidad del Azuay, Cuenca, Ecuador

With the advent of highly effective plant-based medications with few or no side effects, the use of phytomedicines against complex diseases such as cancer is becoming more widespread. The broadly recognized pentacyclic triterpenes known as boswellic acids (BAs) are derived from the oleogum resin, or frankincense, extracted from the plant species of the genus *Boswellia*. The frankincense mixture contains various BA types, each having a different potential and helping treat certain cancers. This review focuses on details regarding the traits of the BAs, their roles as anti-cancer agents, the mechanism underlying their activities, and the function of their semi-synthetic derivatives in managing and treating certain cancers. The review also explores the biological sources of BAs, how they are conserved, and how biotechnology might help preserve and improve *in vitro* BA production. The review concludes that the BAs and their semi-synthetic derivatives are effective against a broad spectrum of cancer cell lines. The detailed information in the review can be helpful for researchers to gain more information about BAs and BA-based medications for efficient and cost-effective cancer treatments.

KEYWORDS

***Boswellia*, cancer, bioactive compounds, apoptosis, triterpenes**

Abbreviations: BA, boswellic acid; BBA, β-boswellic acid; KBA, 11-keto-β-boswellic acid; ABA, acetyl-β-boswellic acid; AKBA, acetyl-11-keto-β-boswellic acid; AMPK, AMP-activated protein kinase; GLUT1, glucose transporter 1 protein; mTOR, mammalian target of rapamycin; TMS, transcranial magnetic stimulation; EGFR, epidermal growth factor receptor; PVP, polyvinylpyrrolidone.

1 Introduction

The discovery of several plant-based chemicals with anti-cancer potential reinstated the ancient traditional knowledge of herbal medicines with the support of scientific knowledge. The identification of compounds such as vinblastine, vincristine, and taxol as anti-cancerous agents laid the fundamentals for the discovery of new phytochemical anti-cancerous agents (Dhyani et al., 2022). In recent years, the finding of phytochemicals with potential anti-cancer activities with no or fewer side effects has been accelerated. One such class of compounds, known as boswellic acids, is extracted from the *Boswellia* genus and is extensively used to treat various other chronic diseases. These include haemolytic, spasmolytic, antiviral, anti-inflammatory, hepatoprotective, gastroprotective, and anti-microbial properties (Sun et al., 2006; Agrawal et al., 2011; Hussain et al., 2017). Boswellic acids (BAs) are pentacyclic triterpenes derived from the frankincense tree. *Boswellia serrata*, popularly referred to as white guggal, Indian olibanum, Salai Guggal, and dhup, is the main source of BAs (Havel et al., 2002; Qurishi et al., 2012), although *B. carteri* (Roy et al., 2019), *B. sacra*, and *B. papyrifera* are additional sources of BAs (Al-Harrasi et al., 2019). Usually, the gum resins of *Boswellia* species were employed for various purposes, such as adhesives, cosmetic preparations, coating materials, and incense used in cultural ceremonies and rituals. It is one of the most important and widely used ingredients in traditional Ayurvedic and Unani remedies, which are exceptionally successful in treating a variety of inflammatory, gastrointestinal, hormonal, and microbiological illnesses (Siddiqui, 2011). The BAs are separated from the gum resin frankincense, which is made up of essential oil, mucous, and a lipophilic portion. The grades and content of this resin vary according to the species of *Boswellia* used to extract it (Saraswati and Agrawal, 2012). The gum resin of *Boswellia* species contains up to 12 different types of BAs among which four major types of BAs are β-BA, A-β-BA, KBA, and AKBA with different pharmacological properties such as anti-cancer, anti-angiogenic, anti-tumour, apoptosis induction, anti-proliferative, and anti-inflammatory, among others (Liu et al., 2002). Nevertheless, not all BAs have an identical activity or potency (Liu et al., 2002; Yadav et al., 2012). For example, KBA and AKBA are the most effective at suppressing cytokine production and inhibiting the enzymes responsible for inflammatory reactions. As a result, these have been described as effective treatments for a variety of chronic conditions (Siddiqui, 2011; Roy et al., 2019).

BAs have been reported to be beneficial in both the prevention and treatment of various cancers such as breast, bladder, cervix, prostate, colorectal, head and neck, liver, lung, and pancreas (Roy et al., 2019). Several semi-synthetic derivatives of the different BAs, that show chemotherapeutic promise against diverse cancerous human cell lines, were also synthesized further to enhance the BAs' anti-cancer action (Liu et al., 2002). Apoptosis, reducing angiogenesis of cancerous cells, obstructing blood flow to the tumour tissue, and down-regulating AKT phosphorylation are some of the mechanisms that BAs use to prevent cancer metastasis, depending on the type of cancer cells targeted (Liu et al., 2002; Uthaman et al., 2012).

This review examines BAs concerning their natural sources, conservation status, and *in vitro* biotechnological production potentials. This review also aims to describe the types of BAs, their chemical properties, semi-synthetic derivatives, and the mechanism of action of these compounds as anti-cancer agents. Scientific evidence supporting their categorization as anti-cancer substances is also presented, along with their modern and traditional applications as valuable drugs. The review will help increase the knowledge about plant-based anti-cancer therapeutics that includes various BAs and their derivatives.

2 General characterization of boswellic acid and its semi-synthetic derivatives

For centuries, frankincense (olibanum) extracted from the *Boswellia* tree, mainly from *B. serrata*, has been used as a source of BAs. Other species studied included *B. sacra, B. papyrifera*, and *B. carteri*, which are also used as BA sources worldwide (Al-Harrasi et al., 2019; Bongers et al., 2019). The resin of the *Boswellia* tree is composed of essential oil (5%–9%) and mucilage (6%–20%), the major component of the BAs, which has been quantified around 25%–35% of the resin acid mixture (Ennet, 2000; Al-Harrasi et al., 2021). BAs are a group of bioactive organic acids containing a pentacyclic triterpene and a β-carboxyl group at the C-4 position. BAs are grouped into two groups: the first one is ursane-type (β-BAs), and the second one is oleanane-type (α-BAs). Ursane-type BAs contain ursane triterpene skeleton-type and include β-boswellic acid (BA), 11-keto-β-boswellic acid (KBA), acetyl-β-boswellic acid (ABA), and acetyl-11-keto-β-boswellic acid (AKBA). Oleanane-type boswellic acid consisted oleanane structure and included α-boswellic acid (α-BA), 11-keto-α-boswellic acid (α-KBA), acetyl-α-boswellic acid (α-ABA), and acetyl-11-keto-α-boswellic acid (α-AKBA) (Shah et al., 2009; Al-Harrasi et al., 2019; Al-Harrasi et al., 2021; Schmiech et al., 2021) (Figure 1).

The resin containing the BAs is isolated from the *Boswellia* tree through wounding and subsequent tapping. These extraction procedures induced a chain of signaling process in the *Boswellia* tree involving gene expression and endogenous BAs production in the wounded location of the tree ultimately resulting in the clumpy frankincense (Khan et al., 2018). However, the BA content in the resin of the *Boswellia* genus varies at inter-species and intra-species levels. Studies showed considerable variation in BAs, their precursor content, and the type of BAs present in the resin of *B. serrata*, *B. sacra*, and *B. papyrifera* (Paul, 2012). For example, in the study of Paul (2012), *B. papyrifera* showed higher β-AKB concentration but lower concentrations of the other BAs and other secondary metabolites, whereas *B. serrata* showed lower β-KBA and β-AKBA concentrations and higher concentrations of α-BA and β-BA. Within a species, the BA content is greatly influenced by the micro- and macroclimatic conditions to which the *Boswellia* trees are subjected (Park et al., 2011). Geographical variations were also observed in various *Boswellia* spp. populations in the BA content of the resin (Al-Harrasi et al., 2018). Even the different tissues of the same tree showed variations in the BA content and the compositions in the studies; for instance, *B. sacra* roots were devoid of the BAs (Paul, 2012), whereas the leaves had trace amounts of β-ABA and β-AKBA. The amyrins are the BAs synthesized by the terpenoid biosynthetic pathway (MVA Pathway), the immediate precursor of the boswellic acids. β-Amyrin is the α-boswellic acid precursor, which is an oleanane, and α-amyrin is the β-boswellic acid

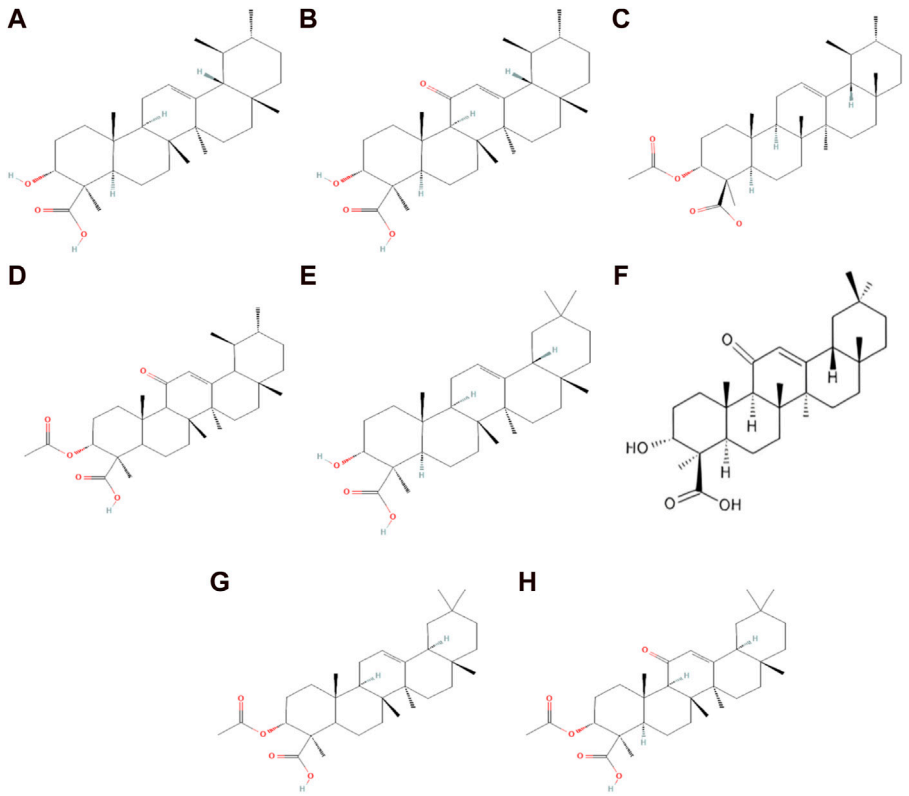

FIGURE 1
Chemical structure of ursane and oleanane-type boswellic acid. **(A)** β-Boswellic acid; **(B)**11-keto-β-boswellic acid; **(C)** acetyl-β-boswellic acid; **(D)** acetyl-11-keto-β-boswellic acid; **(E)** α-boswellic acid; **(F)** 11-keto-α-boswellic acid; **(G)** acetyl-α-boswellic acid; and **(H)** acetyl-11-keto-α-boswellic acid.

TABLE 1 Boswellic acids naturally found in *Boswellia* species.

Compound name	Chemical formula of the compound	Molecular weight of the compound (g/mol)
β-Boswellic acid	$C_{30}H_{48}O_3$	456.7
11-Keto-β-boswellic acid	$C_{30}H_{46}O_4$	470.7
3-Acetyl-β-boswellic acid	$C_{32}H_{50}O_4$	498.7
11-Hydroxy-β-boswellic acid	$C_{30}H_{48}O_4$	472.7
3-Acetyl-11-keto-β-boswellic acid	$C_{32}H_{48}O_5$	512.7
3-*O*-Acetyl-11-hydroxy-β-boswellic acid	$C_{32}H_{50}O_5$	514.7
3-*O*-Acetoxy-11-methoxy-β-boswellic acid	$C_{33}H_{52}O_5$	528.7
9,11-Dehydro-β-boswellic acid	$C_{30}H_{46}O_3$	454.7
3-*O*-Acetyl-9,11-dehydro-β-boswellic acid	$C_{32}H_{48}O_4$	496.7
α-Boswellic acid	$C_{30}H_{48}O_3$	456.7
11-Keto-α-Boswellic Acid	$C_{30}H_{46}O_4$	470.7
3-*O*-Acetyl-9,11-dehydro-α-boswellic acid	$C_{32}H_{48}O_4$	496.7
11-Hydroxy-α-boswellic acid	$C_{30}H_{48}O_4$	472.7
9,11-Dehydro-α-boswellic acid	$C_{30}H_{46}O_3$	454.7
3-*O*-Acetyl-α-boswellic acid	$C_{32}H_{50}O_4$	498.7

TABLE 2 Derivatives of the boswellic acids with their pharmacological action.

Precursor BA	Derivative	Pharmacological actions	Type of study and model	References
KBA	3-*O*-naproxen-β-boswellic acid	Anti-inflammatory potential and anti-arthritic properties	*In vivo* study, carrageenan-induced mice model, carrageenan-induced rat model	Chaturvedi et al. (2015)
KBA	3-*O*-naproxen-11-keto-β-boswellic acid	Anti-inflammatory and anti-arthritic activities	*In vivo* study, carrageenan-induced mice model, carrageenan-induced rat model	Chaturvedi et al. (2015)
KBA	3-*O*-ibuprofen-β-boswellic acid	Anti-inflammatory activity	*In vivo* study, carrageenan-induced mice model, carrageenan-induced rat model	Chaturvedi et al. (2015)
KBA	3-*O*-aspirin-β-boswellic acid	Anti-inflammatory activity	*In vivo* study, carrageenan-induced mice model, carrageenan-induced rat model	Chaturvedi et al. (2015)
KBA	3-*O*-aspirin-11-keto-β-boswellic acid	Anti-inflammatory activity	*In vivo* study, carrageenan-induced mice model, carrageenan-induced rat model	Chaturvedi et al. (2015)
KBA	3-*O*-cinnamyl-11-keto-β-boswellic acid	Anti-inflammatory activity	*In vivo* study, carrageenan-induced mice model, carrageenan-induced rat model	Chaturvedi et al. (2015)
β-BA	11α-Hydroxy-β-boswellic acid	Inhibited 5-lipoxygenase and cathepsin G and promoted apoptosis	*In vitro*, intact human neutrophils and purified cathepsin G	Koeberle et al. (2018)
β-BA	11β-Hydroxy-β-boswellic acid	Weak 5-LO inhibitors	*In vitro*, intact human neutrophils	Koeberle et al. (2018)
β-BA	3-*O*-oxaloyl-β-boswellic acid	Inhibits cathepsin G and promotes apoptosis	*In vitro*, purified cathepsin G	Koeberle et al. (2018)
β-BA	3-*O*-succinoyl-β-boswellic acid	Weak 5-LO inhibitors	*In vitro*, intact human neutrophils	Koeberle et al. (2018)
KBA	3-*O*-succinoyl-11-keto-β-boswellic acid	Weak 5-LO inhibitors	*In vitro*, intact human neutrophils	Koeberle et al. (2018)
β-BA	3-*O*-glutaroyl-β-boswellic acid	Inhibits cathepsin G and promotes apoptosis	*In vitro*, purified cathepsin G	Koeberle et al. (2018)
KBA	3-*O*-glutaroyl-11-keto-β-boswellic acid	Weak 5-LO inhibitors	*In vitro*, intact human neutrophils	Koeberle et al. (2018)
β-BA	3-*O*-carboxymethyl-β-boswellic acid	Inhibits cathepsin G and promotes apoptosis	*In vitro*, purified cathepsin G	Koeberle et al. (2018)
KBA	3-*O*-carboxymethyl-11-keto-β-boswellic acid	Weak 5-LO inhibitors	*In vitro*, intact human neutrophils	Koeberle et al. (2018)
AKBA	2,3-Dehydro-11-keto-β-boswellic acid	Cytotoxic	*In vitro*, human tumour cell lines	Serbian et al. (2018)
AKBA	2α-Hydroxy-11-keto-β-boswellic acid	Cytotoxic	*In vitro*, mouse monocyte–macrophage RAW 264.7 cells	Wang et al. (2013)
AKBA	1α-Hydroxy-2,3-dehydro-11-keto-β-boswellic acid	Cytotoxic	*In vitro*, mouse monocyte–macrophage RAW 264.7 cells	Wang et al. (2013)
AKBA	11-Keto-β-boswellic acid methyl ester	Cytotoxic	*In vitro*, mouse monocyte–macrophage RAW 264.7 cells	Wang et al. (2013)
AKBA	2,3-Dehydro-11-keto-β-boswellic acid methyl ester	Cytotoxic	*In vitro*, mouse monocyte–macrophage RAW 264.7 cells	Wang et al. (2013)
α BA	2α-Cyano-3-en-X-one of methyl boswellates	Growth inhibition of the cancerous cells, cytotoxic, anti-inflammatory, and pro-differentiating activities	*In vitro*, cancer cell lines	Ravanan et al. (2011)
βBA	2β-Cyano-3-en-X-one of the methyl boswellates	Growth inhibition of the cancerous cells, cytotoxic, anti-inflammatory, and pro-differentiating activities	*In vitro*, mouse monocyte–macrophage RAW 264.7 cells	Wang et al. (2013)
βBA	3α-Propionyloxy-β-boswellic acid	Cytotoxicity toward human cancerous cell lines by suppressing the PI3K pathway	*In vitro*, human cancer cell lines and *in vivo*, murine tumour models (Swiss albino mice)	Qurishi et al. (2012)
βBA	3α-Butyryloxy-β-boswellic acid	PI3K-mediated apoptosis	*In vitro*, mouse monocyte–macrophage RAW 264.7 cells	Wang et al. (2013)

(Continued on following page)

TABLE 2 (*Continued*) Derivatives of the boswellic acids with their pharmacological action.

Precursor BA	Derivative	Pharmacological actions	Type of study and model	References
KBA	3-Cinnamoyl-11-keto-β-boswellic acid	Proapoptotic effects and anti-proliferative	*In vitro*, cancer cell lines, and *in vivo*, PC-3 prostate cancer xenografts	Morad et al. (2013)
KBA	7β-Hydroxy-11-keto-β-boswellic acid	NO production inhibition by LPS-induced mechanism without declining cell viability in macrophages (RAW 264.7)	*In vitro*, mouse monocyte–macrophage RAW 264.7 cells	Wang et al. (2013)
KBA	7β,22β-Dihydroxy-11-keto-β-boswellic acid	NO production inhibition by LPS-induced mechanism without declining cell viability in macrophages (RAW 264.7)	*In vitro*, mouse monocyte–macrophage RAW 264.7 cells	Wang et al. (2013)
Acetyl-α-boswellic acid	3α-Acetyl-11-keto-α-boswellic acid	Activates apoptosis in androgen-independent chemo-resistant cancerous cells *in vivo* and *in vitro* by caspase-3 activation and DNA fragmentation induction	*In vitro*, human PC-3 prostate cancer cells and *in vivo*, xenograft model	Büchele et al. (2006)
3-Acetyl-11-keto-β-boswellic acid	7β-Hydroxyl-3-acety-11-keto-β-boswellic acid	NO production inhibition by LPS-induced mechanism without declining cell viability in macrophages (RAW 264.7)	*In vitro*, RAW 264.7 macrophage cells	Sun et al. (2013)
3-Acetyl-11-keto-β-boswellic acid	7β,16α-Dihydroxy-3-acety-11-keto-β-boswellic acid	NO production inhibition by LPS-induced mechanism without declining cell viability in macrophages (RAW 264.7)	*In vitro*, RAW 264.7 macrophage cells	Sun et al. (2013)

precursor, which is an ursane. The different BA compounds extracted from the frankincense (resin) of *Boswellia* are listed in Table 1.

The main problem with most of the BAs is their low bioavailability, particularly for AKBA and KBA, which, in turn, raises questions about the pharmacological relevance of their bioactivities in animal and human research (Du et al., 2015). Synthesis of new derivatives by chemical modification and biotransformation of BAs can be an option (Table 2). BA derivatives have been synthesized for the discovery of new potent drugs, particularly the anti-cancer and tumour suppressors (Meng et al., 2005; Chaturvedi et al., 2015; Koeberle et al., 2018; Serbian et al., 2018; Shamraiz et al., 2020).

3 Mechanism of anti-tumour action of boswellic acid

BAs have been investigated for decades and are found to exhibit robust anti-cancer properties *in vitro* and *in vivo* (Table 3). Different isomers and extracts from the acids exhibit anti-cancer characteristics with distinct mechanisms in many types of cancer. The mechanisms of activity of BAs comprise a variety of targets, including the enzymes of angiogenesis and others such as topoisomerases, 5-lipoxygenase (5-LO), cytochrome P450, and mitogen-activated protein kinase (MAPK, especially p38) which are either promoted or inhibited by BAs (Iram et al., 2017).

B. serrata gum resin extract (methanolic) showed the occurrence of triterpenoids, β-boswellic acid, and its analogues. Huang et al., 2000 reported that b-BA naturally occurring triterpenoids with their derivatives had been part of traditional medicine for cancer treatment (Huang et al., 2000). Several scientific studies have also shown *Boswellia*'s pentacyclic triterpenes as one of the most promising anti-cancer agents (Poeckel and Werz, 2006; Yuan et al., 2013; Al-Bahlani et al., 2020). AKBA and KBA are assessed by active inhibition of topoisomerase I and IIa, which restricts the growth of the cells and their proliferation and induces apoptosis through a pathway dependent on caspase-8 in human leukaemia, hepatoma, colon, and in a wide range of cancer cell lines (Xia et al., 2005; Suhail et al., 2011). Moreover, a chemoproteomic study based on mass spectrometry indicated that b-BAs also interact with the ribosomal proteins, inhibit protein synthesis, and thus further modulate cancer progression (Casapullo et al., 2016). Morphological alterations were noticed in treated HL-60 cells with AKBA, which is a signal of apoptosis of the cells. BA, 3-*O*-acetyl-β-boswellic acid, AKBA, and 3-*O*-acetyl-11-keto-boswellic acid showed anti-tumour activity and inhibition of DNA, RNA, and proteins synthesis in human leukaemia HL60 cells in a dose-dependent manner (Shao et al., 1998; Hoernlein et al., 1999).

AKBA showed cytotoxic action against three treatment-resistance triple-negative breast cancer cell lines (TNBC) and apoptosis in MDA-MB-231 xenografts in the *in vitro* study (Schmiech et al., 2021). AKBA diminished the viability of the cell in H460, H1299, A549, and BEAS-2B cell lines. In A549, cells caused cell cycle arrest at the G0/G1 phase, thus suppressing the clone formation and promoting the cellular apoptosis. It also reduced the expression of LC3A/B-I and LC3A/B-II, along with Beclin-1 proteins and inhibition of the signalling pathway of PI3K/Akt. It also suppressed protein expression and autolysosome formation (Lv et al., 2020). The latest β-isomer synthesized and characterized as 11-keto-boswellic acid (KBA) was discovered to have cytotoxic effects against three treatment-resistant triple-negative breast cancer (TNBC) cell lines *in vitro* and to cause apoptosis in MDA-MB-231 xenografts *in vivo* (Schmiech et al., 2021).

Recently, β-BA has been shown to inhibit precancerous breast lesions by suppressing the glycolysis pathway and reducing ATP production in MCF-10AT cells without damaging normal MCF-10A. It is also observed to suppress glycolysis which activates the

TABLE 3 Scientific studies emphasizing boswellic acids as a promising anti-cancer agent.

Boswellic acids	Type of cancer	Inhibitory activities on cell lines	Techniques to analyse the inhibitory activities	References
BAA (o- and b-boswellic acid acetate)	Metastatic, melanoma, fibrosarcoma	Mouse melanoma cells BI6F10 and human fibrosarcoma cell line HT-1080	MTT proliferation assay, cell viability analysis, gelatin zymography, topoisomerase-II catalytic assay, flow cytometry, and DNA fragmentation	Zhao et al. (2003)
AKBA	Prostate cancer	Inhibited cellular proliferation on LNCaP cell lines associated with reduced androgen receptor expression	Flow cytometry, MTT assay, transient transfection assay, electrophoretic mobility shift assay, and western blot analysis	Yuan et al. (2008)
AKBA	Colon cancer	Initiated apoptosis in HT 29 colon cancer cells	Flow cytometry and caspase assay on cell lines	Liu and Duan (2009)
AKBA	Pancreatic cancer	Induced cellular proliferation inhibition of AsPC-1, BxPC-3, and MIAPaCa-2	MTT proliferation assay, western blot, and immune histochemical analysis PANC-28, an orthotopic mouse model	Park et al. (2011)
BA	Breast cancer	Inhibited MCF-7 cell proliferation and potentiated the cell death	Caspase activity assay, cytokine ELISA assay, superoxide dismutase activity, glutathione essay, and catalase activity	Saraswati and Agrawal (2012)
BA	Colorectal cancer	Orthotopic mouse model	Proliferative index and nuclear factor-κB suppression	Yadav et al. (2012)
BSE (*Boswellia serrata* extract)	Pancreatic cancer	Cytotoxic effect on A375, MIA-PaCa, mouse melanoma, and human pancreatic cancer cell line	DNA fragmentation assay	Uthaman et al. (2012)
BA	Brain tumour	Exhibited antioxidant and analysing anti-inflammatory effects on p65/NF-κB and leukotriene B4 expression	Growth factors and interleukins production (vascular endothelial growth factor, IL-8 and IL-6, MMP-9, and CXCL-12)	Barbarisi et al. (2019)
AKBA	Lung cancer	Inhibited cell growth in A549, H460, H1299, and BEAS-2B cell lines	CCK-8 assay and flow cytometry	Lv et al. (2020)
11-Keto-boswellic acids (KBA)	Breast cancer	Three triple-negative breast cancer (TNBC) cell lines resistant to therapy were used to induce apoptosis in MDA-MB-231 xenografts *in vivo*	High-resolution mass spectrometry (HR-MS) and NMR spectroscopy and HPLC-MS/MS method developed	Schmiech et al. (2021)
KBA and AKBA	Lung cancer	Inhibited cell proliferation in eight cell lines	HPLC analysis, MTT assay, DPPH scavenging, and ABTS assays	Gupta et al. (2022)
β-Boswellic acid	Breast precancerous lesions	MCF-10A and MDA-MB-231 cell lines	Kyoto Encyclopedia of Genes and Genomes (KEGG) analysis, metabolism-related assays, and molecular docking analysis	Bie et al. (2022)

AMPK pathway and inhibits the mTOR pathway to limit MCF-10AT proliferation. In the same study, analysis using molecular docking suggested that the target of β-BA might be GLUT1. The GLUT1 forced expression could rescue the suppression of glycolysis and induce survival checks on MCF-10AT (Bie et al., 2022).

In another study, the effect of β-BA and AKBA has examined in nine human glioma stem-like cells and five glioma-initiating cell lines to analyse the acute growth inhibitory mechanism. The same study includes the anti-clonogenic characteristics along with the application of temozolomide (TMZ) or irradiation. The findings were correlated with previous findings indicating BA cytotoxicity in glioblastoma at low molecular concentrations. A significant synergistic action after application with irradiation and transcranial magnetic stimulation (TMS) was also observed (Schneider and Weller, 2016). These studies have provided insights into the different underlying mechanisms acquired by BAs for their anti-tumour actions. These findings can support the future development of their prospective as anti-inflammatory and anti-cancer drugs. The detailed mechanism of action of BAs as promising anti-cancer agents is depicted in the schematic diagram shown in Figure 2.

4 Studies that confirmed the anti-cancer properties of boswellic acids

BAs extracted from the plant *Boswellia serrata* are considered as the essential active constituents to treat many inflammatory diseases, either acute or chronic. Along with their potential as anti-arthritic, anti-asthmatic, anti-rheumatic, anti-diarrhoeal, and anti-hyperlipidemic, actions they also possess anti-microbial, hepatoprotective, analgesic, immunomodulatory actions, and anti-cancer characteristics. These acids have been found to exhibit very effective anti-inflammatory as well as anti-cancer activities in different models both *in vitro* and *in vivo*. They showed anti-cancer potential against a range of malignant tumours, and many semi-synthetic BAs illustrate outstanding cytotoxic effects (Hussain et al., 2021).

4.1 Cytotoxic effect of boswellic acid on colorectal cancer

Colorectal cancer is a multifaceted disease with epigenetic and genetic mutations in a wide range of oncogenes and tumour

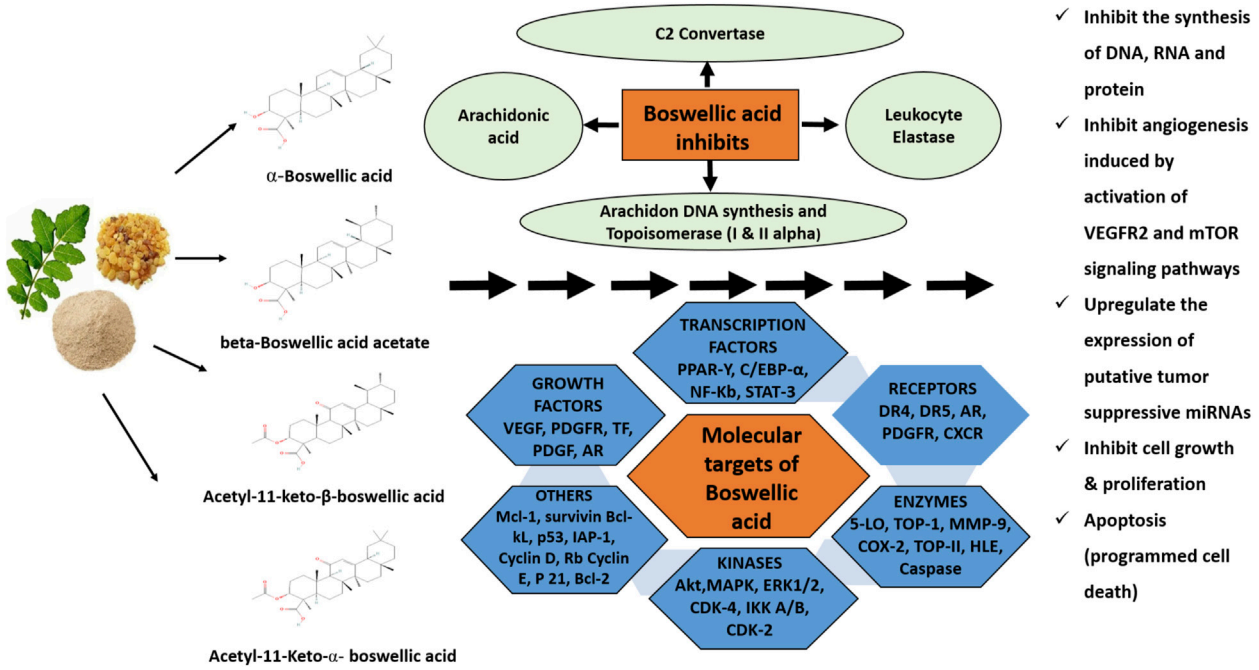

FIGURE 2
Schematic diagram of mechanisms of the boswellic acids extracted from the plant *Boswellia serrata*. These acids exhibit anti-cancer activities against different cancers by acting on numerous targets like 5-lipoxygenase (5-LO), topoisomerases, angiogenesis, and cytochrome p450 enzymes which finally lead to a reduction in cancer cell growth and apoptosis.

suppressor genes (Parmar and Easwaran, 2022). AKBA shows chemo-preventive characteristics capable of targeting principle oncogenic proteins, including 5-lipoxygenase and nuclear factor-kappa B. These BAs are known to modulate specific microRNA (miRNA) pathways due to their chemo-preventive effects. In the pathways, let-7 and miR-200 are both putative tumour-suppressive miRNAs. AKBA showed significantly upregulated expression of both families in various colorectal cancer cell lines. miRNA knockdown has been shown to inhibit let-7 and enable increased cancer cell propagation, migration, and invasion. AKBA modulates the expression of various downstream targets of the miR-200 and let-7 families (vimentin, CDK6, and E-cadherin). Similar findings of inducing modulation of these downstream genes have been observed in CRC cells orthotopically implanted in nude mice. This study gives novel evidence for the ability of BAs to regulate cellular epigenetic mechanisms that emphasise their anti-cancer characteristics and further highlight their potential in the prevention and treatment of CRC (Takahashi et al., 2012).

4.2 Anti-tumor effect of boswellic acid in human colonic adenocarcinoma

Ranjbarnejad et al. (2017) investigated the methanolic extract of Boswellia serrata for its anti-cancer activity on human colon cancer cells. This study establishes that the methanolic extract decreased the expression of cyclooxygenase-2 gene and its terminal end products, such as microsomal prostaglandin E synthase-1 (mPGES-1), vascular endothelial growth factor (VEGF), C-X-C chemokine receptor type 4 (CXCR4), matrix metalloproteinase-2 (MMP-2), MMP-9, and hypoxia-inducible factor-1 (HIF-1). The study, therefore, suggested that the *B. serrata* extract can be a potential agent to inhibit the proliferation, angiogenesis, and migration in colorectal cancer. Similarly, another study (Wang et al., 2018) also finds that BA can be used for the growth suppression of HCT-116 colon cancer cells. With an IC50 value of 15 uM, BA altered the Bax/Bcl-2 ratio in the HCT-116 cells. Therefore, a general understanding can be developed of the usage of BA as an anti-cancerous agent for human colon cancer, provided further *in vivo* detailed studies are performed.

4.3 Role of boswellic acid in growth suppression of human pancreatic tumours and its metastasis

BA acts as a growth suppressor for human pancreatic tumours in a mouse model by interacting with multiple targets and also limiting its metastasis. AKBA activity was studied in an *in vitro* model of orthotopic nude mice against human PaCa; it revealed that AKBA inhibited the proliferation of four PaCa cell lines. It comprised PANC-28, AsPC-1, and with p53 and K-Ras mutations, BxPC-3 with wild-type K-Ras and p53 mutation were also included. AKBA also inhibited the metastasis of the PaCa in the liver, spleen, and lungs in the same mouse model. The study indicated the potential of AKBA as an anti-tumour agent that exhibited an ability to suppress human pancreatic tumour growth and metastasis with multiple target modulations (Park et al., 2011).

4.4 Inhibitory activity of boswellic acids against human leukaemia

Four BAs of *B. serrata*: β-boswellic acid, 11-keto-β-boswellic acid, 3-O-acetyl-β-boswellic acid, and 3-O-acetyl-11-keto-β-boswellic acid were evaluated for their anti-cancer properties. They were examined to restrict the DNA, RNA, and protein synthesis in human leukaemia HL-60 cells. 3-*O*-Acetyl-11-keto-β-boswellic acid significantly inhibited the synthesis of DNA, RNA, and proteins. This compound had an irreversible effect on DNA synthesis, inhibiting the HL-60 cellular growth without affecting cell viability. The result of the study revealed a significant potential of this compound in the regulation of human leukaemia proliferation (Shao et al., 1998).

4.5 Apoptotic effect of boswellic acid in liver cancer cells

Only one study explored the anti-proliferative and apoptotic effect on Hep G2 liver cancer cells of keto-β-boswellic acid and acetyl-keto-β-boswellic acid. Following their application on the cell's DNA synthesis, apoptosis and cell proliferation were examined. The apoptotic pathway was explored employing specific caspase inhibitors, which revealed the decreased cell viability and thymidine amalgamation and enlarged percentage of sub-G1 in the G1 phase. BAs significantly influenced apoptosis, complemented by the activation of these caspase inhibitors. Hence, the study led to the possibility of using the BAs for anti-cancer and anti-proliferation effects in the liver Hep G2 cells (Liu et al., 2002).

4.6 Apoptosis in prostate cancer cells *in vitro* and *in vivo* by boswellic acid

In androgen-independent PC-3 cells, a chemo-resistant prostate cancerous line, acetyl-β-boswellic acid, and acetyl-11-keto-β-boswellic acid inhibited their growth. They promoted the death of the cell *in vitro* as well as *in vivo* models (Syrovets et al., 2005). For analysing apoptosis, parameters like DNA fragmentation and mitochondrial cytochrome C release were examined in cultured PC-3 cells. The underlying molecular mechanism involved the inhibition of signalling of the NF-κB (constitutively activated) by IκB kinase (IKK) activity interruption. The IKK inhibition showed specificity because the signalling through the interferon-stimulated response element remained unchanged. The study was further confirmed in nude mice carrying PC-3 tumours, where the systemic application of AKβBA-γ- cyclodextrin reduced tumour growth. This treatment also activated apoptosis without detectable systemic toxicity. AKβBA and related compounds acting on IKK provide a novel approach for treating chemo-resistant human tumours, including androgen-independent human prostate cancers.

5 Conclusion

BAs and their semi-synthetic derivatives are effective against a broad spectrum of cancer cell lines. They have a minimal potential for resistance due to the multiple ways they operate in the cancer cell lines. The ability of BAs to control cellular epigenetic mechanisms highlights their anti-cancer properties, as they promote apoptosis in cancer cells and inhibit the malignant primary metabolic pathways and DNA, RNA, and protein synthesis. BAs are only present in the *Boswellia* genus, but they display several kinds and contents according to the species. Globally, the survival of the natural sources of frankincense is threatened by over-extraction to obtain BAs and other anthropogenic factors, including climate change. Seed dormancy and slower growth rate make it worse, so more *in vitro* conservation methods are required to protect these plant species. More research is necessary to develop technology for *in vitro* production of BAs from *Boswellia* spp., as well as more clinical trials and scientific studies to validate its anti-cancer potential and obtain novel cancer treatment.

Author contributions

Conceptualization and design were performed by JS-R; investigation, data curation, and writing were performed by VT, RS, PS, and BM; review and editing were performed by PD, ST, AS, WS, AF, MB, and JS-R; validation and supervision were done by JS-R. All authors contributed to the article and approved the submitted version.

Conflict of interest

The authors declare that the research was conducted in the absence of any commercial or financial relationships that could be construed as a potential conflict of interest.

Publisher's note

References

Agrawal, S. S., Saraswati, S., Mathur, R., and Pandey, M. (2011). Antitumor properties of Boswellic acid against Ehrlich ascites cells bearing mouse. *Food Chem. Toxicol.* 49 (9), 1924–1934. doi:10.1016/j.fct.2011.04.007

Al-Bahlani, S., Burney, I. A., Al-Dhahli, B., Al-Kharusi, S., Al-Kharousi, F., Al-Kalbani, A., et al. (2020). Boswellic acid sensitizes gastric cancer cells to Cisplatin-induced apoptosis via p53-mediated pathway. *BMC Pharmacol. Toxicol.* 21, 64–10. doi:10.1186/s40360-020-00442-1

Al-Harrasi, A., Hussain, H., Csuk, R., and Khan, H. (2019). Chemistry of boswellic acids and other terpenoids. In (pp. 9–66). doi:10.1016/B978-0-08-102441-6.00002-5

Al-Harrasi, A., Khan, A. L., Asaf, S., and Al-Rawahi, A. (2019). "Frankincense tree physiology and its responses to wounding stress," in *Biology of genus Boswellia* Editors A. Al-Harrasi, A. L. Khan, S. Asaf, and A. Al-Rawahi (Berlin, Germany: Springer International Publishing), 53–70. doi:10.1007/978-3-030-16725-7_4

Al-Harrasi, A., Khan, A. L., Rehman, N. U., and Csuk, R. (2021). Biosynthetic diversity in triterpene cyclization within the Boswellia genus. *Phytochemistry*, 184, 112660. doi:10.1016/j.phytochem.2021.112660

Al-Harrasi, A., Rehman, N. U., Khan, A. L., Al-Broumi, M., Al-Amri, I., Hussain, J., et al. (2018). Chemical, molecular and structural studies of Boswellia species: β-Boswellic aldehyde and 3-epi-11β-Dihydroxy BA as precursors in biosynthesis of boswellic acids. *PLoS One* 13 (6), e0198666. doi:10.1371/journal.pone.0198666

Barbarisi, M., Barbarisi, A., De Sena, G., Armenia, E., Aurilio, C., Libutti, M., et al. (2019). Boswellic acid has anti-inflammatory effects and enhances the anticancer activities of Temozolomide and Afatinib, an irreversible ErbB family blocker, in human glioblastoma cells. *Phytotherapy Res.* 33 (6), 1670–1682. doi:10.1002/ptr.6354

Bie, F., Zhang, G., Yan, X., Ma, X., Zhan, S., Qiu, Y., et al. (2022). β-Boswellic acid suppresses breast precancerous lesions via GLUT1 targeting-mediated glycolysis inhibition and AMPK pathway activation. *Front. Oncol.* 12, 896904. doi:10.3389/fonc.2022.896904

Bongers, F., Groenendijk, P., Bekele, T., Birhane, E., Damtew, A., Decuyper, M., et al. (2019). Frankincense in peril. *Nat. Sustain.* 2 (7), 602–610. doi:10.1038/s41893-019-0322-2

Büchele, B., Zugmaier, W., Estrada, A., Genze, F., Syrovets, T., Paetz, C., et al. (2006). Characterization of 3alpha-acetyl-11-keto-alpha-boswellic acid, a pentacyclic triterpenoid inducing apoptosis *in vitro* and *in vivo*. *Planta Med.* 72 (14), 1285–1289. doi:10.1055/s-2006-951680

Casapullo, A., Cassiano, C., Capolupo, A., Del Gaudio, F., Esposito, R., Tosco, A., et al. (2016). β-Boswellic acid, a bioactive substance used in food supplements, inhibits protein synthesis by targeting the ribosomal machinery. *J. Mass Spectrom.* 51 (9), 821–827. doi:10.1002/jms.3819

Chaturvedi, D., Dwivedi, P. K., Chaturvedi, A. K., Mishra, N., Siddiqui, H., and Mishra, V. (2015). Semisynthetic hybrids of boswellic acids: A novel class of potential anti-inflammatory and anti-arthritic agents. *Med. Chem. Res.* 24 (7), 2799–2812. doi:10.1007/s00044-015-1331-y

Dhyani, P., Quispe, C., Sharma, E., Bahukhandi, A., Sati, P., Chand Attri, D., et al. (2022). Anticancer potential of alkaloids: a key emphasis to colchicine, vinblastine, vincristine, vindesine, vinorelbine and vincamine. *Cancer Cell International* 22, 206. doi:10.1186/s12935-022-02624-9

Du, Z., Liu, Z., Ning, Z., Liu, Y., Song, Z., Wang, C., et al. (2015). Prospects of boswellic acids as potential pharmaceutics. *Planta medica*. 81 (04), 259–271. doi:10.1055/s-0034-1396313

Ennet, D. (2000). Arzneistoffportrat-Indischer Weihrauch-Pharmazeutische Bewertung der Harzdroge und ihrer Zubereitungen. *Dtsch. Apoth. Ztg.* 140 (16), 105–114.

Gupta, M., Singh, S., Luqman, S., Saikia, D., Thomas, M., Rout, P. K., et al. (2022). Correlation of boswellic acids with antiproliferative, antioxidant and antimicrobial activities of topographically collected Boswellia serrata oleo-gum-resin. *Phytomedicine Plus* 2 (3), 100289. doi:10.1016/j.phyplu.2022.100289

Havel, J., Patocka, J., and Bocaz, G. (2002). Determination of physostigmine and pyridostigmine in pharmaceutical formulations by capillary electrophoresis. *J. Capill. Electrophor. Microchip Technol.* 7 (5-6), 107–112.

Hoernlein, R., Orlikowsky, T., Zehrer, C., Niethammer, D., Sailer, E., Simmet, T., et al. (1999). Acetyl-11-keto-β-boswellic acid induces apoptosis in HL-60 and CCRF-CEM cells and inhibits topoisomerase I. *J. Pharmacol. Exp. Ther.* 288 (2), 613–619.

Huang, M. T., Badmaev, V., Ding, Y., Liu, Y., Xie, J. G., and Ho, C. T. (2000). Anti-tumor and anti-carcinogenic activities of triterpenoid, β-boswellic acid. *Biofactors* 13 (1-4), 225–230. doi:10.1002/biof.5520130135

Hussain, H., Al-Harrasi, A., Csuk, R., Shamraiz, U., Green, I. R., Ahmed, I., et al. (2017). Therapeutic potential of boswellic acids: A patent review (1990-2015). *Expert Opin. Ther. Pat.* 27 (1), 81–90. doi:10.1080/13543776.2017.1235156

Hussain, H., Ali, I., Wang, D., Hakkim, F. L., Westermann, B., Rashan, L., et al. (2021). Boswellic acids: Privileged structures to develop lead compounds for anticancer drug discovery. *Expert Opin. Drug Discov.* 16 (8), 851–867. doi:10.1080/17460441.2021.1892640

Iram, F., Khan, S. A., and Husain, A. (2017). Phytochemistry and potential therapeutic actions of boswellic acids: A mini-review. *Asian Pac. J. Trop. Biomed.* 7 (6), 513–523. doi:10.1016/j.apjtb.2017.05.001

Khan, A. L., Mabood, F., Akber, F., Ali, A., Shahzad, R., Al-Harrasi, A., et al. (2018). Endogenous phytohormones of frankincense producing Boswellia sacra tree populations. *PLOS ONE* 13 (12), e0207910. doi:10.1371/journal.pone.0207910

Koeberle, A., Henkel, A., Verhoff, M., Tausch, L., König, S., Fischer, D., et al. (2018). Triterpene acids from frankincense and semi-synthetic derivatives that inhibit 5-lipoxygenase and cathepsin G. *Molecules* 23 (2), 506. doi:10.3390/molecules23020506

Liu, J.-J., and Duan, R.-D. (2009). LY294002 enhances boswellic acid-induced apoptosis in colon cancer cells. *Anticancer Res.* 29 (8), 2987–2991.

Liu, J.-J., Nilsson, A., Oredsson, S., Badmaev, V., and Duan, R.-D. (2002). Keto-and acetyl-keto-boswellic acids inhibit proliferation and induce apoptosis in Hep G2 cells via a caspase-8 dependent pathway. *Int. J. Mol. Med.* 10 (4), 501–505. doi:10.3892/ijmm.10.4.501

Lv, M., Shao, S., Zhang, Q., Zhuang, X., and Qiao, T. (2020). Acetyl-11-Keto-β-Boswellic acid exerts the anti-cancer effects via cell cycle arrest, apoptosis induction and autophagy suppression in non-small cell lung cancer cells. *OncoTargets Ther.* 13, 733–744. doi:10.2147/OTT.S236346

Meng, Y., Zhao, L., Wang, Z., Liu, D., and Jing, Y. (2005). Synthesis of boswellic acid derivatives and primary research on their activities. *Chin. Chem. Lett.* 16.

Morad, S. A., Schmid, M., Büchele, B., Siehl, H.-U., El Gafaary, M., Lunov, O., et al. (2013). A novel semisynthetic inhibitor of the FRB domain of mammalian target of rapamycin blocks proliferation and triggers apoptosis in chemoresistant prostate cancer cells. *Mol. Pharmacol.* 83 (2), 531–541. doi:10.1124/mol.112.081349

Park, B., Sung, B., Yadav, V. R., Cho, S. G., Liu, M., and Aggarwal, B. B. (2011). Acetyl-11-keto-β-boswellic acid suppresses invasion of pancreatic cancer cells through the downregulation of CXCR4 chemokine receptor expression. *Int. J. cancer* 129 (1), 23–33. doi:10.1002/ijc.25966

Parmar, S., and Easwaran, H. (2022). Genetic and epigenetic dependencies in colorectal cancer development. *Gastroenterol. Rep.* 10, goac035. doi:10.1093/gastro/goac035

Paul, M. (2012). *Chemotaxonomic investigations on resins of the frankincense species Boswellia papyrifera, Boswellia serrata and Boswellia sacra, respectively, Boswellia carterii: A qualitative and quantitative approach by chromatographic and spectroscopic methodology*. Saarbrücken, Saarland, Germany: Saarland University.

Poeckel, D., and Werz, O. (2006). Boswellic acids: Biological actions and molecular targets. *Curr. Med. Chem.* 13 (28), 3359–3369. doi:10.2174/092986706779010333

Qurishi, Y., Hamid, A., Sharma, P. R., Wani, Z. A., Mondhe, D. M., Singh, S. K., et al. (2012). PARP cleavage and perturbance in mitochondrial membrane potential by 3-α-propionyloxy-β-boswellic acid results in cancer cell death and tumor regression in murine models. *Future Oncol.* 8 (7), 867–881. doi:10.2217/fon.12.68

Ranjbarnejad, T., Saidijam, M., Moradkhani, S., and Najafi, R. (2017). Methanolic extract of Boswellia serrata exhibits anti-cancer activities by targeting microsomal prostaglandin E synthase-1 in human colon cancer cells. *Prostagl. other lipid Mediat.* 131, 1–8. doi:10.1016/j.prostaglandins.2017.05.003

Ravanan, P., Singh, S. K., Rao, G., and Kondaiah, P. (2011). Growth inhibitory, apoptotic and anti-inflammatory activities displayed by a novel modified triterpenoid, cyano enone of methyl boswellates. *J. Biosci.* 36 (2), 297–307. doi:10.1007/s12038-011-9056-7

Roy, N. K., Parama, D., Banik, K., Bordoloi, D., Devi, A. K., Thakur, K. K., et al. (2019). An update on pharmacological potential of boswellic acids against chronic diseases. *Int. J. Mol. Sci.* 20 (17), 4101. doi:10.3390/ijms20174101

Saraswati, S., and Agrawal, S. (2012). Antiangiogenic and cytotoxic activity of boswellic acid on breast cancer MCF-7 cells. *Biomed. Prev. Nutr.* 2 (1), 31–37. doi:10.1016/j.bionut.2011.09.006

Schmiech, M., Ulrich, J., Lang, S. J., Büchele, B., Paetz, C., St-Gelais, A., et al. (2021). 11-Keto-α-boswellic acid, a novel triterpenoid from Boswellia spp. with chemotaxonomic potential and antitumor activity against triple-negative breast cancer cells. *Molecules* 26 (2), 366. doi:10.3390/molecules26020366

Schneider, H., and Weller, M. (2016). Boswellic acid activity against glioblastoma stem-like cells. *Oncol. Lett.* 11 (6), 4187–4192. doi:10.3892/ol.2016.4516

Serbian, I., Wolfram, R. K., Fischer, L., Al-Harrasi, A., and Csuk, R. (2018). Hydroxylated boswellic and glycyrrhetinic acid derivatives: Synthesis and cytotoxicity. *Mediterr. J. Chem.* 7 (4), 286–293. doi:10.13171/mjc74181121-csuk

Shah, B. A., Qazi, G. N., and Taneja, S. C. (2009). Boswellic acids: A group of medicinally important compounds. *Nat. Prod. Rep.* 26 (1), 72–89. doi:10.1039/b809437n

Shamraiz, U., Hussain, H., Ur Rehman, N., Al-Shidhani, S., Saeed, A., Khan, H. Y., et al. (2020). Synthesis of new boswellic acid derivatives as potential antiproliferative agents. *Nat. Prod. Res.* 34 (13), 1845–1852. doi:10.1080/14786419.2018.1564295

Shao, Y., Ho, C.-T., Chin, C.-K., Badmaev, V., Ma, W., and Huang, M.-T. (1998). Inhibitory activity of boswellic acids from Boswellia serrata against human leukemia HL-60 cells in culture. *Planta medica*. 64 (04), 328–331. doi:10.1055/s-2006-957444

Siddiqui, M. Z., and Serrata, B. (2003). A potential antiinflammatory agent: an overview. *Indian Journal of Pharmaceutical Sciences* 73 (3), 255–261. doi:10.4103/0250-474X.93507

Suhail, M. M., Wu, W., Cao, A., Mondalek, F. G., Fung, K.-M., Shih, P.-T., et al. (2011). Boswellia sacra essential oil induces tumor cell-specific apoptosis and suppresses tumor aggressiveness in cultured human breast cancer cells. *BMC complementary Altern. Med.* 11, 129–214. doi:10.1186/1472-6882-11-129

Sun, H., Fang, W.-S., Wang, W.-Z., and Hu, C. (2006). Structure-activity relationships of oleanane-and ursane-type triterpenoids. *Bot. Stud.* 47 (4), 339–368.

Sun, Y., Liu, D., Xi, R., Wang, X., Wang, Y., Hou, J., et al. (2013). Microbial transformation of acetyl-11-keto-β-boswellic acid and their inhibitory activity on

LPS-induced NO production. *Bioorg. Med. Chem. Lett.* 23 (5), 1338–1342. doi:10.1016/j.bmcl.2012.12.086

Syrovets, T., Gschwend, J. R. E., Buchele, B., Laumonnier, Y., Zugmaier, W., Genze, F., et al. (2005). Inhibition of IkappaB kinase activity by acetyl-boswellic acids promotes apoptosis in androgen-independent PC-3 prostate cancer cells *in vitro* and *in vivo*. *J. Biol. Chem.* 280 (7), 6170–6180. doi:10.1074/jbc.M409477200

Takahashi, M., Sung, B., Shen, Y., Hur, K., Link, A., Boland, C. R., et al. (2012). Boswellic acid exerts antitumor effects in colorectal cancer cells by modulating expression of the let-7 and miR-200 microRNA family. *Carcinogenesis* 33 (12), 2441–2449. doi:10.1093/carcin/bgs286

Uthaman, S., Snima, K., Annapoorna, M., Ravindranath, K., Nair, S. V., and Lakshmanan, V.-K. (2012). Novel boswellic acids nanoparticles induces cell death in prostate cancer cells. *J. Nat. Prod.* 5, 100–108.

Wang, D., Ge, S., Bai, J., and Song, Y. (2018). Boswellic acid exerts potent anticancer effects in HCT-116 human colon cancer cells mediated via induction of apoptosis, cell cycle arrest, cell migration inhibition and inhibition of PI3K/AKT signalling pathway. *J. BUON* 23 (2), 340–345.

Wang, Y., Sun, Y., Wang, C., Huo, X., Liu, P., Wang, C., et al. (2013). Biotransformation of 11-keto-β-boswellic acid by Cunninghamella blakesleana. *Phytochemistry* 96, 330–336. doi:10.1016/j.phytochem.2013.07.018

Xia, L., Chen, D., Han, R., Fang, Q., Waxman, S., and Jing, Y. (2005). Boswellic acid acetate induces apoptosis through caspase-mediated pathways in myeloid leukemia cells. *Mol. cancer Ther.* 4 (3), 381–388. doi:10.1158/1535-7163.MCT-03-0266

Yadav, V. R., Prasad, S., Sung, B., Gelovani, J. G., Guha, S., Krishnan, S., et al. (2012). Boswellic acid inhibits growth and metastasis of human colorectal cancer in orthotopic mouse model by downregulating inflammatory, proliferative, invasive and angiogenic biomarkers. *Int. J. cancer* 130 (9), 2176–2184. doi:10.1002/ijc.26251

Yuan, H.-Q., Kong, F., Wang, X.-L., Young, C. Y., Hu, X.-Y., and Lou, H.-X. (2008). Inhibitory effect of acetyl-11-keto-β-boswellic acid on androgen receptor by interference of Sp1 binding activity in prostate cancer cells. *Biochem. Pharmacol.* 75 (11), 2112–2121. doi:10.1016/j.bcp.2008.03.005

Yuan, Y., Cui, S.-X., Wang, Y., Ke, H.-N., Wang, R.-Q., Lou, H.-X., et al. (2013). Acetyl-11-keto-beta-boswellic acid (AKBA) prevents human colonic adenocarcinoma growth through modulation of multiple signaling pathways. *Biochim. Biophys. Acta* 1830 (10), 4907–4916. doi:10.1016/j.bbagen.2013.06.039

Zhao, W., Entschladen, F., Liu, H., Niggemann, B., Fang, Q., Zaenker, K. S., et al. (2003). Boswellic acid acetate induces differentiation and apoptosis in highly metastatic melanoma and fibrosarcoma cells. *Cancer Detect. Prev.* 27 (1), 67–75. doi:10.1016/s0361-090x(02)00170-8

frontiers | Frontiers in Pharmacology

TYPE Review
PUBLISHED 28 September 2023
DOI 10.3389/fphar.2023.1250893

OPEN ACCESS

EDITED BY
Visweswara Rao Pasupuleti,
REVA University, India

REVIEWED BY
Kui Zhang,
The University of Chicago, United States
Saurabh Srivastav,
Rice University, United States
Indrani Manna,
University of Calcutta, India
Md. Rizwanullah,
Jamia Hamdard University, India

*CORRESPONDENCE
Jing Zhuang,
13963676719@163.com

RECEIVED 30 June 2023
ACCEPTED 20 September 2023
PUBLISHED 28 September 2023

CITATION
Shen X, Gao C, Li H, Liu C, Wang L, Li Y, Liu R, Sun C and Zhuang J (2023), Natural compounds: Wnt pathway inhibitors with therapeutic potential in lung cancer. *Front. Pharmacol.* 14:1250893. doi: 10.3389/fphar.2023.1250893

Natural compounds: Wnt pathway inhibitors with therapeutic potential in lung cancer

Xuetong Shen[1], Chundi Gao[2], Huayao Li[2], Cun Liu[2], Longyun Wang[3], Ye Li[3], Ruijuan Liu[4], Changgang Sun[2,4] and Jing Zhuang[4]*

[1]College of First Clinical Medicine, Shandong University of Traditional Chinese Medicine, Jinan, China, [2]College of Traditional Chinese Medicine, Weifang Medical University, Weifang, China, [3]State Key Laboratory of Quality Research in Chinese Medicine and Faculty of Chinese Medicine, Macau University of Science and Technology, Taipa, China, [4]Department of Oncology, Weifang Traditional Chinese Hospital, Weifang, China

The Wnt/β-catenin pathway is abnormally activated in most lung cancer tissues and considered to be an accelerator of carcinogenesis and lung cancer progression, which is closely related to increased morbidity rates, malignant progression, and treatment resistance. Although targeting the canonical Wnt/β-catenin pathway shows significant potential for lung cancer therapy, it still faces challenges owing to its complexity, tumor heterogeneity and wide physiological activity. Therefore, it is necessary to elucidate the role of the abnormal activation of the Wnt/β-catenin pathway in lung cancer progression. Moreover, Wnt inhibitors used in lung cancer clinical trials are expected to break existing therapeutic patterns, although their adverse effects limit the treatment window. This is the first study to summarize the research progress on various compounds, including natural products and derivatives, that target the canonical Wnt pathway in lung cancer to develop safer and more targeted drugs or alternatives. Various natural products have been found to inhibit Wnt/β-catenin in various ways, such as through upstream and downstream intervention pathways, and have shown encouraging preclinical anti-tumor efficacy. Their diversity and low toxicity make them a popular research topic, laying the foundation for further combination therapies and drug development.

KEYWORDS

Wnt/β-catenin signaling pathway, lung cancer, natural compounds, therapeutic potential, Wnt inhibitors

Abbreviations: KRAS, Kirsten Rat Sarcoma Viral Oncogene Homologue; RAS, rat sarcoma viral oncogene homolog; FDA, The US Food and Drug Administration; Stat3, signal transducer and activator of transcription 3; CDKN1B, Cyclin-dependent kinase inhibitor 1B; N-cadherin, neural-cadherin; E-cadherin, epithelial-cadherin; ZEB1, zinc-finger E-box binding homeobox 1; ZEB2, zinc-finger E-box binding homeobox 2; HOXB9, homeoboxB9; Oct4, octamer-binding transcription factor 4; BCL-XL, B-cell lymphoma-extra large; ALDH1, aldehyde dehydrogenase 1; BCL2L2, B cell lymphoma-2-like 2; BCL2, B cell lymphoma 2; IL-6, interleukin-6; Src, proto-oncogene tyrosine-protein kinase SRC; FAK, focal adhesion kinase 1; ERK, extracellular signal regulated kinase; HSP90, heat shock protein 90; KK1, Dickkopf-1; p70S6K, 70 kDa ribosomal protein S6 kinase.

1 Introduction

With an estimated 2 million new diagnoses and 176 million deaths worldwide, lung cancer (LC) is the most prevalent malignancy and a major cause of cancer-related deaths (Thai et al., 2021). Its prognosis is one of the worst among all tumor types, with a 5-year survival rate of less than 20% (Allemani et al., 2018; Neal et al., 2019). Despite substantial advancements in disease management, the treatment of advanced LC is fraught with the risk of failure due to solid metastases, drug resistance, and the limited efficacy of current treatment options, including immunotherapy (Miller and Hanna, 2021). Therefore, there is an urgent need to identify new LC targets and develop safe treatment strategies.

The Wnt signal transduction cascade controls multiple embryonic and somatic processes, including cell fate classification, tissue repair, organ formation, and several pathological states (Nusse and Clevers, 2017). Notably, immoderate activation of Wnt signaling has been observed in numerous solid tumors, such as LC, and in other hematological tumors, such as leukemia. This abnormal activation can determine stem cell fate; promote tumorigenesis; and aid in tumor progression, metastatic spread, and drug resistance to chemotherapy, radiotherapy, immunotherapy, and targeting therapy (Ferrarelli, 2017; McMellen et al., 2020; Aguilera and Dawson, 2021; Yu et al., 2022).

Characteristic of adenocarcinomas, especially lung adenocarcinoma (LUAD), are abnormalities in the epigenetic control of the Wnt signaling system (Li et al., 2016a). Compared to normal tissues, the level of β-catenin in LC tissues was also significantly increased and was closely related to the differentiation and lymph node metastasis of LC. In addition, the recurrence rate in patients with high β-catenin expression was significantly higher than that in patients with low β-catenin expression (Liu et al., 2015). Wnt3a, a canonical Wnt pathway ligand, is overexpressed in 43% of squamous cell carcinomas and 51% of adenocarcinomas (Nardi et al., 2018). It was found that the expression of Wnt3a protein was low in normal or grade 1 LC tissues, but remarkably increased in higher-grade samples. Approximately 35%–70% of non-small cell lung cancers (NSCLC) are estimated to have anomalous Wnt signaling, depending on the quantification assay (Xu et al., 2011). Additional studies have confirmed that coercive activation of the Wnt pathway via engineered gene alleles promotes the advancement of KRAS- or BRAF-mutant lung adenomas (Juan et al., 2014; Rogers et al., 2018). The Wnt signaling cascade is a highly promising cancer target, and its diversity and importance provide great opportunities for the development of targeted therapies for LC (Tennis et al., 2007).

Targeted Wnt/β-catenin pathway therapy shows outstanding anti-LC efficacy, and a range of Wnt pathway inhibitors provide great potential for combination therapy in LC, according to preclinical studies conducted in recent years (Okada-Iwasaki et al., 2016; Scarborough et al., 2017). Unfortunately, most existing Wnt inhibitors have limited clinical application due to their non-negligible toxicity and side effects; thus far, no medicines that target this route have received FDA market approval (Krishnamurthy and Kurzrock, 2018; Torres et al., 2019) (Table 1). It is worth noting that acute inhibition of Wnt signaling or systemic elimination of Wnt secretion can affect intestinal homeostasis, leading to severe diarrhea, osteoblast and osteoclast differentiation, bone loss, and other serious side effects (Jung and Park, 2020). For example, the non-specific distribution of Wnt inhibitors leads to the development of diarrhea or fractures that force patients to discontinue treatment (Diamond et al., 2020). Therefore, a better understanding of the mechanism of this pathway will assist in new drug research to further explore new ways of targeting the Wnt/β-catenin pathway specifically or in

TABLE 1 The Wnt pathway inhibitors in LC clinical trials.

Drug	Cancer type	Trial phase	Status	Clinical trial
LGK974	Lung Squamous Cell Cancer and some Malignancies Dependent on Wnt Ligands	I	Active, not recruiting	NCT1351103
OMP-54F28	Solid Tumors	I	Completed	NCT1608867
XNW7201	Advanced Solid Tumors	I	Completed	NCT3901950
CGX1321	Advanced Solid Tumors	I	Recruiting	NCT2675946
RXC004	cancer/Solid Tumors	I	Recruiting	NCT3447470
PRI-724	Advanced Solid Tumors	I	Terminated	NCT1302405
MCLA-158	NSCLC and Advanced/Metastatic Solid Tumors	I/II	Recruiting	NCT03526835
ETC-1922159	Solid Tumor	I	Recruiting	NCT02521844
DKN-01	Adenocarcinoma、Squamous cell carcinoma and other advanced solid tumors with Wnt-activated mutations	I/II	Available	NCT04681248
OMP-18R5	recurrent or advanced (Stage IV) NSCLC	I	Completed	NCT01957007
JS015	Advanced malignant solid tumors	I	Recruiting	CTR20223111
BI-905681	Advanced, unresectable and/or metastatic non-hematologic malignancies	I	Completed	NCT04147247

The data obtained from https://clinicaltrials.gov/ and https://db.pharnexcloud.com/. Last accessed on 30 April 2023.

combination. Therapeutic efficacy and toxicity should be perfectly balanced in treatments that target this route, given its extensive biological activity in LC.

The research prospects for plant-derived medicines are relatively broad owing to the variety of targets, good safety standards, and excellent synergism (Guan et al., 2022; Liu et al., 2022). Furthermore, sub-non-toxic-specific targeting may offer new therapeutic windows for LC therapy. To better understand the impact of the Wnt/β-catenin pathway on LC, we discuss its role in various aspects of tumor progression. With a limited number of potential Wnt inhibitors available in the clinic, this study is the first to systematically summarize the mechanism of action of flavonoids, polyphenols, alkaloids, terpenoids, and other natural products and their derivatives in the intervention of the Wnt signaling pathway in LC to meet the high demand for the development of more secure and manageable Wnt inhibitors. Various classes of compounds can interfere with multiple targets of the Wnt pathway to produce inhibitory effects and show great therapeutic potential when used alone or in combination with other drugs. Additionally, exploring these compounds in combination with existing anti-LC drugs could potentially enhance the effectiveness of current therapies and reduce the risk of drug resistance.

2 Composition and activation of the Wnt/β-catenin pathway

Wnt ligands are cysteine-rich proteins whose family consists of 19 secreted glycoproteins. Wnt ligand-mediated signaling pathways have a variety of physiological functions that have been conserved throughout evolution (Eubelen et al., 2018). Depending on whether they have a direct impact on β-catenin, the three pathways that the Wnt receptor activates are the canonical β-catenin cascade, the non-canonical planar cell polarity pathway, and the Wnt/Ca^{2+} pathway. These three pathways form a network of mutual regulation that finely coordinates various biological activities. Among them, the canonical pathway is closely related to the occurrence and development of LC and the most widely studied pathway; it is also the subject of this review.

The β-catenin-dependent pathway consists of three major components: transduction of Wnt signaling in the membrane, modulation of β-catenin stability in the cytoplasm, and overactivation of Wnt target genes in the nucleus (Nusse and Clevers, 2017). Ligand-related activation of the Wnt/β-catenin signaling pathway is induced by the binding of the Wnt ligand to the co-receptor complex, which includes the transmembrane domain protein frizzled (Fzd) and low-density lipoprotein receptor-related protein (LRP) 5/6. Activation of the Wnt pathway results in initiation intracellular signaling and membrane recruitment of Disheveled (Dsh/Dvl) which induces unsteadiness of the destruction complex made up of axis inhibition protein (Axin), glycogen synthase kinase-3beta (GSK-3β), casein kinase 1alpha (CK1α), and adenmatous polyposis coli (APC). This leads to the stabilization and accumulation of β-catenin in the cytoplasm and its subsequent nuclear localization. B-catenin attaches to T-cell factors/lymphoid-enhancer factors (TCFs/LEFs) in the nucleus and elicits the transcription of Wnt target genes, such as c-myc (Myc), Cyclin D1 (CCND1), and survivin, to regulate cell proliferation, transdifferentiation, apoptosis, and other life processes (Yao et al., 2011; Okada-Iwasaki et al., 2016; Zhao H. et al., 2022). When no Wnt ligand is present, β-catenin is degraded by protein-destroying complexes. β-catenin is markedly degraded after phosphorylation by CK1α and GSK-3β. Dissociative β-catenin is then recognized by the E3 ubiquitin ligase-transducin repeat-containing protein (β-TrCP) and degraded via the ubiquitin-dependent proteasome pathway to maintain low levels of free β-catenin in the Wnt-off state (Stamos and Weis, 2013) (Figure 1).

There are various abnormal Wnt activation modes in malignant tumors, including acquired mutations, decreased expression of pathway inhibitors, and abnormal expression of ligands and receptors (Tortelote et al., 2017). Most sporadic colorectal tumors accumulate APC or β-catenin mutations, leading to abnormal Wnt signaling (Ferrarelli, 2017). Compared with colorectal cancer, activation of Wnt-mediated signaling takes place differently in LC, which is often associated with increased expression of Wnt pathway-activating effectors, such as Dvl and Wnt ligands, and downregulation of negative regulators, such as Axin and Wnt inhibitory factor-1 (WIF-1) (Mazieres et al., 2004; Mazieres et al., 2005; Tennis et al., 2007; Luo et al., 2018). It is clear that the mode of Wnt activation correlates with the type of tumor tissue. Therefore, future efforts to regulate this pathway more effectively may benefit from a clearer understanding of the unique aberrant activation of Wnt in LC.

3 Wnt/β-catenin in LC

Abnormally activated Wnt signalings frequently manifests in a variety of tumors that are widely involved in the occurrence and development of cancer. The Wnt signaling network controls a wide range of biological processes in LC (Katoh and Katoh, 2022). The undesirable activation of the Wnt/β-catenin signaling pathway has been linked to increased cancer prevalence, accelerated malignant progression, poor prognosis, and higher LC-related mortality (Xu et al., 2011; Parsons et al., 2021). Moreover, abnormal activation of the Wnt pathway interferes with stemness, proliferation, angiogenesis, metastasis/invasion treatment resistance, and other critical tumor developmental processes in LC, which are discussed below in light of the significant role of the classical Wnt pathway.

3.1 Maintain the stemness

Cancer stem cells (CSCs) are now considered the main "seeds" in tumorigenesis, development, metastasis and recurrence (Reya et al., 2001). Wnt signaling plays a role in the development of LCs by producing CSCs from non-CSCs or normal stem cells (Chaudhary et al., 2023). For example, the Wnt/β-catenin pathway is involved in the process of tobacco smoke (TS)-induced LC. After prolonged exposure to TS, human bronchial epithelial (HBE) cells are malignantly transformed and acquire CSC-like characteristics. In TS-transformed HBE spherical cells, silencing of β-catenin impeded the tumorsphere and reduced the expression levels of lung CSC markers (Wang J. et al., 2018). Similar to normal lung stem cells, CSCs enlist the Wnt, Notch, and Hedgehog signaling cascades to control stemness (Rowbotham et al., 2022).

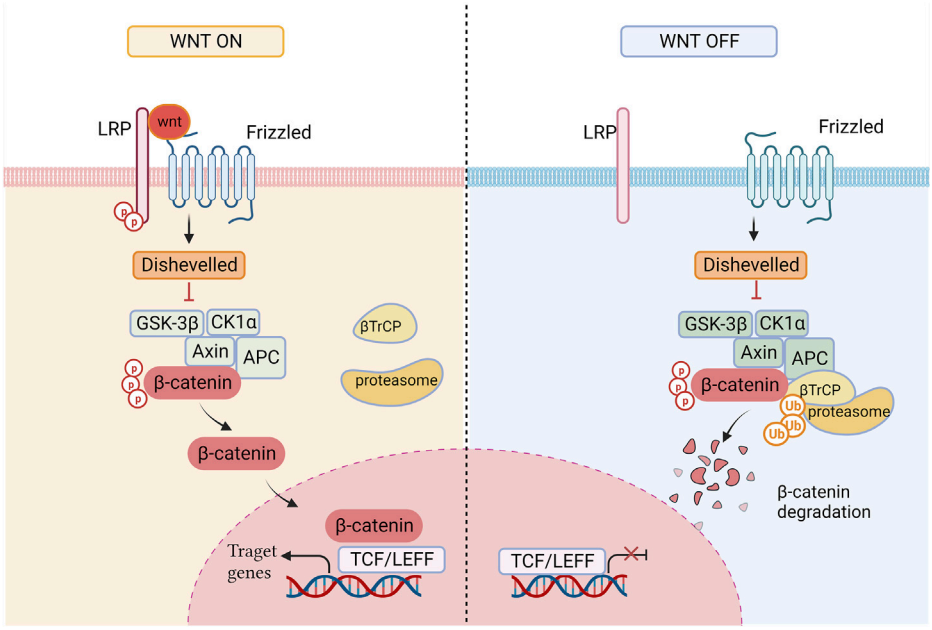

FIGURE 1
The state of the Wnt signaling path on and off. When Wnt ligand is present, the cytoplasmic concentration of β-catenin rises and β-catenin translocates to the nucleus, promoting the expression of target genes; In the Wnt Off state, β-catenin is degraded by ubiquitination.

Wnt/β-catenin signaling is thought to be necessary for maintaining the CSC phenotype. In CSCS, β-catenin dependent Wnt signaling is extremely active and contributes to maintaining the expression of putative lung CSC markers such as cluster of differentiation 44 (CD44) and cluster of differentiation 133 (CD133) (Teng et al., 2010; Zhu J. Y. et al., 2017). Compared to non-CSCs, LEF/TCF-binding elements have higher transcriptional activity, and Wnt signaling is increased in CSCs (Li X. et al., 2020). The high expression of Fzd 4/5 and higher sensitivity to Wnt3a-induced β-catenin dependent Wnt signaling further show that CSCs have heightened expression of Wnt downstream molecules compared with that in non-CSCs (He et al., 2021). In addition, transcription factor Stat3 is required for the proliferation and pluripotency of stem cells, and Stat3 activity is Wnt/β-catenin dependent, which suggests that Wnt signaling can control stem cell fate by affecting other pathways essential for stem cell maintenance (Peron et al., 2020).

Wnt signaling regulates complex biological behaviors that are beneficial for the survival and metastasis of lung CSCs. Through various target genes, Wnt pathway activation can aid CSCs in penetrating adjacent tissues and entering the bloodstream. During this time, tumor cells remain dormant, allowing them to survive and avoid immune monitoring through the adverse feedback of Wnt signaling. When CSCs reach appropriate sites, another burst of Wnt signaling induces successful CSC reinitiation and colonization of secondary organs (Malladi et al., 2016; Kim et al., 2017). In addition, a subset of p53-and KRAS-mutated lung carcinoma cells can serve as Wnt-producing niches for other cancer cell subsets. After treatment with the Wnt pathway inhibitor (LGK974), the lifespan of LC mice increased by nearly 50%, and leucine-rich repeat-containing G-protein-coupled receptor 5 (LGR5)+LUAD cells lost the potential for unlimited proliferation and metastasis similar to stem cells (Tammela et al., 2017). In summary, aberrant Wnt/β-catenin activation maintains LC stem cell-like characteristics and promotes LC progression. The Wnt/β-catenin signaling pathway has been implicated in the regulation of CSCs, although the underlying regulatory pathways of CSCs remain elusive (Cheng et al., 2023).

3.2 Participate in proliferation

Control of the cell cycle by Wnt signaling is responsible for the most mechanisms that promote proliferation during cancer (Pate et al., 2014). Wnt signaling is involved in LC cell cycle regulation in multiple mechanistic layers. Two key cell cycle regulators, Myc and CCND1, are direct target genes of the β-catenin/TCF transcription complex (Shtutman et al., 1999; Tetsu and McCormick, 1999). As one of the most important oncogenic transcription factors, Myc positively regulates multiple key cell cycle effectors including E2F transcription factors, cyclins, and cyclin-dependent kinases (Bretones et al., 2015). Wnt ligands accelerate tumor proliferation in NSCLC, partly by upregulating Myc and CCND1. The Ki-67 proliferation index of Myc-positive LC tissues is significantly higher than that of Myc-negative tissues (Huang et al., 2008). Compared to nearby normal tissues, CCND1 was significantly upregulated in NSCLC tissues and promoted cell proliferation and colony formation (Wu et al., 2020).

LC cells are also tightly regulated by multiple negative regulators and avoidance of these growth suppressors is necessary for tumorigenesis and facilitates cancer progression. Wnt signaling accelerates cell cycle progression by reducing the expression of many key cyclin-dependent kinase inhibitors (CDKNs) (Zhong et al., 2020). Nuclear accumulation of β-catenin in NSCLC is

accompanied by increased cell proliferation. It was also observed that β-catenin expression was inversely correlated with CDKN1B ($p27^{KIP}$), and dysregulation of β-catenin activity was shown to induce p53-dependent growth arrest in LC cells (Kotsinas et al., 2002). In addition, cancer cells acquire a characteristic resistance to apoptosis, which prevents them from dying and maintains uncontrolled proliferation (Jan and Chaudhry, 2019). Wnt3a triggers the canonical Wnt pathway to stop apoptosis caused by decreased levels of caspase-9 and caspase-3 (Wang T. L. et al., 2018). Suppressive Wnt/β-catenin signaling may encourage LC cell death and prevent proliferation through downstream transcription factors such as survivin, an inhibitor of the apoptosis family, although the precise mechanism is still unknown (You et al., 2004).

Tumor cell proliferation and malignant behavior require energy support (Patel and Powell, 2016) and CSCs prefer aerobic glycolytic energy metabolism, enabling constitutive proliferation and resilience to treatment-induced damage (Sancho et al., 2016). The Wnt pathway affects tumor cell energy metabolism through a variety of target genes (Pate et al., 2014). Myc is a major regulator of glycolysis (Dang et al., 2008). Myc-overexpressing LC cells exhibit enhanced aerobic glycolysis, whereas Myc-low cell lines appear to be more dependent on oxidative metabolism (Cargill et al., 2021). Activated Wnt/β-catenin signaling promotes Myc mRNA translation and expression and subsequently increases glycolysis and proliferation of LC cells (Yang X. et al., 2021; Huang et al., 2021).

3.3 Regulate angiogenesis

LC is a highly vascularized tumor and microvessel density (MVD) is the primary characteristic of intratumoral angiogenesis (Daum et al., 2020). Wnt signaling is an important factor in both pathological and physiological angiogenesis (Dejana, 2010). High-level angiogenesis is a crucial event in cancer cell dissemination and distant metastasis (Herbst et al., 2005), and hypoxia is considered a major catalyst for tumor angiogenesis (Brahimi-Horn et al., 2001). Hypoxia in LUAD cells can promote Wnt signaling by stabilizing β-catenin and altering its localization in the nucleus. Meanwhile, overexpression of hypoxia-inducible factors increases the content of β-catenin and enhances the resistance of LC cells to chronic hypoxia-induced stress (Hong et al., 2017). The most significant pro-angiogenic molecules, including members of the vascular endothelial growth factor (VEGF) family, matrix metalloproteinases (MMPs), and multiple chemokines, are regulated by canonical Wnt/β-catenin downstream signaling (Glaw et al., 2010). Numerous genes associated with tumor angiogenesis are expressed more frequently than usual when nuclear-β-catenin levels are elevated (Kasprzak, 2020). VEGF is a major mediator of the tumor microvasculature and is closely linked to the progression, metastasis, and recurrence of NSCLC. Previous studies have reported a positive correlation between β-catenin and VEGF protein expression in patients with NSCLC (Huang et al., 2008; Zhao Y. et al., 2022). In addition, tumor blood vessels are often leaky, poorly differentiated, and regardless of grade; one of the reasons for this phenomenon may be that differential Wnt expression induces modulation of cell morphology and function in LC (Rapp et al., 2017). For example, Wnt5a signaling can induce vasculogenic mimicry (Yao et al., 2014), while Wnt3a-induced Wnt activation is associated with increased angiogenesis (Shukla et al., 2016).

Wnt signaling can also indirectly affect angiogenesis by regulating the tumor microenvironment. For instance, angiogenesis can be induced by tumor-associated macrophages (TAMs) in the tumor microenvironment, which is thought to be the "switch" that first causes tumor angiogenesis (Cassetta and Pollard, 2023). TAMs release a range of pro-angiogenic substances that eventually lead to tumor angiogenesis due to the abnormally active Wnt pathway and autocrine signaling, which simultaneously promote M2 polarization (Cui et al., 2022). It is worth noting that although antiangiogenic therapy brings sufficient benefits to patients, its efficacy of antiangiogenic therapy is limited and is often accompanied by local hypoxia, tumor adaptation, progression, and metastasis (Uribesalgo et al., 2019). Studies have observed that when VEGF is inhibited, feedback activates Wnt signaling to increase the expression of β-catenin and CCND1, leading to a certain degree of upregulation of the proliferation and invasion abilities of human NSCLC A549 cells (Zhang X. X. et al., 2016). This implies that Wnt inhibitors can improve LC treatment when combined with antiangiogenic therapy.

3.4 Related to metastasis/invasion

Metastasis and invasion of the primary tumor and systemic tumor dissemination are the most deleterious events in the development of cancer, which pose challenging therapeutic difficulties and are significant contributors to cancer-related mortality (Hanahan and Weinberg, 2011). Changes that occur during LC initiation and metastasis can be described as epithelial-to-mesenchymal transition (EMT) (Brabletz et al., 2018). EMT-progressing cells exhibit altered phenotypes, lose epithelial features, and express more mesenchymal markers. The activation of EMT during cancer growth enables cancer cells to develop migratory, invasive, and stem cell-like characteristics (Liao and Yang, 2017; O'Leary et al., 2018). It has been demonstrated that Wnt signaling is essential for EMT and that the Wnt/GSK-3β axis regulates the degradation of Snail, an important mediator of EMT (Yook et al., 2005). Wnt signaling also regulates cell adhesion, triggering the adhesion junction protein E-cadherin, and upregulates the expression of the mesenchym-specific marker N-cadherin during EMT (Wu et al., 2017). Transforming growth factor-β (TGF-β), a key element in stimulating the EMT process, upregulated the expression of β-catenin, and the progression of EMT was positively correlated with the activity of Wnt/β-catenin pathway (Luan et al., 2022). Activation of Wnt/β-catenin signaling can also contribute to EMT induction either directly or indirectly by stimulating several EMT-related transcription factors, such as Slug, Twist, ZEB1, ZEB2, and E47 (Shin et al., 2010; Sánchez-Tilló et al., 2011). Notably, Wnt may also affect EMT by affecting CSCs, because the expression of the CSC marker CD44 is associated with the mesenchymal phenotype, suggesting a role in EMT induction and maintenance in LC (Suda et al., 2018).

Cell-cell adhesion and matrix depletion are important steps in the progression of all cancers from localized malignancy to

metastatic disease. Wnt/β-catenin and its downstream products may affect the actin cytoskeleton and destabilize adhesion molecule junctions (Liu et al., 2023). Activation of Wnt/β-catenin signaling can work in conjunction with other oncogenic pathways such as KRAS in lung epithelial cells to produce a more aggressive cancer phenotype by forcing an embryonic distal progenitor phenotype and reducing E-cadherin expression (Pacheco-Pinedo et al., 2011; Hung et al., 2020). Moreover, MMPs enzymes directly regulated by Wnt can promote cancer metastasis by aiding the breakdown of the extracellular matrix and enabling cancer cells to spread throughout the lymphatic and blood arteries of the body (Ku et al., 2015). Wnt signaling may influence the organotropism of LC cells that progress along the metastatic cascade. A metastatic subpopulation isolated from node-derived lung adenocarcinoma cell lines has previously been shown to exhibit highly active Wnt/TCF signaling, and the Wnt/TCF target genes LEF1 and HOXB9 have been shown to promote LUAD cell colonization in the bone and brain (Nguyen et al., 2009). In addition, activation of the Wnt pathway in tumors results in a noninflammatory environment and suppresses immune surveillance through a variety of mechanisms (Du et al., 2023). This suggests that Wnt signaling may indirectly promote tumor growth and metastasis by inhibiting the immune-resistant tumor microenvironment.

3.5 Implicate in medication resistance

Systemic anti-LC treatments face great challenges, and drug resistance is primarily responsible for cancer patient mortality, whether directly or indirectly. The persistence of CSCs, enhanced multidrug resistance (MDR) and the downregulation of apoptosis are important causes of treatment failure (Yuan et al., 2017; Aleksakhina et al., 2019). It has been demonstrated that CSCs are more resistant to standard chemotherapy and radiotherapy. This may be because these cells produce large levels of anti-apoptotic proteins such as Myc, express more genes for drug resistance, and have more effective DNA damage repair (Ayob and Ramasamy, 2018). Several cancers, including LC, exhibit treatment resistance, given that Wnt signaling is crucial for sustaining CSCs (Yang et al., 2016b). Silencing β-catenin abolished Oct4/Nanog-mediated MDR and EMT in NSCLC cells (Liu et al., 2020).

MDR is the primary contributor to cancer chemotherapy failure (Wang et al., 2021). Wnt signaling activation is an important mechanism of chemoresistance in recurrent LC. Activation of Wnt signaling by APC inhibition resulted in chemoresistance in chemosensitive human LC cell lines, and higher Wnt activity was observed *in vitro* derived chemoresistant cell lines (Wagner et al., 2018). Overexpression of MDR-associated transporters is the key mechanism by which the aberrant activation of Wnt/β-catenin signaling results in the induction of cancer MDR (Ghandadi et al., 2019). The level of Wnt/β-catenin activity is positively correlated with resistance to several common chemotherapeutic drugs, such as paclitaxel and cisplatin, and radiation used in the treatment of LC (Yang et al., 2016b; Datta et al., 2019; Li et al., 2022). Frequently used adjuvant chemotherapy agents activate β-catenin-dependent signaling, which results in the upregulation of the expression and activity of multidrug-resistant protein 1 and other multidrug efflux transporters (Vesel et al., 2017). Upregulation of Wnt signaling protects cancer cells from cell cycle arrest or apoptosis which can promote tumor chemoresistance (Yuan et al., 2020). For example, the upregulation of β-catenin signaling may promote cisplatin resistance in LUAD cells through the overexpression of the BCL-XL gene (Zhang J. et al., 2016). Experiments have revealed that blocking Wnt signaling increases the radiosensitivity of LC cells (Wu et al., 2016; Li et al., 2022). Although this protective effect is attributed to downstream effectors of Wnt/β-catenin signaling, the more general mechanism of stress remains unclear (Lee et al., 2013).

Targeted therapy for LC is drug-resistant, partly because of the Wnt pathway. Adenocarcinoma is usually associated with activating mutations in the epidermal growth factor receptor (EGFR) gene and LC patients with activating mutations in the kinase domain of EGFR can be treated with tyrosine kinase inhibitors (TKIs) (Casás-Selves et al., 2012; Nakayama et al., 2014). Cross-regulation of EGFR and Wnt signaling in cancer results in abnormal increases in signaling proteins and transcription factors, leading to the failure of targeted therapies (Tabasum and Singh, 2019). Overexpression of EGFR not only increased the synthesis of Wnt3a, Fzd, and β-catenin, but also deactivated the phosphorylation of multiple Wnt components (Kim N. Y. et al., 2022). Although EGFR inhibitors have not been shown to significantly upregulate Wnt signaling in preclinical investigations, Wnt/β-catenin signaling promotes resistance to EGFR inhibitors in EGFR-mutated LC cells. Previous studies have shown that the canonical Wnt pathway contributes to the maintenance of NSCLC cells during EGFR inhibition and that the efficacy of EGFR inhibitors can be significantly improved by inhibiting various components of the canonical Wnt pathway. Importantly, inhibiting multiple elements of the canonical Wnt pathway can dramatically increase the *in vitro* and *in vivo* effectiveness of EGFR inhibitors (Casás-Selves et al., 2012; Scarborough et al., 2017; Yan et al., 2022). Furthermore, pharmacological reduction of β-catenin nuclear localization inhibited resistance to osimertinib (a third-generation EGFR-TKI) in PC-9 cells resistant to gefitinib (a first-generation EGFR-TKI), and IMU1003, an inhibitor of nuclear localization of β-catenin, significantly reduced the emergence of osimertinib-resistant colonies (Katagiri et al., 2023). This implies that inhibition of nuclear β-catenin function may overcome transgenerational EGFR-TKI resistance.

Aberrant Wnt signaling can inhibit the recruitment of inflammatory anti-tumor T cells and may undermine cancer immunosurveillance, thereby negatively controlling innate immunity, fostering immunoevasion, and boosting resistance to a variety of immunotherapeutics, including immune checkpoint inhibitors (ICIs) (Galluzzi et al., 2019; Hargadon, 2023). Wnt3a overexpression significantly increases the transcriptional activity of the programmed death ligand 1 (PD-L1) promoter reporter (Ma et al., 2022). Molecular screening performed at the time of progression after ICIs treatment in patients with advanced NSCLC revealed molecular alterations in the genes involved in the Wnt

TABLE 2 The intervention for lung cancer Wnt using natural compounds and others.

Group	Name	Mode of action	Effect	Cell type/Modle	References
Flavonoids	EGCG	↓ the expression of p-GSK-3β(Ser9), β-catenin and its downstream target gene c-Myc, ↑GSK-3 expression	↓tumor globular formation. ↓protein and mRNA levels of CSCs markers. ↓proliferation and ↑apoptosis	A549, H1299 cells	Zhu et al. (2017a)
		↑WIF-1 promoter and recovery of WIF-1 expression. ↓β-catenin level and Tcf/Lef reporter activity	potential therapeutic use of reversing the methylation of the WIF-1 promoter	H460, A549 cells	Gao et al. (2009)
	Garcinol	↓phosphorylation of LRP6. ↓β-catenin, Dvl2, Axin2 and Cyclin D1 expression	↓colony formation capacity. ↑cytotoxic death and apoptosis. ↓tumor initiation and growth	H441, A549 cells and H441 CSC mouse xenograft model	Huang et al. (2018)
	Fisetin	↓the expression of various signaling proteins (β-catenin, NF-κB, EGFR, STAT-3) acting on the upstream of EMT	↓EMT program. ↓the migration, invasion potential and stem cell phenotype of LC cells	A549 and H1299 cells	Tabasum and Singh (2019)
	Nobiletin	↓miR-15-5p expression. ↓Wnt/β-catenin	↓stemness and the migration ability. ↑cell apoptosis	A549 and H460 cells	Han et al. (2021)
	TF	↓COX-2, Wnt and β-catenin mRNA expression	↓proliferate and ↑apoptosis of LC cells. ↓tumor growth of mice. ↑survival time of mice	A549 cells, BALB/c nude mouse	Han et al. (2020)
Polyphenols	Curcumin	↓Wnt/β-catenin pathway upregulation mediated by oxidative stress	↓LC cell proliferation	A549	Wang et al. (2018b)
		↓p-GSK3β(Ser9), ↑GSK3β. ↓β-catenin and its downstream c-Myc and Cyclin D1	↓lung CSC proliferation and ↑apoptosis	A549 and H1299 cells	Zhu et al. (2017b)
		↓MTAl-Wnt/β-catenin signal path and ↓downstream targets such as Cyclin D1, and MMP-7	↓proliferation and invasion of NSCLC cells, and ↑G0/G1 phase arrest	95D and A549 cells	Lu et al. (2014)
	RES	↓p-GSK3β(Ser9) β-catenin and c-Myc expression	↓tumor sphere size, expression of CSC specific markers, and activation of Wnt/β-catenin	A549, NCI-H460, NCI-H226 and NCI-H1299 cells, BALB/c nude mice	Xie et al. (2023)
		↑snail stability to reduce Axin2 levels, ↑the binding of β-catenin/TCF to PD-L1 promoter, and of ↑PD-L1 expression	suggesting the role in tumor immune escape	A549 and H1299 cells	Yang et al. (2021a)
	Maclurin	antioxidant activity and ↓Src/FAK-ERK-β-catenin pathway. ↓MMP-2 and MMP-9	↓the migration and invasion of LC cells	A549	Ku et al. (2015)
	Eugenol	regulated the phosphorylation pattern of β-catenin and ↓its nuclear translocation	↓CSC complexity. ↓development of LC and ↑the life span of mice	A549, female Swiss Albino mice	Choudhury et al. (2021)
Alkaloids	Sanguinarine	↓the expressions of Wnt1 and Wnt7b in M2 macrophages	↓tumor growth and angiogenesis in mice	Lewis LC cells, HUVEC, C57BL/6 mice	Cui et al. (2022)
		↓snail and wnt target gene cyclin-D1	↓proliferation, invasion and metastasis of CSC	A549 and H1299 cell lines, nude mice	Yang et al. (2016a)
	Chelerythrine	↓β-catenin cell expression and the localization of β-catenin in the nucleus	↓colony formation and spheroid growth. ↓ability to migrate and invade	NCI-H1703, SK-LU-1, HLCSCs	Heng and Cheah (2020)
	Nuciferine	↑accumulation and stabilization of Axin, ↑degradation of β-catenin and ↓the expression of target genes	↓cell proliferation and apoptosis-resistance. ↓LC growth	A549 and H1299, BALB/c athymic nude (nu/nu) mice	Liu et al. (2015)
	β-asarone	↑GSK-3β expression. ↓protein expression of p-GSK-3β, DVL 2, β-catenin and Cyclin D1. ↓transcriptional activity of β-catenin/TCF	↓tumor cell viability, ↓migration/invasion/adhesion. ↑mitochondria-related apoptosis	A549, NCI-H1299, NCI-H1650 and HCC827 cells	Wang et al. (2018c)

(Continued on following page)

TABLE 2 (*Continued*) The intervention for lung cancer Wnt using natural compounds and others.

Group	Name	Mode of action	Effect	Cell type/Modle	References
	Lycorine	↑GSK-3β expression. ↓β-catenin and EMT	↓growth and metastasis of lung tumors	A549, H460 cells and A549/Luc mice	Sun et al. (2018)
	Daurisoline	↓the stability of β-catenin and ↑the degradation of β-catenin	↑G1 phase cell cycle arrest. ↓the invasion and metastasis potential of tumor cells and tumor growth in mice	A549, Hop62 and H1299 cells. Female BALB/c nude mice	Huang et al. (2020)
	Matrine	↑Let-7b level. ↓CCND1/Wnt signaling pathway and ↓EMT	↓characteristic labeling and renewal of CSCs and ↑the sensitivity 5-FU. ↓the growth and migration	NCI-A549 and NCI-H460 cells	Li et al. (2020b)
	Ligustrazine	↑GSK-3β expression and ↓the activation of Wnt/β-catenin pathway in tumor tissues	↓tumor formation and development in mice	H1650, A549, H1299 and PC-9 cells	Dong et al. (2020)
				Male BALB/c nude mice	
	Fascaplysin	↓expression levels of β-catenin, AXIN2, GSK-3β and C-myc. EMT phenotype was reversed	↓migration of A549 cells	A549 cells	Luo and Xu (2022)
	(1′S, 6R)-nitidumalkaloid B	↓β-catenin, Axin2, and p-GSK-3β↑p-β-catenin expression	↓tumor cell proliferation, ↑arrest cell cycle and apoptosis	A549 cells	Qin et al. (2023)
Terpenoids	TP	↑methylation of histone H3. ↓expression of various wnt inhibitors (including WIF1, FRZB, SFRP1, ENY2, and DKK1)		A549 and H460 cells. Fen1 E160D transgenic mouse	Nardi et al. (2018)
		the expression level of WIF-1 is increased by demethylation of WIF-1 promoter	↓cell proliferation, invasion, migration and anti-apoptosis	A549 and H460 cells	Mao et al. (2018)
		↑phosphorylation of β-catenin and ↓expression of p-GSK3β(ser9)	↓growth and EMT/metastasis of NSCLC cells	NCI-H1299 and NCI-H460 cells	Deng et al. (2021)
		↓the activity of p70S6K. ↑activated GSK-3 to promote β-catenin degradation	↓the EMT of paclitaxel-resistant LUAD cells	A549 and A549/TaxR cells, (BALB)/c nude mice	Tian et al. (2021)
	CuB	↓Wnt3/Wnt3a expression. ↓GSK-3 Inactivated phosphorylation. ↓β-catenin nuclear localization and TCF-1 interaction	↓cell stemness and metastasis. ↓tumor angiogenesis	A549, H1299 and H23 cells. NNK-induced A/J mouse	Shukla et al. (2016)
	Curcumol	↓LRP5/6 phosphorylation, ↑expression of Axin, APC, GSK-3β and p-β-catenin	↓cell proliferation and survival, motility and migration	A549 and H460 cells. BALB/c nude mice	Li et al. (2021)
	FDN	↓Wnt3 and β-catenin expression levels	↑apoptosis and cell cycle arres	A549 cells	Al Saqr et al. (2022)
	EPBS	↓expression of EGFR, Wnt3a and Fzd-1 which triggered the activation of GSK-3β and induced the degradation of β-catenin	regulated the activity of Wnt/β-catenin pathway proteins in cancer cells with EGFR overexpression and EGFR depletion	A549 and PC-9 cells	Kim et al. (2022a)
	Artemisinin	↓Wnt5a/b, LRP6 Dvl2 and β-catenin expression. ↑NKD2 and Axin2 expression	↑G1 phase cell cycle arrest. ↓tumor proliferation and metastasis	A549 and H1299 cells, Female Balb/c-nude mice	Tong et al. (2016)
	PPD25	↓β-catenin, c-myc, cyclin D1, TCF-4. ↓β-catenin/TCF transcriptional activity	↓proliferation, ↑apoptosis	A549 cells	Bi et al. (2009)
Isothiocyanate	BI and PI	↓β-catenin localization in the nucleus	BI more effectively inhibited long-term colony formation. PI more effectively inhibited the growth of tumor	SK-LU-1, HLCSC	Heng and Cheah (2021)
				NCI-H1703 cells line	
Bufadienolides	19-HB	↓β-catenin c-Myc and CCND1	↓tumor cell viability and ↑apoptosis	NCI-H1299, NCI-H838, A549 cell lines, xenograft mouse model	Yu et al. (2021)

(Continued on following page)

TABLE 2 (*Continued*) The intervention for lung cancer Wnt using natural compounds and others.

Group	Name	Mode of action	Effect	Cell type/Modle	References
Plant steroid hormone	Epibrassinolide	↓the level of β-catenin. ↓the mRNA levels for a number of genes (Axin-2, c-Jun, c-Myc, MMP7, MMP9, Nanog	↑cell apoptosis and ↓drug resistance of tumor	VPA17 and H69 SCLC cells	Sadava and Kane (2017)
		Survivin, *etc.*)			
Fungal metabolite	Patulin	↑inhibitors of Wnt pathway, Dkk and WIF-1, ↓Cyclin D1	antiproliferative, proapoptotic, and antimigration effects	A549 cells	Monteillier et al. (2018)
Phenanthrene	Dehydroeffusol	↓expression of β-catenin and its downstream related proteins	↓hypoxic-induced migration and invasion of NSCLC cells	A549 cells	Wei et al. (2020)
Aldehyd	Cinnamaldehyde	↑GSK-3β, p-β-catenin expression. ↓β-catenin, TCF-1 and related genes	↓EMT and growth of NSCLC cells. ↓cell movement and metastasis	A549, YTMLC-90 and NCI-H1299 cells. BALB/c/nu/nu nude mice	Wu et al. (2017)
Carotenoid	Fucoxanthin	↓β-catenin and EMT-associated proteins levels	↓TGF-β1 induced cell migration and invasion and EMT	A549 cells	Luan et al. (2022)
saponin	Ophiopogonin B	↑Axin stabilization to inhibit β-catenin	↓EMT in β-catenin overexpressed cells and↓ movement and metastasis	A549, NCI-H1299 and NCI-H460 cells	Zhang et al. (2021)
Polysaccharide	ASPS	↓the levels of wnt3a, p-GSK-3β and Cyclin D1. ↓the expression of EMT-related markers	↓cell proliferation and metastasis	NCI-H520 cells	Sun et al. (2019)
Derivatives	FV429	↑protein expression of GSK-3β and AXIN. ↓β-catenin nuclear localization	↑G2/M phase arrest induced by paclitaxel	A549 and NCI–H460 cells	Guo et al. (2021)
	MRx102	↑WIF-1 by promoter hypomethylation	had similar effects to triptolide without unwanted toxicity	A549 and H460 cells, NSG Mouse Model	Reno et al. (2016)
	xl, 1c and 8b	↓levels of β-catenin and its downstream targets Cyclin D1, CDK4 and c-myc	↓LC cells and tumor growth	A549 and H460 cells, tumor-bearing mice model	Bi et al. (2014)
	DUD	↑Axin expression and p-β-catenin proteolysis	reversed EMT and inhibited migration	A549 cells	Dai et al. (2020)
	12K	↓LRP5/6 phosphorylation and ↓β-catenin expression and nuclear translocation	↓cell growth and metastasis	A549 cells	Dai et al. (2017)
Extracts	GBEE	↓expression of Wnt3a and β-catenin. ↓levels of VEGF and VEGFR2	↓tumor growth and metastasis. ↓MVD in LC grafts	Lewis LC cells, C57BL/6 nude mice	Han et al. (2016)
	AvL-EtOH	↓Wnt3a, β-catenin and downstream genes	↑Caspase-mediated apoptosis and ↓proliferation	A549 cells	Tiwari et al. (2023)
	Atranorin	↓nuclear import of β-catenin and downstream genes	↓invasion and inhibit tumor growth↓tumorigenesis	A549, H460, H1650 and LLC cells, C57BL/6 mice	Zhou et al. (2017)
Chinese medicinal formulae	Miao	↓the expression of c-myc, AXIN and β-catenin	Miao and cisplatin can synergistically regulate LC cell proliferation and apoptosis	NCI-H446 cells, C57BL/6 nude mice	Li et al. (2020a)
	QYSL	↓Wnt1、Wnt2、Wnt5a、GSK3β、p-GSK-3β、β-catenin and Dvl-1	synergistic anti-tumor effect with cisplatin	Lewis lung carcinoma cell xenografts model in nude mice	Tong et al. (2018)
	FYLM	↓expression of p-EGFR, PRC1 and Wnt pathway-related proteins such as β-catenin, c-Myc and c-Jun	↑EGFR-mutated NSCLC cells sensitive to osimertinib	EGFR triple-mutant Lewis LC cells and xenograft mouse model	Shi et al. (2023)
	FYN	↓GSK-3β and β-catenin	↓proliferation and migration of Osimertinib-resistant cell lines	HCC827OR, PC9OR cells, xenografts model in nude mice	Sang et al. (2022)

pathway, with significantly higher activation of the Wnt pathway in NSCLC during ICIs treatment than before, suggesting a role for this pathway in secondary ICIs resistance (Giroux Leprieur et al., 2020). Inhibition of Wnt signaling, dominated by pharmacological Wnt ligand inhibition, promotes the development of the tumor microenvironment, making it more receptive to checkpoint blocking in patients with LC (DeVito et al., 2021).

4 Intervention of natural products on the canonical Wnt pathway in LC

Targeted Wnt therapy has become an important research direction in the development of cancer drugs; however, it also faces problems such as insufficient targeting and large toxic side effects. Therefore, the search for safer and broader drug sources has become the focus of Wnt-targeting research. Natural products have become valuable effective drug sources owing to their wide range of sources, high bioavailability, good safety, and low cost (Sheremet et al., 2017). In the following section, natural products are classified according to their type to discuss their anti-tumor effects via regulation of the Wnt pathway in LC (Table 2). The natural products we discuss in the article are pure compounds extracted from plants except for the Extracts and Chinese Medicine Formulas section.

4.1 Flavonoids

Flavonoids, which are frequently found in human diets and have biological effects, including antioxidant, antibacterial, and anti-inflammatory properties, can lower the risk of disease and are thought to be natural tumor-preventive agents. The biological activity of flavonoids relies on the structural substitution of the C6-C3-C6 loop (Shen et al., 2022). The following is a review of relevant literature on Epigallocatechin gallate (EGCG), garcinol, fisetin, nobiletin, and total flavonoids (TF) involved:

EGCG, the main bioactive ingredient in green tea, is linked to a number of bioactivities, including, anti-cancer, antioxidant, anti-inflammatory and antibacterial activities (Zhang S. et al., 2023). The inactive form of GSK-3β, which is phosphorylated at Ser9 and inhibited by EGCG, became significantly more abundant in the presence of EGCG, while β-catenin and Myc decreased. EGCG increased apoptosis, prevented lung CSCs from proliferating, and decreased the expression of lung CSCs markers at both the protein and mRNA levels (Zhu J. et al., 2017). Lithium chloride (LiCl) is a typical Wnt activator. By causing its phosphorylation at ser9, LiCl therapy inactivated GSK-3β to enhance β-catenin activation which overrode the inhibitory effects of EGCG on the Wnt pathway, tumor sphere formation, and lung CSC markers. LiCl treatment decreased EGCG's ability of EGCG to inhibit the growth of lung CSCs and induce apoptosis (Zhu J. et al., 2017). In addition, aberrant promoter methylation of WIF-1 is the basic mechanism of epigenetic silencing in human cancers. Previous studies have also shown that EGCG treatment can regain WIF-1 expression by promoter demethylation of WIF-1 in NSCLC cell lines (Mazieres et al., 2004). Additionally, cytosolic β-catenin protein levels are lowered by EGCG, and TCF/LEF reporter activity is suppressed (Gao et al., 2009).

Garcinol, a polyisoprenylated benzophenone derived from *Garcinia indica* Choisy (kokum) fruiting bodies and having anti-inflammatory, antioxidant, acetyltransferase inhibitory, and anti-cancer effects, alters lung CSCs' activity and the aggression that goes along with them. Garcinol interferes with the phosphorylation of LRP6, a shared Wnt and Stat3 receptor, and blocks the activation of the Wnt/β-catenin/Stat3 axis. In NSCLC-produced spheres, garcinol reduced the expression of Dvl2, Axin2, β-catenin, and CCND1, indicating that garcinol can control the Wnt/β-catenin signaling pathway. Garcinol therapy dramatically slowed the formation of tumors in a mouse model of H441 CSC, confirming the above findings *in vivo*. Garcinol was found to modulate the lung CSCs phenotype by modulating Wnt/β-catenin signaling and Stat3 inactivation, thus suggesting that garcinol might be a potential new anti-lung CSC medicinal substance (Huang et al., 2018).

Fisetin (3,3′,4′,7-tetrahydroxyflavone) is a natural bioactive flavonoid present in a variety of fruits and vegetables, displaying a range of pharmacological properties, such as anti-invasive and anti-cancer actions (Sundarraj et al., 2018). Fisetin controls the expression of EMT markers and lowered the expression of several signaling proteins that act upstream of EMT such as β-catenin, EGFR, and Stat3. It also decreases the expression of the invasion markers MMP-2, vimentin, and N-cadherin, thereby limiting the potential of the tumor to metastasize. Both the stem cell-like phenotype of H1299 cells and the expression of the lung CSC markers CD44 and CD133 were downregulated following fisetin treatment. Fisetin also inhibited LC cell proliferation by inducing G1-phase cell cycle arrest instead of cell death (Tabasum and Singh, 2019).

The polymethoxylated flavonoid nobiletin (3′,4′,5,6,7,8-hexamethoxyflavone) is specifically accumulated in citrus fruit peel, with many anti-cancer activities. Nobiletin was found to enhance regulators of Wnt/β-catenin signaling, such as Axin2 and WIF-1, which are related to the inhibition of miR-15-5p expression. Nobiletin significantly reduced the ability of NSCLC cells to form spheres and the expression of proteins linked to cancer stemness, namely, CD133 and ALDH1 (Han et al., 2021). Study also discovered that nobiletin prevented A549 and H460 cells from migrating, demonstrating a strong anti-metastatic effect that may be related to the suppression of cell stemness and EMT induced by the inactivation of the Wnt pathway (Han et al., 2021).

TF isolated from Fructus viticis significantly reduced the mRNA expression levels of cyclooxygenase 2 (COX-2), Wnt, and β-catenin in A549 cells. Further research found that TF promoted the apoptosis of A549 cells by inhibiting the COX-2 mediated Wnt/β-catenin signaling pathway, increasing multiple pro-apoptotic genes expression such as apoptotic peptidase activating factor 1, and lowering expression of anti-apoptotic genes BCL2L2 and BCL2. The ability of A549 cells to proliferate was decreased by TF in a dose-dependent manner; however, this effect was reversed by activating Wnt signaling via COX-2. Additionally, animal studies revealed that TF therapy greatly slowed the growth of mouse tumors, with a tumor inhibition rate of 64.07%, and increased the survival time of the animals (Han et al., 2020).

4.2 Polyphenols

Phenols in large numbers and diverse forms provide a variety of potential benefits to human health. Polyphenols have multiple conjugated double bonds and show strong antioxidant capacities. Therefore, when electrons at certain sites are removed by free radicals, the molecular structure is stabilized by conjugation, thereby protecting the cell (Sharoni et al., 2012). This review discusses curcumin, resveratrol, and other compounds (maclurin and eugenol).

4.2.1 Curcumin

Oxidative stress is one of the most common causes of cellular damage, mainly due to the accumulation of reactive oxygen species (ROS) and other free radicals causing damage to antioxidant enzymes such as superoxide dismutase (SOD) (Sies et al., 2017). Previous studies have demonstrated that the Wnt/β-catenin pathway can be activated by ROS-mediated induction, and that the crosstalk between ROS and the Wnt pathway plays an important role in LC adeno-to-squamous transdifferentiation (Fang et al., 2023). The primary component of turmeric (*Curcuma longa* L.), a commonly used traditional Chinese herbal remedy, is curcumin (diferuloylmethane), which has numerous pharmacological effects, including anti-tumor, anti-inflammatory, antioxidative, and neuroprotective properties (Deng et al., 2022). Curcumin reduced ROS levels, increased SOD and γ-glutamyl cysteine synthetase levels, and inhibited A549 cell growth. Curcumin also significantly reduced the expression of nuclear β-catenin and phosphorylated GSK-3β (p-GSK3-β) in their respective proteins. Curcumin treatment drastically inhibited CCND1 and Myc expression. Pretreatment with an ROS scavenger (NAC) significantly reversed this effect. It is clear that oxidative stress plays a role in curcumin-induced suppression of the Wnt/β-catenin pathway by curcumin (Wang J. Y. et al., 2018).

Another study discovered that curcumin effectively reduces lung CSC activity by suppressing the Wnt/β-catenin and Sonic Hedgehog pathways to diminish tumor sphere formation, downregulate CSC marker expression, inhibit proliferation, and induce apoptosis. LiCl-triggered Wnt/β-catenin activation reversed the anti-tumor effects of curcumin (Zhu J. Y. et al., 2017). Curcumin can reduce the transcription and translation of metastasis-associated protein 1 (MTA1) in LC cells and increase the number of cells in the G0/G1 phase. In addition, MTA1 knockout affected the protein levels of β-catenin, MMP7, and CCND1, which was similar to the effect of curcumin treatment in NSCLC. These results suggest that curcumin inhibits the proliferation and metastasis of 95D and A549 cells by reducing their downstream targets via inactivation of the MTAl-Wnt/β-catenin pathway (Lu et al., 2014). Furthermore, the inhibitory impact of curcumin on NSCLC cells may also be attributed to overexpression of miR-192-5p, which targetd c-Myc and deactivated the Wnt/β-catenin signaling pathway (Pan et al., 2020).

4.2.2 Resveratrol

The bioactive phytochemical resveratrol (RES), which is obtained from a variety of plants, has tumor-suppressing effects on LC. RES successfully reduced IL-6 expression and the levels of the CSC-specific markers CD133, ALDH1A1, and Nanog in NSCLC cell lines. Moreover, RES dose-dependently decreased the expression of β-catenin, p-GSK-3β (Ser9), and Myc and inhibited Wnt/β-catenin signaling *in vivo*, which increased the lifespan of mice and prevented the growth of LC. The addition of LiCl partially counteracts the inhibitory effect of RES on lung CSCs and reverses the inhibition of Wnt/β-catenin signaling by RES (Xie et al., 2023). Interestingly, the Wnt pathway was found to be essential for mediating RES-induced upregulation of PD-L1. In H1299 cells, RES reduced Axin2 levels by increasing Snail stability, leading to breakdown of the destruction complex and enhancing TCF/β-catenin adherence to the PD-L1 promoter. RES dose-dependently increases PD-L1 expression in NSCLC cells at pharmacologically accessible concentrations (<30 μM), and RES treatment strongly inhibits T cell function in a co-culture model (Yang M. et al., 2021). These findings imply that RES may contribute to tumor immune evasion.

These contradictory results may be attributed to the different concentrations of RES. PD-L1 expression was induced after exposure to low doses of resveratrol in H1299 cells. However, at higher doses (>40 μM), RES treatment resulted in a gradual reduction of PD-L1, suggesting that RES can modulate PD-L1 expression in a dose-dependent manner (Yang M. et al., 2021). More importantly, there are two structures of natural RES, cis (3,5,4′-Trihydroxystilbene) and trans (trans-3, 5,4′-trihydroxystilbene), which have significant metabolic differences, and may have different or even opposite effects on cells. Further investigation is required to fully understand the possible advantages and hazards of using RES as an adjuvant cancer therapy (Sundarraj et al., 2018; Jarosova et al., 2020; Jhanji et al., 2021).

4.2.3 Other polyphenols

Morus alba L. and *Garcinia mangostana* L. are sources of the natural compound maclurin ((3,4-dihydroxyphenyl)-(2,4,6-trihydroxyphenyl)methanone), a member of the benzophenone family (Moon et al., 2022). The antioxidant activity of maclurin significantly reduced intracellular ROS levels, leading to the inhibition of Src/FAK and ERK in A549 cells. Subsequently, attenuated GSK-3β and reduced accumulation of nuclear β-catenin were observed after maclurin treatment, which further caused downregulation of transcriptional expression and activation of metastasis-related MMP-2 and MMP-9, leading to the inhibition of migration and invasion of human NCLC cells (Ku et al., 2015).

Eugenol (4-allyl (-2-methoxyphenol)) is abundant in the essential oils of widely used Asian species, such as cloves. Eugenol, a naturally occurring β-catenin inhibitor, is an extremely important chemopreventive agent for LC. Eugenol can sequester β-catenin in the cytoplasm and regulate the phosphorylated form of β-catenin to promote its degradation, thus helping the cellular environment to resemble the normal state. Meticulous molecular analysis clearly revealed GSK-3β-mediated phosphorylation of β-catenin after eugenol treatment, leading to degradation of cytoplasmic β-catenin, which significantly limited its transfer to the nucleus. Eugenol activity reduced the expression of CSC markers regulated by β-catenin (CD44, Oct4, EpCAM, and Notch1). Eugenol successfully slowed the activity of the small-molecule CK1 inhibitor D4476, perpetuating the mandatory phosphorylation of β-catenin by CK1α, thereby pushing it toward degradation and minimizing CSC expression. Eugenol treatment showed tumor-preventing effects and significantly prolonged the lifespan of mice with N-nitrosodiethylamine-induced LC (Choudhury et al., 2021).

4.3 Alkaloids

Natural alkaloids are regarded as valuable sources of anti-cancer medicines because they not only exhibit potent anti-tumor effects when taken alone but also when combined with other anti-tumor agents (Luo et al., 2021). Consequently, alkaloids have attracted considerable interest for tumor treatment.

Sanguinarine, a benzophenanthrodine alkaloid, exerts anti-tumor effects through multiple targets and pathways, such as the CSC and TAM phenotypes. A tappable driver of the immunosuppressive M2-like TAM phenotype is the Wnt signaling pathway, which can be regulated by sanguinarine. In M2 macrophages, sanguinarine reduced the protein expression of the nuclear transcription factor β-catenin as well as the mRNA expression of Wnt1 and Wnt7b. By preventing Wnt signaling in TAMs, sanguinarine controlled M2 macrophage polarization and inhibited angiogenesis, showing potential application value in immunotherapy and anti-angiogenesis therapy for LC (Cui et al., 2022). In addition, sanguinarine inhibited the proliferation, invasion, and metastasis of lung CSC mainly through direct downregulation of Wnt/β-catenin self-renewal pathway and indirect interruption of EMT. Sanguinarine, which can be used to target lung CSC, decreased the expression of β-catenin and downstream CCND1 (Yang et al., 2016a). Moreover, a possible anti-cancer target of sanguinarine *in vitro* is the interaction between β-catenin and LEF1, based on a high-throughput sequencing assay (Chen et al., 2021).

The type III benzophenanthridine alkaloid Fisetin was discovered in medicinal plants including *Chelidonium majus* L. and *Macleaya cordata* (Willd.) R. Br (Liu et al., 2006). The major histology of lung CSCs is sensitive to the growth inhibitor chelerythrine chloride, which inhibits the growth of LC cell lines derived from different proximal/distal origins. By downregulating β-catenin, it suppressed the function of CSCs and triggered apoptosis in a variety of LC cells with diverse histological backgrounds. Chelerythrine chloride caused not only a reduction in average β-catenin cellular expression, but also a reduction in nuclear β-catenin localization in several lung tissues, regardless of tissue origin, and different concentrations could trigger the specific targeting required in different cell lines. This broad applicability of chelidonine chloride as a β-catenin inhibitor would favor its development as an anti-CSC therapy for LC (Heng and Cheah, 2020).

Nuciferine (NF), an alkaloid originally isolated from lotus (*Nelumbo nucifera* Gaertn.) leaves, has therapeutic effects such as anti-obesity, antioxidant, and anti-inflammatory properties (Kim S. M. et al., 2022). Axin protein levels significantly increased in NF-treated cells, but not APC or GSK-3 expression levels, while Axin, APC, or GSK-3 mRNA levels were unaffected. The effect of NF was sufficient to induce the accumulation and stabilization of Axin, which accelerated β-catenin degradation and inhibited Wnt/β-catenin signaling in NSCLC cells. NF effectively inhibited the proliferation of nicotine-pretreated NSCLC cells and exerted chemotherapeutic effects on tumor xenograft growth *in vivo*. NF effectively inhibited the proliferation of NSCLC cells pretreated with nicotine *in vitro* and exerted chemotherapeutic effects on tumor xenograft growth *in vivo* (Liu et al., 2015).

β-asarone (1-propenyl-2,4,5-methoxybenzol), the main bioactive component of *Acorus calamus* L., possesses diverse pharmacological activities, including anti-cancer, antidepressant, antiepileptic, antihyperlipidemic, antithrombotic, and radioprotective activities (Chellian et al., 2017). β-asarone induced a dose-dependent decrease in lung carcinoma cell viability, cell migration, invasion and adhesion, and induced tumor mitochondria-associated apoptosis through an endogenous pathway, which significantly increased the activities of caspase-3 and caspase-9. β-asarone increased the expression of GSK-3β while downregulating the expression of Dvl2, p-GSK-3β (Ser 9), and β-catenin. β-asarone treatment also impaired the transcriptional activity of β-catenin/TCF and the expression of its downstream target genes, including MMP-7, Myc, and CCND1. Restoring Wnt/β-catenin signaling pathway activation by Wnt3a can overcome the anti-LC effect induced by β-Asarone (Wang T. L. et al., 2018).

The natural isoquinoline alkaloid lycorine, which is extracted from the herb *Lycoris radiata* (L'Her.), has many anti-cancer properties. After treatment with lycorine, the expression of GSK-3β was increased, the cellular level of β-catenin was inhibited, and the growth and metastasis of LC were significantly hindered. This is closely related to the inhibition of Wnt/β-catenin signal transduction by lycorine and the reversal of EMT in LC cells (Sun et al., 2018).

Daurisoline, an alkaloid constituent of *Menispermum Dauricum* DC., has excellent anti-inflammatory properties (Zhou et al., 2022). Daurisoline may directly target HSP90, preventing its interaction with β-catenin and accelerating β-catenin's ubiquitin-mediated proteasomal destruction. Daurisoline decreased the expression of the downstream genes Myc and CCND1, resulting in cell cycle arrest at the G1 phase. It also influenced the expression of mesenchymal markers, such as N-cadherin and vimentin, which impair the invasive and metastatic potential of LC cells. Daurisoline inhibits the tumorigenicity of LC both *in vitro* and *in vivo* (Huang et al., 2020).

Matrine is the main bioactive component of *Sophora flavescentis* Ait. and has been widely used clinically in China, either alone or in combination with chemotherapeutic drugs or radiotherapy (Li et al., 2016b). Matrine regulates CSCs renewal in NSCLC in a CCND1/Wnt signaling-dependent manner. By targeting the Wnt/CCND1 pathway to prevent 5-fluorouracil-induced CCND1 accumulation in tumor tissues, matrine sensitized NSCLC cells to the effects of 5-fluorouracil *in vivo* and markedly boosted apoptosis. In addition, matrine alleviated EMT by increasing the expression of E-cadherin and lowering the level of N-cadherin, and CCND1 knockdown in NSCLC cells reduced EMT. Matrine regulates CCND1/Wnt-mediated EMT and decreases the mobility of NSCLC cells (Li X. et al., 2020).

The alkaloid ligustrazine is an active component of the Chinese herbal remedy *Ligusticum chuanxiong* Hort. By increasing the level of GSK-3β, ligustrazine considerably reduced the weight and volume of mouse tumors and significantly blocked the activation of the Wnt/β-catenin pathway in LC tissue. This resulted in the inhibition of tumor growth in mice (Dong et al., 2020).

Natural substances derived from sponges, such as fascaplysin, exhibit promising anti-cancer properties. Fascaplysin blocks the cell cycle of A549 cells by regulating cycle-related proteins such as cyclin D1. Fascaplysin treatment reduced the expression levels of Axin2, GSK-3β, β-catenin, and Myc proteins, which inhibited LC cell migration by hindering Wnt signal transduction and reversing the EMT phenotyp (Luo and Xu, 2022).

(1′S, 6*R*)-nitidumalkaloid B is a novel alkaloid identified from *Zanthoxylum nitidum* (Roxb.) DC. and its antiproliferative activity is partly related to G2/M cell cycle arrest, induction of apoptosis and inhibition of the Wnt/β-catenin signaling pathway. It effectively suppressed the expression of β-catenin, Axin2, and p-GSK-3β but

increased p-β-catenin expression in a concentration-dependent manner. Constitutive relationship analysis suggested that the C-6 substituent of benzophenanthridine alkaloids had a direct effect on its antiproliferative activity (Qin et al., 2023).

4.4 Terpenoids

Terpenoids, also known as isoprenoids, are the most diverse compounds in nature, accounting for approximately one-third of all natural products, and are widely used in the field of medicine. For example, paclitaxel is a widely used chemotherapeutic drug in clinical practic (Christianson, 2017). Recently, some terpenoids have shown beneficial effects on the Wnt pathway in LC.

4.4.1 Triptolide

Triptolide (TP), an important active compound in *Tripterygium wilfordii* Hook. f., is a natural diterpene epoxy compound with strong anti-cancer activity that has been widely studied. TP-induced epigenetic changes in histone H3 methylation and nuclear translocation of β-catenin effectively inhibited Wnt signaling in multiple LC models, thereby inhibiting the proliferation, metastasis, and drug resistance of LC cells. The expression of several Wnt inhibitors, such as WIF-1 and DKK1, significantly increased following treatment with TP (Nardi et al., 2018). After treatment with TP, the demethylation of WIF-1 promoter increased the mRNA and protein levels of WIF-1, which prevented the excessive activation of Wnt pathway and affected the downstream Axin2 and β-catenin expression (Mao et al., 2018). Triptolide treatment promoted β-catenin phosphorylation and decreased p-GSK-3β(ser9) expression, inhibited EMT in the xenograft model and reduced lung metastasis in the tail vein injection model. β-catenin overexpression antagonized the triptolide-mediated inhibition of EMT marker expression and counteracted the triptolide-mediated inhibition of the migration and invasion of LC cells (Deng et al., 2021). TP promoted the degradation of β-catenin by blocking the activity of the protein kinase p70S6K, which was found to inactivate phosphorylated GSK-3 at serine 9/21. By repressing the Wnt/β-catenin pathway, TP reversed EMT in paclitaxel-resistant lung adenocarcinoma cells, offering a prospective use for TP and paclitaxel combination therapy (Tian et al., 2021).

4.4.2 Other terpenoids

Cucurbitacin B (CuB) is a natural plant triterpenoid that inhibits endothelial cell migration, invasion, and angiogenesis in NSCLC. CuB treatment inhibited the expression of Wnt3/Wnt3a, inactivating GSK-3 phosphorylation, and restricted β-catenin nuclear localization to influnce interaction with TCF-1 in NSCLC cells. Downregulation of the Wnt/β-catenin signaling axis conferred the ability of CuB to resist NSCLC stemness and metastasis. Additionally, CuB showed strong antiangiogenic properties both *in vivo* and *in vitro*. This property may be attained by influencing angiogenic mediators such MMP-2, survivin, and VEGF in Wnt target genes (Shukla et al., 2016).

The sesquiterpene Curcumol, a bioactive substance purported to have anti-cancer effects, was isolated from rhizome of various Curcuma species. Curcumol treatment controlled the motility, migration, and proliferation of LC cells by altering the expression of Wnt signaling molecules. Curcumol inhibited the phosphorylation of LRP5/6, although Fzd8 was not altered, thereby greatly increasing the protein expression of downstream Axin, APC and GSK-3β. Thus, the β-catenin protein expression was dramatically reduced while its degree of phosphorylation was significantly higher (Li et al., 2021).

Sesquiterpenoids isolated from Curcuma species also contain furanedienone, which may be a potential adjuvant therapy for the treatment of LC. In A549 cells, furanodienone administration suppressed Wnt3 and β-catenin in a dose-dependent manner, thereby downregulating the Wnt signaling pathway. This was correlated with increased apoptosis and cell cycle arrest (Al Saqr et al., 2022).

Euphorbiasteroid (EPBS), a tricyclic terpenoid extracted from *Euphorbia lathyrism* L., inhibited the expression of EGFR, Wnt3a, and Fzd-1 in NSCLC cells and triggered the activation of GSK-3β, which in turn induced β-catenin degradation. In EGFR-overexpressing and-depleted LC cells, EPBS regulated the constitutive activation of the Wnt/β-catenin pathway, and the nuclear translocation of β-catenin was considerably decreased upon EPBS administration, suggesting that EPBS may be implemented alongside EGFR-TKIs in drug-resistant LC (Kim N. Y. et al., 2022).

The antimalarial compounds artemisinin, dihydroartemisinin, and artesunate halt lung tumor progression by blocking the Wnt/β-catenin pathway. They suppressed Wnt5-a/b protein levels and efficiently lowered the expression of LRP6 and Dvl2 while increasing Axin2 expression. Ultimately, this results in downregulation of β-catenin and inhibition of LC proliferation and metastasis (Tong et al., 2016).

20(S)-25-OCH3-PPD (PPD25), a dammarane-type triterpenoid saponin from the leaves of Panax notoginseng (Burk.) F. H., has been reported to have cytotoxic effects in several human cancer cell lines. PPD25 dose-dependently decreased β-catenin expression and inhibited β-catenin/TCF transcriptional activity in A549 cells. It inhibited the expression of Wnt pathway-associated proteins and effectively suppressed proliferation of LC cells, demonstrating the potential as a chemotherapeutic and/or chemopreventive agent for LC (Bi et al., 2009).

4.5 Other types

Isothiocyanate members reduce the signature activation event of β-catenin nuclear localization in LC cell lines. Phenethylisothiocyanate was more effective in preventing the growth of a multicellular tumor spheroid model that mimicked micrometastases, whereas Benzyl isothiocyanate was better at preventing the Long-term colony formation dependent on CSC viability in Wnt-dependent squamous cells. Therefore, Phenethylisothiocyanate might work as chemotherapy to remove a large tumor and Benzyl isothiocyanate may be a safer alternative to target undifferentiated CSCs (Heng and Cheah, 2021).

19-Hydroxybufalin (19-HB) is a monomer of bufadienolides from the skin of toads. 19-HB reduced β-catenin as well as downstream target genes. It produced safe anti-tumor effects *in vitro* and *in vivo* by decreasing viability and promoting apoptosis of LC cells, and its anti-tumor effects were mediated by inhibition of the Wnt signaling pathway (Yu et al., 2021).

Epibrassinolide is a steroid hormone in plants that acts via membrane receptors and GSK-3 pathway, resulting in stabilization of transcription factors. It significantly reduced β-catenin-dependent cytokinesis, metastasis, and anti-apoptotic gene expression in both drug-resistant (VPA17) and drug-sensitized (H69) small cell LC (SCLC) cells, but had no effect on normal lung epithelial cells (Sadava and Kane, 2017).

Patulin, a metabolite of *Penicillium vulpinum*, exhibited antiproliferative, proapoptotic, and antimigration effects on human LUAD cells through inhibition of the Wnt pathway. It upregulated the expression of two endogenous inhibitors of Wnt pathway, Dkk and WIF-1, and downregulated the expression of CCND1 (Monteillier et al., 2018).

Other compounds, such as dehydroeffusol (Wei et al., 2020), cinnamaldehyde (Wu et al., 2017), fucoxanthin (Luan et al., 2022), ophiopogonin B (Zhang et al., 2021) and acanthopanax senticosus polysaccharide (ASPS) (Sun et al., 2019), can inhibit the Wnt pathway to weaken the EMT process and inhibit tumor metastasis.

4.6 Derivatives

In addition, some derivatives artificially manufactured based on the well-defined structures of pure compounds extracted from plants. Most of them showed better bioavailability and achieved better anti-tumor effects by enhancing efficacy and attenuating toxicity.

FV-429, a derivative of the natural flavonoid wogonin, reprogrammed cancer cell metabolism and reduced fatty acid levels. The combination of FV-429 and paclitaxel not only reduced the levels of Wnt3a, LRP6, and Dvl 2 but also increased the protein expression of GSK-3β and Axin, which blocked the hypoxia-driven nuclear localization of β-catenin. Furthermore, FV-429-regulated fatty acid metabolism enhanced the efficacy of paclitaxel in NSCLC through Wnt-mediated G2/M phase arrest (Guo et al., 2021).

The triptolide derivative MRx102 upregulated WIF-1 in LC cell lines via hypomethylation of its promoter. Interestingly, MRx102 has effects similar to those of triptolide without unwanted toxicity (Reno et al., 2016). Three ginsenoside derivatives, xl, 1c, and 8b, showed good anti-tumor activity against LC, and their anti-growth activity against LC cells partly involved β-catenin-mediated signaling, as these substances reduced the expression of β-catenin and its subsequent targets CCND1, CDK4, and Myc (Bi et al., 2014).

Based on the structure of the natural product taspine, a diphenylurea derivative (DUD) was synthesized using a computer-aided drug design method to reduce the expression and nuclear translocation of β-catenin. DUD significantly upregulated Axin expression and stabilized the β-catenin destruction complex to promote proteasome-mediated protein hydrolysis of phosphorylated β-catenin. DUD reversed EMT process and inhibited LC cell migration via Wnt/β-catenin and PI3K/Akt signaling (Dai et al., 2020). Compound 12k, a derivative of taspine, adversely controlled the Wnt signaling pathway by reducing the nuclear translocation of β-catenin and suppressing the phosphorylation of LRP5/6. Compound 12k downregulated MMP3 and MMP7 expression, which was controlled by β-catenin in A549 cells. Related migration proteins such as VEGF, MMP2, and MMP9 were impaired after 12k treatment (Dai et al., 2017).

4.7 Extracts and Chinese Medicine Formulas

Ginkgo biloba exocarp extract (GBEE) contains a large number of components with bioactivities, such as antioxidant, antibacterial and anti-tumor. Ginkgo biloba seed exocarp polysaccharides and ginkgolic acids are be identified as the main components in GBEE contributing to the anti-tumor effect (Wang et al., 2022). GBEE significantly inhibited the expression of Wnt3a and β-catenin in mice and reduced VEGF and VEGFR2 mRNA levels in LC cells. GBEE inhibits Lewis LC angiogenesis by inhibiting the Wnt/β-catenin-VEGF signaling pathway to suppress MVD in transplant tumors which inhibits tumor growth and suppresses tumor lung metastasis in a dose-dependent manner (Han et al., 2016).

The ethanolic extract of *Artemisia vulgaris* L. (AvL-EtOH) decreased the downstream activation of Wnt3a in A549 cells, thereby inhibiting tumor cell proliferation and promoting caspase cascade activation-induced apoptosis. The gas chromatography-mass spectrometry analysis of AvL-EtOH exhibited 48 peaks of various secondary metabolites such as terpenoids, flavonoids, carbohydrates, coumarins, amino acids, steroids and proteins (Tiwari et al., 2023).

Everniastrum vexans is a secondary metabolite extracted from lichen with anti-migration activity to LC cells, and atranorin is identified as an active subcomponent of this extract. Atranorin inhibited LC cell motility and tumorigenic potential in xenograft tumor model by inhibiting the nuclear import of β-catenin and down-regulating downstream genes expression (Zhou et al., 2017).

Anti-cancer formulas, such as Miao-Yi-Ai-Tang (Miao) and Qiyusanlong (QYSL) decoction, significantly enhance the effect of Cisplatin on LC cells. Miao treatment inhibited the expression of Axin, β-catenin, and Myc, restricting the development of LC. Miao not only had similar effects as cisplatin on LC cells, but also induced an improvement in cisplatin resistance. The simultaneous use of Miao and cisplatin synergistically regulated cell proliferation and apoptosis and enhanced the inhibitory effect on LC cells (Li B. et al., 2020). QYSL inhibited Wnt1, Wnt2, Wnt5a, GSK-3β, p-GSK-3β, β-catenin, and Dvl-1 protein levels and decreased downstream expression of related mRNAs. The combination of chemotherapy drug Cisplatin and a high dose of QYSL decoction significantly enhanced the inhibitory effect on LC (Tong et al., 2018).

The Feiyiliu Mixture (FYLM) and Feiyanning Formula (FYN) are experienced Chinese medicinal formulas. FYLM reduced the expression of phosphorylated EGFR and Wnt pathway-related proteins, such as β-catenin and Myc. FYLM treatment delays the resistance of EGFR-mutant cell lines and EGFR-mutant tumor-bearing mice to osimertinib by inhibiting the Wnt/EGFR pathway (Shi et al., 2023). FYN in combination with osimertinib significantly inhibited the proliferation and migration of drug-resistant NSCLC cell lines. It reduced GSK-3β and β-catenin expression and exerted anti-osimertinib resistance by inhibiting the Wnt/β-catenin pathway (Sang et al., 2022).

Additionally, almost every element of the Wnt signaling pathway, from the synthesis and secretion of Wnt ligands to the

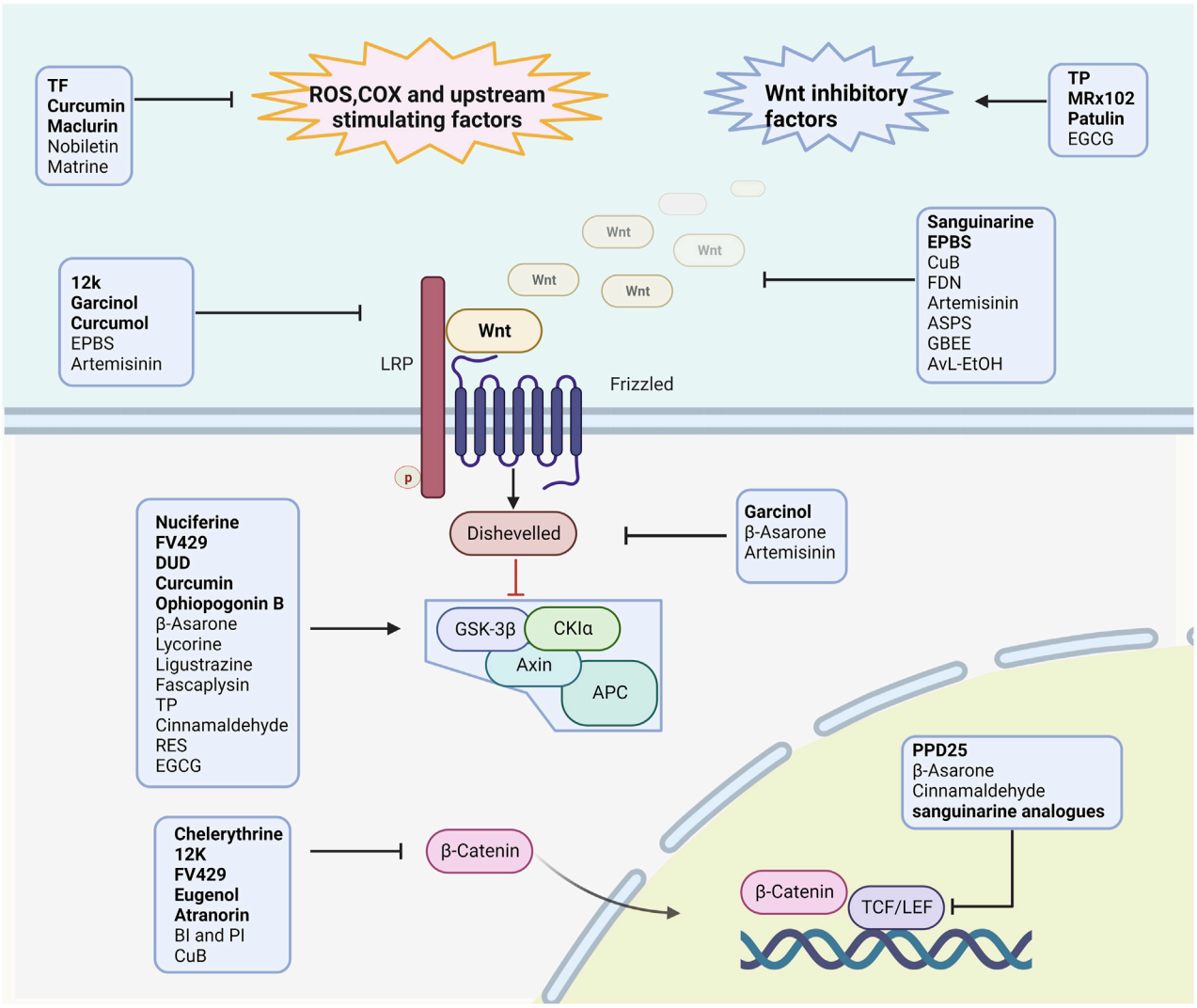

FIGURE 2
The manner in which the studied product acts on the Wnt pathway in lung cancer. Natural compounds and their derivatives inhibit the Wnt signaling pathway by reducing upstream activators such as SOX and COX-2, inhibiting Wnt ligands, inhibiting receptor phosphorylation such as Fzd, inhibiting Dvl, promoting destruction complex stabilization, and inhibiting β-catenin nuclear localization and TCF/LEF transcription factor activity.

transcription of Wnt target genes, has the potential to become a molecular target for cancer therapy (Sheridan, 2018). Natural products and their derivatives could target various components of the canonical Wnt pathway (Figure 2) and have a high safety profile. Some can enhance efficacy or inhibit drug resistance, showing good potential for combination therapy with existing anti-tumor drugs (Table 3). This may be an important breakthrough point to address the limited therapeutic window, and provide new avenues for LC treatment.

5 Drug delivery systems

Although natural products and their derivatives have achieved promising anti-tumor effects in basic research, they still face challenges in clinical applications, such as low solubility, limited oral bioavailability, poor metabolism and insufficient organ targeting. Because of these limitations, most the natural products have to apply to patients with a huge dosage, which may increase the risk of inducing side effects (Atanasov et al., 2021). Therefore, it would be crucial to research effective drug delivery systems (DDSs) for these compounds.

Nanotechnology helps reduce chaotic distribution and direct drug containment in cancer cells through the movement of DDSs to a greater extent, increasing local utilization, maintaining a higher bioactivity and improving metabolic stability (Hu et al., 2017; Maqsoudlou et al., 2022). The immature vascular system with large cellular gaps in LC has enhanced permeability and retention of nanosized DDSs. The smaller capillaries in the lung enable passive lung targeting of DDSs larger than 7 μm in size (Park et al., 2019). It has been suggested that the delivery of Wnt pathway inhibitors to CSCs requires stable liposomal encapsulation and delayed tumor tissue drug release. Liposomal drugs specifically interfere with aberrant Wnt signaling in tumor tissues, resulting

TABLE 3 Effectiveness of subjects in combination with existing drugs.

Name	Anti-LC drugs	Effect of combination	References
Fisetin	Erlotinib	enhance the cytotoxic effect of the drug	Tabasum and Singh (2019)
Matrine	5-fluorouracil	matrine increased the sensitivity of lung CSCs to 5-FU and inhibited the accumulation of CCND1 in tumor tissues induced by 5-FU.	Li et al. (2020b)
TP	Paclitaxel	reversing EMT and impairing tumor growth in paclitaxel-resistant LUAD cells	Tian et al. (2021)
EPBS	-	modulation of Wnt pathway protein activity in EGFR overexpressing and EGFR depleted cancer cells with potential for anti-TKI resistance	Kim et al. (2022a)
Epibrassinolide	Etoposide	the combination index showed synergism between epibrassinolide and etoposide and between epibrassinolide and doxorubicin. Reversing resistance to two chemotherapeutics	Sadava and Kane (2017)
	Doxorubicin		
FV-429	Paclitaxel	remodeling of fatty acid metabolism in hypoxia-induced paclitaxel-resistant NSCLC through inactivation of the Wnt pathway and increasing sensitivity to paclitaxel	Guo et al. (2021)
Miao	Cisplatin	simultaneous treatment can significantly enhance the effect of DDP on LC cells. It can synergistically regulate the proliferation and apoptosis of lung cancer cells	Li et al. (2020a)
OYSL	Cisplatin	treatment with QYSL broth alone was milder compared to DDP, however, the combination of QYSL broth and chemotherapy demonstrated enhanced anti-tumor effects compared to treatment administered alone	Tong et al. (2018)
FYLM	Osimertinib	sensitizing EGFR Del19/T790M/C797S mutant NSCLC cells to osimertinib	Shi et al. (2023)
FYN	Osimertinib	synergistic effect against cell proliferation and migration. Inhibit drug resistance	Sang et al. (2022)

in a focused effect on LGR5^{+} CSCs (Li et al., 2019). Encapsulation in nanoparticles such as liposomes and nanomicelles has solved the problem of poor water solubility and bioavailability of natural products to be a favorable curcumin delivery system for targeting LC (Ibrahim et al., 2018; Zhang et al., 2018). Co-delivery of erlotinib and curcumin by nanomicelles improved anti-tumor effects *in vitro* by reducing Wnt pathway-related gene expression (Bagherian et al., 2021). Liposomes, as the DDSs we are concerned about, have been developed from the initial modification of classical lipid components to long-circulating, environmentally-sensitive and actively-targeted liposomes. It is expected that multifunctional liposomes with high potential for clinical applications can be obtained through organic combinations (Wang L. et al., 2021).

Nanoparticles can be modified to allow delivery of drugs by inhalation, which offers a promising non-invasive therapeutic option for the treatment of LC, such as a nanocomposite system loaded with RES for nebulization, demonstrating higher anti-cancer selectivity index (Wang et al., 2020; Zhang X. et al., 2023). Nanocrystalline materials have good atomization properties and are good carriers for local targeted delivery of natural products with poor water solubility to achieve continuous lung delivery (Lai et al., 2019). Other types of nanocarriers, such as chitosan nanoparticles, mesoporous silica nanoparticles, polymer nanoparticles, *etc.*, have also shown non-negligible development potential, and they not only improve bioavailability *in vivo*, but also enhance the synergistic delivery efficiency of chemotherapeutic agents (Liang et al., 2021). Quercetin and doxorubicin co-delivery using mesoporous silica nanoparticles decreased expression of Wnt16 and P-glycoprotein, thereby reshaping the tumor microenvironment and reversing multidrug resistance (Fang et al., 2018). Nano-delivery systems combining physical, biological and chemical means of targeting have shown promising anti-tumor efficacy and provide templates for multi-technology co-design of DDSs (Lin et al., 2020). However, various DDSs loaded with natural products still need to be explored in-depth preclinical experiments and clinical trials to clarify their safety and efficacy.

6 Summary

Current Wnt studies in LC have focused on LUAD-dominated NSCLC, and markers suggesting efficacy remain inadequately studied, although there have been reports on Wnt ligand-dependent tumor markers (Kleeman et al., 2020). In the future, more attention should be paid to the specific activation modes of Wnt in the LC, such as Wnt effector overexpression and inhibition by Wnt antagonists, which are common alterations in the LC. A fuller understanding of the possible LC-specific mechanisms of Wnt activation and analysis of the conformational relationships between natural product interventions and Wnt will facilitate research on more targeted inhibitors that may reduce the impact of widespread inhibition on normal human function.

Targeted toxicity of existing Wnt inhibitor therapeutic-grade molecules is a major limitation hindering their clinical development (Diamond et al., 2020; Angers, 2021). Compared with chemically synthesized medications, small-molecule compounds of natural product origin are less toxic, more biocompatible, and may present better safety and tolerability in humans. Among them, eugenol was observed to regulate the phosphorylation pattern of β-catenin in tumor cells to near normal, and no excessive inhibition or adverse toxic side effects were observed, indicating its potential as a novel regulator of Wnt (Choudhury et al., 2021). We are interested in this particular way of regulating the Wnt pathway, although we do not have a clear understanding of the constitutive relationship and the deeper mechanism of action of its intervention in the Wnt pathway because of the limited evidence of previous studies.

Therefore, further conformational and experimental studies are required to investigate the mechanism of action and clinical therapeutic effects.

Although the limited number of studies and the incomplete study of Wnt inhibition modalities may have influenced us to draw definite conclusions, we found from the relevant studies that different types of compounds seem to play their own roles in interfering with the Wnt pathway in LC. Polyphenolic compounds, such as curcumin, have an excellent ability to inhibit oxidative stress-mediated upregulation of the abnormal Wnt pathway, an ability not possessed by other compounds. Half of the studied alkaloids and their derivatives could promote the stabilization of β-catenin destructive complex by up-regulating Axin, GSK-3β or downregulating its inactive phosphorylation. Terpenoids appear to act upstream of the Wnt pathway to inhibit it, and most terpenoids and derivatives, such as triptolide, inhibit the Wnt pathway in LC through the upregulation of Wnt antagonists and the downregulation of Wnt ligands. Natural small-molecule products have greatly increased the diversity and potential for drug development, with diverse mechanisms of action, thus allowing them to act on multiple targets of the Wnt pathway in LC and present partial inhibition of some of the more difficult targets, such as c-Myc, which may reduce the risk of future drug resistance.

In the context of the limited clinical studies on existing Wnt inhibitors, our study provides pharmaceutical companies and researchers with safer and more diverse options for the future development of inhibitors targeting the key Wnt pathway in LC, thereby enriching the clinical treatment options for LC.

7 Outlook

The complexity of the molecular interactions of the Wnt/β-catenin pathway and its involvement in different physiological functions make drug discovery challenging (Chatterjee et al., 2022). The introduction of new technologies such as artificial intelligence using, natural language processing, deep learning, and image recognition has greatly improved the efficiency and success rate of drug discovery (Freedman, 2019). Although the development of phytochemicals high-value of is in the spotlight, natural compounds isolated from living organisms currently face difficulties in screening new drugs due to their poor solubility, stability, and pharmacokinetics (Süntar et al., 2021). Nanoparticles and liposomes are useful strategies to overcome the poor absorption, rapid metabolism, and elimination inherent in most natural products; helping to increase their bioavailability and target specific sites, such as the lung. Given the emerging treatment landscape of non-invasive therapy in LC, a precise targeted local therapy should be attempted to reduce the systemic side effects of Wnt inhibitors.

In addition, the direct tumor-killing effect of Wnt inhibitors alone is limited. We are particularly interested in the impact of Wnt in mediating clinically relevant therapies for LC, such as chemotherapy, radiotherapy, EGFR-TKI, immunotherapy, and even antiangiogenic therapy. Therefore, Wnt combination therapy is a good strategy for overcoming drug resistance in LC, and should be an overriding direction for future research. Many naturally occurring small molecules used as Wnt inhibitors have good effects when used in combination with chemotherapy and targeted drugs, with the advantage of inhibiting proliferation and overcoming drug resistance, but the effectiveness and safety of clinical treatment still need to be further determined (Guo et al., 2021; Shah et al., 2021; Tian et al., 2021). The therapeutic treatment of LC could be significantly improved by the discovery of more effective and selective inhibitors of Wnt/β-catenin in combination with other therapies.

Author contributions

XS: Conceptualization, Data curation, Writing—original draft, Investigation. CG: Conceptualization, Data curation. HL and CL: Investigation. LW, YL, RL: Writing—review and editing. CS: Supervision, Validation. JZ: Conceptualization, Data curation, Writing—original draft, Supervision, Validation, Writing—review and editing. All authors contributed to the article and approved the submitted version.

Funding

This work was supported by the National Natural Science Foundation of China (grant number 82174222, 81973677) and Shandong Province Natural Science Foundation (grant number ZR2021MH343).

Acknowledgments

Thanks to all authors for their hard work and important comments.

Conflict of interest

The authors declare that the research was conducted in the absence of any commercial or financial relationships that could be construed as a potential conflict of interest.

Publisher's note

All claims expressed in this article are solely those of the authors and do not necessarily represent those of their affiliated organizations, or those of the publisher, the editors and the reviewers. Any product that may be evaluated in this article, or claim that may be made by its manufacturer, is not guaranteed or endorsed by the publisher.

References

Aguilera, K. Y., and Dawson, D. W. (2021). WNT ligand dependencies in pancreatic cancer. *Front. Cell Dev. Biol.* 9, 671022. doi:10.3389/fcell.2021.671022

Al Saqr, A., Khafagy, E. S., Aldawsari, M. F., Almansour, K., and Abu Lila, A. S. (2022). Screening of apoptosis pathway-mediated anti-proliferative activity of the phytochemical compound furanodienone against human non-small lung cancer A-549 cells. *Life (Basel)* 12 (1), 114. doi:10.3390/life12010114

Aleksakhina, S. N., Kashyap, A., and Imyanitov, E. N. (2019). Mechanisms of acquired tumor drug resistance. *Biochim. Biophys. Acta Rev. Cancer* 1872 (2), 188310. doi:10.1016/j.bbcan.2019.188310

Allemani, C., Matsuda, T., Di Carlo, V., Harewood, R., Matz, M., Nikšić, M., et al. (2018). Global surveillance of trends in cancer survival 2000-14 (CONCORD-3): analysis of individual records for 37 513 025 patients diagnosed with one of 18 cancers from 322 population-based registries in 71 countries. *Lancet* 391 (10125), 1023–1075. doi:10.1016/s0140-6736(17)33326-3

Angers, S. (2021). Wnt signaling inhibition confers induced synthetic lethality to PARP inhibitors. *EMBO Mol. Med.* 13 (4), e14002. doi:10.15252/emmm.202114002

Atanasov, A. G., Zotchev, S. B., Dirsch, V. M., and Supuran, C. T. (2021). Natural products in drug discovery: advances and opportunities. *Nat. Rev. Drug Discov.* 20 (3), 200–216. doi:10.1038/s41573-020-00114-z

Ayob, A. Z., and Ramasamy, T. S. (2018). Cancer stem cells as key drivers of tumour progression. *J. Biomed. Sci.* 25 (1), 20. doi:10.1186/s12929-018-0426-4

Bagherian, A., Roudi, B., Masoudian, N., and Mirzaei, H. (2021). Anti-glioblastoma effects of nanomicelle-curcumin plus erlotinib. *Food Funct.* 12 (21), 10926–10937. doi:10.1039/d1fo01611c

Bi, X., Xia, X., Mou, T., Jiang, B., Fan, D., Wang, P., et al. (2014). Anti-tumor activity of three ginsenoside derivatives in lung cancer is associated with Wnt/β-catenin signaling inhibition. *Eur. J. Pharmacol.* 742, 145–152. doi:10.1016/j.ejphar.2014.08.032

Bi, X., Zhao, Y., Fang, W., and Yang, W. (2009). Anticancer activity of Panax notoginseng extract 20(S)-25-OCH3-PPD: Targetting beta-catenin signalling. *Clin. Exp. Pharmacol. Physiol.* 36 (11), 1074–1078. doi:10.1111/j.1440-1681.2009.05203.x

Brabletz, T., Kalluri, R., Nieto, M. A., and Weinberg, R. A. (2018). EMT in cancer. *Nat. Rev. Cancer* 18 (2), 128–134. doi:10.1038/nrc.2017.118

Brahimi-Horn, C., Berra, E., and Pouysségur, J. (2001). Hypoxia: the tumor's gateway to progression along the angiogenic pathway. *Trends Cell Biol.* 11 (11), S32–S36. doi:10.1016/s0962-8924(01)02126-2

Bretones, G., Delgado, M. D., and León, J. (2015). Myc and cell cycle control. *Biochim. Biophys. Acta* 1849 (5), 506–516. doi:10.1016/j.bbagrm.2014.03.013

Cargill, K. R., Stewart, C. A., Park, E. M., Ramkumar, K., Gay, C. M., Cardnell, R. J., et al. (2021). Targeting MYC-enhanced glycolysis for the treatment of small cell lung cancer. *Cancer Metab.* 9 (1), 33. doi:10.1186/s40170-021-00270-9

Casás-Selves, M., Kim, J., Zhang, Z., Helfrich, B. A., Gao, D., Porter, C. C., et al. (2012). Tankyrase and the canonical Wnt pathway protect lung cancer cells from EGFR inhibition. *Cancer Res.* 72 (16), 4154–4164. doi:10.1158/0008-5472.Can-11-2848

Cassetta, L., and Pollard, J. W. (2023). A timeline of tumour-associated macrophage biology. *Nat. Rev. Cancer* 23 (4), 238–257. doi:10.1038/s41568-022-00547-1

Chatterjee, A., Paul, S., Bisht, B., Bhattacharya, S., Sivasubramaniam, S., and Paul, M. K. (2022). Advances in targeting the WNT/β-catenin signaling pathway in cancer. *Drug Discov. Today* 27 (1), 82–101. doi:10.1016/j.drudis.2021.07.007

Chaudhary, A., Raza, S. S., and Haque, R. (2023). Transcriptional factors targeting in cancer stem cells for tumor modulation. *Semin. Cancer Biol.* 88, 123–137. doi:10.1016/j.semcancer.2022.12.010

Chellian, R., Pandy, V., and Mohamed, Z. (2017). Pharmacology and toxicology of α- and β-asarone: A review of preclinical evidence. *Phytomedicine* 32, 41–58. doi:10.1016/j.phymed.2017.04.003

Chen, Y., Fu, Z., Li, D., Yue, Y., and Liu, X. (2021). Optimizations of a novel fluorescence polarization-based high-throughput screening assay for β-catenin/LEF1 interaction inhibitors. *Anal. Biochem.* 612, 113966. doi:10.1016/j.ab.2020.113966

Cheng, L. H., Hsu, C. C., Tsai, H. W., Liao, W. Y., Yang, P. M., Liao, T. Y., et al. (2023). ASPM activates Hedgehog and wnt signaling to promote small cell lung cancer stemness and progression. *Cancer Res.* 83 (6), 830–844. doi:10.1158/0008-5472.Can-22-2496

Choudhury, P., Barua, A., Roy, A., Pattanayak, R., Bhattacharyya, M., and Saha, P. (2021). Eugenol emerges as an elixir by targeting β-catenin, the central cancer stem cell regulator in lung carcinogenesis: an *in vivo* and *in vitro* rationale. *Food Funct.* 12 (3), 1063–1078. doi:10.1039/d0fo02105a

Christianson, D. W. (2017). Structural and chemical biology of terpenoid cyclases. *Chem. Rev.* 117 (17), 11570–11648. doi:10.1021/acs.chemrev.7b00287

Cui, Y., Luo, Y., Qian, Q., Tian, J., Fang, Z., Wang, X., et al. (2022). Sanguinarine regulates tumor-associated macrophages to prevent lung cancer angiogenesis through the WNT/β-Catenin pathway. *Front. Oncol.* 12, 732860. doi:10.3389/fonc.2022.732860

Dai, B., Fan, M., Yu, R., Su, Q., Wang, B., Yang, T., et al. (2020). Novel diphenyl urea derivative serves as an inhibitor on human lung cancer cell migration by disrupting EMT via Wnt/β-catenin and PI3K/Akt signaling. *Toxicol Vitro* 69, 105000. doi:10.1016/j.tiv.2020.105000

Dai, B., Ma, Y., Yang, T., Wang, W., and Zhang, Y. (2017). Taspine derivative 12k suppressed A549 cell migration through the Wnt/β-catenin and EphrinB2 signaling pathway. *Biomed. Pharmacother.* 87, 102–109. doi:10.1016/j.biopha.2016.12.077

Dang, C. V., Kim, J. W., Gao, P., and Yustein, J. (2008). The interplay between MYC and HIF in cancer. *Nat. Rev. Cancer* 8 (1), 51–56. doi:10.1038/nrc2274

Datta, S., Choudhury, D., Das, A., Mukherjee, D. D., Dasgupta, M., Bandopadhyay, S., et al. (2019). Autophagy inhibition with chloroquine reverts paclitaxel resistance and attenuates metastatic potential in human nonsmall lung adenocarcinoma A549 cells via ROS mediated modulation of β-catenin pathway. *Apoptosis* 24 (5-6), 414–433. doi:10.1007/s10495-019-01526-y

Daum, S., Hagen, H., Naismith, E., Wolf, D., and Pircher, A. (2020). The role of anti-angiogenesis in the treatment landscape of non-small cell lung cancer - new combinational approaches and strategies of neovessel inhibition. *Front. Cell Dev. Biol.* 8, 610903. doi:10.3389/fcell.2020.610903

Dejana, E. (2010). The role of wnt signaling in physiological and pathological angiogenesis. *Circ. Res.* 107 (8), 943–952. doi:10.1161/circresaha.110.223750

Deng, Q. D., Lei, X. P., Zhong, Y. H., Chen, M. S., Ke, Y. Y., Li, Z., et al. (2021). Triptolide suppresses the growth and metastasis of non-small cell lung cancer by inhibiting β-catenin-mediated epithelial-mesenchymal transition. *Acta Pharmacol. Sin.* 42 (9), 1486–1497. doi:10.1038/s41401-021-00657-w

Deng, Z., Dong, Y., Zhou, X., Lu, J. H., and Yue, Z. (2022). Pharmacological modulation of autophagy for Alzheimer's disease therapy: Opportunities and obstacles. *Acta Pharm. Sin. B* 12 (4), 1688–1706. doi:10.1016/j.apsb.2021.12.009

Devito, N. C., Sturdivant, M., Thievanthiran, B., Xiao, C., Plebanek, M. P., Salama, A. K. S., et al. (2021). Pharmacological Wnt ligand inhibition overcomes key tumor-mediated resistance pathways to anti-PD-1 immunotherapy. *Cell Rep.* 35 (5), 109071. doi:10.1016/j.celrep.2021.109071

Diamond, J. R., Becerra, C., Richards, D., Mita, A., Osborne, C., O'shaughnessy, J., et al. (2020). Phase Ib clinical trial of the anti-frizzled antibody vantictumab (OMP-18R5) plus paclitaxel in patients with locally advanced or metastatic HER2-negative breast cancer. *Breast Cancer Res. Treat.* 184 (1), 53–62. doi:10.1007/s10549-020-05817-w

Dong, Y., Yang, Y., Wei, Y., Gao, Y., Jiang, W., and Wang, G. (2020). Ligustrazine eases lung cancer by regulating PTEN and Wnt/β-catenin pathway. *Transl. Cancer Res.* 9 (3), 1742–1751. doi:10.21037/tcr.2020.03.26

Du, W., Menjivar, R. E., Donahue, K. L., Kadiyala, P., Velez-Delgado, A., Brown, K. L., et al. (2023). WNT signaling in the tumor microenvironment promotes immunosuppression in murine pancreatic cancer. *J. Exp. Med.* 220 (1), e20220503. doi:10.1084/jem.20220503

Eubelen, M., Bostaille, N., Cabochette, P., Gauquier, A., Tebabi, P., Dumitru, A. C., et al. (2018). A molecular mechanism for Wnt ligand-specific signaling. *Science* 361, eaat1178. doi:10.1126/science.aat1178

Fang, J., Zhang, S., Xue, X., Zhu, X., Song, S., Wang, B., et al. (2018). Quercetin and doxorubicin co-delivery using mesoporous silica nanoparticles enhance the efficacy of gastric carcinoma chemotherapy. *Int. J. Nanomedicine* 13, 5113–5126. doi:10.2147/ijn.S170862

Fang, Z., Han, X., Chen, Y., Tong, X., Xue, Y., Yao, S., et al. (2023). Oxidative stress-triggered Wnt signaling perturbation characterizes the tipping point of lung adeno-to-squamous transdifferentiation. *Signal Transduct. Target Ther.* 8 (1), 16. doi:10.1038/s41392-022-01227-0

Ferrarelli, L. K. (2017). Treating WNT-driven colorectal cancer. *Science* 356 (6345), 1346–1348. doi:10.1126/science.356.6345.1346-r

Freedman, D. H. (2019). Hunting for new drugs with AI. *Nature* 576 (7787), S49–s53. doi:10.1038/d41586-019-03846-0

Galluzzi, L., Spranger, S., Fuchs, E., and López-Soto, A. (2019). WNT signaling in cancer immunosurveillance. *Trends Cell Biol.* 29 (1), 44–65. doi:10.1016/j.tcb.2018.08.005

Gao, Z., Xu, Z., Hung, M. S., Lin, Y. C., Wang, T., Gong, M., et al. (2009). Promoter demethylation of WIF-1 by epigallocatechin-3-gallate in lung cancer cells. *Anticancer Res.* 29 (6), 2025–2030.

Ghandadi, M., Valadan, R., Mohammadi, H., Akhtari, J., Khodashenas, S., and Ashari, S. (2019). Wnt-β-catenin signaling pathway, the achilles' heels of cancer multidrug resistance. *Curr. Pharm. Des.* 25 (39), 4192–4207. doi:10.2174/1381612825666191112142943

Giroux Leprieur, E., Hélias-Rodzewicz, Z., Takam Kamga, P., Costantini, A., Julie, C., Corjon, A., et al. (2020). Sequential ctDNA whole-exome sequencing in advanced lung adenocarcinoma with initial durable tumor response on immune checkpoint inhibitor and late progression. *J. Immunother. Cancer* 8 (1), e000527. doi:10.1136/jitc-2020-000527

Glaw, J. T., Skalak, T. C., and Peirce, S. M. (2010). Inhibition of canonical Wnt signaling increases microvascular hemorrhaging and venular remodeling in adult rats. *Microcirculation* 17 (5), 348–357. doi:10.1111/j.1549-8719.2010.00036.x

Guan, C., Zhou, X., Li, H., Ma, X., and Zhuang, J. (2022). NF-κB inhibitors gifted by nature: The anticancer promise of polyphenol compounds. *Biomed. Pharmacother.* 156, 113951. doi:10.1016/j.biopha.2022.113951

Guo, Y., Yang, L., Guo, W., Wei, L., and Zhou, Y. (2021). FV-429 enhances the efficacy of paclitaxel in NSCLC by reprogramming HIF-1α-modulated FattyAcid metabolism. *Chem. Biol. Interact.* 350, 109702. doi:10.1016/j.cbi.2021.109702

Han, D., Cao, C., Su, Y., Wang, J., Sun, J., Chen, H., et al. (2016). Ginkgo biloba exocarp extracts inhibits angiogenesis and its effects on Wnt/β-catenin-VEGF signaling pathway in Lewis lung cancer. *J. Ethnopharmacol.* 192, 406–412. doi:10.1016/j.jep.2016.09.018

Han, L., Fang, S., Li, G., Wang, M., and Yu, R. (2020). Total flavonoids suppress lung cancer growth via the COX-2-mediated Wnt/β-catenin signaling pathway. *Oncol. Lett.* 19 (3), 1824–1830. doi:10.3892/ol.2020.11271

Han, S. H., Han, J. H., Chun, W. J., Lee, S. S., Kim, H. S., and Lee, J. W. (2021). Nobiletin inhibits non-small-cell lung cancer by inactivating WNT/β-Catenin signaling through downregulating miR-15-5p. *Evid. Based Complement. Altern. Med.* 2021, 7782963. doi:10.1155/2021/7782963

Hanahan, D., and Weinberg, R. A. (2011). Hallmarks of cancer: the next generation. *Cell* 144 (5), 646–674. doi:10.1016/j.cell.2011.02.013

Hargadon, K. M. (2023). Genetic dysregulation of immunologic and oncogenic signaling pathways associated with tumor-intrinsic immune resistance: a molecular basis for combination targeted therapy-immunotherapy for cancer. *Cell Mol. Life Sci.* 80 (2), 40. doi:10.1007/s00018-023-04689-9

He, Y., Jiang, X., Duan, L., Xiong, Q., Yuan, Y., Liu, P., et al. (2021). LncRNA PKMYT1AR promotes cancer stem cell maintenance in non-small cell lung cancer via activating Wnt signaling pathway. *Mol. Cancer* 20 (1), 156. doi:10.1186/s12943-021-01469-6

Heng, W. S., and Cheah, S. C. (2020). Chelerythrine chloride downregulates β-catenin and inhibits stem cell properties of non-small cell lung carcinoma. *Molecules* 25 (1), 224. doi:10.3390/molecules25010224

Heng, W. S., and Cheah, S. C. (2021). Identification of phytochemical-based β-catenin nuclear localization inhibitor in NSCLC: Differential targeting population from member of isothiocyanates. *Molecules* 26 (2), 399. doi:10.3390/molecules26020399

Herbst, R. S., Onn, A., and Sandler, A. (2005). Angiogenesis and lung cancer: Prognostic and therapeutic implications. *J. Clin. Oncol.* 23 (14), 3243–3256. doi:10.1200/jco.2005.18.853

Hong, C. F., Chen, W. Y., and Wu, C. W. (2017). Upregulation of Wnt signaling under hypoxia promotes lung cancer progression. *Oncol. Rep.* 38 (3), 1706–1714. doi:10.3892/or.2017.5807

Hu, K., Miao, L., Goodwin, T. J., Li, J., Liu, Q., and Huang, L. (2017). Quercetin remodels the tumor microenvironment to improve the permeation, retention, and antitumor effects of nanoparticles. *ACS Nano* 11 (5), 4916–4925. doi:10.1021/acsnano.7b01522

Huang, C. L., Liu, D., Ishikawa, S., Nakashima, T., Nakashima, N., Yokomise, H., et al. (2008). Wnt1 overexpression promotes tumour progression in non-small cell lung cancer. *Eur. J. Cancer* 44 (17), 2680–2688. doi:10.1016/j.ejca.2008.08.004

Huang, J., Tian, F., Song, Y., Cao, M., Yan, S., Lan, X., et al. (2021). A feedback circuit comprising EHD1 and 14-3-3ζ sustains β-catenin/c-Myc-mediated aerobic glycolysis and proliferation in non-small cell lung cancer. *Cancer Lett.* 520, 12–25. doi:10.1016/j.canlet.2021.06.023

Huang, W. C., Kuo, K. T., Adebayo, B. O., Wang, C. H., Chen, Y. J., Jin, K., et al. (2018). Garcinol inhibits cancer stem cell-like phenotype via suppression of the Wnt/β-catenin/STAT3 axis signalling pathway in human non-small cell lung carcinomas. *J. Nutr. Biochem.* 54, 140–150. doi:10.1016/j.jnutbio.2017.12.008

Huang, X. H., Yan, X., Zhang, Q. H., Hong, P., Zhang, W. X., Liu, Y. P., et al. (2020). Direct targeting of HSP90 with daurisoline destabilizes β-catenin to suppress lung cancer tumorigenesis. *Cancer Lett.* 489, 66–78. doi:10.1016/j.canlet.2020.05.024

Hung, P. S., Huang, M. H., Kuo, Y. Y., and Yang, J. C. (2020). The inhibition of wnt restrain KRAS(G12V)-Driven metastasis in non-small-cell lung cancer. *Cancers (Basel)* 12 (4), 837. doi:10.3390/cancers12040837

Ibrahim, S., Tagami, T., Kishi, T., and Ozeki, T. (2018). Curcumin marinosomes as promising nano-drug delivery system for lung cancer. *Int. J. Pharm.* 540 (1-2), 40–49. doi:10.1016/j.ijpharm.2018.01.051

Jan, R., and Chaudhry, G. E. (2019). Understanding apoptosis and apoptotic pathways targeted cancer therapeutics. *Adv. Pharm. Bull.* 9 (2), 205–218. doi:10.15171/apb.2019.024

Jarosova, V., Vesely, O., Doskocil, I., Tomisova, K., Marsik, P., Jaimes, J. D., et al. (2020). Metabolism of cis- and trans-resveratrol and dihydroresveratrol in an intestinal epithelial model. *Nutrients* 12 (3), 595. doi:10.3390/nu12030595

Jhanji, M., Rao, C. N., and Sajish, M. (2021). Towards resolving the enigma of the dichotomy of resveratrol: Cis- and trans-resveratrol have opposite effects on TyrRS-regulated PARP1 activation. *Geroscience* 43 (3), 1171–1200. doi:10.1007/s11357-020-00295-w

Juan, J., Muraguchi, T., Iezza, G., Sears, R. C., and Mcmahon, M. (2014). Diminished WNT -> β-catenin -> c-MYC signaling is a barrier for malignant progression of BRAFV600E-induced lung tumors. *Genes Dev.* 28 (6), 561–575. doi:10.1101/gad.233627.113

Jung, Y. S., and Park, J. I. (2020). Wnt signaling in cancer: therapeutic targeting of wnt signaling beyond β-catenin and the destruction complex. *Exp. Mol. Med.* 52 (2), 183–191. doi:10.1038/s12276-020-0380-6

Kasprzak, A. (2020). Angiogenesis-related functions of wnt signaling in colorectal carcinogenesis. *Cancers (Basel)* 12 (12), 3601. doi:10.3390/cancers12123601

Katagiri, H., Yonezawa, H., Shitamura, S., Sugawara, A., Kawano, T., Maemondo, M., et al. (2023). A Wnt/β-catenin signaling inhibitor, IMU1003, suppresses the emergence of osimertinib-resistant colonies from gefitinib-resistant non-small cell lung cancer cells. *Biochem. Biophys. Res. Commun.* 645, 24–29. doi:10.1016/j.bbrc.2023.01.018

Katoh, M., and Katoh, M. (2022). WNT signaling and cancer stemness. *Essays Biochem.* 66 (4), 319–331. doi:10.1042/ebc20220016

Kim, J. H., Park, S. Y., Jun, Y., Kim, J. Y., and Nam, J. S. (2017). Roles of wnt target genes in the journey of cancer stem cells. *Int. J. Mol. Sci.* 18 (8), 1604. doi:10.3390/ijms18081604

Kim, N. Y., Mohan, C. D., Chinnathambi, A., Alharbi, S. A., Sethi, G., Rangappa, K. S., et al. (2022a). Euphorbiasteroid abrogates EGFR and wnt/β-catenin signaling in non-small-cell lung cancer cells to impart anticancer activity. *Molecules* 27 (12), 3824. doi:10.3390/molecules27123824

Kim, S. M., Park, E. J., and Lee, H. J. (2022b). Nuciferine attenuates lipopolysaccharide-stimulated inflammatory responses by inhibiting p38 MAPK/ATF2 signaling pathways. *Inflammopharmacology* 30 (6), 2373–2383. doi:10.1007/s10787-022-01075-y

Kleeman, S. O., Koelzer, V. H., Jones, H. J., Vazquez, E. G., Davis, H., East, J. E., et al. (2020). Exploiting differential Wnt target gene expression to generate a molecular biomarker for colorectal cancer stratification. *Gut* 69 (6), 1092–1103. doi:10.1136/gutjnl-2019-319126

Kotsinas, A., Evangelou, K., Zacharatos, P., Kittas, C., and Gorgoulis, V. G. (2002). Proliferation, but not apoptosis, is associated with distinct beta-catenin expression patterns in non-small-cell lung carcinomas: Relationship with adenomatous polyposis coli and G(1)-to S-phase cell-cycle regulators. *Am. J. Pathol.* 161 (5), 1619–1634. doi:10.1016/s0002-9440(10)64440-9

Krishnamurthy, N., and Kurzrock, R. (2018). Targeting the Wnt/beta-catenin pathway in cancer: Update on effectors and inhibitors. *Cancer Treat. Rev.* 62, 50–60. doi:10.1016/j.ctrv.2017.11.002

Ku, M. J., Kim, J. H., Lee, J., Cho, J. Y., Chun, T., and Lee, S. Y. (2015). Maclurin suppresses migration and invasion of human non-small-cell lung cancer cells via anti-oxidative activity and inhibition of the Src/FAK-ERK-β-catenin pathway. *Mol. Cell Biochem.* 402 (1-2), 243–252. doi:10.1007/s11010-015-2331-4

Lai, F., Schlich, M., Pireddu, R., Fadda, A. M., and Sinico, C. (2019). Nanocrystals as effective delivery systems of poorly water-soluble natural molecules. *Curr. Med. Chem.* 26 (24), 4657–4680. doi:10.2174/0929867326666181213095809

Lee, S. B., Gong, Y. D., Park, Y. I., and Dong, M. S. (2013). 2,3,6-Trisubstituted quinoxaline derivative, a small molecule inhibitor of the Wnt/beta-catenin signaling pathway, suppresses cell proliferation and enhances radiosensitivity in A549/Wnt2 cells. *Biochem. Biophys. Res. Commun.* 431 (4), 746–752. doi:10.1016/j.bbrc.2013.01.038

Li, B., Zhang, W., Tan, T., Liu, W., Luo, X., Zhang, J., et al. (2020a). Chinese herbal formulas miao-yi-ai-tang inhibits the proliferation and migration of lung cancer cells through targeting β-catenin/AXIN and presents synergistic effect with cisplatin suppressing lung cancer. *Biomed. Res. Int.* 2020, 2761850. doi:10.1155/2020/2761850

Li, C., Liang, Y., Cao, J., Zhang, N., Wei, X., Tu, M., et al. (2019). The delivery of a wnt pathway inhibitor toward CSCs requires stable liposome encapsulation and delayed drug release in tumor tissues. *Mol. Ther.* 27 (9), 1558–1567. doi:10.1016/j.ymthe.2019.06.013

Li, J., Huang, K. L., Zhang, T., Li, H., Zhao, J., and Wang, H. (2016a). Pan-cancer methylation and expression profiling of adenocarcinomas revealed epigenetic silencing in the WNT signaling pathway. *Neoplasma* 63 (2), 208–214. doi:10.4149/205_150601n306

Li, J., Xu, J., Lu, Y., Qiu, L., Xu, W., Lu, B., et al. (2016b). MASM, a matrine derivative, offers radioprotection by modulating lethal total-body irradiation-induced multiple signaling pathways in wistar rats. *Molecules* 21 (5), 649. doi:10.3390/molecules21050649

Li, J., Xu, S., Dong, H., Wu, X., Wang, L. H., and Xu, X. (2022). Altered Wnt5a expression affects radiosensitivity of non-small cell lung cancer via the Wnt/β-catenin pathway. *Exp. Ther. Med.* 23 (1), 5. doi:10.3892/etm.2021.10927

Li, S., Zhou, G., Liu, W., Ye, J., Yuan, F., and Zhang, Z. (2021). Curcumol inhibits lung adenocarcinoma growth and metastasis via inactivation of PI3K/AKT and wnt/-catenin pathway. *Oncol. Res.* 28 (7), 685–700. doi:10.3727/096504020x15917007265498

Li, X., Wang, M., Du, N., Liang, T., Xiao, G. D., Li, K., et al. (2020b). Matrine inhibitory effect on self-renewal and Re-sensitization of 5-FU resistant NSCLC stem cells were through let-7b dependent downregulation of CCND1. *Cell Cycle* 19 (23), 3249–3259. doi:10.1080/15384101.2020.1838791

Liang, Y., Liu, Z. Y., Wang, P. Y., Li, Y. J., Wang, R. R., and Xie, S. Y. (2021). Nanoplatform-based natural products co-delivery system to surmount cancer multidrug-resistant. *J. Control Release* 336, 396–409. doi:10.1016/j.jconrel.2021.06.034

Liao, T. T., and Yang, M. H. (2017). Revisiting epithelial-mesenchymal transition in cancer metastasis: the connection between epithelial plasticity and stemness. *Mol. Oncol.* 11 (7), 792–804. doi:10.1002/1878-0261.12096

Lin, J., Yin, Q., Chen, B., Zhang, H., Mei, D., Fu, J., et al. (2020). A magnetism/laser-auxiliary cascaded drug delivery to pulmonary carcinoma. *Acta Pharm. Sin. B* 10 (8), 1549–1562. doi:10.1016/j.apsb.2019.12.017

Liu, D. X., Hao, S. L., and Yang, W. X. (2023). Crosstalk between β-CATENIN-mediated cell adhesion and the WNT signaling pathway. *DNA Cell Biol.* 42 (1), 1–13. doi:10.1089/dna.2022.0424

Liu, K., Sun, Q., Liu, Q., Li, H., Zhang, W., and Sun, C. (2022). Focus on immune checkpoint PD-1/PD-L1 pathway: New advances of polyphenol phytochemicals in tumor immunotherapy. *Biomed. Pharmacother.* 154, 113618. doi:10.1016/j.biopha.2022.113618

Liu, L., Zhu, H., Liao, Y., Wu, W., Liu, L., Liu, L., et al. (2020). Inhibition of Wnt/β-catenin pathway reverses multi-drug resistance and EMT in Oct4(+)/Nanog(+) NSCLC cells. *Biomed. Pharmacother.* 127, 110225. doi:10.1016/j.biopha.2020.110225

Liu, Q., Liu, Y., Guo, M., Luo, X., and Yao, S. (2006). A simple and sensitive method of nonaqueous capillary electrophoresis with laser-induced native fluorescence detection for the analysis of chelerythrine and sanguinarine in Chinese herbal medicines. *Talanta* 70 (1), 202–207. doi:10.1016/j.talanta.2006.02.049

Liu, W., Yi, D. D., Guo, J. L., Xiang, Z. X., Deng, L. F., and He, L. (2015). Nuciferine, extracted from *Nelumbo nucifera* Gaertn, inhibits tumor-promoting effect of nicotine involving Wnt/β-catenin signaling in non-small cell lung cancer. *J. Ethnopharmacol.* 165, 83–93. doi:10.1016/j.jep.2015.02.015

Lu, Y., Wei, C., and Xi, Z. (2014). Curcumin suppresses proliferation and invasion in non-small cell lung cancer by modulation of MTA1-mediated Wnt/β-catenin pathway. *Vitro Cell Dev. Biol. Anim.* 50 (9), 840–850. doi:10.1007/s11626-014-9779-5

Luan, H., Yan, L., Zhao, Y., Ding, X., and Cao, L. (2022). Fucoxanthin induces apoptosis and reverses epithelial-mesenchymal transition via inhibiting Wnt/β-catenin pathway in lung adenocarcinoma. *Discov. Oncol.* 13 (1), 98. doi:10.1007/s12672-022-00564-4

Luo, L., and Xu, G. (2022). Fascaplysin induces apoptosis and ferroptosis, and enhances anti-PD-1 immunotherapy in non-small cell lung cancer (NSCLC) by promoting PD-L1 expression. *Int. J. Mol. Sci.* 23 (22), 13774. doi:10.3390/ijms232213774

Luo, X., Ye, S., Jiang, Q., Gong, Y., Yuan, Y., Hu, X., et al. (2018). Wnt inhibitory factor-1-mediated autophagy inhibits Wnt/β-catenin signaling by downregulating dishevelled-2 expression in non-small cell lung cancer cells. *Int. J. Oncol.* 53 (2), 904–914. doi:10.3892/ijo.2018.4442

Luo, Y., Yin, S., Lu, J., Zhou, S., Shao, Y., Bao, X., et al. (2021). Tumor microenvironment: a prospective target of natural alkaloids for cancer treatment. *Cancer Cell Int.* 21 (1), 386. doi:10.1186/s12935-021-02085-6

Ma, Y., Marinkova, R., Nenkov, M., Jin, L., Huber, O., Sonnemann, J., et al. (2022). Tumor-Intrinsic PD-L1 exerts an oncogenic function through the activation of the wnt/β-catenin pathway in human non-small cell lung cancer. *Int. J. Mol. Sci.* 23 (19), 11031. doi:10.3390/ijms231911031

Malladi, S., Macalinao, D. G., Jin, X., He, L., Basnet, H., Zou, Y., et al. (2016). Metastatic latency and immune evasion through autocrine inhibition of WNT. *Cell* 165 (1), 45–60. doi:10.1016/j.cell.2016.02.025

Mao, X., Tong, J., Wang, Y., Zhu, Z., Yin, Y., and Wang, Y. (2018). Triptolide exhibits antitumor effects by reversing hypermethylation of WIF-1 in lung cancer cells. *Mol. Med. Rep.* 18 (3), 3041–3049. doi:10.3892/mmr.2018.9263

Maqsoudlou, A., Assadpour, E., Mohebodini, H., and Jafari, S. M. (2022). The influence of nanodelivery systems on the antioxidant activity of natural bioactive compounds. *Crit. Rev. Food Sci. Nutr.* 62 (12), 3208–3231. doi:10.1080/10408398.2020.1863907

Mazieres, J., He, B., You, L., Xu, Z., and Jablons, D. M. (2005). Wnt signaling in lung cancer. *Cancer Lett.* 222 (1), 1–10. doi:10.1016/j.canlet.2004.08.040

Mazieres, J., He, B., You, L., Xu, Z., Lee, A. Y., Mikami, I., et al. (2004). Wnt inhibitory factor-1 is silenced by promoter hypermethylation in human lung cancer. *Cancer Res.* 64 (14), 4717–4720. doi:10.1158/0008-5472.Can-04-1389

Mcmellen, A., Woodruff, E. R., Corr, B. R., Bitler, B. G., and Moroney, M. R. (2020). Wnt signaling in gynecologic malignancies. *Int. J. Mol. Sci.* 21 (12), 4272. doi:10.3390/ijms21124272

Miller, M., and Hanna, N. (2021). Advances in systemic therapy for non-small cell lung cancer. *Bmj* 375, n2363. doi:10.1136/bmj.n2363

Monteillier, A., Allard, P. M., Gindro, K., Wolfender, J. L., and Cuendet, M. (2018). Lung cancer chemopreventive activity of patulin isolated from Penicillium vulpinum. *Molecules* 23 (3), 636. doi:10.3390/molecules23030636

Moon, K. M., Yang, J. H., Lee, M. K., Kwon, E. B., Baek, J., Hwang, T., et al. (2022). Maclurin exhibits antioxidant and anti-tyrosinase activities, suppressing melanogenesis. *Suppressing Melanogenes. Antioxidants (Basel)* 11 (6), 1164. doi:10.3390/antiox11061164

Nakayama, S., Sng, N., Carretero, J., Welner, R., Hayashi, Y., Yamamoto, M., et al. (2014). β-catenin contributes to lung tumor development induced by EGFR mutations. *Cancer Res.* 74 (20), 5891–5902. doi:10.1158/0008-5472.Can-14-0184

Nardi, I., Reno, T., Yun, X., Sztain, T., Wang, J., Dai, H., et al. (2018). Triptolide inhibits Wnt signaling in NSCLC through upregulation of multiple Wnt inhibitory factors via epigenetic modifications to Histone H3. *Int. J. Cancer* 143 (10), 2470–2478. doi:10.1002/ijc.31756

Neal, R. D., Sun, F., Emery, J. D., and Callister, M. E. (2019). Lung cancer. *Bmj* 365, l1725. doi:10.1136/bmj.l1725

Nguyen, D. X., Chiang, A. C., Zhang, X. H., Kim, J. Y., Kris, M. G., Ladanyi, M., et al. (2009). WNT/TCF signaling through LEF1 and HOXB9 mediates lung adenocarcinoma metastasis. *Cell* 138 (1), 51–62. doi:10.1016/j.cell.2009.04.030

Nusse, R., and Clevers, H. (2017). Wnt/β-Catenin signaling, disease, and emerging therapeutic modalities. *Cell* 169 (6), 985–999. doi:10.1016/j.cell.2017.05.016

O'leary, K., Shia, A., and Schmid, P. (2018). Epigenetic regulation of EMT in non-small cell lung cancer. *Curr. Cancer Drug Targets* 18 (1), 89–96. doi:10.2174/1568009617666170203162556

Okada-Iwasaki, R., Takahashi, Y., Watanabe, Y., Ishida, H., Saito, J., Nakai, R., et al. (2016). The discovery and characterization of K-756, a novel wnt/β-catenin pathway inhibitor targeting tankyrase. *Mol. Cancer Ther.* 15 (7), 1525–1534. doi:10.1158/1535-7163.Mct-15-0938

Pacheco-Pinedo, E. C., Durham, A. C., Stewart, K. M., Goss, A. M., Lu, M. M., Demayo, F. J., et al. (2011). Wnt/β-catenin signaling accelerates mouse lung tumorigenesis by imposing an embryonic distal progenitor phenotype on lung epithelium. *J. Clin. Invest.* 121 (5), 1935–1945. doi:10.1172/jci44871

Pan, Y., Sun, Y., Liu, Z., and Zhang, C. (2020). miR-192-5p upregulation mediates the suppression of curcumin in human NSCLC cell proliferation, migration and invasion by targeting c-Myc and inactivating the Wnt/β-catenin signaling pathway. *Mol. Med. Rep.* 22 (2), 1594–1604. doi:10.3892/mmr.2020.11213

Park, J. Y., Park, S., Lee, T. S., Hwang, Y. H., Kim, J. Y., Kang, W. J., et al. (2019). Biodegradable micro-sized discoidal polymeric particles for lung-targeted delivery system. *Biomaterials* 218, 119331. doi:10.1016/j.biomaterials.2019.119331

Parsons, M. J., Tammela, T., and Dow, L. E. (2021). WNT as a driver and dependency in cancer. *Cancer Discov.* 11 (10), 2413–2429. doi:10.1158/2159-8290.Cd-21-0190

Pate, K. T., Stringari, C., Sprowl-Tanio, S., Wang, K., Teslaa, T., Hoverter, N. P., et al. (2014). Wnt signaling directs a metabolic program of glycolysis and angiogenesis in colon cancer. *Embo J.* 33 (13), 1454–1473. doi:10.15252/embj.201488598

Patel, C. H., and Powell, J. D. (2016). Warburg meets epigenetics. *Science* 354 (6311), 419–420. doi:10.1126/science.aak9776

Peron, M., Dinarello, A., Meneghetti, G., Martorano, L., Facchinello, N., Vettori, A., et al. (2020). The stem-like Stat3-responsive cells of zebrafish intestine are Wnt/β-catenin dependent. *Development* 147 (12), dev188987. doi:10.1242/dev.188987

Qin, F., Wang, C. Y., Wang, C. G., Chen, Y., Li, J. J., Li, M. S., et al. (2023). Undescribed isoquinolines from Zanthoxylum nitidum and their antiproliferative effects against human cancer cell lines. *Phytochemistry* 205, 113476. doi:10.1016/j.phytochem.2022.113476

Rapp, J., Jaromi, L., Kvell, K., Miskei, G., and Pongracz, J. E. (2017). WNT signaling - lung cancer is no exception. *Respir. Res.* 18 (1), 167. doi:10.1186/s12931-017-0650-6

Reno, T. A., Tong, S. W., Wu, J., Fidler, J. M., Nelson, R., Kim, J. Y., et al. (2016). The triptolide derivative MRx102 inhibits Wnt pathway activation and has potent anti-tumor effects in lung cancer. *BMC Cancer* 16, 439. doi:10.1186/s12885-016-2487-7

Reya, T., Morrison, S. J., Clarke, M. F., and Weissman, I. L. (2001). Stem cells, cancer, and cancer stem cells. *Nature* 414 (6859), 105–111. doi:10.1038/35102167

Rogers, Z. N., Mcfarland, C. D., Winters, I. P., Seoane, J. A., Brady, J. J., Yoon, S., et al. (2018). Mapping the *in vivo* fitness landscape of lung adenocarcinoma tumor suppression in mice. *Nat. Genet.* 50 (4), 483–486. doi:10.1038/s41588-018-0083-2

Rowbotham, S. P., Goruganthu, M. U. L., Arasada, R. R., Wang, W. Z., Carbone, D. P., and Kim, C. F. (2022). Lung cancer stem cells and their clinical implications. *Cold Spring Harb. Perspect. Med.* 12 (4), a041270. doi:10.1101/cshperspect.a041270

Sadava, D., and Kane, S. E. (2017). The effect of brassinolide, a plant steroid hormone, on drug resistant small-cell lung carcinoma cells. *Biochem. Biophys. Res. Commun.* 493 (1), 783–787. doi:10.1016/j.bbrc.2017.08.094

Sánchez-Tilló, E., De Barrios, O., Siles, L., Cuatrecasas, M., Castells, A., and Postigo, A. (2011). β-catenin/TCF4 complex induces the epithelial-to-mesenchymal transition (EMT)-activator ZEB1 to regulate tumor invasiveness. *Proc. Natl. Acad. Sci. U. S. A.* 108 (48), 19204–19209. doi:10.1073/pnas.1108977108

Sancho, P., Barneda, D., and Heeschen, C. (2016). Hallmarks of cancer stem cell metabolism. *Br. J. Cancer* 114 (12), 1305–1312. doi:10.1038/bjc.2016.152

Sang, S., Sun, C., Ding, R., Jiang, J., Han, Y., Gan, S., et al. (2022). Feiyanning formula modulates the molecular mechanism of osimertinib resistance in lung cancer by regulating the Wnt/β-catenin pathway. *Front. Pharmacol.* 13, 1019451. doi:10.3389/fphar.2022.1019451

Scarborough, H. A., Helfrich, B. A., Casás-Selves, M., Schuller, A. G., Grosskurth, S. E., Kim, J., et al. (2017). AZ1366: An inhibitor of tankyrase and the canonical wnt pathway that limits the persistence of non-small cell lung cancer cells following EGFR inhibition. *Clin. Cancer Res.* 23 (6), 1531–1541. doi:10.1158/1078-0432.Ccr-16-1179

Shah, K., Panchal, S., and Patel, B. (2021). Porcupine inhibitors: Novel and emerging anti-cancer therapeutics targeting the Wnt signaling pathway. *Pharmacol. Res.* 167, 105532. doi:10.1016/j.phrs.2021.105532

Sharoni, Y., Linnewiel-Hermoni, K., Khanin, M., Salman, H., Veprik, A., Danilenko, M., et al. (2012). Carotenoids and apocarotenoids in cellular signaling related to cancer: a review. *Mol. Nutr. Food Res.* 56 (2), 259–269. doi:10.1002/mnfr.201100311

Shen, N., Wang, T., Gan, Q., Liu, S., Wang, L., and Jin, B. (2022). Plant flavonoids: Classification, distribution, biosynthesis, and antioxidant activity. *Food Chem.* 383, 132531. doi:10.1016/j.foodchem.2022.132531

Sheremet, M., Kapoor, S., Schröder, P., Kumar, K., Ziegler, S., and Waldmann, H. (2017). Small molecules inspired by the natural product withanolides as potent inhibitors of wnt signaling. *Chembiochem* 18 (18), 1797–1806. doi:10.1002/cbic.201700260

Sheridan, C. (2018). Wnt is back in drugmakers' sights, but is it druggable? *Nat. Biotechnol.* 36 (11), 1028–1029. doi:10.1038/nbt1118-1028

Shi, J., Hao, S., Liu, X., Li, Y., and Zheng, X. (2023). Feiyiliu Mixture sensitizes EGFR(Del19/T790M/C797S) mutant non-small cell lung cancer to osimertinib by attenuating the PRC1/Wnt/EGFR pathway. *Front. Pharmacol.* 14, 1093017. doi:10.3389/fphar.2023.1093017

Shin, S. Y., Rath, O., Zebisch, A., Choo, S. M., Kolch, W., and Cho, K. H. (2010). Functional roles of multiple feedback loops in extracellular signal-regulated kinase and Wnt signaling pathways that regulate epithelial-mesenchymal transition. *Cancer Res.* 70 (17), 6715–6724. doi:10.1158/0008-5472.Can-10-1377

Shtutman, M., Zhurinsky, J., Simcha, I., Albanese, C., D'amico, M., Pestell, R., et al. (1999). The cyclin D1 gene is a target of the beta-catenin/LEF-1 pathway. *Proc. Natl. Acad. Sci. U. S. A.* 96 (10), 5522–5527. doi:10.1073/pnas.96.10.5522

Shukla, S., Sinha, S., Khan, S., Kumar, S., Singh, K., Mitra, K., et al. (2016). Cucurbitacin B inhibits the stemness and metastatic abilities of NSCLC via downregulation of canonical Wnt/β-catenin signaling axis. *Sci. Rep.* 6, 21860. doi:10.1038/srep21860

Sies, H., Berndt, C., and Jones, D. P. (2017). Oxidative stress. *Annu. Rev. Biochem.* 86, 715–748. doi:10.1146/annurev-biochem-061516-045037

Stamos, J. L., and Weis, W. I. (2013). The β-catenin destruction complex. *Cold Spring Harb. Perspect. Biol.* 5 (1), a007898. doi:10.1101/cshperspect.a007898

Suda, K., Murakami, I., Yu, H., Kim, J., Tan, A. C., Mizuuchi, H., et al. (2018). CD44 facilitates epithelial-to-mesenchymal transition phenotypic change at acquisition of resistance to EGFR kinase inhibitors in lung cancer. *Mol. Cancer Ther.* 17 (10), 2257–2265. doi:10.1158/1535-7163.Mct-17-1279

Sun, D., Chen, J., Hu, H., Lin, S., Jin, L., Luo, L., et al. (2019). Acanthopanax senticosus polysaccharide suppressing proliferation and metastasis of the human non-small cell lung cancer NCI-H520 cells is associated with Wnt/β-catenin signaling. *Neoplasma* 66 (4), 555–563. doi:10.4149/neo_2018_180913N689

Sun, Y., Wu, P., Sun, Y., Sharopov, F. S., Yang, Q., Chen, F., et al. (2018). Lycorine possesses notable anticancer potentials in on-small cell lung carcinoma cells via blocking Wnt/β-catenin signaling and epithelial-mesenchymal transition (EMT). *Biochem. Biophys. Res. Commun.* 495 (1), 911–921. doi:10.1016/j.bbrc.2017.11.032

Sundarraj, K., Raghunath, A., and Perumal, E. (2018). A review on the chemotherapeutic potential of fisetin: *In vitro* evidences. *Biomed. Pharmacother.* 97, 928–940. doi:10.1016/j.biopha.2017.10.164

Süntar, I., Çetinkaya, S., Haydaroğlu Ü, S., and Habtemariam, S. (2021). Bioproduction process of natural products and biopharmaceuticals: Biotechnological aspects. *Biotechnol. Adv.* 50, 107768. doi:10.1016/j.biotechadv.2021.107768

Tabasum, S., and Singh, R. P. (2019). Fisetin suppresses migration, invasion and stem-cell-like phenotype of human non-small cell lung carcinoma cells via attenuation of epithelial to mesenchymal transition. *Chem. Biol. Interact.* 303, 14–21. doi:10.1016/j.cbi.2019.02.020

Tammela, T., Sanchez-Rivera, F. J., Cetinbas, N. M., Wu, K., Joshi, N. S., Helenius, K., et al. (2017). A Wnt-producing niche drives proliferative potential and progression in lung adenocarcinoma. *Nature* 545 (7654), 355–359. doi:10.1038/nature22334

Teng, Y., Wang, X., Wang, Y., and Ma, D. (2010). Wnt/beta-catenin signaling regulates cancer stem cells in lung cancer A549 cells. *Biochem. Biophys. Res. Commun.* 392 (3), 373–379. doi:10.1016/j.bbrc.2010.01.028

Tennis, M., Van Scoyk, M., and Winn, R. A. (2007). Role of the wnt signaling pathway and lung cancer. *J. Thorac. Oncol.* 2 (10), 889–892. doi:10.1097/JTO.0b013e318153fdb1

Tetsu, O., and Mccormick, F. (1999). Beta-catenin regulates expression of cyclin D1 in colon carcinoma cells. *Nature* 398 (6726), 422–426. doi:10.1038/18884

Thai, A. A., Solomon, B. J., Sequist, L. V., Gainor, J. F., and Heist, R. S. (2021). Lung cancer. *Lancet* 398 (10299), 535–554. doi:10.1016/s0140-6736(21)00312-3

Tian, Y., Li, P., Xiao, Z., Zhou, J., Xue, X., Jiang, N., et al. (2021). Triptolide inhibits epithelial-mesenchymal transition phenotype through the p70S6k/GSK3/β-catenin signaling pathway in taxol-resistant human lung adenocarcinoma. *Transl. Lung Cancer Res.* 10 (2), 1007–1019. doi:10.21037/tlcr-21-145

Tiwari, R. K., Ahmad, A., Khan, A. F., Al-Keridis, L. A., Saeed, M., Alshammari, N., et al. (2023). Ethanolic extract of Artemisia vulgaris leaf promotes apoptotic cell death in non-small-cell lung carcinoma A549 cells through inhibition of the wnt signaling pathway. *Metabolites* 13 (4), 480. doi:10.3390/metabo13040480

Tong, J. B., Zhang, X. X., Wang, X. H., Zeng, S. J., Wang, D. Y., Zhang, Z. Q., et al. (2018). Qiyusanlong decoction suppresses lung cancer in mice via Wnt/β-catenin pathway. *Mol. Med. Rep.* 17 (4), 5320–5327. doi:10.3892/mmr.2018.8478

Tong, Y., Liu, Y., Zheng, H., Zheng, L., Liu, W., Wu, J., et al. (2016). Artemisinin and its derivatives can significantly inhibit lung tumorigenesis and tumor metastasis through Wnt/β-catenin signaling. *Oncotarget* 7 (21), 31413–31428. doi:10.18632/oncotarget.8920

Torres, V. I., Godoy, J. A., and Inestrosa, N. C. (2019). Modulating wnt signaling at the root: Porcupine and wnt acylation. *Pharmacol. Ther.* 198, 34–45. doi:10.1016/j.pharmthera.2019.02.009

Tortelote, G. G., Reis, R. R., De Almeida Mendes, F., and Abreu, J. G. (2017). Complexity of the Wnt/β-catenin pathway: Searching for an activation model. *Cell Signal* 40, 30–43. doi:10.1016/j.cellsig.2017.08.008

Uribesalgo, I., Hoffmann, D., Zhang, Y., Kavirayani, A., Lazovic, J., Berta, J., et al. (2019). Apelin inhibition prevents resistance and metastasis associated with anti-angiogenic therapy. *EMBO Mol. Med.* 11 (8), e9266. doi:10.15252/emmm.201809266

Vesel, M., Rapp, J., Feller, D., Kiss, E., Jaromi, L., Meggyes, M., et al. (2017). ABCB1 and ABCG2 drug transporters are differentially expressed in non-small cell lung cancers (NSCLC) and expression is modified by cisplatin treatment via altered Wnt signaling. *Respir. Res.* 18 (1), 52. doi:10.1186/s12931-017-0537-6

Wagner, A. H., Devarakonda, S., Skidmore, Z. L., Krysiak, K., Ramu, A., Trani, L., et al. (2018). Recurrent WNT pathway alterations are frequent in relapsed small cell lung cancer. *Nat. Commun.* 9 (1), 3787. doi:10.1038/s41467-018-06162-9

Wang, H., Shi, M., Cao, F., and Su, E. (2022). Ginkgo biloba seed exocarp: A waste resource with abundant active substances and other components for potential applications. *Food Res. Int.* 160, 111637. doi:10.1016/j.foodres.2022.111637

Wang, J., Chen, J., Jiang, Y., Shi, Y., Zhu, J., Xie, C., et al. (2018a). Wnt/β-catenin modulates chronic tobacco smoke exposure-induced acquisition of pulmonary cancer stem cell properties and diallyl trisulfide intervention. *Toxicol. Lett.* 291, 70–76. doi:10.1016/j.toxlet.2018.04.003

Wang, J. Q., Yang, Y., Cai, C. Y., Teng, Q. X., Cui, Q., Lin, J., et al. (2021a). Multidrug resistance proteins (MRPs): Structure, function and the overcoming of cancer multidrug resistance. *Drug Resist Updat* 54, 100743. doi:10.1016/j.drup.2021.100743

Wang, J. Y., Wang, X., Wang, X. J., Zheng, B. Z., Wang, Y., Wang, X., et al. (2018b). Curcumin inhibits the growth via Wnt/β-catenin pathway in non-small-cell lung cancer cells. *Eur. Rev. Med. Pharmacol. Sci.* 22 (21), 7492–7499. doi:10.26355/eurrev_201811_16290

Wang, L., Yin, Q., Liu, C., Tang, Y., Sun, C., and Zhuang, J. (2021b). Nanoformulations of ursolic acid: A modern natural anticancer molecule. *Front. Pharmacol.* 12, 706121. doi:10.3389/fphar.2021.706121

Wang, T. L., Ouyang, C. S., and Lin, L. Z. (2018c). β-Asarone suppresses Wnt/β-catenin signaling to reduce viability, inhibit migration/invasion/adhesion and induce mitochondria-related apoptosis in lung cancer cells. *Biomed. Pharmacother.* 106, 821–830. doi:10.1016/j.biopha.2018.07.009

Wang, X., Parvathaneni, V., Shukla, S. K., Kulkarni, N. S., Muth, A., Kunda, N. K., et al. (2020). Inhalable resveratrol-cyclodextrin complex loaded biodegradable nanoparticles for enhanced efficacy against non-small cell lung cancer. *Int. J. Biol. Macromol.* 164, 638–650. doi:10.1016/j.ijbiomac.2020.07.124

Wei, H., Zhang, F., Wang, J., Zhao, M., Hou, T., and Li, L. (2020). Dehydroeffusol inhibits hypoxia-induced epithelial-mesenchymal transition in non-small cell lung cancer cells through the inactivation of Wnt/β-catenin pathway. *Biosci. Rep.* 40 (5). doi:10.1042/bsr20194284

Wu, C., Zhu, X. T., Xia, L., Wang, L., Yu, W., Guo, Q., et al. (2020). High expression of long noncoding RNA PCNA-AS1 promotes non-small-cell lung cancer cell proliferation and oncogenic activity via upregulating CCND1. *J. Cancer* 11 (7), 1959–1967. doi:10.7150/jca.39087

Wu, C., Zhuang, Y., Jiang, S., Tian, F., Teng, Y., Chen, X., et al. (2017). Cinnamaldehyde induces apoptosis and reverses epithelial-mesenchymal transition through inhibition of Wnt/β-catenin pathway in non-small cell lung cancer. *Int. J. Biochem. Cell Biol.* 84, 58–74. doi:10.1016/j.biocel.2017.01.005

Wu, D., Li, L., and Yan, W. (2016). Knockdown of TC-1 enhances radiosensitivity of non-small cell lung cancer via the Wnt/β-catenin pathway. *Biol. Open* 5 (4), 492–498. doi:10.1242/bio.017608

Xie, C., Liang, C., Wang, R., Yi, K., Zhou, X., Li, X., et al. (2023). Resveratrol suppresses lung cancer by targeting cancer stem-like cells and regulating tumor microenvironment. *J. Nutr. Biochem.* 112, 109211. doi:10.1016/j.jnutbio.2022.109211

Xu, X., Sun, P. L., Li, J. Z., Jheon, S., Lee, C. T., and Chung, J. H. (2011). Aberrant Wnt1/β-catenin expression is an independent poor prognostic marker of non-small cell lung cancer after surgery. *J. Thorac. Oncol.* 6 (4), 716–724. doi:10.1097/JTO.0b013e31820c5189

Yan, R., Fan, X., Xiao, Z., Liu, H., Huang, X., Liu, J., et al. (2022). Inhibition of DCLK1 sensitizes resistant lung adenocarcinomas to EGFR-TKI through suppression of Wnt/β-Catenin activity and cancer stemness. *Cancer Lett.* 531, 83–97. doi:10.1016/j.canlet.2022.01.030

Yang, J., Fang, Z., Wu, J., Yin, X., Fang, Y., Zhao, F., et al. (2016a). Construction and application of a lung cancer stem cell model: antitumor drug screening and molecular

mechanism of the inhibitory effects of sanguinarine. *Tumour Biol.* 37 (10), 13871–13883. doi:10.1007/s13277-016-5152-5

Yang, J., Zhang, K., Wu, J., Shi, J., Xue, J., Li, J., et al. (2016b). Wnt5a increases properties of lung cancer stem cells and resistance to cisplatin through activation of Wnt5a/PKC signaling pathway. *Stem Cells Int.* 2016, 1690896. doi:10.1155/2016/1690896

Yang, M., Li, Z., Tao, J., Hu, H., Li, Z., Zhang, Z., et al. (2021a). Resveratrol induces PD-L1 expression through snail-driven activation of Wnt pathway in lung cancer cells. *J. Cancer Res. Clin. Oncol.* 147 (4), 1101–1113. doi:10.1007/s00432-021-03510-z

Yang, X., Shao, F., Guo, D., Wang, W., Wang, J., Zhu, R., et al. (2021b). WNT/β-catenin-suppressed FTO expression increases m(6)A of c-Myc mRNA to promote tumor cell glycolysis and tumorigenesis. *Cell Death Dis.* 12 (5), 462. doi:10.1038/s41419-021-03739-z

Yao, H., Ashihara, E., and Maekawa, T. (2011). Targeting the Wnt/β-catenin signaling pathway in human cancers. *Expert Opin. Ther. Targets* 15 (7), 873–887. doi:10.1517/14728222.2011.577418

Yao, L., Sun, B., Zhao, X., Zhao, X., Gu, Q., Dong, X., et al. (2014). Overexpression of Wnt5a promotes angiogenesis in NSCLC. *Biomed. Res. Int.* 2014, 832562. doi:10.1155/2014/832562

Yook, J. I., Li, X. Y., Ota, I., Fearon, E. R., and Weiss, S. J. (2005). Wnt-dependent regulation of the E-cadherin repressor snail. *J. Biol. Chem.* 280 (12), 11740–11748. doi:10.1074/jbc.M413878200

You, L., He, B., Xu, Z., Uematsu, K., Mazieres, J., Mikami, I., et al. (2004). Inhibition of Wnt-2-mediated signaling induces programmed cell death in non-small-cell lung cancer cells. *Oncogene* 23 (36), 6170–6174. doi:10.1038/sj.onc.1207844

Yu, S., Han, R., and Gan, R. (2022). The wnt/β-catenin signalling pathway in haematological neoplasms. *Biomark. Res.* 10 (1), 74. doi:10.1186/s40364-022-00418-9

Yu, W., Zhang, X., Zhang, W., Xiong, M., Lin, Y., Chang, M., et al. (2021). 19-Hydroxybufalin inhibits non-small cell lung cancer cell proliferation and promotes cell apoptosis via the Wnt/β-catenin pathway. *Exp. Hematol. Oncol.* 10 (1), 48. doi:10.1186/s40164-021-00243-0

Yuan, R., Hou, Y., Sun, W., Yu, J., Liu, X., Niu, Y., et al. (2017). Natural products to prevent drug resistance in cancer chemotherapy: a review. *Ann. N. Y. Acad. Sci.* 1401 (1), 19–27. doi:10.1111/nyas.13387

Yuan, S., Tao, F., Zhang, X., Zhang, Y., Sun, X., and Wu, D. (2020). Role of wnt/β-catenin signaling in the chemoresistance modulation of colorectal cancer. *Biomed. Res. Int.* 2020, 9390878. doi:10.1155/2020/9390878

Zhang, J., Liu, J., Li, H., and Wang, J. (2016a). β-Catenin signaling pathway regulates cisplatin resistance in lung adenocarcinoma cells by upregulating Bcl-xl. *Mol. Med. Rep.* 13 (3), 2543–2551. doi:10.3892/mmr.2016.4882

Zhang, S., Li, H., Li, L., Gao, Q., Gu, L., Hu, C., et al. (2021). Ophiopogonin B inhibits migration and invasion in non-small cell lung cancer cells through enhancing the interaction between Axin and β-catenin. *J. Cancer* 12 (20), 6274–6284. doi:10.7150/jca.60066

Zhang, S., Mao, B., Cui, S., Zhang, Q., Zhao, J., Tang, X., et al. (2023a). Absorption, metabolism, bioactivity, and biotransformation of epigallocatechin gallate. *Crit. Rev. Food Sci. Nutr.*, 1–21. doi:10.1080/10408398.2023.2170972

Zhang, T., Chen, Y., Ge, Y., Hu, Y., Li, M., and Jin, Y. (2018). Inhalation treatment of primary lung cancer using liposomal curcumin dry powder inhalers. *Acta Pharm. Sin. B* 8 (3), 440–448. doi:10.1016/j.apsb.2018.03.004

Zhang, X., Li, Y., Wu, Z., Li, J., Li, J., Deng, S., et al. (2023b). Development of carboxymethyl chitosan-coated zein/soy lecithin nanoparticles for the delivery of resveratrol. *Food Funct.* 14 (3), 1636–1647. doi:10.1039/d2fo03180a

Zhang, X. X., Zhang, L. L., Yang, H. L., and Wang, X. W. (2016b). Mechanism of Wnt/β-catenin signaling pathway in enhanced malignant phenotype of non-small cell lung cancer induced by anti-angiogenesis therapy. *Asian Pac J. Trop. Med.* 9 (1), 58–62. doi:10.1016/j.apjtm.2015.12.012

Zhao, H., Ming, T., Tang, S., Ren, S., Yang, H., Liu, M., et al. (2022a). Wnt signaling in colorectal cancer: Pathogenic role and therapeutic target. *Mol. Cancer* 21 (1), 144. doi:10.1186/s12943-022-01616-7

Zhao, Y., Guo, S., Deng, J., Shen, J., Du, F., Wu, X., et al. (2022b). VEGF/VEGFR-targeted therapy and immunotherapy in non-small cell lung cancer: Targeting the tumor microenvironment. *Int. J. Biol. Sci.* 18 (9), 3845–3858. doi:10.7150/ijbs.70958

Zhong, Z., Yu, J., Virshup, D. M., and Madan, B. (2020). Wnts and the hallmarks of cancer. *Cancer Metastasis Rev.* 39 (3), 625–645. doi:10.1007/s10555-020-09887-6

Zhou, J., Wu, H., Hou, J., Wang, J., Wang, J., Li, M., et al. (2022). Daurisoline alleviated experimental colitis *in vivo* and *in vitro*: Involvement of NF-κB and Wnt/β-Catenin pathway. *Int. Immunopharmacol.* 108, 108714. doi:10.1016/j.intimp.2022.108714

Zhou, R., Yang, Y., Park, S. Y., Nguyen, T. T., Seo, Y. W., Lee, K. H., et al. (2017). The lichen secondary metabolite atranorin suppresses lung cancer cell motility and tumorigenesis. *Sci. Rep.* 7 (1), 8136. doi:10.1038/s41598-017-08225-1

Zhu, J., Jiang, Y., Yang, X., Wang, S., Xie, C., Li, X., et al. (2017a). Wnt/β-catenin pathway mediates (-)-Epigallocatechin-3-gallate (EGCG) inhibition of lung cancer stem cells. *Biochem. Biophys. Res. Commun.* 482 (1), 15–21. doi:10.1016/j.bbrc.2016.11.038

Zhu, J. Y., Yang, X., Chen, Y., Jiang, Y., Wang, S. J., Li, Y., et al. (2017b). Curcumin suppresses lung cancer stem cells via inhibiting wnt/β-catenin and sonic Hedgehog pathways. *Phytother. Res.* 31 (4), 680–688. doi:10.1002/ptr.5791

frontiers | Frontiers in Pharmacology

TYPE Original Research
PUBLISHED 17 October 2023
DOI 10.3389/fphar.2023.1194578

Check for updates

OPEN ACCESS

EDITED BY
Vijayakumar Sekar,
Shandong University, China

REVIEWED BY
Partha Roy,
Gandhi Institute of Technology and Management (GITAM), India
Vishwambhar Bhandare,
Shivaji University, India
Sutapa Mukherjee,
Chittaranjan National Cancer Institute (CNCI), India

*CORRESPONDENCE
Lamya Ahmed Al-Keridis,
laalkeridis@pnu.edu.sa
Irfan Ahmad Ansari,
ahmadirfan.amu@gmail.com

RECEIVED 27 March 2023
ACCEPTED 22 September 2023
PUBLISHED 17 October 2023

CITATION
Mishra P, Ali Ahmad MF, Al-Keridis LA, Saeed M, Alshammari N, Alabdallah NM, Tiwari RK, Ahmad A, Verma M, Fatima S and Ansari IA (2023), Methotrexate-conjugated zinc oxide nanoparticles exert a substantially improved cytotoxic effect on lung cancer cells by inducing apoptosis.
Front. Pharmacol. 14:1194578.
doi: 10.3389/fphar.2023.1194578

Methotrexate-conjugated zinc oxide nanoparticles exert a substantially improved cytotoxic effect on lung cancer cells by inducing apoptosis

Prakriti Mishra[1], Mohd Faizan Ali Ahmad[1], Lamya Ahmed Al-Keridis[2]*, Mohd Saeed[3], Nawaf Alshammari[3], Nadiyah M. Alabdallah[4,5], Rohit Kumar Tiwari[1,6], Afza Ahmad[1], Mahima Verma[1], Shireen Fatima[1] and Irfan Ahmad Ansari[1]*

[1]Department of Biosciences Integral University Lucknow, Lucknow, India, [2]Biology Department, Faculty of Science, Princess Nourah Bint Abdulrahman University, Riyadh, Saudi Arabia, [3]Department of Biology, College of Science, University of Hail, Hail, Saudi Arabia, [4]Department of Biology, College of Science, Imam Abdulrahman Bin Faisal University, Dammam, Saudi Arabia, [5]Basic and Applied Scientific Research Centre, Imam Abdulrahman Bin Faisal University, Dammam, Saudi Arabia, [6]Department of Clinical Research, School of Allied Health Sciences, Sharda University, Uttar Pradesh, India

In the current study, we report the synthesis of methotrexate-conjugated zinc oxide nanoparticles (MTX-ZnONPs) and their high efficacy against lung cancer cells. Conjugation of MTX with ZnONPs was authenticated by UV-vis spectroscopy, dynamic light scattering (DLS), Fourier-transform infrared (FTIR) spectroscopy, and transmission electron microscopy (TEM). This drug-nanoconjugate also showed high drug-loading efficiency. The therapeutic efficacy of MTX-ZnONPs was further tested *in vitro* against A549 cells, and the results of MTT and LDH release assays showed that MTX-ZnONPs, in addition to free MTX, were efficient in exerting cytotoxic effect on A549 cells; however, the effectiveness of MTX-ZnONPs was found to be considerably enhanced at very low doses compared to that of free MTX. Moreover, ZnONPs alone significantly inhibited the cell viability of A549 cells at a much higher concentration compared to MTX-ZnONPs and MTX. Furthermore, the cytomorphology of A549 cells was characterized by cellular shrinkage and detachment from the surface in all the treatment groups. Similarly, A549 cells, in all the treatment groups, showed fragmented and condensed nuclei, indicating the initiation of apoptosis. Mitochondrial membrane potential (ψ_m) in A549 cells showed a gradual loss in all the treatment groups. Results of the qualitative and quantitative analyses depicted increased reactive oxygen species (ROS) levels in A549 cells. The results of the caspase activity assay showed that MTX-ZnONPs andfree MTX caused significant activation of caspase-9, -8, and -3 in A549 cells; however, the effect of MTX-ZnONPs was more profound at very low doses compared to that of free MTX. Thus, our results showed high efficacy of MTX-ZnONPs, suggesting efficient intracellular delivery of the drug by ZnONPs as nanocarriers.

KEYWORDS

zinc oxide, nanoparticles, methotrexate, lung cancer, A549, reactive oxygen species, caspases

Introduction

Despite recent advancements in molecularly targeted therapy that have fundamentally transformed the therapeutic strategies for lung cancer, chemotherapy is still a key component of lung cancer treatment (Lee, 2019). Whether administered alone or in conjunction with other treatment options, chemotherapy has benefitted patients with early- and late-stage lung cancer in terms of survival and quality of life. Combination therapy with other classes of anticancer agents and new drug delivery systems haves shown promising results, and these are currently the focus of ongoing research. The ultimate objective of researchers is to increase therapeutic efficacy and reduce the potential risks associated with a drug.

Methotrexate (MTX) is a well-established drug, widely used in numerous cancer treatments, psoriasis, and rheumatological diseases (Khan et al., 2012). Currently, many forms of cancer, such as osteosarcoma, acute lymphoblastic leukemia, acute myeloid leukemia, meningeal leukemia and lymphoma, non-lymphoma, Hodgkin's lymphoma, breast cancer, and bladder cancer, are treated with MTX in conjunction with other drugs (Frei et al., 1975; Evans et al., 1986; Huennekens, 1994; Crews et al., 2004). MTX is a folic acid analog that inhibits dihydrofolate reductase activity, thereby disrupting cellular folate metabolism (Aghajanzadeh et al., 2018). MTX has been shown to exhibit therapeutic efficacy against numerous types of cancer cells that have overexpress folate receptors on their surface (Duthie, 2001).

The bioavailability of chemotherapeutic drugs, which can cause severe toxicities and off-target side effects, is one of the major challenges in cancer chemotherapy (Gewirtz et al., 2010). One plausible approach to overcome these challenges is the design of a nanocarrier that can selectively deliver cytotoxic doses of therapeutic drugs to cancer cells (Nosrati et al., 2017; Aghajanzadeh et al., 2018; Zamani et al., 2018). Zinc oxide nanoparticles (ZnONPs), one of the nanocarriers used for drug delivery and cancer therapy, have attracted significant interest in drug delivery systems (Barui et al., 2018). ZnONPs are considered as potential candidates for drug delivery due to their easy synthesis from low-cost precursors, biocompatibility, and effective cellular internalization through endocytosis (Duncan and Richardson, 2012; Singh et al., 2020).

When compared to conventional methods, formulation and targeting techniques for MTX using controlled release carriers, multi-articulate approaches, prodrugs, and drug conjugates, have been found to increase bioavailability, minimize adverse effects, and maximize clinical effectiveness (Khan et al., 2012). Previous studies have reported high expression of folate receptors on lung cancer cells (Nunez et al., 2012; O'Shannessy et al., 2012). Moreover, MTX has some affinity for folate receptors because of its structural similarity with folic acid (Xie et al., 2018). Moreover, there is no report to date showing the conjugation of MTX with ZnONPs. Therefore, we hypothesized that due to the high expression of folate receptors on lung cancer cells, MTX-conjugated nanoparticles could potentially be efficiently internalized inside cancer cells and show an increased cytotoxic effect against lung cancer cells. Accordingly, to test this hypothesis, we synthesized and investigated the efficacy of MTX-conjugated ZnO nanoparticles (MTX-ZnONPs) against an A549 non-small cell lung adenocarcinoma cell line.

Materials and methods

Materials

Methotrexate, 1-ethyl-3-(3-dimethyl) carbodiimide (EDC), 2′,7′-dichlorodihydrofluorescein diacetate (H_2DCFDA), 4′,6-diamidino-2-phenylindole (DAPI), 3-(4,5-dimethylthiazol-2-yl)-2,5-diphenyltetrazolium bromide (MTT), and Rhodamine 123 were purchased from Sigma-Aldrich (St. Louis, United States). Dulbecco's Modified Eagle Medium, antibiotic–antimycotic solution (penicillin, streptomycin, and amphotericin B), fetal bovine serum (FBS), and LDH Cytotoxicity Assay Kit were procured from Gibco (Thermo Fisher Scientific, Waltham, United States). Caspase-9, -8, and -3 assay kits were procured from BioVision(Milpitas, United States). All other chemicals were of analytical grade.

Methods

Biosynthesis and characterization of ZnONPs

The synthesis process of the fungus (*Aspergillus niger OL*636020)-mediated ZnONPs and their characterization by FTIR, DLS, zeta potential, TEM, and UV-vis spectroscopy analysis were discussed in our previous publication [13].

Conjugation of MTX with ZnONPs

MTX was conjugated with biogenically synthesized ZnONPs. The conjugation was achieved using an EDC coupler, which reacts with carboxyl groups present on ZnONPs and the amino group of MTX to produce MTX-ZnONPs. Briefly, 1 mL of the reaction mixture was prepared by adding 50 mM HEPES buffer, MTX (3 mg/mL), 800 μL of ZnONP suspension, and 5 mM EDC. The mixture was incubated for 5 h at 30°C. Finally, MTX-ZnONPs were separated via centrifugation at 10,000 rpm for 10 min.

Drug loading efficiency of ZnONPs

The loading percentage of MTX on ZnONPs was determined by measuring the absorbance before and after conjugation at 302 nm. The loading efficiency of the nanoparticle was calculated using the following formula:

$$Percent\ Loading\ of\ MTX\ on\ ZnONPs = [(\mathrm{A} - \mathrm{B})] \times \frac{100}{A},$$

where A represents the absorbance of the whole drug added to ZnONPs and B represents the absorbance of the unbound drug in the supernatant of the drug–nanoparticle conjugate solution.

Characterization of MTX-conjugated ZnONPs

MTX-ZnONPs were characterized by UV-vis spectrophotometry (Shimadzu dual-beam spectrophotometer, model UV-1601 PC, 1 nm

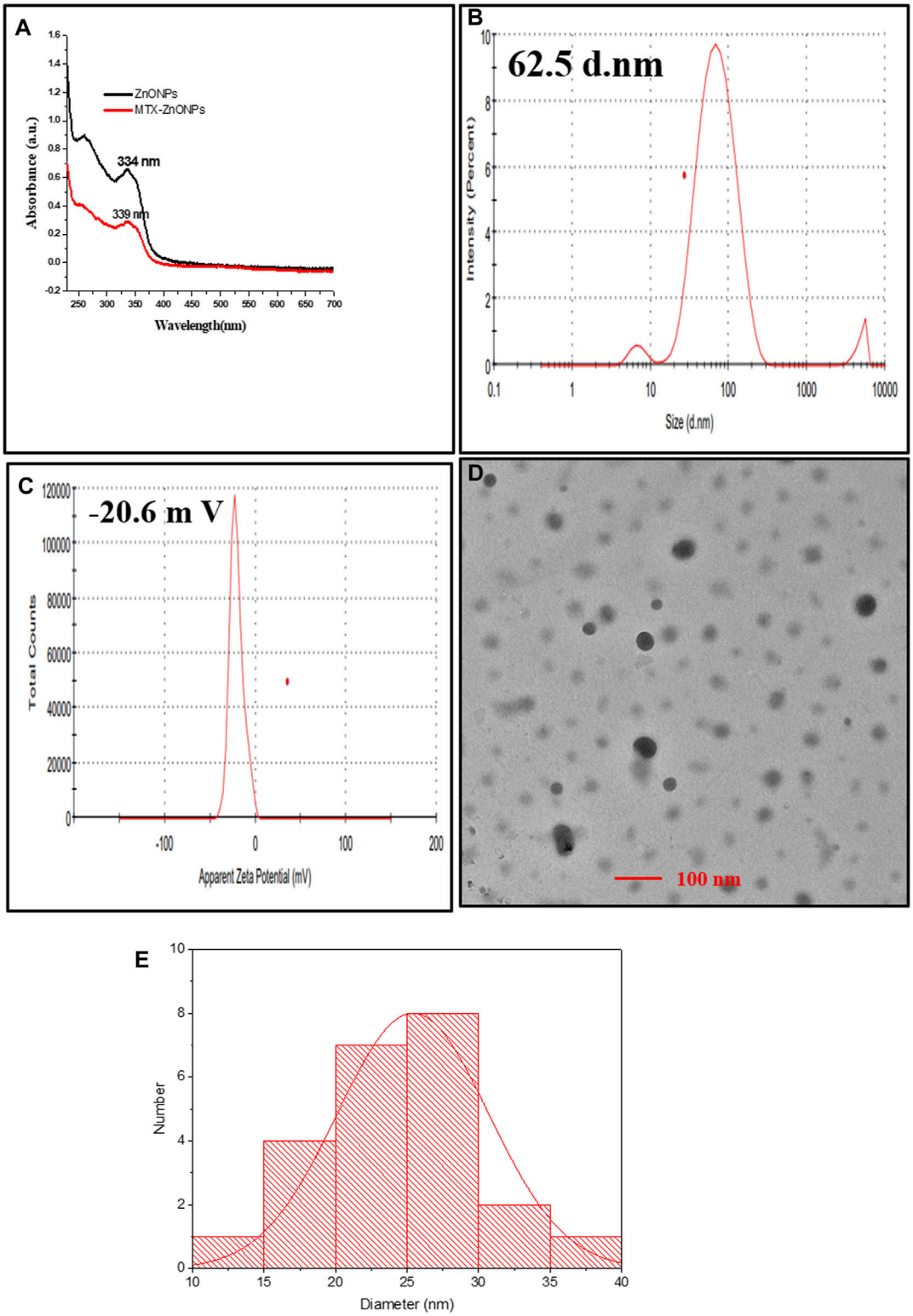

FIGURE 1
Characterization of MTX-ZnONPs under **(A)** UV-visible spectra (339 nm), **(B)** hydrodynamic diameter (62.5 nm), **(C)** zeta potential (−20.6 mV), and **(D)** transmission electron microscopy (size 25.4 nm). **(E)** Size distribution graph showing the size of MTX-ZnONPs (25.407 ± 5.295 nm).

resolution. Kyoto, Japan). The mean particle size and zeta potential of MTX-ZnONPs were determined using a particle size analyzer (Zetasizer Nano-ZS, Model ZEN3600, Malvern Instruments Ltd., Malvern, United Kingdom) [(Gomathy and Sabarinathan, 2010), 15]. Transmission electron microscope (Tecnai™ G2 Spirit Bio-TWIN, FEI, Hillsboro, United States) was used to investigate the size of the

inorganic core at a accelerating voltage of 80 kV (Khan S. et al., 2018). The binding confirmation of MTX on the surface of ZnONPs was analyzed by Fourier-transform infrared spectroscopy (FTIR) (Shimadzu FTIR-8201 PC infrared spectrophotometer) operating in the diffuse reflectance mode at a resolution of 4 cm^{-1}. A total of 256 scans of the ZnONPs film (400–4,000 cm^{-1} range) were acquired to obtain good signal-to-noise ratios.

Cell culture

A549 cells were purchased from the National Centre for Cell Science (NCCS), Pune, India. The cells were cultured in DMEM, supplemented with 10% FBS and 1% antibiotic–antimycotic solution, in a humidified atmosphere containing 5% CO_2 at 37°C.

Assessment of cytotoxicity

To assess the cytotoxic effect of MTX-ZnONPs andMTX and ZnONPs alone, A549 cells (5×10^3 per well) were treated with various doses of MTX-ZnONPs and MTX and ZnONPs alone, for 24 h. Then, 10 μL of MTT dye (5 mg/mL in PBS) was added to each well, followed by incubation for 2 h. Later, 100 μL DMSO was added to each well to solubilize the formazan crystals formed by viable cells. Finally, the absorbance of each well was measured at 570 nm using a microplate reader (Bio-Rad, United States). The results were expressed as percent cell viability, which was calculated using the following formula:

$$Cell\ viability\ (\%) = \frac{Average\ of\ At}{Average\ of\ Ac} \times 100,$$

where At and Ac are the absorbances of the treated and untreated control wells, respectively.

LDH cytotoxicity assay

Briefly, A549 cells (5×10^3 per well) were placed in a 96-well plate, then co-cultured with various doses of MTX-ZnONPs and MTX and ZnONPs alone for 24 h. Subsequently, LDH activity was measured in all the treatment groups, as per the manufacturer's instructions. Then, the percent cytotoxicity in A549 cells in all the treatment groups, was calculated using the following formula:

$$\%\,Cytotoxicity = \frac{(Drug\ Treated\ LDH\ activity) - (Spontaneous\ LDH\ activity)}{Maximum\ LDH\ activity - Spontaneous\ LDH\ activity} \times 100.$$

Examination of the morphological alterations

Briefly, A549 cells (5×10^3 per well) were co-cultured with isoeffective doses (IC_{25}, IC_{50}, and IC_{75}) of MTX-ZnONPs, MTX alone, and ZnONPs alone for 24 h. Subsequently, the changes in cellular morphology of cells in all the treatment groups were examined, and images were taken using the relief phase channel of the FLoid imaging station (ThermoScientific, United States).

Assessment of nuclear changes

Nuclear changes in A549 cells were assessed by staining with DAPI dye. The cells (1×10^4 per well) were treated with isoeffective doses of MTX-ZnONPs, MTX alone, and ZnONPs alone for 24 h, followed by washing with PBS and fixing in 4% paraformaldehyde for 10 min. Cells were permeabilized with permeabilizing buffer (0.25% Triton X-100) and, subsequently, stained with DAPI dye (300 nM). Finally, the cells were observed under a blue filter using the FLoid imaging station (ThermoScientific, United States).

Analysis of mitochondrial membrane potential (ΔΨm)

Mitochondrial membrane potential in lung cancer cells was examined via Rhodamine 123 staining. Briefly, A549 cells (1×10^5 cells per well) were grown in a 24-well plate, followed by treatment with isoeffective concentrations of MTX-ZnONPs and MTX and ZnONPs alone for 24 h. Later, the cells were washed and stained with Rhodamine 123 (300 nM) for 30 min in the dark, and photomicrographs were taken using a FLoid imaging station (ThermoScientific, United States).

Detection and quantification of cytosolic reactive oxygen species (ROS)

The cytosolic ROS in A549 cells was detected by a fluorogenic dye (H_2DCFDA). Briefly, A549 cells (5×10^4 per well) were treated with isoeffective doses of MTX-ZnONPs as well as MTX and ZnONPs alone for 6 h. Thereafter, the cells were stained with H_2DCFDA (25 μM) for 30 min at 37°C, followed by washing of excess dye with phosphate-buffered saline (PBS). Finally, photomicrographs were captured using the green fluorescence channel of a FLoid imaging station (Thermo Scientific, United States).

For the quantification of cytosolic ROS, A549 cells (1×10^4 per well) in a 96-well black-bottomed culture plate were treated with various doses of MTX-ZnONPs, MTX alone, and ZnONPs alone for 6 h, followed by incubation with H_2DCFDA (25 μM) for 30 min at 37°C. Fluorescence intensity was measured using a multi-well microplate reader (Synergy H1 hybrid multi-mode microplate reader, BioTek, United States). Values were shown as percent DCF fluorescence relative to the untreated control.

To further confirm the role of ROS in drug–nanoparticle conjugate-induced apoptosis, A549 cells were pretreated with 5 mM NAC for 2 h, followed by various doses of MTX-ZnONPs, MTX alone, and ZnONPs alone for another 24 h. Thereafter, cell viability was determined in each treatment group by MTT assay.

Measurement of caspase activity

The activation of caspases in A549 cells was determined using caspase-9, -8, and -3 assay kits to find out the mode of apoptosis in lung cancer cells. Briefly, A549 cells (1×10^6) were co-cultured with various doses of MTX-ZnONPs, MTX alone, and ZnONPs alone for 24 h. Later, caspase activity was measured as per the manufacturer's protocol.

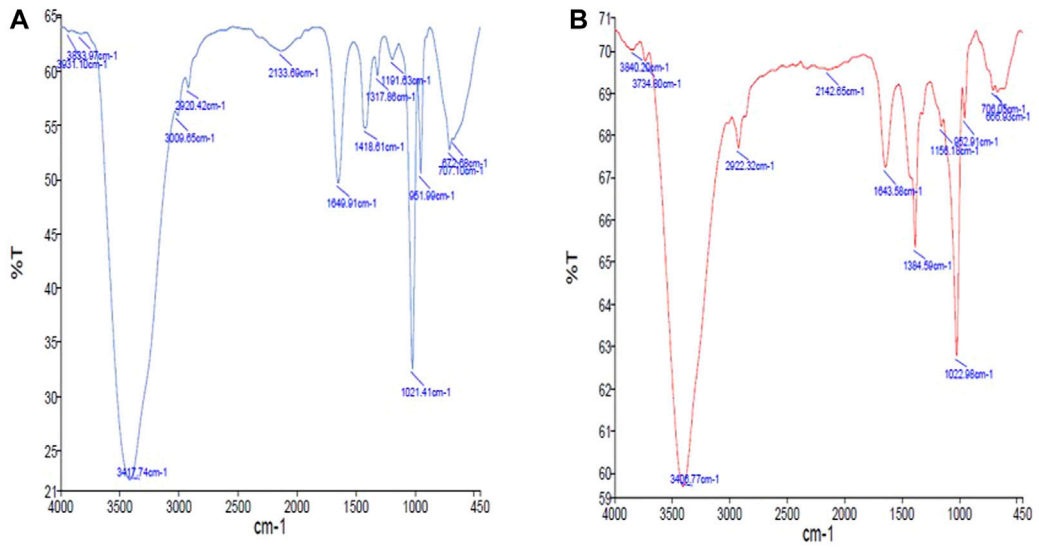

FIGURE 2
FTIR spectra of **(A)** methotrexate and **(B)** MTX-ZnONPs.

Evaluation of the effect of caspase inhibitors

Caspase-3 inhibitor was used to confirm the activation of caspases and ultimately program cell death in lung cancer cells due to drug–nanoparticle conjugate treatment. Briefly, A549 cells were pretreated with 50 μM of each caspase inhibitor for 2 h, followed by treatment with various doses of MTX-ZnONPs, MTX alone, and ZnONPs alone for another 24 h. Finally, cell survival in each treatment group was evaluated using the MTT assay.

Statistical analysis

The data are represented as the mean ± SEM of three separate experiments that were carried out in triplicate. One-way ANOVA with Dunnett's *post hoc* test, two-way ANOVA with Bonferroni's *post hoc* test, and paired *t*-test (GraphPad Prism 8.0) were used to determine significance in various treatment groups (*$p < 0.05$, **$p < 0.01$, and ***$p < 0.001$ denote significant differences between means of various treatment groups).

Results

Characterization of drug–nanoparticle conjugates

Conjugation of MTX with ZnONPs was characterized by observing the spectra of drug–nanoparticle conjugate solution, which depicted a shift of the characteristic wavelength of ZnONPs (334 nm to 339 nm) (Figure 1A). Furthermore, the hydrodynamic diameter of drug–nanoparticle conjugates was found to be 62.5 nm, which was higher than that of ZnONPs (53.28 nm) (Figure 1B). The zeta potential of MTX-ZnONPs was observed to be −20.6 mV, slightly higher than that of ZnONPs (−21.4 mV), which describes the good stability of drug-nanoconjugate (Figure 1C). The average size and shape of the MTX-ZnONPs were further validated by TEM. The average size of drug–nanoparticle conjugates, as shown in the size distribution graph, was 25.4 nm, which was greater than that of ZnONPs (17.2 nm) (Figures 1D,E). Moreover, the shape of drug-nanoconjugates was spherical, and they were found to be monodispersed.

The FTIR spectrum of ZnONPs was shown in our previously published article [13]. In the FTIR spectrum of MTX, the bend peaks of –OH, $-NH_2$, and –COOH groups were observed at 3,417 cm^{-1}, 1,649 cm^{-1}, and 2,133 cm^{-1}, respectively (Figure 2B). The stretch peak of the aromatic ring was observed at 2,920 cm^{-1}. The FTIR spectrum of the prepared MTX-ZnONPs exhibited strong absorption bands at 3,406 cm^{-1}, corresponding to the -OH group stretching (Figure 2C). A new peak was observed at 1,643 cm^{-1}, corresponding to the bend peak of the N-H bond. A new peak was also observed at 1,022 cm^{-1}, corresponding to the stretchof C-N of the peptide bond, which confirmed the conjugation. Interestingly, in the spectrum of MTX-ZnONPs, the stretch peak of the aromatic ring of MTX was observed at 2,922 cm^{-1}. The presence of these peaks in MTX-ZnONPs confirmed the conjugation of MTX with ZnONPs.

Percent drug loading

The amount of MTX conjugated with ZnONPs was shown as percent drug loading or drug loading efficiency, which was found to be 82.04% ± 3.78%. Thus, the result showed high conjugation of MTX with ZnONPs.

Cytotoxicity assay

As shown in Figure 4.3, MTX-ZnONPs (100–800 ng/mL) significantly reduced the viability of A549 cells after 24 h of

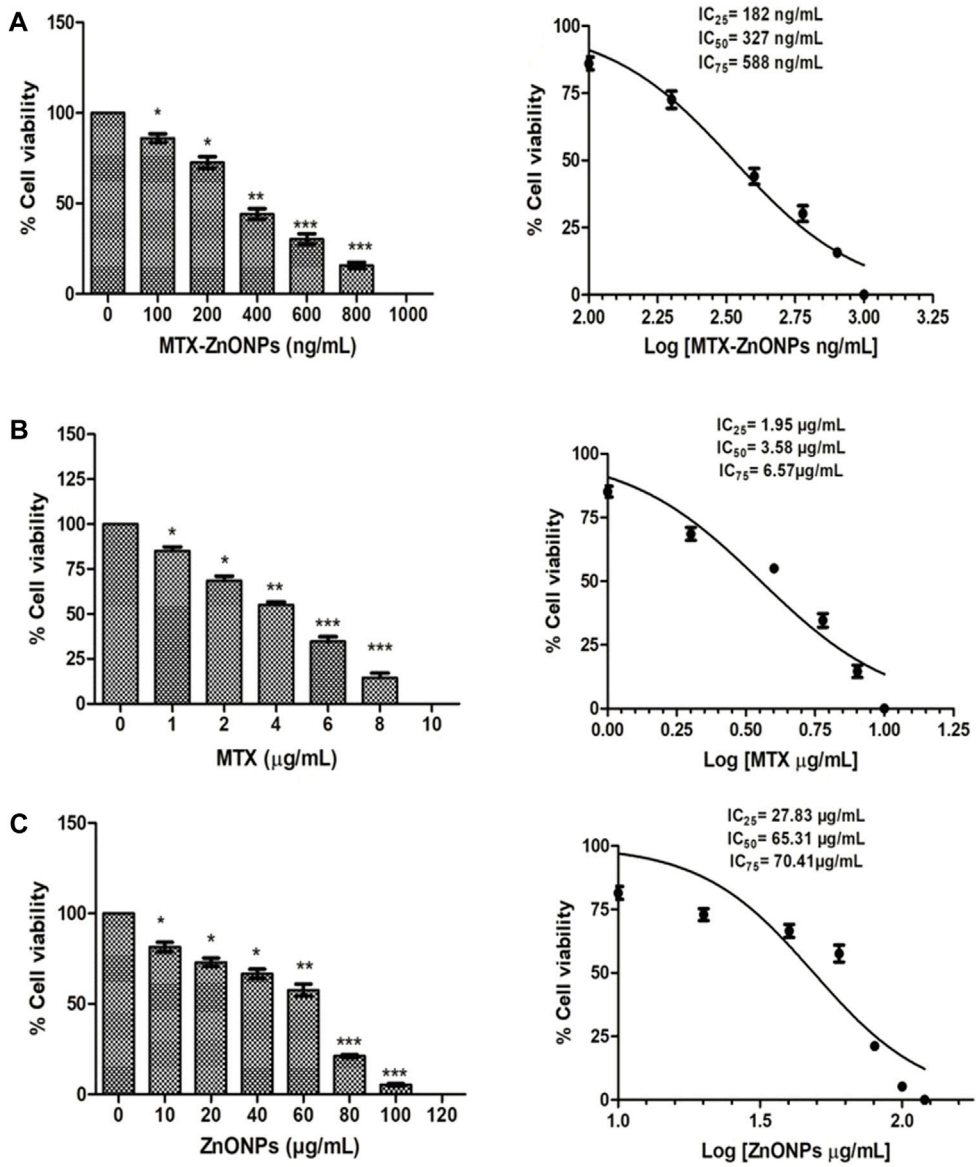

FIGURE 3
Percent cell viability of A549 cells treated with **(A)** MTX-ZnONPs, **(B)** MTX alone, and **(C)** ZnONPs alone for 24 h assessed by MTT assay. The results presented are the mean ± SEM of three independent experiments performed in triplicate. Significance among different dosage groups were determined using one-way ANOVA followed by Dunnett's *post hoc* test (where $*p < 0.05$, $**p < 0.01$, and $***p < 0.001$ represent significant differences compared with vehicle control).

treatment. The cell viability was found to be 86.07% ± 2.37%, 72.6% ± 3.20%, 44.10% ± 2.94%, 30.20% ± 2.93%, and 15.69% ± 1.69% at the doses of 100, 200, 400, 600, and 800 ng/mL MTX-ZnONPs, respectively (Figure 3A). Similarly, MTX alone also significantly inhibited the survival of A549 cells, and the viability was found to be 85.14% ± 2.12%, 68.57% ± 2.54%, 55.03% ± 1.61%, 34.63% ± 2.65%, and 14.59% ± 2.42% at the doses of 1, 2, 4, 6, and 8 μg/mL MTX, respectively (Figure 3B). However, cytotoxic doses of ZnONPs alone for A549 cells were found to be in the range of 10–100 μg/mL, and the cell viability was found to be 81.48% ± 2.53%, 72.97% ± 2.31%, 66.54% ± 2.62%, 57.62% ± 3.32%, 21.18% ± 0.79%, and 5.32 ± 0.55 at the doses of 10, 20, 40, 60, 80, and 100 μg/mL ZnONPs, respectively (Figure 3C). Furthermore, we also performed the cytotoxicity assay of ZnONPs against normal 3T3 cells and found that ZnONPs also significantly inhibited the growth of 3T3 cells at a dose of 10–100 μg/mL (Supplementary Figure S1).

The isoeffective concentrations (IC_{25}, IC_{50}, and IC_{75}) of MTX-ZnONPs were found to be 182 ng/mL, 327 ng/mL, and 588 ng/mL, respectively. Similarly, the IC_{25}, IC_{50}, and IC_{75} of MTX alone were 1.95 μg/mL, 3.58 μg/mL, and 6.57 μg/mL, respectively. However, the IC_{25}, IC_{50}, and IC_{75} of ZnONPs alone were 27.83 μg/mL, 65.30 μg/mL, and 70.41 μg/mL, respectively. According to the aforementioned data, the IC_{25} of MTX-ZnONPs was found to be reduced by approximately 10.71-fold, while the IC_{50} was reduced by approximately 10.95-fold compared to MTX alone. Thus, the isoeffective concentrations of MTX-ZnONPs were significantly

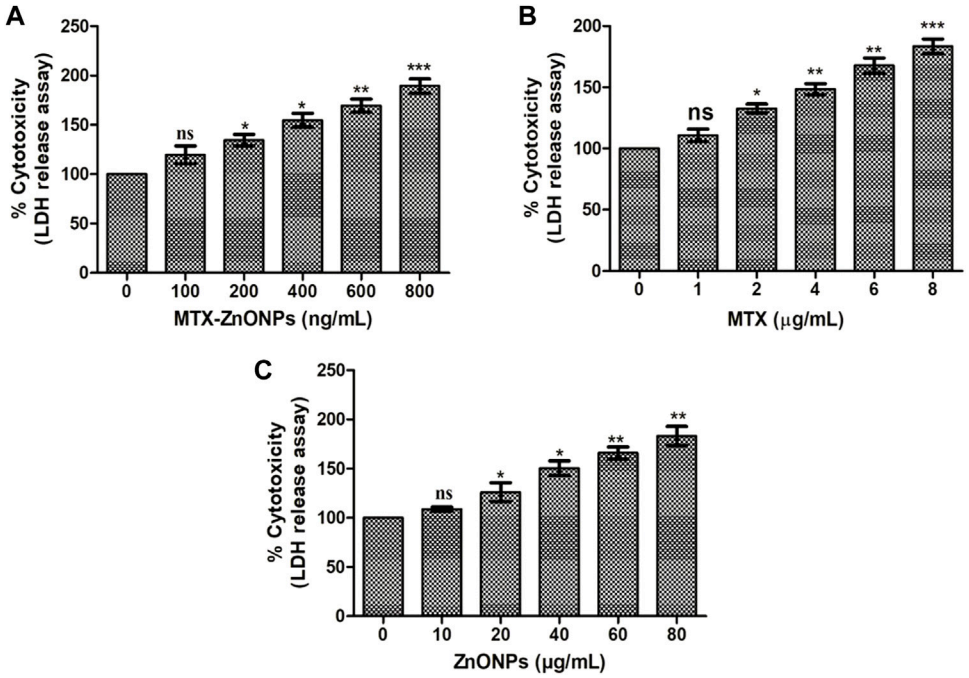

FIGURE 4
Percent cytotoxicity of A549 cells treated with different doses of **(A)** MTX-ZnONPs, **(B)** MTX alone, and **(C)** ZnONPs alone for 24 h assessed by LDH release assay. The results presented are the mean ± SEM of three independent experiments performed in triplicate. Significance among different dosage groups were determined using one-way ANOVA followed by Dunnett's *post hoc* test (where $*p < 0.05$, $**p < 0.01$, and $***p < 0.001$ represent significant differences compared with vehicle control).

reduced compared to MTX alone, which substantiated that MTX-ZnONPs exhibited a similar effect on A549 non-small cell lung cancer cells at a much lower concentration compared to MTX. The results also emphasized the efficient delivery of drug-conjugated ZnONPs.

LDH release assay

The result of the LDH assay revealed that treatment of A549 cells with MTX-ZnONPs for 24 h resulted in a significant amount of cell death, and the percent cytotoxicity was found to be 19.52% ± 5.22%, 34.45% ± 3.37%, 54.78% ± 4.02%, 69.44% ± 3.84%, and 89.40% ± 4.14% at the doses of 100, 200, 400, 600, and 800 ng/mL, respectively (Figure 4A). Similarly, MTX alone also caused significant cell death in A549 cells, and the percent cytotoxicity was found to be 10.65% ± 2.96%, 32.58% ± 2.12%, 48.45% ± 2.60%, 67.77% ± 3.53%, and 83.40% ± 3.47% at the doses of 1, 2, 4, 6, and 8 μg/mL, respectively (Figure 4B). Furthermore, ZnONPs alone exerted a cytotoxic effect on A549 cells only at a dose of 10–80 μg/mL (Figure 4C). Thus, the aforementioned results further established that, at similar doses, drug-nanoconjugate treatment led to a greater amount of death in A549 cells compared to drug alone treatment. This assay also indicated the effective intracellular delivery of the drug via zinc oxide nanocarriers.

Morphological alterations

To analyze morphological alterations in lung cancer cells, A549 cells were treated with isoeffective doses of MTX-ZnONPs, and MTX and ZnONPs alone. The morphology of A549 cells was significantly altered in all the treated groups after 24 h of treatment with IC_{25} (MTX-ZnONPs 182 ng/mL; MTX 1.95 μg/mL; and ZnONPs 27.83 μg/mL), IC_{50} (MTX-ZnONPs 327 ng/mL; MTX 3.58 μg/mL; and ZnONPs 65.3 μg/mL), and IC_{75} (MTX-ZnONPs 588 ng/mL; MTX 6.57 μg/mL; and ZnONPs 70.41 μg/mL) concentrations. A well-spread flattened morphology of cells was observed in the untreated control group, while a round morphology with cell shrinkage was observed in all the treatment groups. Membrane blebbing and lysis were also observed in some proportion of cells among all the treated groups, suggesting their cytotoxicity at the respective doses (Figure 5). As the treatment doses were increased from IC_{25} to IC_{75}, the morphological alterations in A549 cells gradually increased in all the treated groups. As observed previously, MTX-ZnONPs induced similar changes in the cytomorphology of A549 cells at much lower doses compared with MTX, which also indicated the effective delivery of the drug by the carrier nanoparticles.

Nuclear alterations

After treatment with IC_{25}, IC_{50}, and IC_{75} of MTX-ZnONPs, MTX alone, and ZnONPs alone for 24 h, substantial nuclear condensation and fragmentation in A549 cells were observed in all the treatment groups, whereas normal nuclear morphology was observed in the untreated control group (Figure 6). As the treatment doses were increased from IC_{25} to IC_{75}, the nuclear alterations in A549 cells gradually increased in all the treatment groups. The result showed that MTX-ZnONPs exhibited corresponding nuclear

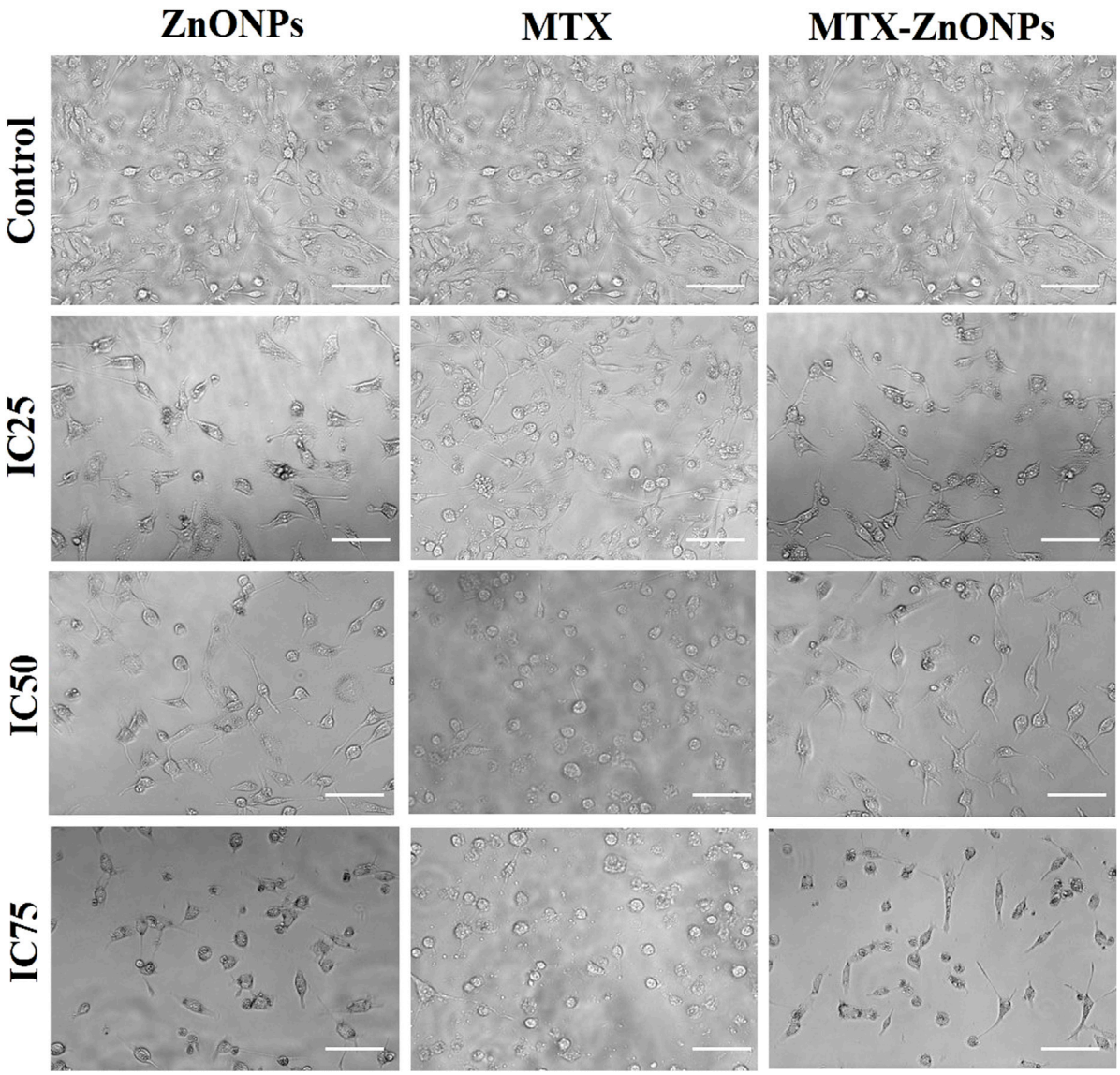

FIGURE 5
Cytomorphological images of A549 cells treated with IC_{25} (ZnONPs 27.83 μg/mL; MTX 1.95 μg/mL; and MTX-ZnONPs 182 ng/mL), IC_{50} (ZnONPs 65.30 μg/mL; MTX 3.58 μg/mL; and MTX-ZnONPs 327 ng/mL), and IC_{75} (ZnONPs 70.41 μg/mL; MTX 6.57 μg/mL; and MTX-ZnONPs 588 ng/mL) concentrations for 24 h analyzed by phase contrast microscopy. Images shown are representative of three independent experiments performed in triplicate (magnification ×20; scale bar 100 μm). The control image was reused in each treatment group.

changes in A549 cells at much lower concentrations compared to MTX. Furthermore, the nuclear condensation in A549 cells suggested the initiation of apoptosis induced by the drug.

Disrupted mitochondrial membrane potential (ΔΨm)

After treatment with IC_{25}, IC_{50}, and IC_{75} of MTX-ZnONPs, MTX alone, and ZnONPs alone for 24 h, A549 cells exhibited a significant loss of ΔΨm in all the treatment groups (Figure 7). The fluorescence intensity of Rhodamine 123 in A549 cells, in all the treatment groups, was proportional to ΔΨm. Maximum fluorescence intensity was observed in the untreated control group, while reduced fluorescence was observed in all the treatment groups. As the treatment doses were increased from IC_{25} to IC_{75}, the Rhodamine 123 fluorescence in A549 cells gradually decreased in all the treatment groups. Our result demonstrated that MTX-ZnONPs caused an equivalent reduction in ΔΨm in A549 cells at much reduced concentrations compared with MTX. Moreover, the loss of ΔΨm in A549 cells indicated the initiation of the intrinsic pathway of apoptosis caused by the aforementioned drug.

Augmented ROS production

The intracellular ROS level was found to be enhanced in A549 cells treated with IC_{25}, IC_{50}, and IC_{75} of MTX-ZnONPs,

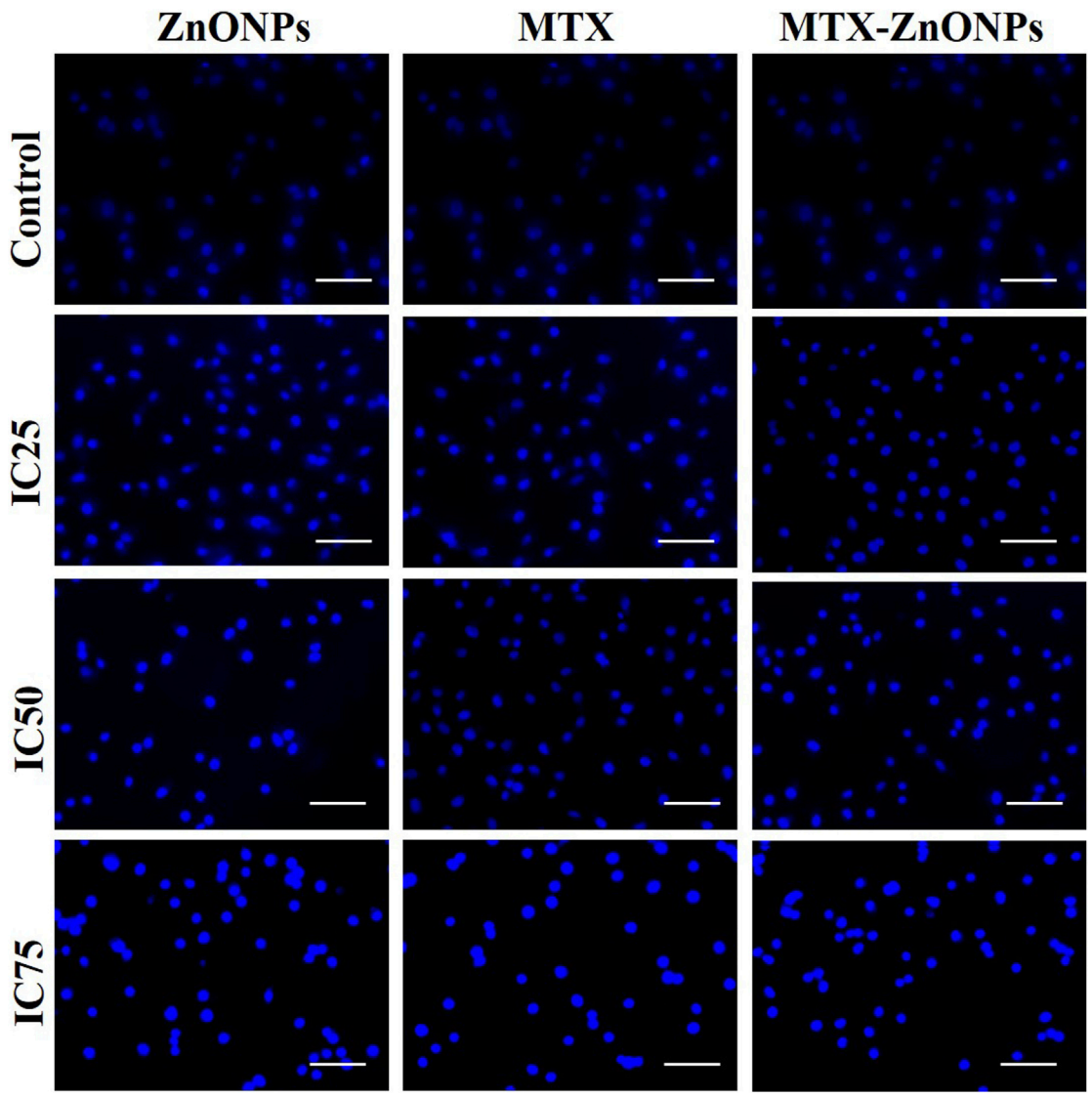

FIGURE 6
Nuclear morphology of DAPI-stained nuclei of A549 cells treated at IC_{25} (ZnONPs 27.83 μg/mL; MTX 1.95 μg/mL; and MTX-ZnONPs 182 ng/mL), IC_{50} (ZnONPs 65.30 μg/mL; MTX 3.58 μg/mL; and MTX-ZnONPs 327 ng/mL), and IC_{75} (ZnONPs 70.41 μg/mL; MTX 6.57 μg/mL; and MTX-ZnONPs 588 ng/mL) concentrations for 24 h analyzed by fluorescence microscopy. Images shown are representative of three independent experiments (scale bar: 100 μm; magnification: ×20). The control image was reused in each treatment group.

MTX alone, and ZnONPs alone for 24 h (Figure 8). The DCF fluorescence intensity in A549 cells was proportional to the level of ROS in all the treatment groups. The untreated control cells demonstrated insignificant fluorescence, while augmented fluorescence was observed in all the treatment groups. As the treatment doses were increased from IC_{25} to IC_{75}, the intracellular ROS level in A549 cells gradually increased in all the treatment groups. The result showed that MTX-ZnONPs caused a similar increment in cellular ROS production in A549 cells at much lower concentrations compared to MTX. Moreover, the enhanced ROS production in A549 cells indicated the activation of the apoptotic pathway induced by the drug.

In an additional experiment, we also quantified the amount of ROS produced in lung cancer cells treated with MTX-ZnONPs and MTX and ZnONPs alone. The result demonstrated a dose-dependent increase of DCF fluorescence in A549 cells treated with MTX-ZnONPs, which was found to be 13.38% ± 2.96%, 28.29% ± 3.47%, 50.35% ± 4.68%, 64.84% ± 4.06%, and 82.62% ± 4.12% at the doses of 100, 200, 400, 600, and 800 ng/mL, respectively (Figure 9A). Similarly, MTX alone also caused a significant augmentation of DCF fluorescence in A549 cells, which was found to be 13.47% ± 3.49%, 33.34% ± 3.39%, 52.78% ± 3.49%, 71.21% ± 3.74%, and 80.17% ± 3.87% at the doses of 1, 2, 4, 6, and 8 μg/mL, respectively (Figure 9B). Furthermore, ZnONPs alone exhibited significant DCF fluorescence in A549 cells at a dose of 10–80 μg/mL (Figure 9C). Our result demonstrated that, at similar doses, MTX-ZnONP treatment led to the generation of a greater

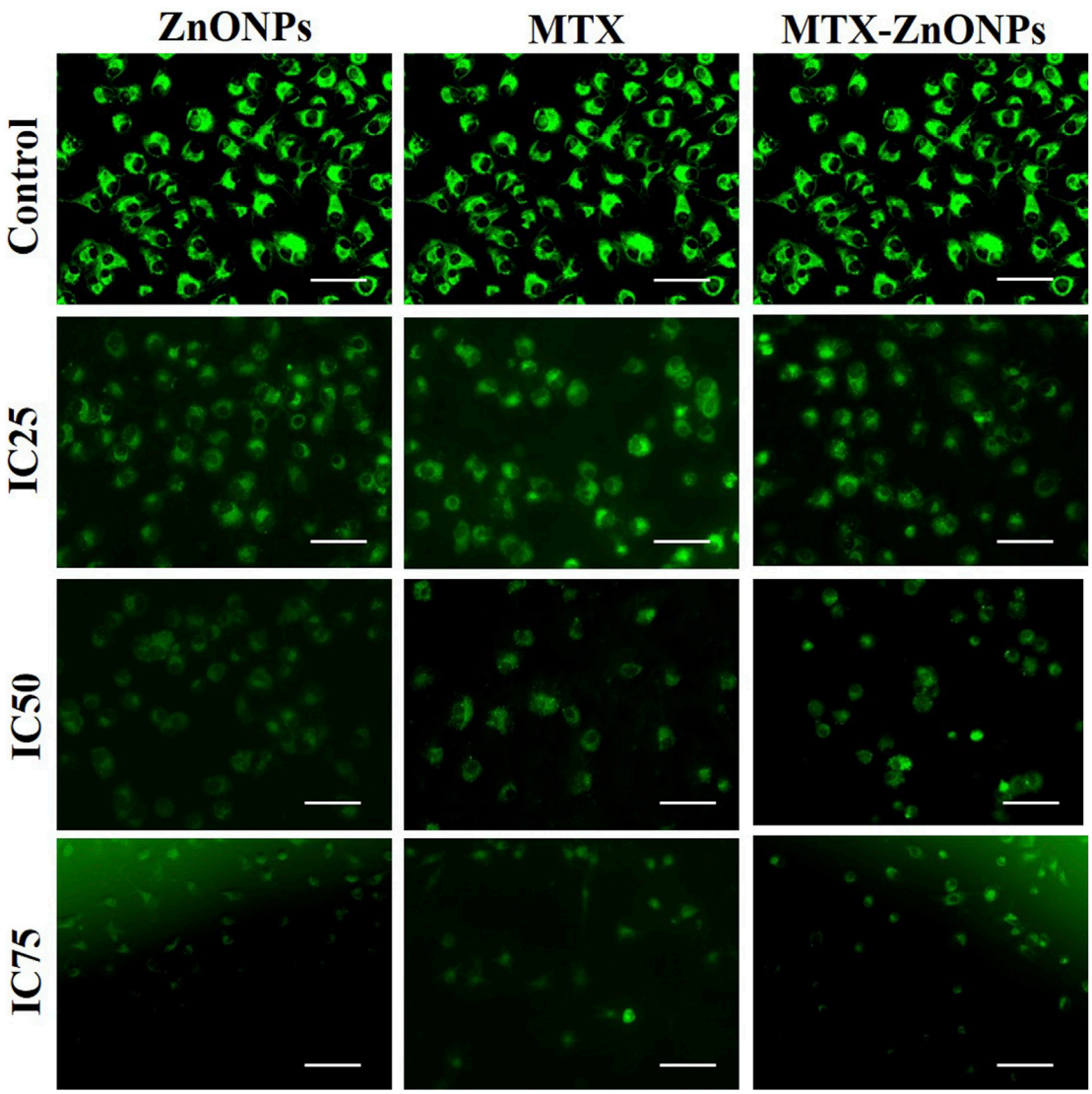

FIGURE 7
Qualitative assessment of mitochondrial membrane potential in Rhodamine 123-stained A549 cells treated at IC_{25} (ZnONPs 27.83 μg/mL; MTX 1.95 μg/mL; and MTX-ZnONPs 182 ng/mL), IC_{50} (ZnONPs 65.30 μg/mL; MTX 3.58 μg/mL; and MTX-ZnONPs 327 ng/mL), and IC_{75} (ZnONPs 70.41 μg/mL; MTX 6.57 μg/mL; and MTX-ZnONPs 588 ng/mL) concentrations for 24 h analyzed by fluorescence microscopy. Images shown are representative of three independent experiments (scale bar: 100 μm; magnification: ×20). The control image was reused in each treatment group.

amount of ROS in A549 cells compared to treatment with MTX alone.

NAC reduced cytotoxicity

Pretreatment of NAC considerably reduced the cytotoxicity in A549 cells caused by MTX-ZnONPs, MTX alone, and ZnONPs alone (Figure 10). Our findings authenticated the fact that an enhanced level of ROS in all the treatment groups was critical for apoptosis in A549 cells. However, it was interesting to note that the cytotoxicity of MTX-ZnONPs, and MTX and ZnONPs alone, was not completely abrogated by NAC, which implicated the involvement of some ROS-independent apoptotic pathways in all the treatment groups.

Activation of caspases

To determine whether apoptosis in lung cancer cells was due to the activation of caspase-dependent or caspase-independent pathways, caspase activities were determined in A549 cells treated with the effective doses of MTX-ZnONPs and MTX and ZnONPs alone. The caspase-9 activity in the MTX-ZnONP-treated group was substantially augmented by 15.17% ± 2.01%, 32.70% ± 4.05%, 56.94% ± 4.33%, 73.50% ± 3.14%, and 91.54% ± 1.86% compared to the untreated control at the doses of 100, 200, 400, 600, and 800 ng/mL, respectively (Figure 11A). Similarly, MTX alone also exhibited significantly increased caspase-9 activity in A549 cells by 10.94% ± 2.81%, 20.03% ± 4.06%, 39.61% ± 4.14%, 64.17% ± 3.28%, and 87.87% ± 3.42% at the doses of 1, 2, 4, 6, and 8 μg/mL, respectively (Figure 11B). Furthermore, the activity of caspase-3

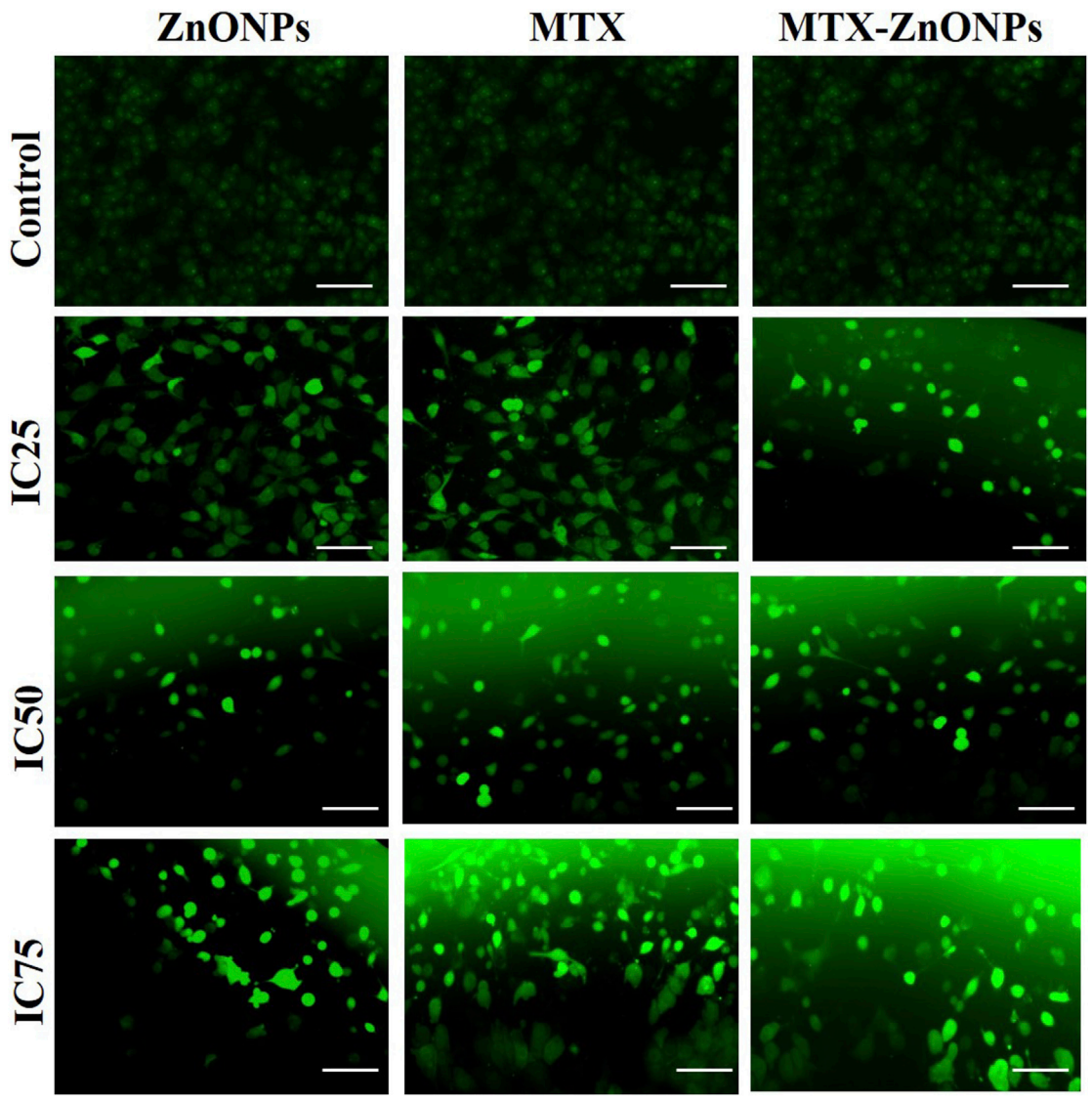

FIGURE 8
Qualitative evaluation of ROS in H_2DCFDA-stained A549 cells treated at IC_{25} (ZnONPs 27.83 μg/mL; MTX 1.95 μg/mL; and MTX-ZnONPs 182 ng/mL), IC_{50} (ZnONPs 65.30 μg/mL; MTX 3.58 μg/mL; and MTX-ZnONPs 327 ng/mL), and IC_{75} (ZnONPs 70.41 μg/mL; MTX 6.57 μg/mL; and MTX-ZnONPs 588 ng/mL) concentrations for 24 h analyzed by fluorescence microscopy. Images shown are representative of three independent experiments (scale bar: 100 μm; magnification: ×20). The control image was reused in each treatment group.

was significantly enhanced in MTX-ZnONP-treated A549 cells by 19.49% ± 3.13%, 32.41% ± 2.97%, 56.89% ± 5.43%, 72.35% ± 4.39%, and 88.08% ± 4.62% at the doses of 100, 200, 400, 600, and 800 ng/mL, respectively (Figure 11A). Similarly, MTX alone also exhibited substantially elevated caspase-3 activity in A549 cells by 14.49% ± 3.26%, 24.97% ± 4.23%, 42.81% ± 3.99%, 71.30% ± 5.37%, and 91.46% ± 3.44% at the doses of 1, 2, 4, 6, and 8 μg/mL, respectively (Figure 11B). The caspase-8 activity in A549 cells treated with MTX-ZnONPs was substantially augmented by 18.82% ± 1.80%, 29.30% ± 3.67%, 55.81% ± 5.64%, 67.96% ± 2.26%, and 86.33% ± 4.08% at the doses of 100, 200, 400, 600, and 800 ng/mL, respectively (Figure 11A). Likewise, MTX alone also exhibited significantly increased caspase-8 activity in A549 cells by 13.16% ± 2.68%, 22.97% ± 2.46%, 40.81% ± 3.96%, 65.23% ± 4.28%, and 88.66% ± 3.08% at the doses of 1, 2, 4, 6, and 8 μg/mL, respectively (Figure 11B). Additionally, ZnONPs alone did not exhibit any significant activity of caspase-8 in A549 cells after 24 h of treatment (Figure 11C). Our results demonstrated that, at similar doses, the MTX-ZnONP-treated group showed prominent caspase-9, -8, and -3 activities in A549 cells compared to that treated with MTX alone. Thus, our results established that MTX induced caspase-dependent apoptosis in lung cancer cells via the activation of both intrinsic and extrinsic pathways.

Caspase inhibitors reduced the cytotoxicity

Our results demonstrated that the caspase-3 inhibitor considerably attenuated the cytotoxicity in all the treatment groups, substantiating the activation of caspases in A549 cells

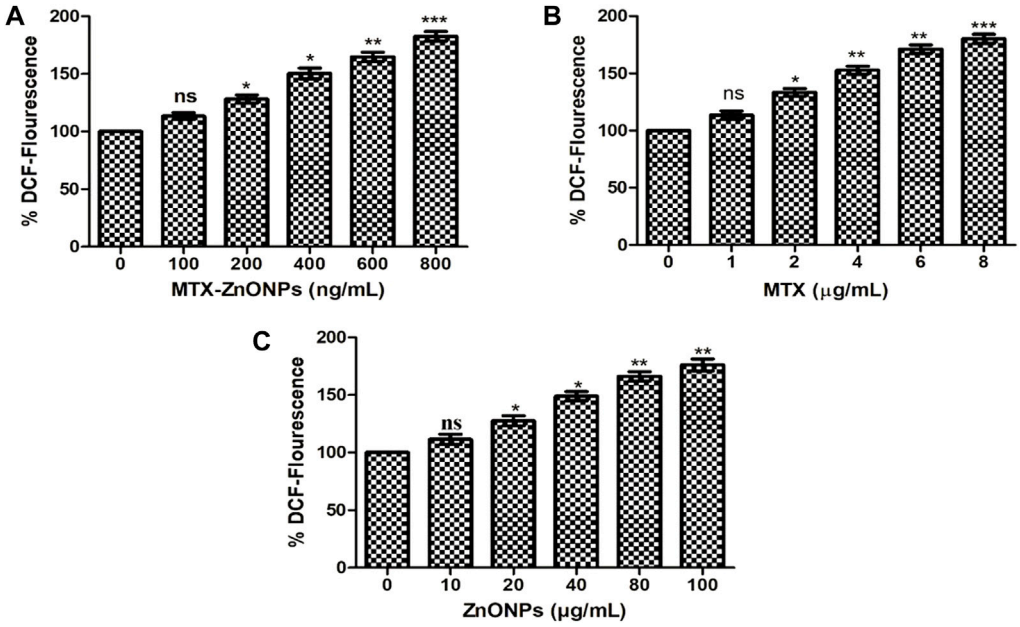

FIGURE 9
Quantitative determination of ROS in H_2DCFDA-stained A549 cells treated with different concentrations of **(A)** MTX-ZnONPs, **(B)** MTX alone, and **(C)** ZnONPs alone for 24 h. The results presented are the mean ± SEM of three independent experiments performed in triplicate. Significance among different dosage groups were determined using one-way ANOVA followed by Dunnett's *post hoc* test (where $*p < 0.05$, $**p < 0.01$, and $***p < 0.001$ represent significant differences compared with vehicle control).

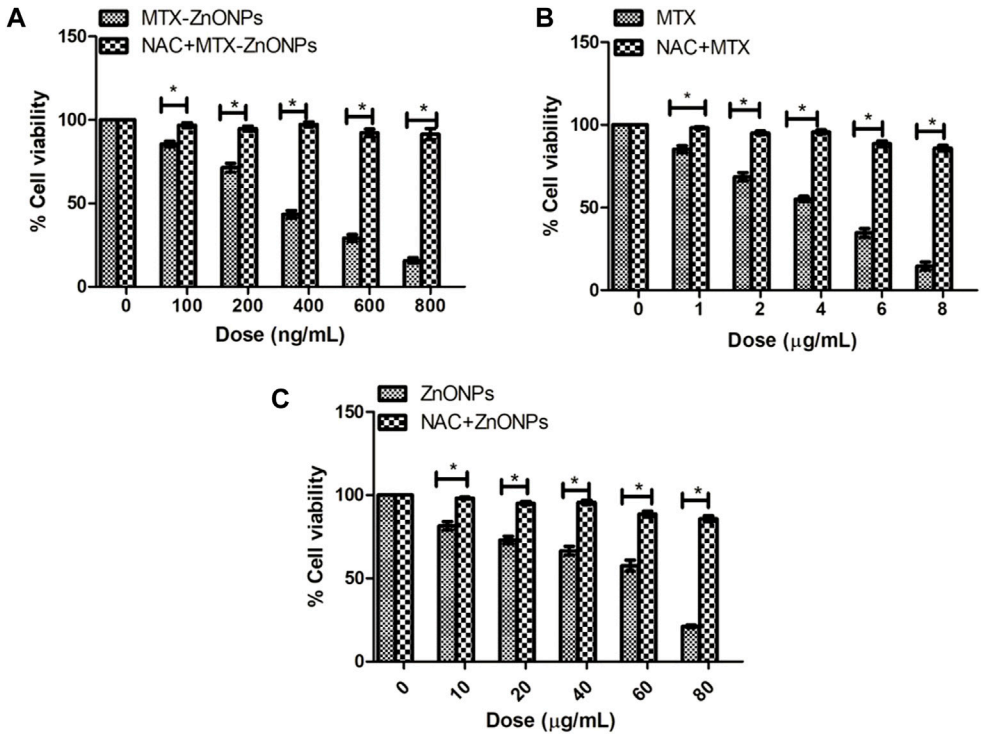

FIGURE 10
Percent cell viability of A549 cells, pretreated with NAC (5 mM), followed by treatment with different doses of **(A)** MTX-ZnONPs, **(B)** MTX alone, and **(C)** ZnONPs alone for 24 h assessed by MTT assay. The results presented are the mean ± SEM of three independent experiments performed in triplicate. Significance among two treatment groups were determined using two-tailed paired *t*-test (where $*p < 0.05$ represents significant difference between means of both treatment groups).

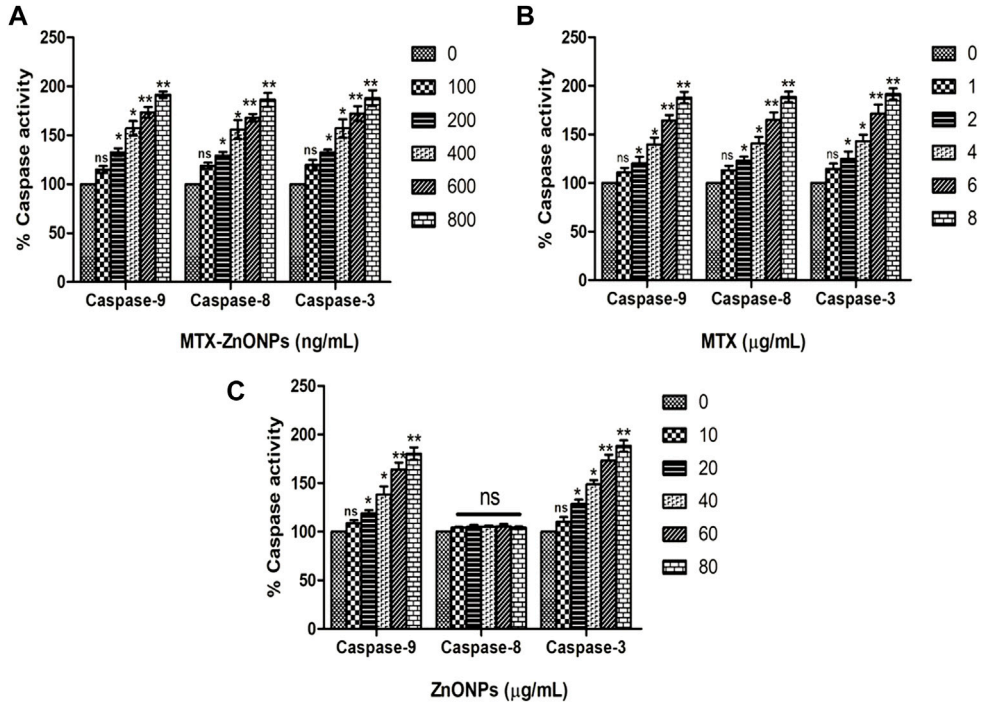

FIGURE 11
Percent caspase-9, -8, and -3 activities in A549 cells treated with different concentrations of **(A)** MTX-ZnONPs, **(B)** MTX alone, and **(C)** ZnONPs alone for 24 h. The results presented are the mean ± SEM of three independent experiments performed in triplicate. Significance among different dosage groups were determined using one-way ANOVA followed by Dunnett's *post hoc* test (where $*p < 0.05$, $**p < 0.01$, and $***p < 0.001$ represent significant differences compared with vehicle control).

(Figure 12). Interestingly, the caspase-3 inhibitor did not completely reduce the cytotoxicity in all the treatment groups, which indicates a minor role of a caspase-independent pathway of apoptosis in A549 cells along with the caspase-dependent pathway.

Discussion

Since standard chemotherapeutic agents often exhibit serious side effects during chemotherapy, their dosage can be reduced by coupling them with some carrier or delivery agent to minimize the side effects of these drugs. This type of conjugation of drugs with some carrier will help deliver drugs directly to the cancer cells. Thus, a lower dose of the drug will be more effective than a higher therapeutic dose (Zhang et al., 2018). In this regard, nanotechnology can offer good drug-delivery options. The biocompatibility and exceptional physicochemical properties of ZnONPs have shown their potential in the diagnosis and treatment of various types of cancer (Hanley et al., 2008; Deng et al., 2009). ZnONPs have been shown to exhibit cytotoxicity in cancer cells by inducing intracellular ROS production and abrogation of $\Delta\Psi m$, ultimately leading to the activation of caspases and apoptosis (Anjum et al., 2021). For the effective use of ZnONPs, their surface needs to be modified with certain capping (Kalpana et al., 2018; Xu et al., 2018). In this regard, the green synthesis of ZnONPs has received increasing attention recently (Lv et al., 2017). In the current study, biogenically synthesized ZnONPs were conjugated with the antifolate drug MTX, and their cytotoxic efficacy was determined against lung cancer cells.

We have discussed the biogenic synthesis of ZnONPs using a fungus, later identified as an *A. niger* strain, in the previous publication (Mishra et al., 2017; Mishra et al., 2022). In the current study, we have successfully shown the conjugation of MTX with biogenically synthesized ZnONPs. The conjugation of MTX with ZnONPs was authenticated by UV-vis spectroscopy, DLS, FTIR, and TEM. The drug-nanoconjugate showed high drug-loading efficiency, which indicated the efficiency of ZnONPs as drug carriers. We utilized EDC chemistry to conjugate MTX with ZnONPs. The drug–nanoparticle conjugates were highly stable due to the amide linkage of MTX with ZnONPs.

The cytotoxic efficacy of MTX-ZnONPs was further tested *in vitro* on a non-small cell lung cancer cell line, and the results of MTT and LDH release assays showed that MTX-ZnONPs (at the dose of 100–800 ng/mL) and MTX (at the dose of 1–8 μg/mL) were efficient in suppressing the growth of A549 cells; however, the efficacy of MTX-ZnONPs was found to be substantially enhanced at very low doses compared to that of MTX. The most plausible reason behind this enhanced activity of MTX-ZnONPs may be the high drug-loading efficiency of the biogenic nanocarrier and effective delivery of the drug, which could significantly increase the intracellular concentration of MTX, thus enhancing the inhibition of cancer cell proliferation. Interestingly, human folate receptors have been reported to take up MTX-loaded nanoparticles into cells to a better degree than MTX and are most likely to be released only in the acidic environment of lysosomes (Xie et al.,

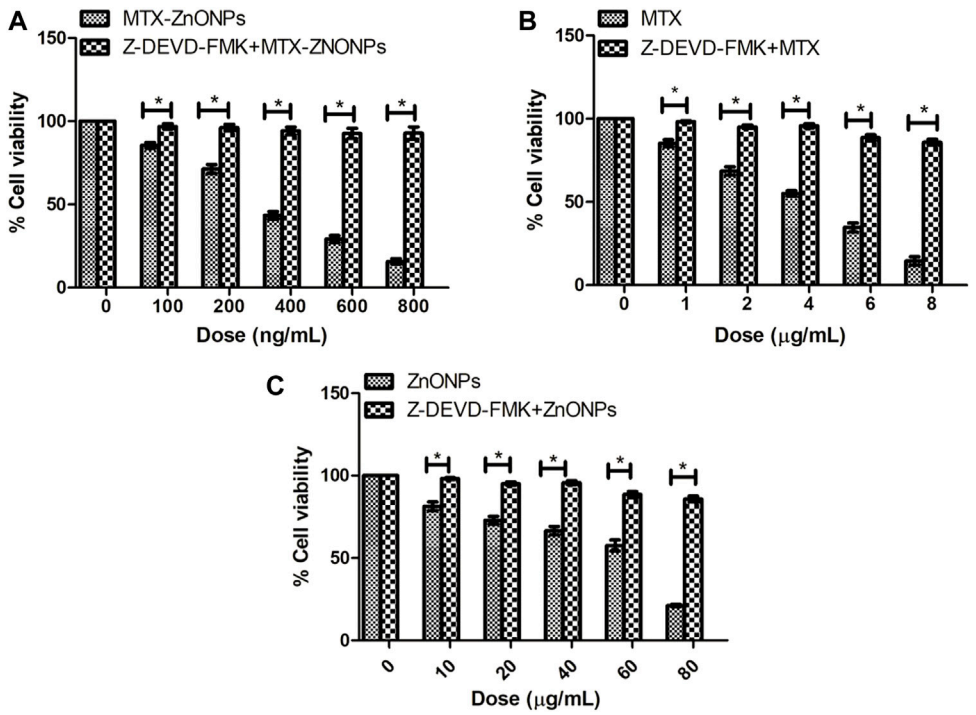

FIGURE 12
Percent cell viability of A549 cells, pretreated with caspase-3 inhibitor Z-DEVD-FMK (50 μM), followed by treatment with different doses of **(A)** MTX-ZnONPs, **(B)** MTX alone, and **(C)** ZnONPs alone for 24 h assessed by MTT assay. The results presented are the mean ± SEM of three independent experiments performed in triplicate. Significance among two treatment groups were determined using two-tailed paired *t*-test (where $*p < 0.05$ represents significant difference between means of both treatment groups).

2018). Due to the high expression of the folate receptor on the target cancer cells, MTX-ZnONPs could possibly be internalized inside cancer cells easily and efficiently (Figure 13). Our results were in agreement with a previous study where MTX was conjugated with iron oxide nanoparticles (IONPs) as a drug delivery system to study its cytotoxic effect on cancer cells (Nosrati et al., 2018). Moreover, ZnONPs alone significantly inhibited the cell viability of A549 cells at a much higher concentration (at a dose of 10–80 μg/mL) compared to MTX-ZnONPs and MTX, which suggested the intrinsic cytotoxic properties of ZnONPs against lung cancer cells at higher concentrations. Previously, the cytotoxic property of ZnONPs was demonstrated in cancer cells, which corroborated our finding (Anjum et al., 2021). Furthermore, our results have also shown a significant cytotoxicity effect of ZnONPs against normal 3T3 cells at a dose range of 10–100 μg/mL (Supplementary Figure S1). This signified that ZnONPs are cytotoxic not only to A549 cells but also to 3T3 cells at this dose range (Pinho et al., 2020).

When conjugated with MTX, these ZnONPs intriguingly exhibited a similar degree of effect at much lower doses (100–800 ng/mL). This observation might be due to drug alone or the nanocarrier. So, to confirm this observation, we again performed the cell viability assay of A549 cells treated with free ZnONPs at 100–800 ng/mL doses, which showed that ZnONPs were not cytotoxic to A549 cells at the indicated doses (Supplementary Figure S2). This result suggested the non-toxic behavior of free ZnONPs at much lower doses, which could be articulated to be its good nanocarrier property.

Furthermore, cytomorphological analysis performed at isoeffective concentrations by phase contrast microscopy revealed significant changes in the morphology of A549 cells in all the treatment groups, which were evident by cell shrinkage and detachment from the surface, forming clusters. Similarly, the nuclear changes in A549 cells in all the treatment groups, analyzed at isoeffective doses by a fluorescent dye DAPI, revealed fragmented and condensed nuclei, indicating initiation of apoptosis. Interestingly, at isoeffective concentrations, ZnONPs alone exerted similar effects on A549 cells compared to MTX-ZnONPs and MTX alone, which indicated the inherent cytotoxic properties of ZnONPs against lung cancer cells at higher concentrations (Figure 8). Moreover, the results also showed that MTX-ZnONPs exerted similar morphological changes in lung cancer cells at very low doses compared to MTX.

As described previously, the reduction in mitochondrial membrane potential ($\Delta\psi_m$) is an important event during the activation of the intrinsic pathway of apoptosis (Khan I. et al., 2018). Thus, $\Delta\psi_m$ in A549 cells in all the treatment groups, analyzed at isoeffective doses by using a cationic fluorescent dye Rhodamine 123, showed a gradual decrease. ZnONPs alone caused an equivalent reduction in $\Delta\psi_m$ in A549 cells compared to MTX-ZnONPs and MTX alone, which suggested the apoptotic potential of ZnONPs against lung cancer cells at higher doses. Furthermore, the results also showed that MTX-ZnONPs reduced the $\Delta\psi_m$ in lung cancer cells at very low concentrations compared to MTX, suggesting efficient delivery of the drug inside the cell.

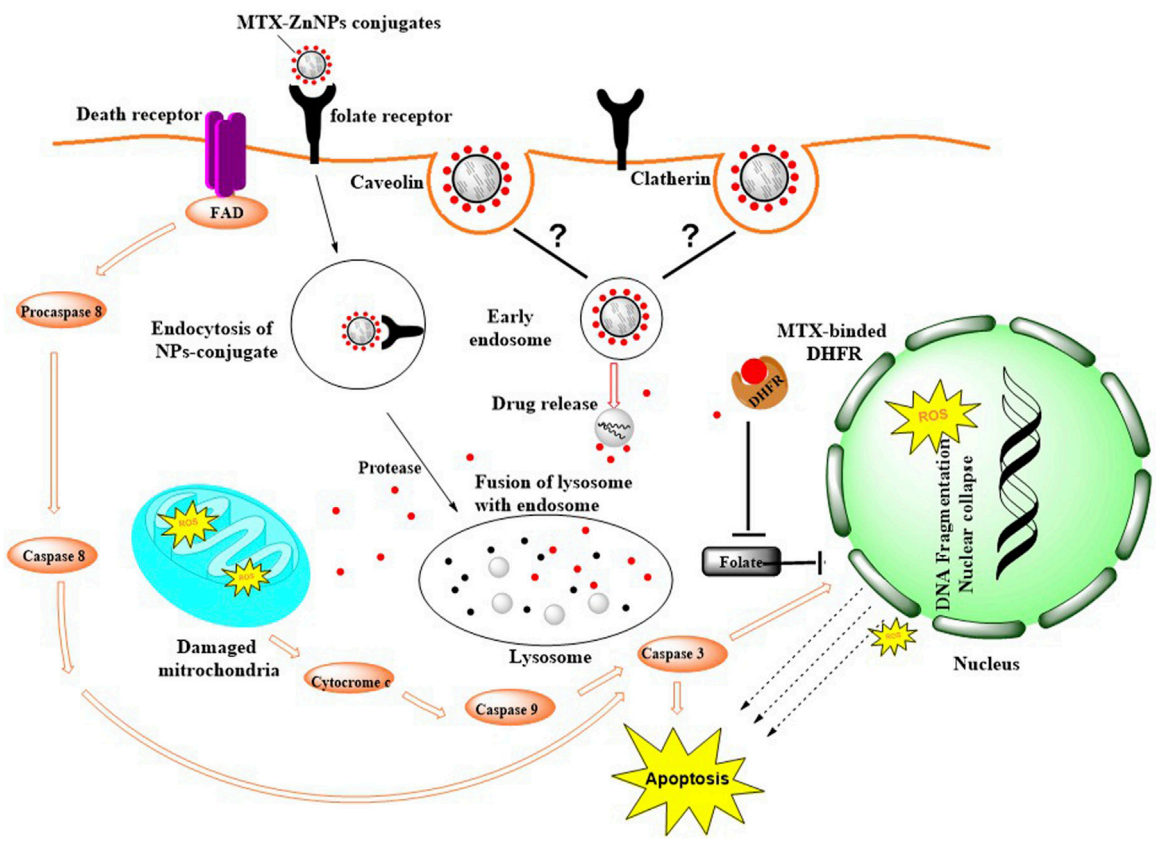

FIGURE 13
Possible mode of internalization of MTX-ZnONPs via caveolin-mediated or clathrin-mediated endocytosis and mechanism of action of MTX in A549 cells.

Many anticancer drugs exert their therapeutic effect on cancer cells by augmenting the production of cytosolic ROS (Doroshow, 1986; Oh et al., 2007). ROS have been implicated in many cellular functions, such as apoptosis (Nakazato et al., 2007). Results of qualitative analysis of ROS, analyzed at isoeffective doses in A549 cells in all the treatment groups, depicted an augmented intracellular ROS level. Intriguingly, ZnONPs alone induced a similar amount of ROS generation in A549 cells compared to MTX-ZnONPs and MTX at isoeffective doses, which suggested that ZnONPs alone caused ROS-dependent apoptosis in lung cancer cells at higher doses. Furthermore, the results also showed that MTX-ZnONPs induced a similar amount of ROS in lung cancer cells at very low concentrations compared to MTX. Thus, our results suggested that MTX primarily caused ROS-mediated cell death in A549 cells.

Additionally, the results of quantitative analysis of ROS revealed that MTX-ZnONPs (at the dose of 100–800 ng/mL) and MTX alone (at the dose of 1–8 μg/mL) were effective in augmenting the intracellular ROS level in A549 cells; however, the effect of MTX-ZnONPs was more profound at very low doses compared to that of MTX. Moreover, ZnONPs alone substantially elevated the ROS level in A549 cells at much higher concentrations (10–80 μg/mL) compared to MTX-ZnONPs and MTX alone, which illustrated that the cytotoxic property of ZnONPs was due to ROS-mediated programmed cell death in lung cancer cells at higher concentrations. To corroborate the production of ROS in all the treatment groups, cell survival was estimated in lung cancer cells pretreated with NAC. It was observed that NAC significantly ameliorated the cell viability in all the treatment groups, authenticating the crucial role of ROS-mediated apoptosis in A549 cells. Interestingly, NAC did not completely ameliorate the survival of A549 cells in all the treatment groups, which indicated the role of ROS-independent pathways of apoptosis in A549 cells. Thus, our results showed that MTX could induce apoptosis in lung cancer cells via both ROS-dependent and ROS-independent pathways.

It has been well established that caspase-8 and caspase-9 play indispensable roles in the activation of the extrinsic and intrinsic apoptotic pathways, respectively (Ona et al., 1999). Moreover, caspase-3 is the chief executor of apoptosis by cleaving and dismantling the cellular structures (Bakar et al., 2010). Therefore, to confirm whether the cell death induced in lung cancer cells in all the treatment groups was due to the extrinsic or intrinsic pathway of apoptosis, caspase activities were determined in A549 cells. The results showed that MTX-ZnONPs (at the dose of 100–800 ng/mL) and MTX alone (at the dose of 1–8 μg/mL) caused significant activation of caspase-9, -8, and -3 in A549 cells; however, the effect of MTX-ZnONPs was more profound at very low doses compared to that of MTX. These results suggested that MTX induced apoptosis in A549 cells via both extrinsic and intrinsic pathways. Moreover, ZnONPs alone substantially activated caspase-

9 and -3 in A549 cells at much higher concentrations (10–80 μg/mL) compared to MTX-ZnONPs (at the dose of 100–800 ng/mL) and MTX alone (at the dose of 1–8 μg/mL), while there was no significant activation of caspase-8, illustrating the activation of only the mitochondrial pathway of programmed cell death in lung cancer cells treated with ZnONPs at higher concentrations.

To validate the activation of caspases in lung cancer cells, cell survival was estimated in all the treatment groups pretreated with the caspase-3 inhibitor. The results showed that pre-treatment with the caspase-3 inhibitor significantly ameliorated the cell viability, demonstrating the instigation of caspases during programmed cell death in A549 cells in all the treatment groups. Intriguingly, pretreatment with a caspase-3 inhibitor did not completely ameliorate cell viability in lung cancer cells, indicating the activation of a caspase-independent pathway of apoptosis in A549 cells. Thus, our results showed that MTX could induce apoptosis in lung cancer cells via both caspase-dependent and caspase-independent pathways.

Conclusion

In conclusion, the results of the current study have illustrated the conjugation of MTX with ZnONPs with high drug-loading efficiency. Moreover, the cytotoxic efficiency of MTX-ZnONPs was found to be enhanced compared to MTX alone in lung cancer cells. ZnONPs exhibited significant toxicity against lung cancer cells only at very high doses compared to the effective doses of drug-nanoconjugates, which suggested that the high therapeutic efficiency of MTX-ZnONPs was due to intracellular delivery of MTX. Thus, our results emphasized the efficient delivery of MTX to lung cancer cells via ZnONPs as nanocarriers.

Data availability statement

The original contributions presented in the study are included in the article/Supplementary Material; further inquiries can be directed to the corresponding authors.

Author contributions

Conceptualization: IA and PM; methodology: PM and MFA; software: IA, MS, and NA; validation: MS, PM, MFA, MV, SF, AA, and NA; formal analysis: LK, NMA, MS, and NA; investigation: PM and AA; resources: MS, NMA, LK, and IA; data curation: IA; writing—original draft preparation: PM; writing—review and editing: IA; visualization: IA, MS, and LK; supervision: IA and LK; project administration: IA, MS, and LK.

Acknowledgments

The authors are thankful to the Princess Nourah bint Abdulrahman University researcher supporting program number (PNURSP2023R82), Princess Nourah bint Abdulrahman University, Riyadh, Saudia Arabia.

Conflict of interest

The authors declare that the research was conducted in the absence of any commercial or financial relationships that could be construed as a potential conflict of interest.

Publisher's note

Supplementary material

The Supplementary Material for this article can be found online at: https://www.frontiersin.org/articles/10.3389/fphar.2023.1194578/full#supplementary-material

SUPPLEMENTARY FIGURE S1
Percent cell viability of 3T3 cells treated with different doses of ZnONPs for 24 h assessed by MTT assay. The results presented are the mean ± SEM of three independent experiments performed in triplicate. Significance among different dosage groups were determined using one-way ANOVA followed by Dunnett's *post hoc* test (where $*p < 0.05$, $**p < 0.01$, and $***p < 0.001$ represent significant differences compared with vehicle control).

SUPPLEMENTARY FIGURE S2
Percent cell viability of A549 cells in all the treatment groups treated with the effective doses of MTX-ZnONPs (100–800 ng/mL) for 24 h. The results presented are the mean ± SEM of three independent experiments performed in triplicate. Significance in different treatment groups at different doses were determined using two-way ANOVA with Bonferroni's *post hoc* tests (where $*p < 0.05$, $**p < 0.01$, and $***p < 0.001$ represent significant differences between means of different treatment groups at different doses).

References

Aghajanzadeh, M., Zamani, M., Molavi, H., Khieri Manjili, H., Danafar, H., and Shojaei, A. (2018). Preparation of metal–organic frameworks UiO-66 for adsorptive removal of methotrexate from aqueous solution. *J. Inorg. Organomet. Polym. Mater.* 28 (1), 177–186. doi:10.1007/s10904-017-0709-3

Anjum, S., Hashim, M., Malik, S. A., Khan, M., Lorenzo, J. M., Abbasi, B. H., et al. (2021). Recent advances in zinc oxide nanoparticles (ZnO NPs) for cancer diagnosis, target drug delivery, and treatment. *Cancers* 13 (18), 4570. doi:10.3390/cancers13184570

Bakar, M. F. A., Mohamad, M., Rahmat, A., Burr, S. A., and Fry, J. R. (2010). Cytotoxicity, cell cycle arrest, and apoptosis in breast cancer cell lines exposed to an extract of the seed kernel of Mangifera pajang (bambangan). *Food Chem. Toxicol.* 48 (6), 1688–1697. doi:10.1016/j.fct.2010.03.046

Barui, A. K., Kotcherlakota, R., and Patra, C. R. (2018). "Biomedical applications of zinc oxide nanoparticles," in *Inorganic frameworks as smart nanomedicines* (Amsterdam, Netherlands: Elsevier), 239–278.

Crews, K. R., Liu, T., Rodriguez-Galindo, C., Tan, M., Meyer, W. H., Panetta, J. C., et al. (2004). High-dose methotrexate pharmacokinetics and outcome of children and young adults with osteosarcoma. *Cancer Interdiscip. Int. J. Am. Cancer Soc.* 100 (8), 1724–1733. doi:10.1002/cncr.20152

Deng, X., Luan, Q., Chen, W., Wang, Y., Wu, M., Zhang, H., et al. (2009). Nanosized zinc oxide particles induce neural stem cell apoptosis. *Nanotechnology* 20 (11), 115101. doi:10.1088/0957-4484/20/11/115101

Doroshow, J. H. (1986). Role of hydrogen peroxide and hydroxyl radical formation in the killing of Ehrlich tumor cells by anticancer quinones. *Proc. Natl. Acad. Sci.* 83 (12), 4514–4518. doi:10.1073/pnas.83.12.4514

Duncan, R., and Richardson, S. C. W. (2012). Endocytosis and intracellular trafficking as gateways for nanomedicine delivery: opportunities and challenges. *Mol. Pharm.* 9 (9), 2380–2402. doi:10.1021/mp300293n

Duthie, S. J. (2001). Folic-acid-mediated inhibition of human colon-cancer cell growth. *Nutrition* 17 (9), 736–737. doi:10.1016/s0899-9007(01)00595-0

Evans, W. E., Crom, W. R., Abromowitch, M., Dodge, R., Look, A. T., Bowman, W. P., et al. (1986). Clinical pharmacodynamics of high-dose methotrexate in acute lymphocytic leukemia. Identification of a relation between concentration and effect. *N. Engl. J. Med.* 314 (8), 471–477. doi:10.1056/NEJM198602203140803

Frei, E., III, Jaffe, N., Tattersall, M. H. N., Pitman, S., and Parker, L. (1975). New approaches to cancer chemotherapy with methotrexate. *N. Engl. J. Med.* 292 (16), 846–851. doi:10.1056/NEJM197504172921607

Gewirtz, D. A., Bristol, M. L., and Yalowich, J. C. (2010). Toxicity issues in cancer drug development. *Curr. Opin. investigational drugs (London, Engl. 2000)* 11 (6), 612–614.

Gomathy, M., and Sabarinathan, K. G. (2010). Microbial mechanisms of heavy metal tolerance-a review. *Agric. Rev.* 31 (2).

Hanley, C., Layne, J., Punnoose, A., Reddy, K., Coombs, I., Coombs, A., et al. (2008). Preferential killing of cancer cells and activated human T cells using ZnO nanoparticles. *Nanotechnology* 19 (29), 295103. doi:10.1088/0957-4484/19/29/295103

Huennekens, F. M. (1994). The methotrexate story: A paradigm for development of cancer chemotherapeutic agents. *Adv. enzyme Regul.* 34, 397–419. doi:10.1016/0065-2571(94)90025-6

Kalpana, V. N., Kataru, B. A. S., Sravani, N., Vigneshwari, T., Panneerselvam, A., and Rajeswari, V. D. (2018). Biosynthesis of zinc oxide nanoparticles using culture filtrates of Aspergillus Niger: antimicrobial textiles and dye degradation studies. *OpenNano* 3, 48–55. doi:10.1016/j.onano.2018.06.001

Khan, I., Khan, F., Farooqui, A., and Ansari, I. A. (2018a). Andrographolide exhibits anticancer potential against human colon cancer cells by inducing cell cycle arrest and programmed cell death via augmentation of intracellular reactive oxygen species level. *Nutr. cancer* 70 (5), 787–803. doi:10.1080/01635581.2018.1470649

Khan, S., Ahmad, K., Ahmad, A., Raish, M., Jan, B. L., Khan, A., et al. (2018b). Biogenic pentagonal silver nanoparticles for safer and more effective antibacterial therapeutics. *Int. J. nanomedicine* 13, 7789–7799. doi:10.2147/IJN.S168224

Khan, Z. A., Tripathi, R., and Mishra, B. (2012). Methotrexate: A detailed review on drug delivery and clinical aspects. *Expert Opin. drug Deliv.* 9 (2), 151–169. doi:10.1517/17425247.2012.642362

Lee, S. H. (2019). Chemotherapy for lung cancer in the era of personalized medicine. *Tuberc. Respir. Dis.* 82 (3), 179–189. doi:10.4046/trd.2018.0068

Lv, Y., Liu, R., Xie, S., Zheng, X., Mao, J., Cai, Y., et al. (2017). Calcein-acetoxymethy ester enhances the antitumor effects of doxorubicin in nonsmall cell lung cancer by regulating the TopBP1/p53RR pathway. *Anti-cancer drugs* 28 (8), 861–868. doi:10.1097/CAD.0000000000000527

Mishra, P., Ahmad, A., Al-Keridis, L. A., Alshammari, N., Alabdallah, N. M., Muzammil, K., et al. (2022). Doxorubicin-conjugated zinc oxide nanoparticles, biogenically synthesised using a fungus Aspergillus Niger, exhibit high therapeutic efficacy against lung cancer cells. *Molecules* 27 (8), 2590. doi:10.3390/molecules27082590

Mishra, P. K., Mishra, H., Ekielski, A., Talegaonkar, S., and Vaidya, B. (2017). Zinc oxide nanoparticles: A promising nanomaterial for biomedical applications. *Drug Discov. today* 22 (12), 1825–1834. doi:10.1016/j.drudis.2017.08.006

Nakazato, T., Sagawa, M., Yamato, K., Xian, M., Yamamoto, T., Suematsu, M., et al. (2007). Myeloperoxidase is a key regulator of oxidative stress–mediated apoptosis in myeloid leukemic cells. *Clin. Cancer Res.* 13 (18), 5436–5445. doi:10.1158/1078-0432.CCR-07-0481

Nosrati, H., Salehiabar, M., Davaran, S., Danafar, H., and Manjili, H. K. (2018). Methotrexate-conjugated L-lysine coated iron oxide magnetic nanoparticles for inhibition of MCF-7 breast cancer cells. *Drug Dev. industrial Pharm.* 44 (6), 886–894. doi:10.1080/03639045.2017.1417422

Nosrati, H., Salehiabar, M., Davaran, S., Ramazani, A., Manjili, H. K., and Danafar, H. (2017). New advances strategies for surface functionalization of iron oxide magnetic nano particles (IONPs). *Res. Chem. Intermed.* 43 (12), 7423–7442. doi:10.1007/s11164-017-3084-3

Nunez, M. I., Behrens, C., Woods, D. M., Lin, H., Suraokar, M., Kadara, H., et al. (2012). High expression of folate receptor alpha in lung cancer correlates with adenocarcinoma histology and EGFR [corrected] mutation. *J. Thorac. Oncol.* 7 (5), 833–840. doi:10.1097/JTO.0b013e31824de09c

Oh, S. Y., Sohn, Y. W., Park, J. W., Park, H. J., Jeon, H. M., Kim, T. K., et al. (2007). Selective cell death of oncogenic Akt-transduced brain cancer cells by etoposide through reactive oxygen species–mediated damage. *Mol. cancer Ther.* 6 (8), 2178–2187. doi:10.1158/1535-7163.MCT-07-0111

Ona, V. O., Li, M., Vonsattel, J. P. G., Andrews, L. J., Khan, S. Q., Chung, W. M., et al. (1999). Inhibition of caspase-1 slows disease progression in a mouse model of Huntington's disease. *Nature* 399 (6733), 263–267. doi:10.1038/20446

O'Shannessy, D. J., Yu, G., Smale, R., Fu, Y. S., Singhal, S., Thiel, R. P., et al. (2012). Folate receptor alpha expression in lung cancer: diagnostic and prognostic significance. *Oncotarget* 3 (4), 414–425. doi:10.18632/oncotarget.489

Pinho, A. R., Martins, F., Costa, M. E. V., Senos, A. M. R., da Cruz e Silva, O. A. B., Pereira, M. de L., et al. (2020). *In vitro* cytotoxicity effects of zinc oxide nanoparticles on spermatogonia cells. *Cells* 9 (5), 1081. doi:10.3390/cells9051081

Singh, T. A., Das, J., and Sil, P. C. (2020). Zinc oxide nanoparticles: A comprehensive review on its synthesis, anticancer and drug delivery applications as well as health risks. *Adv. colloid interface Sci.* 286, 102317. doi:10.1016/j.cis.2020.102317

Xie, J., Fan, Z., Li, Y., Zhang, Y., Yu, F., Su, G., et al. (2018). Design of pH-sensitive methotrexate prodrug-targeted curcumin nanoparticles for efficient dual-drug delivery and combination cancer therapy. *Int. J. nanomedicine* 13, 1381–1398. doi:10.2147/IJN.S152312

Xu, S., Sun, T., Xu, Q., Duan, C., Dai, Y., Wang, L., et al. (2018). Preparation and antibiofilm properties of zinc oxide/porous anodic alumina composite films. *Nanoscale Res. Lett.* 13 (1), 201–212. doi:10.1186/s11671-018-2568-4

Zamani, M., Rostami, M., Aghajanzadeh, M., Kheiri Manjili, H., Rostamizadeh, K., and Danafar, H. (2018). Mesoporous titanium dioxide@ zinc oxide–graphene oxide nanocarriers for colon-specific drug delivery. *J. Mater. Sci.* 53 (3), 1634–1645. doi:10.1007/s10853-017-1673-6

Zhang, T., Chen, Y., Ge, Y., Hu, Y., Li, M., and Jin, Y. (2018). Inhalation treatment of primary lung cancer using liposomal curcumin dry powder inhalers. *Acta Pharm. Sin. B* 8 (3), 440–448. doi:10.1016/j.apsb.2018.03.004

frontiers | Frontiers in Pharmacology

TYPE Original Research
PUBLISHED 30 October 2023
DOI 10.3389/fphar.2023.1269895

OPEN ACCESS

EDITED BY
Mohd Adnan,
University of Hail, Saudi Arabia

REVIEWED BY
Xin Wang,
Affiliated Hospital of Shandong University of Traditional Chinese Medicine, China
Lan Bai,
Sichuan Academy of Medical Sciences and Sichuan Provincial People's Hospital, China
Huanyu Guan,
Chinese Academy of Medical Sciences and Peking Union Medical College, China

*CORRESPONDENCE
Xiaoyan Jiang,
jiangxiaoyan1121@163.com

†These authors have contributed equally to this work

RECEIVED 31 July 2023
ACCEPTED 16 October 2023
PUBLISHED 30 October 2023

CITATION
Lv H, Jia X, Yang H, Zhu X, Zhao Z and Jiang X (2023), Prediction of the mechanism for the combination of diallyl trisulfide and cisplatin against gastric cancer: a network pharmacology study and pharmacological evaluation. *Front. Pharmacol.* 14:1269895. doi: 10.3389/fphar.2023.1269895

Prediction of the mechanism for the combination of diallyl trisulfide and cisplatin against gastric cancer: a network pharmacology study and pharmacological evaluation

Huaiyou Lv[1,2,3†], Xiumei Jia[3†], Huatian Yang[2], Xiaosong Zhu[2,4], Zhongxi Zhao[2] and Xiaoyan Jiang[1,2*]

[1]Department of Pharmacy, Qilu Hospital of Shandong University, Jinan, Shandong, China, [2]Department of Pharmaceutics, Shandong University, Jinan, Shandong, China, [3]Department of Pharmacy, Yantai Yuhuangding Hospital Affiliated to Qingdao University, Yantai, Shandong, China, [4]Department of Infection Management, Linyi People's Hospital, Linyi, Shandong, China

Background: In this research, we aimed to explore the efficacy of diallyl trisulfide (DATS) combined with cisplatin (DDP) for gastric cancer treatment and its underlying mechanism based on network pharmacology.

Methods: First, the pharmacological mechanism by which DATS combined with DDP acts against gastric cancer was predicted using network pharmacology. The TTD, GeneCards, and OMIM databases were used to extract drug and disease targets. The David Bioinformatics Resources 6.8 database was used to conduct GO and KEGG analyses. We investigated the efficacy of DATS combined with DDP against gastric cancer in SGC7901 cells and a xenograft model. Furthermore, the specific mechanism of DATS combined with DDP, inferred by network pharmacology, was identified by Western blotting and immunohistochemistry.

Results: The combination of DDP and DATS significantly increased cytotoxicity and cell apoptosis compared to the DATS or DDP treatment group *in vitro*. In addition, continuous intraperitoneal injection of DATS markedly improved the tumor inhibitory effect of DDP in the SGC-7901 tumor-bearing mouse model. Furthermore, network pharmacology and experimental validation studies revealed that the combination of DATS and DDP synergistically enhanced antitumor activity by regulating endoplasmic reticulum stress and inhibiting STAT3/PKC-δ and MAPK signaling pathways.

Conclusion: Our study showed that the combination of DATS and DDP could exert outstanding therapeutic effects in gastric cancer. Moreover, network pharmacology coupled with experimental validation revealed the molecular mechanisms of combination therapy for gastric cancer. This study offers a new adjuvant strategy based on DATS and DDP for the treatment of gastric cancer.

KEYWORDS

gastric cancer, diallyl trisulfide, cisplatin, network pharmacology, MAPK/STAT3/PKC-δ, endoplasmic reticulum stress

1 Introduction

Gastric cancer (GC) is the fifth most confirmed malignant tumor worldwide, with an annual increase of more than 1 million cases. Owing to its advanced stage at diagnosis, it has become the third leading cause of cancer-related deaths (Sung et al., 2021). Continuous chemotherapy based on first-line platinum and fluoropyrimidine has been used in the treatment of advanced gastric cancer. Cis-diaminedichloroplatinum II (DDP, cisplatin) is a widely used first-line chemotherapy drug and the main treatment strategy for patients with advanced GC, and has been shown to effectively improve the survival rate of patients with advanced GC (Shah, 2015; Sasaki et al., 2017). However, DDP exhibits drug resistance and significant organ toxicity, such as nephrotoxicity, ototoxicity, hepatotoxicity, and gastrointestinal toxicities (Ghosh, 2019). After several cycles of chemotherapy with DDP, approximately one-third of the patients developed renal dysfunction (Merouani et al., 1996), and half of the patients showed acquired drug resistance. Therefore, various new adjuvant approaches are urgently needed to protect normal organs from damage and enhance the therapeutic effect of DDP on gastric cancer cells or tumors, which could provide new ideas to improve DDP-based cancer treatment.

Garlic (*Allium sativum*) is an ancient cultivated plant that possesses the dual-purpose characteristics of food and medicine. Epidemiological and research studies have demonstrated that many active components of garlic have preventive and suppressive effects on various types of tumors (Iciek et al., 2009; Tsubura et al., 2011; Jin et al., 2013; Yan et al., 2014). Recent research has shown that basic treatment with *H. pylori* (H.pylori) and garlic supplementation for 7 years significantly decreased the risk of death from gastric cancer (Li et al., 2019). Garlic extract products possess activity against *Helicobacter pylori* and gastric inflammation, which promotes its potential role in the treatment of peptic ulcer diseases (Sivam, 2001). Moreover, garlic powder, aged garlic extract, and some organosulfur compounds (s-allylcysteine, diallyl disulfide, and diallyl sulfide) have been reported to exhibit antioxidant effects that can ameliorate the nephrotoxic effects of DDP (Dwivedi et al., 1996; Chiarandini Fiore et al., 2008; Razo-Rodriguez et al., 2008; Gomez-Sierra et al., 2014; Nasr and Saleh, 2014). Diallyl trisulfide (DATS), a major bioactive compound in garlic, has multiple health benefits such as anticancer, anti-inflammatory, and immunomodulatory effects. Due to the existence of a triple sulfur bond (-S-S-S-) structure, DATS was reported to be more effective than single and double sulfur-containing compounds in antitumor activity and chemical detoxification defense functions (Tsai et al., 2005; Lai et al., 2013). In addition, DATS has been proven to have a variety of active metabolites *in vivo* in drug metabolism and pharmacokinetics (DMPK) studies, which might offer better protective and therapeutic effects depending on multiple target strategies (Gao et al., 2013). Nevertheless, existing research on garlic organic sulfur compounds has focused on their anti-tumor and anti-oxidation properties. Based on the characteristics of garlic ingredients in dietary therapy, it is worth exploring in-depth in the joint treatment strategy.

Network pharmacology, as a new scientific approach for drug combinatorial research, has the characteristics of constructing "drug-gene-target-disease" networks based on biological properties, analyzing the linkages between drugs, proteins/genes, and diseases, and predicting the mechanism of action of small molecule drugs on diseases (Nogales et al., 2022). Network pharmacology offers brilliant prospects for multiple disease treatments rather than targeting a single disease target. Given its systematic and comprehensive characteristics, more and more research on the active substances in herbal medicines and their mechanisms of action on disease targets were based on network pharmacology (Li et al., 2022).

In this study, we attempted to apply network pharmacology to predict the mechanism of action of DATS combined with DDP against gastric cancer and then validated its protective effect as well as the possible mechanism through pharmacological experiments *in vitro* and *in vivo*. This research revealed the effects and molecular mechanism of the combination of DATS and DDP, which could provide novel ideas for chemotherapy of gastric cancer.

2 Materials and methods

2.1 Drugs and chemicals

DATS (98% purity) was availible from AIKE Biotechnology (Chengdu, China). DDP was obtained from Qilu Pharmaceutical (Jinan, China). Antibodies against Akt, phospho-Akt, phospho-ERK1/2, ERK1/2, phospho-p38, p38, phospho-JNK, JNK, and PKC-δ were obtained from Cell Signaling Technology (Danvers, MA, United States). Antibodies against XBP1, IRE1α, Calnexin and GAPDH were purchased from Beyotime Biotechnology (Shanghai, China). The apoptosis detection kit, cell mitochondrial membrane potential assay kit (TMRE), Annexin V-FITC apoptosis detection kit, TUNEL staining kit, Cell Counting Kit-8 (CCK-8) and calcium ion fluorescent probes (Fluo 3-AM) were purchased from Servicebio Biotechnology (Wuhan, China). Transwell Chambers and Matrigel were obtained from Corning (New York, NY, United States).

2.2 Collection of gene symbols for gastric cancer and construction of protein-protein interaction (PPI) networks

First, the targets of DDP combined with DATS were identified by importing the chemical structures into the SwissTargetPrediction data library (http://www.swisstargetprediction.ch/). After standardizing the target names by the UniProt database (https://www.uniprot.org/), the underlying gene targets for gastric cancer were selected from the following three databases, GeneCards (https://www.genecards.org/), TTD (http://db.idrblab.net/ttd/), and OMIM databases (http://omim.org/). Next, the protein-protein interaction (PPI) network of DDP combined with DATS treatment in gastric cancer was obtained by uploading the selected intersecting genes of 3 databases into STRING 11.0 (http://stringdb.org/cgi/input.pl).

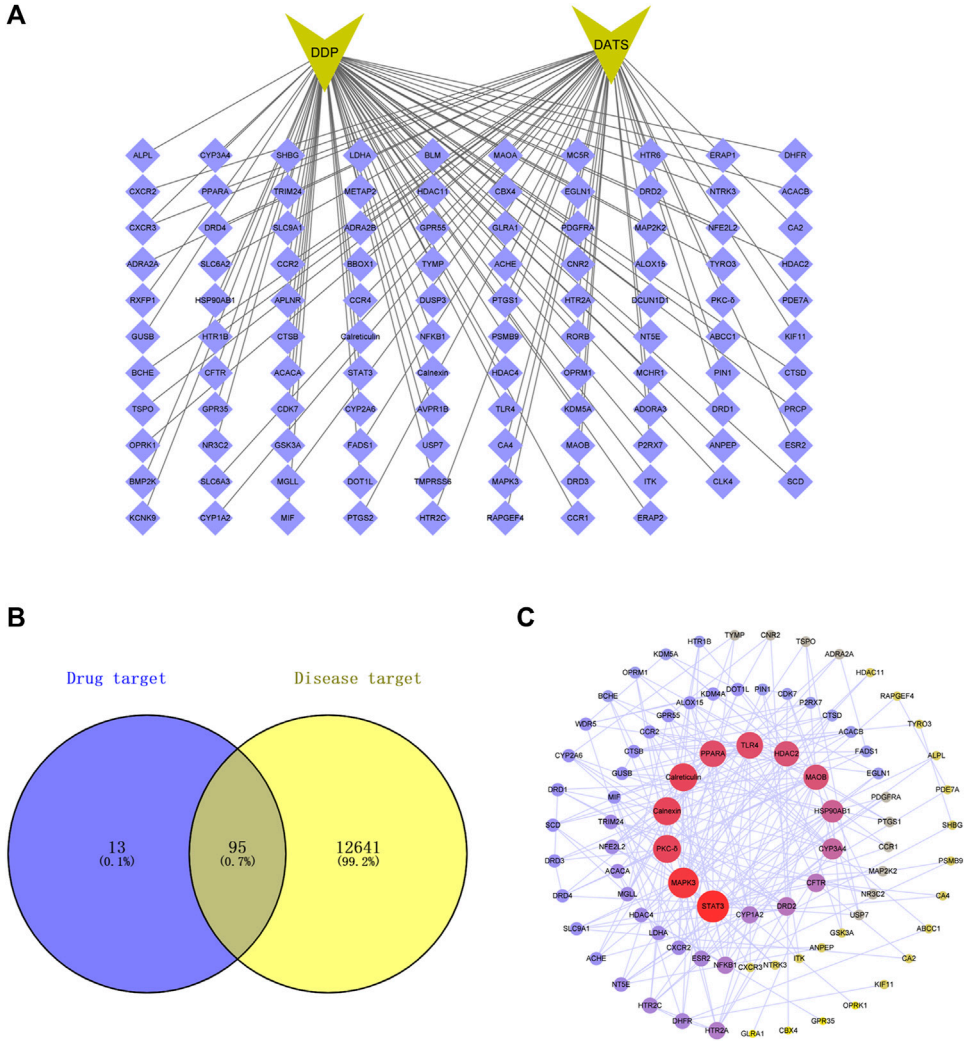

FIGURE 1
Protein-protein interaction (PPI) networks of potential targets for the DDP combined DATS treatment of GC. **(A)** Top 100 targets of DATS combined DDP in SwissTargetPrediction; **(B)** 95 targets of DATS combined DDP related to GC by Venn diagram; **(C)** PPI networks of potential targets for DATS combined DDP against GC.

2.3 Definition of target pathway by building networks

The drug target network was constructed by Cytoscape 3.7.1 software to explore the molecular mechanism of DDP combined with DATS against GC. The potential pathways of DDP combined with DATS against GC were analyzed using gene ontology (GO) enrichment and KEGG pathway analyses using the David Bioinformatics Resources 6.8 database (https://david.ncifcrf.gov/).

2.4 Cell culture and cell proliferation

SGC-7901 cells were used as a gastric cancer model and were obtained from Cobioer Biotechnology (Beijing, China). SGC-7901 cells were cultured in RMPI-1640 medium with 10% fetal bovine serum (BioInd, Israel) at 37°C in a 5% CO_2 incubator. The percentage inhibition of cell growth for 24 h by different concentrations of DATS and DDP was determined using the CCK-8 kit and following its instructions with 450 nm absorbance by a Microplate Reader (Safire2, TECAN, France). The combination index (CI) analysed by Calcusyn 2.1 software (Biosoft, Cambridge, United Kingdom) was used to reveal the interaction between DATS and DDP. CI < 1 indicated synergistic interactions (Chou, 2010).

2.5 Cell apoptosis

SGC-7901 cells were cultured in six-well plates and treated with the indicated doses of DATS, DDP, or their combination for 48 h. The cells were collected and stained with apoptosis detection kit according to the manufacturer's instructions. To evaluate apoptosis, the cells were analyzed by flow cytometry (Beckman FC 500, United States of America) and calculated using FlowJo software.

2.6 Cell migration assay

The migration of SGC-7901 cells was examined by transwell cell migration and scratch assays. For transwell, the matrigel was diluted at a ratio of 1:8 with serum-free medium, and 40 μL diluted matrigel was spread on the upper layer of the chamber. SGC-7901 cells were adjusted to 5×10^5 cells ml^{-1} using serum-free medium, then 100 μL cells and 100 μL drugs were added to the upper layer of the chamber, and 500 μL medium with 10% FBS was added to the lower layer of the chamber. After 48 h of incubation at 37°C, cells were fixed with 4% paraformaldehyde. After removing the cells in the upper compartment, the cells were stained with 0.1% crystal violet. The migrating cells were recorded under the microscope. Finally, photographs were taken using an inverted microscope. The number of cells migrating between the chambers was calculated using the ImageJ software. The scratch test was performed according to a standard protocol (Chou, 2010).

2.7 Calcium ion and mitochondrial membrane potential detections

SGC-7901 cells were plated on glass coverslips and incubated for 24 h. The cells were washed twice with PBS, fixed with 4% formaldehyde for 15 min, permeabilized with 0.2% TritonX-100 for 20 min, and blocked with 5% BSA for 0.5 h. After incubation with Fluo-3 AM and TMRE at 4°C for 1 h, the cells were washed thrice, followed by incubation with Hoechst for 5 min. Finally, images were obtained using an LSM900 confocal laser microscope (Carl Zeiss AG, Germany). The fluorescence intensity was quantified using flow cytometry.

2.8 Western blot

SGC-7901 cells were harvested and lysed in lysis buffer. Total protein was extracted and loaded into each well of 8%–10% SDS-PAGE gel and blotted onto PVDF membranes. The membranes were incubated with primary antibodies (1:1000 dilution) overnight at 4°C after blocking. After washing with TBST buffer three times, incubation with 1:5000 dilution of secondary antibodies linked to horseradish peroxidase (Bioss, China) were carried out for 2 h. Finally, the blots were visualized using ECL Plus reagent (Millipore Corp, Bedford, MA, United States). GAPDH was used to assess the amount of the reference protein in each lane. The relative protein levels were analyzed using AlphaView SA software.

2.9 *In vivo* tumor xenograft experiment

Female athymic nude mice (16–18 g) were purchased from the Institute of Laboratory Animal Sciences (Beijing, China). 5×10^6 SGC-7901 cells in 100 μL PBS were injected subcutaneously into the armpit of the right forelimb of the mice. As the tumor volume (TV) reached approximately 100 mm^3, four groups of mice ($n = 6$) were randomly divided and injected intraperitoneally with vehicle, DATS, DDP, and their combination: (i) vehicle (Control group), every day; (ii) DATS, 30 mg/kg every day; (iii) DDP, 4 mg/kg every 7 days; (iv) DATS+DDP, 4 mg/kg of DDP every 7 days, and 30 mg/kg of DATS every day. Tumor length (a), width (b), and body weight (BW) were recorded every 4 days, and TV was calculated as follows: $TV = (a \times b^2)/2$. After 32 days, the mice were sacrificed, and the main tissues were acquired for further assessment.

2.10 Histopathologic analysis

Tumor tissues were fixed in paraformaldehyde and embedded in paraffin. Sections were made and stained with hematoxylin and eosin to evaluate histopathological changes from three independent images using an Olympus microscope (Tokyo, Japan).

2.11 Immunohistochemistry and TUNEL assay

The immunohistochemical expression of calnexin, PKC-δ, XBP1, and p-JNK was determined. A series of xylene and ethanol aqueous solutions were used to dewax and rehydrate paraffin sections. After blocking, the sections were treated with microwaves to repair the antigen and expose antigenic determinants. After serum blocking, the paraffin sections were incubated with the primary antibody at a 1:100 dilution at 37°C in a humidified chamber for 2 h and then incubated with the diluted secondary antibody for 1 h. The specific binding antibodies in the sections were developed using DAB substrate and hematoxylin counterstain. While, according to the instructions from the TUNEL staining kit, DNA of tissue sections was also counterstained by DAPI. Images were acquired by an Olympus microscope (Tokyo, Japan).

2.12 Statistical analysis

Data were showed as mean ± SD and statistically evaluated by one-way ANOVA based on GraphPad Prism 6.0 statistical software. The significant differences between groups was evaluated by Unpaired *t*-test, with $p < 0.05$ the criterion for statistical significance.

3 Results

3.1 Construction of PPI network of DDP and DATS against GC

As shown in Figure 1, the top 108 targets of DATS combined with DDP were selected from SwissTargetPrediction data (Figure 1A) while 12641 targets for GC were gathered from 3 databases. Consequently, 95 overlapping targets related to DATS, DDP, and GC were identified (Figure 1B). Protein intersections were then performed by mapping the targets of DATS combined with DDP on GC in the STRING database. Three topological features (betweenness centrality, degree and closeness centrality) focused on identification of the key targets in the network. A total of 45 points were identified as key targets in the network, including Calnexin, STAT3, PKC-δ and Calreticulin (Figure 1C).

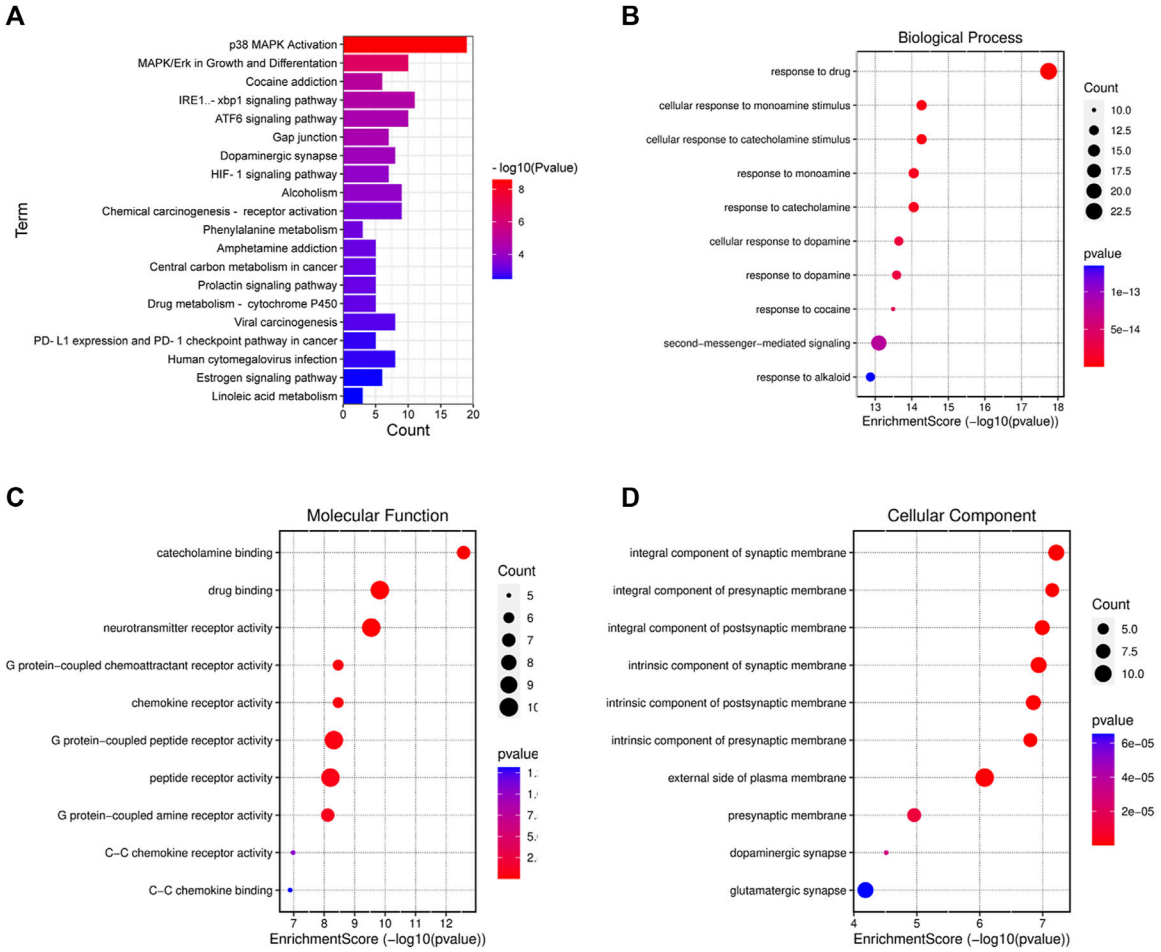

FIGURE 2
Diagrams of mechanistic analyses of **(A)** Pathways enrichment; **(B)** Biological process enrichment; **(C)** Molecular function enrichment; **(D)** Cellular component enrichment.

3.2 KEGG and GO enrichment analysis

To confirm the biological properties of the relevant targets of DATS combined with DDP on GC in detail, KEGG and GO enrichment analysis was performed as shown in Figure 2. Through KEGG pathway enrichment, 83 related pathways were identified, of which the top twenty pathways are shown in Figure 2A.The P38/MAPK, IRE1/XBP1, and ATF6 signaling pathways are the three main pathways closely associated with proliferation and endoplasmic reticulum stress in GC.

GO analysis showed that 133 genes were selected among 2684 GO entries ($p < 0.05$), consisting of 2181 biological progress (BP), 215 cellular components (CC), and 288 molecular functions (MF). The top 10 entries of biological progress, cellular components, and molecular functions among the selected 133 genes are shown in Figures 2B–D, respectively. The potential targets among the top biological processes were primarily focused on the response to the drug and the cellular response to monoamine stimulus. In addition, the potential cellular targets were mainly focused on the integral components of the synaptic and presynaptic membranes. The major molecular functions are related to catecholamine and drug binding.

3.3 Effects of DATS and DDP on the proliferation and apoptosis of SGC-7901 cells

To determine the potential anticancer activity of DATS and DDP in combination, the CCK-8 assay was used to evaluate cell viability after treatment with DATS alone or in combination with DDP by CCK-8 assay. As shown in Figure 3A, DATS treatment (50–400 μM) resulted in dose-dependent growth inhibition of SGC-7901 cells, which increased from 16.20% ± 6.56% to 45.48% ± 6.91%. Nevertheless, when combined with 3 μg/mL DDP, the inhibition rate of DATS against SGC-7901 cells increased from 59.5% to 72.7%, which showed that DATS and DDP in combination significantly enhanced the cytotoxicity of SGC-7901 cells in comparison with DATS alone. In addition, CI values calculated using Comsyn software showed a strong synergy for the combination of DATS and DDP (CI < 1; Figure 3B). To explore the influence of the combination of DATS and DDP on apoptosis (Jiang et al., 2017), cell apoptosis was evaluated using flow cytometry. As shown in Figures 3C, D, compared to the two monotherapy groups, the combination treatment dramatically increased the apoptosis ratio in SGC-7901 cells. Apoptosis rate in the combination group was enhanced to

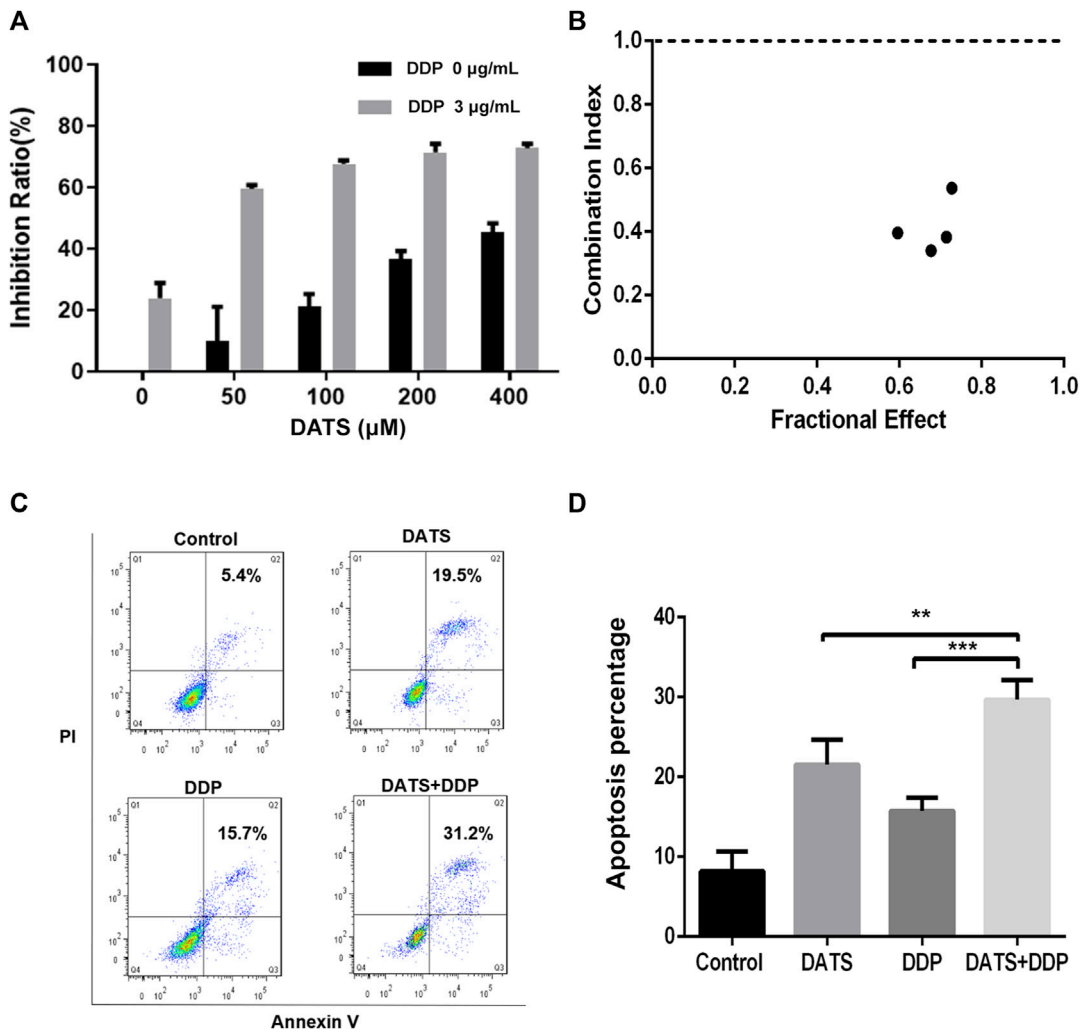

FIGURE 3
DATS synergistically enhanced the effects of cell growth inhibition and apoptosis of DDP in SGC-7901 cells. **(A)** The inhibition rate of SGC-7901 cells; **(B)** The CI values of DATS and DDP; **(C)** Apoptosis of SGC-7901 cells; **(D)** Apoptosis ratio of SGC-7901 cells after different treatments. Data are shown as mean ± SD (n = 3). Compared with the DATS+DDP group, $*p < 0.05$, $**p < 0.01$, $***p < 0.001$.

29.7% ± 2.4%, which was much higher than that in the two monotherapy groups (21.6% ± 2.0% for DATS and 13.9% ± 2.5% for DDP).

3.4 Effects of DATS and DDP on the metastasis of SGC-7901 cells

To explore whether DATS and DDP affect GC metastasis, the effects of DATS and DDP in combination on cell invasion and migration were evaluated. Both the DATS and DDP groups exhibited the ability to inhibit cell migration compared with the control group. Interestingly, we observed that the inhibition of migration in the combination group was stronger than that of either DATS or DDP alone ($***p < 0.001$, $**p < 0.01$, respectively) (Figures 4A, C). In addition, as can be seen in Figures 4B, D, compared with the control group, the number of cells invading the bottom of the vesicles was significantly reduced after DATS and DDP treatment, and this effect was remarkably enhanced in the co-treatment group of DATS and DDP as compared with the groups of single treatment.

3.5 DATS and DDP cooperated to increase endoplasmic reticulum stress in SGC-7901 cells

Calcium ions are essential for the stability of the endoplasmic reticulum, and abnormal concentrations of calcium ions trigger endoplasmic reticulum stress, resulting in apoptosis. Changes in mitochondrial membrane potential are closely related to ER function of the endoplasmic reticulum. Therefore, the levels of calcium ions and mitochondrial membrane potential were evaluated to determine the effects of DATS+DDP on endoplasmic reticulum stress. As shown in Figure 5A, when DATS and DDP were used in combination, the mitochondrial membrane potential decreased significantly compared to both the DATS and DDP groups, according to the fluorescence

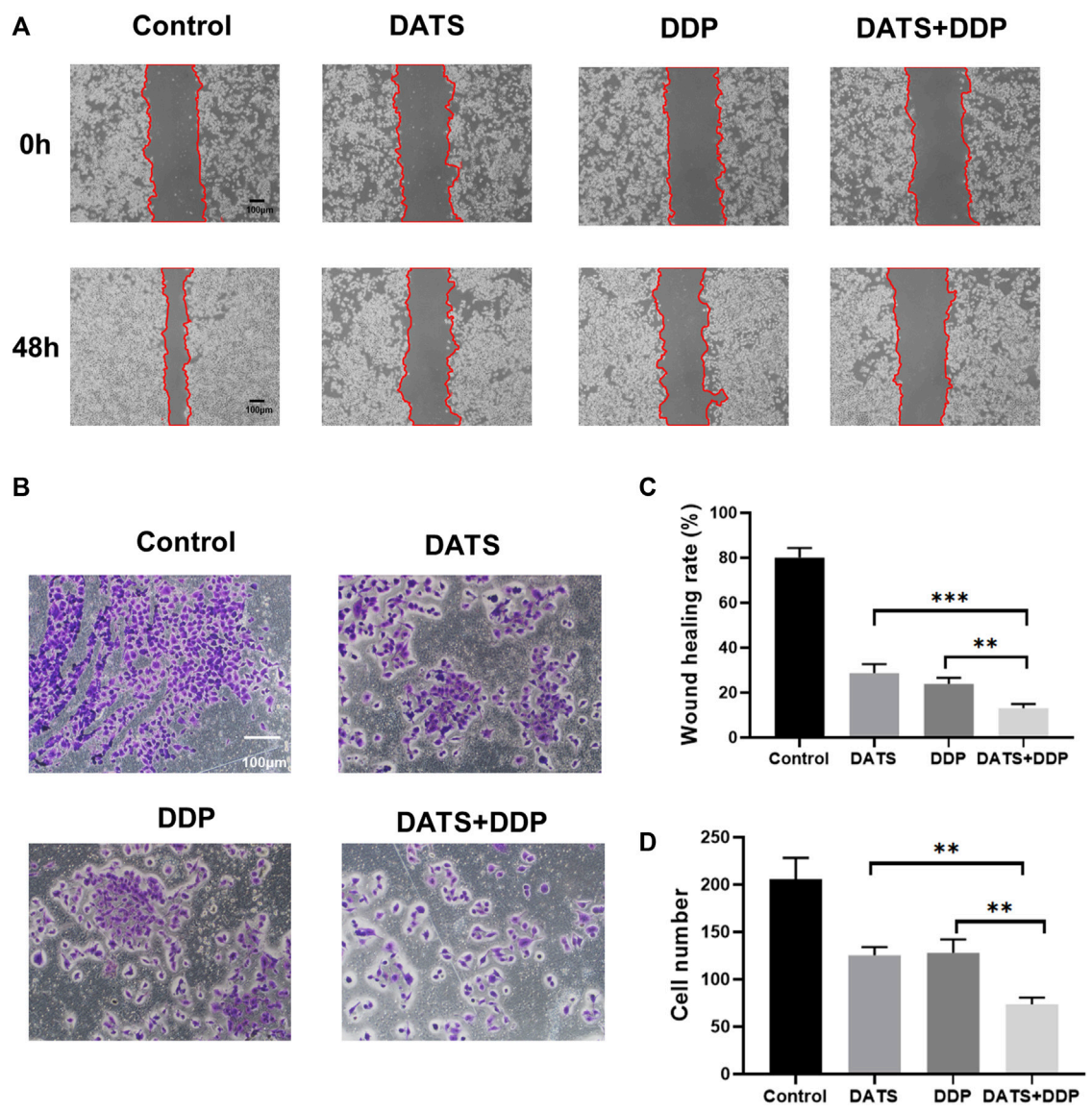

FIGURE 4
DATS synergistically enhanced the anti-migration of DDP in SGC-7901 cells. **(A)** The effects of DATS+DDP on the migration of SGC-7901 cells; **(B)** The effect of DATS+DDP on the Invasion ability of SGC-7901 cells. **(C)** Wound healing rate. **(D)** Cell number. Data are shown as the mean ± SD (n = 3). Compared to the DATS+DDP group, *p < 0.05, **p < 0.01, ***p < 0.001.

intensity of TMRE by flow cytometry (**p < 0.01, Figure 5B). Besides, the content of intracellular calcium ions (shown as fluorescence intensity of Fluo-3 a.m.) in the DATS+DDP group increased dramatically compared to that in the DATS and DDP groups (**p < 0.01, ***p < 0.001, respectively, Figure 5C). These results suggest that co-treatment with DATS and DDP triggers endoplasmic reticulum stress in SGC-7901 cells.

3.6 DATS and DDP regulated MAPK pathway, STAT3/PKC-δ and endoplasmic reticulum stress

To verify the predictions of network pharmacology, the MAPK pathway, STAT3/PKC-δ, and endoplasmic reticulum stress were detected by Western blotting. The MAPK pathway was validated using p-p38, p-ERK, and p-JNK. STAT3/PKC-δ are closely related to the proliferation and invasion of GC cells. In addition, IRE1α, XBP1, and calnexin have been reported to be key proteins in endoplasmic reticulum stress generation (Wang et al., 2013). As important nodes for the combined effects of DATS and DDP, they have been explored using network pharmacology. Our results showed that the expression of the relevant proteins (p-p38, p-ERK, p-JNK, STAT3, and PKC-δ) was remarkably reduced after DDP or DATS treatment. Compared to the monotherapy groups, a considerable decrease in (p-p38, p-ERK, p-JNK, STAT3, and PKC-δ) was observed in the DDP and DATS groups (Figures 6A, C, D, F). IRE1α expression significantly increased after treatment with DDP+DATS (Figures 6B, E). Additionally, the levels of XBP1 and Calnexin showed a trend similar to that of IRE1α (Figures 6B, E).

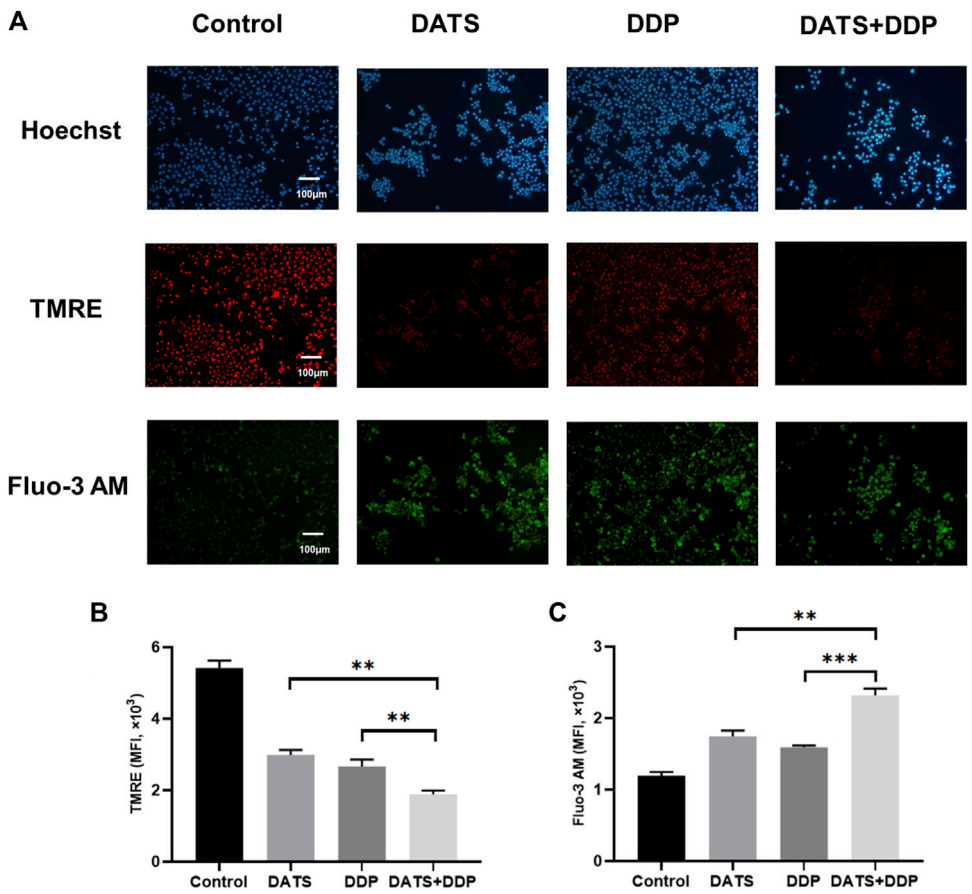

FIGURE 5
The effect of DATS and DDP on endoplasmic reticulum stress in SGC-7901 cells. **(A)** Representative immunofluorescence images of TMRE and Fluo-3 AM in SGC-7901 cells; **(B)** The expression of TMRE in SGC-7901 cells; **(C)** The expression of Fluo-3 AM in SGC-7901 cells. Data are shown as mean ± SD (n = 3). Compared with the DATS+DDP group, $*p < 0.05$, $**p < 0.01$, $***p < 0.001$.

3.7 DATS combined with DDP synergistically inhibited SGC-7901 tumor growth *in vivo*

An SGC-7901 subcutaneous xenograft model in nude mice was established to further evaluate the *in vivo* effects of combined exposure. We observed that 30 mg/kg DATS and 4 mg/kg DDP effectively inhibited SGC-7901 xenograft after a 32-day treatment. In addition, the combined treatment showed a stronger inhibitory effect on TV and tumor weight (Figures 7A–C) than the DATS and DDP groups. Representative H&E-stained tumor sections demonstrated an increase in the area of cell-cell contact loss and tissue disintegration in the DATS, DDP, and the combined group, compared to the control group (Figure 7D), and notable necrosis and the fewest tumor cell infiltration were observed in DATS and DDP-treated tumor tissues. Compared to the control group, more TUNEL-positive cells were stained in the monotherapy groups. Additionally, the number of apoptotic tumor cells in the combination group was substantially higher than that in the DATS and DDP groups ($***p < 0.001$ and $**p < 0.01$, respectively) (Figures 7E, F). Therefore, DATS synergistically enhanced the effect of DDP on tumor growth inhibition and apoptosis *in vivo*.

3.8 Combined treatment of DATS and DDP regulated MAPK pathway, STAT3/PKC-δ and endoplasmic reticulum stress *in vivo*

To verify the mechanism of the combination of DATS and DDP, the expression of p-JNK, Calnexin, XBP1 and PKC-δ was detected by immunohistochemistry. As shown in Figure 8, the expression of p-JNK and PKC-δ was decreased by DDP and DATS alone, while the expression of XBP1 and Calnexin, as signs of endoplasmic reticulum stress, was elevated compared to control group. In addition, the above changes were enhanced under the combined treatment of DATS and DDP compared with the groups treated with DATS or DDP alone.

4 Discussion

Garlic has been used in alternative medicine to treat a variety of diseases such as cardiovascular and cerebrovascular diseases (Sobenin et al., 2019), antigenic microbial infections, and several tumors (Nicastro et al., 2015; Mondal et al., 2022). DATS, the main component of garlic, was reported to exert anti-GC activity and

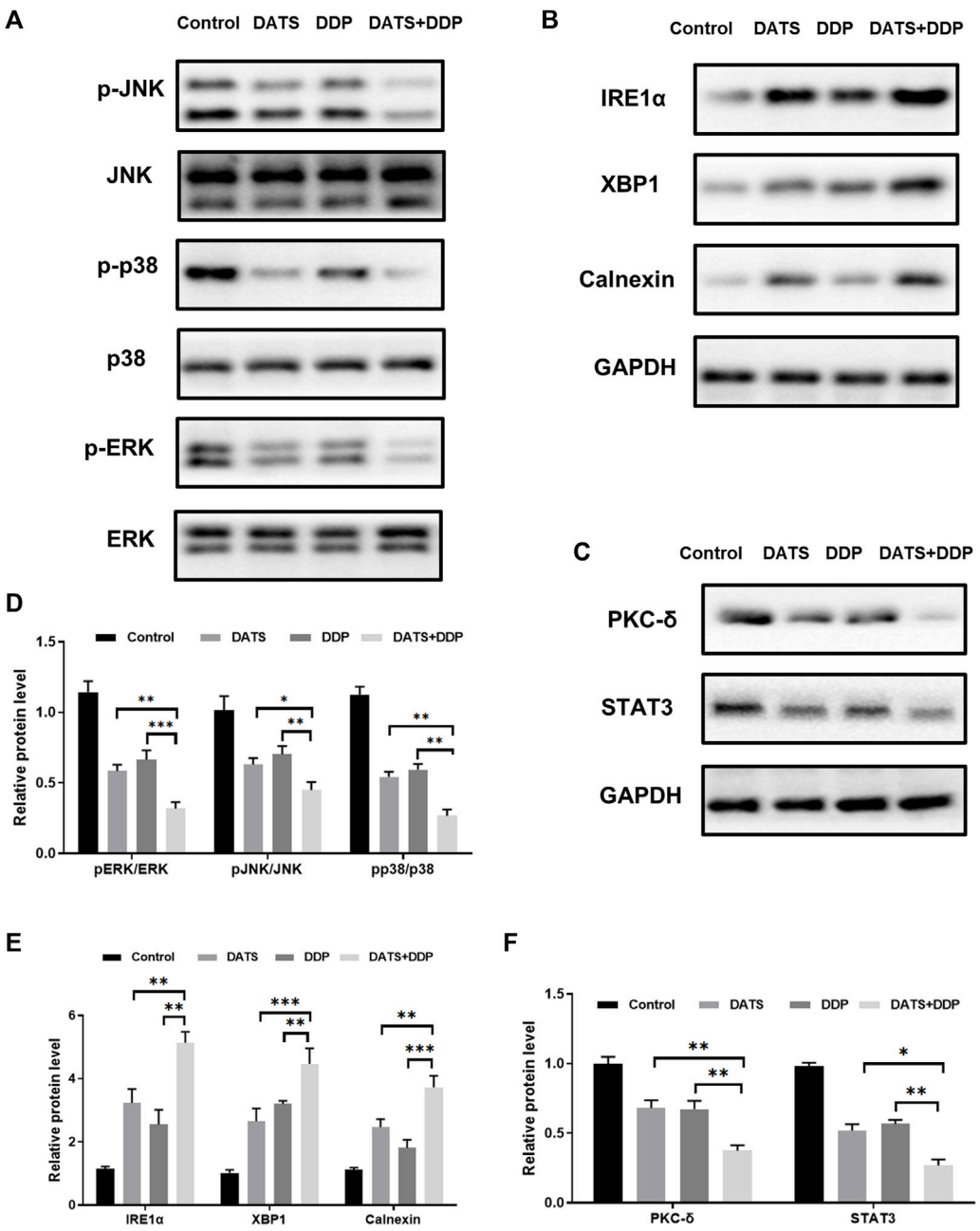

FIGURE 6
Effects of DATS and DDP on protein expressions of p-p38, p-ERK, p-JNK, STAT3, PKC-δ, IRE1α, XBP1 and Calnexin in SGC7901 cells. **(A)** p38, p-p38, ERK, p-ERK, JNK and p-JNK gel electrophoresis bands; **(B)** IRE1α, XBP1 and Calnexin gel electrophoresis bands; **(C)** STAT3 and PKC-δ gel electrophoresis bands; **(D)** p-p38, p-ERK and p-JNK protein expression; **(E)** IRE1α, XBP1 and Calnexin protein expression; **(F)** STAT3 and PKC-δ protein expression. Data are shown as mean ± SD (n = 3). Compared with the DATS and DDP group, *p < 0.05, **p < 0.01, ***p < 0.001.

enhance the chemosensitivity to GC of chemotherapeutic agent (Izdebska et al., 2016). DDP is the first-line drug used clinically for the treatment of GC, but its therapeutic effect is often affected by drug-resistance-associated problems (Fu et al., 2021). In addition, the use of high-dose DDP often causes strong side effects in patients (Dasari and Tchounwou, 2014). Therefore, by combining DATS with DDP, adverse effects may be improved by lowering the dose of DDP. On one hand, it is a promising way to reduce the development of tumor resistance by producing a synergistic anti-tumor effect. In our study, the synergistic therapeutic ability of DATS was found to enhance the anti-tumor effect of DDP in SGC-7901 cells and tumor-bearing models.

In terms of the molecular mechanism, the predictions of network pharmacology confirmed DATS played an important role in GC treatment combined with DDP in multiple pathways. PPI network analysis indicated combination of DATS and DDP may exert therapeutic effects on modulation of endoplasmic reticulum (ER) stress and STAT3/PKC-δ and MAPK signaling

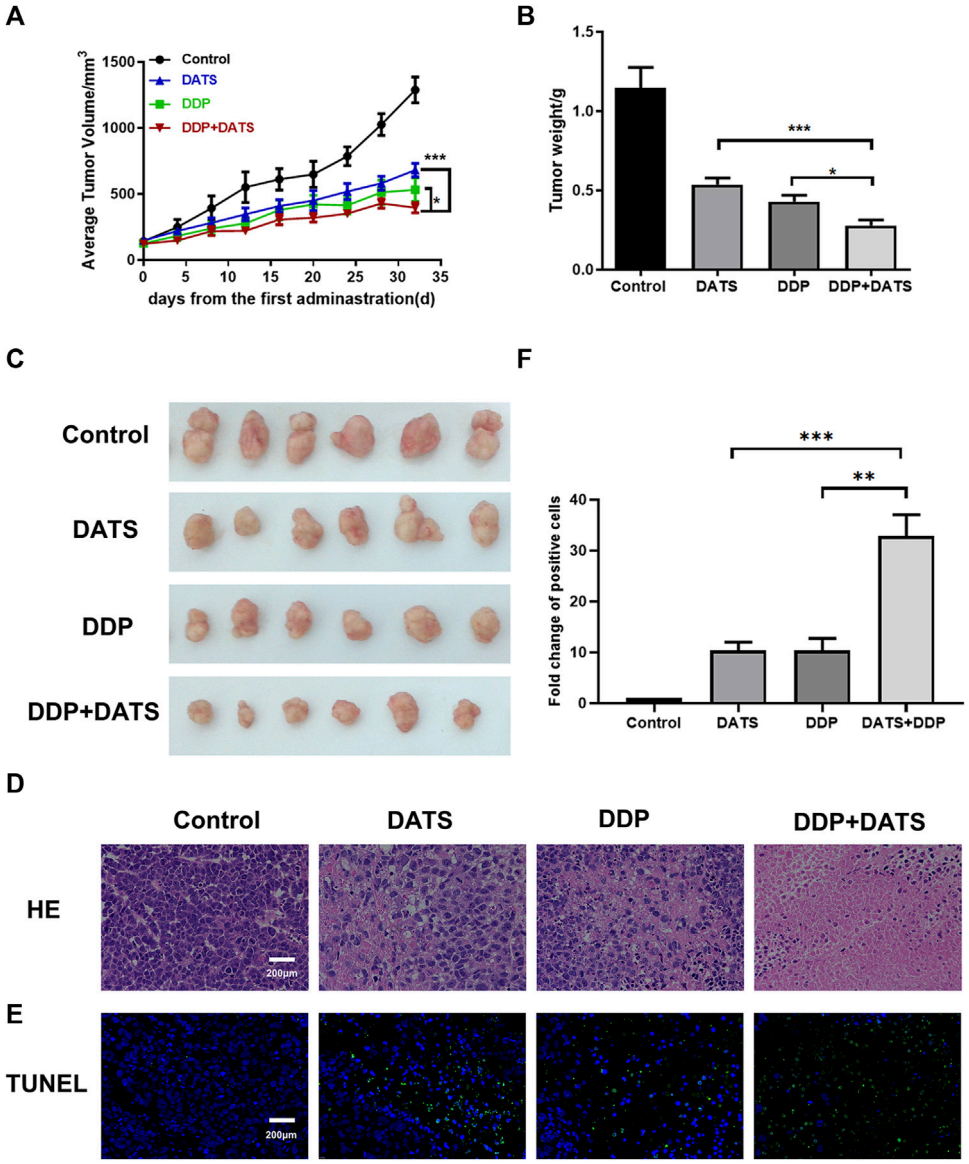

FIGURE 7
In vivo treatment of DATS and DDP in SGC-7901 tumor-bearing mice. **(A)** Average tumor volume; **(B)** Tumor weight; **(C)** Tumor morphology of mice; **(D)** HE staining results of tumor tissues; **(E)** TUNEL apoptosis results of tumor tissues; **(F)** Analysis of TUNEL-positive cells. Data are shown as mean ± SD (n = 6). Compared with the DATS+DDP group, $^{*}p < 0.05$, $^{**}p < 0.01$, $^{***}p < 0.001$.

pathways, which was consistent with the KEGG pathway and GO analyses. The results offered preliminary insights into the mechanism of action of DATS combined with DDP against GC. Experimental mechanistic studies were performed to validate the protective effects of DATS combined with DDP against GC and its possible mechanism.

Mitogen activated protein kinase (MAPK) plays a critical role in progression of GC and drug resistance. Previous studies have suggested that activation in p38-MAPK pathway may be responsible for modulating multidrug resistance in the SGC-7901/VCR cell line (Guo et al., 2008). The role of garlic components in the MAPK pathway has also been partially reported (Chang et al., 2011). In addition, sustained activation of STAT3 maintains self-renewal of tumor stem cells, making tumors prone to recurrence, metastasis, and drug resistance (Aziz et al., 2007). Therefore, STAT3 plays an important role in tumor cell transformation, infiltration, metastasis, and progression. Moreover, STAT3 can continue to activate downstream PKC-δ and promote tumor survival in multiple ways. In our study, DATS combined with DDP synergistically enhanced cell growth inhibition, induction of cell apoptosis, inhibition of MAPK signaling phosphorylation, and STAT3/PKC-δ.

When cells are exposed to stress conditions such as nutrient deficiency, hypoxia, calcium imbalance, and oxidative stress, unfolded or misfolded proteins accumulate in the endoplasmic reticulum, resulting in ER stress (Oakes and Papa, 2015). If ER stress persists or is exacerbated, ER stress shifts from a pro-survival state to a pro-apoptotic state (Ferri and Kroemer, 2001). Therefore,

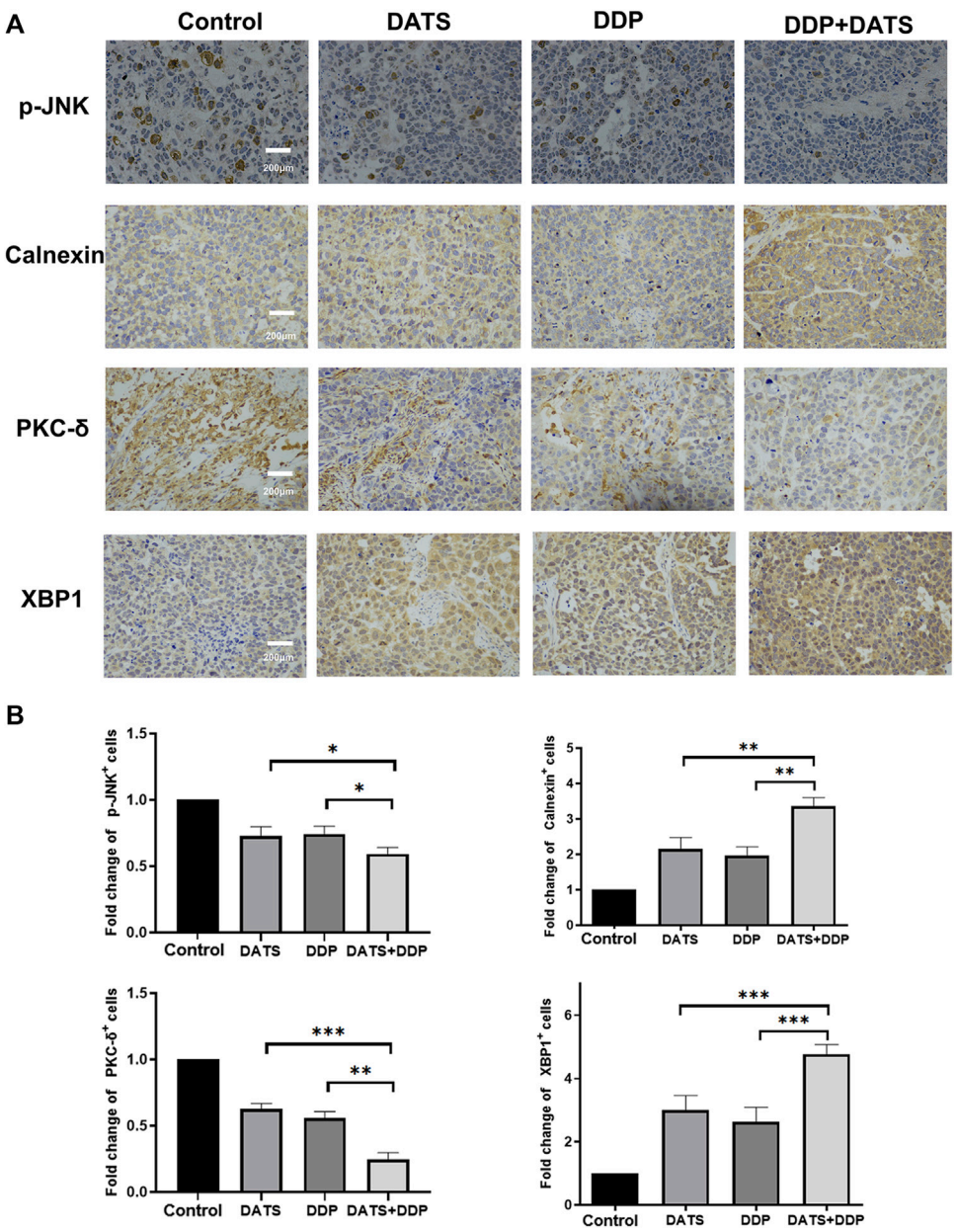

FIGURE 8
DATS and DDP regulated p-JNK, Calnexin, XBP1 and PKC-δ in SGC-7901 tumor-bearing mice. **(A)** Immunohistochemical detection of p-JNK, Calnexin, PKC-δ and XBP1 in tumor tissues; **(B)** Analysis of positive cells of p-JNK, Calnexin, PKC-δ and XBP1. Data are shown as mean ± SD (n = 3). Compared with the DATS+DDP group, *p < 0.05, **p < 0.01, ***p < 0.001.

promoting ER stress to initiate the apoptotic pathway is an anticancer therapeutic strategy (Yadav et al., 2014). In addition, persistent aggravation of ER stress also inhibits the MAPK pathway and STAT3 expression (Kim and Kim, 2018). In particular, studies focusing on cross-linking between natural products and existing chemotherapeutic agents via ER stress between apoptosis in cancer are of increasing interest (López-Antón et al., 2006; Law et al., 2010; Shi et al., 2016). It has been shown that certain drugs can induce apoptosis by inducing sustained activation of IRE1α-XBP1 and increased expression of calnexin thereby sustaining ER activation (Cubillos-Ruiz et al., 2015; Ryan et al., 2016; Wang et al., 2018). In our study, DATS combined with DDP synergistically enhanced the inhibition of ER stress.

In summary, the findings of our research confirmed that DATS increased the chemosensitivity to cisplatin in the treatment of GC, and its mechanism may be related to the MAPK pathway, STAT3/PKC-δ, and endoplasmic reticulum stress. These results suggest that DATS combined with DDP may be a new therapeutic strategy for the clinical treatment of GC. However, this study only focused on the synergistic anti-tumor activity and mechanism of DATS and DDP in normal gastric cancer cells, lacking relevant data on drug resistance and requiring further exploration.

Data availability statement

The raw data supporting the conclusions of this article will be made available by the authors, without undue reservation.

Ethics statement

The animal study was approved by Animal Care and Use Committee of Shandong University. The study was conducted in accordance with the local legislation and institutional requirements.

Author contributions

HL: Data curation, Investigation, Methodology, Software, Supervision, Writing–original draft. XuJ: Investigation, Methodology, Resources, Supervision, Writing–review and editing. HY: Writing-review and editing, Validation and Visualization. XZ: Data curation, Formal Analysis, Supervision, Writing–review and editing. ZZ: Writing–review and editing and Resources. XaJ: Funding acquisition, Supervision, Writing–review and editing.

Funding

The authors declare financial support was received for the research, authorship, and/or publication of this article. The National Natural Science Foundation of China (Grant No. 81903718) and Natural Science Foundation of Shandong Province (Grant No. ZR2019BH058) give fund supports to our work.

Conflict of interest

The authors declare that the research was conducted in the absence of any commercial or financial relationships that could be construed as a potential conflict of interest.

Publisher's note

All claims expressed in this article are solely those of the authors and do not necessarily represent those of their affiliated organizations, or those of the publisher, the editors and the reviewers. Any product that may be evaluated in this article, or claim that may be made by its manufacturer, is not guaranteed or endorsed by the publisher.

References

Aziz, M. H., Manoharan, H. T., Sand, J. M., and Verma, A. K. (2007). Protein kinase Cepsilon interacts with Stat3 and regulates its activation that is essential for the development of skin cancer. *Mol. Carcinog.* 46 (8), 646–653. doi:10.1002/mc.20356

Chang, S. H., Liu, C. J., Kuo, C. H., Chen, H., Lin, W. Y., Teng, K. Y., et al. (2011). Garlic oil alleviates MAPKs- and IL-6-mediated diabetes-related cardiac hypertrophy in STZ-induced DM rats. *Evid. Based Complement. Altern. Med.* 2011, 950150. doi:10.1093/ecam/neq075

Chiarandini Fiore, J. P., Fanelli, S. L., de Ferreyra, E. C., and Castro, J. A. (2008). Diallyl disulfide prevention of cis-Diamminedichloroplatinum-induced nephrotoxicity and leukopenia in rats: potential adjuvant effects. *Nutr. Cancer* 60 (6), 784–791. doi:10.1080/01635580802100869

Chou, T. C. (2010). Drug combination studies and their synergy quantification using the Chou-Talalay method. *Cancer Res.* 70 (2), 440–446. doi:10.1158/0008-5472.CAN-09-1947

Cubillos-Ruiz, J. R., Silberman, P. C., Rutkowski, M. R., Chopra, S., Perales-Puchalt, A., Song, M., et al. (2015). ER stress sensor XBP1 controls anti-tumor immunity by disrupting dendritic cell homeostasis. *Cell* 161 (7), 1527–1538. doi:10.1016/j.cell.2015.05.025

Dasari, S., and Tchounwou, P. B. (2014). Cisplatin in cancer therapy: molecular mechanisms of action. *Eur. J. Pharmacol.* 740, 364–378. doi:10.1016/j.ejphar.2014.07.025

Dwivedi, C., Abu-Ghazaleh, A., and Guenther, J. (1996). Effects of diallyl sulfide and diallyl disulfide on cisplatin-induced changes in glutathione and glutathione-S-transferase activity. *Anticancer Drugs* 7 (7), 792–794. doi:10.1097/00001813-199609000-00012

Ferri, K. F., and Kroemer, G. (2001). Organelle-specific initiation of cell death pathways. *Nat. Cell Biol.* 3 (11), E255–E263. doi:10.1038/ncb1101-e255

Fu, D., Wang, C., Yu, L., and Yu, R. (2021). Induction of ferroptosis by ATF3 elevation alleviates cisplatin resistance in gastric cancer by restraining Nrf2/Keap1/xCT signaling. *Cell Mol. Biol. Lett.* 26 (1), 26. doi:10.1186/s11658-021-00271-y

Gao, C., Jiang, X., Wang, H., Zhao, Z., and Wang, W. (2013). Drug metabolism and pharmacokinetics of organosulfur compounds from garlic. *J. Drug Metabolism Toxicol.* 4, 1–10. doi:10.4172/2157-7609.1000159

Ghosh, S. (2019). Cisplatin: the first metal based anticancer drug. *Bioorg Chem.* 88, 102925. doi:10.1016/j.bioorg.2019.102925

Gomez-Sierra, T., Molina-Jijon, E., Tapia, E., Hernandez-Pando, R., Garcia-Nino, W. R., Maldonado, P. D., et al. (2014). S-allylcysteine prevents cisplatin-induced nephrotoxicity and oxidative stress. *J. Pharm. Pharmacol.* 66 (9), 1271–1281. doi:10.1111/jphp.12263

Guo, X., Ma, N., Wang, J., Song, J., Bu, X., Cheng, Y., et al. (2008). Increased p38-MAPK is responsible for chemotherapy resistance in human gastric cancer cells. *BMC Cancer* 8, 375. doi:10.1186/1471-2407-8-375

Iciek, M., Kwiecien, I., and Wlodek, L. (2009). Biological properties of garlic and garlic-derived organosulfur compounds. *Environ. Mol. Mutagen* 50 (3), 247–265. doi:10.1002/em.20474

Izdebska, M., Grzanka, D., Gagat, M., Halas-Wisniewska, M., and Grzanka, A. (2016). Downregulation of importin-9 protects MCF-7 cells against apoptosis induced by the combination of garlic-derived alliin and paclitaxel. *Oncol. Rep.* 35 (5), 3084–3093. doi:10.3892/or.2016.4628

Jiang, X., Zhu, X., Huang, W., Xu, H., Zhao, Z., Li, S., et al. (2017). Garlic-derived organosulfur compound exerts antitumor efficacy via activation of MAPK pathway and modulation of cytokines in SGC-7901 tumor-bearing mice. *Int. Immunopharmacol.* 48, 135–145. doi:10.1016/j.intimp.2017.05.004

Jin, Z. Y., Wu, M., Han, R. Q., Zhang, X. F., Wang, X. S., Liu, A. M., et al. (2013). Raw garlic consumption as a protective factor for lung cancer, a population-based case-control study in a Chinese population. *Cancer Prev. Res. (Phila)* 6 (7), 711–718. doi:10.1158/1940-6207.CAPR-13-0015

Kim, C., and Kim, B. (2018). Anti-cancer natural products and their bioactive compounds inducing ER stress-mediated apoptosis: a review. *Nutrients* 10 (8), 1021. doi:10.3390/nu10081021

Lai, K. C., Hsu, S. C., Kuo, C. L., Yang, J. S., Ma, C. Y., Lu, H. F., et al. (2013). Diallyl sulfide, diallyl disulfide, and diallyl trisulfide inhibit migration and invasion in human colon cancer colo 205 cells through the inhibition of matrix metalloproteinase-2, -7, and -9 expressions. *Environ. Toxicol.* 28 (9), 479–488. doi:10.1002/tox.20737

Law, B. Y., Wang, M., Ma, D. L., Al-Mousa, F., Michelangeli, F., Cheng, S. H., et al. (2010). Alisol B, a novel inhibitor of the sarcoplasmic/endoplasmic reticulum Ca(2+) ATPase pump, induces autophagy, endoplasmic reticulum stress, and apoptosis. *Mol. Cancer Ther.* 9 (3), 718–730. doi:10.1158/1535-7163.Mct-09-0700

Li, W. Q., Zhang, J. Y., Ma, J. L., Li, Z. X., Zhang, L., Zhang, Y., et al. (2019). Effects of *Helicobacter pylori* treatment and vitamin and garlic supplementation on gastric cancer incidence and mortality: follow-up of a randomized intervention trial. *BMJ* 366, l5016. doi:10.1136/bmj.l5016

Li, X., Wei, S., Niu, S., Ma, X., Li, H., Jing, M., et al. (2022). Network pharmacology prediction and molecular docking-based strategy to explore the potential mechanism of Huanglian Jiedu Decoction against sepsis. *Comput. Biol. Med.* 144, 105389. doi:10.1016/j.compbiomed.2022.105389

López-Antón, N., Rudy, A., Barth, N., Schmitz, M. L., Pettit, G. R., Schulze-Osthoff, K., et al. (2006). The marine product cephalostatin 1 activates an endoplasmic reticulum stress-specific and apoptosome-independent apoptotic signaling pathway. *J. Biol. Chem.* 281 (44), 33078–33086. doi:10.1074/jbc.M607904200

Merouani, A., Shpall, E. J., Jones, R. B., Archer, P. G., and Schrier, R. W. (1996). Renal function in high dose chemotherapy and autologous hematopoietic cell support treatment for breast cancer. *Kidney Int.* 50 (3), 1026–1031. doi:10.1038/ki.1996.405

Mondal, A., Banerjee, S., Bose, S., Mazumder, S., Haber, R. A., Farzaei, M. H., et al. (2022). Garlic constituents for cancer prevention and therapy: from phytochemistry to novel formulations. *Pharmacol. Res.* 175, 105837. doi:10.1016/j.phrs.2021.105837

Nasr, A. Y., and Saleh, H. A. (2014). Aged garlic extract protects against oxidative stress and renal changes in cisplatin-treated adult male rats. *Cancer Cell Int.* 14 (1), 92. doi:10.1186/s12935-014-0092-x

Nicastro, H. L., Ross, S. A., and Milner, J. A. (2015). Garlic and onions: their cancer prevention properties. *Cancer Prev. Res. (Phila)* 8 (3), 181–189. doi:10.1158/1940-6207.CAPR-14-0172

Nogales, C., Mamdouh, Z. M., List, M., Kiel, C., Casas, A. I., and Schmidt, H. (2022). Network pharmacology: curing causal mechanisms instead of treating symptoms. *Trends Pharmacol. Sci.* 43 (2), 136–150. doi:10.1016/j.tips.2021.11.004

Oakes, S. A., and Papa, F. R. (2015). The role of endoplasmic reticulum stress in human pathology. *Annu. Rev. Pathol.* 10, 173–194. doi:10.1146/annurev-pathol-012513-104649

Razo-Rodriguez, A. C., Chirino, Y. I., Sanchez-Gonzalez, D. J., Martinez-Martinez, C. M., Cruz, C., and Pedraza-Chaverri, J. (2008). Garlic powder ameliorates cisplatin-induced nephrotoxicity and oxidative stress. *J. Med. Food* 11 (3), 582–586. doi:10.1089/jmf.2008.0033

Ryan, D., Carberry, S., Murphy, A. C., Lindner, A. U., Fay, J., Hector, S., et al. (2016). Calnexin, an ER stress-induced protein, is a prognostic marker and potential therapeutic target in colorectal cancer. *J. Transl. Med.* 14 (1), 196. doi:10.1186/s12967-016-0948-z

Sasaki, K., Onodera, S., Otsuka, K., Satomura, H., Kurayama, E., Kubo, T., et al. (2017). Validity of neoadjuvant chemotherapy with docetaxel, cisplatin, and S-1 for resectable locally advanced gastric cancer. *Med. Oncol.* 34 (8), 139. doi:10.1007/s12032-017-0997-z

Shah, M. A. (2015). Update on metastatic gastric and esophageal cancers. *J. Clin. Oncol.* 33 (16), 1760–1769. doi:10.1200/JCO.2014.60.1799

Shi, S., Tan, P., Yan, B., Gao, R., Zhao, J., Wang, J., et al. (2016). ER stress and autophagy are involved in the apoptosis induced by cisplatin in human lung cancer cells. *Oncol. Rep.* 35 (5), 2606–2614. doi:10.3892/or.2016.4680

Sivam, G. P. (2001). Protection against *Helicobacter pylori* and other bacterial infections by garlic. *J. Nutr.* 131 (3), 1106S–1108S. doi:10.1093/jn/131.3.1106S

Sobenin, I. A., Myasoedova, V. A., Iltchuk, M. I., Zhang, D. W., and Orekhov, A. N. (2019). Therapeutic effects of garlic in cardiovascular atherosclerotic disease. *Chin. J. Nat. Med.* 17 (10), 721–728. doi:10.1016/S1875-5364(19)30088-3

Sung, H., Ferlay, J., Siegel, R. L., Laversanne, M., Soerjomataram, I., Jemal, A., et al. (2021). Global cancer statistics 2020: GLOBOCAN estimates of incidence and mortality worldwide for 36 cancers in 185 countries. *CA Cancer J. Clin.* 71 (3), 209–249. doi:10.3322/caac.21660

Tsai, C. W., Yang, J. J., Chen, H. W., Sheen, L. Y., and Lii, C. K. (2005). Garlic organosulfur compounds upregulate the expression of the pi class of glutathione S-transferase in rat primary hepatocytes. *J. Nutr.* 135 (11), 2560–2565. doi:10.1093/jn/135.11.2560

Tsubura, A., Lai, Y. C., Kuwata, M., Uehara, N., and Yoshizawa, K. (2011). Anticancer effects of garlic and garlic-derived compounds for breast cancer control. *Anticancer Agents Med. Chem.* 11 (3), 249–253. doi:10.2174/187152011795347441

Wang, F., Reece, E. A., and Yang, P. (2013). Superoxide dismutase 1 overexpression in mice abolishes maternal diabetes-induced endoplasmic reticulum stress in diabetic embryopathy. *Am. J. Obstet. Gynecol.* 209 (4), 345.e341–e7. doi:10.1016/j.ajog.2013.06.037

Wang, Y., Guo, S. H., Shang, X. J., Yu, L. S., Zhu, J. W., Zhao, A., et al. (2018). Triptolide induces Sertoli cell apoptosis in mice via ROS/JNK-dependent activation of the mitochondrial pathway and inhibition of Nrf2-mediated antioxidant response. *Acta Pharmacol. Sin.* 39 (2), 311–327. doi:10.1038/aps.2017.95

Yadav, R. K., Chae, S. W., Kim, H. R., and Chae, H. J. (2014). Endoplasmic reticulum stress and cancer. *J. Cancer Prev.* 19 (2), 75–88. doi:10.15430/jcp.2014.19.2.75

Yan, S., Li, B., Bai, Z. Z., Wu, J. Q., Xie, D. W., Ma, Y. C., et al. (2014). Clinical epidemiology of gastric cancer in Hehuang valley of China: a 10-year epidemiological study of gastric cancer. *World J. Gastroenterol.* 20 (30), 10486–10494. doi:10.3748/wjg.v20.i30.10486

Frontiers in Pharmacology

Explores the interactions between chemicals and living beings

The most cited journal in its field, which advances access to pharmacological discoveries to prevent and treat human disease.

Discover the latest Research Topics

See more →

Frontiers

Avenue du Tribunal-Fédéral 34
1005 Lausanne, Switzerland
frontiersin.org

Contact us

+41 (0)21 510 17 00
frontiersin.org/about/contact